

# **IRE Transactions**

PERIODICAL  
UNIVERSITY OF HAWAII  
LIBRARY



## **ON MILITARY ELECTRONICS**

Volume MIL-4

APRIL-JULY, 1960

Numbers 2-3

U. S. ARMY SPACE ISSUE

PART I—ARMY PROJECT JUNO I AND II

PART II—ARMY COMMUNICATION SATELLITE ACTIVITIES

PART III—ARMY ROLE IN OTHER SPACE ACTIVITIES

PART IV—ARMY SATELLITE AND SPACE PROBE TRACKING

~~TK 7800~~  
~~524~~

UG-485  
A1113

PUBLISHED BY THE

**PROFESSIONAL GROUP ON MILITARY ELECTRONICS**

## **IRE PROFESSIONAL GROUP ON MILITARY ELECTRONICS**

### **Administrative Committee**

#### **Chairman**

HENRY RANDALL

#### **Vice-Chairmen**

E. C. CALLAHAN (East Coast)

L. A. G. VER TEEN (West Coast)

#### **Secretary**

L. SULLIVAN

#### **Treasurer**

C. L. ENGLEMAN

A. S. BROWN

J. H. DAVITT

M. H. SCHRENK

J. F. BYRNE

S. W. HERWALD

C. A. STROM

W. E. CLEAVES

P. C. MUNROE

A. J. WILDE

W. L. DOXEY

J. C. MYERS

E. G. WITTING

H. DAVIS

D. R. RHODES

D. N. YATES

#### **Editors**

J. Q. BRANTLEY, JR.

D. R. RHODES

## **IRE TRANSACTIONS® ON MILITARY ELECTRONICS**

Published by the Institute of Radio Engineers, Inc., for the Professional Group on Military Electronics at 1 East 79th Street, New York 21, New York. Responsibility for the contents rests upon the authors, and not upon the IRE, the Group, or its members. Individual copies available for sale to IRE-PGMIL members at \$5.75; to IRE members at \$8.60; and to nonmembers at \$17.25.

COPYRIGHT © 1960—THE INSTITUTE OF RADIO ENGINEERS, INC.

Printed in U.S.A.

All rights, including translation, are reserved by the IRE. Requests for republication privileges should be addressed to the Institute of Radio Engineers, 1 E. 79th St., New York 21, N. Y.



## TABLE OF CONTENTS

Frontispiece.....	Hans K. Ziegler	62
Guest Editorial.....	Hans K. Ziegler	63

## PART I—ARMY PROJECT JUNO I AND II

Army Activities in Space—A History.....	Ernst Stuhlinger	64
General Description and Design of the Configuration of the Juno I and Juno II Launching Vehicles.....	Bill B. Greever	70
Explorer Satellite Electronics.....	W. K. Victor, H. L. Richter and J. P. Eyraud	78
Considerations to the Development of Explorer VII Satellite.....	Josef Boehm	86
Scientific Objectives of Explorer VII.....	A. W. Thompson	93
Problems Concerning the Thermal Design of Explorer Satellites.....	Gerhard B. Heller	98
Army Role in Project Argus.....	R. D. Shelton and A. W. Thompson	112
The Impact of the Argus Experiment on Hydromagnetic-Wave Research.....	Hans A. Bomke	120
Pioneer III and IV Space Probes.....	H. Curtis and D. Schneiderman	123
Early Orbit Determination Scheme for the Juno Space Vehicle.....	F. Kurtz and F. Speer	129
Outlay of Trajectories for the Army's Juno I and Juno II Program.....	O. Jean	145
Deep Space Communications.....	W. D. Merrick, E. Reichtin, R. Stevens and W. K. Victor	158
Lunar Circumnavigation.....	H. O. Ruppe and C. L. Barker, Jr.	163
Evolution of the Saturn Booster Telemetry System.....	James E. Rorex	169

## PART II—ARMY COMMUNICATION SATELLITE ACTIVITIES

The Significance of Military Communication Satellites.....	Clifford D. May, Jr.	176
Concerning Optimum Frequencies for Space Vehicle Communication.....	S. Perlman, W. J. Russell, Jr. and F. H. Dickson	184
Project SCORE: Signal Communication by Orbiting Relay Equipment.....	Samuel P. Brown	193
A Delayed-Repeater Satellite Communication System of Advanced Design.....	T. P. Mottley, D. H. Marx and W. P. Teetsel	195
Progressive Communication Satellite Systems Design.....	J. E. Bartow, D. L. Jacoby and G. N. Krassner	208

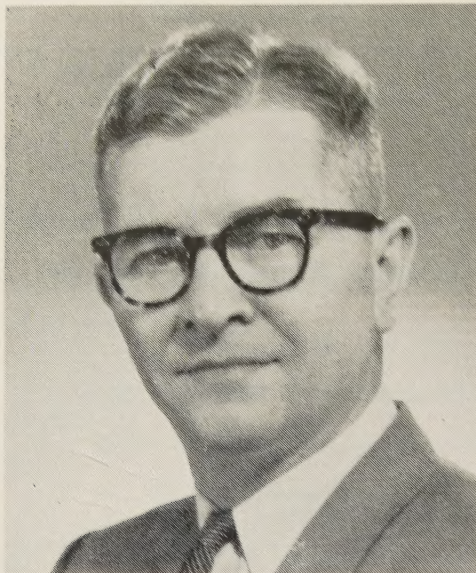
## PART III—ARMY ROLE IN OTHER SPACE ACTIVITIES

USASRD Upper-Air Research with Rockets.....	H. J. aufm Kampe and J. R. Walsh	216
Upper Atmospheric Research at the Ballistic Research Laboratories.....	John C. Mester	222
The Radar Beacon Comes Into Its Own.....	Perry L. White	228
Preliminary Radar Performance Data on Passive Rocket-Borne Wind Sensors.....	Norman J. Beyers	230
Automatic Meteorological Data Collecting System.....	R. Thomas and M. McLardie	234
Rocket Sounding of High Atmosphere Meteorological Parameters.....	K. R. Jenkins, W. L. Webb and G. Q. Clark	238
Automatic Rocket Impact Predictor.....	Louis D. Duncan	243
The Satellite Vanguard II: Cloud Cover Experiment.....	R. A. Hanel, J. Licht, W. Nordberg, R. A. Stampfl and W. G. Stroud	245
TIROS—The System and Its Evolution.....	H. I. Butler and S. Sternberg	248
Surveying and Mapping from Space.....	Charles S. Spooner, Jr.	256
Radio Interferometry Applied to Geodesy.....	Werner D. Kahn	259
Application of Electronic Distance Measuring Equipment in Surveying.....	Thelma A. Robinson	263
Semi-Active Correlation Radar Employing Satellite-Borne Illumination.....	O. E. Rittenbach and W. Fishbein	268
Artificial Ionospheres for Communications.....	F. F. Marmo and A. Engelman	270
Basic Research Efforts in Astrobiology.....	R. S. Young and J. L. Johnson	284
Bio-Telemetry in the Nose Cones of U. S. Army Jupiter Missiles.....	S. J. Gerathewohl, S. W. Downs, Jr., G. A. Champlin and E. S. Wilbarger, Jr.	288
Recovery System Development.....	R. M. Barraza and W. G. Huber	303
Electronic Components for Space Instrumentation.....	James P. McNaull	308
Power Sources Designed For Space.....	W. Shorr, D. Linden and A. F. Daniel	313
Launching Procedures for Space Vehicles.....	Daniel D. Collins	317

## PART IV—ARMY SATELLITE AND SPACE PROBE TRACKING

From an Early Sputnik Diary.....	Harold A. Zahl	320
Army Participation in Project Vanguard.....	W. E. Smitherman	323
The Signal Corps Astro-Observation Center, Fort Monmouth, N. J.....	L. H. Manamon and A. S. Gross	327
Tracking in Space by DOPLOC.....	L. G. deBey	332
Orbit Determination from Single Pass Doppler Observations.....	R. B. Patton, Jr.	336
Comparison of Precalculated Orbital Elements of the Army Explorer Satellites with the Actual Elements Derived from Observations.....	H. G. L. Krause and R. N. DeWitt	345
Tracking Experiments with Pioneer IV.....	T. A. Barr and C. A. Lundquist	355
Review of USASRD Satellite Propagation Studies.....	P. R. Arendt	359
Analysis of Satellite Motion from Radio Reception.....	Friedrich O. Vonbun	361
World-Wide Clock Synchronization.....	F. H. Reder and G. M. R. Winkler	366
Contributors.....		377





## Hans K. Ziegler

Hans K. Ziegler (SM'56) was born on March 1, 1911, in Munich, Germany. He received the following degrees from the Technical University of Munich: the German equivalents of B.S. in 1932, M.S. in 1934, and the Ph.D. in 1936, all in electrical engineering.

Between 1934 and 1936 Dr. Ziegler was the German equivalent of an Assistant Professor in Electrical Engineering at the Technical University, Munich, pursuing research in dielectrics and in the theory of nonlinear circuits. In 1936 he accepted a research position with the Rosenthal Isolatoren G.M.B.H. in Selb, Germany, a subsidiary of the AEG, where he spent the first three years in research of dielectrics, high-voltage phenomena, lightning, high-current arcs, and energy transmission. Soon after the beginning of World War II, he was appointed Chief of the Research and Development Department of the company and his work shifted to military electronics for the German Army and Air Force. Electronic fuze systems for bombs, shells, and mines, proximity fuze systems and many other aspects of military electronics and communications, and associated components, were his major assignment.

After the war he was invited by the U. S. Government to come to this country and in March, 1947, he joined the Army Signal Corps Laboratory at Fort Monmouth, N.J., where he has been for the past thirteen years.

In 1954 he became a United States citizen.

For eight years he was a Scientific Consultant to what is now the Electronic Components Research Department of the Army Signal Corps Laboratory, and has made major research contributions to the field of energy generation and conversion, and to the electronic components field. In 1955

he was assigned to the Office of the Director of Research to guide the Laboratory's Space Electronics and Geophysical Programs. In 1956 he was appointed Assistant Director of Research, with research in meteorology and electronic components added to his assignments.

In late 1958 he became Director of the newly established Astro-Electronics Division. Under his leadership, since 1955, the Army Signal Corps has produced major contributions to space electronics, among which are the first solar power supply for Satellite 1958 Beta, the SCORE communications electronics for Satellite 1958 Zeta, and the Vanguard cloud cover electronics for Satellite 1959 Alpha. It has technically supervised further the TIROS electronics for Satellite 1960 Beta and presently is developing various advanced satellite communication systems.

During the IGY, he was a Defense Department Delegate to the Technical Panel on the Earth Satellite Program of the NAS and a U. S. Delegate at the 5th CSAGI conference at Moscow, 1958.

In August, 1959, the Signal Corps appointed Dr. Ziegler to the position of Chief Scientist of the U. S. Army Signal Research and Development Laboratory at Fort Monmouth.

He has published numerous scientific and technical papers, holds a number of patents, and is a frequent speaker, lecturer, and moderator to the scientific community throughout this country and abroad.

Dr. Ziegler is the 1960-61 President of the Armed Forces Communications and Electronics Association Fort Monmouth Chapter, and also serves on various military and civilian committees and panels.



## Guest Editorial

HANS K. ZIEGLER

OVER the past 100 years the United States Army has established a proud record of pioneering on many scientific and technological frontiers. The experience of each war in retrospect has generated an energetic and imaginative drive for progress which has allowed it to set many outstandingly significant milestones of success, to make this country safer, improve our mode of living, and enhance the Nation's prestige in the world. These accomplishments not only cover many aspects of electronics, but also very much include the physical, chemical, engineering, biological and medical sciences. In some instances the results of the progressive undertakings grew to such magnitude and importance that the Nation decided to establish organizations devoted completely to the newly-created disciplines or potentials.

The U. S. Weather Bureau's transfer in 1890 to the Department of the Interior after origination by the Army in 1870; the establishment of the U. S. Air Force as an independent third military service in 1947 as the result of the Army's forward-looking initiation of an Aeronautical Division of the Signal Corps in 1907, and its 40 years aggressive effort in the aviation field; the foundation for the activities of the Atomic Energy Commission as an outgrowth of the Manhattan Project (for which the Army had an important responsibility)—these are only a few examples of the Nation's trend to utilize the Army as a trail blazer into new areas of science and technology.

The advent of the Space Age found the Army well prepared. Its own capabilities gained in years of endeavor in the scientific and engineering fields—supplemented by the Free World's most experienced rocket and missile team under Dr. Wernher von Braun—enabling it to establish an unsurpassed record of achievements in many aspects of our military and civilian space effort.

The Army's first successful electronic contact with the moon in 1946 from the Diana Radar at Fort Monmouth, N.J., extended man's information beyond the earth's environment and paved the way for later space-age electronics.

In 1949 a V2 rocket with WAC Corporal second stage, fired at White Sands, New Mexico, reached up 250 miles and provided the first physical penetration into outer space.

In 1956 a Jupiter C test firing exhibited a performance which obviously had the inherent capabilities of launching an earth satellite.

In 1957 another Jupiter C test firing furnished the first solution to the re-entry problem—the nose cone which President Eisenhower proudly displayed in his talk to the Nation.

In January, 1958, the Army launched Explorer I, the first satellite of the United States and the Free World.

In March, 1959, the Army placed the first U. S. satellite, PIONEER IV, into orbit around the sun.

In addition to these and other launching successes, it has contributed many firsts to the payload electronics of various satellites. The first solar power supply was provided for the small IGY satellite Vanguard I in 1958. The first satellite communications system, Project SCORE, transmitting the President's 1958 Christmas message to the world, was an Army project. So was the first cloud cover electronics carried by the IGY satellite Vanguard II in 1959.

In the biological field, after a journey into outer space, the first recovery of live premates, Able and Baker, was an Army achievement.

These are only a few of the outstanding milestones associated with a wealth of new scientific information found along the long road of Army space activities. The accompanying papers are an attempt to give the reader a cross section through the past and some of the future contemplated work, much of which has been and will be conducted in close cooperation with other military and civilian agencies and industry. All of this work is closely related to the field of electronics.

This issue is arranged in four parts to tell the story of JUNO I and II satellites and space probes, of the Communications Satellites, of the many other space endeavors, and the story of the satellite tracking effort. Acknowledgment is due to all who have contributed and helped to make this publication possible.

The Army has its own important role in space—as other military services have. The utilization of space technology in the future fulfillment of its assigned missions in the areas of communications: air defense, reconnaissance (including meteorology) and mapping, will be an indispensable requirement, for which proper implementation is on the way.

The Army is indeed proud of its major part in launching the United States space effort and will continue in this field consistent with its roles and missions. But perhaps more important, the imagination which has led to so many of our Nation's "firsts" is now aggressively at work, and, inevitably, new concepts or potentials of great importance and significance will come out of its laboratories—concepts vital to superior defense, and as history has so often demonstrated, concepts which also lead to better living.



# Army Activities in Space—A History\*

ERNST STUHLINGER†

**Summary**—This paper presents an account of the Army's role in missile development and achievements. It begins by giving a short historical account of the Army's missile and space program. It then gives an explanation of the Army's present role in missiles and space. Finally it gives a few proposals for the future. Also included is a list of "Firsts" that are credited to the Army in its role of missile and space achievements.

This paper also gives the achievements and capabilities of the Redstone, Jupiter and modified Jupiter (JUNO I and JUNO II) vehicles, and some of the capabilities of the Saturn vehicle.

THE first encounter of the U. S. Army with space above balloon altitudes dates back to 1946. The captured components of a number of German V-2 missiles were assembled at that time in the hangars of White Sands Proving Ground in New Mexico, and from the spring of 1946 until the summer of 1951 approximately 70 of the big rockets were launched, most of them successfully.

The primary purpose of these launchings was to familiarize the troops, and also the potential future missile manufacturers, with the peculiarities of guided missiles. However, it quickly became apparent that these huge rocket vehicles with their empty warhead compartments offered a unique and unprecedented opportunity to carry scientific instruments to altitudes of a hundred miles and above.

The Army offered free rides into space to the developers of flight instruments, and to scientists all over the country. It did not take long before the test firings at White Sands represented a scientific program of the first order. The Naval Research Laboratory developed and operated a telemetry system. Many research teams from companies and universities prepared instruments, and an impressive number of scientific data were obtained and published during those years.

An "Upper Atmosphere Research Panel" was established in 1946 under the excellent chairmanship of Dr. James Van Allen from the State University of Iowa. This panel organized the experimental work and gave advice and guidance for its evaluation. A direct outgrowth of this panel is the scientific forum, the Rocket and Satellite Research Panel, where measurements and discoveries from space probes are first discussed. Many of its present members are veterans of the old V-2 days in White Sands who look back not only over a most distinguished record of accomplishments in space science, but also over a remarkably long period of stability of their space exploration program.

\* Manuscript received by the PGMIL, February 1, 1960.

† Research Projects Lab., Army Ballistic Missile Agency, Redstone Arsenal, Huntsville, Ala.

One outstanding achievement of this rocket firing program was the "Bumper Project," in which the Army and the Jet Propulsion Laboratory teamed up to combine the V-2 and a Corporal rocket into a two-stage missile. The nose cone of this vehicle, which carried a number of measuring instruments, reached an unprecedented altitude of 250 miles in February, 1949. The first Corporal, developed by the Jet Propulsion Laboratory under Army auspices, was launched in 1947.

Shortly after World War II, the Army started experimenting in the field of radio signal propagation through outer space. On January 10, 1946, the Signal Corps Engineering Laboratories beamed a radar signal towards the moon and received the reflected signal two seconds later. A radar frequency of 111.5 mc and a power of at first 3 kw, and later 7 kw, was used. Distinct echos were detected 22 times in 111 attempts. Since those early experiments, considerable progress has been made in the Moon relay project. Venus, also, was successfully used as a reflector. Many anomalies in propagation and reflection are still unresolved, but significant strides toward interplanetary communication and navigation were achieved.

While the test firings of the old V-2 missiles were underway at White Sands Proving Ground, the Army built up its guided missile development team very quietly at Fort Bliss, Tex. Major General Toftoy, then Colonel, who had organized the transfer of Dr. von Braun and a number of his associates from Germany to the Fort Bliss post between fall, 1945 and summer, 1946, directed the activities of the organization from Washington. There was no missile project assigned to the team at that time, but the development of a number of guidance and control components was begun which proved of paramount importance a few years later. Based on former experience, air bearing gyroscopes and floating gyroscopes were considered as stabilizing elements for guidance systems. A number of laboratory tests indicated that the air bearing type would lead more quickly to a highly accurate, but rugged system with a short warm up time and adjustment period. The team concentrated its effort on the development of the air bearing system; and when, about the fall of 1952, the Redstone missile approached its completion, a stabilized guidance platform was available with air-bearing gyros, air-bearing accelerometers, and air-bearing adjustment pendulums. Modified versions of this platform are used in the Jupiter and Pershing missiles. In all three cases, the accuracies of the platforms and of the accelerometers are so high that they are not the governing factors for the over-all target accuracies of the missiles.



Along with the development of a stabilized platform, work on advanced electric and electronic components was initiated at an early time. Magnetic amplifier research started in 1947, with the result that by 1953 the tactical version of the Redstone missile did not contain one electron tube, a definite gain in over-all reliability. In 1951, a novel and then little-known device, the transistor, was introduced in the laboratory. Two years later, a transistor amplifier made its maiden flight in a Redstone as part of an automatic program device, with full success. This was probably the first flight for any transistor in a rocket. Today, any one of the big tactical or space missiles contains hundreds or even thousands of transistors.

The year 1950 stands out in the history of the Army as the year of the first big missile project assignment, the Redstone. While the development of the 200-mile vehicle progressed rapidly, some advanced thinking concentrated on missiles for 500, 1000, and more miles. It became evident that the warhead of these missiles required some kind of thermal protection during re-entry through the atmosphere. One relatively simple way of simulating the heat influx during descent, at least approximately, is to expose a sample nose cone to the jet of a stationary rocket engine. Tests of this kind began at Redstone Arsenal, Huntsville, Ala., in 1953. Some early experiments with metal structures, sweat-cooling arrangements, and impregnated plastics showed little promise, but definite progress was made with fiber-reinforced plastics. Material of this kind, developed by the General Electric Company for jet vanes, proved fairly successful in static nose-cone tests, and also in flight tests performed by the Martin Company on Viking rockets. Satisfactory results were finally achieved with fiberglass and a special resin binder. When the Jupiter project was initiated in 1955, the nose-cone development project had progressed to a point where a fiberglass nose could definitely be planned for Jupiter. A scale model of a Jupiter nose, reduced in size by a factor of 3, was successfully flown on an experimental three-stage Jupiter C vehicle over a range of 1160 nautical miles, in September, 1957. After recovery from the Atlantic Ocean, it was carefully investigated, and the fiberglass techniques proved to be feasible and sound. President Eisenhower, in November, 1957, exhibited this scale nose cone in his news conference, along with his announcement that the IRBM re-entry problem had been successfully solved.

While the Jupiter Project was in its early beginning, a significant change occurred with the Army team. On February 1, 1956, the Guided Missile Development Division of Redstone Arsenal was transferred into the Army Ballistic Missile Agency under the command of Maj. Gen. J. B. Medaris. The agency grew quickly in personnel, and the outcome of the subsequent struggles for the Jupiter IRBM Project proved that it had also grown considerably in national stature. In 1958, the Army Ordnance Missile Command was established under Major General Medaris.

The Command included the Army Ballistic Missile Agency, the Army Rocket and Guided Missile Agency, the Jet Propulsion Laboratory in Pasadena, Calif., and the White Sands Proving Ground.

In the meantime, the Jupiter missile neared its completion. The first test flight, early in 1957, failed because of unexpectedly high temperatures around the electric circuits of the tail section. This problem could be solved quickly by more effective heat protection of the missile base. The second flight was unsuccessful because of a detrimental influence of fuel sloshing on the stability of the missile. Although some sloshing effect had been expected, its full impact was much greater than anticipated. A crash program to solve the problem was quickly initiated, and on May 31, 1957, the first successful Jupiter flight could be accomplished. The recovery technique developed earlier for the scaled-down nose cone proved to be successful also for full-scale nose cones. The first fiberglass nose of a Jupiter, after a successful flight over 1200 nautical miles, was recovered completely intact early in 1958.

The possibility of putting an artificial satellite into an orbit around the earth had been known for many years. After the Redstone missile had made its first successful test flights, the launching of a satellite became feasible. In 1954, Dr. W. von Braun of the Guided Missile Development Division wrote a study report on a satellite-carrying vehicle consisting of a Redstone and three upper stages of Loki rockets. Together with members of the Naval Office of Research and scientists experienced in high-altitude rocket research, the Army started work on this "Project Orbiter." Later on, the Navy withdrew its support, and the Army teamed up with the Jet Propulsion Laboratory. The Loki rockets were replaced by scaled-down Sergeant rockets, and the launching of a 15-pound satellite in the fall of 1956 appeared definitely possible. During spring 1955, the Naval Research Laboratory worked out another proposal for a satellite, which later was named "Vanguard." A special committee was established which decided, in the summer of 1955, that "Vanguard" would be the national satellite project.

The Army, in the following years, contributed essentially to the Vanguard Project by developing electronic equipment and measuring instruments at the Signal Corps laboratories at Fort Monmouth, N. J., and by establishing and operating Minitrack ground stations through the Corps of Engineers and the Signal Corps. Shortly after Project Vanguard had been officially initiated, the Army was directed to work out plans for a 1500-mile Intermediate Range Ballistic Missile, the Jupiter. Since the Army team at Redstone Arsenal was no longer an official participant in the national satellite program, it was a logical decision to convert the four-stage vehicle of "Project Orbiter" into a three-stage test vehicle for the Jupiter nose-cone development. With the fourth stage containing



a dummy load, the first test vehicle of the Jupiter-C series was fired as a joint Army-JPL project on September 20, 1956. It was a complete success, covering a range of 2960 nautical miles and attaining an altitude of approximately 690 miles.

The early theoretical work on satellites, the development of the multistage Jupiter-C, and the re-entry test flights gave the Army-JPL team an excellent preparedness for an assignment which General Medaris received in November, 1957, a few days after Sputnik II had been put in orbit: the directive to launch an instrumented satellite as soon as possible. The Jet Propulsion Laboratory furnished the upper stages. Dr. Van Allen provided the cosmic ray instrumentation. The Naval Research Laboratory and JPL supplied transmitters for tracking and telemetry. The Vanguard team pitched in with its Minitrack ground stations in addition to JPL's Microlock system. The Smithsonian Institute helped with orbit computations. On January 31, 1958, Explorer I began its long journey around the earth. A second successful satellite, Explorer III, followed in March, 1958, and a third one, Explorer IV, in July, 1958.

The discovery of the Radiation Belts by the Explorers is undoubtedly the finest and most exciting accomplishment of the International Geophysical Year. While the radiation counters of Explorer IV were in operation, a series of three high-altitude atomic explosions were set off in the South Atlantic. This project, later publicly known as "Project Argus," was undertaken to study the long-time radiation effects of atomic bombs which are exploded at high altitudes. It was expected that electrons, both from the initial blast and from radioactive decay of the fission fragments, would be trapped by the magnetic field of the earth, and would oscillate between the magnetic poles along the field lines on cork screw trajectories for days and even months. The theory had been worked out by Drs. Christofilos and Panovsky. The measurements confirmed the theory by providing data on the density of the artificial electron cloud, its growth in thickness, its spreading around the earth, and its lifetime. Even though many of the details of a possible artificial radiation belt are still unknown, the Argus experiment proved very helpful for the prediction of electron densities that can be created artificially at high altitudes, and of their possible effects on radio and radar communications on earth.

In December, 1958, the Army-JPL-Van Allen team made its first attempt at the Moon, with a Juno II vehicle consisting of a Jupiter as booster and the same upper stages which had been successfully used on the Redstone for the re-entry tests, and the Explorers. The vehicle, called Pioneer III, failed as a lunar probe, but is considered a scientific success as it provided excellent data on radiation intensities as far out as 65,000 miles, and it proved that there are two distinct belts of very intense radiation. The second attempt in March 1959, Pioneer IV,

was a success. The 15-pound package, again providing excellent radiation data, passed the Moon at a distance of 37,000 miles and entered into a planetary orbit around the sun.

Towards the end of 1958, one of the Jupiters which were prepared for nose-cone recovery carried, in a special capsule, a live squirrel monkey provided by the Naval School of Aviation Medicine in Pensacola, Fla. All the body functions, like breathing rate, heart rate, cardiogram, and temperatures, which were telemetered back to the ground, indicated that the animal was in good shape during the flight until the end when trouble in the re-entry gear developed. This particular nose cone could not be recovered, and the little monkey found an early grave in the Atlantic.

A second monkey-carrying Jupiter took off on May, 28, 1959. An American-born rhesus monkey had been provided by the Army Surgeon General, and a South American squirrel monkey by the Naval School of Aviation Medicine in Pensacola. This time, recovery was a full success, not only for the biomedical project planners, but particularly for the two brave space-traveling monkeys. Their fame sped quickly around the globe, and they were readily promoted to the most enviable status of Army and Navy VIP's. The same Jupiter nose carried a selection of biomedical and biophysical specimens which had been prepared by members of the Army Medical Research Laboratory at Ft. Knox, Ky., of the Army Ballistic Missile Agency, and of the Florida State University at Tallahassee. Even though these experiments may have not as much public appeal as the monkeys, they will prove very valuable for our understanding of life functions in outer space.

A 90-pound satellite, carrying a collection of eight major physical experiments and powered by solar cells, was prepared for a Juno II launching under the sponsorship of the National Aeronautics and Space Administration (NASA) as a continuation of the American IGY effort. The first firing, in the summer of 1959, failed several seconds after lift-off because of a short between two diodes in the electric power supply circuit. The second attempt, in October, was a full success. The desired orbit was achieved very closely, and at the time of this writing, all the instruments still transmit strong signals.

The Juno II series will contain four more satellites, all of them to be launched during 1960. They are equipped with instrumentation to measure the radiations of the Great Belts,  $\gamma$ -radiation from the Sun, ionic space charges at satellite altitudes, electric fields in outer space, and the influence of ionospheric layers on wave propagation.

The National Aeronautics and Space Administration, in 1958, initiated a program to put man in space. Known as Project Mercury, it will climax in manned satellite flight with, of course, recovery of the pilot. A number of short ballistic flights are planned prior to orbital flight of the



capsule with the man. The Army team, late in 1958, was directed to prepare eight flights of the capsule with Redstone vehicles. The Redstone missile was selected because of its outstanding record of reliability, and because it is aerodynamically stable. Even if the engine should fail during ascent, separation of the capsule with subsequent recovery could be achieved without difficulty. If the engine of an unstable missile fails, immediate tumbling is unavoidable, which normally renders safe separation of the forward section impossible.

It is planned to fly empty and manned capsules. Redstone flights with manned capsules will give future human satellite pilots a first impression and feeling of capsule flight under weightlessness.

The wisdom of exposing a pilot to a short ballistic flight before he boards a satellite has been questioned. However, it should not be forgotten that the chances for a full success of the first manned satellite flight will be much better if it is preceded by a few manned ballistic flights over shorter distances. The functioning of capsule equipment, the efficient handling of manual controls, the use of instruments for observations, and the operation of the recovery system, are functions which will certainly undergo countless improvements after each flight. The specific need for such improvements will show even during short ballistic flights. Why, then, should not a number of short flights, which are much safer for the pilot and much less costly than satellite flights, precede orbital launchings?

The Army team at Huntsville contributed essentially to another long-range research and development project: electric propulsion. Since 1953, theoretical studies on feasibility and performance have been carried out by members of ABMA. Experimental work on ion propulsion systems and arc jet systems was initiated during recent years at several companies under contracts which are technically supervised by ABMA.

The most ambitious space vehicle in our country, the 1.5-million-pound Saturn, was assigned to the Army team by the Advanced Research Projects Agency during the summer of 1958. It will be capable of carrying a 15- to 20-ton payload into a low orbit, one or two tons softly to the lunar surface, a few tons around the moon and back to earth, and about one ton to the vicinity of the nearer planets.

Sponsorship of Project Saturn was transferred from ARPA to NASA in October, 1959. A more elaborate description of Saturn will be given in a later paper.

Under the auspices of the Advanced Research Projects Agency, the Army Ballistic Missile Agency and the Signal

Corps are presently engaged in a joint study project for a large satellite to be boosted into a 22,000-mile high, 24-hour orbit by a multistage Saturn vehicle. This satellite proposes elaborate communication equipment for world wide microwave traffic.

Since early 1959, members of the Army team have actively participated in the Lunar Working Group of the National Aeronautics and Space Administration. A detailed study of a lunar exploration program, based on the Saturn as carrier, is presently underway at ABMA. The program provides for the soft landing of an instrumented package on the lunar surface; for the landing, and subsequent operation, of a vehicle capable of traveling over 50 to 100 miles of lunar terrain; for the circumnavigation of the moon with a manned vehicle prepared for return and recovery on earth; and for a project involving manned lunar landing and return. The latter project requires a refueling operation in a low earth orbit.

When the Saturn Project was initiated in 1958, the first flight of a lunar vehicle appeared to be possible in 1963. Subsequent reduction in funds forced a delay in schedule which at present amounts to about one year.

The President decided in October, 1959, that, subject to Congressional approval, the Army team under the technical direction of Dr. von Braun will be transferred to the National Aeronautics and Space Administration. This transfer will conclude an exciting chapter of Army history, teeming with life, and often climaxing in most gratifying accomplishments. It should always be remembered, though, that in none of these accomplishments the Army was alone. There was always powerful help and brilliant cooperation from other services and organizations. When the first American V-2's were launched, back in 1946, the Navy prepared and operated the telemeter. The Explorer satellites were tracked by the Navy Minitrack Systems, and computed by the Smithsonian Institution. Explorers IV and VII carried instrumentation prepared by the Navy and the Air Force. The nose-cone recovery operations were joint ventures with the Air Force, the Navy, and the Marine Corps. The primate experiment was carried out jointly by Army and Navy. All of the Atlantic Missile Range launchings were accomplished under the splendid hospitality, and with the most efficient support, of the Patrick Air Force Base under Major General Yates. It is confidently hoped that this spirit of cooperation will further be enjoyed mutually by the missile teams of the services and at NASA, because it will be one of the most important ingredients in our great national space program of the future.

*(See pp. 68-69 for Appendices I and II)*



## APPENDIX I

## THE ARMY'S RECORD IN THE MISSILE AND SPACE VEHICLE FIELD

First successful firing of a ballistic missile. A Corporal was launched at White Sands, New Mexico, in May 1947.

First penetration of outer space. In using a German V-2 to boost a second stage WAC Corporal at White Sands on February 24, 1949, it also marked the first time that the stacked stage principle was successfully used. The WAC Corporal reached an altitude of 250 miles, a record which was unequaled for eight years.

First intercept of an airplane by a guided missile. A Nike-Ajax shot down a remotely-controlled plane at White Sands on November 27, 1951.

First U. S. inertial guidance system development completed for long-range ballistic missiles in 1953.

First successful launching of a U. S.-developed heavy ballistic missile, the Redstone, on August 20, 1953.

First operational air defense guided missile, the Nike-Ajax, was placed on site near Washington, D. C., in December, 1953.

First ballistic missile to be placed in the hands of troops. The 259th Field Artillery Missile Battalion (Corporal) was formed at Fort Bliss, Texas, in November, 1954.

First long-range firing of a U. S. ballistic missile on September 20, 1956. This was the 3,000-mile flight of the JUPITER C (Composite Re-entry Test Vehicle).

First successful launching of a U. S. Intermediate Range Ballistic Missile. The 500-mile JUPITER IRBM was fired for the first time at the Atlantic Missile Range, Cape Canaveral, Florida, on May 31, 1957.

First recovery intact of an object launched into outer space and the first solution to the aerodynamic heating problem of re-entry. A scale model JUPITER IRBM nose cone launched with a JUPITER C (Composite Re-entry Test Vehicle) was recovered from the South Atlantic August 7, 1957, and was shown by the President on television in November, 1957.

First free world satellite, EXPLORER I, placed in orbit around the earth. It was launched from Cape Canaveral, Florida, on January 31, 1958, by a JUPITER C—only 83 days after the order to try was received.

First intercept of a high altitude target by a guided missile when in 1958, a Nike-Hercules destroyed a rocket-launched parachute target at an altitude of more than 100,000 feet and 35 miles from its launching site.

First intercept of an F-80 jet flying at tree-top level, and below the effective range of conventional radar by a Hawk guided missile in May, 1958.

First recovery intact of a full-scale IRBM nose cone—May 17, 1958. It was launched with a JUPITER missile.

First complete and highly accurate Inertial Guidance System developed—July 17, 1958.

First deep space radiation measurements made by Pioneer III at an altitude of 65,000 miles on December 8, 1958.

First to maintain deep space telemetry to a distance of 400,000 miles—with Pioneer IV on March 8, 1959.

First successful U. S. effort to send animals into space and recover them, on May 28, 1959, as a forerunner to manned space trips. Monkeys Able and Baker were sent out 300 miles to a distance of 1500 miles to determine effects on life of 10,000 miles per hour speeds, 38 g acceleration, and 9 minutes of weightlessness.

First to place a really sophisticated satellite in orbit. Explorer VII was launched on October 13, 1959 to obtain data on earth heat radiation, x-ray radiation from the sun, solar aspect cell for attitude determination, intensity of cosmic ray particles and their variation with time, space performance of silicon solar cells, surface temperatures on the satellite, micrometeorite impacts, and other scientific problems.

Now building the SATURN booster with 1,500,000-pound thrust, the most powerful booster stage under development.

## APPENDIX II

## ARMY ORBITAL AND SPACE LAUNCHES

Satellite and Vehicle	Launched and Initial Orbit	Orbiting Weight	Communications	Payload Instrumentation	Information Obtained
Explorer I 1958 Alpha Jupiter C	January 31, 1958 Apogee 1573 SM Perigee 224 SM Period, 114 minutes Life expectancy, 3-5 years	30.8 pounds 80 inches, long 6 inches, diameter  Payload weight, 18.13 pounds	A. 108 mc, 10 mw Stopped, May 23, 1958  B. 108.03 mc, 60 mw Stopped, February 11, 1958 Resumed, February 24, 1958 Stopped, February 28, 1958  1 Turnstile antenna 1 Dipole antenna  Mercury batteries	1. Cosmic ray intensity measurements  2. Erosion grid and microphone for micrometeorite measurements  3. Temperature measurements of nose cone, fore and aft skin, and internal areas	Confirmed predicted cosmic radiation levels up to 600 miles altitude.  Measured frequency of impacts and size of micrometeorites.  Provided information relative to earth's bulge and gravity.  Obtained data on extreme altitude atmospheric density.  Confirmed success of method to control temperature of satellite's interior.  Count rates above 600 miles altitude were very irregular and were later learned to be the result of very intense trapped radiation about the earth.
Explorer II Jupiter C	March 5, 1958 Failed to orbit. Last stage did not ignite. Flight time 885 seconds.	31.5 pounds 80 inches long 6 inches diameter  Payload weight, 18.5 pounds.	A. 108 mc, 10 mw  B. 108.03 mc, 60 mw  1 Turnstile antenna 1 Dipole antenna	As Explorer I with addition of a recorder which permitted playback of previously recorded data upon ground command. This command was given when satellite was within range of ground receiving stations. Permitted world-wide coverage between the latitudes which the satellite circled. Microphone and temperature measurement in nose cone were left out.	This launch revealed a structural failure in the igniter support of the last stage. Support was strengthened and no similar failures were experienced in subsequent launches.
Explorer III 1956 Gamma Jupiter C	March 26, 1958 Apogee, 1740 SM Perigee, 119 SM Period, 115.8 minutes Down, June 28, 1958	Duplicate of Explorer II except that the turnstile antenna had been replaced with a dipole antenna.	Duplicate of Explorer II  A. Stopped, May 10, 1958 Resumed, May 18, 1958 Stopped, June 16, 1958  B. Stopped May 14, 1958 Resumed Erratically May 22, 1958 Stopped June 5, 1958	Duplicate of Explorer II	Additional data on information obtained from Explorer I. Particularly on the cosmic ray and trapped particle zones atmospheric density studies.



## APPENDIX II (Continued)

Satellite and Vehicle	Launched and Initial Orbit	Orbiting Weight	Communications	Payload Instrumentation	Information Obtained
Explorer IV 1958 Epsilon Jupiter C	July 26, 1958 Apogee, 1373 SM Perigee, 163 SM Period, 110 minutes	37.1 pounds 80.39 inches long 6.25 inches diameter  Payload weight, 25.8 pounds	A. 108 mc, 10 mw Stopped September 9, 1958  B. 108.3 mc, 30 mw Telemetry stopped, September 19, 1958 Transmitter stopped, October 6, 1958	1. 2 Geiger-Mueller counters 2. 2 Scintillation counters 3. Internal temperature measurements transmitted by sub-carrier center frequency shift.	Measured cosmic rays and trapped radiation over a wide range of levels and energies. Also explored a far greater volume of space as regards latitude and altitude than Explorers I and III.  Collected data on trapped electrons resulting from argus high-altitude nuclear explosions.
Explorer V Jupiter C	August 24, 1958 Failed to orbit. At first stage separation, the booster rammed the instrument compartment. Flight time 659 seconds	37.1 pounds 80.39 inches long 6.25 inches diameter  Payload weight, 25.8 pounds	Duplicate of Explorer IV	Duplicate of Explorer IV	Improved separation devices were designed for future flights.
Explorer attempt Jupiter C with "Apogee kick" fifth stage added.	October 22, 1958 Failed to orbit. Rotational spin vibrations of the cluster caused the payload to drop off at 112 seconds	9.26 pounds 12 feet diameter when inflated	108.3 mc, 24 mw  This transmitter was to act as a radio beacon to facilitate initial path prediction and acquisition of the balloon by optical means.	12 foot inflatable  Mylar balloon  Aluminum coated	One of the missions of this flight was to place a high-visibility balloon in orbit, in order to provide high-altitude atmospheric-density data and to serve as a radar target.
Explorer attempt Juno II	July 16, 1959 Failed to orbit. At lift-off, the vehicle deviated sharply to the left and was destroyed at 5½ seconds after lift-off. Failure of the guidance inverter caused open loop drift of the control system.	Duplicate of Explorer VII	Duplicate of Explorer VII	Duplicate of Explorer VII	Inverters were modified so as to prevent future similar failures.
Pioneer III Juno II Lunar probe	December 6, 1958 Reached an altitude of 63,580 miles and returned to earth after 38 hours flight.	15.25 pounds 23 inches long 10 inches maximum diameter	960.05 mc, 180 mw  3 Subcarriers	2 G-M radiation counter tubes  Internal temperature measurements. Test of de-spin hardware.	Discovered 2 radiation belts around the earth.  Obtained further information of cosmic ray and trapped particle intensity.  Contributed information on high-velocity trajectories towards cis-lunar space.
Explorer attempt Juno II	August 14, 1959 Failed to orbit.	Duplicate of October 1958 Explorer attempt	Duplicate of October 22, 1958 Explorer attempt	Duplicate of October 22, 1958 Explorer attempt	
Pioneer IV Juno II Lunar probe	March 3, 1958 Passed within 3700 miles of the moon and proceeded into solar orbit.	Duplicate of Pioneer III	Duplicate of Pioneer III	Duplicate of Pioneer III and, additionally, a measurement of the power output of the radio transmitter.	Provided data on attenuation of radio signals whose transmission path is through outer space. The satellite's radio transmitter was tracked until the batteries were depleted at a distance of 407,000 miles from earth.  Radiation data support and enlarge data obtained by Explorers and Pioneer III.  Further data on space high-velocity trajectories.
Explorer VII Juno II	October 13, 1959 Apogee, 681 SM Perigee, 345 SM Period, 101.3	91.5 pounds  Double-truncated cone	A. 108 mc, 15 mw  B. 20 mc, 600 mw  Transmitter to be cut off one year after launching.	1. Heat radiation experiments to study the transfer of heat radiation between the earth and the surrounding space. 2. Lyman Alpha and x-ray experiments to measure the spectral intensity of the Lyman Alpha line and x-ray radiation from the sun. 3. Solar aspect cell to determine the attitude of the satellite relative to the sun. 4. Ion chamber to measure intensity of three classes of heavy primary cosmic ray particles. 5. Measurement of intensity of primary and secondary cosmic ray and intensity variations of the trapped radiation over a period of time. 6. Solar cell experiment to determine the effect of the spatial environment on the performance of exposed silicon solar cells. 7. Temperature measurements at five localized positions on the satellite. 8. Micrometeorite experiment to detect micrometeorite impacts of the order of 10 microns or greater diameters.	



# General Description and Design of the Configuration of the Juno I and Juno II Launching Vehicles\*

BILL B. GREEVER†

**Summary**—The Juno I Vehicle consists of a modified Redstone Booster with three solid propellant upper stages. The second and third stages are made up by clustering the same rocket used as the fourth stage. The upper stages are contained in a spinning launcher. The spinning provides stability during flight. The Juno II vehicle uses the same upper stages as the Juno I and the booster is a modified Jupiter. The Juno I has put 25 pounds of payload into orbit. The Juno II can carry a 90-pound satellite or 15 pounds in an escape mission. Both vehicles were conceived to provide a quick and economical space vehicle; and as such the design was not optimum in all cases. Problems were created by this approach, such as dispersion of the upper stages as a function of spin speed, heavier payloads which require reinforcing the cluster structure, protecting the missile from aerodynamic heating on some missions, and raising the natural frequency of the cluster structure. These and other problems had to be solved as the Juno program progressed.

## INTRODUCTION

THE free world's first earth satellite was hurled aloft from Cape Canaveral, Fla., on January 31, 1958, by a Jupiter C Vehicle. About a year later a Juno II Vehicle (the Jupiter C's big brother) boosted the first free world's man-made planet past the moon to its orbit around the sun. Many small but important events had to precede these two major accomplishments. Let us see how these vehicles came into being; how they were designed and fabricated; and some of the problems that had to be solved to make them possible.

The Jupiter C (Jupiter Composite Re-entry Test Vehicle) is a staged vehicle almost 69 feet long, developed by the Army to test proposed solutions to the aerodynamic heating of missile nose cones when re-entering the earth's atmosphere. When the Jupiter C was used to carry satellites, a fourth stage was added and the vehicle became known as the Juno I.

The Juno I main stage is a modified Redstone Ballistic Missile, and is about 56 feet long and 70 inches in diameter. The second, third, and fourth stages are solid propellant motors. The Jupiter C was made almost completely by modifying hardware that already existed. The fuel tanks on the Redstone were lengthened to increase propellants capacity for Jupiter C configuration. The Jupiter C was thus a relatively low cost vehicle from a design standpoint.

The first launching of this hybrid bird was on September 26, 1956. There were only three stages, but it hurled a payload more than 3000 miles downrange from Cape Canaveral. This was the first flight test of the composite

missile, and a completely successful one. On August 7, 1957, the Jupiter C propelled a scale model nose cone of the Jupiter more than 1200 miles downrange with a summit altitude of more than 600 miles. An earlier flight fell short of this range and recovery was not accomplished. However, the later flight was on the target, and Navy recovery ships picked up the floating nose cone after parachutes had lowered it into the water. Results from the re-entry of the nose cone proved to be sufficient to complete the design of the Jupiter nose cone. Several more Jupiter C vehicles were available for re-entry tests but further tests were deemed unnecessary.

Late in 1957, the Advanced Research Projects Agency requested that the Army use the Jupiter C as part of the United States' participation in the International Geophysical year. Hence, Explorer I was placed into orbit on January 31, 1958. The second attempt on March 5, 1958 was unsuccessful; however, a spare vehicle was available and was used to launch Explorer III into orbit on March 26, 1958. The total Juno I firings are listed below.

<i>Payload</i>	<i>Launched</i>	<i>Record</i>
Explorer I	January 31, 1958	Success
Explorer II	March 5, 1958	Failed
Explorer III	March 26, 1958	Success
Explorer IV	July 26, 1958	Success
Explorer V	August 24, 1958	Failed
Explorer VI	October 22, 1958	Failed

Juno I was initially developed and fabricated by the Army Ballistic Missile Agency, and the Jet Propulsion Laboratory (JPL). The Missile Agency provided the main stage, the guidance and control system, and fired the vehicle; JPL provided the high-speed upper assembly.

The booster is a modified Redstone Ballistic Missile. The fuel tanks are elongated to carry the maximum amount of fuel. The instrument compartment was redesigned to taper its diameter down so that the launcher, or spinning bucket, which houses the upper stages, could be mounted on top.

The Juno II vehicle is very closely related to the Juno I in that the same high-speed stages and launcher are used, and a modified Jupiter ICBM is used as a booster or first stage instead of the Redstone. The Juno II is far from optimum with respect to staging; but as such, it provided a quick way to more than triple payload-carrying capabilities as compared to the Juno I. In addition, the Juno II provided the capability of putting a 15-pound payload in the vicinity of the moon. Very little design time was involved in providing this additional capability. The Jupiter ICBM was well along in its development program

\* Manuscript received by the PGMIL, February 1, 1960.

† U. S. Army Ballistic Missile Agency, Redstone Arsenal, Huntsville, Ala.



and was available in sufficient quantities to support a space program without disrupting the military program.

Both the Juno I and Juno II vehicles were conceived as a quick and economical means of putting up a satellite or lunar probe. The Juno I program was completed in October, 1958. The Juno II has several missions yet to be accomplished; but it is rapidly being obsoleted by the missile state of the art. Both vehicles could have been designed to accomplish more, but the philosophy was to provide a space vehicle in a short time with a minimum amount of expense. The philosophy under which these vehicles were conceived implies that there were problems. The mating of pieces which were not necessarily designed to mate is difficult in any case. These are the kind of problems that will be discussed here.

### JUNO I AND JUNO II DESIGN

The Juno I Vehicle consisted of four stages: a liquid propellant first stage, high-speed clusters of solid propellant rockets for the second and third stages, and a single solid propellant rocket, for the fourth stage. The payload was attached to the top of the fourth stage.

The first stage was a Redstone Missile modified as follows: the over-all length was increased 96 inches to provide greater fuel capacity; weight was reduced by using aluminum replacements for steel wherever practical; drop-off external ground connecting cables were used instead of inside cables; a smaller, lighter weight instrument compartment was designed; some tactical instrumentation was eliminated; spring force was used for separation of the propulsion unit rather than pneumatic cylinders; and skin thickness of containers was reduced.

The first stage of the first missiles was powered by a mixture of liquid oxygen (LOX) and alcohol. To obtain greater burnout velocity and thus increased specific impulse and engine thrust, other fuels were investigated. An improved fuel was developed which could be accommodated without major modification to the existing booster stage. An improved high-performance fuel, called hydyne, was developed, consisting of 60-per cent unsymmetrical dimethylhydrazine and 40-per cent diethylene triamine, and having the same density as the alcohol mixture. Since the densities of the LOX-fuel mixtures were the same for both hydyne and alcohol, the standard fuel and oxidizer tankage of the booster stage could be used without modification when hydyne was employed in lieu of alcohol.

During the booster-powered flight phase, the missile attitude is controlled by an autopilot system. The system controls pitch, yaw, and roll of the missile up to the engine cutoff point, through gyro and associated electronic and servo mechanisms which activate the jet vanes and air rudder. During the burning phase of booster flight, the missile is tilted with respect to earth fixed vertical. Shortly after burnout of the first stage, the Juno I booster is separated from the rocket body containing the instrument compartment of the rocket and the high-speed solid pro-

pellant stages. During the free flight following separation of stage 1, the rocket body must be tilted so it is horizontal at apex. Free flight control is achieved by four pairs of air jet nozzles which are attached to the instrument compartment.

Telemetry equipment included in the missile is used to monitor performance and furnish other flight data. The PAM/FM/FM system is used. The carrier is modulated with 16 standard subcarriers, with one or more of the subcarriers commutated. The composite wave is used to frequency modulate the carrier, which is amplified and then radiated from slot antennas on the missile to the various receiving stations.

The Juno II Missile is composed of a Jupiter intermediate range ballistic missile without the nose cone, vernier motor, and spin rockets. The container section length is increased thirty-six inches to increase engine burning time. A cluster assembly, shroud, shroud support, and payload are added forward of the instrument compartment. The upper stages and launcher, which contains the upper stages, are identical to the unit used on Juno I. The Juno II measures approximately 76 feet in length, and weighs about 60 tons when fueled.

A specially designed shroud covers the launching vehicle's upper three stages and payload. The two primary purposes of the shroud are: to provide a rigid support for the angle-of-attack meter placed out ahead of the missile to give it refined guidance during its first moments of flight; and to protect the upper stages and payload from aerodynamic heating during the powered flight. Aerodynamic heating is considerably greater in the Juno II than in a Juno I flight. This is caused by a much higher acceleration of the missile, and a lower initial trajectory which carries it through more of the dense atmosphere. The shroud becomes heated during ascent to about 500°F on some trajectories.

The Juno II propulsion system operates on RP-1 (kerosene) and liquid oxygen (LOX). The vehicle is controlled in pitch and yaw by gimbaling the engine chamber. Roll control is achieved by a hydraulically actuated swivel nozzle on the gas generator turbine exhaust.

The Juno II has a delta-minimum inertial guidance scheme. It is an advanced and improved version of the system used on the Redstone Ballistic Missile, and the missile is controlled much in the same manner as the Juno I.

The missile is oriented in the direction of the target after being placed on the launching pad. The stabilized platform is aligned precisely to the target. From the blockhouse, data for a precalculated trajectory are recorded on a tape in the guidance computer on board the missile. This trajectory can be changed by remote control to within 20 minutes of firing time.

Figs. 1 and 2 show the configuration of Juno I and II, respectively. Fig. 1 shows Explorer IV just after lift off and on its way to placing the payload in orbit. Fig. 2 is missile 11, the first moon probe, just before it was fired.





Fig. 1—Explorer IV at liftoff.

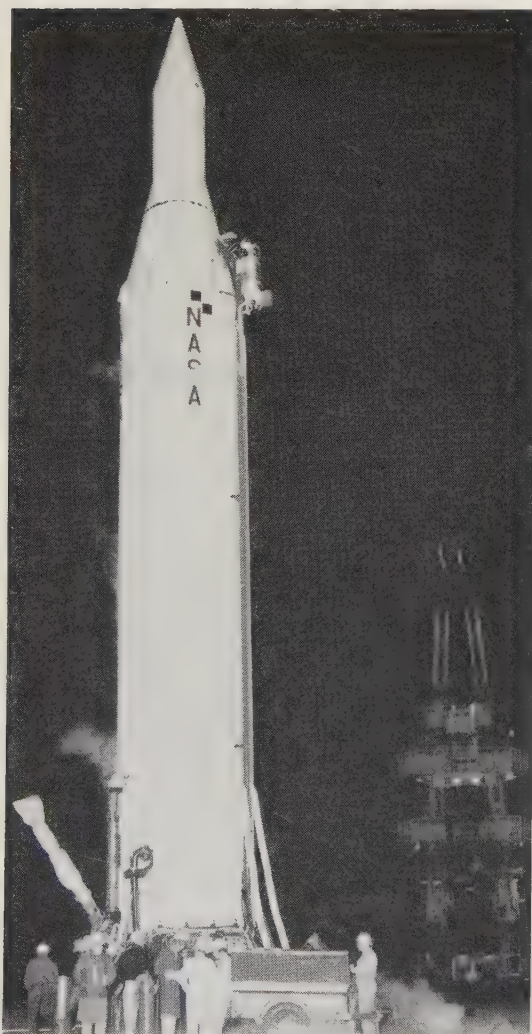


Fig. 2—Pioneer III just before launching.

## CLUSTER DESIGN AND RELATED PROBLEMS

The clusters of upper stages for both Juno I and Juno II have the same hardware. The cluster consists of four major components: the launcher, or cylindrical tub which contains the upper stages; the second stage which contains the 11 solid propellant motors; the third stage of three motors; and a single motor fourth stage. Fig. 3 shows an exploded view of the cluster.

The spinning tub or launcher, consists of a hollow shaft mounted in ball bearings and supported by the instrument compartment of the booster; a webbed base plate; and a cylindrical outer shell that contains the high-speed cluster assemblies.

The 11 solid propellant motors of the second stage are each approximately 4 feet in length, and 6 inches in diameter. They are held together by three transverse bulkheads and further supported by three circumferential steel rings to which each motor case is welded. Each bulkhead is made from one solid piece of flat aluminum alloy stock in which 11 evenly spaced holes are machined so the bulkhead will fit snugly over the motor rings. The circumferential rings are bolted to the bulkheads, which are designed to support the rocket motors against radial loads imposed by the spinning motion of the rockets. The forward bulkheads also transmits thrust loads between the 11 motors and the other parts of the structure.

The forward bulkhead has four supporting lugs equally spaced around the outside circumference. These lugs are designed to fit into matching slots near the forward edge of the launching tub, and serve to support the forward portion of the ring structure against transverse loads. No thrust loads are carried by these lugs.

Near the inner circumference on the front face of the forward bulkhead are three equally spaced supports which are used to hold the stage-3 assembly. These supports are fitted together with adjusting screws to permit alignment of stage 3 and transmit both thrust and transverse loads from the forward bulkhead of stages 2 and 3.

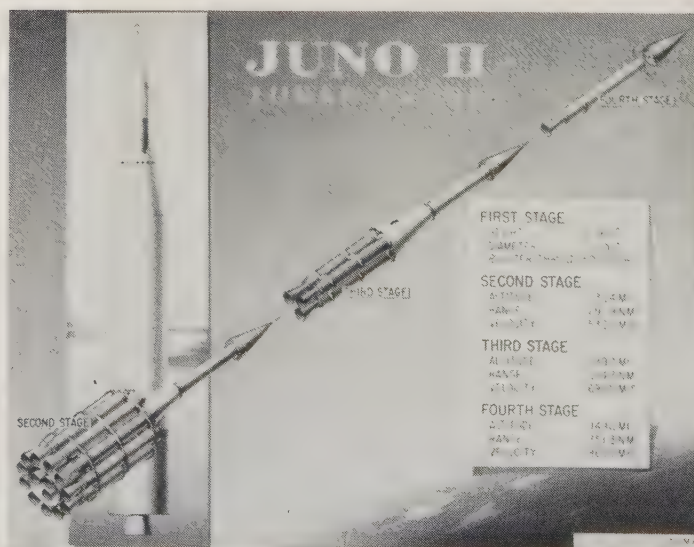


Fig. 3—Exploded view of the cluster.



The inner circumference of the forward bulkhead extends slightly aft. To this cylindrical section a tube is bolted which runs from the forward bulkhead to a point slightly behind the nozzles of the motors. This tube transmits thrust loads from the booster to the high-speed stages. The thrust load tube is bolted to the inner circumference of each of the three bulkheads. This tube is constructed from three pieces of aluminum sheet, fastened together by screws on overlap joints running lengthwise. The tube is reinforced by three aluminum doubles between the center and forward bulkheads.

The stage 3 assembly consists of two structures, the cluster of three motors held together by three transverse bulkheads, and a conical shell which extends forward of the front bulkhead. This conical shell supports the fourth stage. The front bulkhead of stage 3 has three equally spaced lugs around its inner circumference which fits into three supports of the front face of the stage-2 forward bulkhead. The conical shell, fabricated from an aluminum spinning, is bolted to the forward bulkhead of the stage-3 assembly, and stiffened by a steel ring at the forward end. Another ring in the cone is made as a webbed aluminum structure, riveted to the conical support section. These two rings in the stage-3 cone, support the single motor of the 4th stage. Three 5¼-inch-diameter exhaust holes are cut into the cone support forward of the stage 3 rockets, to permit access to the motor heads for the installation of the igniters. The center of each stage 3 bulkhead is cut out in a triangular shape, which permits a 1½-inch diameter cylinder to run through the stage 3 centerline. The cylinder contains the batteries and the timer assembly for ignition.

Because the launching tub and high-speed stages are spun at high rotational speeds (450 to 750 rpm), it is essential that these parts be dynamically balanced to eliminate excessive vibration. Dynamic balancing was accomplished by the addition of weights at the appropriate locations in the following steps: balancing of launching tub; installing and aligning of stage 2 within the tub; balancing of the composite mass of the tub and stage 2; installing and aligning of stage 3 in the stage 2 cylinder; and balancing of the composite mass of the tub and stages 2 and 3. A long series of special tests were conducted to evaluate the spinning assembly containing the high-speed clusters. Special equipment was designed and built to balance the spinning assembly.

The choice of motors for the high-speed stages was based primarily on reliability. Because the stages were to be made up of a relatively large number of small rocket motors, it was vitally important that the reliability of the individual motors be high. As a by-product of the development work of another program at the Jet Propulsion Laboratory, a small solid propellant motor was available in which considerable confidence had been established.

An extensive test program was undertaken on the rocket motors to solve three important problems on the motor design.

1) Because the stage-2 motors would be located well

away from the spin axis in the spinning assembly, the effects which the centrifugal forces might have on the integrity of the propellant grain or the uniformity of the combustion had to be determined.

2) The extreme directional accuracy required in the launching of the high-speed stages made it necessary for the thrust axis misalignment and mass unbalance to be kept at a minimum during the launching of these stages. Tests were required to ensure that variations in ignition time, thrust, and total impulse of the different motors could be kept within the allowable limits.

3) As the high-speed stages would be required to ignite in a near vacuum, characteristic of altitudes greater than 200 miles, the reliability of ignition under such conditions had to be demonstrated.

Spin tests were carried out to determine the structural rigidity of the solid propellant grain and the deflection of the motor case. It was proven that the grain was sufficiently rigid to withstand the spinning loads. The deflection of the loaded motor case under the spinning loads was measured by placing strain gages on the outside of the case. Although there was some deflection, it was not considered sufficient to cause any difficulty.

The requirement for minimum thrust and mass unbalance could be met by special care in processing the propellant, to keep the motor-to-motor variation in thrust and impulse within acceptable limits.

The ignition system was designed with safety as the first consideration, and reliability next in importance. For safety, the system had to be shielded from stray radio frequencies and power surges, and the final connecting of battery circuits to igniters had to be done as late as possible in the missile preflight work. To ensure reliability, duplicate circuits, batteries, switches, etc., were used wherever possible.

Spinning the high-speed stages is necessary to equalize thrust differences among the motors in the cluster. Regulation of the spin rate is essential for two reasons:

1) The missile mode should not be excited by the cluster frequency. Therefore, the rotational speed of the cluster must vary so as not to interfere with the missile mode which changes with fuel consumption in the powered phase of the flight.

2) The cluster speed has to be kept constant after the powered flight ends. Reaction torques caused by speed changes of the cluster might overtax the roll control system, and force the missile off course. A programmed speed regulator was developed to perform these two tasks.

The cluster is driven by two dc aircraft motors rated 28 volts, 135 amperes, 7700 rpm, and 3.5 hp. The motors work in parallel by means of a toothed belt. A synchro, connected by a flexible coupling to the motor shaft, provides the data for the speed regulator and an indication for a counter for accurate speed measurement. The load on the motors varies from missile take off to free flight, depending on acceleration and aerodynamic pressure. The normal motor load is about 60 per cent of its full load capacity; that is, when it is not accelerating or under aero-



dynamic pressure. When the cluster is accelerated during flight, the motor loads exceed 200 per cent for a short period. Early tests proved this relatively small motor could withstand high overloads for a short period of time. Thus, by using the small motor, and overloading it through the acceleration period, a good bit of weight was saved.

#### PERFORMANCE AND FLIGHT MECHANICS

Payload carrying capability of the Juno I and Juno II Vehicles can best be shown by tabulation of the payloads that have been flown. (See Table I.)

TABLE I

	Payload	Payload Weight (pounds)	Perigee (miles)	Apogee (miles)
Juno I	Explorer I	18.11	223	1580
	Explorer III	18.51	117	1740
	Explorer IV	25	161	1388
Juno II	Pioneer III (Lunar)	15	—	—
	Explorer VII	91.5	345	681

Structural limitations in the cluster prohibit heavier payloads on the Juno II Vehicle even though the vehicle performance is sufficient to carry 15 or 20 pounds more in a minimum orbit.

The Juno I's were fired vertically. During the burning time of the first-stage engine, the vehicle tilts into the trajectory. A few seconds after the engine cuts off, the booster is separated from the instrument compartment by igniting explosive bolts. Coil springs push the two bodies apart. After separation the instrument compartment, with the high speed stages mounted on top, continues to tilt so that it will be in a horizontal position (with respect to the Earth) when it reaches apex. (Apex is defined as that point on the trajectory where the velocity component radial to the Earth is zero.) At this point the stages are fired in sequence to bring the speed up to the requirements for orbiting the satellite.

Several methods of predicting the time of apex were considered and evaluated. Final selection was based on the inherent accuracy capabilities, adaptability to existing facilities, and minimization of computer and other requirements involving additional facilities.

The time required for a ballistic missile to travel from one point on its trajectory to any other point on its trajectory may be computed, provided that the velocity vector and position of the missile in its elliptical path are known for the first point. Prediction of time of apex requires only the measurements of the initial conditions and the computation of the time interval from the initial point to the apex. Selection of the initial point presents no problem, but the measurement of the initial conditions is more difficult. The direct computation of apex time is impractical within the time permitted, without extensive computer facilities. It was decided that a precalculated trajectory would be used. Corrections to the computed apex could then be made in accordance with measured deviations from the assumed initial conditions. The problem of predicting

the time of apex then became one of obtaining the data on the actual initial conditions with the necessary accuracy, and in a form suitable for use.

To determine actual initial conditions, the weighted value of the error was calculated for each possible deviation from the assumed initial conditions. The error in position, with respect to the surface of the earth, has a comparatively minor effect, thus allowing considerable latitude in the measurement of the initial point. In contrast, the velocity must be measured with a high order of accuracy both in magnitude and angle. The error in measurement of magnitude alone must be held within 50 meters per second to attain an apex. The time of apex must be computed with an error of less than 5 seconds or else the upper stages will be fired in the wrong direction, and the flight will be a failure.

Early flights of the Juno I Vehicle proved that the predicted trajectory was close enough to the actual trajectory so that a timer could be used to fire the stages at apex. This simplified the launch procedure.

The Juno II flight pattern is very similar to that of the Juno I. The vehicle is fired vertically and during the booster burning period it begins its tilting program. At burnout of the first stage propellants, the instrument compartment and upper stages separate from the booster. At separation, four small lateral kick rockets (contained in the booster) are fired to slow down the booster and move it to one side. This eliminates any possibility of the booster bumping or interfering with the flight of the separated upper stages.

Shortly after separation, the nose cone of the shroud is removed by explosive bolts and springs, and a lateral kick rocket moves it to the side and out of the way of the upper stages.

The cluster flight begins when the program device in the booster sends the firing signal to the second stage. About nine seconds after second stage ignition, the third stage fires. Nine seconds later, the fourth stage fires. If the payload is to be separated from the burned out fourth stage motor case, it can be done about 13 seconds after fourth stage ignition. On large payloads, this separation time is increased to about 2 minutes to make sure the fourth stage has no thrust when separated to prevent bumping between payload and fourth stage.

Fig. 4 illustrates the major steps of flight mechanics.

#### PROBLEM AREAS FROM FLIGHT RESULTS

The Juno I vehicle experienced three failures in flight. Explorer II failed to go into orbit because the fourth stage did not ignite. Exhaustive tests after the flight did not reveal any reason why the fourth stage should have failed to ignite.

Explorer V did not attain orbital speed because the cluster was fired slightly down and hard to the left. The powered flight of the booster was normal. After separation of the instrument compartment, the spatial attitude control system controlled the missile properly for several seconds, then rather large attitude deviations developed in all three planes. It appears that the booster must have overtaken



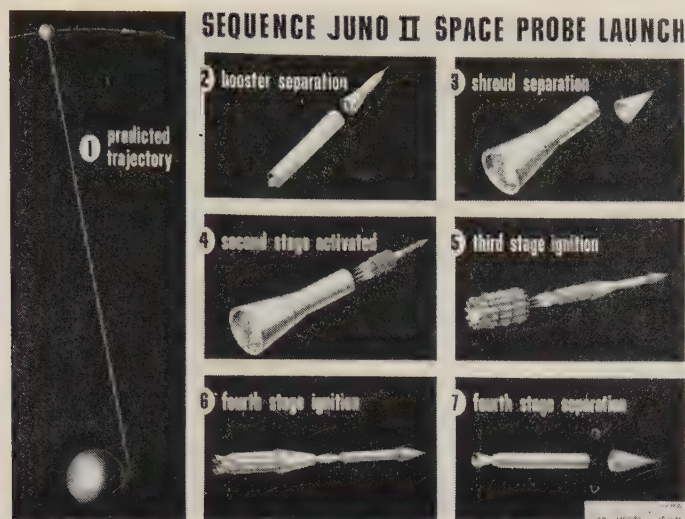


Fig. 4—Major steps in flight mechanics of Juno II.

and collided with the instrument compartment. This could be caused by a long "tail-off" of engine chamber pressure or external venting from the tanks. The net result of the collision was permanent disturbances to the guidance reference which aimed the cluster flight in the wrong direction. Flight studies were started to relocate vents and to place retrorockets on the booster to prevent the booster from overtaking the instrument compartment after separation on future flights.

Explorer VI was launched on October 22, 1958 from Cape Canaveral. It failed to orbit. Reasons for the failure were never completely clear, but the following events did occur. The first one-and-a-half minutes of flight were normal. Then vibrations started to build up in the cluster as shown by accelerometers mounted at the base of the rotational launcher. After about two minutes of Flight time, there was an increase in the current drawn by the launching tub drive motors. Coincidentally with this load increase, the cluster spin speed began to drop sharply. All evidence indicates that the payload, still attached to the fourth stage, broke off from the cluster. About a minute later the remaining part of the cluster apparently broke up and disintegrated. Though cause of the failure could not be determined, three possible causes acting singly or in combination were:

- 1) The cluster structure could have been forced into resonance with its natural frequency causing excessive vibration,
- 2) Thermal buckling and differential expansion effects caused by aerodynamic heating,
- 3) Unbalance in the cluster caused by failure of a payload component.

The Juno II vehicle has experienced three failures in flight. Pioneer III was the first Juno II flight and the first attempt by the Army at a moon shoot. Several malfunctions caused a velocity deficit of about 440 meters per second which kept the probe from escaping from the earth. However, the probe did travel to a height of 67,543 miles from the center of the earth, and extremely valuable data was gathered on the Van Allen radiation belt.

Main engine cutoff occurred several seconds earlier than predicted. The cutoff signal was given by the propellant depletion switch and cutoff occurred at the same time that the depletion switch was armed. All evidence indicated that the depletion switch had failed earlier and when armed, it erroneously gave a cutoff signal.

Additional discrepancies developed during the cluster flight which cost about 80 meters per second in velocity and caused trajectory angle deviations of about  $1^\circ$  in pitch and almost  $5^\circ$  in yaw. The most probable cause for the cluster deviations is a torque caused by an early or late thrust decay in one of the cluster rockets, details of which will be discussed later.

Experience gained from Pioneer III resulted in several changes in the depletion switch system and increasing of the cluster spin speed for future flights.

The third Juno II flight carrying the 91- $\frac{1}{2}$  pound IGY satellite, blew up after about 5 seconds of flight. Telemetering records showed that the main power converter was shorted. This is the converter that supplies power to the guidance system. With no guidance and control, the missile flight became erratic shortly after lift off. The missile began to roll and tumble, and started to break up after about five seconds of flight. The missile was then ordered to be destroyed. The converter has since been redesigned to prevent such a recurrence of events.

Missile 19B with the 12-foot inflatable sphere failed to orbit for two reasons. First, an apparent mixture ratio shift in the booster phase of flight caused fuel depletion to occur several seconds early and resulted in a velocity deficit of about 370 meters per second at cutoff. Second, a hole in the pressurized instrument compartment caused pressure loss and a subsequent loss in missile attitude control. The loss of instrument compartment pressure and attitude control caused the cluster to fly to the right and almost straight up with consequent failure to place the payload in orbit.

Among other problems encountered during the Juno programs was the spin speed of the upper stages. This was a problem from the outset of the Juno I program. A high spin speed is desirable to equalize thrust differences among the motors in the cluster and keep the dispersion of the stages to a minimum. Conversely, it is desirable to separate the missile mode and the frequency of the spin as far as possible. This latter requirement normally demands lower spin speeds. These two conflicting requirements necessitate a compromise.

Early tests established a maximum spin rate of 750 rpm. Even at this speed there are loads in the order of 300g at the outer circumference of the second stage.

There was no way to run tests to establish the lowest practical spin speed, so early flights were spun at a high rate but without coming too close to the natural frequency of the missile. This meant starting the spin speed at about 500 rpm at liftoff of the missile, and increasing the speed during flight, since, as the missile propellant tanks emptied, the natural frequency of the missile was raised. This program of spin speeds worked satisfactorily for the Juno I Vehicle. At the beginning of the Juno II



program the problem had to be reconsidered because the natural frequency of the Juno II Vehicle is lower than that of the Juno I Vehicle. One of two things had to be done. Either the spin speed had to be lowered, or the structure had to be "beefed up" to raise the natural frequency. On the first Juno II flight (Pioneer III) the spin program was established at 450 rpm as a compromise of the frequency problem. Flight results from this first flight indicated that dispersion of the cluster flight was excessive. The injection velocity vector was about  $5^\circ$  off the predicted path. Fig. 5 shows a typical frequency curve for Juno II.

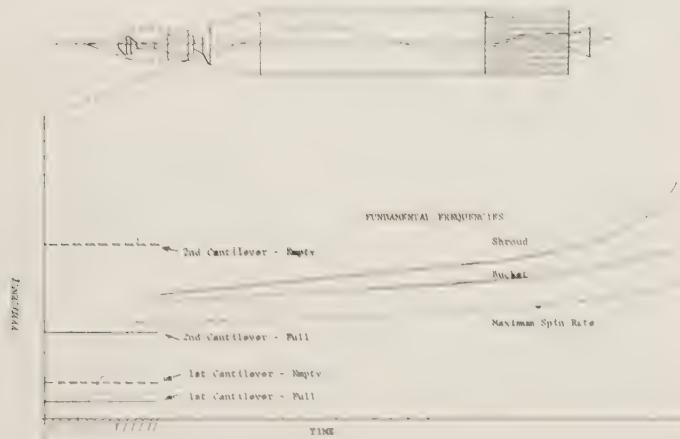


Fig. 5—Typical natural frequencies and allowable spin rates for Juno II.

The most likely explanation for this deviation seems to be an uneven burnout of one or more of the motors in stage two. Angular deviations of this nature can be reduced quadratically by increasing spin. However, the natural frequency of the Juno II Vehicle will not permit spin speeds in excess of 600 rpm. About 10-msec time delay of one rocket of stage 2 yields the angular rate required to cause the observed deviation. Angular disturbances such as these not only cause an error in the flight path direction, but also degrade the over-all performance by reducing the total velocity.

The second flight of a Juno II Vehicle (Pioneer IV) was spun at 600 rpm. The cluster was spinning at 450 rpm at liftoff and was programmed to 600 rpm at about 135 seconds of flight time after the fuel tanks were emptied sufficiently to raise the natural frequency safely above the 600 rpm frequency. The success of Pioneer IV proved this spin program satisfactory. Cluster deviations were reduced to a tolerable limit.

The third Juno II attempt was scheduled to carry a 91-pound satellite. The spin program had to be reviewed again. Tests indicated that the cluster could not withstand spin speeds in excess of 500 rpm with a payload of 90 pounds. However, the mass moment of inertia ratio of cluster and payload indicated that the cluster dispersion problem would not be as serious as had been experienced with lighter payloads.

Further tests on the cluster with the heavy payload showed that the fourth stage did not have sufficient struc-

tural rigidity to carry the heavy payload at 500 rpm. Two problem areas had to be overcome to carry the 90 pound payload: first, the fourth stage had to be reinforced; and second, the entire cluster had to be stiffened to raise its natural frequency. These two problems came into being because the cluster was not originally designed to carry payloads as heavy as 90 pounds. Redesign of the cluster would have been the best solution to both problems, but time and money overruled this solution and made it necessary to put a couple of "crutches" under the old cluster design.

The first "crutch" evolved to look like a 12-inch diameter aluminum cylinder which encased the fourth stage and attached to the fourth stage support cone and the top of the fourth stage. This cylinder was reinforced with cylindrical rings, and tests proved the structural rigidity in the fourth stage area to be in the order of twice the original value. This raised the natural frequency of the cluster some, but not enough. The second "crutch" was not so easy because, it required raising the natural frequency of the cluster several cycles per second without any major redesign of the structure and without appreciably increasing the weight of the cluster.

The weakest areas in the cluster with respect to flexing were the cluster support (the support which attached the cluster to the Jupiter), the base casting of the bucket which contains the stages, and the skin of the bucket. To change any of these would mean major redesign and retooling. Additionally, these parts had already been fabricated for the remaining Juno II shots.

The only apparent solution to meet all the requirements was to support the rotating cluster with rollers, so six rollers were mounted to the shroud support which encircles the cluster. The rollers contact the launcher at the top support ring. This roller support system raises the natural frequency of the cluster in the order of 2 to 3 cps, depending on the payload weight. The first roller design was an aluminum wheel with rubber bonded to the surface, but tests showed that rubber could not withstand the high surface speed and heat. Rollers made out of nylon are able to withstand the high surface speeds imposed.

The roller fix solved the natural frequency problem but produced a few new problems. Adjusting rollers to the right preload required about one hour. This necessitated an additional hour in the count-down time. The bearing which carries the roller is mounted in a leaf-type spring which allows flexing of the roller to adjust to out-of-roundness of the launcher support ring. The spring is in turn tied into the shroud support structure. The preloading of the spring takes into account the out-of-roundness of the launcher and expansion of the shroud support caused by aerodynamic heating in the ascending phase of flight. Adjusting of the rollers has to be done with care and precision. Uneven roller loads may cause distortion of the launcher and thus disturb the alignment of the second stage. Alignment of the payload can also be disturbed by uneven roller loads.

Another problem area created by the rollers is the addi-



tional load imposed upon the spin motors which drive the cluster. This additional load is in the order of 10 per cent increase under nominal conditions.

The spin motors can tolerate the roller load but accelerating the cluster is naturally slower and spin speed cannot be increased in large steps.

The spinning cluster and the shroud which encases it present problems in the RF area of payload design. Placing the shroud over the payload is like putting the transmitter under a can. To overcome this problem, the shroud was designed to provide two rings of RF windows around the middle of the shroud support. The windows are made of fiberglass and are located in the region where the payload sits on the cluster. These windows allow the transmitter signals to pass through the shroud so that the payload can be checked out before the missile is launched, and so that the transmitter signals can be received during the powered phase of flight before the shroud is ejected. The spinning cluster creates interference with RF signals and in some cases, where low power is used, the payload has to be checked out on the spinning cluster, and under the shroud. Modifications have to be made to fit each case.

The two attempts at a lunar probe with the Juno II vehicle required special effort in several areas. Early studies of the payload indicated it would have to weigh about 15 pounds to make technical sense. The standard Juno II vehicle did not have a 15-pound capability as a moon probe. Several changes had to be made to have the 15-pound capability. First, the vehicle was stripped of every piece of nonessential equipment. About 500 pounds must be removed from the booster to gain one pound of payload. Obviously, this was not a very profitable area but it helped some. The big payoff in weight saving is in the upper stages. The Jet Propulsion Laboratory was successful in manufacturing the fourth stage motor case from titanium, with a weight saving of about two pounds. Weight saving in the fourth stage is a one-to-one ratio with the payload, therefore, two pounds were gained in the payload.

Another profitable area for improving performance and, thus payload weight on a lunar shot, is to fly a lower trajectory. However, this method of gaining payload weight adds problems of its own. Trajectories were calculated to see how flat the trajectory would have to be to get the required payload weight after utilizing all the other weight saving methods. The resultant trajectory was so low with respect to the earth, that it meant the missile would have to fly longer through the atmosphere. Aerodynamic heating studies of this trajectory revealed that the material limit of the upper portion of the missile would be exceeded from a temperature standpoint. Three methods considered for thermal protection of the missile skin were:

- 1) Increase skin thickness,
- 2) Cover existing surface with a thin coat of insulating material,
- 3) A sandwich-type construction of thin steel and fiberglass insulation fastened to the existing aluminum structure.

Preliminary calculations indicated methods 1) and 3) to be less desirable than method 2) because of fabrication problems and excessive weight. The problem was thus reduced to the selection of material and the proper thickness to satisfy temperature requirements. A fiberglass paint was chosen because of simplicity of application and temperature insulation properties. It was applied in layers and built up to thickness between 1 and 2 mm, depending upon the location on the missile skin.

A boom is attached to the shroud nose cone shell and the steel angle-of-attack meter is fastened to the front of the boom. Calculations revealed that the welds holding the angle-of-attack meter vanes would be destroyed by aerodynamic heating, but at a time during flight when it was no longer needed for guidance purposes. Tests were run to assure that the falling vane would not puncture the missile skin.

Flights during the latter part of the Juno I program indicated that retrorockets were needed on the booster to prevent it from overtaking the instrument compartment and upper stages, after separation. Consequently, retrorockets were installed on the Juno II vehicles. The retrorockets used were solid propellant Honest John spin rockets. Four of these were placed in the tail section area of the booster. They are canted at an angle with respect to vertical, to give the booster a side thrust vector as well as a backward thrust. The canting is done to move the booster out of the path of the upper stages and instrument compartment in case the retrorockets cannot overcome the overtaking force of the booster. The retrorockets are covered with a small dog-house type of structure to protect them from aerodynamic heating; and specially designed mounting brackets protect them from the heavy vibration in the tail section area.

This covers some of the interesting problems connected with the flights of the Juno vehicle.

#### CONCLUSION

Neither the Juno I nor the Juno II Vehicles were optimum with respect to staging. They were both conceived as a quick and economical means of putting up a satellite or lunar probe. The Juno II has several missions yet to be accomplished, but it is rapidly being obsoleted by the missile state-of-the-art. Both vehicles have served their purpose well, as the record shows. The free world's first satellite and space probe are now history.

Many problems are created in attempting to use vehicles for purposes other than what they were designed for. The end result is generally inadequate capability and performance.

Spinning a mass as large and as heavy as the upper stages and launcher has very definite limitations from a spin speed standpoint, and guidance accuracy improves as the spin speed becomes higher.

The high acceleration and vibration of the solid propellant stages create some difficult problems for the payload designer. More instrumentation could be put in the payload if the structure could be made lighter.



## Explorer Satellite Electronics\*

W. K. VICTOR†, H. L. RICHTER†, AND J. P. EYRAUD†

**Summary**—A discussion is presented of the design restrictions and the philosophy which enabled the Explorer satellites to be first during the IGY to reveal the presence of a belt of intense cosmic radiation encircling the earth's equator. In addition, an indication of the amount and momentum of cosmic dust in the solar system was obtained from the Explorers. Methods used to obtain reliability in the transducing and communications system are described, together with interpretations of space-environment information as deduced from the narrow-band telemetry.

### INTRODUCTION

**D**URING the International Geophysical Year, the United States Army, in cooperation with the Jet Propulsion Laboratory, placed three Explorer satellites in orbit around the earth. Telemetered data from Explorers I, III, and IV provided much unexpected new knowledge and an increased understanding of the hazardous space environment encountered above the earth's atmosphere. National Academy of Sciences IGY instruments were adapted to the payload structure of Explorer I and III (Fig. 1) by engineers and technicians at JPL; Explorer IV was assembled at the Army Ballistic Missile Agency. Most of the scalars, telemetering oscillators, and transmitters used had been designed and assembled at JPL. A satellite tracking network was based on a sensitive Microlock communication system originally developed by JPL for long-range tracking of tiny radio beacons inside re-entry nose cones.

### DESIGN RESTRICTIONS IMPOSED BY THE VEHICLE AND ORBIT

In 1957, the most reliable American rocket vehicle capable of boosting a satellite up to a 200-mile orbit altitude was the Army's Redstone guided missile. For the upper high-speed stages, another thoroughly tested Army rocket was available, a scaled-down version of the JPL-developed solid-propellant Sergeant missile. Both of these rockets had, however, been built for rugged tactical field handling and were structurally much heavier than if they had been designed specifically for satellite launching. On the other hand, the structure was proven trustworthy. Because of the structural weight, the maximum possible ratio of orbitable weight to launching weight was only about 1 to 1000. This ratio meant that the final-stage rocket case and in-

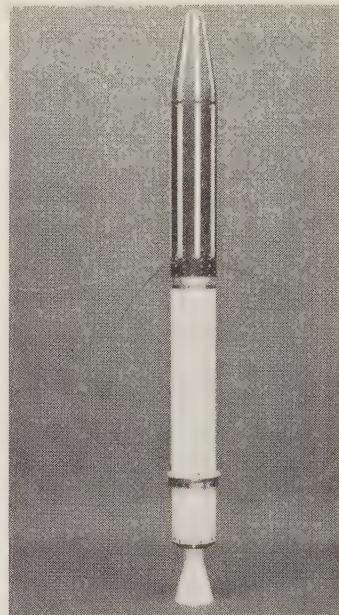


Fig. 1—The United States' first earth satellite, Explorer I.

strumented payload together could weigh no more than 31 pounds. Of this weight, the rocket motor case used 12.7 pounds and the cylindrical instrument housing used 7.5 pounds. Only 10.7 pounds could be allotted for all the instruments, the transmitters, the batteries, and their supporting structures. Severe restrictions were thus placed on individual component weights, battery power drain, and information bandwidth.

Internal temperatures of Explorer payloads had to be maintained within a range of  $-5$  to  $60^{\circ}\text{C}$  in order to avoid freezing the mercury batteries or overheating the germanium transistors. Earth satellites are, however, subject to abrupt and severe temperature excursions about once every hour as they pass from direct sunlight into the earth's shadow and back into sunlight again. To slow down the heat-transfer rate between the steel shell and the internal payload electronics, Micarta was used for all supporting structures. Furthermore, to produce as long a thermal time constant as possible for all components, all electronics, including batteries, were thermally connected with one another. For midnight launchings, it was calculated that about 25 per cent of the stainless steel outer surface should be coated with a heat-reflecting material to keep the average internal temperature at an optimum low operating level. Therefore, the nose and cylindrical shell of the instrument container were flame-sprayed with eight equally spaced aluminium oxide stripes.

Temperature data telemetered from the Explorers

\* Manuscript received by the PGMIL, February 1, 1960. This paper presents the results of one phase of research carried out at the Jet Propulsion Lab., California Inst. Tech., under Contract No. NASw-6, sponsored by the National Aeronautics and Space Administration. Portions of the report were originated under studies conducted for the Dept. of Army Ordnance Corps under Contract No. DA-04-498-Ord 18.

† Jet Propulsion Lab., California Inst. Tech., Pasadena, Calif.



showed that the design objective had been met. Although the external shell temperatures fluctuated between  $-25$  and  $75^{\circ}\text{C}$ , the instruments remained within the safe  $0$  to  $35^{\circ}\text{C}$  range. The temperature of the satellite nose cone never rose above  $40^{\circ}\text{C}$ .

#### EXPLORER IGY INSTRUMENTATION

The choice of instruments for the Explorers was critical in determining success. The instruments had to be scientifically valuable, capable of withstanding the comparatively rigorous vibration and spin environment of the Explorer rocket, and ready for immediate incorporation in November, 1957. The final selection was made by the IGY with the agreement of the experimenters, JPL, and the Army Ordnance Missile Command.

A careful arrangement and mounting of these instruments was required for reasons of thermal and mechanical symmetry. Arrangement of the instrumentation in Explorer I is shown in Fig. 2. The instrumentation included: 1) a Geiger-Mueller tube with its scaling circuit, which had been designed by Dr. James A. Van Allen of the State University of Iowa to measure the intensity of high-energy cosmic radiation; 2) four temperature-measuring devices, three on the outer shell of the satellite and one inside; 3) a sensitive microphone placed in contact with the shell, designed to respond to the impacts of micrometeorites; and 4) 12 external wire-grid erosion detectors, which had been designed by Dr. M. Dubin of the Air Force Cambridge Research Center to measure by their fracture the impact of micrometeorites. Since the maximum counting rate anticipated for cosmic rays was about 17 counts per second, it was believed that a maximum reading rate of 80 counts per second would be adequate. As it turned out, this rate was exceeded during each orbit.

Explorer III, shown in Fig. 3, was designed to make more sophisticated measurements of cosmic-ray intensity. It carried the same type of Geiger-Mueller tube as Explorer I, but the information this time was stored on a magnetic tape. The tiny tape recorder (Fig. 4), whose maximum recording rate was 128 counts per second, was designed by George Ludwig of SUL. Once during each orbit around the earth, when the satellite passed over one of the Minitrack receiving stations, a coded interrogation signal was transmitted to a special Minitrack receiver in the satellite. Upon receipt of this signal, a playback of the tape recorder was initiated. In approximately 5 seconds, all of the cosmic-ray information gathered from one orbit around the earth was transmitted back to the Minitrack ground station. The transmitter used in the satellite for this operation was similar to the high-power transmitter of Explorer I.

Explorer IV, although still tiny by Russian standards, was nevertheless a fairly complex space laboratory. It carried a thin cesium iodide scintillation counter with a very thin window for detecting low-energy particles, a plastic scintillator for somewhat higher energy particles, a Geiger

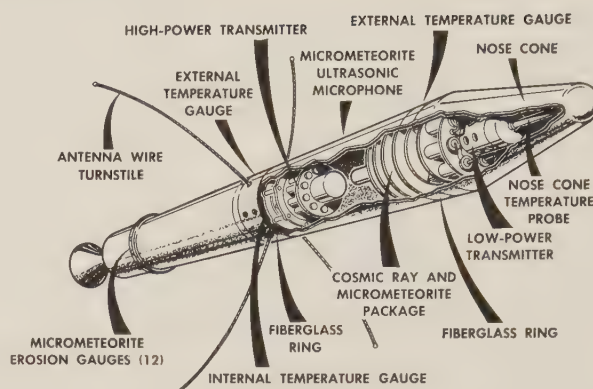


Fig. 2—Instrumentation installed in Explorer I.

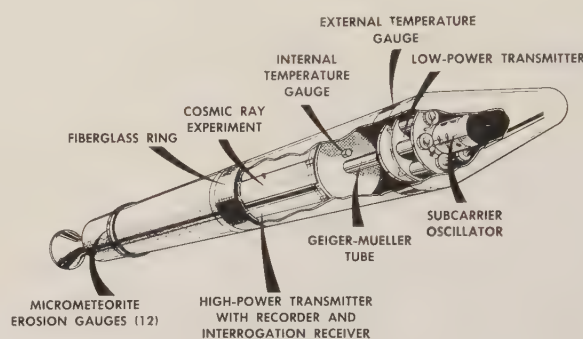


Fig. 3—Instrumentation installed in Explorer III.

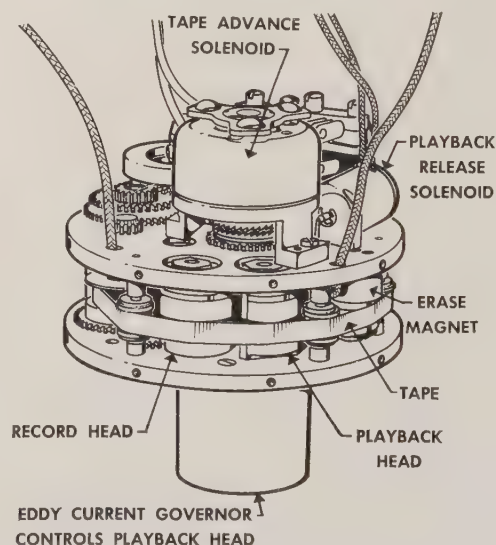


Fig. 4—Tape recorder for cosmic-ray data flown in Explorer III.

counter for still higher energy particles, and a lead-shielded Geiger counter for very high energy particles. The Geiger counters were reduced in size by a factor of 25, and more scaling stages were included by Dr. Van Allen to avoid the saturation problems which plagued the earlier two Explorers.

Block diagrams of the telemetering systems flown in the Explorer I satellite are shown in Fig. 5.



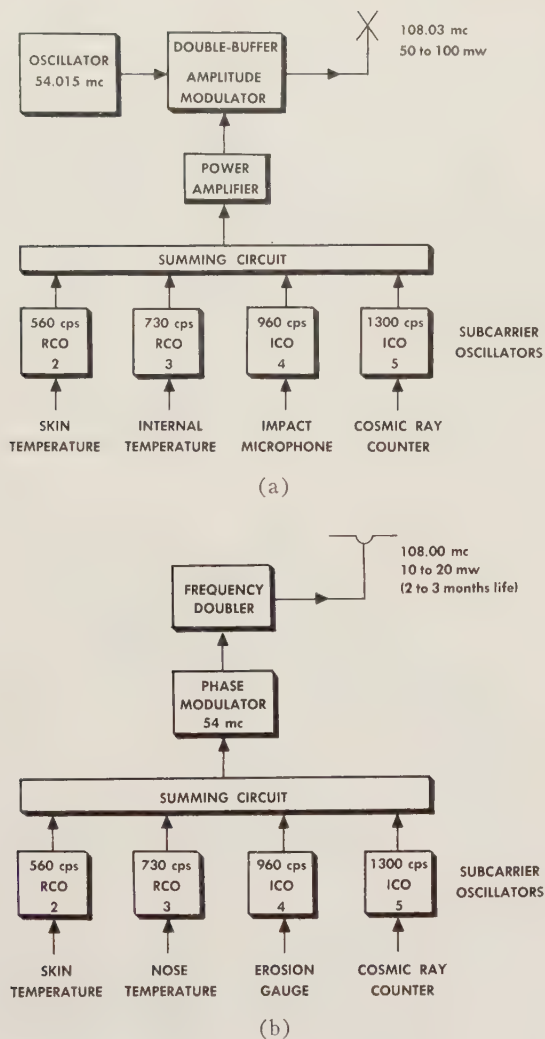


Fig. 5—Telemetry systems flown in Explorer I.

#### COSMIC-RAY INSTRUMENTATION AND MEASUREMENTS

The measurements of high-intensity radiation, carried out in Explorers I, III, and IV, were under the direction of Dr. Van Allen and his colleagues of the State University of Iowa who were responsible for the experiment design and for the scientific conclusions abstracted here. The intensity of cosmic radiation was measured by a standard Geiger-Mueller tube. An electronic scaling circuit was attached to the tube. In Explorer I, the output of a scale of 32 was telemetered directly. The maximum scaler counting rate was 4000 counts per second; but the reduced telemetered data were readable only between 0.14 pulse per second (one change of state per 2-minute pass) and 80 pulses per second.

In Explorer III, the tape-recorded information was handled as follows. A tuning fork and scaling circuit put out one pulse every second. This output is diagramed in the first line at the top of Fig. 6(a). The scaling circuit associated with the Geiger-Mueller tube put out one pulse for every 128 counts of the tube, as indicated for a possible case by the second line in Fig. 6(a). Since the tape was advanced only once a second, the maximum rate that

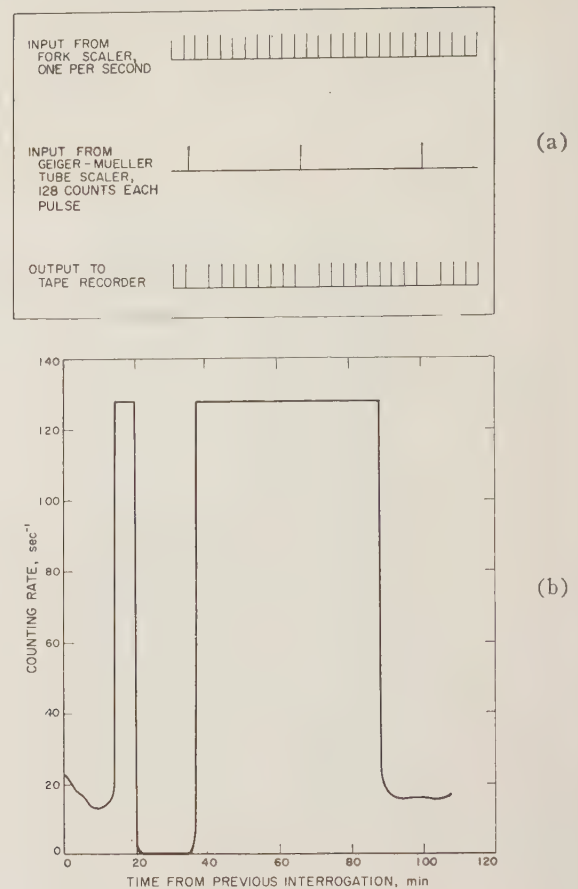


Fig. 6—Cosmic-ray data: (a) pulse inputs to recorder; (b) typical reduced counting rates for one complete orbit.

could be recorded was 128 counts per second. Each pulse from the tuning fork was recorded on the tape unless it happened to follow an output from the Geiger-Mueller tube scaling circuit. In this latter case, the pulse from the cosmic-ray counting circuit blocked the next succeeding timer pulse. The result of this mixture was a series of pulses with some missing, as shown by the third line in Fig. 6(a). The frequency of cosmic rays is then 128 divided by the number of timing pulses from blank to blank. Because of dead-time effects, when the counting rate is above 20,000 counts per second, the G-M tube responses become too weak to trigger the scaling circuit.

From a scientific viewpoint, the most startling information which has been generated by the Explorer satellites is the new cosmic-ray data. If a cosmic-ray Geiger counter is taken upward by rocket or balloon from the earth's surface to a point out in space, the intensity measured by the counter increases to a maximum of about 20 counts per second at an altitude of 6 miles, then decreases to about 1 count per second at an altitude of about 50 miles. Above this altitude, it was expected to increase slowly to an asymptotic value of about 2 counts per second at about 600 miles. When numerous tape recordings of Explorer I telemetry showed a sharp rise in cosmic-ray counting rate to the unbelievable 80-count-per-second rate, followed by an abrupt drop to zero for 5 to 15 minutes while the satel-



lite was near apogee, it was at first presumed that the scaler was not functioning properly.

When the first cosmic-ray recordings from Explorer III started coming in, it seemed again that the scaler was not functioning properly. Reduced data from a typical Explorer III recording are shown in Fig. 6(b). For the first 15 minutes, the counting rate coincides closely with that expected. Suddenly there is a jump to the maximum possible recorder counting rate, 128 counts per second. This is followed by an abrupt decrease to a zero counting rate. After about 15 minutes when no counts at all were being recorded, the rate again jumps to the maximum possible value. This continues for the next half hour when the count again suddenly falls to its expected level. This peculiar behavior was reproduced on almost every orbit, and each time over some portion of the orbit the counting rate appeared to be close to that expected.

An analysis of several orbits shows that the sudden increase in counting rate and subsequent blocking of the counter occurred as the satellite approached its apogee and passed up through an altitude limit of approximately 600 miles. The counting rate returned to that expected as the satellite came back down through this limit on its way toward perigee. By testing a spare payload, it was found that saturation occurred at a counting rate of 20,000 counts per second, which was 1000 times that expected. This intense radiation could not be electromagnetic. The 0.023-inch steel shell of the satellite and the 0.05-inch steel walls of the counting tube form a shield with a density of 1.5 g/cm<sup>2</sup>. Photons with energies high enough to penetrate this quantity of material should have been noticed at much lower altitudes. Certainly they would have been recorded long before this by balloon flights and high-altitude rocket observations; but no such observations had been reported. On the other hand, high-altitude rocket measurements in the auroral zone had detected a similar type of radiation. Measurements on a spare payload indicated that the penetrating radiation could be produced by electrically charged particles such as electrons with energies above 3 mev or protons above 20 mev. It was not possible, on the basis of the results of the single Geiger-Mueller tube, to determine which of the many possible atomic particles was responsible for the intense radiation field. Therefore, more definitive measurements were made in Explorer IV. The experiments were again under the direction of Dr. Van Allen, but the payload implementation (with the sole exception of the JPL Microlock beacon) was accomplished by the Army Ballistic Missile Agency. The scientific conclusions reported here are again due to Dr. Van Allen.

The cosmic-ray detectors in Explorer IV consisted of two small Geiger counters and two scintillation counters. One of the Geiger counters was unshielded and responded to any particle which could penetrate the 0.023-inch stainless steel shell of the satellite and the 0.05-inch stainless steel casing of the Geiger tube. The other Geiger tube was shielded with 1/16-inch-thick (1 g/cm<sup>2</sup>) lead sheet. One of the two scintillation counters recorded a pulse each time

a particle passed through it; the other counter measured the energy of the particles which came to rest in it. Both of these scintillation counters were shielded by lead except for one window each, where the shielding was made as light as possible and placed next to a hole cut in the steel shell of the satellite.

The results of the first two Explorers were confirmed by the detectors in Explorer IV. Again the intense field of radiation at altitudes above 600 miles were observed. The number of particles passing through the unshielded Geiger tube showed a density of about 12,000 particles/cm<sup>2</sup>/second/sterad. At least 60 per cent of these particles had enough energy to penetrate the lead shield around the other Geiger counter.

In addition to these very energetic particles, the scintillation counters revealed that there is an even greater density of particles with low energy. At the northern or southern limits of the trajectory, these low-energy particles predominate. Here, the flux of particles of low energy at an altitude of about 1400 miles is about 80,000/second/cm<sup>2</sup>/sterad.

To put this information in terms of another number, radiation intensities in excess of 100 roentgens per hour have been observed by the satellites, and this intensity increased steadily with altitude, with no indication of any leveling off at altitudes reached by the Explorers. It remained for the moon probes, Pioneers III and IV, to discover how far away from the earth the dangerous radiation belt extended and what the maximum counting rate might be.

#### MICROMETEORITE INSTRUMENTATION AND MEASUREMENTS

The measurements of micrometeorite densities in Explorers I and III were carried out under the direction of Dr. E. Manring and Dr. M. Dubin of the Air Force Cambridge Research Center. Two types of micrometeorite detectors were used in Explorer I: a parallel combination of 12 wire-grid detectors (Fig. 7) and an ultrasonic impact microphone, in spring contact with the steel shell, and its associated amplifier (Fig. 8).

In the grid-type detector, the severing of a wire in one of the grid structures by a micrometeorite of sufficient size and velocity resulted in a small step increase in resistance. This change of resistance, when sensed by the resistance-controlled oscillator, produced a step increase in subcarrier frequency. To assure accuracy, a flight erosion gauge with a multiple-switching network was used for calibration.

Frequency-vs-temperature data for the impact microphone were obtained by subjecting both the beacon and the microphone equipment to oven and refrigerator temperatures. Thus, if the scaler output voltage varied with temperature, it was automatically included in the frequency calibration.

Ultrasonic microphone sensitivity was determined by dropping glass beads of known size and density on the





Fig. 7—Wire-gauge micrometeorite detector.

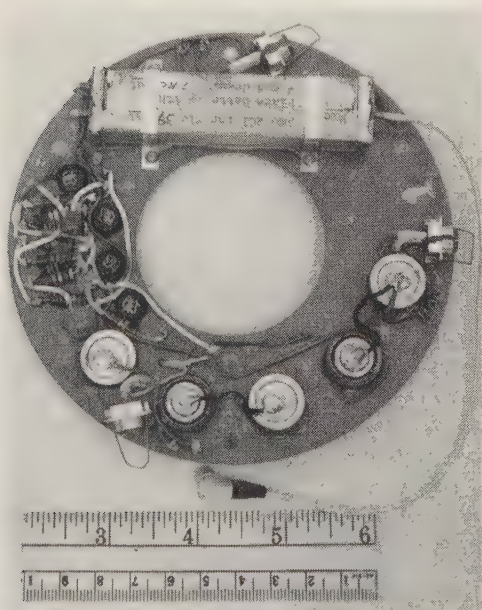


Fig. 8—Micrometeorite microphone and amplifier.

satellite shell from various heights. With the height necessary to actuate the scaler and the size of the glass beads known, the required momentum averaged over the entire shell was found to be 0.002 g-cm/second. Therefore, if a velocity of 40 km/second (velocity of the earth) is assumed for a micrometeorite, the minimum detectable particle mass is found to be  $5 \times 10^{-10}$  g. As an additional check, shaped explosive charges were fired at the steel shell to simulate high-velocity-particle impact.

In the data which have been reduced from the Explorer I high-power transmitter, which carried data from the ultrasonic microphone, 145 impacts were recorded during a telemetry time of 79,000 seconds from January 31 to Feb-

ruary 12, 1958. This result indicates that the average influx of particles 4 microns or more in diameter (one-fifth the diameter of human hair) was approximately 0.01 particle/m<sup>2</sup>/second. Almost all impacts were observed between midnight and noon, satellite local time. Only on one day out of 12 were a number of hits observed at any other time. From these results it appears that the average speed of the dust particles in space may be less than the speed of the earth in its orbit, so that the earth appears to be sweeping through a cloud of dust. Only on one day was a shower recorded in which the speed of the particles was greater than that of the earth, allowing them to catch up to the earth from behind. Daily variations in flux up to a factor of 10 were observed.

The low-power transmitters on both Explorers I and III carried the data from the wire gauges, consisting of a set of 12 cards (each 1 cm<sup>2</sup> in area) wound with two layers of fine wire. No more than one (and perhaps none) of the wire gauges was broken during the lifetime of the telemetering system on Explorer I. This information permits an upper limit to be established for the influx of particles of 10 microns diameter or larger. This limit is 0.001 particle/m<sup>2</sup>/second during the lifetime of the experiment, from January 31 to April 14.

Data received from Explorer III showed no wire gauges broken from March 26 until May 6. Between 2243 Greenwich Mean Time on May 6 and 0232 GMT on May 7, two of the wire gauges were fractured. Then both transmitters of Explorer III started to function erratically about May 8, only about 6 weeks after launching and long before expected battery exhaustion. The signals became erratic at the same time on both transmitters, which was very curious, since the two transmitters were completely independent. These symptoms were consistent with an assumption of physical damage. All of the micrometeorite data before this time were taken in a period of normal background activity. No meteor showers were encountered. However, the shower Eta Aquarides, which has been associated with Halley's Comet, occurs during the early part of May and reaches its most intense activity on about May 6.

#### TELEMETERING SUBCARRIER OSCILLATORS

Both the resistance-controlled and current-controlled subcarrier oscillators used in the Explorer satellites were self-contained (Fig. 9), using four mercury cell batteries each. Each consumed about 2.5 mw. The type of resistance-controlled oscillator used in Explorer I is shown in Fig. 9(a). The current-controlled oscillator, shown in Fig. 9(b), used time-control reactance modulation for controlling oscillator frequency. This method was made possible by the characteristics of the transistor. The operating frequency of a conventional LC oscillator can be altered by introducing an alternating current that is of the same frequency but is 90° out of phase with the oscillator voltage. The frequency shift thus produced is proportional to the amount of additional current introduced into the tuned circuit.



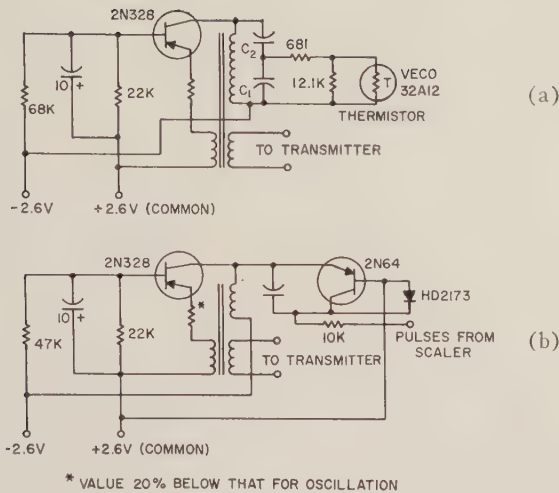


Fig. 9—Subcarrier oscillators used in Explorer satellites.

Oscillator frequency shift can be obtained using a transistor as a time-controlled reactance modulator. The portion of the cycle during which this reactive current is introduced can be controlled by direct current introduced into the control transistor. By this new method, frequency modulation is achieved with minimum dependence upon temperature-sensitive parameters.

#### MICROLOCK COMMUNICATIONS SYSTEM

Beginning in 1953, the Jet Propulsion Laboratory had studied and developed simple light-weight radio transmitters and ultrasensitive receivers. Weighing only about 1 pound with their batteries, the tiny transmitters could serve in small satellites as continuous tracking beacons for about 2 months. It was even possible to add several FM telemetry channels to the carrier signal (Fig. 5) to convey environmental data. It also was necessary to use highly sensitive and complex receiving equipment on the ground. A phase-locked receiver developed by JPL for Army missile instrumentation purposes was adopted for the purpose. This combination of a minimum-weight transmitter with a phase-locked ground receiver was named the Microlock communication system (Fig. 10). To permit tracking of satellites approaching from any direction, a helical quasi-omnidirectional receiving antenna was used.

Microlock tracking stations, located on the east and west coasts of the Americas, Nigeria, and Singapore, picked up the signals and recorded them together with accurate time signals on magnetic tape. These tapes were then flown to various data reduction centers, the principal one being at the Jet Propulsion Laboratory in Pasadena. When the magnetic tapes were received at these centers, the telemetered data were reduced onto Sanborn tapes, advancing at a 1-mm/second rate. An analog record (Fig. 11), as well as digital printouts of counted audio frequencies, was thus made available. The reduced data were then turned over to IGY scientists familiar with the characteristics of the instruments on board the satellite. They, in turn, could interpret the frequency measurements in

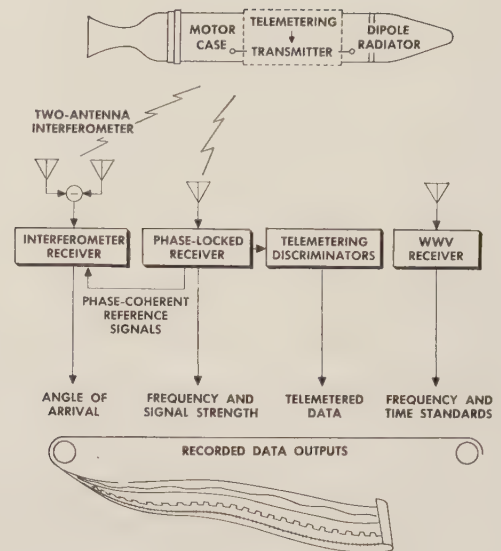


Fig. 10—Microlock communication system used in tracking Explorer satellites.

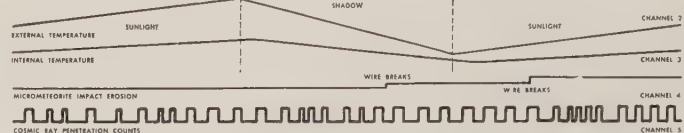


Fig. 11—Typical recordings of Explorer telemetry.

terms of the actual measured quantities which had been observed by the satellite in its orbit above the earth.

#### MICROLOCK GROUND RECEIVER

The performance of any signal detection system can be maximized only by using all available *a priori* information concerning signal frequency, strength, polarization, and bandwidth as well as receiver noise level. One means of employing some of the *a priori* information about the most probable received signal characteristics from a rapidly moving satellite is correlation detection. The method of mechanizing correlation detection used by JPL in the Microlock receiving system is the phase-locked loop (Fig. 12), which is particularly applicable when the transmitted signal is a pure sine wave. In the phase-locked loop, the local estimate of the transmitted signal is generated by a voltage-controlled oscillator (VCO), and the mathematical operation of multiplication is performed by the phase detector. This phase detector provides a dc output voltage which is proportional to the phase difference between the incoming signal and the local estimate generated by the VCO. The dc error voltage is separated from noise by the low-pass filter (integrator) to provide a control voltage to the VCO. In this way, the phase-locked loop is an electronic servomechanism which accomplishes signal detection using only linear mixing. This system provides memory by virtue of the voltage stored on the integrating capacitor in the low-pass filter. This voltage is always a "best guess" of the present signal frequency and is re-



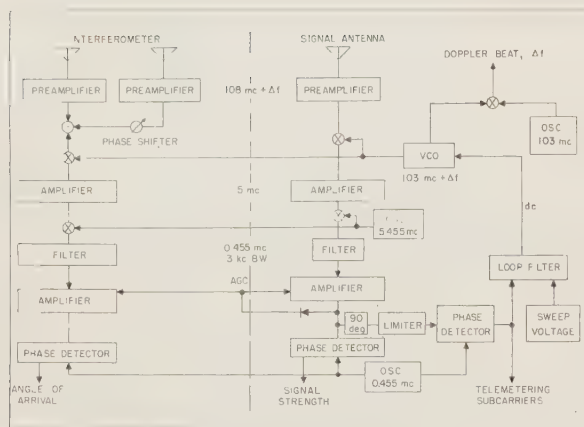


Fig. 12—Microlock phase-locked ground receiver and interferometer.

tained for some seconds after disappearance of the signal, thus providing means for re-acquiring the signal should it appear again at the same frequency. The design of a phase-locked loop for a particular application requires detailed knowledge of target dynamics and their effect on signal characteristics, since the dynamic tracking characteristics and noise bandwidth of the phase-locked servo-loop are affected.

In a second channel, the signal is shifted in phase by  $90^\circ$ , so that it is in phase with the VCO output. The phase detector in this channel then produces a dc voltage which is proportional to the signal amplitude. In this manner, the signal is completely detected by the phase-locked loop; *i.e.*, the frequency, phase, and amplitude are determined.

In this description of the phase-locked loop, it is assumed that the loop is initially locked. Initial acquisition of the signal may be accomplished by slowly sweeping the VCO frequency across the signal frequency. As the beat between the signal and the VCO output goes to zero, the system acquires phase lock and thereafter retains synchronism unless the signal level becomes so small that the available control voltage can no longer overcome the effects of the small amount of noise which appears at the output of the low-pass filter.

#### SATELLITE TRANSMITTERS

Two similar but independent transmitters (Fig. 13) were used in each of the Explorers. This arrangement provided additional reliability in the form of redundancy so that orbit parameters could be accurately determined. One transmitter operated at 108.03 mc with an output of 60 mw, and the lower power unit operated at 108.00 mc and 10 mw. Information on the space environment was sent back on four standard FM/FM telemetry channels. The frequency of the audio signal was modulated by changes of resistance or current in the measuring instruments in the satellite.

The higher power (60-mw) unit, using amplitude modulation, made it possible for nonprofessional radio receiving equipment around the world to record telemetry signals of cosmic events as they occurred while Explorers

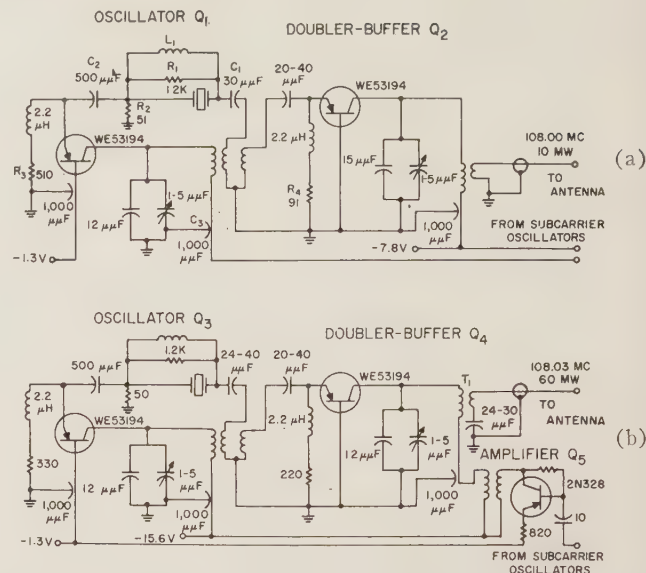


Fig. 13—Transmitters used in explorer satellites: (a) low-power transmitter; (b) high-power transmitter.

were above the local horizon. Because of the higher power drain, the mercury battery power supply could operate this transmitter continuously for only about 2 weeks, but the 10-mw Microlock transmitter could provide telemetry and tracking data for over 2 months. This tiny 10-mw unit was continuously heard by Microlock tracking stations for as long as 35 minutes during a pass near the satellite apogee altitude of 1500 miles.

Fig. 13(a) shows a schematic diagram of the low-power Microlock transmitter. This 10-mw transmitter is powered by a battery of 6 mercury cells from which it draws approximately a 5-ma current at about 8 volts. Phase modulation of the carrier signal with four standard FM/FM channels of telemetry is produced by varying the voltage applied to the collector of oscillator  $Q_1$ . This circuit produces in the stable crystal-controlled oscillator about a  $14^\circ$  index of phase modulation. A conversion efficiency of 25 per cent was obtained with class C operation. The high-power transmitter of Fig. 13(b) is similar to the low-power unit. Amplitude modulation is produced by varying the voltage applied to the collector of the doubler-buffer transistor. An audio voltage of about an 8-volt peak produces a 50 per cent amplitude modulation of the carrier signal.

One of the Explorer transmitters stopped operation at the expected time of battery exhaustion, only to return to the air again after a few days of silence. It is believed that this phenomenon was due to the particular arrangement of the batteries which supplied the collector and emitter currents in combination with the oscillator circuit itself. When the battery supplying both the collector and emitter current was power-depleted but still capable of producing a back voltage due to finite internal resistance, oscillations stopped. However, dc current continued to flow from the collector-only batteries. After a few days the collector-



emitter battery probably changed its characteristics enough to appear as a true short circuit. Thereupon, the collector batteries, which still had some residual power, started transmitter operation with a different operating mode for the oscillator.

#### SATELLITE ANTENNAS

In Explorer I, the output of the high-power transmitter was fed through a phasing and matching network into four flexible-wire turnstile antennas, mounted perpendicular to the cylindrical case at 90° intervals. The nearly omnidirectional radiation pattern thus produced was believed desirable because of the random payload orientations. Some pattern dissymmetry made it possible to determine satellite spin rate from received RF signal strength records.

During the second orbit pass of Explorer I, a very slow periodic fluctuation in signal strength became noticeable, in addition to the flutter caused by the 750-rpm rotation rate. By the end of the first orbit, it was already evident that the 750-rpm axial rotation was being damped out. A slow precession soon transferred the rotation axis to an end-over-end tumble with a 9-rpm rate. The change in motion was due to mechanical energy losses in the whip antennas under the condition that satellite momentum had to be conserved. To reduce the large signal-strength fluctuations resulting from this changing motion so early in the broadcasting lifetime, it was decided to eliminate whip antennas in Explorer III. Instead, the rocket motor case was electrically matched to the instrument carrier case to act as a dipole radiator. Explorer III did not begin to tumble until the end of the third day, after its orbital parameters had been firmly established.

The tumbling phenomenon had a valuable byproduct. In explaining the signal-strength variations, an analytical technique was developed which permits a surprisingly accurate determination of vehicle attitude using only ground measurements. The technique has been exploited in describing the performance of the high-speed rocket cluster

and in specifying final spin orientation of the Explorer and Pioneer payloads. The tumbling action also served to demonstrate the remarkable property of the Microlock system to perform well even under comparatively severe signal-strength fluctuations, a design criterion derived from the previous JPL telemetering philosophy.

Both scientifically and technologically, the Explorer electronics was considered successful.

#### PREFLIGHT TESTING

No statistical information concerning the expected reliability of the new component units was available at the time of the Explorer flights. The severe environmental specifications and the high reliability required for the Explorer satellite instrumentation prescribed that all components be subjected to 100 per cent flight-acceptance and type-approval tests. Flight-acceptance tests, applied to all units prepared for flight, including spares, were designed to subject the components to an environment simulating that encountered in space flight. The type-approval tests, applied to a sample payload, were designed to verify that the payload design was capable of surviving an environment more severe than that expected, as well as surviving the flight-acceptance test and then the space flight.

The second phase of the testing program consisted of subjecting the payload shell to temperatures fluctuating between -30°C and 120°C, an environment similar to that expected during flight. A safe temperature cycle of several hours demonstrated that the internal temperature variation was within the range desired, 0 to 45°C. Noise vibration of 15 g simulated the vibration produced by the burning of the fourth-stage rocket motor. Centrifuge tests to 100 g were used to simulate the linear acceleration during the firing of the fourth-stage motor. Spin tests at 750 rpm duplicated the expected final-stage spin rate. Simulated altitude tests in the vacuum chamber were used to check out the high-voltage circuitry. In this test it was found necessary to provide additional high-voltage breakdown protection in the form of plastic foam potting.



# Considerations to the Development of Explorer VII Satellite\*

JOSEF BOEHM†

**Summary**—The development of the orbiting carrier Explorer VII is presented. It is shown how the many requirements inherent to the mission were incorporated into one satellite system. The design parameters are discussed. Particular emphasis is devoted to the testing of the satellite with regard to functional and environmental conditions.

## I. INTRODUCTION

THE SATELLITE was engineered to contribute a most suitable carrier for the variety of scientific experiments of the Explorer VII mission. The complexity of this orbiting vehicle, the applied light-weight design, and the advanced technology of microminiaturization mark this satellite. It is the most efficient and sophisticated orbital carrier ever placed in orbit by the United States. The Explorer VII project was sponsored by the National Aeronautics and Space Administration.

To simplify the apparent complexity, great efforts went into establishing a clear layout scheme which would guarantee exact and unbiased measurements.

The design gathered form by consideration of a series of parameters which resulted partly from the specific mission and partly from the Juno-II rocket system of four stages. Requirements such as the satellite orientation, appropriate mounting possibilities for the sensors, sufficient area for solar cell arrays, and temperature control emerged directly from the task of Explorer VII. The booster system subjected the satellite to high static, dynamic, and centrifugal accelerations. The forces involved formulated the basic structural design. Weight limitation imposed by the capability of the booster has necessitated extreme light-weight design. In order to avoid excessive and unbearable balancing weights, the satellite was built symmetrical about the spin axis.

Two antenna systems, a 20-mc telemetry transmitter and a 108-mc tracking transmitter, presented most challenging mechanical design problems. The thermal calculations combined with thermal testing were of decisive influence to the design by yielding satisfactory radiation and conductivity conditions for the satellite.

A broad and thorough test program helped acquire the indispensable reliability.

## II. ORIENTATION IN SPACE

Several scientific experiments and one antenna system required our maintaining the orientation of the spin axis as established at injection. This was accomplished by spin-

stabilization. Because of weight and power limitation, the use of an active attitude-control system was out of the question. An oblate inertia distribution about the spin axis was chosen in order to assure stable orientation of the satellite at energy dissipation.<sup>1</sup> To nullify nutation, special damping was artificially introduced. The 20-mc antenna system with its long wires lent itself very favorably to the generation of additional nutation damping. To gain this damping, the antenna wires were run through a one-step telescoping Teflon tube which protrudes through the cylindrical center section of the satellite and reaches over the range of maximum bending of the wires during oscillation.<sup>2</sup> The moment of inertia ratio of approximately 1.24:1, with respect to the spin axis and a lateral axis through the center of gravity, was finally realized by separating the empty shell of the fourth-stage motor from the satellite body. (See Fig. 1.)

The unchanged orientation of the spin axis can be preserved only under the assumption that there are no external torques acting on the satellite. This assumption does not fully correspond to the actual conditions. The perturbing torques resulting from magnetic induction, differential gravity, etc., will produce a slowly increasing deviation from the original orientation of the spin axis. The

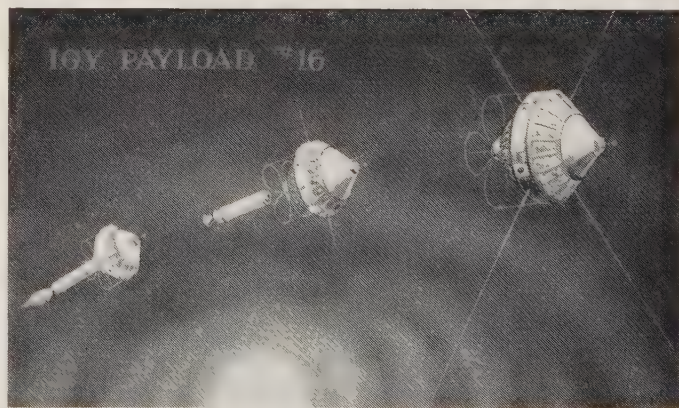


Fig. 1—Three flight phases of Explorer VII: (a) Last stage of booster system propels the satellite, 20-mc antenna wires not yet unreeled; (b) separation of last stage has taken place, antenna wires are extending; (c) orbiting satellite with fully unreeled wires.

<sup>1</sup> M. E. Kuebler, "Behavior of a Spinning Body in Space Whose Moment of Inertia Ratio Is Changed from a Rod to a Disk Shaped Body by Extended Masses," Electro-Mechanical Engrg. Branch, Guidance and Control Lab., Dev. Ops. Div., ABMA, Huntsville, Ala., Internal Rept.; 1958.

<sup>2</sup> J. A. Chambers, "Experimental Determination of Bending Energies and Fatigue Resistance 20 MC Antenna Systems: IGY-Satellite (AM#16)," Electro-Mechanical Engrg. Branch, Guidance and Control Lab., Dev. Ops. Div., ABMA, Huntsville, Ala., Internal Rept.; 1959.

\* Manuscript received by the PGMIL, February 1, 1960.

† Guidance and Control Lab., Dev. Ops. Div., U. S. Army Ballistic Missile Agency, Huntsville, Ala.

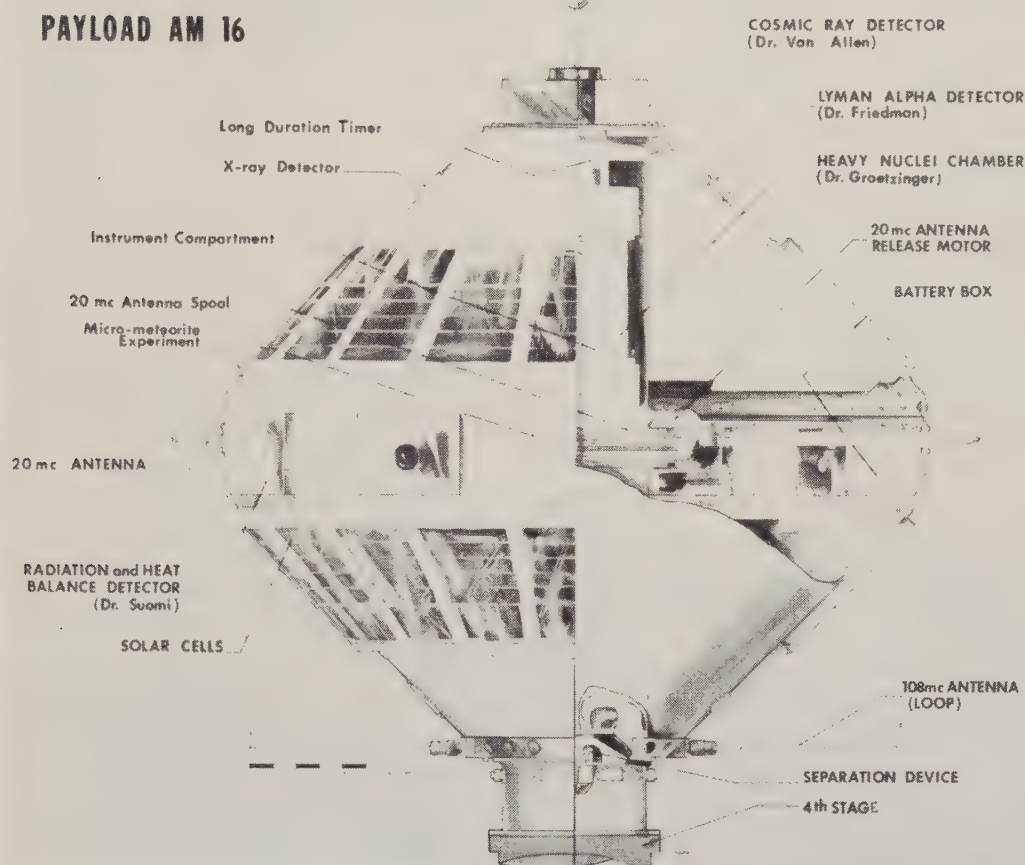


Fig. 2—Partial cutaway view of Explorer VII.

rate of change is not yet positively known. It is anticipated that the orientation change can be established to a reasonable degree of accuracy by comparison of the analytical results with corresponding Explorer VII measurements.

### III. LAYOUT AND DESIGN

The design parameter of conspicuous influence to the shape of the satellite was the orientation in space. As mentioned above, an oblate mass distribution about the main axis of the spin-stabilized body had to be provided. We accomplished the desired inertia distribution by placing the relatively heavy batteries at great distance from the spin axis. The components of the instrumentation were shaped in modules six inches in diameter and of varying thickness. These modules were assembled to a column, which was held together by two rods and inserted in a cylindrical aluminum housing. The instrument column with its shell was concentrically arranged about the spin axis, Figs. 2 and 3. The external over-all configuration was composed of a truncated double cone joined by a cylindrical center section. The connection between the centrally placed instrument housing and the outer center ring was obtained by four spokes which sustained the centrifugal forces because of spin, and also furnished support for the eight battery packs which were equally distributed at equal

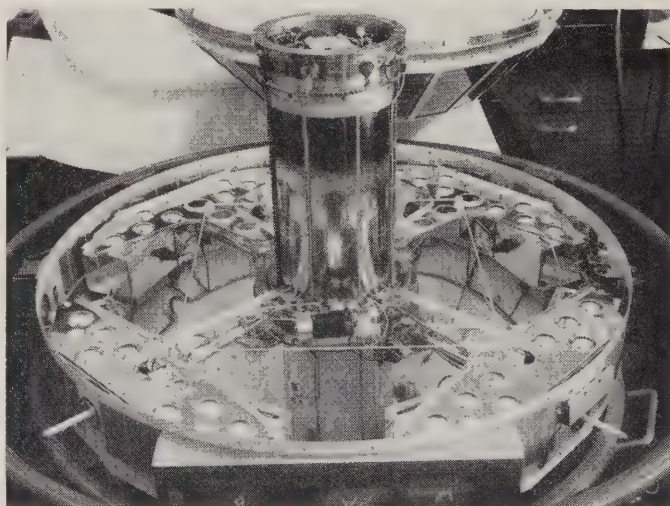


Fig. 3—Inside of Explorer VII; top cone is removed.

radial distance from the spin axis.

The top and the lower truncated conical shell, made of laminated polyester fiberglass, had to hold the center ring in position, and therewith the heavy batteries, during the impact of the thrust forces. These shells were at the same time exposed to the centrifugal load due to spin. The stress calculations were checked by simulating the load condition



by a sled test. The truncated cones were attached at the narrow opening to the rigid center column. At the wide opening, the cones were connected to profiled aluminum rings which formed a good transition of the thrust through the center ring and sustained at the same time the centrifugal load.

The over-all dimensions of the orbital carrier were 30 inches in width at the equator and approximately 30 inches in length.

The indicated method of packaging the instrumentation proved to be of noticeable advantage with regard to accessibility and exchangeability of components.

The total weight of Explorer VI at launch was 92.3 pounds, with the following weight breakdown:

Structure	29.6 pounds
Instrument package	14.4 pounds
Battery supply	15.9 pounds
Solar cell arrays	18.2 pounds
Separation device	2.8 pounds
Detectors and sensors	3.0 pounds
Balancing weights	0.7 pound
Antenna systems	
108-mc	2.2 pounds
20-mc	3.5 pounds
Potting and wiring	1.1 pounds
Surface coating and paint	.9 pound
	<hr/>
	92.3 pounds

The wiring network of the satellite was centralized in a separate distributor module at the forward end of the center column. The column wiring was concentrated in a channel which was shaped by grooves provided in each module of the instrument column. For efficient exchangeability, each instrument module was wired separately. The wires of one module were soldered to the module terminals and were equipped with a plug at the other end for convenient connection and disconnection to and from the network center. All electrical connections between the components of the instrument column and the sensing elements, batteries, solar power supply, antenna release motor, etc., were most practically obtained by means of this central distributor.

The slope of the shell cones had to furnish sufficient mounting area for the solar power supply.<sup>3</sup> The 45° slope was chosen to permit adequate solar energy interception at all possible angles of sunlight incidence. Fig. 2 shows the solar cell rings as they have been wrapped around the forward and the backward cone shell. The arrays of silicon solar cells, protected by fused silica glass against destruction by radiation and/or micrometeorites, have been laid out for a nonoriented satellite.<sup>4</sup>

<sup>3</sup> The solar-power supply for Explorer VII was designed and furnished to the ABMA by the USASRD.

<sup>4</sup> P. Youngblood, "Solar Cells for Satellite Power Supplies," Electrical Network Systems Branch, Guidance and Control Lab., Dev. Ops. Div., ABMA, Huntsville, Ala., Rept. No. DG-TN-18-58; 1958.

The shape of the satellite had to present also appropriate attachment possibilities for the various sensors of the experiments. They had to be protected from shading by the satellite itself. See Fig. 2 which illustrates distinctly the over-all arrangement of instrumentation and the location of the sensors.

Explorer VII is supposed to orbit for 20 years. The active lifetime was scheduled to be one year. This will be accomplished by an on-board timer which will automatically switch off the 20-mc transmitter after one year of operation time. The timer<sup>5</sup> was placed on the upper side of the wiring center. (See Fig. 2.)

As indicated before, the dynamic stability makes it mandatory that separation of the empty shell of the last-stage rocket motor from the satellite occur after burnout. In order to avoid having the shell hit the satellite after separation or enter the area of the antenna wires because of tiny impulses generated by outgassing and afterburning, it was decided to set the separation approximately two minutes after burnout. The timing was initiated by a timer in the third-stage rocket cluster. After two minutes, the delay timer caused the ignition of the explosive charges in the separation device and also started the antenna mechanism motor. It was necessary to assure instantaneous separation that would not produce an undue reaction to the satellite. A component was designed to this specification and was installed as a package, preloaded and sealed, between the satellite and the fourth-stage rocket motor.<sup>6</sup> The separation took place at the very moment when the six clamps located on the periphery of the separation device were ejected simultaneously and the spring force in the center of the device could push. The spring action effected separation of the two bodies in space. Two squibs, in redundant arrangement and fired by the above-mentioned delay timer, provided the force to unlock and accelerate the six clamp rods and dislodged the wedge-type clamps on the periphery, thus allowing the upper and lower halves of the device to separate.

The choice of fiberglass as material for the shell was influenced by the intent to minimize the eddy currents caused by the orbiter's spin in the earth's magnetic field. Large spin decay had to be avoided. The fiberglass, a thermal insulator, increased the temperature-control problems. Careful consideration was devoted to the selection of proper materials for vacuum condition.

#### IV. MECHANICAL ANTENNA DESIGN

A wave-propagation pattern about the equatorial plane of the satellite was accomplished for the 20-mc transmitter by an extendible flexible wire turnstile antenna system. In order to obtain efficient transmission, the antenna expert asked for a radial-wire length of approximately 12

<sup>5</sup> Developed and manufactured by the Bulova Watch Co., New York, N. Y.

<sup>6</sup> H. Wagner, "Development and Testing of IGY Satellite Separation Device," Electro-Mechanical Engrg. Branch, Guidance and Control Lab., Dev. Ops. Div., ABMA, Huntsville, Ala., Rept. No. DG-TR-7-60; 1960.

feet. During the ascending propelled flight phase, the space around the payload was limited by the protective shroud; therefore, an extended antenna system of desired dimensions was not applicable. Furthermore, the accelerations would not permit even the use of a light-weight rigid antenna of such size. Only an extendible antenna system was workable. The four antenna wires, each approximately 12 feet in length, were stored by winding them into separate grooves on a common drum which was bearing-supported and motor-driven. (See Fig. 2.) The wires were unreeled simultaneously at nearly constant speed.<sup>7</sup> The release started at the exact time the separation of the last stage shell took place. The drum was located around the cylindrical housing of the instrument column in such a way that the plane of the antenna-wire array went through the center of gravity of the satellite. Each wire was precisely counter-balanced by the one diametrically opposite. The flexible-wire antenna system was completely compatible with a satellite of oblate inertia distribution. Another factor implicit in the application of this antenna system was the need for nutation damping. How this nutation damping capability was obtained has been discussed in Section II. The release velocity of the antenna wires was controlled by a worm-gear assembly driven through a reduction-gear train and release motor. Three limit switches correctly controlled the power switch and the extended wire length. The wires were chosen with regard to electrical characteristics, high tensile strength, and sufficient internal damping.<sup>2</sup> The type of wire selected for this purpose had an 0.085-inch outside diameter, and consisted of a twisted-fiberglass core and a silver-plated copper-braided jacket, plus a wall of extruded Teflon. (See Fig. 4.)

A stationary loop antenna with four loops was provided for the 108-mc transmitter. The base of the satellite offered the most favorable mounting location for this antenna. The loops, approximately 10 inches in diameter, were supported by light strings in order to avoid shape deviation under the influence of thrust and centrifugal accelerations. (See Figs. 1 and 2.)

#### V. THERMAL DESIGN

Sensing elements, instrumentation, and power supply components imposed temperature restrictions upon the satellite in orbit. Proper operation was guaranteed only when the temperature fluctuations were held within prescribed temperature ranges. Therefore, the instrumentation and the batteries could not be exposed to temperatures lower than 0°C or higher than plus 60°C. Thermal considerations have greatly influenced the design of the satellite.<sup>8</sup> The internal instruments and the batteries were

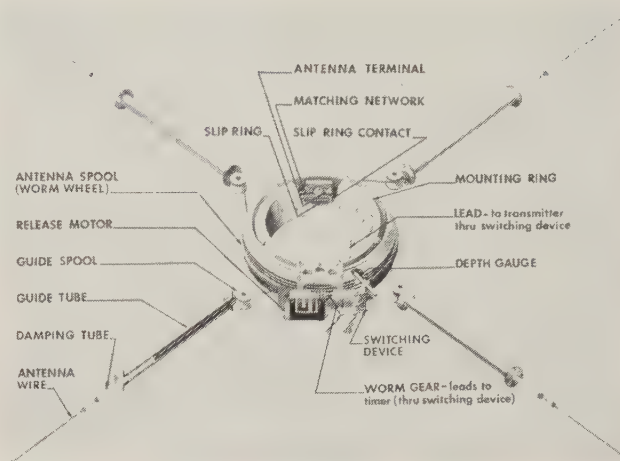


Fig. 4—20-mc antenna system.

insulated from the exterior hull of the carrier. The batteries were metallically connected to the instrument column by four spokes, but were thermally detached from the skin of the satellite by Kel-F spacers placed between the battery boxes and an aluminum ring composing a main structural element of the satellite shell at the equator.

By provision of suitable emissivities on the outer skin surfaces, the desired thermal balance was achieved, implying that acceptable internal average temperatures could be expected. The fact that the material of the shell was a thermal insulator demanded that the outside of the shell be covered by a metal foil in order to reduce the temperature gradients along the skin and to secure the necessary emissivities. The employed aluminum foil was interrupted by 0.125-inch gaps to reduce the effect of magnetic damping by eddy currents. The satellite configuration and the shell material made it inevitable that the radiation exchange was directed so as to 1) increase to the utmost the radiation exchange between the two truncated cones and 2) diminish as much as possible the undesirable energy exchange between the cones and the instrument column and batteries. In order to attain this guided radiation exchange, the inside of the truncated cones was coated with Rokide ( $\text{TiO}_2$ ) and all surfaces of the instrument column, battery supports and battery boxes were covered with gold foil or were made of polished aluminum. A passive temperature-control system was employed in such manner; the obvious simplicity inherent in this system meant greater reliability. The array of solar cells occasioned an additional thermal problem because of the used shell material and the shape of the satellite; a "greenhouse" effect resulted from the fused silica glass covering the solar cells. This problem posed great difficulties in obtaining a satisfactory solution. It became imperative to radiate from the rear side of the cells via a detour into space.

#### VI. ENVIRONMENTAL AND FUNCTIONAL TESTING

A most vital prerequisite for the successful performance of Explorer VII was comprehensive and rigorous testing with respect to functions and to environmental conditions.

<sup>7</sup> M. E. Kuebler, "Spin Reduction of a Satellite by Extension of Masses on Strings. Feasibility Study of the 20 MC Antenna System for the IGY-Satellite (#16)." Electro-Mechanical Engrg. Branch, Guidance and Control Lab., Dev. Ops. Div., ABMA, Huntsville, Ala., Internal Rept.; 1959.

<sup>8</sup> B. P. Jones, "Thermal Design Tests of the IGY Satellite (Payload for Missile No. 16)," Res. Projects Lab., Dev. Ops. Div., ABMA, Huntsville, Ala., Rept. No. DV-TM-23-59; 1959.



The test program reflected to optimum extent simulation of all expected environmental conditions to be faced by the satellite during the ascending phase of its trajectory and while in orbit. Exhaustive functional tests were in particular performed with the individual component systems of the satellite.

The applied test procedure provided first tests with prototype models, and second, so-called flight acceptance tests with the actual flight satellite. The prototype models completely resembled the flight satellite. Accordingly, separate test specifications were prepared for prototype acceptance and flight acceptance. The prototype specifications contained well-founded safety factors, *e.g.*, 20 per cent to 50 per cent safety was used for the dynamic environments. The flight satellite was subjected to basically the same series of tests under substantially lessened rigourousness. The main intent of these tests was to investigate the satellite after final assembly in order to determine the extent of "human error."

Several prototypes were manufactured to be available for mechanical, electrical, etc., tests, which were often run in parallel.

Findings of the prototype testing were evaluated, and were reflected, when necessary, in corresponding modifications which were given consideration before the manufacture of the flight satellite.

The Juno-II rocket system with the cluster rotating at 450 rpm imposed stringent balancing requirements. The radial distance of the center of gravity of the 92.3-pound satellite body on top of the last-stage motor (six inches in diameter), was to be smaller than 0.005 inch. The dynamic tests were performed with a highly sensitive special balancing apparatus. Because of the rotationally-symmetric design, the balancing weights which had to be added cost only a relatively small weight penalty.

Another essential phase of the test program represented the testing of the effects of static and dynamic accelerations produced by spin, thrust, initial shock, and vibrations. The satellite was spun on a spin mechanism at a rate of 600 rpm for at least five minutes. Functional operation of the payload instrumentation was monitored during the spin period. This was to prove 1) the structural adequacy of the satellite, and further 2) the perfect functioning of the instrumentation and the complete power supply under spin.

The entire satellite was subjected on a centrifuge to accelerations caused by the thrust of the Jupiter booster and the cluster rockets. Instrumentation and power supply were checked before and after a three-minute exposure to acceleration. By spinning the satellite on the centrifuge, we superimposed centrifugal acceleration on thrust acceleration.

To simulate the acceleration conditions during propelled flight, the instrument column of the satellite was spun on the revolving centrifuge. It was necessary to abstain from exposing the entire satellite to this test because of the unacceptable gyroscopic torques which would have resulted

from the prescribed spin rpm and the necessary angular velocity of the centrifuge.

The initial shock influence particularly resulting from the three solid-propellant rocket stages was checked by a linear accelerator. Thirty shock exposures to about 25g and 10 milliseconds duration were imparted to the instrument column.

The test apparatus used was a newly developed linear accelerator, working cyclically on a pneumatic principle.<sup>9</sup> We tested the behavior of the satellite, with regard to the structure and the operation of the instrumentation under the impact of rocket vibrations, by vibrating the satellite in three directions about three mutually perpendicular axes, one of which was the spin axis. The tests were performed on a MB Co. vibration table, Model C25HB.

The test specifications for vibrations in thrust direction for prototype and flight acceptance testing are given in Table I, for purposes of comparison.

TABLE I

	Acceleration Level rms (g's)	Duration (second)	Bandwidth (cps)
Prototype	20	120	20-1500
Flight satellite	3	8	20-1500

This example illustrates clearly how we attempted to avoid fatigue effects on the flight satellite.

The orbital environments were simulated with respect to vacuum and temperature, after the satellite was exposed to launch environments. For obvious reasons, the condition of weightlessness could not be simulated. The instrumentation and power supply (except solar cells) worked in near vacuum over the anticipated range of temperature. The thermal characteristics of the satellite were determined to enable prediction of orbital temperature ranges by analysis. Liquid nitrogen and a special electric heating blanket were used in a vacuum chamber, to cool the satellite to a low temperature and to heat it up by a heat-step which could be directed to all or part of the satellite's surface. In this way, internal conductive and radiative coefficients of the satellite were determined and evaluated in order to calculate, in connection with the surface emissivity ratios, the temperatures for certain orbital data.

The satellite's operation capability over longer duration in space was investigated by our subjecting the satellite to a vacuum of  $5 \times 10^{-5}$  mm of mercury at an instrumentation temperature of  $0^{\circ}\text{C}^{+10^{\circ}}$  and plus  $60^{\circ}\text{C}^{-10^{\circ}}$ , respectively, for two weeks. For one week each of the above-shown temperatures was applied, these representing the extremes of the permissible temperature range. During this so-called vacuum-temperature "soak" test, the functioning of all the experiments (except solar cells) was continuously monitored.

<sup>9</sup> Developed jointly by the Guidance and Control Lab. of ABMA and the Franklin Institute, Philadelphia, Pa.

The significance of the vacuum tests became very apparent when an oil film was found which deposited also on reflective radiation insulation surface producing an unacceptable increase of thermal transfer to the instrument column and batteries. The oil film seems to have been caused by partial volatilization of wire insulation. It appears that wires with insulation material not containing plasticizers like Teflon, Kel-F, etc., should be given preference.

A special rocket-sled test was planned and performed so that we could investigate and check the stress conditions of the double-cone structure of Explorer VII. (See Fig. 5.)<sup>10</sup> This test was carried out on a rather short sled track only approximately 0.8 mile long. Two successive and equal linear impulses were given the mass of sled and load by 2-plus-2 loki rockets, each of 3200-pound thrust and approximately 0.83-second thrust duration. The velocity of the sled was broken and slightly reversed by the simultaneous firing of four rockets of the same kind in opposite directions.

By this "shuttle" sled method, it was possible to impart to the spinning satellite on the sled a simulated thrust acceleration of approximately 35 g's and 0.83-second duration. 22 g's occurred as greatest thrust acceleration at the end of the second stage during the actual flight. Strain-gauges were used to measure the deformation of the satellite structure which was recorded by on-board devices.

Typical of the way in which functional testing was executed were the following two tests performed with component systems. Both devices, the described separation device and the 20-mc antenna release mechanism, had to work perfectly. The malfunction of one or both during the actual flight would have resulted in a total failure of the Explorer VII mission.

This separation device, after all its parts had been checked very critically, was tested under closely simulated flight conditions so that we could observe the dynamic behavior of the complete system consisting of satellite and empty shell of last stage motor. A satellite mock-up of true mass distribution was suspended at its center of gravity, with low friction, by a cord. This way, the approach to six degrees of motion freedom was quite optimized. A rocket dummy, also representing an actual mass distribution, was attached to the dummy satellite by the separation device to be tested. (See Fig. 6). After the system was spun up to the cluster rpm of 450 and nutation was artificially imparted, the separation mechanism was actuated. It was found that the applied mechanical scheme was sound and reliable. The separation was instantaneous and without noticeable reaction to the satellite body.<sup>11</sup>

<sup>10</sup> The test was designed and fabricated by ABMA and operated by the Army Rocket and Guided Missile Agency at Redstone Arsenal.

<sup>11</sup> H. M. Pfaff, chief of Mechanical Systems Section, Electro-Mechanical Engrg. Branch, Guidance and Control Lab., Dev. Ops. Div. ABMA, Huntsville, Ala., proposed this test. He also contributed in many respects to the success of the Explorer VII project.

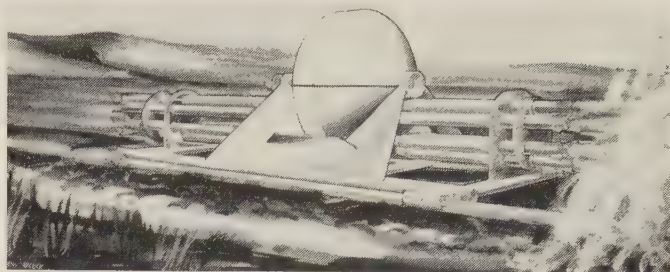


Fig. 5—Acceleration test sled.

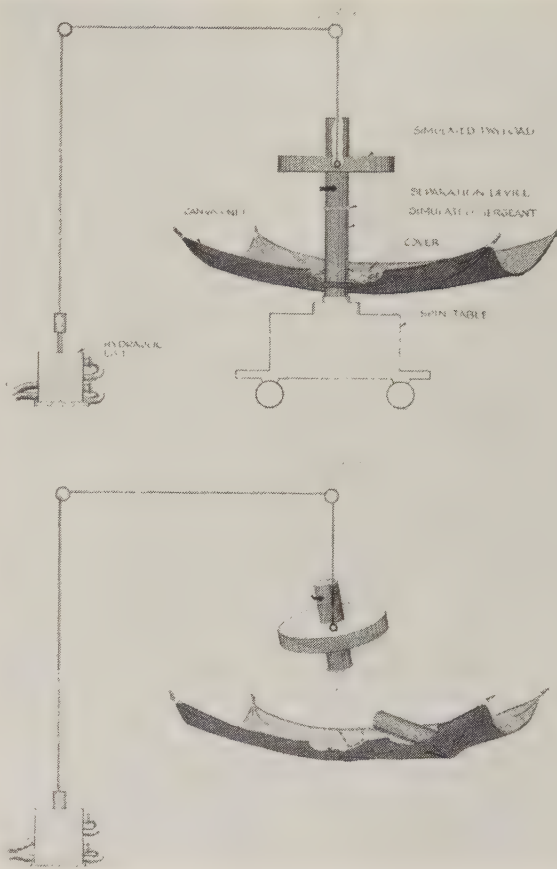


Fig. 6—Schematic of separation test equipment.

The extendible 20-mc antenna system, as shown in Fig. 4, was also tested under a close simulation of possible flight conditions.<sup>12</sup> The test program was based on full-scale operation of the antenna system in a large vacuum chamber, a 41-foot diameter sphere, at one to two millimeters of mercury. The satellite was similarly suspended as for the separation test. The motion of the wires and the satellite were observed. Nutation of varying amount was generated by the dropping of weights onto the simulated satellite. The operation of the mechanical system to full wire extension, with and without nutation, the damping capability of the extended wires, the wire release velocity, and the spin decrease caused by inertia increase by change of mass dis-

<sup>12</sup> The tests were performed and operated by the National Aeronautics and Space Administration at Langley Field, Va.



tribution were studied and checked. The antenna release system was accepted for flight after a considerable number of operations had been performed satisfactorily from every point of evaluation.<sup>13</sup> The test program outlined above was based on the philosophy that high reliability is achieved not only by suitable design but also by the quality of the tests.

## VII. RESULTS AND CONCLUSION

Explorer VII has already furnished a wealth of usable scientific measurements. These data will contribute much to our knowledge about synoptic meteorology and radiation conditions in the earth's adjacent space. It appears that this satellite operated perfectly. This would signify that all the individual component systems functioned correctly. The separation took place approximately two minutes after burnout of the last-stage rocket. At the same time, the four wires started to unreel and were released with the proper velocity to shape, in approximately 18 seconds, the full antenna array of 24-foot diameter for the 20-mc transmission system. The load switches which first paralleled the antenna wires with the dummy load resistance, and then disconnected the resistive load, thus giving full transmitter output to the antenna system, occurred as intended a few fractions of a second before the release motor cutoff. The number of revolutions of the satellite before release of the wires was approximately 420. After change of mass distribution by the antenna array, the rpm decreased to the expected value of approximately 360. The spin decay amounted to not more than 4.1 per cent of the original value after two and a half months of orbiting in the earth's magnetic field. Because of the anticipated exponential course of spin drop, it is ascertained that sufficient angular velocity about the spin axis for stabilization and for the 20-mc antenna operation will be provided. The separation and the unfolding of the antenna array occurred at a very small nutation.

The communication systems furnished good and unbiased data. Both transmitters operated with the expected signal strength. The 108-mc transmitter discontinued at the end of its planned life time of approximately seven weeks.

<sup>13</sup>L. L. Mitchum, "Test Report for IGY Satellite Antenna Release," Electro-Mechanical Engrg. Branch, Guidance and Control Lab., Dev. Ops. Div., ABMA, Huntsville, Ala., Internal Rept.; 1959.

The operation of Explorer VII has shown that the solar cell arrays were suitably laid out and that the recharging mechanism between solar power and chemical power satisfies the power requirements under all orbital conditions.

The thermal design proved to be adequate to keep the temperature, at all locations on the outside surface and inside of the satellite, well within the prescribed and tolerable temperature limitations. As mentioned before, a temperature range between 0°C and plus 60°C was permissible for the instrumentation. Thus, after three months of orbiting, measurements indicate that the temperature of the 20-mc transmitter, located centrally within the instrument column, was never lower than plus 16°C and never higher than plus 41°C.

Summarizing, it can be concluded that the design objectives of the Explorer VII mission have been met. The component and system designs, as applied, satisfied the presented requirements. Adequate reliability was established by design and by subjecting the satellite to the test program and test procedure outlined above. It is felt that the knowledge and experience gained by developing Explorer VII is a sound basis for future work in the field of space technology.

## ACKNOWLEDGMENT

Explorer VII was predominantly developed in the Guidance and Control Laboratory, Development Operations Division, Army Ballistic Missile Agency, Huntsville, Alabama. Contributions came from the following branches of this laboratory: Electro-Mechanical Engineering Branch: mechanical system, design engineering, packaging, and testing; Missile Instrumentation Development Branch: telemetry and tracking systems, and associated electronics for complete communications systems; Electrical Network Systems Branch: wiring, solar cells, battery systems and timers; Pilot Manufacturing Development Branch: manufacturing of prototypes and flight satellites and their assembly; Applied Research Branch: performance of tests. In addition, the Missile Instrumentation Development Branch and Applied Research Branch were responsible for the coordination with experiment sponsors, and were responsible that these components met the specifications. Other essential contributions were furnished by Research Projects Laboratory: temperature control; and by Structures and Mechanics Laboratory: selection of materials, coating and performance of tests.

# Scientific Objectives of Explorer VII\*

A. W. THOMPSON†

**Summary**—This paper presents a description and the results of experiments conducted and carried aboard the Explorer VII satellite. Experiments covered are: radiation balance, heavy primary cosmic ray, Lyman-alpha X ray, the cosmic ray, exposed solar cell, micrometeorite, the earth radiation balance, and temperature measurement. A brief description of the power source and telemetering frequencies used on the satellite for the transmission of scientific information is also given.

AT THE request of Dr. Richard Porter, Chairman, United States Technical Panel on Earth Satellites of the National Committee for the IGY, Army Ballistic Missile personnel met with sponsors of five hard-core International Geophysical Year experiments to determine which, and how many of the experiments could be carried in a satellite launched with a Juno II type satellite launching vehicle.

In order to determine which of the experiments should be selected, the sponsor of each experiment described his experiment. Next a chart (Fig. 1) was formed which

dropped. Of the five hard-core experiments considered, the Cloud Cover Experiment developed under IGY sponsorship by the United States Army Signal Research Development Laboratory with W. G. Stroud as project leader, was found to require a reduction in spin from 360 rpm at injection to some 12 rpm for operation and the telemetering bandwidth was considerably greater than the others. The O'Sullivan visibility sphere was quite heavy and did not complement the rest of the experiments. Therefore, these two experiments were eliminated.

The experiments, with their sponsors, selected for the satellite were:

Earth Radiation Balance—Dr. Vern Suomi;

Intensity of Heavy Primary Cosmic Radiation—Dr. Gerhart Groetzinger;

Lyman-Alpha and X-Ray Intensity—Dr. Herbert Friedman;

Cosmic-Ray Count—Dr. James Van Allen.

Experiment	Desired Maximum Latitude	Attitude	Spin	Weight	Power Requirements	Voltage	Bandwidth Requirements
Van Allen	51°	No difference	No difference	1 pound	40 mw	5.4	1 cps
Groetzinger	35-51°	No difference	No difference	4 pounds	40 mw	5.4	10 cps
Friedman	51°	No difference	No difference	1½ pounds	125 mw	3.4 2.7 1.35 —9	20 cps
Suomi	51°	Spin stabilized	No difference	2½ pounds	90 mw	6	2-200 cps
Stroud	35-51°	Spin stabilized	Needs damping	2½ pounds	75 mw	1.2	3000 cps
O'Sullivan	—	Spin stabilized	No difference	10 pounds	—	—	—
Transmitter Power Requirements					2 watts for telemetering 50 mw for tracking		

Fig. 1—Chart of each sponsor's description of his experiment. All concerned agreed that they could meet the schedule deadlines. If a 20-mc continuous-wave telemeter transmitter were used, no tape recorders would be required. It was also agreed that if temperatures were maintained between  $\pm 10^{\circ}\text{C}$  to  $+60^{\circ}\text{C}$ , there would be no temperature problems.

showed such factors as optimum orbit parameters, power requirements, telemetering bandwidth required, satellite spin requirement and proposed weights. Another Vanguard experiment, the O'Sullivan visibility sphere, was also considered.

Since not more than four major experiments could be included in the satellite for reasons of weight and complexity, two of the proposed experiments had to be

During this meeting it was also decided to use solar energy instead of batteries for the power to insure a long and useful lifetime for the instrumentation, and to transmit the scientific information on a 20-mc frequency. This frequency was selected because it is in a frequency spectrum where many people, widely distributed around the world, have receivers and not because it was considered optimum for satellite telemetering. It was also decided to use a battery-powered 108-mc tracking beacon which would operate for several months.

The development of this satellite was interrupted by the

\* Manuscript received by the PGMIL, February 1, 1960.

† U. S. Army Ballistic Missile Agency, Redstone Arsenal, Huntsville, Ala.



high-priority Explorers IV and V (ARGUS) program, and a corresponding delay in the launch date was introduced. This delay allowed the introduction of several temperature measurements sponsored by ABMA, an unprotected solar cell experiment sponsored jointly by USASRDL and ABMA, and a micrometeorite experiment sponsored by Herman La Gow of NRL (presently of NASA). The micrometeorite experiment was added to the 108-mc transmitter battery power supply and its data along with data from a temperature measurement were transmitted over the 108-mc transmitter.

#### THE RADIATION BALANCE EXPERIMENT

This experiment was proposed by Dr. Harry Wexler of the U.S. Weather Bureau and is sponsored by Dr. Suomi, University of Wisconsin. Its scientific purpose is to aid meteorologists in their understanding of weather. The radiation balance of the earth system is nearly constant over the entire earth for a period of several years. However, the earth receives more energy from the sun near the equator than it radiates into space, and it radiates more energy into space from the poles than it receives from the sun. This means that energy must be transferred from the lower latitudes to the higher latitudes by means of ocean currents and the atmosphere. The transfer of this energy will be studied in this experiment by measurement of the following:

- 1) the direct radiation from the sun;
- 2) the fraction of this radiation that is diffusely reflected by earth, clouds, and atmosphere; and
- 3) the fraction of radiation that is converted into heat by the earth and is ultimately reradiated back to space in the far infrared portion of the spectrum.

Several sensing elements were designed to measure the different quantities needed: two are hemispheres painted *black* to measure total energy at all wavelengths; one hemisphere is painted *white* to measure radiations in the longer wavelengths while reflecting short wavelengths; one hemisphere has a Tabor coating to make it absorb only short-wave radiation and is shielded from the sun by half of a cylindrical shield. The other sensor is a black sphere sitting at the end of a small rod extended from the top of the satellite. Table I shows the values of absorptivity for these surfaces as a function of wavelength and wavefront type.

TABLE I  
VALUES OF ABSORPTIVITY FOR VARIOUS COATINGS

Surface	Short-Wave Beam Radiation	Short-Wave Diffuse Radiation	Long-Wave Radiation
Black paint	0.95	0.95	0.95
Lead carbonate White paint	0.05	0.95	0.95
Tabor coating	0.90	0.90	0.10

Each sensor contains a thermistor which is switched in sequence to a blocking oscillator. The pulses of the blocking oscillator are scaled 1024 to 1 and are coded to modulate the 730-cps subcarrier oscillator; the 560-cps subcarrier oscillator is modulated by an on-board reference timer.

#### HEAVY PRIMARY COSMIC RAY EXPERIMENT

The experiment was sponsored by the late Dr. Groetzing of Research Institute for Advanced Studies (RIAS) and is now sponsored by Dr. Martin Pomerantz of Bartol Research Foundation and Dr. Philip Schwed of RIAS. The scientific objective of this experiment is to investigate the heavy primary cosmic rays which consist of heavy atoms stripped of their external electrons and endowed with very high energies. One hopes to learn the chemical composition of the sources of cosmic radiation and something of the conditions in cosmic space. The equipment employs an ion chamber to count cosmic rays in three classes. The three ranges have limits determined by the atomic numbers "*Q*" of specific atoms carbon, fluorine, and sulphur whose numbers are 6, 9, and 16 respectively. Any particle with a number equal to or greater than 6 will be counted in one channel, equal to or greater than 9 in another, and equal or greater than 16 in the remaining channel. The principle of detection is based upon the fact that all the primary particles to be countered will be completely ionized nuclei having relativistic velocities (greater than 0.9 times the velocity of light). To a good approximation, the ionization per unit path length produced by such a particle in traversing a gas is independent of its energy, but proportional to the square of its charge, *i.e.*, in the present case to the square of its atomic number. The ionization chamber employed to detect these particles is effectively an instrument for detecting the ionization per unit path length produced whenever a charged particle passes through the argon gas which fills this chamber. The chamber is a cylinder 11 cm in diameter by 18 cm long, filed with argon gas at 9 atmospheric pressure, with a 0.01 wire along the axis of the cylinder charged to a potential of 370 volts with respect to the walls of the cylinder. The total charge reaching the central wire is therefore proportional to the total ionization generated by the particle in question and hence measures the charge of the particle. In the circuit employed here, the pulse of electron current in the chamber is converted to a voltage pulse by a resistance capacity network, the pulse height being approximately 0.3 volts for a *Q* of 6, 1.2 volts for a *Q* of 9, and 2.7 volts for a *Q* of 16. The pulses are separated by amplitude discrimination and fed to scaler circuits. The output of the scaler circuits are converted to dc voltages which in turn are multiplexed on to the 960-cps voltage-controlled oscillator.

#### LYMAN-ALPHA X-RAY EXPERIMENT

This experiment is sponsored by Dr. Friedman of NRL and will measure the solar emissions at the ultraviolet 1216-Å line and X rays in the 15- to 3-Å range during

normal and active solar periods. The Lyman-alpha radiation intensity will be measured by means of two photo-sensitive ion chambers which are cylindrical in shape, some  $\frac{3}{4}$  inch in diameter by  $1\frac{1}{4}$  inches long. The chambers are located one in each hemisphere, one above the other and making an angle of  $\pm 45^\circ$  from the equator of the satellite. The chamber is fitted with a window made of lithium fluoride which transmits wavelengths longer than 1040 Å and is filled with nitric oxide gas pressurized to 15–25-mm Hg, which is ionized by wavelengths shorter than 1340 Å. This means that the chamber is sensitive to radiation between 1040 Å and 1340 Å. The only radiation of noticeable intensity in this band is the Lyman-alpha line of atomic hydrogen at 1216 Å. This chamber is operated at a potential of 45 volts with a current output in the order of  $2 \times 10^{-11}$  amperes at the expected radiation intensity.

The X-ray instrument is similar in size and shape to the Lyman-alpha detector. It is filled with argon gas at 692-mm Hg pressure, has a 15-mil beryllium window, and is sensitive to radiation wavelengths from 15 to 3 angstroms. The X-ray detectors are located  $180^\circ$  from the Lyman-alpha detectors and their current output is in the order of  $10^{-13}$  amperes to  $10^{-10}$  amperes. A photocell is included to determine the aspect of the satellite relative to the sun.

The outputs of the Lyman-alpha ion chamber, the X-ray ion chamber, and the photocell are multiplexed into the 960-cps subcarrier oscillator.

The sensitivity range of the ion chambers and their speed of response are adequate for monitoring the normal level of Lyman-alpha radiation and the increase expected with flare activity.

#### THE COSMIC-RAY EXPERIMENT

This experiment is sponsored by Dr. Van Allen, State University of Iowa. The scientific objective of this experiment is to:

- 1) measure the cosmic-ray intensity and the high-intensity radiation over a large portion of the earth's surface; and
- 2) provide a survey of the temporal variations in cosmic-ray and high-intensity radiations.

Two GM tubes will be carried on the satellite to measure the cosmic ray count. The output of an Anton 302 (same as Explorer IV) tube with no special shielding will be scaled 2048 to 1 and will map the radiation belt. The output of an Anton 112 GM tube with a lead shield (approximately 1 mm thick) will be scaled by 128 to 1 to give the cosmic-ray count below the belt. The output of both scalers will key a 4-step SCO with a center frequency of 1300 cps.

#### TEMPERATURE MEASUREMENTS

This experiment is sponsored by Mr. Gerhard Heller, ABMA. In previous satellites, the temperature data have resulted from indirect measurements. These data are not

considered adequate to explain the temperature history of the satellites to date. Therefore, special planning has resulted in adding several temperatures, in addition to those which are part of the Suomi and La Gow experiments, to measure temperature variations in the following:

- 1) a very isolated skin area;
- 2) a solar cell cluster;
- 3) inside the 20-mc transmitter;
- 4) in a battery pack;
- 5) one of the Van Allen GM tubes; and
- 6) gold hemisphere on equator.

These data will be telemetered with the Suomi data.

#### EXPOSED SOLAR CELL EXPERIMENT

The purpose of this experiment is to determine the effect of space environment on unprotected photovoltaic energy convertors. A patch made up of 10 Hoffman-type 52 C cells connected in series, loaded by a 100-ohm resistor, were placed on the equator of the satellite. The voltage, expected to reach a maximum of 5 volts, developed across the 100-ohm resistor, will vary greatly as a cosine function of the angle which the surface of the patch makes with respect to the sun. This voltage is multiplexed into the 960-cps subcarrier oscillator for telemetry.

By observing the voltage variations over a period of several months and applying proper correction factors for aspect and temperature one should be able to obtain the stated objective of the experiment.

#### MICROMETEORITE EXPERIMENT

Sponsored by Herman La Gow, NASA, this experiment was designed to measure the incidence of micrometeorite particles in the 10-micron or larger ranges.

The basic detector is a glass cylinder, approximately 5 mm in diameter and 6 mm long, the walls of which are mirrorized. The exposed end of the cylinder is frosted and covered with an opaque surface; the other end has an evaporated CdS surface. Three of these detectors are used in the experiment and the opaque surface is different in each.

One detector which is designed to detect surface sputtering and micrometeorites has a 1-mil mylar window with a coating of evaporated aluminum on its outer surface. Of the other two detectors which detect micrometeorites, only one has a window made up of 1-mil mylar coated with aluminum on both sides and the other a 1-mil aluminum window; this sensor has a very small hole for calibration purposes.

The CdS cell resistance is temperature dependent and a thermistor is used to measure the temperature of one of the cells.

The resistance of the three detectors, a 20,000-ohm calibration resistor, a 100,000-ohm calibration resistor, and the thermistor, are multiplexed on a 730-cps subcarrier oscillator which modulates the 108-mc transmitter.



## RESULTS

The Explorer VII was launched at 11:31 A.M. EST, October 13, 1959. As of November 28, the perigee was 346 miles and the apogee was 673 miles. The firing azimuth was such that the desired  $51^\circ$  latitude orbit was reached. An orbital lifetime of about 20 years is anticipated.

A working group, made up of the people concerned with the satellite, met December 29 and 30 at NASA Headquarters, Washington, D. C., to discuss the results of the satellite data to date. The working group session ended in a press conference which is summarized as follows.

*The Earth Radiation Balance Experiment*

This experiment is making some 4000 radiation observations daily; of these, some 400 to a 1000 are being collected for analysis. The analysis of the data to date shows that in the sunlight portion of the earth, large (about a thousand miles across) clouds or storm areas show up readily, and on the dark side of the earth, one can detect positions where cold or warm air exists. Large changes in heat loss have been observed over small areas of the earth, such changes as one would expect in going from the equator to the poles.

Much additional data analysis remains to be done, but the results thus far are very encouraging.

*Intensity of Heavy Primary Cosmic Radiation*

This is the first occasion on which this sort of detector has been used in a satellite experiment, and results to date have shown that the desired performance was indeed attained. Specifically, one has been able to determine the rate of arrival of particles of various energies at different geographic locations. In fact, the count rate in the energy range  $Q \approx 6$  or greater per square centimeter at the high latitudes is approximately ten times as great as at the equator. It is expected that the final analysis of the fluctuations of counts with sun storms will extend our knowledge of the effects of solar influence on cosmic radiations.

*Lyman-Alpha and X-Ray Intensity*

The detectors of this experiment have been almost exclusively saturated with trapped particle radiation. Therefore very few solar X-ray or Lyman-alpha data have been collected. However, the experiment is giving information on the lower energy particles trapped in the earth's magnetic field. This will aid in understanding the structure of the inner part of the radiation belt.

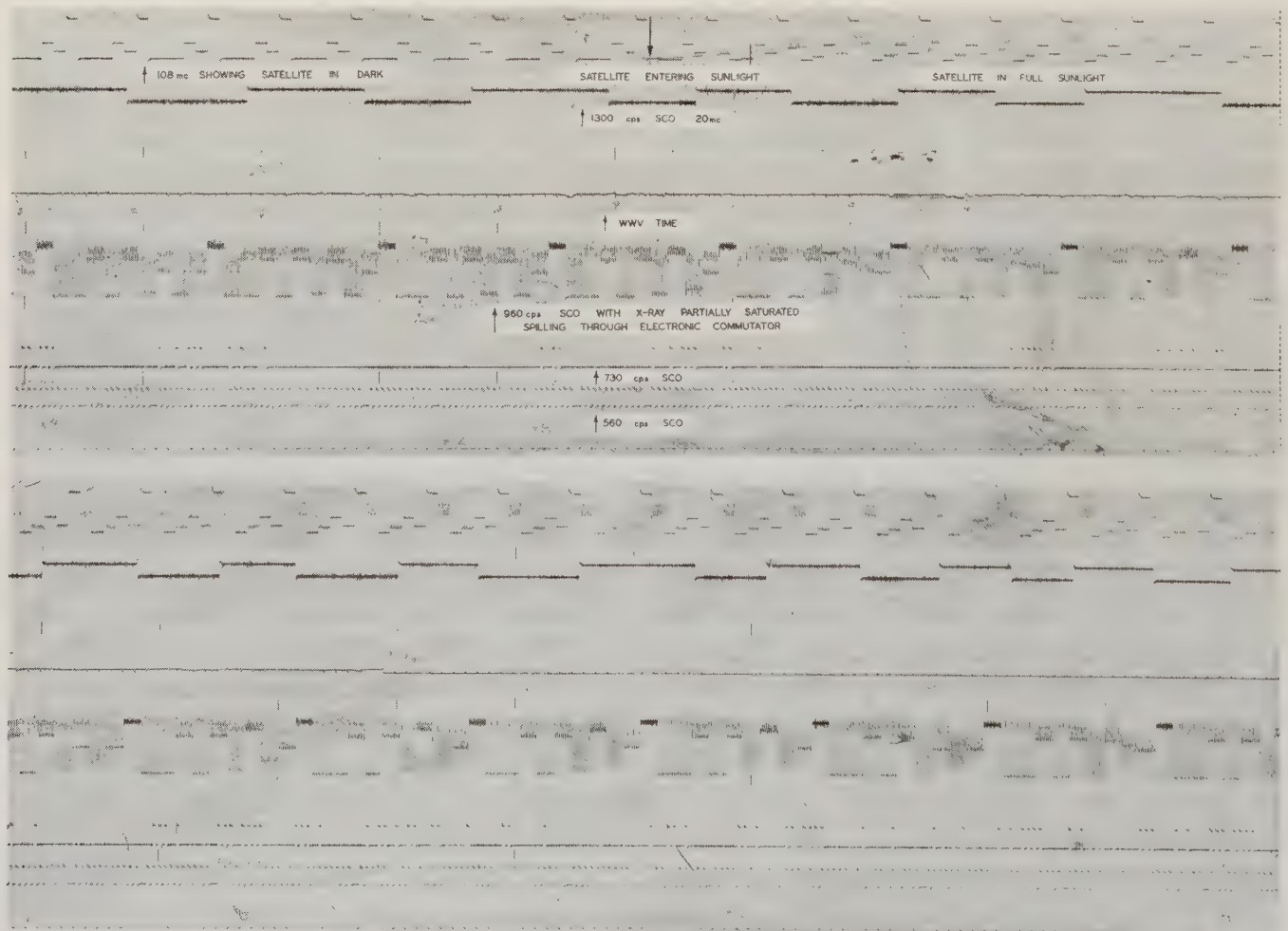


Fig. 2—Telemetry playback showing both 20- and 108-mc telemetry in phase from the earth's shadow to full sunlight.

### Cosmic-Ray Count

This experiment has thus far resulted in some very interesting data on the short-time effects on the outer radiation zone by geomagnetic storms, and on the Forebush decrease of cosmic-ray intensity which is associated with geomagnetic storms.

As the satellite data continues, it is expected that the long-time effects will be very valuable.

### Temperature Measurements

The thermal design of the satellite has proven to be well within the temperature ranges required and are treated in detail by Heller elsewhere in this issue.<sup>1</sup>

### Micrometeorite Experiment

Analysis of the telemetered records to date show that approximately one-half of one per cent of the area of one cell was admitting sunlight. This puncture occurred during the launch phase and is not expected to have been from a

micrometeorite. No further penetration or erosions have been noted to date.

This 108-mc transmitter was last tracked on December 4, 1959. The exhaustion of the chemical batteries is the reason that the transmitter went off the air.

### Unprotected Solar Cells

The unprotected solar cells are still operating properly. This indicates that there is very little damage to solar cells from space environment in the orbit of this satellite. It must be noted, however, that the apogee of this satellite does not extend into the high-energy radiation belts. Therefore, the effect of high-energy particles on unprotected solar cells must await future experiments.

### Telemetry Playbacks from Explorer VII

Figs. 2 and 3 are samples of actual recordings made at the ABMA Huntsville receiving station. Fig. 2 represents a pass where the satellite was in the dark and entered sunlight. Some 23 seconds are required from the time that the sensors of the micrometeorite experiment first detect sunlight until they show the sunlight at full strength. On this same pass, it is interesting to note that 11 of the Suomi

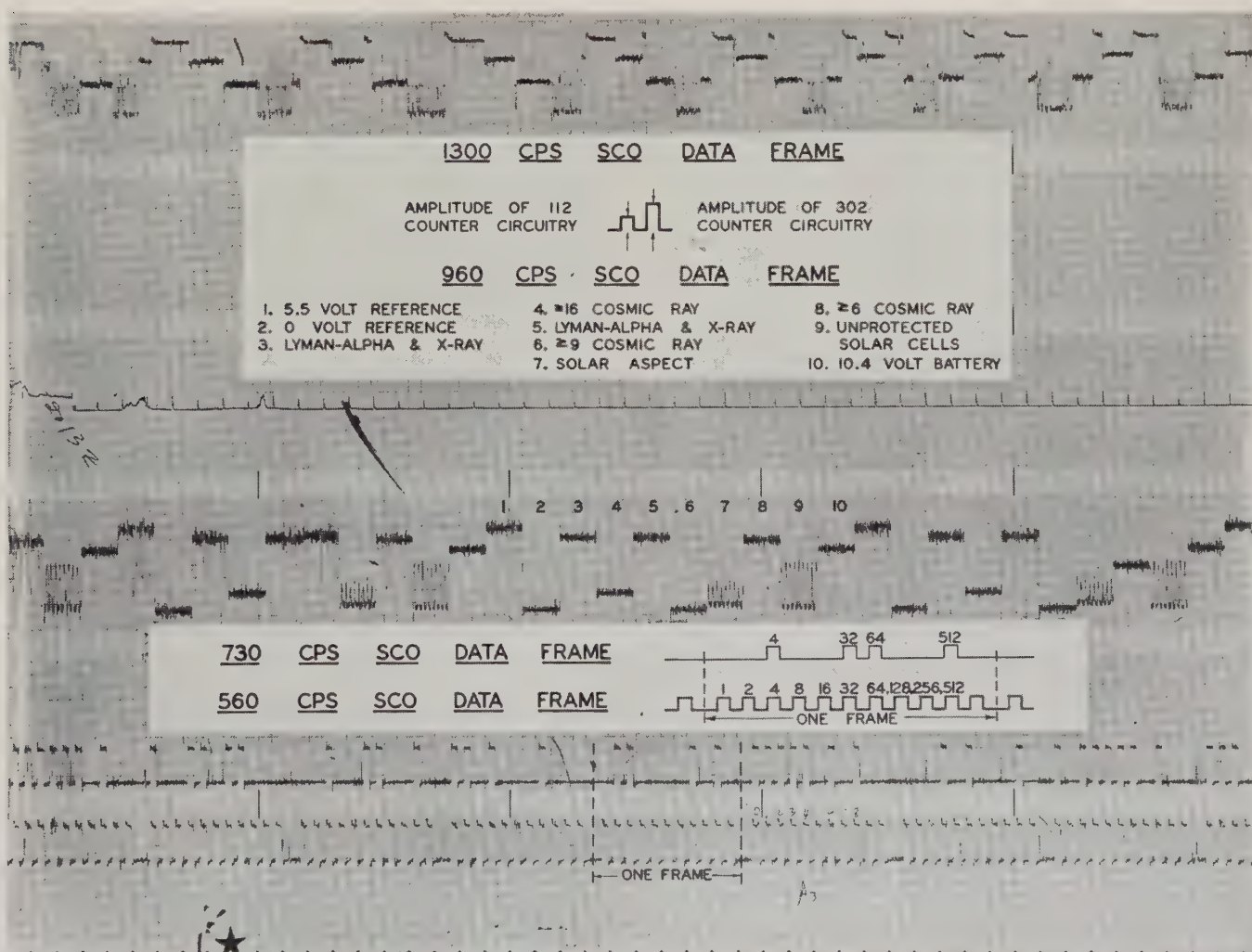


Fig. 3—Telemetry playback of 20-mc telemetry only illustrating effect of trapped radiation of fully-saturated 960 SCO.



data frames represent "0" count rate, as would be expected from the satellite's being in the earth's shadow.

The 1300-cps subcarrier is indicating the Anton 112 cosmic-ray counts only during this period of time and the 960-cps subcarrier is rendered inoperative by the fact that the solar X-ray sensors are being driven, by trapped radiation, slightly beyond their normal operating levels and are spilling through the electronic commutator.

The reason for the spilling through of the output from the solar X-ray sensor to the other data sampled by the electronic commutator of the 960 SCO in Fig. 2, and not

in Fig. 3, is that the saturated output voltage from the sensor is less than the near saturation voltage, and a limiting diode included in the output circuitry of the solar X-ray amplifier fails to limit completely this overshoot under certain near-saturated conditions.

Fig. 3 represents a daytime pass from the Huntsville station when the solar X-ray channel is completely saturated and therefore not spilling over. Both the Van Allen Anton 302 and 112 are counting on this record, which indicates that the satellite is within the trapped radiation region.

## Problems Concerning the Thermal Design of Explorer Satellites\*

GERHARD B. HELLER†

**Summary**—The thermal control of the Explorer satellites that were launched by Development Operations Division of the Army Ballistic Missile Agency is described. Explorers I through V were launched under the direction of the Department of Defense, and Explorer VII under the sponsorship of NASA. The thermal design of these satellites was based on a study of environmental conditions, and the effect of many parameters was determined in a computer program to find their influence on the thermal equilibrium. Methods have been improved from satellite to satellite. A description is given of the thermal design of Explorer VII, the most recent one of these satellites which had to fulfil the temperature and attitude requirements of seven experiments. A nearly spherical shape was found to fulfil these requirements best. A new principle was introduced that allowed the radiative heat transfer through the interior of the satellite, but kept the instruments and batteries well insulated from this internal heat flux.

A thermal testing program carried out in a vacuum chamber with a prototype of Explorer VII is described and some examples of measuring results are given. This testing program proved to be extremely valuable to test the soundness of the thermal design, to find and eliminate bugs, and to measure thermal coefficients for flight correlation.

Temperature measurements of the Explorers allowed conclusions to be drawn on the behavior of these satellites in space. Explorer IV showed strong temperature fluctuations. These were explained by rotation of the direction of the spin momentum vector from its original direction in space due to external forces acting on the satellite. Preliminary results of temperature measurements of Explorer VII have already shown that the thermal design works well. The satellite has operated for nearly three months with all experiments functioning. Some examples of the preliminary evaluation of the thermal experiment of Explorer VII are given. A more detailed analysis and correlation with ground tests, other temperature sensors and with results of the University of Wisconsin radiation experiment is in progress.

### I. INTRODUCTION

**I**NSTRUMENTS aboard satellites must experience only temperatures within a relatively narrow range in order to gather and transmit data reliably and accurately. Investigation disclosed that such instrument temperatures depend upon more than 20 parameters. These parameters may be divided into three distinct groups:

- 1) Satellite environment, which includes the general radiation environment, orbital characteristics, position of the sun, and attitude of a satellite.
- 2) Satellite configuration, which includes size, shape, and thermal design of the satellite.
- 3) Material properties, which include surface treatments, surface coatings, heat conductivity, heat absorptivity, and heat emissivity of all satellite components.

A series of thermal tests in vacuum was performed on each complete Explorer prototype to evaluate their thermal design. Various heat transfer coefficients, time constants of various components, and temperature-time histories under transient conditions were thus determined.

By selecting the time of day for launching, a satellite incorporating passive thermal control can accomplish reliable data transmission throughout its planned life span.

Telemetered temperature measurements from the first Explorers have been evaluated and have increased our knowledge of satellite environment and the accuracy of control methods used. Temperature measurements from Explorer VII are presently being received. They have already furnished very valuable results. Temperature measurements were able to yield information on the change of the satellite momentum vector. Continuous data evaluation will enable improved thermal design and more accurate checks on attitude definition of satellites.

\* Manuscript received by the PGMIL, February 1, 1960.

† U. S. Army Ballistic Missile Agency, Redstone Arsenal, Huntsville, Ala.

## II. PARAMETER STUDIES

### A. Satellite Environment

The temperature environment of an earth satellite is dependent upon heat radiated from the sun and earth, and, in some cases, aerodynamic drag. Table I gives the aerodynamic heat flux of circular and eccentric orbits for various minimum altitudes.

The aerodynamic heating is negligible for eccentric satellites with perigee equal or greater than 250 km, and circular satellites of greater than 300 km.

TABLE I

Altitude	Density (Smithsonian) (kg sec <sup>2</sup> ) m <sup>4</sup>	Heat Flux by Heating Kcal/m <sup>2</sup> h	Average Heat Flux by Aero- dynamic Heating for Orbit with Eccentricity
		Circular orbit	$e=0.13$
100	$8 \times 10^{-8}$	170,000	17,000
150	$6 \times 10^{-10}$	1,300	130
200	$7.5 \times 10^{-11}$	160	16
250	$1.8 \times 10^{-11}$	39	3.9
300	$7 \times 10^{-12}$	15	1.5
350	$3.3 \times 10^{-12}$	7.1	0.7
400	$1.7 \times 10^{-12}$	3.7	0.4
450	$1.0 \times 10^{-12}$	2.2	0.2
500	$6 \times 10^{-13}$	1.2	0.1

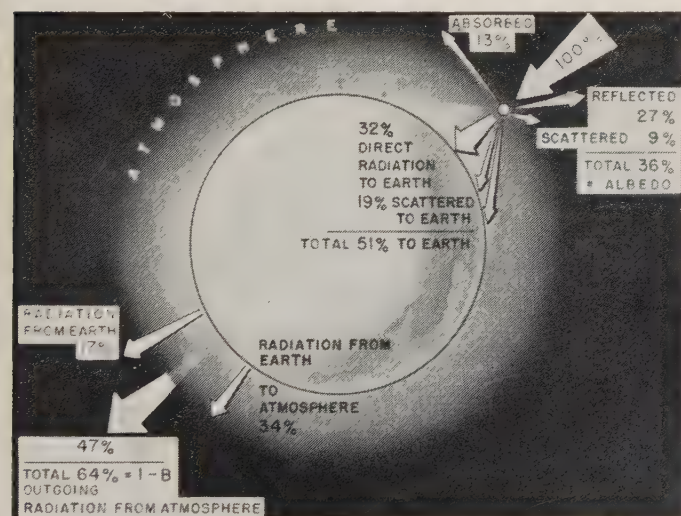


Fig. 1—Radiation equilibrium in space.

For such satellites, the thermal environment is determined exclusively by radiation from the sun and the earth. Fig. 1 illustrates the radiation household of the earth. The incoming radiation from the sun, or solar constant, is 100 per cent. 36 per cent of this radiation leaves the atmosphere because of reflection and scattering. This albedo of the planet Earth has basically the same spectral distribution as the incoming radiation. Since the albedo varies with the cloud cover and land and sea areas, a variation between 24 per cent and 54 per cent has been used for temperature considerations. Using the average value of the albedo (36 per cent) we find that 64 per cent of the

solar radiation has been absorbed by the atmosphere and the earth's surface. This energy is reradiated as infrared light, 17 per cent being radiated directly from the earth and 47 per cent from the atmosphere. There are slight differences in the spectral distribution of these infrared radiations due to day and night, latitude, and seasons; however, they are close enough together to allow us to use the spectral distributions of a black body at 255°K as a mean value. Forthcoming results from the thermal balance experiment of Explorer VII will allow us to improve on the environment of radiation affecting a satellite.

The temperature of a satellite is determined by four modes of radiation: 1) direct radiation from the sun, 2) reflected solar radiation, 3) infrared radiation from earth and atmosphere, and 4) infrared radiation from the skin of the satellite. We had to place the satellite within this given environment and operate it for two or three months for Explorers I through V and for one year for Explorer VII without exceeding the temperature limits imposed by the instrumentation. Maximum temperatures that could occur in this environment are 400 to 450°K, and minimum temperatures of about 200°K can be expected. The problem is to find out whether this range can be reduced to meet the instrument requirements.

### B. Orbital Parameters

In order to establish the thermal environment of a particular satellite based on its planned orbit and variations during its orbiting time, the orbital characteristics, expressed by parameters in equatorial spherical coordinates, must be considered. The parameters used are:

$i$  = inclination of orbit to equatorial plane,

$e$  = eccentricity of orbit,

$R_p$  = radius of perigee,

$\omega$  = argument of perigee,

$\Omega$  = right ascension of ascending node, and

$M$  = mean anomaly from injection point of satellite to initial perigee.

$\nu$  = true anomaly from satellite position to perigee.

The inclination  $i$  is determined by the firing azimuth and the geocentric latitude of the firing site (which for the Atlantic Missile Range is 28.45°). Variations of the inclination are due to angular dispersion in yaw of the high speed stage, errors in booster trajectory and cutoff flight direction, and changes in final velocity.

It turned out that the variations of  $i$  are important in the determination of the time the satellite is in sunlight. Time in sunlight is covered as a separate topic below.

The eccentricity  $e$  is determined mainly by the altitude of the booster apex, the injection velocity after fourth stage burn-out, the error angle in pitch due to timing error of upper stage ignition, and cluster dispersion in pitch. The eccentricity is also dependent on time after launching because the friction caused by interaction with air molecules at perigee of each revolution decreases the eccentricity.



The radius of perigee is equal to the booster apex for zero error angle in pitch. Any error angle decreases the perigee altitude. The effect of various perigee altitudes on the long time temperature balance was studied. The argument of perigee is the spherical angle measured from the ascending node to perigee in the orbital plane. For a given set of booster characteristics and upper stage performance,  $\omega$  is a constant if the pitch error angle is zero. The influence of variations of  $\omega$  has been studied in connection with simultaneous changes of  $e$  and  $R_p$ . The right ascension  $\Omega$  of the ascending node, a function of the day and hour of the launching, is an important factor because it determines the plane of the orbit in space and thus its inclination to the ecliptic and the angular distance to the position of the sun within the ecliptic. Changes of  $\Omega$  through  $360^\circ$  have been studied. In addition to the variation of the initial values of  $\omega$  and  $\Omega$ , it has to be considered that these angles are time dependent (regression of nodes and progression of line of apsides).

The mean anomaly  $M$  from injection point of the satellite to the perigee of the first revolution is proportional to the time difference between injection point and perigee. For zero error angle in pitch,  $M$  is zero.

### C. Time in Sunlight

An important factor that influences the satellite temperature is the time in sunlight. An analysis of the satellite crossover points in and out of sunlight for each revolution as a function of the orbital characteristics and the position of the sun was made. For the Explorer type satellites, the time in sunlight may vary between 63 and 100 percent. According to Krause,<sup>1</sup> the shadow angle is given by

$$\sin X = \frac{\sin \beta}{\cos \delta} \quad (1)$$

where

$X$  = angle between 0600-1800 hours line and crossover from shadow to sunlight or from sunlight to shadow,

$\beta$  = angle at center of earth between satellite and tangent to earth,

$\delta$  = angular distance of sun from orbital plane.

The position of the sun has been entered by using its mean motion in the ecliptic, and its motion in the equatorial plane has been obtained by coordinate transformation.

For orbiting during an extended period of time, it has to be considered that the orbital characteristics change. First order perturbation theory as developed by Krause and by Cunningham has been applied to compute these changes. Only secular changes have been considered, because the small periodic changes have only negligible effect on the temperature problem. For this purpose, three time-dependent angles  $\Omega$ ,  $\phi$ , and  $\alpha$  have been derived as functions of the hours of launching  $H_0$  and the day of launch-

ing  $D_0$ . The changes with respect to time are expressed by the linearized equations:

$$\Omega = \Omega_0 + k_1(D - D_0), \quad (2)$$

$$\phi = \phi_0 + k_2(D - D_0), \quad (3)$$

$$\alpha = \alpha_0 + k_3(D - D_0), \quad (4)$$

where  $k_1$ ,  $k_2$ ,  $k_3$ , are constants,  $D - D_0$  is the number of days after launching,  $\phi$  is the time angle measured in the orbital plane between the 0600 and 1800 hours line and the perigee, and  $\alpha$  is the right ascension of the sun. For the conditions of Explorer VII, the coefficients are

$$k_1 = -4.208^\circ \text{ per day (rotation of orbital plane),}$$

$$k_2 = 3.405^\circ \text{ per day (rotation of line of apsides),}$$

$$k_3 = .9856^\circ \text{ per day (mean motion of sun).}$$

From the crossover points of the Satellite in and out of the sunlight, the time can be computed by introduction of the eccentric anomaly  $E$  and the use of Kepler's equation

$$T_x = \frac{T_1 - T_2}{\tau} = \frac{1}{2\pi} (E_1 - e \sin E_1) - (E_2 - e \sin E_2) \quad (5)$$

The time in sunlight was computed for orbital characteristics of each Explorer as a function of day of firing  $D_0$  and hour of firing  $H_0$ . The 704 computer program was run for a simulated orbiting time of 60 days to 1 year for each combination of  $D_0$  and  $H_0$ . Fig. 2 shows the results for Explorer IV's orbit. The maximum values obtained at any point during the first 60 days of orbiting are plotted in Fig. 2 as a function of  $D_0$  and  $H_0$ . The percentage time in sunlight is used as the parameter like altitude lines on maps. For the selection of a firing time, variations of the initial orbital conditions had to be analyzed. The following effects were found. The areas of high time in sunlight values increase with the increase of:

- 1) the eccentricity of the orbit,
- 2) the injection altitude,
- 3) inclination angle, and

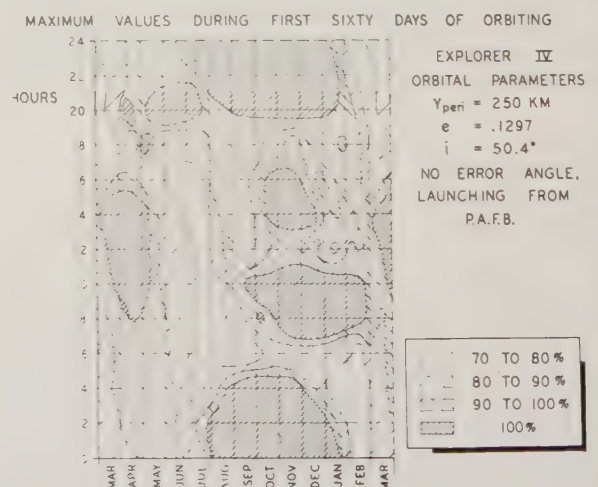


Fig. 2—Time in sunlight vs day of firing  $D_0$ , and hour of firing  $H_0$ , for Explorer IV.

<sup>1</sup> H. G. L. Krause, "The Secular and Periodic Perturbations of the Orbit of an Artificial Earth Satellite," paper presented at the VII Internatl. Aston. Congress, Rome, Italy; September 17-22, 1956.

- 4) error angle in pitch both plus and minus, and in yaw to the left for firing from PAFB.

The effect of eccentricity has been described elsewhere.<sup>2,3</sup> Fig. 3 shows the time in sunlight curve for Explorer VII.

#### D. Attitude of Satellite

The parameters previously discussed are those defining the time-dependent spatial position of the satellite with respect to the sun and earth. Equally important is the time-dependent attitude of the satellite with respect to the same sources.

The attitude angle of satellite axis with respect to the sun is determined by the original coordinates with respect to the horizon coordinate system. In this system, the attitude angle of the rotational momentum vector is zero and the angular direction is given by the azimuth. The initial attitude can be computed from these coordinates and the position angles of the sun as function of the day  $D_0$  and hour  $H_0$  of launching.

Changes of the attitude angle to the sun with time are dependent on the movements of the sun with respect to the original launching plane and not on other time variable changes of this orbit. It is assumed that the initial momentum vector of the spinning satellite is maintained in space. Exchange of angular momentum from the longitudinal axis to an axis of greatest moment of inertia has been considered. However, this initial concept has been refined on the basis of results obtained from the first Explorer measurements.

The initial attitude of the satellite to the direction of the sun is easily determined from the direction of the velocity vector at injection into orbit and the known direction of the sun. This holds true for a spin-stabilized satellite whose spin axis is aligned horizontally to the earth at the injection point and whose angular dispersion is negligible. These conditions were fairly well satisfied for Explorers I, III, and IV at the time of injection. Discussion of the attitude of Explorer IV has been presented in Heller,<sup>2</sup> Figs. 7 and 8, as a function of the day  $D_0$  and the hour of firing  $H_0$ . The initial attitude angle will change due to the relative motion of the sun. This is shown in Fig. 4 for Explorer VII as a function of the number of days after the firing. For Fig. 4, the injection conditions of the actual firing have been used. It is the theoretical curve for zero angular deviations. A curve based on actual attitude measurements has not been established yet, but measurements have been received, and their evaluation is in progress to determine any deviations from the theoretical curve. For the pencil-shaped Explorer satellites I through V, the spin axis is not stable since it

has the smallest moment of inertia. The initial momentum vector was considered unchanged in space (pointing toward the same fixed star). However, an exchange of momentum from the minor axis of inertia to a major axis of inertia had to be considered in the analysis (see Fig. 5). It can be shown that such a momentum transfer is possible, if the energy equation can be satisfied. Since the spin around a major axis of inertia means a reduction of the spin rate, this mode of rotation corresponds to a lower energy level. The transfer of momentum, therefore, takes place if rotational energy is dissipated by internal friction. It was assumed prior to Explorer I that this transfer should take place during the active lifetime of the satellite instrumentation. By evaluation of temperature measurements of Explorer I it has been proven that the spin axis

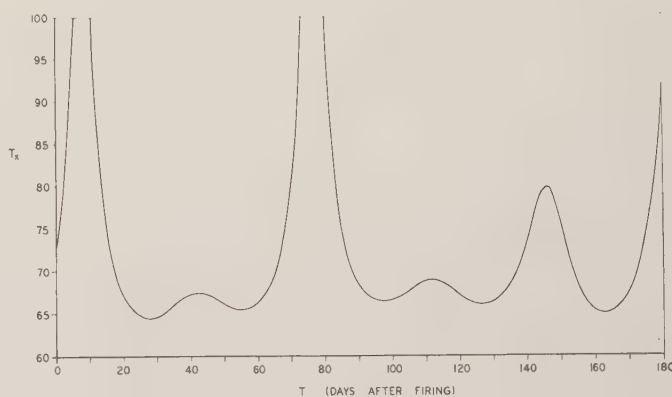


Fig. 3—Time in sunlight of Explorer VII.

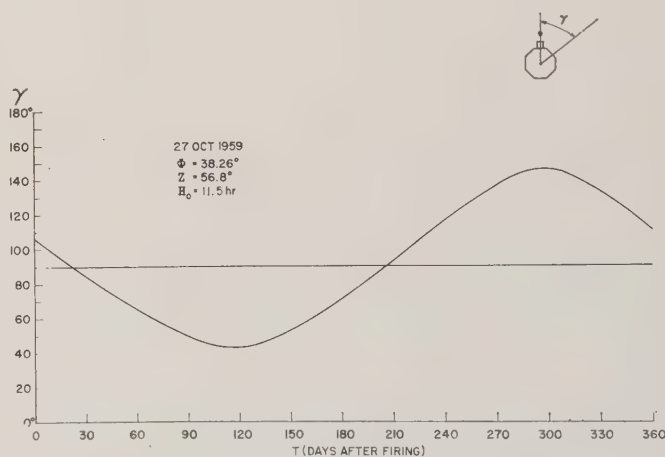


Fig. 4—Theoretical attitude of Explorer VII.

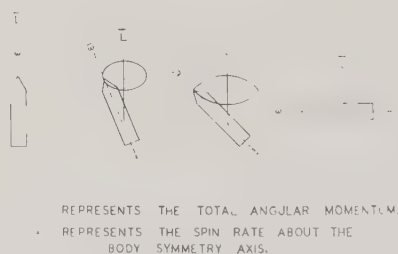


Fig. 5—Evolution of Explorer motion.

<sup>2</sup> G. Heller, "The Explorer, the explorer story and the temperature control of the satellite package," in "Ten Steps into Space," Mono. No. 6, pub. by J. Franklin Inst., Philadelphia, Pa.; December, 1958.

<sup>3</sup> G. Heller, "Thermal Control of the Explorer Satellites," paper presented at the ARS Semi-Annual Meeting, San Diego, Calif., June 8-11, 1959; submitted to the ARS Journal.



changed from its initial mode of spin to a flat spin quite rapidly (during the first day).<sup>1</sup> This was the first case in which temperature measurements were used to determine the behavior of the satellite in space. Further analysis of other Explorers showed that due to the internal damping, the flat spin was reached in all cases. In Explorers III and IV, it took about 10 days. These satellites did not have the flexible antenna wires, and the dissipation of energy took much longer. The cause for this dissipation is assumed to be inelastic flexing and damped vibrations inside the satellite. External forces on the satellite to be considered are tidal forces, magnetic forces, and forces caused by interaction with the atmosphere. The long-time vector sum of changes can have a decisive effect on the thermal design and was, therefore, considered for the basic design philosophy of Explorer IV.

### E. Radiation Equilibrium

The temperature of a satellite further depends on its ability to reradiate a portion of the heat received by it. The temperature can be controlled within limits by completely passive means.

The temperatures of the satellite depend on the emissivities of the skin with respect to short wave solar radiation and infrared radiation from earth and from satellite skin, and on the coefficients of solar radiation (solar constant), albedo and earth radiation.

For the simplest case of an instrument package insulated from a metal skin of cylindrical shape, two simultaneous differential equations have to be solved:

$$A_1\alpha SD_1 + A_2\alpha BS D_2 + A_3\epsilon ES - A_4\epsilon\sigma T_s^4 - C_5\dot{T}_i - C_6\dot{T}_s + Q = 0, \quad (6)$$

$$C_6\dot{T}_s = C_7(T_s - T_i) + C_8\sigma(T_s^4 - T_i^4). \quad (7)$$

These two equations describe with a good degree of approximation the situation for Explorers I through V. For the case of Explorer VII the thermal situation was simulated by the solution of 12 simultaneous equations. The validity of each approach was checked by an error analysis and by thermal tests.

In the above equations the definition of the symbol is as follows:

- $A_1$  = projected area with respect to sun direction,
- $\alpha$  = absorptivity for solar radiation,
- $S$  = solar constant,
- $D_1$  = step function ( $D_1=1$  for sunlight,  $D_1=0$  for shadow),
- $A_2$  = effective area of satellite with respect to albedo,
- $D_2$  = step function ( $D_2=1$  for orbit in hemisphere  $\pm 90^\circ$  from sun direction,  $D_2=0$  for orbit in hemisphere opposite sun direction),
- $B$  = albedo of earth,
- $A_3$  = effective area of satellite with respect to earth radiation,
- $\epsilon$  = emissivity with respect to infrared radiation,
- $E$  = ratio of IR heat flux from earth to solar constant

- $A_4$  = total surface area of satellite,
- $\sigma$  = Boltzman constant,
- $T_s$  = skin temperature,
- $C_5$  = heat capacity of skin,
- $\dot{T}_s$  = rate of temperature change of skin,
- $C_6$  = heat capacity of instruments,
- $T_i$  = instrument temperature,
- $\dot{T}_i$  = rate of temperature change of instruments,
- $Q$  = heat release of instruments,
- $C_7$  = heat transfer coefficient by conduction,
- $C_8$  = heat transfer coefficient by radiation.

The areas are obtained from

$$A_1 = A_1^0 \sin \gamma \quad (8)$$

$$A_2 = A_1^0 f(\zeta) \left[ 1 - \sqrt{\frac{2R_0H + H^2}{R_0^2 + 2R_0H + H^2}} \right] \cos \theta \quad (9)$$

$$A_3 = A_1^0 f(\zeta) \left[ 1 - \sqrt{\frac{2R_0H + H^2}{R_0^2 + 2R_0H + H^2}} \right] \quad (10)$$

where

- $A_1^0$  = maximum area of cylinder as seen from side,
- $\gamma$  = attitude angle to sun,

$f(\zeta)$  = function of attitude angle  $\zeta$  of satellite axis to radius vector to center of earth (it was approximated by a 5-power polynomial of  $\cos \zeta$ ),

$R_0$  = radius of earth at equator,

$H$  = altitude of satellite,

$\theta$  = angle of radius vector and direction to sun

The ratio of emissivities  $\alpha/\epsilon$  was found to be of decisive influence on the control of the mean satellite temperature, if heat capacity and conductivity effects are negligible.<sup>4</sup>

The effect of the ratio of emissivities  $\alpha/\epsilon$  is illustrated in Fig. 6. The average satellite temperature is plotted vs  $\alpha/\epsilon$  for various times in sunlight as parameters for one set of area exposed to sun and radiation conditions.

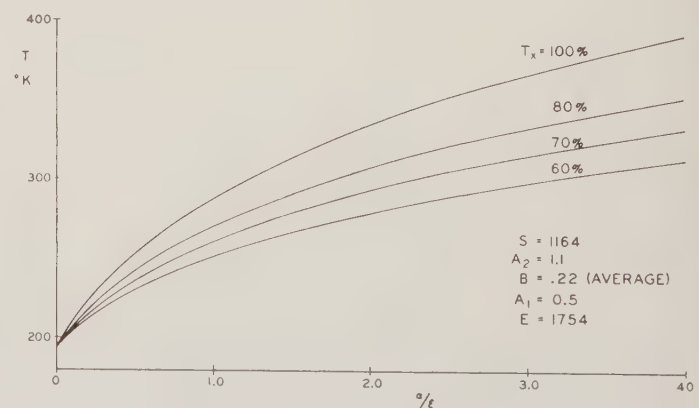


Fig. 6—Satellite temperatures as a function of the ratio of emissivities.

<sup>4</sup> A. R. Hibbs, "The Temperature of an Orbiting Missile," Jet Propulsion Labs., Calif. Inst. Tech., Pasadena, Rept. No. 20-294; March 28, 1956.

Table II gives values for a number of additional cases (sets of conditions). As cases 3) and 6) show, temperatures of areas with zero exposure to the sun can run quite low. If the low temperature is a requirement as in the case of tanks of cryogenics, low temperature should be assured by a low ratio of emissivities and for longer exposures by insulation. In the neighborhood of a planet like Earth, Venus, or Mars, satellite temperatures do not drop appreciably below  $-70^{\circ}\text{C}$  because of the heat flux from albedo and IR radiation.

Case 2) of Table II is of special interest for the first Explorer satellites. The area of  $A_1 = 0.637$  is the minimum mean exposure of a cylinder whose rotation mode is the flat spin. Without tumbling or shift to flat spin, minimum values as shown in cases 3) and 6) would apply.

A comparison of cases 4) and 5) shows the variations of temperatures between the maximum and minimum case for an exposed area  $A_1 = 1$ . At  $\alpha/\epsilon = 1$  this difference is  $36^{\circ}\text{C}$ . It should be noted that it includes a change of the effective area to IR radiation and albedo. This last term is a function of satellite altitude. It would average out for

the mean temperature and the total difference would be somewhat reduced.

#### F. Emissivities

The study of emissivities was considered an essential part of the assignment for the thermal control of satellites. Theoretical work at the Research Projects Laboratory of ABMA was supplemented by experimental work at Baird-Atomic, the National Bureau of Standards, and later on Arthur D. Little Co. Similar studies were made at the Jet Propulsion Lab in cooperation with the University of California at Berkeley. Literature values of emissivities cannot be used safely for satellite application, mainly because the measuring conditions under which the emissivities were determined are not clearly defined.

The areas of investigation include the following:

1) Dependence of emissivity on wavelength. Determination of the spectral emissivities of a number of substances has allowed to compute the temperature dependence of the infrared radiation of the Explorers. Measurements of the spectral emissivities up to wavelengths of 60 microns has

TABLE II  
TEMPERATURE OF CYLINDRICAL SATELLITES AS A FUNCTION OF THE RATIO OF EMISSIVITIES.  
TIME IN SUNLIGHT FOR SIX SETS OF TYPICAL ENVIRONMENTAL CONDITIONS

$\alpha/\epsilon$ \ Time in Sunlight, Per Cent	100	80	70	60	$\alpha/\epsilon$ \ Time in Sunlight, Per Cent	100	80	70	60
Case 1) $A_1 = 1.0$ and Average Radiation Conditions					Case 4) $A_1 = 1$ and Maximum Radiation Conditions				
0	195	195	195	195	0	212	212	212	212
0.5	289	271	261	252	0.5	303	284	276	265
1	334	307	293	279	1	350	323	308	294
2	392	353	333	313	2	409	370	350	331
4	465	409	382	355	4	490	431	402	375
Case 2) $A_1 = 0.637$ and Average Radiation Conditions					Case 5) $A_1 = 1$ and Minimum Radiation Conditions				
0	195	195	195	195	0	180	180	180	180
0.5	262	250	243	236	0.5	269	252	243	234
1	299	280	270	259	1	314	288	274	261
2	350	320	304	288	2	369	331	312	293
4	411	367	345	324	4	436	383	358	332
Case 3) $A_1 = 0$ and Average Radiation Conditions					Case 6) $A_1 = 0$ and Minimum Radiation Conditions				
0	195	195	195	195	0	180	180	180	180
0.5	220	215	212	210	0.5	191	188	187	186
1	239	231	226	222	1	201	196	194	192
2	266	252	245	238	2	217	209	205	202
4	305	283	272	260	4	242	230	223	217

Where

$A_1$  = ratio of area exposed to sun to maximum area. The radiation conditions are defined by:

	Average	Max.	Min.	Kcal $m^2h$
Solar constant	1164	1205	1123	
Effective albedo	0.22	0.44	0.08	
Ratio of earth radiation to solar constant	0.175	0.193	0.158	
Effective area with respect to IR radiation from earth	1.1	1.3	0.9	



not been achieved yet. However, total emissivity beyond 35 microns has been determined by the use of a filter that cuts out all radiation below 35 microns. Fig. 7 shows the spectral emissivity of Hoffman solar cells. It is interesting to note that the mean effective emissivity above 35 microns is appreciably below the last IR measurement at 13.5 microns.

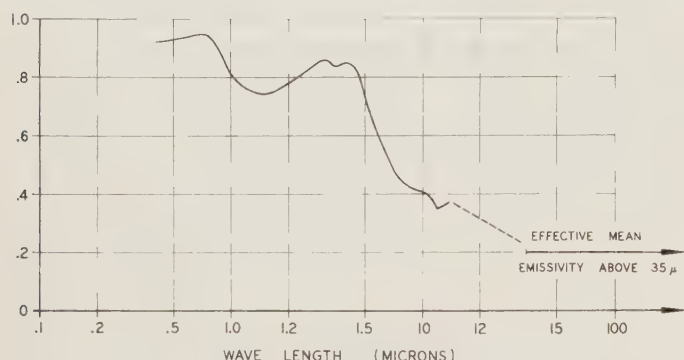


Fig. 7—Spectral emissivity of Hoffman solar cells.

2) Dependence of spectral emissivity on temperature. This dependency is small, if temperature changes of less than 100°C are considered. This relationship allows a correction to emissivity computation for solar radiation and the infrared radiation from the earth to the satellite and from the satellite to space.

3) Dependence of emissivity on the surface characteristics. A number of sandblasted and polished metal surfaces have been investigated. The surface characteristics are described as carefully as possible in terms of preparation of the surface. Emissivities differ strongly depending on the procedure of preparing the surface. Polished gold, *e.g.*, that has been polished by a buffing technique using jewelers' rouge, has an emissivity of 7 per cent at 10 microns, and polished gold obtained by a vaporization technique has a corresponding emissivity of 2 per cent. Great care has been exercised to define clearly the surfaces to be used in satellites and to obtain reproducible and reliable values of emissivities.

4) Closely related to the previous subject is the change of emissivities by environmental conditions in space. The study includes the effect of micrometeorites on all kinds of surfaces. The largest change is to be expected with polished surfaces. The simulation of such effects and their relationship to emissivities and temperatures of satellite is the purpose of experimental programs sponsored by ABMA at research institutes.

5) The emissivity of paints is under extensive investigation at ABMA. Advantage is seen in the ease of application and the possibility of continuous variations of desired characteristics by varying the composition. The main problem is the ultraviolet sensitivity. It has been solved for short time missile application. Work continues on the long-time application for satellites, especially of white paints with a low ratio of solar to IR emissivities. Paints have not

been used yet on outside surfaces of satellites for thermal control, pending the outcome of research work.

6) The angular dependence of the emissivity is different for metallic surfaces and metal oxides. It has to be known for all cases where the radiative transfer includes geometries with relative angles of surfaces different from 0° (different from parallel surfaces). In most cases the validity of Lambert's law has been assumed for the computation of emissivities and geometry factors, especially if the angular effects are relatively small.

7) Polarization effects in connection with emissivities have been studied. The thermal design of the Explorers was such that these effects did not enter in the considerations.

8) Investigation of the emissivity of surfaces whose characteristic is determined by optically thin coatings. Such coatings include the silicon monoxide coating on aluminum as used in telescope mirrors of astronomical observatories, and dark mirror coatings that absorb visible light, but are reflective for one or several bands in the infrared region.

9) The emissivity of solar cells was studied. This information was required for Explorer VII which is powered by solar cells in addition to batteries (see Fig. 7).

Research in all these areas is continuing.

The thermal control of the Explorer satellite had to be done before results from all the research efforts mentioned above were available. The thermal design was, therefore, planned such that the least variations of emissivities could be expected due to environmental effects or due to nonreproducibility of surface characteristics. Table III shows the surfaces used in the various Explorers, their emissivities for solar and IR radiation, and the ratio of emissivities.

TABLE III  
EMISSIVITIES OF SURFACE ELEMENTS OF EXPLORER SATELLITES

Material	Absorptivity for Solar Radiation	Emissivity for IR Radiation at 10 Microns	Ratio of Emissivities
<i>Explorers I and III</i>			
Stainless Steel Sandblasted	0.81	0.42	1.92
Rokide A on Stainless Steel	0.33	0.75	0.44
Fiberglas	0.85	0.75	1.13
<i>Explorer IV</i>			
Stainless Steel, Sandblasted	0.75	0.46	1.63
Fiberglas	0.85	0.75	1.13
<i>Explorer VII</i>			
Sandblasted Aluminum	0.42	0.21	2.00
Polished Aluminum	0.31	0.07	4.43
Sandblasted Magnesium	0.63	0.54	1.17
Rokide A	0.15	0.77	0.195
Gray TiO <sub>2</sub> Paint	0.87	0.87	1.00
White TiO <sub>2</sub> Paint	0.19	0.94	0.20
Solar Cells	0.8	0.4	2.00
Sauereisen Cement	0.34	0.88	0.39
Fused Silica*	0.06	0.84	*
Gold Foil	0.21	0.09	2.35
Gold Sensor	0.212	0.07	3.0

\* Ratio of emissivities does not apply because fused silica is not opaque for visible light.

### III. THE THERMAL DESIGN OF EXPLORER VII

#### A. Requirements of Temperatures and Attitude

1) The temperature of the instrument package in the central column should stay within the range between  $0^{\circ}$  and  $60^{\circ}\text{C}$  (the upper limit is more critical than the lower one). This and all other requirements have to be fulfilled throughout the planned lifetime of the instrumentation and experiments of one year.

2) The temperature of the solar cells should not exceed  $85^{\circ}\text{C}$ . This limit is imposed by the power requirement. Solar cells are not damaged at higher temperatures; however, their efficiency drops to one half for a temperature increase of  $80^{\circ}\text{C}$ .

3) The temperature range of batteries is  $0^{\circ}$  to  $60^{\circ}\text{C}$ . Both limits are critical, because of possible loss of rechargeability at the upper limit and the freezing-out below  $0^{\circ}\text{C}$ .

4) The temperature limits of the sensors of the scientific experiments are wider than transmitter and battery limits. No lower temperature limit was imposed; the upper limit for most of the sensors is  $85^{\circ}\text{C}$ . This is a severe requirement because the sensors are imbedded in the skin, which is subject to strong diurnal variations and whose temperature range is correspondingly wide.

5) The temperature limits should be maintained throughout the one-year instrument life at all possible attitudes of the sun with respect to the satellite. The attitude requirements of the instruments are an important consideration because both these requirements and the thermal requirements had to be fulfilled.

6) The radiation balance sensors of the University of Wisconsin work best if the sun is in the plane of the satellite's equator. With respect to the hemispherical white and black sensors, the sun can have considerable deviations from this position. However, the hemispherical sensors are mounted on mirror surfaces and any effects from mirror reflectivity and its change with time are small, if the sun is in the plane of the satellite's equator. The shielded Tabor sphere works within a range of  $\pm 45^{\circ}$  deviation of the sun from the equator. The sun attitude measurement of NRL operates in a range of  $\pm 60^{\circ}$  from the equator; however, a small initial angle is desirable. The Lyman Alpha and X-ray experiments of Dr. Friedman work at any angle, because they are redundant with one set of sensors in each of the halves of the satellite. At sun angles greater than  $45^{\circ}$  only one set would see the sun.

#### B. Thermal Design

In order to fulfill these somewhat conflicting requirements, the thermal design had to deviate from previous Explorer satellites. Because of the long instrument lifetime, no attempts were made to avoid 100 per cent sunlight. The problem was rather to find initial conditions that give throughout one year desirable combinations of time in sunlight, attitude of sun to the satellite's equator, and minimum deviations of satellite temperatures. A com-

puter program was run for a simulated lifetime of one year with a great number of variations of initial orbital characteristics, their time changes, environmental conditions, and various shapes and design parameters. A spherical satellite shape was found to fulfill best the various requirements and time changes. The mechanical design arrived at an early spherical shape, consisting of two cone frustums connected by a cylindrical piece which became the satellite equator. It was found that the thermal requirements can be fulfilled by passive control. Active control by variation of surfaces was considered, but it was found to be unnecessary. The instrument column in the axis of Explorer VII is insulated from the skin, but metallically connected to the battery packs by four aluminum spokes. The batteries are insulated from the skin by Kel-F spacers between the battery boxes and an aluminum ring, which is part of the skin. One of the essential features of the Explorer VII thermal design is the equalization between upper and lower satellite shell. Equalization around the equator is effectively provided by the spin of the satellite of 360 rpm. The equalization between the half shells is done by radiative transfer. Conductive transfer through the fiberglass shells and the glued-on aluminum foil is not sufficient to conduct heat from one shell to the other, if the sun's position is over one shell (more than  $45^{\circ}$  from the equator). The inside of the fiberglass shells are painted with a titanium dioxide paint with an IR emissivity of 95 per cent. This reduces the skin temperature from a possible maximum of  $127^{\circ}$  to  $69^{\circ}\text{C}$  for standard environmental conditions. This coupling of thermal equilibrium of the shells by infrared radiation that goes through the satellite made it necessary to provide excellent radiative insulation of all interior metal parts connected to batteries or instrument column. This insulation was achieved by gold foil on the instrument column and aluminum foil on the battery packs, and by polishing all aluminum parts such as spokes, battery housing, etc. The radiative heat transfer through the satellite made it possible to fulfill the temperature requirements of the sensors imbedded in an insulating fiberglass skin. Some of the sensors required polished metal surfaces that would run hot if completely insulated. By painting such sensors white on the back side the excess heat could be radiated away. The paint which was used fulfilled the requirements of high IR emissivity and extremely small electrical conductivity. An additional problem of Explorer VII is that a great part of the surface is covered by solar cells whose surface characteristics cannot be changed to meet thermal requirements. As Fig. 7 shows, the solar cells have a high emissivity in the visible region and a low value in the infrared. The problem of inherent high temperatures is made more severe by a "hot house" effect caused by the protective covers of fused silica glass, and by the fact that the fiberglass shell of the satellite provides insulation which prevents excess heat to be conducted away. The internal heat exchange through the satellite contributes to the reduction of temperature extremes. However, the part of the skin underneath the aluminum



tray on which the cell are mounted acts as a partial radiation shield toward the inside and the fused silica windows act as partial radiation shields toward the outside. The solution was found by covering the aluminum frame and all adjacent metal parts with Rockide A which absorbs little solar radiation, but with an IR emissivity of 80 per cent emits effectively at the solar cell temperature. A temperature gradient of  $10^\circ$  necessary to conduct the heat away was considered tolerable. The expected maximum temperature came out as  $85^\circ$ , which is the upper limit. The fiberglass shells on the cones and the cylindrical equator were covered by areas of aluminum foil. Small gaps were left between these areas to minimize magnetic damping by eddy current induced in the magnetic field of the earth. The aluminum foils were sandblasted on the outside to maintain a proper ratio of emissivities. The aluminum foil contributed to some extent to temperature equalization and avoidance of hot spots. All exposed fiberglass areas were painted with a gray paint. The purpose of this was to protect the fiberglass against radiation damage in the space environment. It has a small effect on the thermal balance of Explorer VII.

By comparison, the thermal design of Explorer I is much simpler. As a result of earlier studies, the thermal design of Explorer I was pursued on the following concepts: 1) the temperature control was passive, *i.e.*, no variable surfaces nor heat exchange equipment were incorporated; and 2) the instrument package was insulated from the satellite skin to minimize short-time fluctuations during one revolution.

The satellite consisted of two parts separated by insulation—the cylinder and the cone. The surface properties were adjusted in such a way that the average temperatures in both parts were about the same. The insulation between skin and instruments had to strike a happy medium between two extremes. If it was too good, the internal heat release would cause the package to overheat. Without insulation, the instruments would take part in the strong temperature variations of the skin.

### C. Computation of Theoretical Temperatures

Temperatures were computed for twelve points in the Explorer VII satellite. The twelve simultaneous differential equations contain coupling terms due to conductive and radiative heat transfer similar to (6) and (7). The twelve temperatures are in the following locations:

- 1) temperature of the Van Allen experiment box;
- 2) transmitter temperature on upper end of satellite;
- 3) temperature at lower end of instrument column;
- 4) skin temperature at lower end in center (point where Sergeant motor is attached);
- 5) battery temperature;
- 6) equator skin temperature;
- 7) solar cells, lower hemisphere;

- 8) fiberglass shell, lower hemisphere;
- 9) solar cells, upper hemisphere;
- 10) fiberglass shell, upper hemisphere;
- 11) fused silica, upper hemisphere;
- 12) fused silica, lower hemisphere.

The radiative coupling terms affect a number of the differential equations. The physical model had to be chosen carefully to make possible a numerical solution by electronic computer methods. Various physical models were tried out and their radiative geometry factors determined. By analytical means the best approximation to the difficult problem was determined and entered into the final computer program. This program has been kept flexible so that additional terms can be added to analyze their relative importance. The same program is being used in analyzing the telemetered measuring results, to clarify unexpected occurrences, and to correlate theoretical and experimental results.

The program provides for variations in the time in sunlight, orbital characteristics, the sun's position, variations in internal power dissipation, and changes of properties of insulating materials and surface emissivities. Table IV gives the range of expected temperatures of Explorer VII.

TABLE IV  
THEORETICAL TEMPERATURE RANGE OF EXPLORER VII

Position	Temperature, $^\circ\text{C}$
A) Temperature Covered by Measurement Channels.	
1) Skin on Fiberglass Shell	-21 to 79
2) Solar Cells	-27 to 84
3) Transmitter	7 to 57
4) Batteries	2 to 57
5) Van Allen Box	-22 to 80
6) Gold Hemisphere Experiment	-35 to 120
7) Skin on Equator (University of Wisconsin Experiment)	-13 to 52
B) Temperatures Not Measured in Flight.	
1) Fused Silica	-70 to 19
2) Thrust End of Satellite	-10 to 138

These extremes are obtained by combining the simultaneous occurrence of maximum or minimum conditions. A fluctuation of  $10^\circ$  due to environmental conditions is included. Evaluation of Explorer VII results will allow reduction in computed temperature limits in future satellites, because of a better knowledge of the variations of the environment.

### D. Prototype Testing

The prototype testing of satellites proved to be an important part of the preparation for flight. Many aspects came up during the tests that were not predictable by theoretical or analytical means. It can be stated that the elimination of trouble areas found in these tests helped to make

Explorer VII reliable. The prototype tests were planned with three main purposes in mind: 1) to check out the soundness of the thermal design concept, 2) to determine material properties, insulation coefficient, and heat radiation factors in order to arrive at the final design criteria; and 3) to measure time constants and equilibrium temperatures that can be correlated with the 704 computer programs and that serve as a basis for evaluating the temperature measurements that are part of the planned program for Explorer VII. Fig. 8 shows schematically the test setup for three types of tests. The sketches show cross sections of the payload. The heating is done by electric blankets that are applied in the cross-hatched areas. The application of the blankets is shown in Fig. 9. This illustration shows the heating blanket in place, and a back-up aluminum foil is just being placed over it. Test setups I and II allow for heating of the payload from one side only. The nonheated side radiates freely into the vacuum chamber whose walls are kept at liquid nitrogen temperature or have reflective aluminum foils. Test setup III is a test

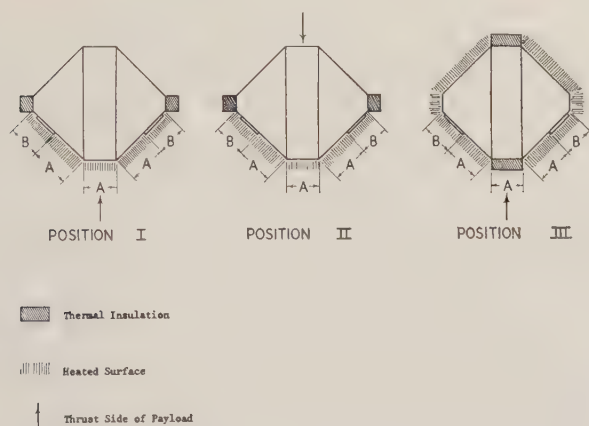


Fig. 8—Schematic test setup for prototype testing.

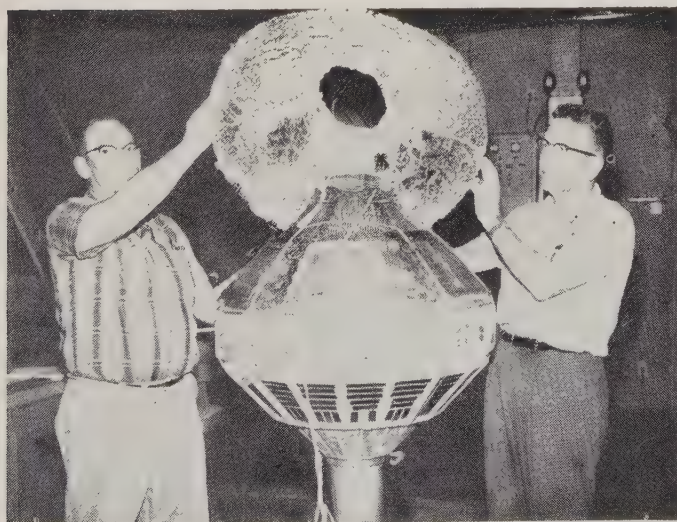


Fig. 9—Preparation of a thermal prototype test of Explorer VII.

to determine transfer coefficients. In all thermal tests the payload was brought to a uniform temperature and then heat was applied as a step function or the nearest approximation to it. Fig. 10 is an idealized plot of temperatures vs time. The skin temperature follows the step function. The internal temperature curves have a different shape especially near time zero for radiation or for conductive transfer, as shown by two typical curves. The tests were conducted at a vacuum between  $2 \times 10^{-6}$  and  $6 \times 10^{-3}$  mm mercury. The step function was very well approximated by a rise of the skin temperature (curve 21 in Fig. 11) in three minutes. Control oscillations as the ones shown occurred in early tests, but were eliminated after experience was gained. The interior temperatures reflect the oscillations of the applied temperature. The temperature measurements shown are;

- 21—skin temperature (heat applied),
- 6—inside skin at equator,
- 8—solar cell temperature on heated shell,
- 9—skin under solar cell,
- 3—transmitter inside instrument column (same location as in flight),
- 24—battery temperature (same location as in flight).

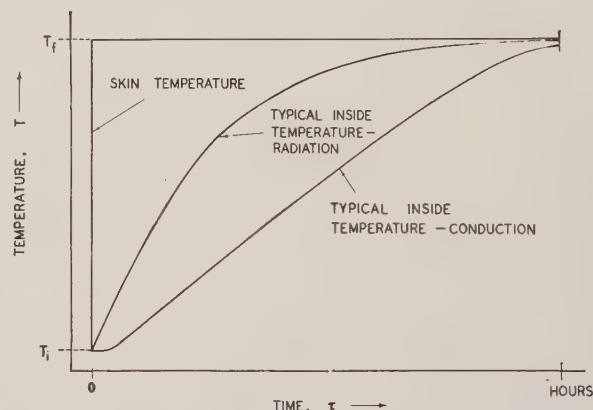


Fig. 10—Temperature vs time during thermal tests, schematic.

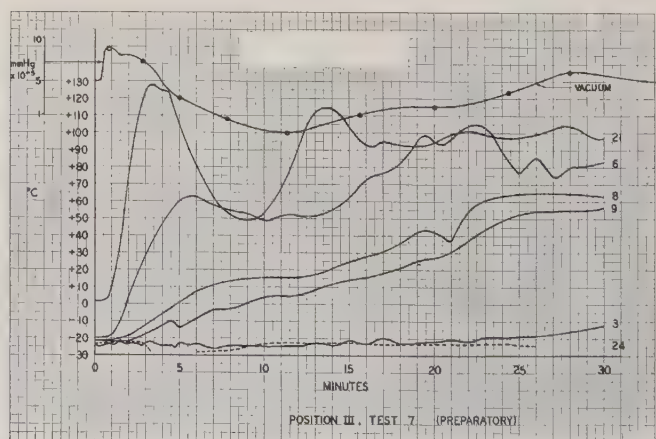


Fig. 11—Measuring results of a thermal test of Explorer VII.



A test with small control oscillations and well-defined conditions is shown in Fig. 12. The upper curve is a skin temperature of the opposite shell (no. 12) and the lower curve is a skin temperature at the equator (no. 6). The effect of outgassing of satellite components and condensation of the gas on colder parts of the internal structure were detected during other tests. The transition from the predominantly conductive transfer to radiative transfer occurred at about 60 minutes when the satellite temperatures had increased to some critical value. Two effects of the outgassing had to be considered: 1) transfer by the gas convection, and 2) increased radiative transfer because of the condensate on the polished metal surfaces.

In order to determine transfer coefficients and time constants, it was necessary to run a series of three tests with each test setup. In each of these tests a different initial temperature and a different temperature jump was used. This produces differences in the radiative terms because of the different fourth-power temperature expressions and differences in the conductive term due to variations of heat conductivity with temperature. From these it was possible to arrive at radiative and conductive transfer coefficients between various parts of the satellite. Fig. 12 shows that in this type of test the opposite skin reaches an equilibrium of  $30^{\circ}$ , and the equator of  $26^{\circ}\text{C}$ . This means that radiative equilibrium was maintained by a temperature of  $70^{\circ}$  of one shell and  $30^{\circ}$  of the other, with the heat entering on the hot side passing through the satellite and being radiated to the cold chamber walls by the cold satellite shell.

On the basis of the thermal prototype tests a number of design changes were introduced to eliminate trouble areas as, *e.g.*, the replacement of all organic materials that had shown high outgassing rates. Other changes were introduced to adjust the thermal coefficients to the proper values.

One important problem of flight payloads turned out to be the protection of the sensitive optical surfaces against handling, and every surface is sensitive. All sandblasted aluminum surfaces were covered with a removable plastic. The protective gray paint on all exposed fiberglass surfaces was applied one day before the launching, thus minimizing the danger of changes by handling. The titanium oxide paint that covered all inside fiberglass surfaces was re-touched during the last two days and paint was applied on the inside of sensors located in the skin where necessary. The most difficult problem was the protection of the Rokide A on the frame surrounding the solar cells. During the extensive testing of the flight payloads, the originally white Rokide surfaces became gray. Measurements of emissivities and computation revealed that the payload might run hotter than desired by up to  $10^{\circ}$ . It was not known whether the space environment would cause a darkening by carbonization or a bleaching by ultraviolet radiation. Preliminary results from Explorer VII have shown that apparently a bleaching of the organic dirty spots has taken place, because results check nearly with precomputed values for the original Rokide A. Efforts

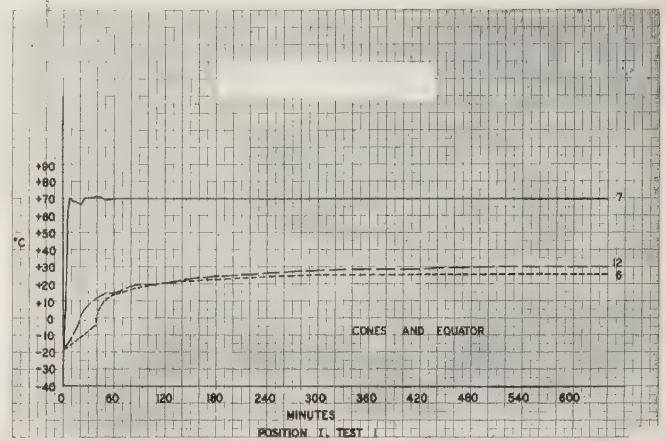


Fig. 12—Temperature vs time of Explorer VII, vacuum chamber test.

will be made to improve the handling methods on future satellites.

#### IV. TEMPERATURE MEASUREMENTS

Explorer VII is the satellite of the Explorers with the most complete coverage by temperature measurements. The radiation balance experiment of the University of Wisconsin comprises seven measurements—one temperature measurement is connected with the NASA micrometeorite, and six temperature measurements are part of the ABMA experiment. All temperature measurements work well, and continued results are obtained from all measurements except the NASA experiment which was planned only to be received during the active time of the 108-mc transmitter and ceased to furnish telemeter data on December 4, 1959.

Fig. 13 shows a schematic of the payload, and the location of the fourteen temperature measurements. All temperatures other than the NASA-sponsored measurement are transmitted via telemetry of the 20-mc transmitter. Temperature sensors are thermistors whose output changes the frequency of a blocking oscillator built by the University of Wisconsin. The number of cycles during a 5-second interval is converted to binary digits which are telemetered in the form of pulses. The ABMA tracking station has received passes up to eighteen minutes in length with readable telemetry. All temperature measurements are working well.

The temperature measurements, although each set was incorporated into the scientific experimentation program for a different purpose, supplement each other. The temperature measurement of the La Gow micrometeorite sensor (NASA) allowed a check on the battery temperature, because the sensor was insulated from the skin, but connected to the battery housing by two copper bars. The mirror temperatures of the Suomi experiment (University of Wisconsin) are closely connected to the skin temperature of the equator and can be evaluated by the use of a computer program.

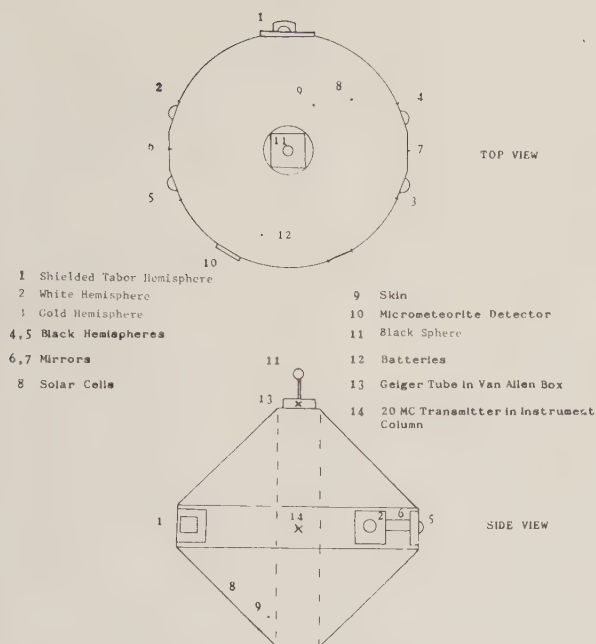


Fig. 13—Location of temperature measurements in Explorer VII.

## V. RESULTS OF THE ABMA EXPLORER TEMPERATURE MEASUREMENTS

Some of the results of earlier Army Explorers have been published elsewhere.<sup>2,3,5</sup> Table V summarizes the results.

Explorer III<sup>3</sup> was the first satellite that operated in 100 per cent sunlight during its instrumental lifetime. Since the mean operating temperature was low, the passive temperature control operated well at the upper limit, but could not be kept in temperature limits at the lower end.

Explorer IV showed temperature measurements with improved accuracy and consistency of results compared to earlier Explorers. Fig. 14 shows a plot of temperatures as obtained from telemetry received by the ABMA tracking station. The calibrated temperature sensitivity of the sub-carrier oscillator of channel III was used for the evaluation. There is a systematic error between the high and low frequency of the channel. Since this difference remains constant, the value of the measurement is sufficient to warrant further analysis. The arithmetic mean value of the two measurements came close to the initial temperature at the time of launching.

The strong temperature fluctuations constituted a new phenomenon that did not find an easy explanation, because no strong variations could be expected from either time in sunlight considerations or from surface changes. Since the surface selected for this satellite was sandblasted stainless steel, the possibility of surface changes had to be excluded. One strong possibility was the change of the rotational momentum vector in space due to external forces.

TABLE V  
TRANSMITTER TEMPERATURE OF EXPLORERS

Explorer	Mean Design Temperature	Measured Maximum	Measured Minimum
I	20°C	40	0
III	20°C	41	0*
IV	40°C	55	19

\* The actual temperature of Explorer III was lower, but no measurements were obtained because the transmitter ceased to operate, probably due to freezing out of the batteries.

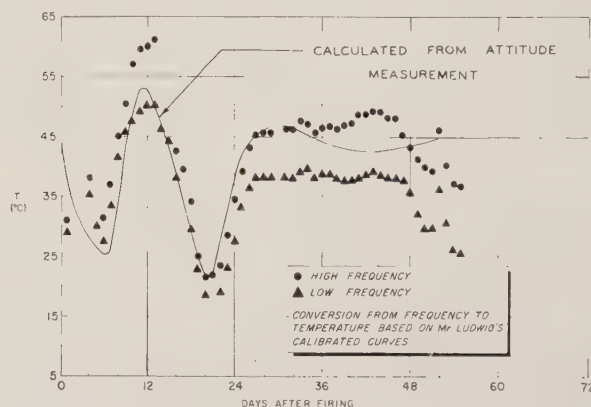


Fig. 14—Measured temperatures of Explorer IV.

The first rapid drop of temperature can be explained by the change of the initial mode of rotation about the minor moment of inertia axis to a tumbling mode that finally ends in a flat spin (see Fig. 5). The correlation of results shows that even during this first period of six days the momentum vector changed. The initial angle between the momentum vector and the sun's direction was 75°, resulting in a 97 per cent exposure area. After six days the expected value was 71°. From the temperature measurements follows the fact that the angle had increased to 77°. This is only a small change. After the flat spin had fully developed, the temperature changes indicate a fast momentum vector rotation of up to 15° per day. The temperatures fluctuated between a position corresponding to 100 per cent exposed area (*i.e.*, maximum cross section obtained if the momentum vector points toward the sun), and 63.7 per cent (momentum vector perpendicular to direction of sun).

One independent corroboration of these results was attempted by analyzing signal strength measurements from various stations who had received Explorer IV signals.<sup>6,7</sup> Fig. 15 shows the results of the analysis obtained from these records. The change of the momentum vector could be followed throughout 53 days as indicated. The relatively small initial angle increased to more than 150° during the

<sup>6</sup> R. J. Naumann, "The Determination of Satellite Spatial Orientation," paper presented at the Army Science Conference, West Point, N. Y.; June 22-29, 1959.

<sup>7</sup> R. J. Naumann, "Recent Information Gained from Satellite Orientation Measurements," paper presented at the Fourth Symposium on Ballistic Missiles and Space Technology, University of California at Los Angeles; August 24-27, 1959.

<sup>5</sup> E. P. Buwalda and A. R. Hibbs, "Satellite Temperature Measurements for 1958 Alpha-Explorer I," Jet Propulsion Labs., Calif. Inst. Tech., Pasadena, External Pub. No. 481; April 23, 1958.



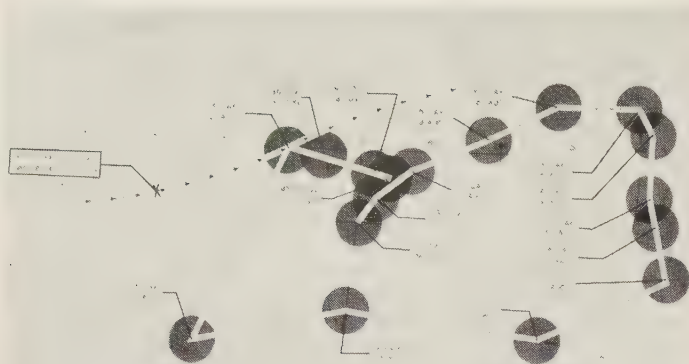


Fig. 15—Position of sun relative to the momentum vector of Explorer IV.

first fourteen days. Temperatures computed from these attitude values and other known input information are plotted in Fig. 14, together with the temperature measurements. The good agreement made it attractive to analyze the results with respect to forces which cause such attitude changes of satellites. The problem is considered of importance for our knowledge of the satellite environment and the problems encountered in their effects on attitude and temperature control.

Forces that are studied include magnetic and aerodynamic forces. Special attention is focused on gravitational forces and their integrated effects. Integration is done by the use of electronic computers with the Explorer IV ephemeris of the Smithsonian Astrophysical Observatory as an input. For a discussion of the problems and the present status see Lundquist and Naumann.<sup>8</sup>

## VI. RESULTS OF EXPLORER VII

All temperature measurements have functioned properly during nearly three months of operation up to the present time. Results have been evaluated from telemetry records of the ABMA Station on Madkin Mountain. From these records it is already apparent that the thermal control is functioning properly. During the nearly constant conditions in the second month of operation the battery is 6° below the transmitter temperature (see Fig. 16). During the first period of 100 per cent sun light (Fig. 17) the battery temperature is 13° higher than the transmitter temperature. This fact was not predicted, and a preliminary analysis indicates that it is connected with the circuitry of the payload. Further study and simulated ground testing is necessary before final conclusions can be drawn. The transmitter temperature has a nearly constant value of 19°C for 66 per cent of sunlight as it occurred during the time from the thirtieth to the sixtieth day after launch (see

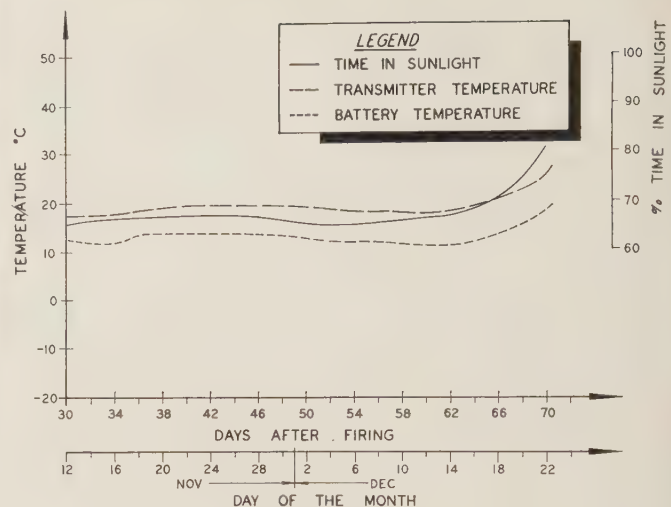


Fig. 16—Comparison of temperatures measured in transmitter and battery of Explorer VII with theoretical temperatures.

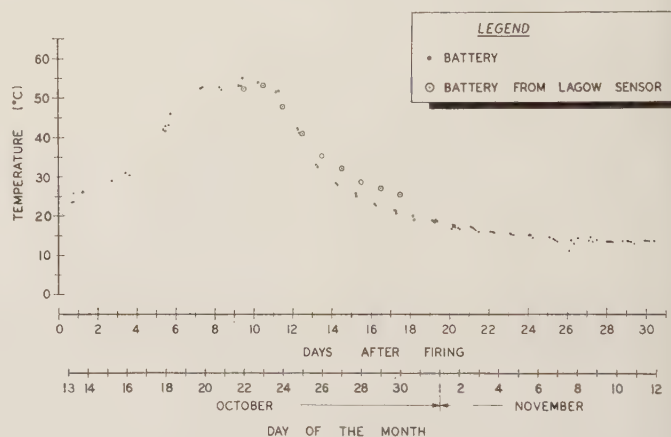


Fig. 17—Telemetered battery temperatures of Explorer VII.

Fig. 16). During this period the time in sunlight varied between 64.4 and 67.8 per cent and the transmitter temperature varied  $\pm 1^\circ$  around a mean value of 19°.

Maximum temperatures of the transmitter occur when Explorer VII is in 100 per cent sunlight. Fig. 3 shows that two such periods occurred up to the present time, the first from October 18–24, 1959, and the second from December 25, 1959 to January 1, 1960. Temperature measured during the first period was constant at 41°C and during the second period at 38°C. Fig. 18 is a plot of ABMA temperature measurements of the transmitter. The graph also shows a time in sunlight curve. Its scale is chosen such that the two curves coincide for theoretical temperature and theoretical time in sunlight as obtained from a computer program. It is interesting to note that there are only small deviations, and that these deviations are mainly due to a time lag of the measurements behind the computed values which were determined for equilibrium conditions at each point. The time constant of this lag seems to be greater than the time constant determined in a vacuum chamber during the prototype test program. The reason for this is still under study.

<sup>8</sup> C. A. Lundquist and R. J. Naumann, "Orbital and Rotational Motion of a Rigid Satellite," paper to be presented at the 1960 Jet Propulsion Labs. Seminar in Tracking Problems and Orbit Determination, Calif. Inst. Tech., Pasadena; February 22–26, 1960.

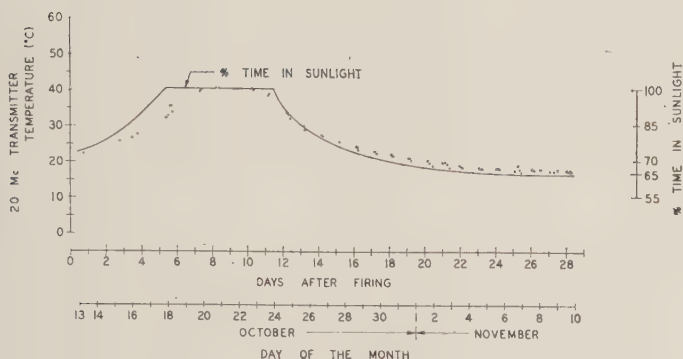


Fig. 18—Measured temperatures of transmitter of Explorer VII.

The battery temperatures shown in Fig. 17 also follow closely the time in sunlight curve. However, deviations from precalculated values are considerable, and the time lag is less than the time lag of the transmitter temperature.

Fig. 16 shows a rise of both transmitter and battery temperatures after 64 days of orbiting. Comparison with Fig. 3 indicates that this is the time when the rise to the second 100 per cent sunlight period starts. The close correlation of transmitter temperatures to the time in sunlight curve is due to the fact that the transmitter temperature is well insulated from the skin and is, therefore, only little effected by the strong fluctuations during each daylight and shadow cycle or other environmental conditions. The heat transfer time constant as determined by thermal tests is much longer than the period of 101.3 minutes of Explorer VII. The dependency of the transmitter temperature on the sun's attitude is small. According to Fig. 4, this attitude changes less than a degree per day. For the evaluation of long-time changes of the transmitter temperature, attitude and other factors have to be considered. It can be concluded from Fig. 18 that the thermal control of Explorer VII worked well. Fig. 17 shows, in addition, the battery temperature measurements obtained from the telemetered temperature of the LaGow micrometeorite experiment. During 100 per cent sunlight the correlation to the battery temperature is very good. After October 25, 1959 the time in sunlight had dropped to 85 per cent and lower, and the temperature of the LaGow sensor is consistently above the battery temperature. Both temperature measurements are affected by the satellite attitude and environmental conditions as indicated by a slight scatter of data. It has been found that temperatures are lower if the measuring point is obtained during the shadow period, and higher if the satellite is in sunlight; however, this is only a small change of  $2^{\circ}$  to  $3^{\circ}\text{C}$ . Much stronger changes are experienced by the temperature of the skin or by the temperature of sensors and solar cells located on the satellite surface, and insulated from the inside mass. Figs. 19 and 20 show skin temperatures and Geiger counter temperatures obtained from the ABMA tracking station data. A correlation has been attempted by plotting all data vs the time after the satellite enters the shadow of the earth. The legend on Figs. 19 and 20 gives the points of maximum and minimum time in sunlight and the corresponding positions of the sun relative to

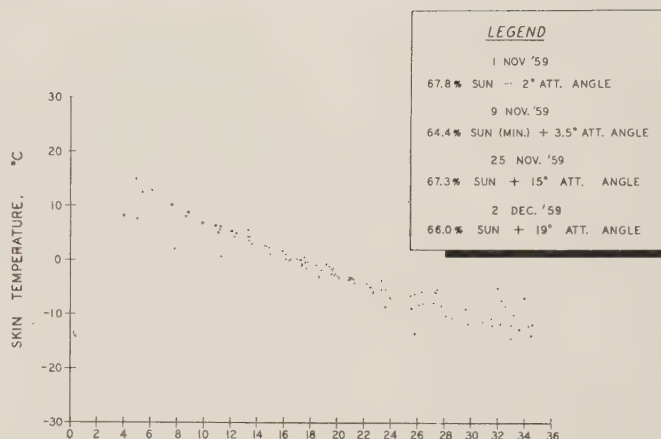


Fig. 19—Skin temperatures of Explorer VII vs time after entering shadow.

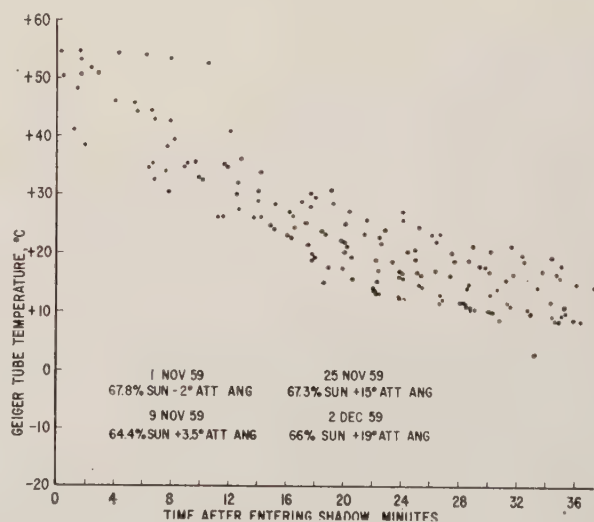


Fig. 20—Geiger counter temperatures of Explorer VII vs time after entering shadow.

the satellite equator (theoretical positions were used pending the evaluation of the attitude sensor of Explorer VII). It can be noted that variations of the conditions during the period of evaluation are small. The scatter of data is greater in the case of the Geiger counters of the Van Allen experiment. A better correlation is possible only if all variations of parameters are taken into account by using inputs from measurements and a computer program.

Even stronger temperature variations are encountered by the gold hemisphere sensor located on the equator of the satellite. Fig. 21 shows the temperature variation computed for a complete daylight-shadow cycle. The time in sunlight used is 68.3 per cent and the angle between spin axis and sun's position is  $67.5^{\circ}$ . Measuring points from two different passes are shown. The points agree qualitatively with the theoretical curve. The evaluation of this experiment promises to yield interesting results. The gold sensor is markedly affected by albedo variations. Evaluation will require correlation with other temperature measurements with preflight data and the University of Wisconsin radiation experiment.



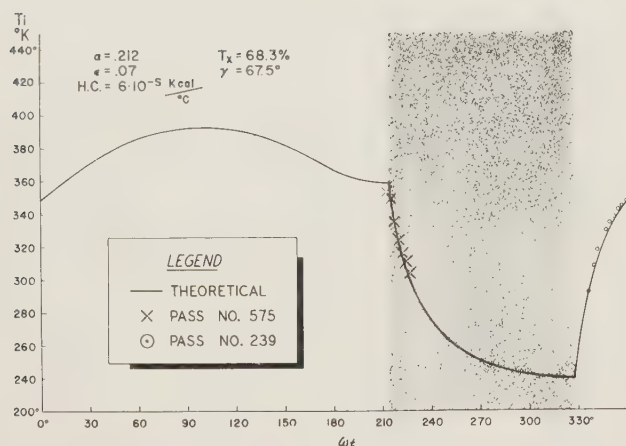


Fig. 21—Temperature of gold hemisphere of Explorer VII.

The short account given of the thermal experiment of Explorer VII is not complete and the evaluation is presently still in progress. It can be stated, however, that results have already shown that the thermal control worked well and that the thermal experiment has been successful.

#### VII. ACKNOWLEDGMENT

The thermal control of the Explorer satellites discussed in this paper is considered a part of the team effort of ABMA. This specific aspect has many contributors from various labs of ABMA, for Explorer I from Jet Propulsion Labs., and for Explorer VII from Dr. Suomi of the University of Wisconsin. My immediate coworkers on the thermal control aspects were K. Schocken, W. P. Jones, R. J. Naumann, W. C. Snoddy, and C. D. Cochran.

## Army Role in Project Argus\*

R. D. SHELTON† AND A. W. THOMPSON†

**Summary**—Argus was a code name given to a project which was to utilize atomic bursts at high altitudes to inject electrons artificially into the magnetic field of the earth, and to observe their movements by means of satellite borne instrumentation.

The Army Ballistic Missile Agency (ABMA) was assigned the over-all project direction for the satellite program including development of the instrumentation, construction, and testing and launching of the satellite. Also, ABMA was given post flight responsibility for tracking, telemetering, orbital computations, and data reduction.

This paper presents an account of the events leading up to the project, and ABMA's program in carrying out its responsibilities. Also included are test results for project Argus.

#### HISTORICAL SKETCH

AS EARLY as 1900, physicists were aware of ubiquitous ionizing radiation, and by 1912 an ionization chamber carried to altitudes by a balloon, provided data which showed that the radiation increased with altitude.<sup>1</sup> Later, because of the theoretical work of Stormer<sup>2</sup> and Vallarta<sup>3</sup> and the verification of the east-west effect by means of directional counting, it was generally agreed that the primary cosmic radiation consisted of positively

charged particles, which came from outer space, and which were subject to deflection by the magnetic field of the earth. Experimentation with detectors carried to high altitudes by balloons has continued, and with the development of rockets, numerous experiments have been carried aloft by this means.

Since the thermonuclear effort began in earnest<sup>4</sup> in 1953, a number of people interested in cosmic rays and nuclear physics found themselves attempting various means of confining plasmas by means of intense magnetic fields. One device of particular interest was the magnetic mirror machine developed at the Lawrence Radiation Laboratory. This device based the containment scheme on the principle that moving charged particles tend to be reflected as they travel into more intense magnetic fields. The magnetic field of the earth provides a magnetic mirror machine on a grand scale.

Christofilos<sup>5</sup> was stimulated by the launching of the first Sputnik on October 4, 1957 and by his interest in containment devices in the thermonuclear effort, to propose that electrons be artificially injected into the magnetic field of the earth at high altitudes, by means of atomic bombs, and that their movements be observed by means of satellite-

\* Manuscript received by the PGMIL, February 1, 1960.

† U. S. Army Ballistic Missile Agency, Redstone Arsenal, Huntsville, Ala.

<sup>1</sup> D. Halliday, "Introductory Nuclear Physics," John Wiley and Sons, Inc., New York, N. Y., p. 415; 1957.

<sup>2</sup> K. Stormer, "Sur un Probleme Relats aux Movement des L'Espace Cosmiques," *Videnskapsselskobets Skrifter. I. Mat. naturvi. Kl.*, vol. 14, 1913.

<sup>3</sup> M. G. Vallarta, "On the Energy of Cosmic Radiation Allowed by the Earth's Magnetic Field," *Phys. Rev.*, vol. 74, p. 1837; 1948.

<sup>4</sup> A. Bishop, "Project Sherwood," Addison-Wesley Publishing Co., Inc., Reading, Mass., p. 78; 1958.

<sup>5</sup> N. C. Christofilos, "The Argus Experiment," Symposium on Scientific Effects of Artificially Introduced Radiations at High Altitudes, IGY Rept. Ser. No. 9, National Academy of Sciences—National Research Council, Washington, D.C., p. 1144; 1959.

borne instrumentation. The preliminary calculations and the proposal for this experiment, later known under the code name Argus, were completed in January, 1958. Shortly thereafter, the Army was successful in launching the first U.S. satellite, Explorer I, which had as its primary purpose the study of cosmic radiation in the vicinity of the earth.

The observations with this satellite, as well as with Explorer III, another of the Army series, led to the discovery of a new phenomena,<sup>6</sup> the existence of a high-intensity corpuscular radiation region about the earth. This discovery of the radiation surrounding the earth stimulated interest in the proposal of Christofilos to the extent shown in the following excerpt from a published release by J. C. Haggerty on March 26, 1959.

The fate of the entire enterprise was laid before the President's Science Advisory Committee since it was clear that the undertaking involved a mixture of a scientific and military interest. At the suggestion of the President's Advisory Committee, a group of representatives of the scientific community and the defense community were brought together to appraise all aspects of the matter. It was decided in latter April 1958 to proceed with the Argus experiments as a major national undertaking. The operational and technological management of the project was vested in the new Advanced Research Projects Agency of the Department of Defense. In his capacity of Chief Scientist, Herbert York directed the program for that agency.

On May 2, 1958 the Department of the Army directed ABMA to participate in the proposed Argus test. In addition to supplying the satellite launching vehicle, ABMA was assigned over-all project direction for the satellite program, including development of the instrumentation, construction, testing and launching of the satellite. Also included in this package were the post-flight responsibility for tracking, telemetering, orbital computation and data reduction. Later, ABMA received a directive to conduct a quick look program to determine, and to report to the Armed Forces Special Weapons Projects (AFSWP), in the shortest possible time following a burst, the effectiveness of the nuclear burst.

During the week following the May 2 directive, the Jupiter C Missiles, numbers 44 and 47, which had been scheduled to place high-visibility inflatable spheres in orbit, were rescheduled to launch satellites instrumented to measure the Argus effect. Work on the Juno II type lunar probe, satellite vehicles, and the heavy International Geophysical Year satellite (later known as Explorer VII) was postponed in favor of the more urgent work on the Argus project. Jet Propulsion Laboratory contributed its full support with the upper stages, satellite shells and some components of the instrumentation. State University of Iowa initiated a high-priority program under contract with the Army to develop, test, and fabricate detectors for the expected radiation.

An organizational meeting was held at SUI on May 10 during which detailed plans for the Argus satellite pay-

loads evolved. In that meeting, test schedules and final delivery of the satellite components were established and responsibilities assigned. The crash program was then underway, and in less than three months (July 26, 1958) Explorer IV was launched.

#### SATELLITE PROJECT ORGANIZATION

The Argus satellite project involved six major areas of effort:

- 1) fabrication, checkout, and launching of the carrier vehicles,
- 2) design, fabrication, and environmental testing of the satellites,
- 3) development, design, fabrication, environmental testing, and calibration of the radiation detectors,
- 4) organization and operation of the data collection system,
- 5) computation of ephemeris,
- 6) assembly of data and evaluation of results.

For the launching vehicles, ABMA provided the booster, the spin launchers, the guidance and control equipment, while Jet Propulsion Laboratory furnished the solid propellant motors for the upper stages, and the steel shells for the satellites.

For the satellite, the detectors and scaler circuitry were obtained from the State University of Iowa, Iowa City, the subcarrier oscillators and microlock transmitters were obtained from Jet Propulsion Laboratory, the Naval Research Laboratory (NRL) furnished the minitrack transmitter, and the power supplies were obtained from the Signal Corps.

ABMA performed the satellite engineering, packaging of all the instruments, environmental and spin testing, antenna measurements, passive temperature control, and checkout.

In addition to those ground stations established by NRL and JPL for the earlier satellites, additional stations were required to insure world wide coverage of the scheduled experiment. ABMA arranged with the Naval Ordnance Test Station, the Signal Corps, Army Map Service, Ballistic Research Laboratory, Stanford Research Institute, and various universities, for the additional stations.

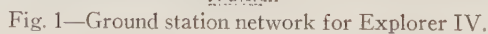
In addition to the normal function of the NRL Vanguard Computation Center, which was to furnish satellite position predictions to the tracking stations, a program for orbital determination was established with Smithsonian Astrophysical Observatory, Cambridge, Mass.

The resulting wide spread network of ground receiving stations used in the Argus experiment is shown in Fig. 1.

The flow of data from the receiving stations is shown in Fig. 2. The ground station network was sufficient to collect 234 cases where Explorer IV penetrated, or intercepted, the three Argus shells. Fig. 3 represents the points where data were collected. Fig. 4 is a sample of a telemetry playback, and it illustrates how the count rate changed as the satellite passed through the Argus belt.

<sup>6</sup> J. Van Allen, *Trans. Amer. Geophys. Union*, vol. 39, pp. 767-769; 1958.





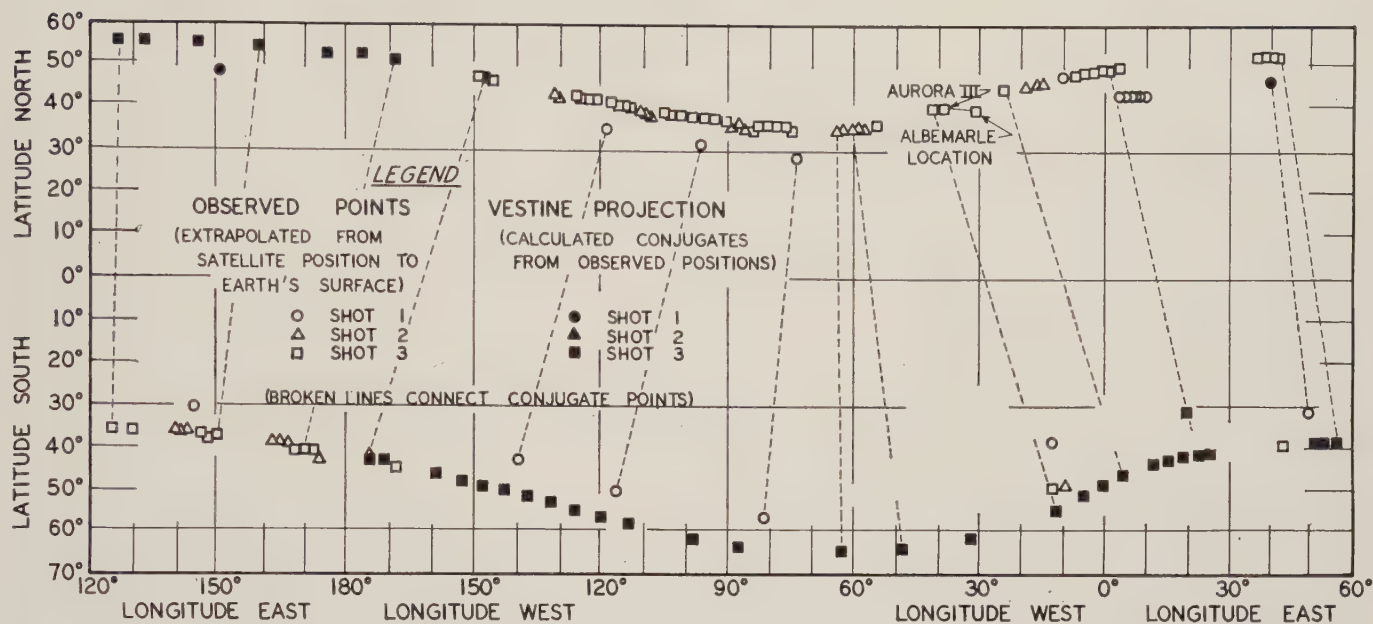


Fig. 3—Argus intercepts extrapolated to surface of earth with predicted mirror points.

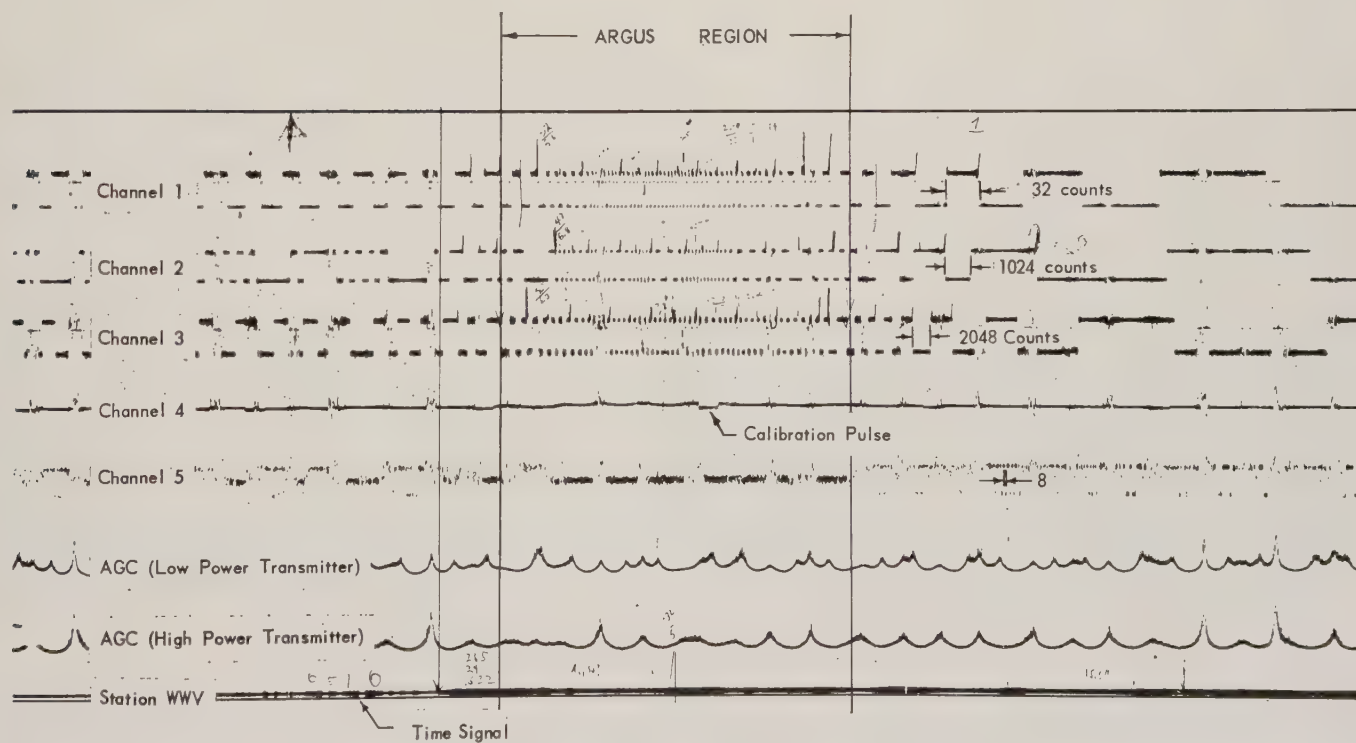


Fig. 4—Telemetry playback showing Argus intercept.



A comparison of the records from the stations operating during the lifetime of the satellite illustrates several important factors. If a beamed antenna is to be used to collect data from a continuous transmitter, the antenna should be steerable. However, a broad-beam width, low-gained antenna may be used if the receiver is extremely sensitive. An example of this was the Van Buren, Maine station, operated by the Signal Corps, which used a  $2\frac{1}{2}$  turn Helix set on a horizontal ground plane.

Stations which were very simple<sup>7</sup> as compared to either the minitrack or microlock type, such as those located in Johannesburg, South Africa, and at Bonn and Heidelberg in Germany provided excellent data.

A functional diagram of the payload is given in Fig. 5. Two transmitters were used. One, a 25-mw transmitter, was amplitude-modulated for use with minitrack stations, and the other, a 10 mw transmitter, was phase-modulated for use with the microlock stations. After the phase-modulated transmitter battery depletion, the microlock stations were able to receive excellent data from the phase modulation inherent in the amplitude modulated minitrack transmitter.

To accomplish the rapid data evaluation assignment, the Army Ballistic Missile Agency established and operated a high quality ground receiving station on the Redstone Arsenal. This station used a microlock type 108-mc receiver and directional antennae which were directed by an operator watching a field strength indicator. The range over which data were received from this station is represented by selected passes shown in Fig. 6. Table I shows the significant data on the passes.

During the periods when bursts were scheduled the telemetry playback station operated on a 24-hour basis so that the magnetic tapes from the ground station would be processed to permanent records for data reduction in the

shortest possible time. The result was that the evaluation group had the strip chart data in their hands within an hour or so after the end of a satellite pass.

Two special study groups were established, one group for special orbital problems and the other to do quick reduction and preliminary evaluation of the satellite records.

Before the first Argus nuclear detonation, the general characteristics of the radiation background were determined, and within three hours after the first Argus nuclear detonation, the success of the experiment, verified by two successive satellite passes, was reported by ABMA to Armed Forces Special Weapons Projects (now Defense Atomic Support Agency or DASA).

By continuing the rapid processing of data and by improving the satellite ephemeris with successive Doppler readings made at the local stations, the satellite position in orbit was established to an accuracy estimated to be in the order of  $\pm 0.8$  seconds of time. After study of the results from the first two bursts, the location of the initial lune of radiation resulting from the third Argus shot in the southern hemisphere was predicted with sufficient accuracy to permit the prior location of observers at the conjugate point in the northern hemisphere. As a result, the officers and crew of the USS Albermarle were able to observe, visually and with various types of equipment, many of the related phenomena associated with the ARGUS experiment.

On January 30, 1959, a report by members of ABMA to Armed Forces Special Weapons Projects contained the following information.

- 1) Each Argus shot has resulted in the creation of an easily detectable shell of high energy electrons about the earth, much as shown in Fig. 7.
- 2) The shells of radiation were quite constant in position, but showed a decay as time elapsed.
- 3) The configuration of the shell of artificial radiation showed a definite correlation with the magnetic field of the earth, as shown in Fig. 8.

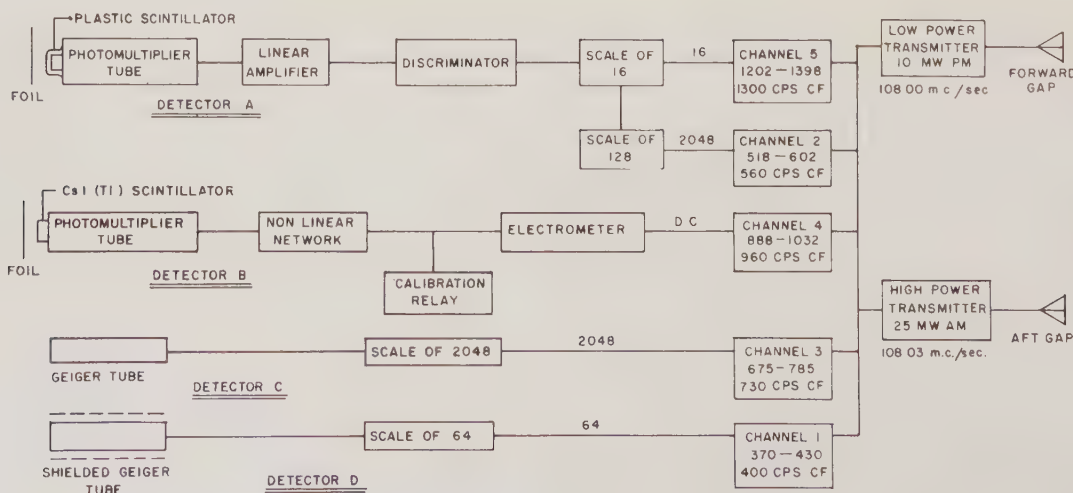


Fig. 5—Explorer IV functional diagram.

<sup>7</sup> These stations consisted of a Yagi antenna, Tape Tone Converter, the Signal Corps' R-390 receiver, a dual channel recorder, and a time signal receiver.

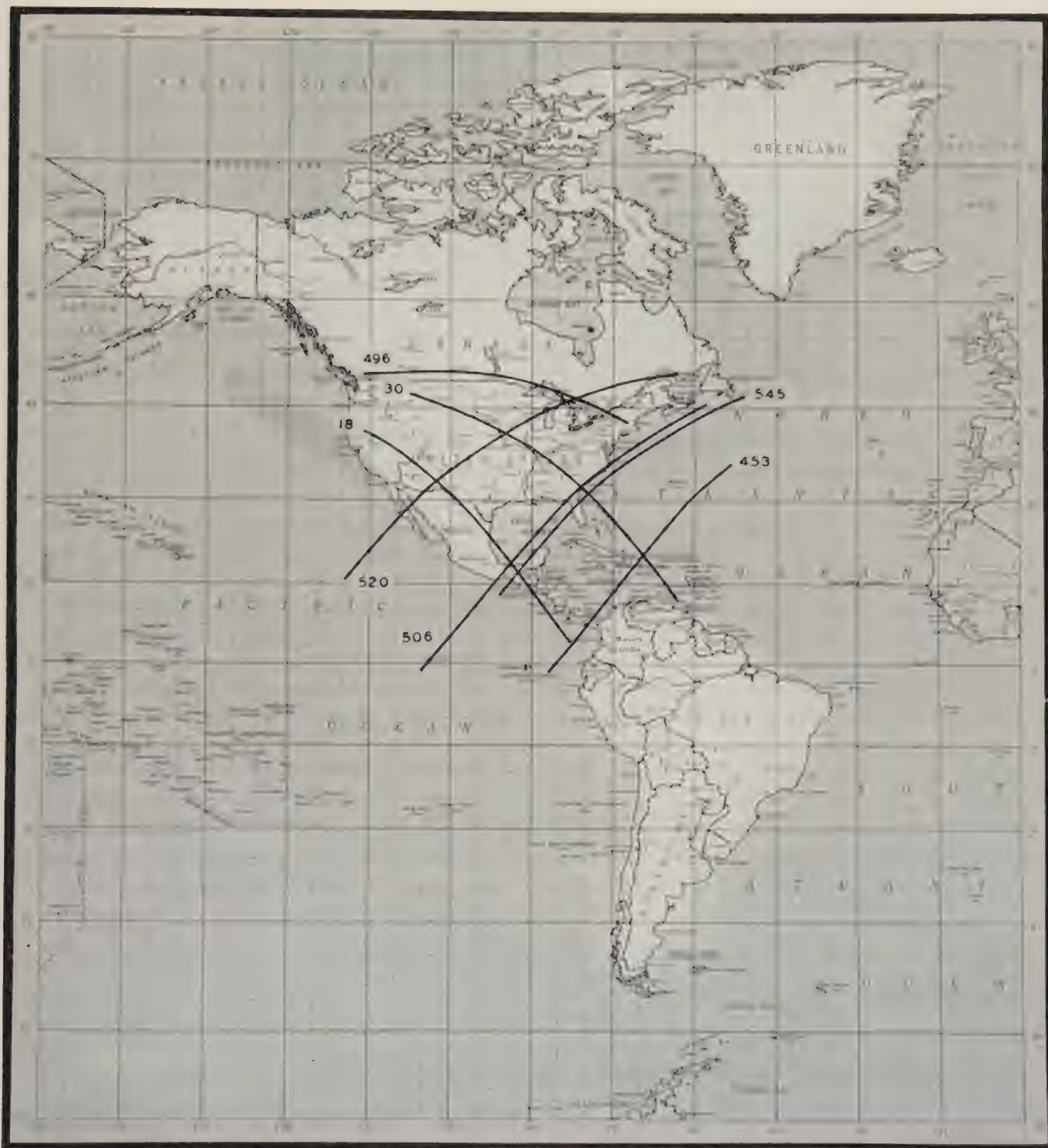


Fig. 6—Selected Explorer IV passes recorded at ABMA station.

TABLE I

Pass	Longitude		Latitude	Height (KM)	Pass	Longitude		Latitude	Height (KM)
18	Acquired	239.40	41.03	802.1	506	Acquired	250.90	0.16	2034.7
	Lost	268.42	16.24	1403.5		Lost	302.12	45.51	1109.8
30	Acquired	247.92	47.37	583.1	520	Acquired	236.13	16.07	1859.6
	Lost	296.62	13.02	1429.9		Lost	296.28	49.94	921.2
453	Acquired	273.86	- 1.34	1959.8	545	Acquired	264.31	13.45	1952.4
	Lost	306.08	35.08	1237.3		Lost	309.34	46.65	1199.8
496	Acquired	240.46	50.08	829.6					
	Lost	288.04	42.70	420.8					



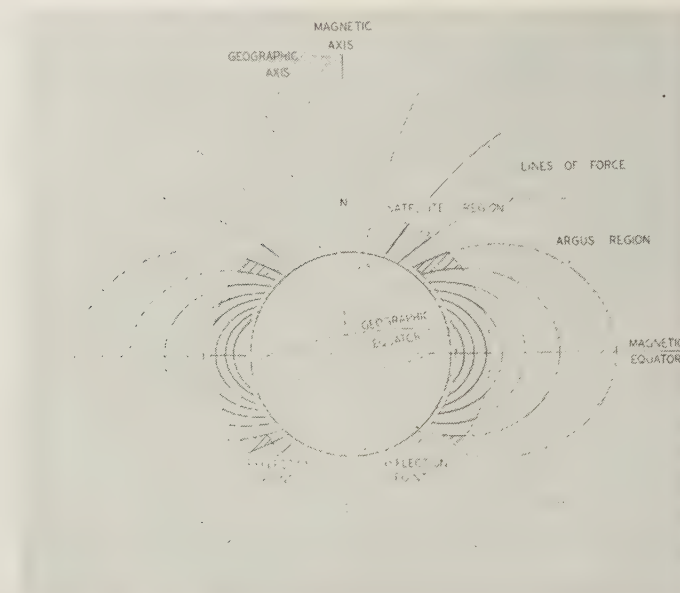


Fig. 7—Earth and magnetic field assumed to be generated by an eccentric magnetic dipole.

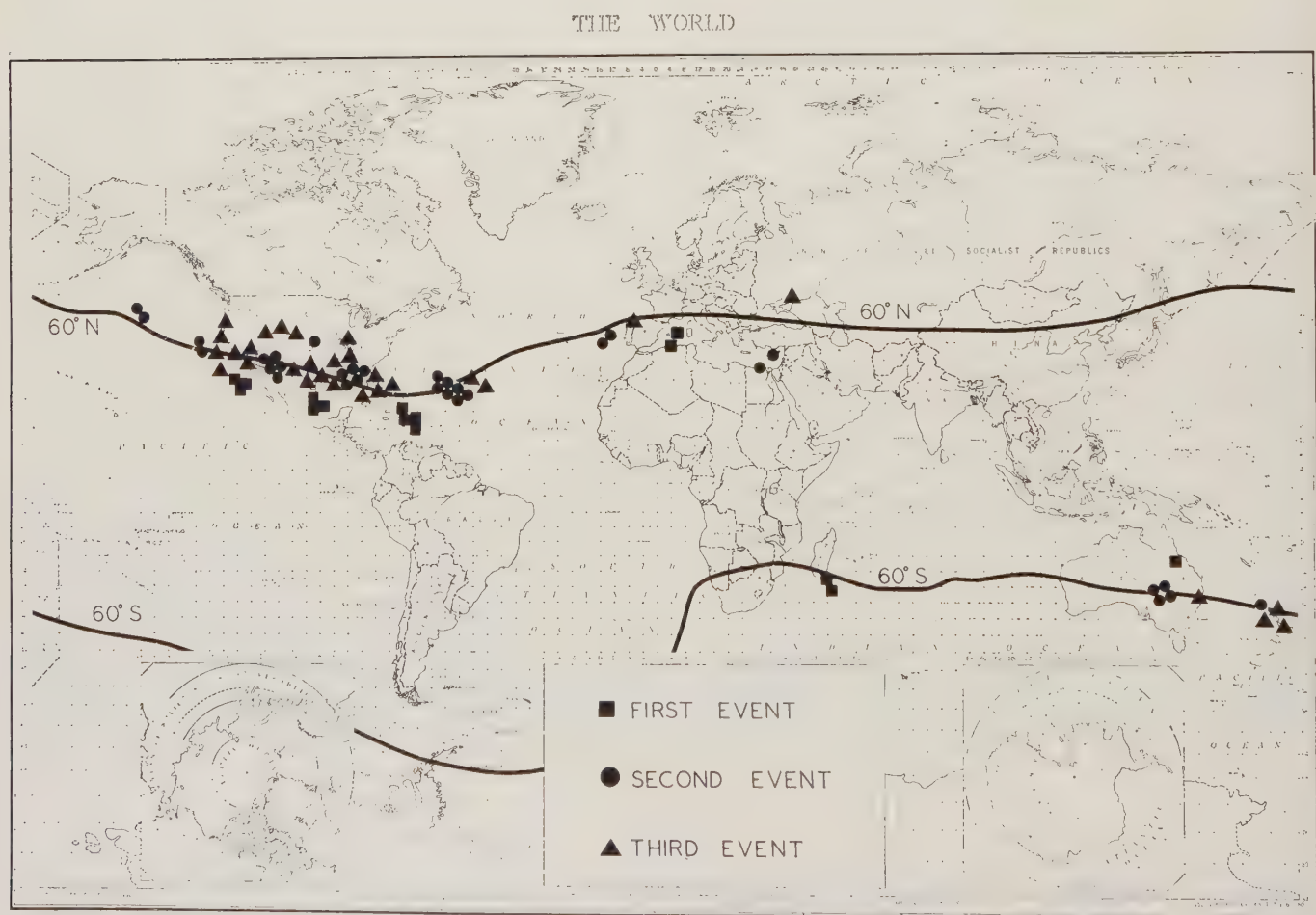


Fig. 8—Illustrative Argus data points collected by the satellite.

After the initial evaluation of the satellite data, members<sup>8</sup> of ABMA attended the Second Argus Working Group at Livermore, at which the collection of data from various sources was reviewed and studied. By assuming the

<sup>8</sup> E. Stuhlinger, A. Weber, C. Lundquist, and R. Shelton.

eccentric dipole model for the earth's magnetic field and by developing a machine code to extrapolate the satellite observations along the magnetic lines of force to the ground, Major R. Pennington obtained data tables from which the observed readings of Fig. 3 were drawn. Fig. 3 illustrates

in a striking fashion several important aspects of the Argus experiment. As mentioned previously, the location of the different shots were separated. The conjugate points calculated by E. H. Vestine fall nicely into the observed pattern. By using the model of the earth's magnetic field provided by E. Vestine<sup>9</sup> and the results of a machine program by W. Karzas, in which he calculated the intensity of the

<sup>9</sup>E. Vestine and W. Sible, "Lines of Force of the Geomagnetic Field in Space," Rand Corp., Santa Monica, Calif., no. R-1541; 1958.

magnetic field at the points at which the satellite traversed the Argus shells, Lt. Comdr. D. Chandler and R. Shelton arrived at the method of data presentation illustrated by Figs. 9 and 10.

Fig. 9 shows excellent consistency for the third Argus shot, considering the facts that the data points came from many geographic locations on the earth, that the tumbling and rolling motion of the satellite introduced some uncertainty into the measured count rates, and that a  $1/t$  decay law is implicit in the ordinate. This plot revealed the

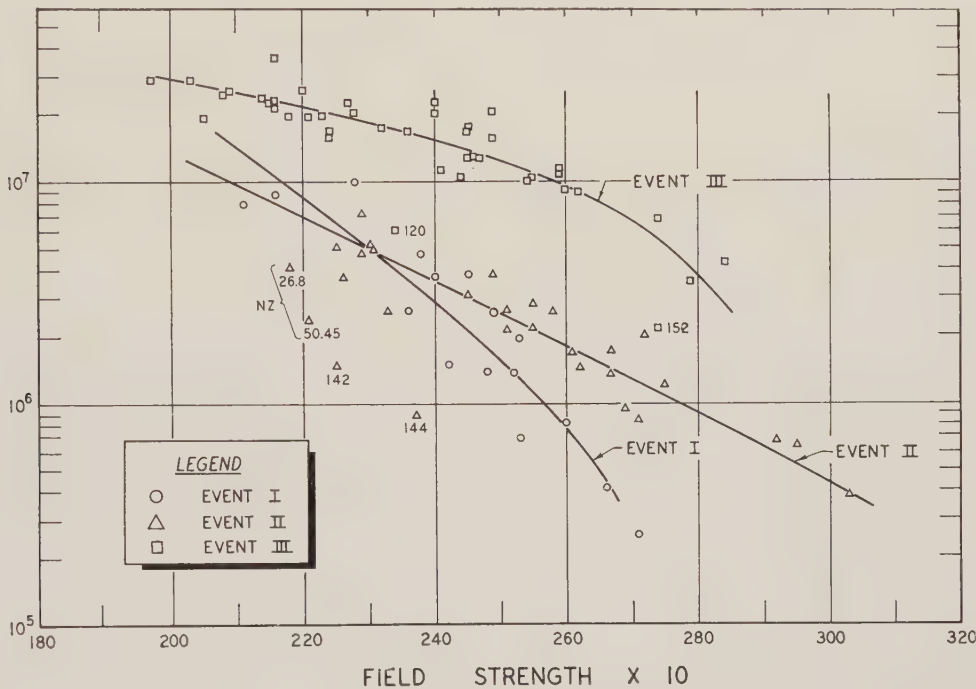


Fig. 9—A plot of the product of count rate of channel three on Explorer IV, the thickness of the Argus radiation belt, and time elapsed since the Argus shot vs magnetic strength in milligrams at the location of the satellite penetration of the Argus shell.

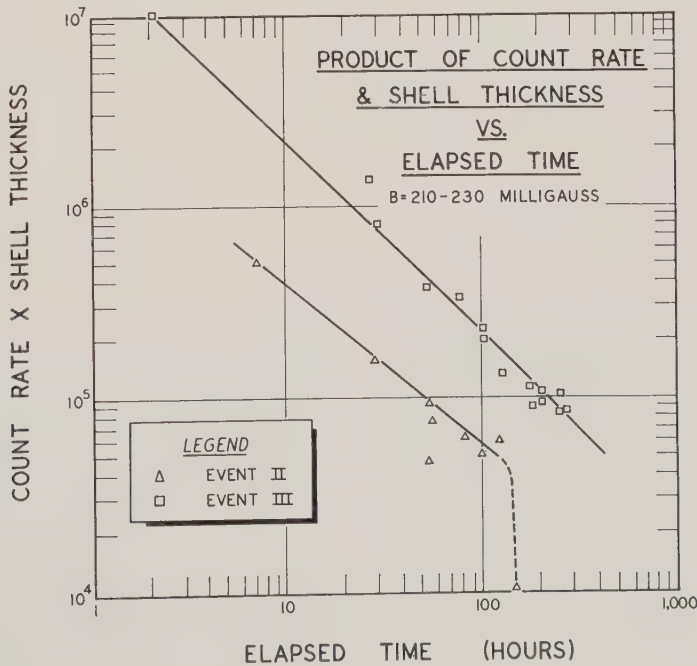


Fig. 10—A plot of the product of count rate and shell thickness vs elapsed time for the second and third Argus events.



important fact that electrons were injected for some distance along the field lines rather than just in the immediate neighborhood of the nuclear burst, and explained somewhat the large auroral displays observed at the conjugate point of the third Argus shot.

Fig. 10 illustrates the manner in which the radiation resulting from shots I and III decayed. This is in agreement with the  $1/t$  decay law predicted from theoretical considerations.<sup>10</sup>

The data from the Argus experiment is under continuing study. In closing, it is appropriate to point out the importance of satellites in geophysical and scientific research by quoting from statements by Porter and Christofilos at

<sup>10</sup> I. Welch and W. Whitaker, "Theory of Geomagnetically Trapped Electrons From An Artificial Source," Symposium on Scientific Effects of Artificially Introduced Radiations at High Altitudes, IGY Rept. Ser. No. 9, National Academy of Sciences—National Research Council, Washington, D.C., p. 1202; 1959.

the Symposium on Scientific Effects of Artificially Introduced Radiations at High Altitudes,

For the first time in history, geophysical phenomena on a world wide scale were being measured and related to a quantitatively known cause—namely, the injection of a known quantity of electrons of known energies at a known position and at a known time.<sup>11</sup> . . . The experiment was successful in all respects, except that Explorer V was not placed into orbit. However, the one satellite available, Explorer IV, yielded most of the important information, although valuable information resulted from other observations.<sup>12-14</sup>

<sup>11</sup> R. W. Porter, Symposium on Scientific Effects of Artificially Introduced Radiations at High Altitudes, IGY Rept. Ser. No. 9, National Academy of Sciences—National Research Council, Washington, D.C., p. 1143; 1959.

<sup>12</sup> L. Allen, et al., "Project Jason Measurements of Trapped Electrons from a Nuclear Device by Sounding Rockets," Symposium on Scientific Effects of Artificially Introduced Radiations at High Altitudes, IGY Rept. Ser. No. 9, National Academy of Sciences—National Research Council, Washington, D.C.; 1959.

<sup>13</sup> N. Christofilos, *op. cit.*, pp. 1144-1152.

<sup>14</sup> I. Welch and W. Whitaker, *op. cit.*, p. 1147.

## The Impact of the Argus Experiment on Hydromagnetic-Wave Research\*

HANS A. BOMKE†

**Summary**—The Argus series of high-altitude nuclear explosions has provided us with the means of studying hydromagnetic-wave effects under known and controllable conditions. These explosions have enabled us to compare, for the first time, quantitative experimental data with theoretical considerations.

Analysis of the world-wide hydromagnetic-wave effects led to the discovery of an interesting duct-like mechanism for the propagation of hydromagnetic waves at altitudes between 2000 and 3000 km. This mechanism is essential for the efficient propagation of hydromagnetic waves over global distances.

### INTRODUCTION

EXPERIMENTATION conducted by scientists of the U. S. Army Signal Research and Development Laboratory (USASRD) during the Hardtack and Argus series of 1958 has resulted in the development of significant new information concerning the excitation and propagation of hydromagnetic waves at great altitudes. In addition, this work has made it possible to verify experimentally certain basic concepts of hydromagnetic-wave theory.

In 1942, the Swedish astrophysicist H. Alfvén [1] had shown theoretically that, in a highly conductive fluid in

the presence of a magnetic field, mechanical displacements of a volume element perpendicular to the magnetic field will propagate with a well-defined velocity in the same direction as the magnetic field. This phenomenon is now called a hydromagnetic (or Alfvén) wave.

The hydromagnetic-wave velocity is given by the formula  $V = H/\sqrt{4\pi\rho}$ , where  $H$  is the magnetic field and  $\rho$  is the density of the conductive fluid. In normal conductive fluids, the wave velocity is quite small because of the relatively high densities. For example, in liquid mercury, even with  $H$  as large as 1000 gauss, the wave velocity is only 75 cm/second. On the other hand, with very low  $\rho$ , such as in the very tenuous plasma that exists at great altitudes, hydromagnetic-wave velocities of more than 1000 km/second are possible.

In general, we can state that easily observable hydromagnetic waves are present only in large volumes of very tenuous plasmas, such as in the atmospheres of the sun and the stars, in interplanetary space, and in the very high atmosphere of the earth. We advance two physical reasons for this statement. First, the magnetic forces that interact with the mechanical motion of conductive matter are rather weak, becoming predominant as compared with other effects only if very large volumes are involved. Second, the

\* Manuscript received by the PGMIL, February 1, 1960.

† U. S. Army Signal Res. Dev. Lab., Fort Monmouth, N. J.

electrical conductivity of matter, under normal temperature and pressure conditions, is so low that the electric currents produced by the displacement of conductive matter in the presence of a magnetic field are quickly damped out. Thus, these currents cause only short, transient effects instead of quasistationary hydromagnetic waves. Because of the large volume requirement, as stated above, laboratory experiments on hydromagnetic waves have been few and inconclusive.

Although we recognize the vital relationship between hydromagnetic effects and natural astrophysical and geophysical phenomena, such as sun spots, aurorae borealis, magnetic storms, etc., the latter are highly complicated phenomena and poorly understood. Moreover, hydromagnetic-wave theory becomes very complex when the consideration is not restricted to the simple case of a constant-density incompressible fluid in a constant, parallel magnetic field. For example, in 1952 van de Hulst [2] showed that, in compressible conductive fluids, we have two longitudinal hydromagnetic modes in addition to the transverse mode originally studied by Alfvén. These newer modes consist of a so-called modified Alfvén wave, which is faster than the original Alfvén wave, and a so-called retarded sound wave, which propagates more slowly than sound speed. The theory becomes even more complex under conditions of strongly inhomogeneous densities and magnetic fields, which are always present in natural astrophysical and geophysical phenomena.

EXPERIMENTATION

The high-altitude nuclear experiments, therefore, provided an excellent opportunity of gaining a better understanding of hydromagnetic-wave physics in general, and of outer-space hydromagnetic-wave propagation in particular.

magnetometers for the detection of hydromagnetic effects caused by the explosions. Accordingly, we developed an unconventional magnetometer system that had unprecedented sensitivity. This system consisted of a large wire loop, of about 100 km<sup>2</sup> in area, laid out on the ground. The large extent of the loop provided for effective averaging out and cancellation of undesired out-of-phase local magnetic disturbances caused by electric equipment and ignition systems, whereas the desired geomagnetic-field fluctuations excited the entire loop in phase. In practice, the signal-to-noise ratio of our large loop was extremely favorable, thus permitting reliable operation at high sensitivity, namely, 10<sup>-8</sup> to 10<sup>-9</sup> gauss at a frequency of about one cps.

RESULTS

During the high-altitude nuclear tests of 1958, W. Berthold and A. Harris [3] of USASRDL operated two such magnetometers: one in Wharton Tract, southern New Jersey, and the other in Grand Canyon, Ariz. The use of WWV time signals allowed a synchronization of the two recorders with an accuracy better than 0.1 second. Berthold and Harris obtained, at both stations, signals that had originated from the Argus explosions. Both stations received two signals: a fast one, which arrived about four seconds postshot; and a slow one, which arrived about four to five times later than the fast signal. The same two signals were also recorded by an earth-current station operated in Maine by G. Carp and A. Schwartz of USASRDL, by two European stations (Uppsala, Sweden and Reykjavik, Iceland) by arrangement with Prof. H. Benioff (California Institute of Technology), and by an Azores station operated under the supervision of P. Newman [4] of the U. S. Air Force. The experimental results are given in Table I.

TABLE I  
EXPERIMENTAL RESULTS

Site	Geomagnetic Latitude ( $\phi_2$ )	Geomagnetic Longitude ( $\lambda_2$ )	Observed Time (Fast Mode) (seconds)	Calculated Time (Fast Mode) (seconds)	Observed Time (Slow Mode) (seconds)	Calculated Time (Slow Mode) (seconds)
Azores	47N	49E	4.2	3.9	10.8	12.0
Uppsala	58N	106E	4.3	4.6	15.7	17.4
Reykjavik	70N	71E	4.6	4.6	17.8	18.7
Maine	57N	359E	4.5	4.5	17.7	16.7
New Jersey	51N	353E	4.7	4.5	18.3	16.4
Arizona	44N	310E	5.0	5.3	26.0	24.8

In 1957, during the planning stages of the high-altitude nuclear tests, we had concluded that the highly diamagnetic, rapidly expanding, completely ionized fireball should act as a magnetically opaque piston with respect to the earth's magnetic field, and should produce a noticeable excitation of hydromagnetic waves. We estimated that the conversion of bomb energy into hydromagnetic energy should be in the order of per cents. However, the dearth of knowledge about hydromagnetic-wave excitation and propagation prompted us to recommend the use of very sensitive

The high accuracy of the experimental data made it possible to make a quantitative comparison with theoretical computations of expected travel times of hydromagnetic waves. This comparison allowed us to draw several significant conclusions. First, the fast signal is the modified Alfvén wave predicted by van de Hulst. Second, the slow signal fits the predicted travel pattern of the transverse Alfvén wave. However, the physical mechanism that produces this excitation is not understood in detail, and therefore our interpretation of the slow signal is tentative.



Third, the propagation path of both signals is governed by Fermat's principle of the shortest possible propagation time, and can be described by the Euler-Lagrange equation. In accordance with the Fermat principle, hydromagnetic waves propagate essentially near the height of maximum hydromagnetic-wave velocity in the upper atmosphere: at about 3000 km. The refractive properties of the upper atmosphere impart a duct-like quality to this region of maximum hydromagnetic-wave velocity, and the duct provides the means of bending hydromagnetic waves in approximately great-circle paths to remote parts of the world. Within the latitudes over which our observations extended, the hydromagnetic-wave propagation paths form a nearly concentric shell around the earth. Nearer the poles, however, the shell should theoretically be elongated in the direction of the earth's magnetic axis. However, we need more data to substantiate this hypothesis. Fourth, detailed analysis of the data shows that the fast mode propagates at an average altitude of 3000 km, whereas the slow mode follows a lower duct at about 1700 km. The postulated hydromagnetic-wave propagation duct at an altitude between 2000 and 3000 km can also be deduced from general geometrical optics and the known electron-density profile of the upper atmosphere. These considerations make possible a theoretical computation of the expected times of arrival for the fast and the slow modes (see Table I). A comparison of theoretical with experimental values shows very good agreement, which is strong evidence in favor of the postulated hydromagnetic-wave duct.

The fact that the observed travel times for the fast mode are not noticeably greater than the calculated travel times implies additional deductions concerning the hydromagnetic waves, namely: both the excitation mechanism and the coupling-to-ground mechanism should be very fast compared to the travel time in the duct. With respect to the excitation mechanism, the assumption of extremely fast injection agrees with our present knowledge of the rapid expansion of a high-altitude atomic fireball. Estimates indicate that after 0.3 or 0.5 second, the expanding fireball ceases to act like a piston on the earth's magnetic field. This would explain both the observed oscillation period of about one second, and the extremely rapid injection of hydromagnetic energy into the duct. Concerning the

coupling-to-ground mechanism, we know that hydromagnetic waves are limited to areas of high electric conductivity, and therefore they cannot reach the earth's lower atmosphere. Accordingly, we must seek a mechanism that is capable of transmitting to the ground the magnetic-field fluctuations that travel as hydromagnetic waves through the upper atmosphere. This mechanism is conventional electromagnetic interaction, for the ground stations are within a wavelength of the ionosphere (owing to the great length of the hydromagnetic waves). Since this electromagnetic interaction propagates with almost light speed through the nonconductive lower atmosphere, the ground station will receive the signal at about the same time as the wave passes overhead.

#### CONCLUSIONS

The Argus experiments have given a decided impetus to hydromagnetic research in general, and to further exploration of the properties of the boundary zone between the exosphere and outer space. The fragmentary data obtained during the Argus events have helped us to formulate a rather clear concept of hydromagnetic-wave propagation. High-altitude explosions indeed offer an excellent tool for outer-space exploration by means of hydromagnetic-wave investigation, and it is hoped that further high-altitude experiments will be conducted to help us close many of the remaining gaps in this important area of space physics.

#### ACKNOWLEDGMENT

The author acknowledges the assistance of Dr. W. J. Ramm, S. Goldblatt, and Lt. V. Klemas of USASRD in conducting the theoretical studies. A paper summarizing the chief results of the studies was published in *Nature* in January, 1960 [5].

#### REFERENCES

- [1] H. Alfvén, "Cosmical Electrodynamics," Clarendon Press, Oxford, Eng.; 1950.
- [2] H. van de Hulst, "Problems of Cosmical Aerodynamics," Central Air Documents Office, Dayton, Ohio, ch. 7; 1951.
- [3] W. Berthold, *et al.*, "World-wide hydromagnetic effects due to Argus," (to be published).
- [4] P. Newman, "Optical electromagnetic and satellite observations of high-altitude nuclear detonations, part I," *J. Geophys. Res.*, vol. 64, pp. 923-932; August, 1959.
- [5] H. A. Bomke, *et al.*, "Global hydromagnetic wave ducts in the exosphere," *Nature*, vol. 185, pp. 299-300; January, 1960.

# Pioneer III and IV Space Probes\*

H. CURTIS† AND D. SCHNEIDERMAN†

**Summary**—A description of the over-all objectives of the Pioneer III and IV experiments is presented. Included is an analysis of the payload design philosophy, a description of the flight hardware, and a synopsis of the results of the experiments.

## INTRODUCTION

EARLY in 1958 the Army Ballistic Missile Agency (ABMA) and the Jet Propulsion Laboratory (JPL) were asked to prepare a space probe for National Aeronautics and Space Administration as part of the United States' participation in the International Geophysical Year. It was the responsibility of ABMA to provide the booster and guidance sections; JPL was asked to prepare the high-speed propulsion stages, the payload, and its associated ground tracking and telemetering equipment. This combined effort resulted in the successful launching of Pioneer III on December 6, 1958, and Pioneer IV on March 3, 1959 (Fig. 1).

A description of the design considerations and mechanization of the Pioneer III and IV space probes will be given. Pioneers III and IV were nearly identical in design; however, certain detailed differences in mechanization did appear as improvements on Pioneer IV.

The prime objectives of the Pioneer space probe experiments were:

- 1) to establish a trajectory in the vicinity of the moon,
- 2) to make a significant scientific measurement,
- 3) to advance space technology.

Specific design of the payload was subject to several important engineering constraints. Payload weight was limited to 15 pounds by the available vehicle and the required trajectory. The mechanical environment (up to 85-g linear acceleration, 600-rpm rotation, and severe shock and vibration) during launching of the high-speed stages imposed severe structural requirements. Thermal balance considerations during the coast period of the trajectory required accurate surface emissivity control.

Because of the weight limitations and the accuracy with which the trajectory was to be established, it was decided that the mission could best be satisfied by a spin-stabilized payload. The stringent weight requirement also made it necessary to tailor the structure closely to the over-all electrical and mechanical needs. This optimization exacted a penalty by minimizing the versatility of the unit. To provide a maximum moment of inertia about the spin

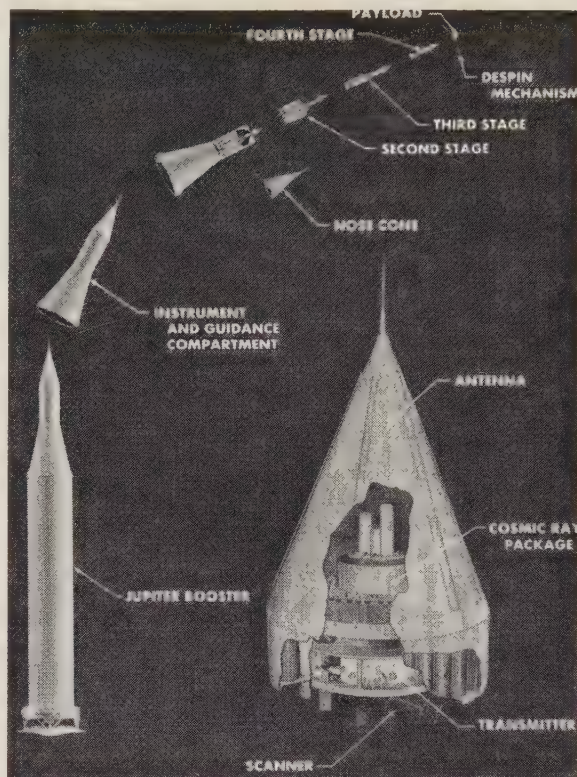


Fig. 1—Pioneer III.

axis (so that tumbling would not occur), and an acceptable antenna pattern, the payload configuration itself was limited.

Working within these limitations, a payload having the configuration shown in Figs. 2 and 3 was evolved. The payload was a gold-plated, conical-shaped instrument package, housing a small battery-powered radio transmitter, a cosmic-ray experiment with its associated electronic circuitry, and such developmental devices as an optical trigger, a hydraulic timer, and a despin mechanism.

## COMMUNICATIONS SYSTEM

The communications system employed in the Pioneer III and IV experiments utilized an extremely low-power transmitter. Ground reception used advanced phase-lock techniques for narrow-band detection of both the carrier and subcarrier signals.

To aid in tracking and communications over extended ranges (lunar and beyond), an 85-foot-diameter receiving antenna was employed. This tracking and communications system, known as the TRACE system,<sup>1</sup> is the outgrowth of earlier JPL-developed Microlock techniques.

\* Manuscript received by the PGMIL, February 1, 1960. Portions of the following report were originated under studies conducted for the Department of Army Ordnance Corps under Contract No. DA-04-495-Ord 18. Such studies are now conducted for the National Aeronautics and Space Administration under Contract No. NASw-6.

† Jet Propulsion Lab., Calif. Inst. Tech., Pasadena, Calif.

<sup>1</sup> M. H. Brockman, H. R. Buchanan, R. L. Choate, and L. R. Malling, "Extra-terrestrial radio tracking and communication," *Proc. IRE*, vol. 8, pp. 643-654; April, 1960.



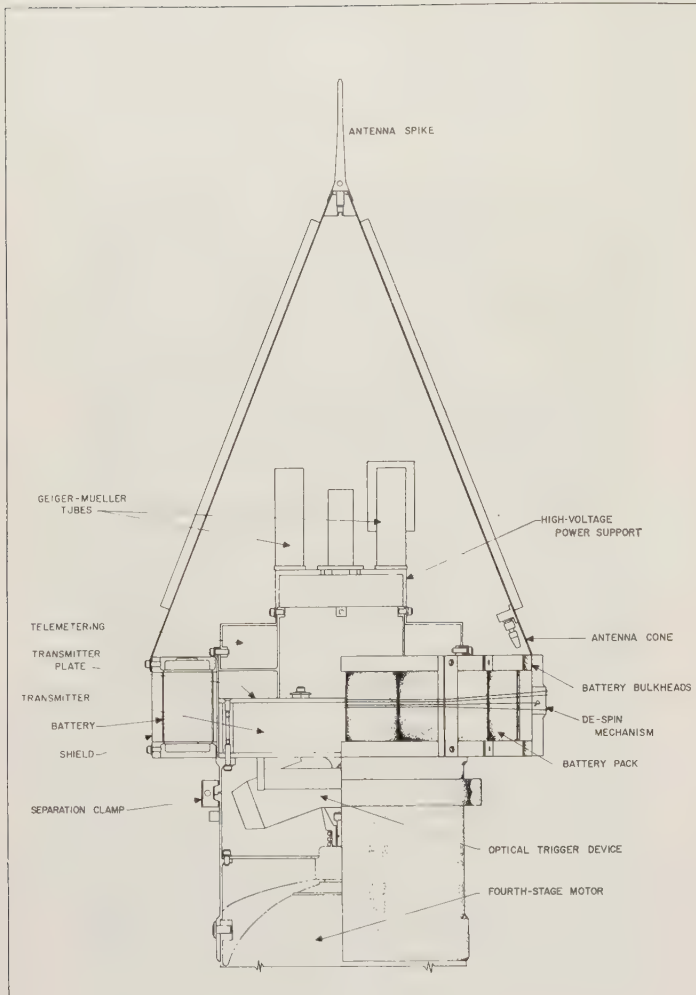


Fig. 2—Pioneer IV.

While the TRACE system was especially established for this series of experiments, it now forms the backbone of the NASA Deep Space Tracking Network.

The airborne portion of the communication system incorporated in the Pioneer space probes consisted essentially of three elements: the audio-subcarrier oscillators, of which there were three, assigned RDB channels 1, 2 and 3; the transmitter, which was phase-modulated by the three subcarrier oscillators, and radiated approximately 180 mw of power at a frequency of 960.05 mc; and the antenna, which has a maximum lobe gain of 2.5 db over isotropic.

Choice of this operating frequency for the TRACE space communications system was affected by propagation characteristics within the ionosphere and stratosphere and by galactic, circuit, and other noise considerations. The frequency used in Pioneers III and IV constitutes a compromise between the theoretical optimum and practical considerations.

#### Subcarrier oscillator

The subcarrier voltage-controlled oscillators were transistorized units developed by JPL for previous programs. It was only necessary to repackaging them into the highly-integrated structure.

#### Transmitter

The complete transmitter assembly includes a crystal oscillator (40 mc), frequency multipliers, a modulator, and a final power-output-amplifier stage, packaged as shown in Fig. 4. A block diagram of this unit is shown in Fig. 5. It should be noted that all stages are transis-

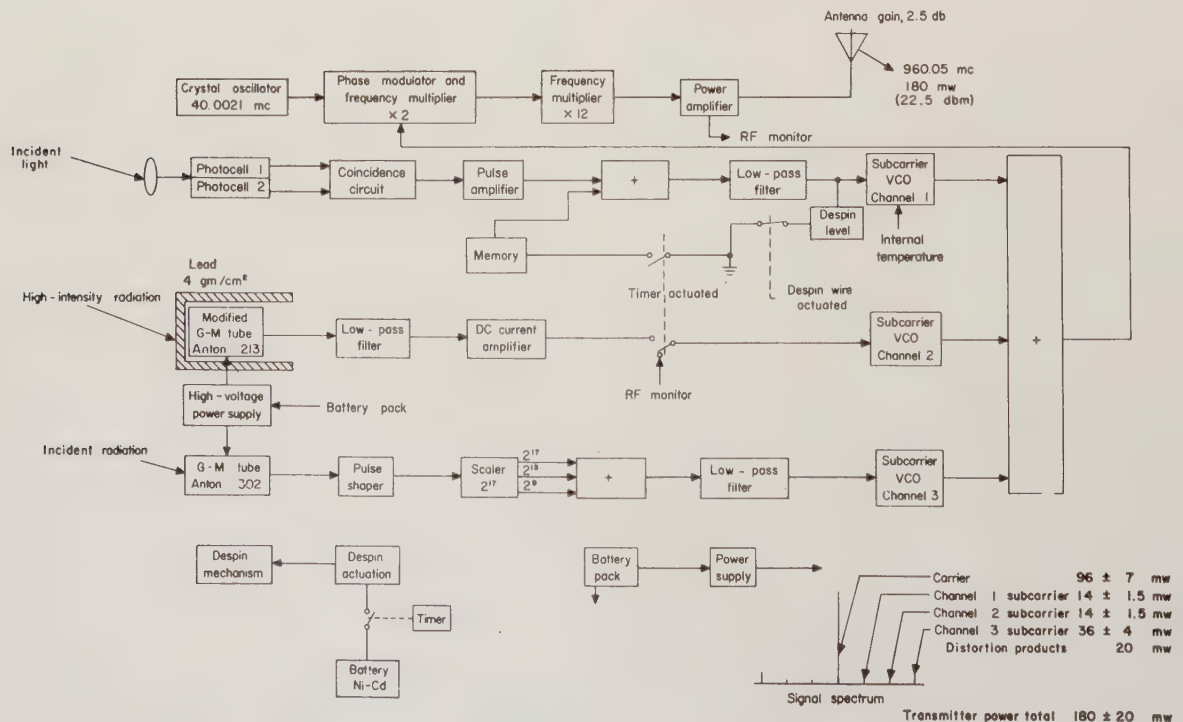


Fig. 3—Block diagram of Pioneer IV.

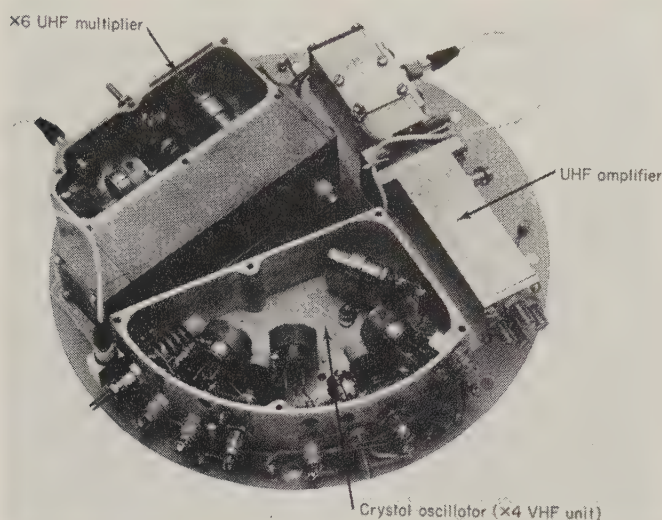


Fig. 4—Pioneer IV transmitter.

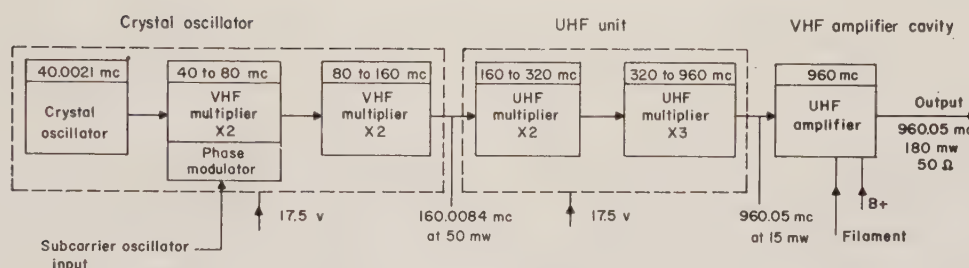


Fig. 5—Block diagram of transmitter.

torized with the exception of the final amplifier. The only vacuum tube is a subminiature ceramic UHF triode (GE-7077). Silver-plated magnesium was extensively used in the fabrication of the cavities and chassis for this unit.

### Antenna

The selection of the space-probe antenna was determined by the following criteria: lightness of weight and mechanical rigidity, reliability (simplicity), optimum gain, and antenna pattern. To meet these requirements, several antenna configurations were investigated. The final flight configuration chosen, an unsymmetrical dipole, is shown in Fig. 6.

The antenna was constructed from 0.016-inch-thick laminated epoxy cloth which was formed into a conic section having a base diameter of 9-1/4 inches and a height of 12 inches. The cone was flashed with silver and then plated with gold. In effect, the gold-plated cone acted as a ground plane reflector for a 3-inch quarter-wavelength aluminum probe which was mounted on the top of the cone. The epoxy antenna cone also acted as a protective cover for the payload instrumentation.

Because there was some uncertainty in the exact payload orientation in space for a given trajectory, a study was made of the viewing angle between the payload spin axis and a line going from the payload to the observer (Fig. 7). For several reasons this angle ( $\alpha$ ) can be pre-

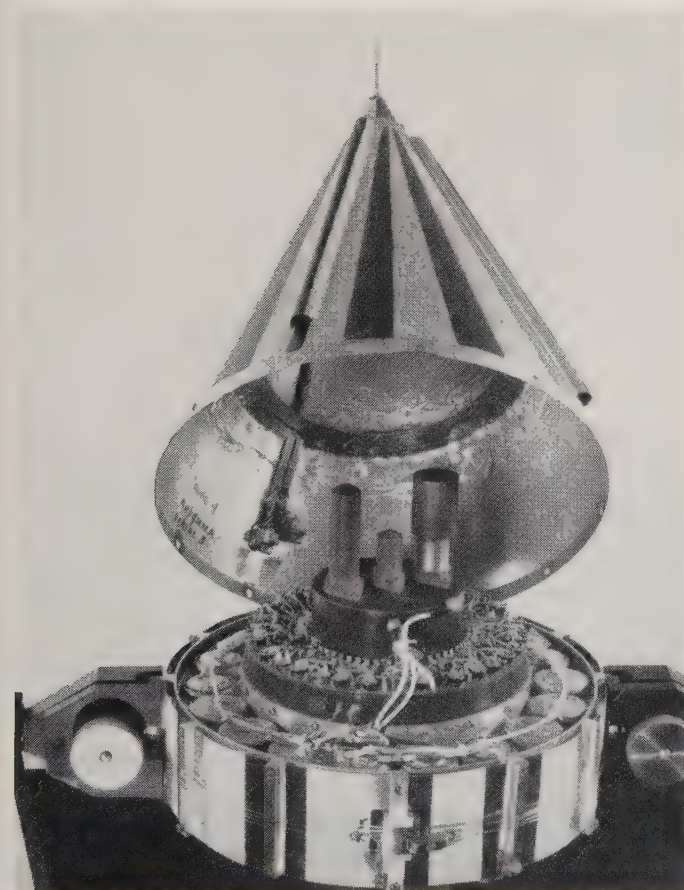


Fig. 6—Internal view of Pioneer IV.



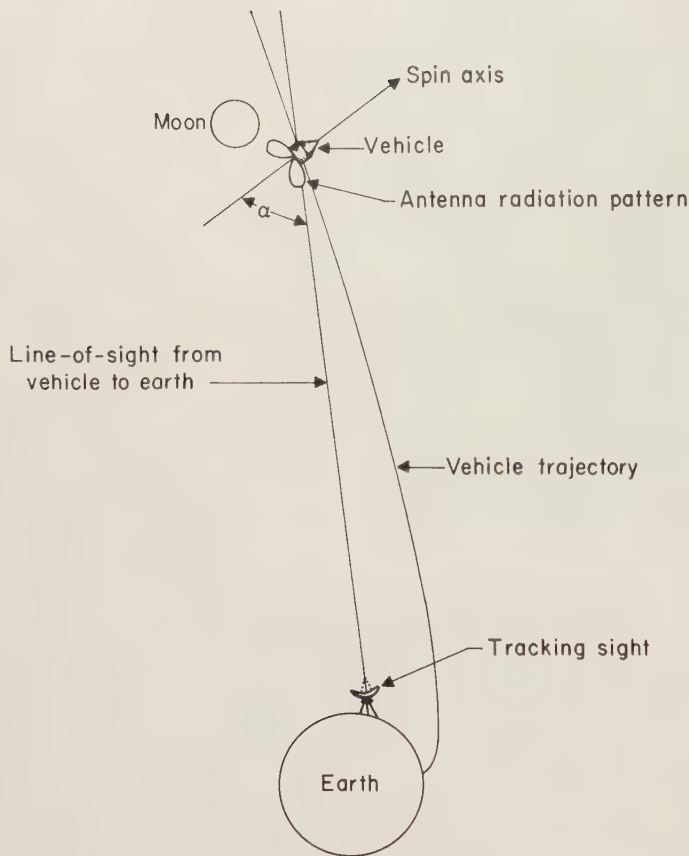


Fig. 7—Antenna look angle.

dicted only with moderate accuracy. Since  $\alpha$  is the function of a particular trajectory, it is necessary to have the antenna beamwidth large enough to cover variations between trajectories. Since the payload was spin-stabilized, perturbing torques applied to the payload in space tend to induce anomalous payload motions. Such torques may arise in separation from the final-stage motor, in despin of the payload, or from unforeseen sources. The flight antenna radiation pattern is shown in Fig. 8.

#### Electrical power

The battery pack supplying power to all the electronics of the probe contained eighteen Mallory RM-42R mercury cells. These cells were chosen because of their relatively high watt-hour per pound output, good regulation, and high reliability characteristics. The batteries were arranged in a ring around the base of the payload structure (Fig. 6) in order to provide the maximum possible moment of inertia about the payload axis. In order to allow extensive testing of the payload with a representative flight-battery source, it was necessary to arrange the battery pack as a replaceable assembly so that a fresh battery pack could be installed just prior to launch. Electrically, the batteries were arranged in three groups of six batteries, each group providing a nominal 7.2-volt output. Power for the scaler circuits and transmitter was derived by means of a static converter which produced 17.5 volts and 130-volt B+ output. In addition, a regulator circuit

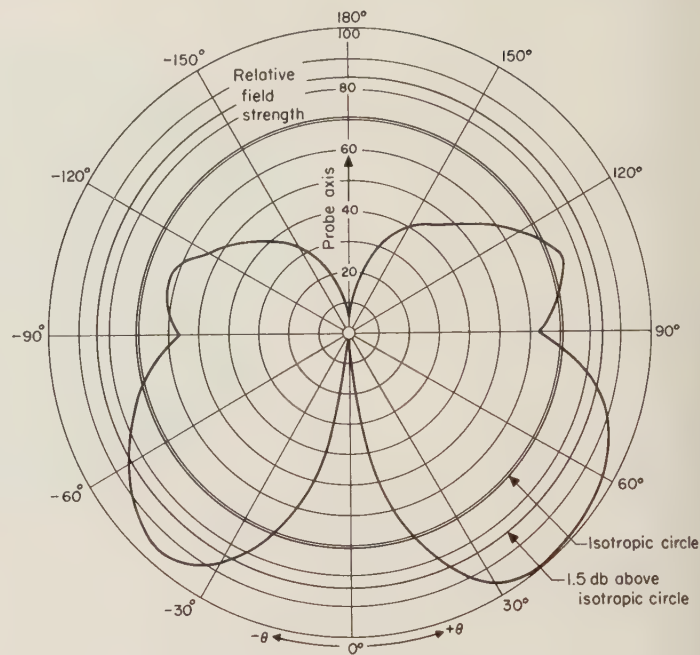


Fig. 8—Pioneer IV antenna pattern.

was incorporated which provided 6.4 volts for the filament of the final amplifier of the transmitter and 5.5 volts for the dc amplifier circuitry associated with the Anton 213 Geiger tube.

#### OPTICAL TRIGGER EXPERIMENT

Future space missions will involve the photographing of some galactic body. In anticipation of such a need, three devices were included in Pioneers III and IV which could be of later use. The first of these was an optical trigger which could be used to trigger a camera when the probe was in an appropriate position in respect to the moon. The second was a despin mechanism to reduce the angular velocity of the probe to a value compatible with probable photographic exposure times. A third device, a hydraulic timer, was developed to control arming of the trigger mechanism and initiation of the despin operation.

#### Optical trigger

The optical trigger device was located at the rear of the payload and was exposed to space after the probe was separated from the fourth propulsion stage. This trigger consisted of a lens system, two photoelectric cells, and logic elements which served to create a pulse when an object of sufficient angular size was in the proper part of the field of vision of the trigger mechanism. This device was designed to trigger when the probe passed within an appropriate distance from the moon. The trajectory was chosen to provide an intercept when the lunar surface was properly illuminated. The portion of the moon which would initiate the trigger action was dependent upon the geometry between the payload spin axis, the angle of the trigger in the payload, and the trajectory. This in combination with the arming timer would enable the trigger

to operate only after the payload had passed the moon.

For the Pioneer III and IV experiments, the optical trigger device (Fig. 2) was intended to operate as follows. After the probe separated from the fourth stage, the optical trigger was exposed and viewed the earth. As the optical trigger scanned the light side of the earth, it generated a pulse alternately switching a bistable multivibrator. The output of the multivibrator was then passed to the channel 1 subcarrier VCO, where it appeared as a square-wave frequency variation of 5-cps magnitude at each earth sighting. However, prior to despin, the rotational speed of the probe was too high to permit the system to respond to this switching rate and the output settled out at an intermediate frequency. Shortly after separation, the hydraulic timer actuated the despin mechanism which slowed the probe's rotational speed to approximately 5 rpm. A memory circuit which was part of the optical trigger mechanism was not armed until the probe was in flight about 18 hours. At this time, if the probe was on trajectory, the earth would subtend an angle to the probe which would not be sufficiently large to stimulate the optical trigger. As an indication that the trigger had been activated by the moon, the trigger's memory circuit shifted the output frequency of the VCO by a discrete increment upon first sighting after arming. Each alternate sighting of the moon would then be indicated by a square-wave output generated around the newly established baseline.

#### *Despin mechanism*

As mentioned previously, a payload despin technique was required to accommodate a possible future photographic mission by a spin-stabilized payload. For this purpose the final spin rate must be low (about 5 rpm) but greater than zero. A zero spin rate would fail to provide spin stabilization of the space instrument. It would also fail to guarantee detection of the moon during the time of intercept, since the detector might be facing away from the moon.

The initial high spin rate was necessitated by the need to stabilize the high-speed stages of the Juno II vehicle. Consideration of techniques to provide an initial spin rate for the payload lower than the spin rates of the stages upon which it rested were abandoned in favor of techniques that reduced the spin rate in flight.

The probe was revolving at approximately 600 rpm at the time of its separation from stage 4. It was to continue to revolve at this speed for approximately 10 hours. Upon activation of the despin release assembly by the hydraulic timer, the despin mechanism slowed the probe revolution rate in less than  $\frac{1}{4}$ -second to 1 per cent of the spin rate that existed just prior to despinning.

The despin mechanism (Fig. 6) consisted of two 6-g counterweights on 60-inch-long nichrome wires. Each wire was attached to the payload by an eyelet which pivoted on a hook mounted on the center-of-gravity plane of the probe,  $180^\circ$  opposed. In their preflight position, the counterweight wires were wrapped around the probe

and the counterweights were locked into their static position by a pin. Upon activation of the release assembly, the counterweights swung out, unwrapping the wires. In the early stages of despinning, the wires were tangentially suspended, and as the probe spin rate decreased to that desired, the wire positions progressed from tangential to radial. In the final stage, the wires reached a radial position which caused the eyelets to pivot off the hooks, releasing the wire-counterweight assemblies to fly off into space carrying with them most of the rotational kinetic energy originally stored in the payload.

The despin release assembly on Pioneer IV was actuated by the firing of an explosive device which received its firing signal from the hydraulic timer switch closure. The firing current was provided by a separate 4-volt battery pack.

#### *Hydraulic timer*

To meet the requirements of the initiating operation of the despin and optical trigger experiments at some predetermined time after launch, a timer was required. Studies revealed that this switching could most reliably be accomplished by a hydraulic timer. The key to the reliability of this unit is its simplicity of operation and design. The timer operated as a closed hydraulic system. A spring-loaded plunger forced a column of silicone fluid through a capillary tube 30-inches long. The flow rate of the fluid through the system controlled the rate of motion of the plunger. The placing of the spring-loaded switches along the plunger shaft controlled the interval and sequence.

The timer was designed to be started 3.5 hours before launch, to release the despin mechanism electrically 13.5 hours later, and after 21.5 hours of running time, to arm the optical trigger.

#### TEMPERATURE CONTROL

Temperature control (Fig. 6) of Pioneers III and IV was achieved by controlling the absorptivity and emissivity ratio of the surface of the payload. Since solar heat input would change as a function of the angle between the probe axis and the probe-sun line, which in turn depends on the trajectory used and firing date, it was necessary to have readily-controllable average-surface characteristics. This was accomplished by having a basic gold-plated surface with overlaid black or white paint in a striped pattern as required.

#### RADIATION EXPERIMENT

The scientific aspects of the radiation experiment (Fig. 2) were determined by Dr. James A. Van Allen of the State University of Iowa, Iowa City, who also participated in the design and calibration of this portion of the payload. This experiment (Fig. 6) employed two Geiger-Mueller tubes, the first an Anton-type 302 tube, whose output was counted by a seventeen-stage binary scaler. This length of counter was chosen to prevent high-count information from being severely attenuated by the narrow



bandwidth of communications system. In order to cover the extreme dynamic ranges expected in counting rates within the design bandwidth of the communications system, a unique data processing scheme was employed. By passing the outputs of the ninth, thirteenth, and seventeenth stages of the scaler through suitable weighting networks and then linearly combining them to give different peak-to-peak amplitudes, an output as is shown in Fig. 9 was achieved.

A second Geiger-Mueller tube, Anton-type 213, served two different purposes on Pioneers III and IV. On Pioneer III its function was to provide coverage in the high-intensity region of radiation. On Pioneer IV, it was shielded by a 4-g/cm<sup>2</sup>-lead shield, and its function was to provide a degree of discrimination against lower-energy particles. This was an attempt to determine the nature and the quantity of the particles. In operation, the pulses obtained from the Anton-type 213 tube were integrated in a low-pass filter and the average voltage thus formed was fed to the channel 2 subcarrier oscillator through a unity-voltage-gain power amplifier.

The Geiger tubes encased in their flight containers and the scaling circuits are shown in Fig. 6. In the center of the scaling circuitry is a cylinder containing a potted high-voltage power supply which also served to mount the Geiger tubes. The small cylinder mounted on the center of this power supply is the voltage reference tube for the high-voltage system.

## RESULTS

Pioneer III did not achieve escape velocity. However, it reached an altitude of 63,500 miles from the earth and obtained some very valuable radiation data during its flight of 38 hours and 6 minutes. Pioneer III was tracked as it re-entered the earth's atmosphere, at a speed in excess of 23,000 mph, where it burned up from aerodynamic heating at an estimated altitude of 55 miles above the earth, at 19:51 GMT on December 7, 1958.

Pioneer IV came within 37,300 miles of the moon 41 hours after launch. The probe's transmitter continually radiated an intelligible signal for 82 hours and 6 minutes before its batteries were depleted. At the time of the batteries' exhaustion, the probe was more than 407,000 miles from the earth and being tracked by the 85-foot dish of the JPL Goldstone tracking station. Pioneer IV is now in a heliocentric orbit having a perihelion of 91.7 million miles, an aphelion of 106.1 million miles, a period of 394.75 days, and an indefinite orbital life.

Telemetry data from Pioneer IV indicated that 11 hours and 20 minutes after launch, the payload's rotational speed was reduced from 420 to 11 rpm, indicating action of the despin mechanism.

The light sensor which was to have been triggered by reflected light from the moon was not triggered since it was designed to work at a maximum range of 20,000 miles.

After launch, as the payload moved out of the shadow of the earth, the temperature very rapidly reached its

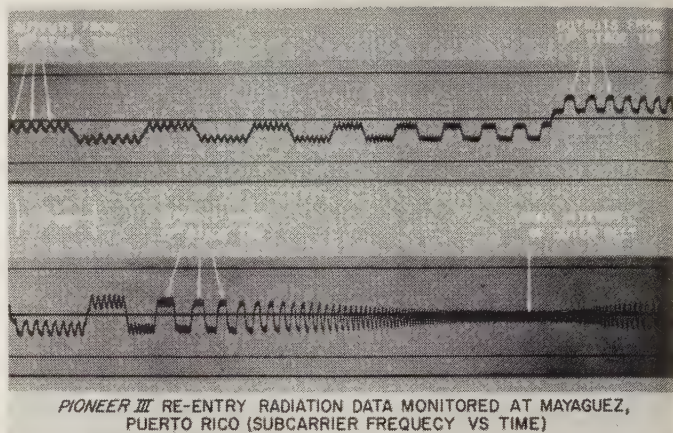


Fig. 9—Pioneer III radiation data as monitored at Puerto Rico.

steady-state value. For Pioneer III, the value so obtained was 38°C, and for Pioneer IV the value was 42°C. The results of these measurements not only verified the payload thermal design but also demonstrated the adequacy of the measurements used to determine radiative properties of the materials involved.

The measurement of high-intensity radiation carried out with the Explorer satellites and Pioneers III and IV was under the direction of Dr. Van Allen. Analyses of the results of these measurements have been made by Dr. Van Allen and his associates and have been reported to the U. S. National Committee for the IGY.<sup>2-4</sup>

At altitudes below about 1000 km, the radiation measurements indicated a cosmic-ray intensity which agreed with extrapolations made on the basis of experiments with high-altitude rockets and balloons. However, using Explorer satellite data above 1000 km, a sudden anomalous increase in cosmic-ray activity was noted.

These observations, begun with the Explorer satellites, were projected to extreme altitudes by the measurements taken on board Pioneers III and IV. A diagram of the probable shape of these two belts is shown in Fig. 10. This diagram shows the trajectory of Pioneer III plotted in geomagnetic coordinates. Counting rates at distinct points along the trajectory are indicated by the contour lines drawn through those points. At low altitudes, these contour lines coincide with those discovered by the Explorer satellites. At high altitudes the contour lines are drawn to fit reasonably the data obtained from Pioneer III. The contour lines in regions not actually traversed by this probe are speculative but are drawn consistent with both

<sup>2</sup> J. A. Van Allen, G. H. Ludwig, E. C. Ray, and C. E. McIlwain, "Observation of High Intensity Radiation by Satellites 1958 Alpha and Gamma," State University of Iowa, Iowa City; May 1, 1958.

<sup>3</sup> J. A. Van Allen, G. H. Ludwig, and C. E. McIlwain, "Radiation Observations with Satellite 1958 Epsilon," State University of Iowa, Iowa City; May, 1958.

<sup>4</sup> J. A. Van Allen, and L. A. Frank, "Survey of Radiation Around the Earth to a Radial Distance of 107,400 Kilometers," State University of Iowa, Iowa City; January, 1959.

## PIONEER III RADIATION SURVEY

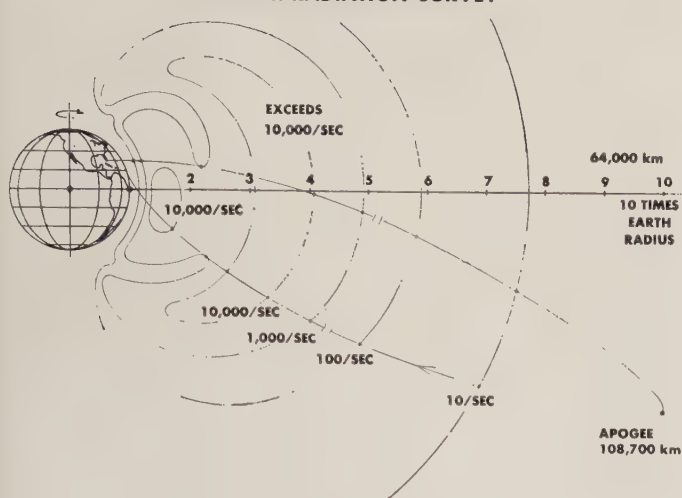


Fig. 10—Van Allen Radiation belts.

the Explorer and Pioneer III data.

Although the peak intensity of both radiation belts encountered by Pioneer IV appears to occur at the same altitudes as those encountered by Pioneer III, the extension of the belt beyond this maximum is quite different for these two probes. For Pioneer III the belt appears to end at an altitude of approximately 60,000 km following a steady decrease in counting rate to an apparent asymptotic value. Beyond that, the counting rate is very nearly

constant. For Pioneer IV, quite different results were obtained. Not only does the belt appear to extend to much greater altitudes, apparently not terminating until an altitude of about 91,000 km is reached, but furthermore, as the edge of the belt is approached, the decrease of radiation is not at all steady. The data taken during the remaining flight of Pioneer IV from the apparent limit of the radiation belt at 91,000 km out to the limit at which radio signals were received—660,000 km—show only minor fluctuations which appear to be within the expectations of statistics.

It must be remembered that the nature and structure of the radiation zones, as represented by the data so far obtained, depend critically upon the nature of the detectors used in the probes. Different detectors sensitive to different energies and types of radiation might give quite different results. A complete picture of radiation activity above the earth's atmosphere can be constructed only when much more detailed observations have been made with additional rocket flights into this most interesting region.

Although all detailed objectives were not achieved, Pioneers III and IV provided much useful scientific and technological information, specifically in the measurement of the Van Allen radiation belts and in the development of advanced communications techniques. Indeed, the lessons learned in the design of the United States' first space vehicle have proven invaluable in the preparation of the next generation of spacecraft.

## Early Orbit Determination Scheme for the Juno Space Vehicle\*

F. KURTZ† AND F. SPEER†

**Summary**—The present status (1959–1960) of the ABMA Early Orbit Determination scheme for the Juno space vehicle is described.

The design of the scheme was essentially influenced by three factors: 1) its origin centered around post flight vehicle analysis; 2) the flexibility required for accepting varied kinds of data; and 3) the potential of high speed computers concentrated in the ABMA Computation Laboratory.

The scheme is outlined and the evaluation techniques used for the various steps of the orbit determination are discussed in detail.

### I. INTRODUCTION

IT IS the purpose of this paper to describe the Army Ballistic Missile Agency (ABMA) orbit determination scheme at its present state of development. Although varying payload missions, modified tracking

instrumentation, and improved techniques are continually changing features of the over-all scheme, the basic philosophy remains.

While there are a number of good and precise methods available for the orbit determination of artificial satellites and space probes (reference is made especially to the highly advanced but specialized Jet Propulsion Laboratory program [1]), the ABMA orbit determination has some distinct features which reflect the missions for which it was designed and the facilities directly available to ABMA.

First, this method was primarily intended to analyze the vehicle performance, and therefore, concentrated essentially on the power flight up to and including injection into orbit. Second, because ABMA lacked substantial orbital tracking instrumentation, it was mandatory to maintain an extreme degree of flexibility and

\* Manuscript received by the PGMIL, February 1, 1960.

† U. S. Army Ballistic Missile Agency, Redstone Arsenal, Huntsville, Ala.



versatility as to kind and format of tracking data to be accepted from other agencies. Third, the unusual potential of advanced electronic computers available in the ABMA Computation Laboratory influenced the scheme.

It is desirable to know about the vehicle performance approximately in real time. Thus, a distinction began to develop between the "Quick Look" and the precision determination of the injection point. It was realized that the Quick Look fulfills all requirements of an early orbit determination scheme, providing information which could be offered to other agencies as the initial point for long term tracking and orbit determination.

The present state of the scheme is characterized by the first generation of satellites with payloads between 20 and 100 pounds. A single miniaturized radio transmitter was all that could be afforded to make these flights worthwhile scientific experiments. The lack of high quality tracking had to be compensated for by masses of lower quality data, which presented a problem even to the fastest and most advanced electronic computers.

Most of the incoming tracking data still consist of range rates (one-way Doppler frequencies), which have a low specific information content and require a very high transmitter frequency stability.

In all flight tests, the programmed flight path is known to a high degree of accuracy. All deviations from this standard flight are due exclusively to unpredictable disturbances. Excluding major failures, these deviations are small enough to permit the application of linear perturbation theory to every step of the orbit determination scheme.

The scheme, consisting of two major phases—the injection phase and the orbital phase—has been successfully applied to five satellite and two lunar probe flights.

The responsibilities and efforts in tracking the Juno space vehicle were somewhat varied. In the beginning the Juno I (Explorer) early orbit determination was carried out as a joint operation of the Jet Propulsion Laboratory (JPL) and ABMA, with the former agency primarily responsible. ABMA efforts were directed to post flight analysis of the vehicle performance, in particular that of the cluster [2]. The early phase of the Juno II orbit determination was characterized by the successful operation of the Goldstone tracking station and the JPL mechanized tracking program.

Beginning with Juno II AM-16, however, the orbit determination task was transferred to ABMA. This necessitated the modification of the post flight analysis scheme into a real time orbit determination. The basic philosophy of the ABMA orbit determination scheme is:

- 1) Utilize tracking during the power flight and the injection phase to the highest possible extent.
- 2) Accept all available kinds of data from as many stations as possible.
- 3) Subdivide the data processing and the correction procedure to best utilize all ABMA high speed computers.

- 4) Complete the initial orbit determination within approximately two orbits and discontinue the operation when sufficiently precise initial conditions are obtained.

## II. EVALUATION SCHEME

The entire orbit determination scheme has been viewed as a continuous process designed to obtain accurate orbital elements and injection conditions at the earliest possible moment. Succeeding phases in the scheme are planned to improve previous results, while remaining as independent as possible of preceding steps. All steps are designed to yield as much information as possible, whether partial or complete with respect to the orbital elements, as an aid to the following correction phases and the interpretation of later data.

There are six time periods which are dictated by the launching sequence of the satellite carrying vehicle: countdown, booster flight, coasting period, cluster flight, early free flight, first orbit. These will be discussed below in connection with the orbit determination scheme which is shown graphically in Fig. 1.

To understand better the six time periods a brief description of the basic vehicles may be useful. The first stage is a modified Redstone or Jupiter missile for Juno I and Juno II, respectively. Both booster vehicles are lengthened from their tactical configurations to permit longer burning times. On top of the booster is an instrumented conical section which houses the flight control equipment, the spatial attitude control and the spin motors for the clustered upper stages. This section separates after booster engine cutoff and coasts to the programmed ignition point of the second stage. It constitutes the attitude controlled launching platform of the upper stages.

The upper stages for both Juno I and Juno II type vehicles are assemblies of scaled down (1/5) solid propellant Sergeant rockets grouped into a spinning cluster. This cluster contains eleven rockets for stage II, three rockets for stage III, and one rocket for stage IV. The burning time for each stage is about six seconds, with short coast periods between the stages.

### A. Countdown

During the countdown all necessary communication lines are opened. It is desirable to have one teletype line to each of the key stations. Additional telephone connections are opened temporarily as emergency links in case of teletype failure. The tracking frequency of the payload transmitter is obtained from Missile Firing Laboratory (MFL), ABMA, and given to all stations at X-60 and X-15 minutes. All stations within this network have, by this time, received specific tracking instructions based on the predicted flight path. A micro-lock station, for instance, obtains elevation, azimuth and frequency increment as a function of time after liftoff. After the liftoff event has been communicated to all stations, a first orbit is calculated entirely on the

Phase of Flight	Source of Information	Location	Information Received ABMA	Results Obtained by ABMA	Time Obtained (After Liftoff)
Countdown	Launching operations	AMR	Liftoff time	Orbit No. 1, based on actual liftoff and pre-calculated trajectory	5 minutes
Booster Flight	ABMA interferometer Booster telemetry FPS—16 radar	AMR (AMR Redstone C. Hatteras AMR	Cutoff conditions	Booster performance (velocity, attitude)	
Coasting Flight	FPS—16 radar and IBM—709 computation	AMR	Stage II ignition conditions	Orbit No. 2, based on actual ignition II and standard cluster flight	15 minutes
Cluster Flight	Microlock stations	AMR Redstone C. Hatteras* Bermuda* Ft. Monmouth Van Buren* Aberdeen	Cluster slant velocity increments	Orbit No. 3, based on actual injection conditions from cluster evaluation	Approximately 90 minutes (depending on data)
Early Free Flight	North Bound: Millstone Hill radar	Westford, Mass.	Payload positions	Orbit No. 4, based on Millstone Hill radar observations or Minitrack data	Approximately 90 minutes (depending on data)
	South Bound: Africa Minitrack	Johannesburg	Meridian, crossing time		
First Orbit Pass	Microlock stations Minitrack stations Goldstone 85-foot dish	Continental U.S. Bermuda San Diego Blossom Point Goldstone	Time of closest approach Time of meridian crossing Payload tracking angles and Doppler	Orbit No. 5, based on period correction from first observed pass Orbit No. 6, based on all observations of first orbit	Approximately 2 hours (depending on orbit) Approximately 3 hours
	Millstone Hill radar	Westford	Payload positions		

\* Mobile stations—present locations given.

Fig. 1—ABMA early orbit determination (Juno II).

basis of the precalculated flight path. This "orbit number one," printed with actual times, is convenient for tracking predictions to the stations in the event of a near standard flight and is important as a basis for search patterns in case no further information is obtained from the satellite.

### B. Booster Flight

The booster serves as the launching platform for the spin stabilized upper stages. All the guidance elements are part of this first stage. Regardless of possible performance variations or meteorological influences, the position, velocity and attitude of the vehicle at the instant of second stage ignition must be very near the precalculated conditions.

For this reason a real time record of the booster flight performance is important. The first stage is conventionally tracked by FPS/16 (C-band) radar (beacon or skin). The radar output is fed directly into the IBM-709 computer as part of the routine Atlantic Missile Range (AMR) launch operations. Originally designed for impact prediction, this setup is also capable of computing position and velocity at any time after cutoff.

A substantial amount of inflight measurements is telemetered from the instrument compartment of the booster to ground receiving stations at Cape Canaveral,

Redstone, and other required locations.

The ground stations have a real time display (brush records) for a dozen or more of the most important telemetry channels. A quick analysis gives answers to the following questions:

Did the booster achieve the predicted velocity?

Was the booster performance normal?

Did separation and other vital mechanical functions occur properly?

Was the attitude properly controlled?

Did the second stage ignite at the right time?

Knowledge of these facts has no immediate effect on orbit calculation other than to give an indication of whether or not booster errors are present. However, it is of great value for the interpretation of later tracking results.

In addition to the AMR radar tracking, there is, for flight safety purposes, an interferometer type tracking system using both the Dovap beacon (74 mc) and the telemeter carrier frequency of the booster. The Doppler slant velocity and two angles are compared with the predicted quantities in real time. Should the AMR radar fail, these tracking results are used for first order corrections of the standard flight to yield approximate conditions at ignition of stage II.



### C. Coasting Period

Since the spin stabilized upper stages are fired into one space-fixed direction, the resulting orbital perigee can never be much higher than the altitude at ignition of stage II. The booster cutoff altitude is much too low to be acceptable as initial perigee. Therefore, a substantial coast period is programmed between booster cutoff and ignition of stage II.

Shortly after cutoff the instrumented part of the booster is separated from the empty thrust unit. Essentially, it follows a vacuum ballistic flight, and, by means of small control nozzles, maintains the proper attitude of the rotating cluster until ignition of stage II. The length of the coasting period depends on the desired orbital shape and trajectory layout.

The most important part of the FPS/16 radar tracking takes place early after cutoff. In most cases, less than one minute of tracking is sufficient to establish reliable initial conditions for the free flight. From these initial conditions, the AMR computer calculates the entire ballistic trajectory of the vehicle. Position coordinates and velocity components may be printed at any desired time.

In most cases, ignition of stage II is given by a preset timer. Consequently, the AMR computer can print ignition conditions shortly after cutoff, even before the ignition event occurs. In cases in which ignition time is not known beforehand, it has to be evaluated from the real time telemeter display and transmitted to the AMR computer.

As soon as ignition conditions are known and found compatible with the telemetered information received, a cluster trajectory and a second orbit (number two) are computed in the evaluation center. In these calculations a standard cluster flight is tied to actual ignition conditions and actual ignition time. "Orbit number two" is very valuable in conjunction with the cluster analysis which follows. If the observed velocity increments of the cluster flight are close to the calculated cluster trajectory, orbit number two is a good approximation of the actual flight and is obtained in a minimum of time. Depending on the availability of ignition conditions, this orbit is complete about twenty minutes after launch.

A last important check during this phase concerns the attitude of the entire vehicle immediately prior to ignition of stage II. Noticeable deviations in either pitch or yaw have to be taken into account in the next evaluation phase, the cluster flight.

### D. Cluster Flight

The cluster flight is the crucial phase of the entire launch operation. A very substantial velocity contribution is imparted to the payload within a very short time, necessitating high load factors. There is only the open loop control of spin stabilization, and very little onboard instrumentation to monitor the behavior of the cluster stages.

Therefore, special efforts have been made to develop a tracking system especially suited for this short but important flight phase. At present, there are a total of seven special microlock tracking stations available, three of which are mobile. The four permanent stations are located at Cape Canaveral, Fla.; Huntsville, Ala.; Fort Monmouth, N. J.; and Aberdeen, Md. (Fig. 2).

The basic tracking principle is spherical velocity tracking (one-way Doppler). Its main disadvantages are the limited stability of the transmitter frequency and data reduction difficulties, while its main advantages are simplicity and good tracking geometry (long base lines).

Since one of the permanent tracking sites, the Redstone station, is physically close to the evaluation center, a real time audio signal reflecting the Doppler shift can be displayed within the evaluation center from this station. This is the first qualitative information received about the general functioning of the upper stages. Any large deviation from standard flight will be evident on this early record, *e.g.*, failure of one stage to fire.

A corresponding arrangement may be made with another microlock tracking station which is closest to the predicted injection point. Here and in Redstone the phase modulated telemeter signals are displayed in real time to permit immediate conclusions concerning certain payload functions, *e.g.*, separation, spin reduction, etc. This information is immediately communicated to the evaluation center.

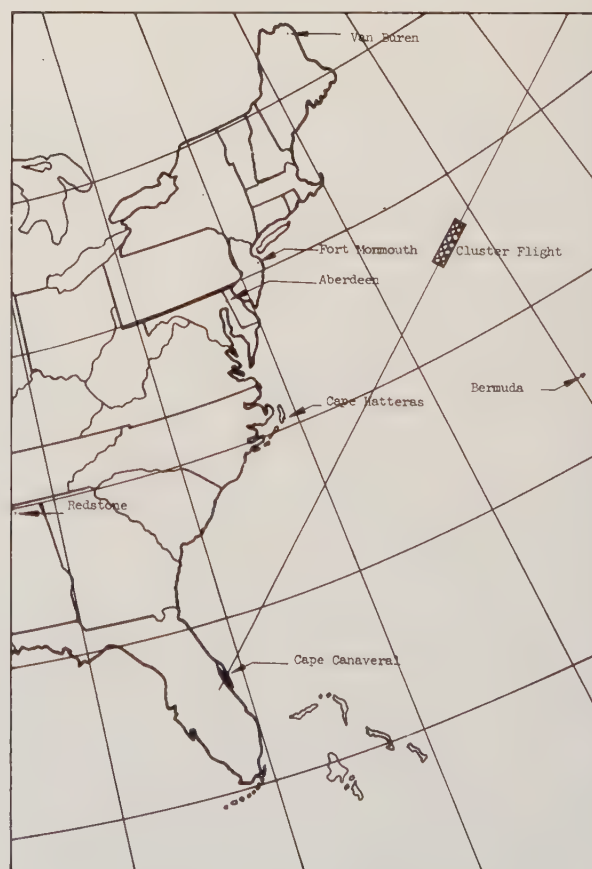


Fig. 2—Cluster station locations.

The Doppler frequencies are received at the evaluation center by teletype in one-second steps and are automatically plotted in order to find qualitative irregularities, *e.g.*, failure of ignition and gross errors. After determining and defining ignition and injection times, respectively, the total frequency difference between these two time points is evaluated and fed into one of the IBM-704 computers. In comparing the predicted increments with those actually measured, the computer performs a number of differential correction steps, modifying the computed trajectory to minimize the error. Since the tracking situation is often rather marginal with respect to signal strength and elevation angle, the possibility of gross errors exists. As excessive errors would considerably damage the least square solution, an automatic sorting process has been designed which eliminates such gross errors.

The final results of the cluster flight phase, both cluster performance and injection point, are printed by the IBM-704. The latter conditions are immediately utilized for running "orbit number three," the first completely "actual" orbit.

At this point the first major step of the early orbit determination is completed. The results should be available approximately sixty minutes after launch. About thirty minutes of this time are required to receive all microlock data.

#### *E. Early Free Flight*

During the early orbit phase additional microlock data is obtained by the East Coast stations tracking the satellite after injection until loss of signal. This information generally has been insufficient to permit an independent orbit determination. However, large deviations in flight path may be detected and the functioning of the payload telemetry can be monitored during this period.

A truly independent and powerful source of orbital information is the Millstone Hill Radar operated by M.I.T. This large radar dish possesses the power and receiver sensitivity necessary to skin track even the relatively small target presented by the Juno II payloads. Millstone is capable of the accuracy necessary to permit determination of complete injection conditions from a short time period of data, the possible tracking period after injection being normally from five to fifteen minutes, depending on the particular mission. The problem of acquisition of the satellite by the radar is a serious one, however, in view of the separation of the missile into several pieces shortly before injection (as the upper stages burn), the smallest and most rapidly moving piece always being the one desired.

The result of the Millstone Hill tracking, "orbit number four," should be available approximately twenty minutes after reception of the complete data message. Therefore, the cluster evaluation and the Millstone Hill determination are processed simultaneously on separate IBM-704 computers. Both results should be available

for comparison at approximately the same time, fifty minutes after liftoff.

If no gross errors are present and the two orbits, numbers three and four, are of comparable quality, the decision as to which one is preferred is postponed until after first pass data become available.

#### *F. Reacquisition*

About one hour elapses between completion of the injection phase evaluation and the first appearance of low-altitude, low-eccentricity orbit satellites over the West Coast. Within this time, path predictions are prepared and communicated to the stations.

The final adjustment of the initial conditions is done in two steps, which may be called the period correction and full correction, respectively. There are several reasons for this peculiarity. The period correction requires only one exact timing of a closest approach or a meridian crossing, preferably in the extreme West of the continent. This time is a fairly accurate measure of the total velocity amount and is comparatively insensitive to position errors and velocity angle deviations. Such an early time can be received and utilized in a special correction process within a very short time, while the satellite is still passing over the continent.

Also, this simple adjustment provides a better basis for the subsequent full correction than the earlier approximation. If, for instance, Doppler frequencies as a function of time are used for the corrections, it is important to have predicted and observed inflection points as closely together as possible.

Finally, from the standpoint of computer efficiency, it is advantageous to run the period correction first. It requires only one additional variational orbit calculation to generate the partial derivative with respect to the total velocity. Omitting this step would necessitate one to three more iterative steps for the full correction, with at least three additional variational orbit calculations for each iteration.

Thus, the period correction is considered important because it saves valuable time, it improves the linearity of partial derivatives with respect to Doppler frequencies, and it offers a superior computational efficiency. The actual input for this special program are the observed times of closest approach or of meridian crossing for any number of stations. The result is a correction coefficient common to all three velocity components at injection (leaving the angles invariable) which is automatically followed by a new orbit computation, "orbit number five."

At this time, sufficient information usually is available to justify an official statement about success or failure of the mission. The main orbital parameters are known within comparatively narrow limits. Good predictions for the following passes can be made to tracking stations all over the world.

The remaining problem is now a more precise determination of injection conditions, not only for orbit



determination, but for assessment of vehicle performance in terms of derivations from the predicted. This is particularly interesting for the performance analysis of the upper stages. The comparatively crude velocity tracking by the microlock stations can be improved considerably if start and end points of the cluster flight are precisely known by other means.

From a computational standpoint the full correction is the most crucial evaluation phase for the following reasons: 1) extreme flexibility in accepting data of all kinds, in every format, and with different weights is required; 2) large amounts of data must be accepted; 3) the highest possible accuracy is required; and 4) computational speed is still an important factor.

The full correction normally used at this stage is a differential correction process applied to the velocity and the two velocity angles at injection. The necessary partial derivatives of the actual observations available for the correction process are obtained by variational orbit calculations for each of the three initial parameters.

The magnitude of the variations which generate the partial derivatives is optimized for each particular flight mission. The choice of correction parameters (velocity amount and two angles) represents at least a relative optimum for the correction process. It is superior to the method of correcting Cartesian velocity components in an arbitrary coordinate system.

The restriction to three unknowns was made after it was found in several actual evaluations that at present the injection position is determined better by the AMR range instrumentation than by orbital observations. Of course, this is to be understood only as a general rule. Exceptions are clearly indicated if C-band radar should fail or if very good power flight tracking from Millstone Hill should be available.

The following types of data are used as input for the correction deck:

- Range (Radar),
- Rate of range (Microlock Doppler),
- Azimuth and elevation (Millstone Hill),
- Hour angle and declination (Goldstone),
- Time of Doppler inflection (Microlock),
- Maximum Doppler slope (Microlock),
- Time of meridian crossing (Minitrack).

The whole correction process includes the computation of a standard orbit, of three variational orbits, the differencing of actual and "standard" observations, the least squares solution, and the printout of the new orbit with all desired orbital parameters. The total time required for this process is twenty minutes (300 observations).

Provided that enough data are available and that the previous evaluation steps have at least partially succeeded, only one full correction is needed for the purposes mentioned above. To check the accuracy a second correction step is added as a matter of routine. In such a

case new partials are always calculated, although there is the option to re-use the previously established partials.

### III. EVALUATION TECHNIQUES

The basic evaluation scheme has been outlined in Section II. In this section the techniques utilized in the scheme will be examined in greater detail. The computation and data handling scheme and its division between manual and machine operations are shown in Fig. 3.

#### A. Powered Phase—Booster and Cluster Flight

1) *Method of Tracking:* The evaluation steps performed during power and coast flight of the booster are described in Section II, B and C. Here the evaluation center serves primarily as the recipient of reduced and interpreted results. The information is important to the orbit scheme, but not a product of the scheme.

The primary function of the evaluation center begins with ignition of the upper stages. The short cluster flight produces a large change in the velocity vector but a relatively small change in position (decreasing the value of angle measurements), and is tracked by utilization of the Doppler shift observed in the signal broadcast by the payload transmitter.

2) *Cluster Doppler Data:* The Doppler effect is an apparent shift in the frequency of a signal, due to the relative motion between the observer and the source. For all practical purposes the frequency shift  $\Delta f$  measured by an observer is

$$\Delta f = (f_r - f_0) = \frac{f_0}{c} \dot{s}$$

$$f_r = f_0 \left( 1 + \frac{\dot{s}}{c} \right) \quad (1)$$

where

- $f_r$  is the absolute frequency received by an observer,
- $f_0$  is the frequency transmitted by the source,
- $c$  is the propagation velocity of electromagnetic waves,
- $\dot{s}$  is the relative velocity between observer and source (small compared with  $c$ ).

The quantity  $\dot{s}$  may be called the slant velocity, the rate of change of the path of the radio signal between observer and source. This path would be a straight line were it not for refraction and reflection phenomena.

In the simplest picture, for a transmitter moving with an instantaneous velocity  $v$ , a given receiver measures by the Doppler shift only a certain component of  $v$ , the component along the line of sight between observer and transmitter.

A schematic plot of received frequency vs time during cluster burning for a typical station is shown in Fig. 4. This plot is typical of the one-way Doppler data obtained during cluster flight. The most significant features of these data are the three steps seen. At the

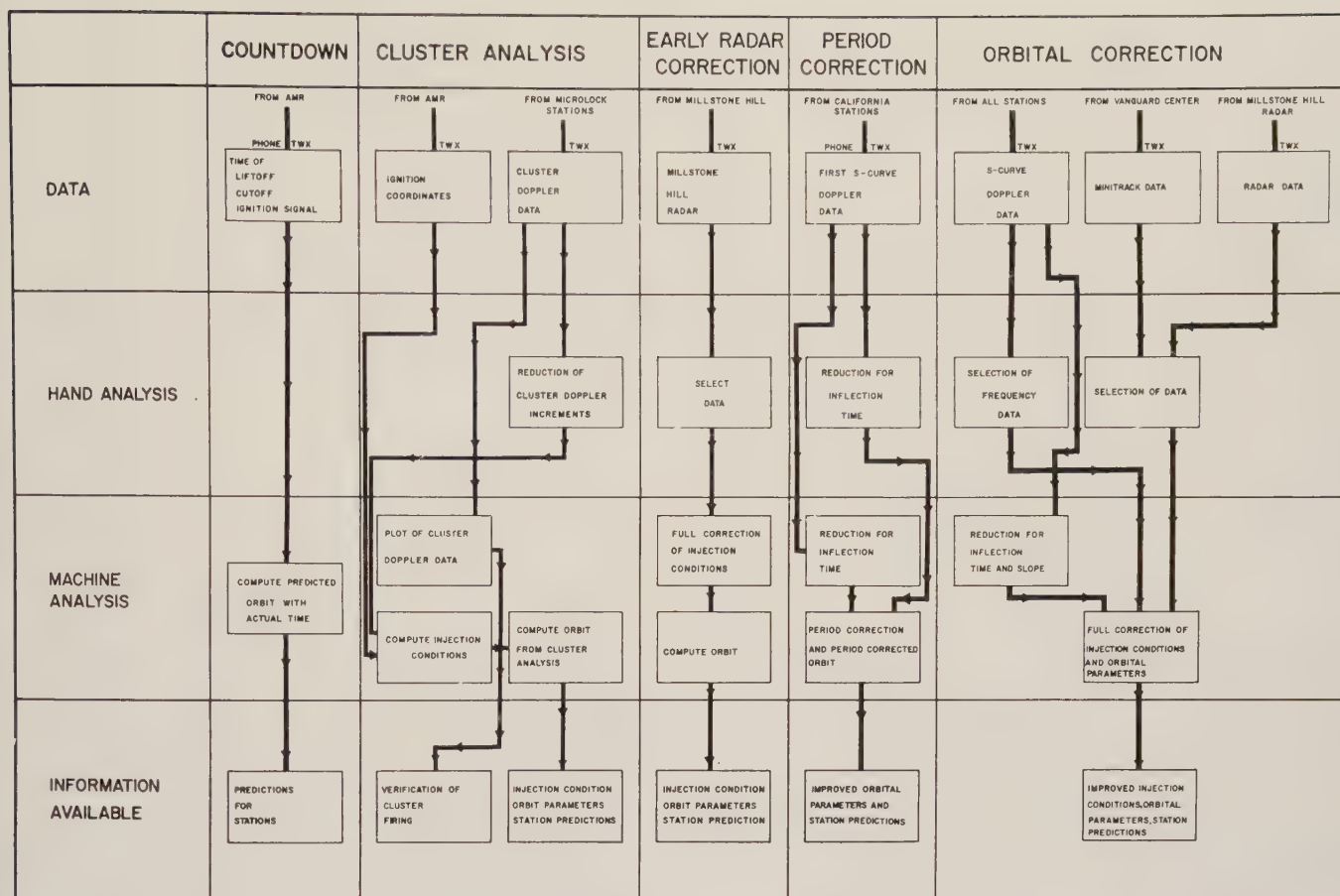


Fig. 3—Cluster and free flight reduction process.

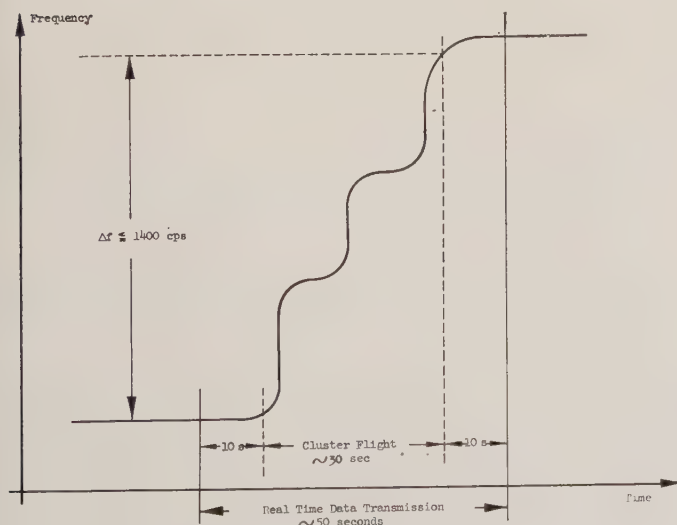


Fig. 4—Cluster Doppler data (108 mc).

ignition time of stage II, the relatively flat frequency function rises steeply as the stage accelerates. The function flattens again during the coast period between burnout of stage II and ignition of stage III, forming the first step. Stage III forms a second step, and stage IV results in a third step.

3) *Data Reduction:* In addition to the simply obtained information concerning firing of the three stages, a more

detailed analysis utilizing the magnitude of the steps in the Doppler shift permits a solution for the coordinate and velocity vectors of the payload at burnout of stage IV. For this purpose, the Doppler shift is measured by the various tracking stations and recorded digitally as a function of time, normally at one-second intervals. This digital information is then transmitted via teletype to the evaluation center.

At the center, the Doppler shift  $\Delta f$  from ignition of stage II until burnout of stage IV is extracted from the data. This extraction is presently performed by hand because of difficulties involving data quality and transmission problems, normally requiring about thirty minutes for the reduction of all data received. It is anticipated that this problem will be handled on the IBM-709 in the near future, reducing reduction time to less than five minutes after reception of data in the evaluation center.

The problems to be solved for machine reduction are severe. The rapid, irregular change in the Doppler frequency during cluster burning combined with low elevation angles and signal levels often causes tracking stations to lose signal lock momentarily, creating gaps or bad points in the data. Special smoothing and extrapolation techniques must be developed to fill in such gaps, as well as variations in data arising from oscillations of the transmitter frequency, shifts in the trans-



mitter frequency, erroneous points, and the normal errors of data transmission.

Further, the Doppler increments must be taken between physically corresponding points. Therefore the ignition point has to be determined individually for each station from the Doppler data, since each station measures time increments very accurately, but errors of up to several seconds arise in the digitally coded absolute time.

For detailed post flight analysis of upper stage performance, the Doppler increment during burning of each stage is extracted and utilized. However, for the early orbit determination it is only necessary to measure the total increment observed during burning of three stages. The reason for this and the principle of the injection point determination follow.

Neglecting refraction, the Doppler shift  $f$  observed by a given station at ignition of stage II is

$$f = \frac{f_0}{c} \dot{s}_{\text{ign}}, \quad (2)$$

where

$$\dot{s}_{\text{ign}} = \frac{\mathbf{r} \cdot \dot{\mathbf{r}}}{|\mathbf{r}|},$$

and  $\mathbf{r}$  is the line of sight vector between the station and transmitter at ignition.

Similarly, the Doppler shift  $f'$  at injection is

$$f' = \frac{f_0}{c} \dot{s}_{\text{inj}}, \quad (3)$$

and the Doppler increment during burning of the upper stages is

$$\delta f = f' - f = \frac{f_0}{c} (\dot{s}_{\text{inj}} - \dot{s}_{\text{ign}}). \quad (4)$$

It is seen that

$$\delta f = F(\mathbf{r}_{\text{inj}}, \dot{\mathbf{r}}_{\text{inj}}) - F(\mathbf{r}_{\text{ign}}, \dot{\mathbf{r}}_{\text{ign}}), \quad (5)$$

where all other parameters may be considered known. However, since the position and velocity of the missile at ignition of stage II are known from range instrumentation, in terms of unknowns the function  $\delta f$  reduces to

$$\delta f = F(\mathbf{r}_{\text{inj}}, \dot{\mathbf{r}}_{\text{inj}}). \quad (6)$$

Since  $\mathbf{r}$  and  $\dot{\mathbf{r}}$  are each three component vectors, the function  $F$  is known, and the quantity  $\delta f$  is measured, there are six unknowns in (6). Given accurate  $\delta f$ 's observed by six stations, it would be possible to solve for  $\mathbf{r}$  and  $\dot{\mathbf{r}}$ .

However, an additional restraint is present since the injection conditions are related to the ignition II conditions by the laws of motion. Thus,

$$F(\mathbf{r}_{\text{inj}}, \dot{\mathbf{r}}_{\text{inj}}) = G(\mathbf{r}_{\text{ign}}, \dot{\mathbf{r}}_{\text{ign}}, I, \alpha, \beta), \quad (7)$$

where  $I$  is the average effective thrust magnitude, and  $\alpha$  and  $\beta$  are the average thrust directions during burning of the stages. The injection conditions are relatively insensitive to the exact time history of  $\alpha$  and  $\beta$ , and to small deviations of  $I$  from the predicted. Hence only the average effective thrust magnitude and the average thrust directions need be considered unknown, while the nominal time history is used.

This is also the reason that only the total Doppler increments during cluster burning are needed for determination of injection conditions, rather than the stage by stage increments required for a more exact flight history.

Thus, (6) reduces to

$$\delta f = G(I, \alpha, \beta). \quad (8)$$

Since there are now only three unknowns, only three observations are required for the solution for  $I$ ,  $\alpha$ , and  $\beta$ . The injection conditions may then be computed from  $\mathbf{r}_{\text{ign}}$ ,  $\dot{\mathbf{r}}_{\text{ign}}$ ,  $I$ ,  $\alpha$ , and  $\beta$ .

It should be understood that  $I$ ,  $\alpha$ , and  $\beta$ , while interpretable in terms of mean deviation of the thrust performance of the total cluster stages as an entity, are only artificial parameters leading to a close estimation of the injection conditions. They in no way represent the true attitude motion or thrust history of the upper stages.

4) *Method of Solution*: The method utilized for the solution for injection conditions is the method of differential corrections, used in connection with a simplified trajectory computation program. Thus it is assumed that

$$\delta f_{\text{observed}} = \delta f_{\text{nominal}} + \frac{\partial f}{\partial \alpha} \delta \alpha + \frac{\partial f}{\partial \beta} \delta \beta + \frac{\partial f}{\partial I} \delta I, \quad (9)$$

where  $\delta f_{\text{nominal}}$  is the value of  $\delta f$  predicted from a nominal trajectory, and  $\delta \alpha$ ,  $\delta \beta$ , and  $\delta I$  are corrections to be applied to the nominal trajectory values  $I$ ,  $\alpha$ , and  $\beta$  to produce  $\delta f_{\text{observed}}$ .

The partials required are obtained by the method of successive perturbations; that is,  $\delta f_{\text{nominal}}$  is calculated from (8),

$$\delta f_{\text{nominal}} = G(I_0, \alpha_0, \beta_0).$$

Then, a perturbed value  $\delta f_{\text{pert}}$  is computed as

$$\delta f_{\text{pert}} = G(I_0, \alpha_0, \beta_0 + \Delta \beta).$$

The desired partial is then taken as

$$\frac{\partial f}{\partial \beta} = \frac{\delta f_{\text{pert}} - \delta f_{\text{nom}}}{\Delta \beta}. \quad (10)$$

Partials are computed similarly for  $I$  and  $\alpha$ . Thus, (9) requires the computation of four trajectories, one nominal and three having perturbations in  $I$ ,  $\alpha$ , and  $\beta$ .

The perturbation sizes  $\Delta \alpha$ ,  $\Delta \beta$ , and  $\Delta I$  for computation of the partials are optimized to obtain the most accurate partials, normally as small as possible without encountering numerical errors. The perturbation sizes

in present use are  $0.1^\circ$  for  $\Delta\alpha$ ,  $0.1^\circ$  for  $\Delta\beta$ , and 0.5 per cent of the nominal thrust for  $I$ .

Because the method of differential corrections is based upon the solution of linear equations, and because the Doppler increment functions being solved are linear only for small deviations, an iterative process must be used. That is, the solution for  $I_1$ ,  $\alpha_1$ , and  $\beta_1$  from a set of equations of the form of (9) are regarded as new  $I_0$ ,  $\alpha_0$ , and  $\beta_0$  for an improved trajectory, the partials are recomputed, and the new equations are solved for  $I_2$ ,  $\alpha_2$ , and  $\beta_2$ . This process is repeated until  $I_n$ ,  $\alpha_n$ ,  $\beta_n$  are sufficiently close to  $I_{n-1}$ ,  $\alpha_{n-1}$ ,  $\beta_{n-1}$ .

It is observed that only three observations producing equations of the form of (9) above are required to solve for injection conditions. If, in addition, the assumption of a nominal effective impulse  $I$  of the upper stages ( $\delta I = 0$ ) were acceptable, only two observations are needed. This is possible if the actual specific impulse of the cluster rockets is nominal, and if the precessional motion of the cluster is small. It should be noted that even though the actual specific impulse of the upper stage rockets is exactly nominal, the artificial impulse  $I$  need not be nominal. This is due to the assumption that  $I$  (and  $\alpha$  and  $\beta$ ) are parameters of a three-stage cluster flight having no change in thrust direction within or between stages. In actual flight, deviations arise generally from precessional motion of the spin stabilized cluster, causing the true thrust direction to be a complex function of time. This results in a loss of effective thrust, or a change in the quantity  $I$ , if the mean thrust directions  $\alpha$  and  $\beta$  are considered. Therefore as a rule three stations are required.

Although only three equations are mathematically sufficient, it is more reliable and accurate to utilize as many observations and as many equations as are available, solving the equations simultaneously by the method of least squares. At the present time, five or six sets of data are generally available.

5) *Elimination of Gross Errors*: One major problem is encountered, however, in this application. The method of least squares assumes a normal error distribution and works best for large quantities of data where the normal distribution may perhaps be expected. Even with numerous data points, however, a few gross errors, of perhaps ten or fifteen sigma level, will completely destroy the least square solution. In the case of the cluster Doppler increments where less than ten observations are available, one gross error is sufficient to spoil the solution.

Of the five Juno I and II missiles to which the method has been fully applied, in all cases a gross error was present in at least one station, for reasons not always fully understood. Therefore, it is necessary to provide a fast and simple means of detecting gross errors. The probability of such gross errors also emphasizes the need for a sufficient redundancy of tracking stations to insure a sufficient number of good observations for a solution.

The detection of gross errors has been achieved in the following way. All data obtained from  $n$  stations are used, and all possible ( $\binom{n}{3}$ ) sets of three-observation solutions are obtained. All the solutions obtained are compared and arranged in groups of solutions which agree within specified limits. It has been found that whereas all combinations of good observations give the same answer within certain limits, different combinations containing the same grossly wrong observation usually give quite different solutions. Thus, the largest group of consistent solutions will normally contain all the good data, while the solutions containing bad data fall in small or single-member groups. A least square solution obtained with all stations appearing in the largest group then has a high degree of reliability.

It will be noted that because three-station solutions are normally required, at least four good observations must be available for the grouping process to work. The method has been found to require no restrictive time expenditure for up to ten sets of data.

Another method commonly used for rejection of gross errors is the least square solution followed by the rejection of all data whose fit to the solution exceeds a certain sigma level. This method was found to be less efficient and reliable than the grouping procedure when less than ten observations were available.

6) *Experimental Results*: The method of cluster flight analysis described above, which is the sole means of tracking the Juno upper stages, has proved quite effective in an extended form for the detailed flight evaluation which follows each space flight. However, certain difficulties have been encountered in its use as a fast real time method.

The principal difficulties experienced thus far have been: 1) the reliability and quality of data received, or more specifically, lack of sufficient tracking stations; 2) stability of the satellite transmitter; and 3) data transmission and reduction difficulties. Sufficient tracking stations are now in operation; the stability of the transmitter has been a serious problem in only one flight, where large frequency shifts were present; rapid data transmission and reduction remain the principal problem.

The problem of data quality may be seen in Table I which summarizes the data experienced on past Juno vehicles beginning with the Juno I vehicle C-29 (Explorer I). The real time method was first applied to Juno I C-44 (Explorer IV).

7) *Optimization of Station Locations*: Three micro-lock stations are mobile and can be placed for best efficiency according to individual flight missions.

The location of tracking stations used in relation to a particular trajectory exhibits strong influence on the results obtained [5]. Possible station locations are limited by consideration of the altitude and range of the cluster flight with respect to the stations. An adequate elevation angle is required to insure acquisition of the payload signal and to minimize refraction effects. New



TABLE I  
CLUSTER TRACKING RESULTS—ERROR IN OBSERVED SLANT VELOCITY INCREMENTS (m/s)

Station	C-29	C-26	C-24	C-44	C-47	AM-11†	AM-14	AM-19B	AM-19A
Aberdeen	—	—	+40	+42	X	X	X	-11	X
Cape Canaveral	-20	+67	-46	-5	-2	-36	+8	-22	?
Fort Monmouth	—	—	-2	-33	-621	—	—	+8	X
Redstone Arsenal	—	—	-29	+38	-3	X	-223	+44	?
Mobile No. 1 (V)	—	—	—	X	X	—	—	-6	X
Mobile No. 2	—	—	—	—	—	-54(M)	+21(G)	+14(B)	X
Mobile No. 3	—	—	—	—	—	-72(F)	+300(F)	-12(C)	X

( ) Location Identification:

B Bermuda  
C Cape Hatteras  
F Fort Stewart  
G Grand Bahama Island  
M Miami  
V Van Buren

† Because of conversion from 960 mc frequency, stations actually measured only 1/18 of indicated error.

— Station not in operation  
X Station failed to track  
? Incomplete solution

sites for the mobile stations are also limited to existing tracking installations for reasons of support and communication.

Within the restrictions mentioned, however, a wide range of geometrical situations exist which strongly affect the accuracy of the solution. A geometrical quality factor may be defined in the following manner.  $N$  simultaneous equations of the forms of (9) can be made to yield solutions of the form

$$\begin{aligned}\delta I &= \sum_N \gamma_{IN} \delta f_N, \\ \delta \alpha &= \sum_N \gamma_{\alpha N} \delta f_N, \\ \delta \beta &= \sum_N \gamma_{\beta N} \delta f_N,\end{aligned}\quad (11)$$

where  $\delta f_N$  is the observed frequency increment for the  $N$ th station, and the  $\gamma$ 's are computed coefficients.

The coefficients  $\gamma$  will be functions such as

$$\gamma_{IN} = \gamma(\mathbf{r}_{ign}, \dot{\mathbf{r}}_{ign}, I_0, \alpha_0, \beta_0, \mathbf{r}_{s1}, \mathbf{r}_{s2}, \dots, \mathbf{r}_{sN}). \quad (12)$$

That is, each coefficient is a function of the upper stage trajectory, defined by the ignition and thrust conditions, and of the coordinates of the  $N$  stations,  $\mathbf{r}_{s1}, \mathbf{r}_{s2}, \dots, \mathbf{r}_{sN}$ .

For a particular trajectory and particular stations, the error  $\epsilon_I$  in the calculated quantity  $\delta I$  is

$$\epsilon_I = \sum_N \gamma_{IN} \epsilon_{fN}, \quad (13)$$

where  $\epsilon_{fN}$  is the error in the observed frequency increment for the  $N$ th station. If the errors  $\epsilon_{fN}$  are normally distributed with a mean error  $\sigma_{fN}$ , the mean error  $\sigma_I$  in  $\delta I$  may be taken as

$$\sigma_I = \sigma_{fN} \sqrt{\sum_N \gamma_{IN}^2} = \sigma_{fN} \Gamma_I. \quad (14)$$

Similar expressions apply for the errors in  $\alpha$  and  $\beta$ .

It is seen then that for any given error  $\sigma_{fN}$  in the observed frequency increments, the errors in the desired quantities  $I$ ,  $\alpha$ , and  $\beta$  are directly dependent upon the coefficients  $\gamma$  and hence upon the trajectory parameters

and station coordinates. Since satellite trajectories are normally determined by stronger factors than improvement of tracking, the trajectory parameters for a given flight must be considered as fixed. However, tracking accuracy may be improved by proper location of stations.

$\Gamma_I$ ,  $\Gamma_\alpha$ , and  $\Gamma_\beta$  may then be taken as geometrical error factors to be minimized by proper selection of station locations. In practice,  $\Gamma_I$  is found to be relatively smaller in physical effect than  $\Gamma_\alpha$  and  $\Gamma_\beta$  by several orders of magnitude, so for convenience an over-all error factor  $\bar{\Gamma}$  may be considered where

$$\bar{\Gamma} = \sqrt{\Gamma_\alpha^2 + \Gamma_\beta^2}. \quad (15)$$

It is also found that  $\bar{\Gamma}$  is little affected by the number of stations  $N$  considered in the solution, being determined essentially by the best three-station sub-group for  $N$  greater than three. Hence it is necessary only to minimize  $\bar{\Gamma}$  for all possible three-station groups. The consideration of three-station combinations is further desirable because of the limited number of stations and the possibility of gross errors in the observations, which make the three- or four-station solution the most probable in the actual event.

The effect of station geometry may be seen in Table II, where the relative error factor  $\bar{\Gamma}$  is given for various station combinations for the trajectory of the Juno II vehicle AM-16. The station locations are shown in Fig. 2, and are identified at the end of Table II. It may be seen that by the inclusion of the Bermuda station, the possible error factor is reduced by a factor of roughly three. This means that with a given observational error, the results obtained with a Bermuda station may be three times as accurate as without; or, to achieve a given accuracy, the observational error may be three times as large with a Bermuda station as without.

No attempt has been made to optimize station locations in the absolute sense; the approach has been rather to choose the best available locations within the limits of other considerations as mentioned previously.

TABLE II  
CLUSTER STATION OPTIMIZATION FOR EXPLORER VII

Stations*	$\bar{\Gamma}^\dagger$	Stations	$\bar{\Gamma}$
VB-RS-BER	31	CH-RS-BRL	99
VB-BRL-BER	32	AMR-RS-FM	100
AMR-VB-BER	35	AMR-RS-BER	107
AMR-FM-BER	45	AMR-RS-BRL	129
RS-FM-BER	52	AMR-CH-RS	157
AMR-BRL-BER	54	CH-VB-BRL	160
CH-FM-BER	58	CH-BRL-FM	269
RS-BRL-BER	75	AMR-BRL-FM	319
CH-BRL-BER	84	VB-RS-BRL	395
CH-RS-FM	88	VB-BRL-FM	564

\* Station Identification:

AMR—Atlantic Missile Range, Fla.

BER—Bermuda.

BRL—Aberdeen, Md.

CH—Cape Hatteras, N. C.

FM—Fort Monmouth, N. J.

RS—Redstone Arsenal, Ala.

VB—Van Buren, Me.

† For explanation of  $\bar{\Gamma}$  see (15).

## B. Orbital Phase

1) *Basic Method*: The basic method utilized throughout the orbital analysis is that of differential correction of the orbital parameters [6]. Beginning with the best orbital characteristics available after the power flight analysis, successive corrections yielding improved parameters are applied, based on the increasing sum of the tracking data available.

The corrections are computed as follows. An orbital computation is assumed available which permits the accurate prediction of the value of any desired observed quantity (e.g., range or elevation angle at some time) to some required accuracy, given the parameters of the orbit  $X_j$ . The observation  $\alpha_i$  is then a function of the orbital parameters  $X_j$ .

$$\alpha_i = \alpha_i(X_j, t). \quad (16)$$

Assuming approximate orbital parameters  $X_j^0$ , an observed quantity  $\alpha_i^{\text{obs}}$  is assumed related to the predicted value  $\alpha_i^{st}$ , where

$$\alpha_i^{st} = \alpha_i(X_j^0),$$

by the Taylor expansion

$$\alpha_i^{\text{obs}} = \alpha_i^{st} + \sum_j \left[ \frac{\partial \alpha_i}{\partial X_j} \right]_{X_j^0} \delta X_j, \quad (17)$$

where  $\delta X_j$  are the corrections to be applied to the  $X_j^0$  to yield improved parameters  $X_j'$  of the true orbit, and higher order terms are neglected.

Because (17) assumes that the observable function  $\alpha$  is linear in each  $X_j$ , which is not true, the  $X_j'$  are improved but not completely correct parameters, and the correction process must be iterated. The  $X_j'$  are used to compute new  $\alpha_i^{st}$  and new  $\partial \alpha_i / \partial X_j$ , and new  $\delta X_j'$  are obtained. This process is repeated until the corrections converge (i.e.,  $\delta X_j \rightarrow 0$ ), and the final parameters obtained are

$$X_j' = X_j^0 + \sum \delta X_j. \quad (18)$$

The correction process does converge for most practical cases, assuming observations of sufficient accuracy and information content, and initial parameters of reasonable nearness to the actual parameters.

The minimum number of observations required to solve for the  $X_j$  is of course  $j_{\text{max}}$ , the number of  $X_j$ 's. Because of the quality and type of data normally obtained, overdetermination becomes a necessity, and the number of observations  $i_{\text{max}}$  used is usually much larger than  $j_{\text{max}}$ . The overdetermined set of linear equations of the form (17) is solved by the method of least squares.

The partials  $\partial \alpha_i / \partial X_j$  are computed by the method of successive perturbations. That is, in addition to the predicted value

$$\alpha_i^{st} = \alpha_i(X_j^0),$$

$j_{\text{max}}$  perturbed values  $\alpha_i^{st}$  are computed for each  $\alpha_i$ ,

$$\alpha_i^{st} = \alpha_i(X_1, X_2, \dots, X_j + \Delta X_j, \dots, X_{j_{\text{max}}}).$$

The partials are then approximated as

$$\left[ \frac{\partial \alpha_i}{\partial X_j} \right]_{X_j^0} \cong \frac{\alpha_i^{st} - \alpha_i^{st}}{\Delta X_j}. \quad (19)$$

The size of the perturbations  $\Delta X_j$  must be chosen correctly to obtain the most accurate partials, normally as small as possible without encountering numerical difficulties.

The perturbation sizes must be optimized according to the parameters chosen for correction and the data used for the correction. For larger perturbation sizes the partials change value rapidly due to the invalidity of (19). For very small perturbation sizes, the partials again change value due to round off in the numerical calculations.

An alternative method is to obtain approximate analytic expressions for the partials as a function of the time of observation and initial parameters. The method of successive perturbations, while in some cases more time consuming than the use of analytic expressions (since it requires the computation of  $j_{\text{max}} + 1$  orbits), was chosen because of its flexibility in accepting varied data types, and its relative simplicity in development and programming.

2) *Orbital Parameters*: The orbital parameters chosen for correction are the coordinates and velocity of the satellite at some time after completion of all thrust, defined as the orbital injection point. The reason for this choice lies in the connection of the orbital determination with the power flight analysis and in the mission of evaluation of vehicle performance. The system chosen may be immediately interpreted in terms of missile performance, and this interpretation in turn permits a physical feeling for the reality of results indicated by the orbital correction scheme.

Also, in all cases except the early orbit correction with radar data [Section III, B, 3)], it has been found advantageous to solve for only the velocity vector, the



injection coordinates being more accurately determined from the power flight analysis than from orbital data. This point is covered more thoroughly in Section III, B, 5 concerning the final orbital phase.

The specific injection quantities chosen are the Cartesian coordinates of the satellite at injection in an earth-fixed system with origin at the center of the earth, the magnitude of the earth-fixed velocity at injection and the elevation and azimuth angles of this velocity vector. This system of coordinates is denoted as the perturbation system. An error in velocity elevation  $\epsilon$  corresponds roughly in missile terminology to an error in the local pitch velocity angle, and an error in the velocity azimuth angle  $\alpha$  to the missile yaw velocity angle.

While the above system of coordinates has not been optimized, it has proven convenient, satisfactory, and at least a relative optimum in comparison with some other systems. For instance, if the same correction utilizing Doppler data from five stations during one revolution of a satellite in an Explorer VII type orbit is made in the perturbation system just described and in a completely Cartesian system (space-fixed Ephemeris system), the following results shown in Table III are obtained.

TABLE III  
COMPARISON OF CORRECTION CONVERGENCE (ERROR  
REMAINING AFTER ONE CORRECTION)

Correction in Perturbation System	Correction in Ephemeris System	Results in Ephemeris System Transformed to Perturbation System
V 0.1 m/sec $\alpha$ 0.03 deg $\epsilon$ 0.00 deg	$\dot{X}$ 10.8 m/sec $\dot{Y}$ 20.3 m/sec $\dot{Z}$ 16.4 m/sec	V 2.6 m/sec $\alpha$ 0.22 deg $\epsilon$ 0.03 deg

It may be seen that making the correction in the perturbation system affords a larger initial correction, and hence more rapid convergence of the correction process. Ninety-nine per cent of the initial injection error is removed in one iteration in the perturbation system, while two or three iterations are required in the Ephemeris system.

While for practical purposes the same ultimate accuracy is obtained in either system, the correction process performs more efficiently (more rapid convergence) in the perturbation system. The general conclusion is that the relation between orbital parameters and observations is more nearly satisfied by the linear equations used if the coordinate system is properly chosen. Work is now in progress for determining an absolute optimum coordinate system for given circumstances.

3) *Early Orbit Phase:* During the early orbit phase the Doppler data acquired is generally insufficient for a complete orbit determination. When used, the Doppler is treated by the normal processes described in Section III, C, 1).

The data obtained by Millstone Hill Radar, if the

acquisition problem is solved, requires special treatment, however. The possible tracking period after injection varies from five to fifteen minutes.

The data is supplied in the form of range, azimuth, and elevation. The data is smoothed by Millstone before transmission to the evaluation center, and has an estimated residual error of 8 km in range and  $0.2^\circ$  in the angles.

Radar acquisition during power flight is complicated by a number of separation events during the staging process. The smaller and faster vehicle part has to be skin tracked after each separation. Therefore, it is rather important to provide Millstone Hill with precise acquisition instructions prior to each flight.

Once the payload is acquired, the data processing and transmission via teletype is automatic. The data message is to be expected about fifteen minutes after loss of skin track. At ABMA, the perforated teletype tape is fed into a tape-to-IBM-card converter. The cards are used as input for the orbit correction deck, using orbit number two as an initial estimate. All six parameters of the injection point (position and velocity components) are corrected simultaneously. This is preferable because the complete angle and range data obtained immediately after injection determine both position and velocity. For a typical satellite such as Explorer VII, 5.5 minutes of Millstone data beginning at the injection point will determine the injection point within 2 km in coordinates, 10 m/sec in velocity magnitude, and  $0.15^\circ$  in the direction of the velocity vector.

After loss of signal by the tracking stations on the western edge of the Atlantic, normally no further information is available to the evaluation center until the satellite again approaches the United States at the completion of its first orbit. The silent period has a duration of approximately sixty to ninety minutes.

Predictions are computed for the first orbital pass for all stations in the form needed, based on the most accurate and reliable parameters then available from the evaluation scheme. Predictions to microlock stations equipped with omnidirectional antennas consist of predicted crossover time only, and are sent manually. Predictions to stations requiring more detailed information, as, for instance, antenna pointing angles as a function of time, are sent through a mechanized scheme. The IBM-704 computer punches the predicted data required (e.g., time, hour angle and declination for the Goldstone dish) into IBM cards, which are then converted to punched teletype tape and automatically transmitted.

4) *Reacquisition Phase:* The end of the silent phase occurs when the signal of the satellite is received by the westernmost station tied into the tracking net, generally located in southern California. This initial reacquisition confirms that the satellite is in orbit and that the transmitter is still functioning properly. The first station to reacquire is followed rapidly by other stations located in the southwestern United States.

In addition to simple verification of orbit, a refine-

ment of orbital parameters may occur immediately during the reacquisition phase. Comparison of actual signal acquisition times with those predicted from the launch and early orbit tracking reveals the accuracy of earlier information. Should early results be in error, considerable improvement may be obtained without awaiting the transmission of complete tracking data. This improvement is obtained by use of the inflection time of the Doppler curve recorded by the first microlock stations, or the time of meridian crossing in the case of minitrack stations, to determine the injection velocity magnitude. The inflection and meridian crossing times are quantities which may be obtained quickly and simply with fair accuracy at the tracking stations. They require the transmission of one number only, a time, rather than a mass of data. The time elapse between injection into orbit and the inflection time or meridian crossing for a given station is primarily a measure of the injection velocity magnitude, being relatively insensitive to small velocity angle errors.

Thus, for the Explorer VII orbit, an error of 3.6 m/sec in velocity magnitude would cause a shift of 10 seconds in the inflection time for the Goldstone station, while an error of  $6.7^\circ$  in velocity pitch angle or  $1.3^\circ$  in yaw angle would be required for the same shift.

The correction for the velocity magnitude (called for historic reasons a period correction) is accomplished by the differential correction procedure described previously, solving for the one unknown with one or more observed times, inflection or meridian crossings, or a combination of both. The method of averages is used whereby the velocities indicated by each observation are averaged, and the average taken as the result. The methods of averages and of least squares are essentially equivalent in this particular case of few observations and nearly identical partials, and the method of averages was chosen only for computational simplicity.

The accuracy of the rough observed times which are quickly available varies greatly according to individual circumstances. If, however, one inflection time is used with an accuracy of perhaps 5 seconds and the injection velocity angle deviations are small ( $<1.0^\circ$ ), the velocity magnitude may usually be determined within 5 m/sec.

5) *Final Orbital Phase:* As the orbiting satellite crosses the continental United States, the major portion of the data available for early orbit determination is acquired. One or two revolutions across the United States normally yield sufficient data for an orbit for vehicle evaluation and tracking acquisition purposes, independent of results of the early evaluation phases.

In the final orbital phase, all data available are used in a full differential correction of injection conditions. The parameters corrected are normally chosen as the magnitude and direction of the injection velocity vector. Again the injection coordinates are not corrected because they are nearly always determined more accurately from the power flight analysis. The velocity vector is less well determined in the power flight analysis, and

its determination is more sensitive than that of the coordinates to partial failure of the early phases of the evaluation process. Further, the orbital data obtained two or more hours after injection, particularly the Doppler data, are relatively insensitive to variations of injection position of the magnitude of a few kilometers.

Thus, utilizing Doppler frequency data from five stations on the first pass, and assuming a standard deviation of 10 cps in the data, the average standard deviation in the resulting injection coordinates is about 10 km. The estimated average error for the injection coordinates from the power flight analysis is only 5 km.

Two practical advantages are also gained by restricting the correction to the velocity vector alone. One is computing time saved by elimination of the calculation of the three orbital trajectories necessary for the partial derivatives in the method of successive perturbations. The second advantage is increased stability and more rapid convergence of the correction due to elimination of the less sensitive parameters.

The majority of the data received in the orbital phase is Doppler frequency, although angle data from Goldstone are now available on 108 and 960 mc, and radar data (angles and range) are available from Millstone Hill if acquisition is achieved. The techniques used with the Doppler data will be treated first.

### C. Orbital Data Techniques

1) *Doppler Data:* The Doppler data received by a tracking station during the passage of an orbiting satellite is commonly known as an S curve, from the characteristic shape the frequency function takes. Fig. 5 shows a plot of a typical set of orbital Doppler data.

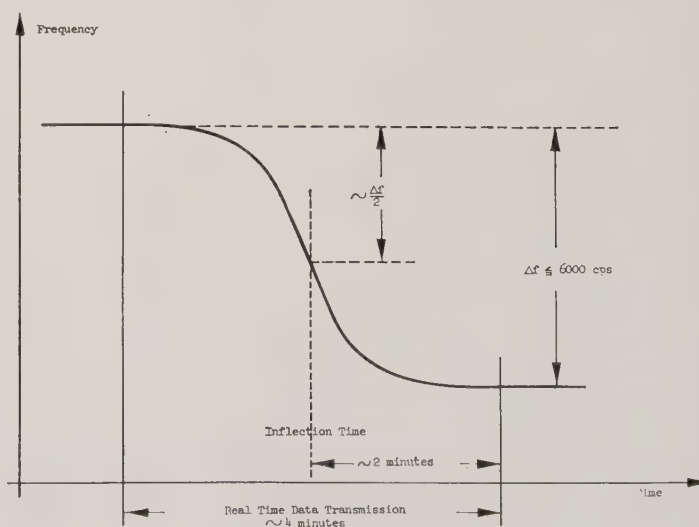


Fig. 5—Orbital Doppler data (108 mc).

Two basic approaches exist for utilization of Doppler orbital pass data. The first consists of smoothing the Doppler S curve and extracting a few characteristic quantities, usually taken as the inflection time and inflection (maximum) slope of the curve, which are then



used in the differential correction process. The second and preferred approach uses the raw Doppler frequency as a function of time, smoothed or unsmoothed, directly in the correction program.

a) *Inflection time and slope*: The first approach, extraction of inflection time and slope, has a decided advantage for use in the period correction as described in Section III, B, 4). For full correction purposes, the advantages of the use of time and slope lie in part in the convenience of dealing with two data points per crossing, rather than a larger number of frequencies. Also advantageous is the strong effective smoothing resulting from the extraction of only two quantities from the entire pass, enabling the use of poor data. The disadvantages are the loss of some of the information content of the complete *S* curve (discussed below), the length of time required to obtain highly accurate times and slopes, and the requirement of having Doppler data both before and after the inflection time in order to achieve accuracy.

The simplest manner of obtaining the inflection time and slope from a Doppler curve consists of plotting the first differences of the Doppler frequency points (see Fig. 6). The first differences, of course, reach a maximum at the inflection time. The inflection slope may then be read as the ordinate of the maximum of the first difference curve.

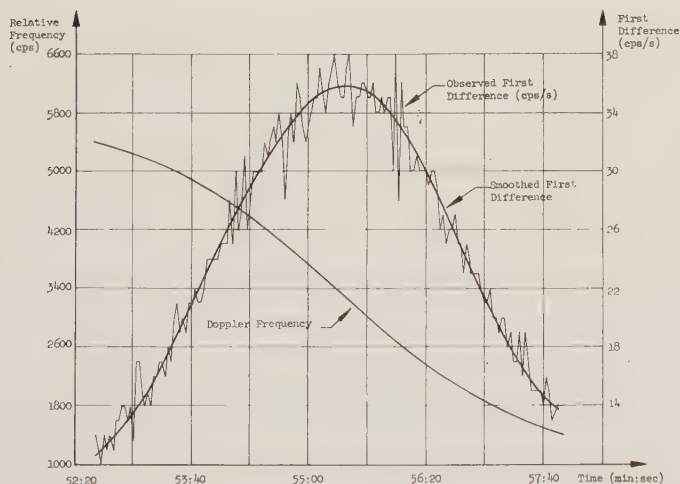


Fig. 6—First differences of orbital Doppler data.

The difficulty encountered in this method is also seen in Fig. 6. If the Doppler frequencies have much dispersion, the maximum of the first difference curve becomes difficult to ascertain by inspection, on both the ordinate and abscissa. Also as the sharpness of the first difference peak is largely a function of the magnitude of the inflection slope, which in turn is largely a measure of the close-approach distance from satellite to tracking station, the inflection time may be read accurately only on data from fairly close passes.

The above difficulties limit the accuracy of this

method, particularly under real time operating conditions; however, its simplicity and relative speed are advantages. This method is used for evaluation of the first passes received at initial reacquisition (see Section III, B, 4) for period correction purposes, for evaluation of early results, and as a first step for the more exact determination. The accuracy attained under normal conditions is  $\pm 5$  seconds for inflection time and  $\pm 2$  cps/sec for inflection slope. The time required for manually processing one *S* curve by the first difference method is approximately 5 minutes for a two-man team; a similar rough reduction performed by two men utilizing a small digital computer is slightly faster.

Other simple methods, e.g., utilizing the approximately skewsymmetric properties of most *S* curves to find the symmetry point, have been investigated, but found less reliable and generally less accurate than the first difference approach.

For accurate early orbit determination with inflection times and slopes, where only a limited number of *S* curves are available, it is necessary to extract more exact data from the curves. This is achieved by fitting a least squares polynomial to the raw Doppler data, and obtaining the inflection time and slope of the polynomial.

The procedure followed for the polynomial fitting begins with the manual determination of rough inflection time as described above. Simultaneously with the rough determination, the punched teletype tape containing the Doppler data is converted to punched cards for input to the IBM-704 computer, one time point to the card. Data cards covering a time period of between 90 and 180 seconds centered about the rough inflection time are selected, rapidly scanned for gross transmission and punching errors, and fed to the IBM-704 computer. The computer fits an  $n$  degree (normally third degree) polynomial to the input data in the sense of least squares, yielding as output the smoothed frequency values, the inflection time and slope of the fitted polynomial, and the standard deviation of the raw data from the polynomial. If the standard deviation of the data exceeds a specified input value, raw data points are removed from each end of the *S* curve (reducing the length of time coverage). The fitting process is then repeated until the standard deviation of the fit falls below the specified limit, or until the total number of data points being fitted is reduced to a specified minimum. Normally a standard deviation of 15 cps and a minimum of thirty seconds of data is required.

The reduction of the number of data points being fitted is desirable for two reasons; one inherent in the method, the other a product of observational inaccuracy. The first and primary reason is brought about by the normal use of a third-degree polynomial. This polynomial has been determined to approximate best the center portion of typical *S* curves; however, the total amount of the curve that can be successfully fitted by a third-degree polynomial depends (primarily) upon

the steepness or maximum slope. Thus for steep curves (close passes), only the central region of the curve can be fitted, while for more moderate slopes, a wider region can be successfully covered. To insure maximum accuracy, the intent is to fit the maximum amount of raw data compatible with the required degree of the polynomial and a required precision of fit.

The second reason for the reduction in points fitted is to eliminate points of large dispersion, which normally occur primarily on the outer limbs of the curve.

Through the least squares fitting process, an accuracy of 1.0 second in inflection time and  $\pm 0.3$  cps/sec in inflection slope may be obtained for average data. Five passes on one crossing of the United States, reduced to this accuracy, are sufficient for an injection point determination of 1 m/sec in velocity and  $0.3^\circ$  in direction, for an orbit like that of Explorer VII.

Although accuracy is gained by the least square fitting process, it is at considerable expense of time, as well as loss of information. Since only the central portion of the  $S$  curve is fitted, and only two quantities extracted from this fit, any further information content of the total  $S$  curve is discarded.

The possibility of using the third characteristic of the polynomial (second derivative of the frequencies) was discarded because it would involve an impractical amount of computation.

b) *Direct use of Doppler frequency:* The second approach to the use of Doppler  $S$  curves requires the use of the raw frequency differences (as defined below) as a function of time directly in the differential correction procedures, and affords a considerable gain in efficiency and accuracy.

Thus the same five passes on one crossing of the United States used as an example above yield an accuracy of 0.2 m/sec in velocity magnitude and  $0.06^\circ$  in velocity direction when the direct use of frequency is made, assuming a standard deviation of  $\pm 10$  cps in all data. This accuracy is five times better than that obtained from the same data with inflection times and slopes.

Two difficulties are encountered in the direct use of raw Doppler data. Many microlock stations are not equipped to determine accurately and quickly the true frequency they are receiving, but obtain easily only the so-called VCO or "beat" frequency. This frequency exhibits the same shifts as a function of time as the true received frequency (assuming no local equipment shifts), and differs from the received frequency only by some constant additive factor, a function of the reference oscillator frequencies of the station.

While some stations are equipped to accurately determine this factor, little is gained for tracking purposes by doing so because of the following second difficulty. The instability of most Juno satellite transmitters is such that during injection of the satellite into orbit, when various accelerations and changes in temperature affect the transmitter, the transmitted frequency may

exhibit substantial drifts and shifts. These drifts are usually negligible over a short length of time, but the cumulative effect over an orbit is quite significant.

Thus, the absolute frequency  $f_r$  received by a tracking station is

$$f_r(t) = f_0 + \Delta f(t) + \left( \frac{f_0 + \Delta f(t)}{c} \right) \dot{s}(t) + f_R(t), \quad (20)$$

where

$f_0$  = nominal transmitter frequency (measured before flight),

$\Delta f(t)$  = any drifts occurring in the transmitter frequency since the measurement  $f_0$ ,

$c$  = velocity of light,

$f_R(t)$  = any refraction and other effects, expressed for simplicity as an additive term,

$\dot{s}$  = radial velocity of satellite from station.

Since  $\Delta f(t)$  is an unknown function, this frequency must be compared for the correction process against a computed frequency  $f_c$

$$f_c(t) = f_0 + \left( \frac{f_0}{c} \right) \dot{s}_c(t) + f_{cr}(t). \quad (21)$$

Here  $f_{cr}$  is a computed refraction effect, and  $\dot{s}_c$  is the calculated radial velocity.

Thus, the direct use of  $f_r$ , even if measured by a tracking station, is of little value unless some account is made of the drift term  $\Delta f(t)$ , which is not negligible.

The above two difficulties are largely eliminated in the following manner. Rather than comparing  $f_r(t)$  and  $f_c(t)$  in the correction process, the quantities  $\Delta f_r$  and  $\Delta f_c$  are used, where

$$\begin{aligned} \Delta f_r(t) &= f_r(t) - f_r(t') \\ &= [\Delta f(t) - \Delta f(t')] + \left[ \frac{\Delta f(t)\dot{s}(t) - \Delta f(t')\dot{s}(t')}{c} \right] \\ &\quad + \frac{f_0}{c} [\dot{s}(t) - \dot{s}(t')] + [f_R(t) - f_R(t')], \end{aligned} \quad (22)$$

$$\Delta f_c(t) = \frac{f_0}{c} [\dot{s}_c(t) - \dot{s}_c(t')] + [f_{cr}(t) - f_{cr}(t')]. \quad (23)$$

The first bracket on the right of (22) is negligible if  $t'$  is sufficiently close to  $t$  [ $\Delta f(t) - \Delta f(t') \rightarrow 0$ ]. The second bracket on the right of (22) is usually negligible in comparison with the third bracket on the right. Neglecting these two brackets in (22),  $\Delta f_r$  and  $\Delta f_c$  are seen to be directly comparable.

Practically, the procedure above amounts to performing the correction not with the true Doppler frequency, but with the change in Doppler frequency occurring after some arbitrary reference time. In this manner the effect of all drifts in transmitter frequency occurring before the reference time is minimized, and



only the VCO frequency need be measured by tracking stations.

One further difficulty is now encountered in the use of frequencies in this manner. The function  $\Delta f_r$  is nearly constant for times more than one minute before or after the inflection time of the  $S$  curve, since the  $S$  curve becomes nearly flat on the outer limbs. The frequency data used is of course centered about the observed inflection time. If the observed and calculated (based on the approximate parameters being corrected) inflection times differ by more than one minute, the  $\Delta f_c$  function, calculated at the observed times, is almost constant, and the partial derivatives of  $\Delta f_c$  with respect to the parameters are almost zero. The correction process converges slowly and poorly.

This problem is eliminated through use of the period correction, which insures that observed and calculated inflection times agree within a few seconds. Under this condition the observed and calculated  $S$  curves have a close overlap, and the correction process performs efficiently.

Utilizing the above principles, the frequency correction data is utilized in the following manner. From each available  $S$  curve, frequency points are chosen centered about the observed inflection time and covering a total time span of about  $\pm 60$  seconds. The exact time span used is chosen according to characteristics of the satellite pass over the station, primarily in consideration of refraction effects. The data sampling rate during the time span is roughly one frequency every eight to ten seconds, leading to a total number of about fifteen frequencies per  $S$  curve. These frequencies are then used as input to the correction desk, where the first time point of each  $S$  curve is regarded as the reference point for the curve and the change in frequency from this time point is utilized for the correction.

The refraction correction  $f_{cr}$ , shown for simplicity as an additive term in (21) above, is not at present included in the correction process. If only data received at elevation angles greater than ten degrees are used, refraction effects are generally small, and are neglected. The time span of the data used from a given  $S$  curve is chosen, therefore, to enforce the condition that the elevation angle at reception of all time points used be greater than ten degrees. Depending upon the relative geometry of station and orbit, this criterion results in the use of data from one to two minutes on either side of the inflection point. No more than two minutes is normally used even if the elevation angle is satisfactory. The time span, which may usually be determined in a general manner and within sufficient limits for a given station from the predicted orbit, imposes no large demand on the data handling scheme.

The majority of the Doppler frequency data received at the evaluation center is not transmitted by automatic electronic readout, but manually by teletype operators.

Because of the resulting variations in data and format, automatic data handling equipment is at present used only partially in processing the data. Automatic conversion from teletype tape to punched cards is performed where possible in the curve-fitting procedure for inflection time and slope, since a mass of frequency data must be fed to the computer for fitting. For direct correction with raw frequency data, the desired sampled frequency points (about fifteen to an  $S$  curve) are extracted manually from the printed teletype messages, and key punched for input to the computer. Since relatively few points are taken from each set of data, little time is lost by this method in comparison to the time required to extract the desired sampled cards from the mass of cards obtained after complete conversion of the teletype tape.

2) *Angle and Range Data:* In the present state of tracking, experience has shown that angle and range data, when available, are much more powerful than one-way Doppler frequency for the purposes of orbit determination. However, the present sources (excluding interferometric angles) of sufficiently accurate angle and range data are limited particularly in real time and at the common satellite frequencies and sizes. For this reason no extensive data scheme is at present in use for these data types. The procedures used are as follows.

Angle and range data are usually received from automatic transmission equipment and hence have uniform format and a minimum of gross data errors. The punched teletype tape is converted to punched cards, and the cards used for input to the correction program. The conversion process is monitored for removal of obvious errors. Before use as input, the data cards are sampled at a rate chosen from consideration of the total data available, the total time period covered, the quantity of other data available, and the capacity of the correction program. The minimum of data judged necessary to obtain representative data samples is used in order to reduce the burden of computation.

Refraction corrections are presently not made, but the data used is limited to that obtained at elevation angles above ten degrees. Any known observational biases may be removed where significant by input to the correction program.

#### BIBLIOGRAPHY

- [1] JPL Space Programs Summary No. 2, NASA, pp. 2-5; April 1, 1959 (Secret).
- [2] F. Kurtz, "Summary of Cluster Deviations," Army Ballistic Missile Agency, DA-TN-36-59; April 15, 1959 (Confidential).
- [3] JPL Space Programs Summary No. 2, NASA, pp. 27-38; April 1, 1959 (Secret).
- [4] JPL Space Programs Summary No. 3, NASA, pp. 27-53; June 1, 1959 (Secret).
- [5] P. Clugston and F. Kurtz, "Optimization of Microlock Station Locations for Cluster Tracking," Army Ballistic Missile Agency, DA-TN-30-59; March 30, 1959.
- [6] R. Zurmühl, "Praktische Mathematik für Ingenieure und Physiker," Springer-Verlag, Berlin, Germany, pp. 238-260; 1953.

# Outlay of Trajectories for the Army's Juno I and Juno II Program\*

O. JEAN†

**Summary**—This paper presents a description of the factors associated with establishing trajectories for the Juno I and Juno II program. It gives a description of the following orbital elements: inclination, eccentricity, semi-major axis, right ascension of the ascending node, argument of perigee, and time of perigee passage. Also included is a detailed description of the trajectory arrangement for the Lunar Probe, and a list of the elliptical characteristics for the Explorer VII trajectory.

THE theoretical possibility of projecting an artificial earth-circling satellite or earth-escape projectile into space has been known for years. The limitation of achieving these goals was a carrier vehicle capable of producing the thrust necessary to obtain orbital velocity.

When the Defense Department announced in the fall of 1957 that the Army was to participate in the scientific program of the International Geophysical Year, the Army had a vehicle available that was capable of projecting a satellite into orbit.

The Army's Jupiter development program had created the need for a re-entry test vehicle. A composite re-entry test vehicle, Jupiter C, had been designed with the capabilities of propelling a scale model of the Jupiter Nose Cone along a 1500 nautical mile trajectory. The Jupiter C test vehicle consisted of three stages, an elongated Redstone booster for the first stage and two high speed, solid propellant stages for Stage II and Stage III. The high speed stages were bundled fast-burning solid propellant rocket motors, 47 inches long and 6 inches in diameter. The second stage had an arrangement of eleven motors and the third stage, three motors. By adding a fourth stage of one motor, the test vehicle had orbital capabilities.

The Juno I program utilized the three solid propellant stages to supplement the velocity of the elongated Redstone booster.

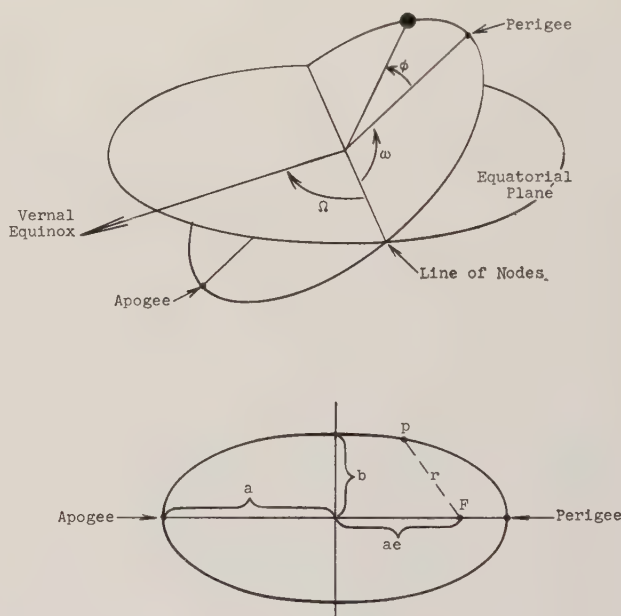
## JUNO I PROGRAM (EARTH-CIRCLING SATELLITES)

One of the first technical problems to be considered in planning an earth satellite project is that of orbit selection. The orbit and motion within the orbit of a satellite can be defined by six values called orbital elements.

- 1) Inclination ( $i$ ): This is the angle between the orbital plane and the equatorial plane.
- 2) Eccentricity ( $e$ ): Defining the shape of the orbit.
- 3) Semi-Major axis ( $a$ ): Defining the size of the orbit.

- 4) Right ascension of the ascending node ( $\Omega$ ): Orienting the orbital plane in the solar system. It is the angle between vernal equinox and the intersection of the orbital and equatorial plane.
- 5) Argument of perigee ( $\omega$ ): Orienting the orbit within the orbital plane. It is the angle measured from the line of nodes to perigee.
- 6) Time of perigee passage ( $\tau$ ): Describing the motion of the satellite in its orbital plane.

Fig. 1 gives the geometry of the characteristic elements.



SCHEMATICS OF THE ELLIPTIC CHARACTERISTICS

Fig. 1—Schematic of the elliptic characteristics:  $e$  = eccentricity;  $a$  = semi-major axis;  $b$  = semi-minor axis;  $p$  = a point on the orbit path;  $F$  = focus;  $r$  = radius vector.

In establishing trajectories up to the point of orbital injection, and the trajectory of the first orbital pass, only three of the above elements need to be considered; these are the elements that affect the performance of the carrier vehicle.

**Inclination:** The satellite travels in the centrally-directed force field of the earth so that the plane of its orbit passes through the center of the earth. Therefore, the path of the probe is a great circle or great ellipse. If the earth were stationary, and disregarding perturbations, the orbit of the probe would geographically reproduce itself on successive revolutions. But due to the rotation of the earth,

\* Manuscript received by the PGMIL, February 2, 1960.

† U. S. Army Ballistic Missile Agency, Redstone Arsenal, Huntsville, Ala.



the satellite orbit will shift westward in longitude for each revolution. Fig. 2 shows the longitudinal shift for Explorer I satellite. The equatorial satellite is an exception. If the period of a satellite orbiting in the equatorial plane has the same period and sense of rotation as the earth's rotational period, the satellite will remain not only in the plane of the equator but will remain over a given longitude.

The inclination of the orbital plane to the equatorial plane is dependent on injection latitude and injection azimuth. The inclination can be computed by a simple rule of spherical trigonometry;

$$\cos i = \sin A_i \cos \phi_i$$

where  $A_i$  is the injection azimuth measured from north and  $\phi_i$  is the injection latitude.

The firing azimuth is so chosen that the largest number of tracking and telemetering stations will be in position to monitor data from the satellite. The firing direction must be selected in a direction such that no habitated land area will be in danger from the propelled phase of the operation. This limits the propelled phase and resulting impact of burnt-out stages to occur over water. From Cape Canaveral a safe azimuth grid is from approximately 40 degrees east from north to 110 degrees east from north. Another consideration in choosing firing direction is the velocity increment gained due to the rotation of the earth. A due east firing from Cape Canaveral gives the satellite an unpaid for increase in velocity of about 410 meters per second. This is approximately 5 per cent of the necessary orbital velocity.

The orbital inclinations obtainable from Cape Canaveral are limited by azimuth and latitude restrictions to about 28.5 degrees to 51 degrees. (For values refer to Juno I and Juno II programs.) Neither a circumpolar nor equa-

torial orbit can be achieved. (An equatorial or polar orbit could be arranged if a "dog-legging" maneuver is introduced. "Dog-legging" is turning the velocity vector due north for a polar orbit or turning into the equatorial plane for an equatorial orbit. This maneuver is very expensive.)

**Semi-Major Axis:** The size of the ellipse is dependent upon the semi-major axis which in turn is dependent upon the amount of energy of the ellipse. The total energy of the ellipse is equal to the kinetic plus potential

$$2E = v^2 - 2gr$$

where  $E$  is the energy per unit mass,  $v$  the velocity at a point ( $P$ ) on the ellipse,  $r$  the distance from center of earth (one focus of the ellipse) to point  $P$ , and  $g$  is the gravitational acceleration at point  $P$ .

The semi-major axis becomes

$$a = \frac{g_0 r_0^2}{2gr - v^2}$$

where the subscript (0) refers to sea level values.

The two important parameters contained in the equation for the semi-major axis are the altitude of injection into the ellipse and the velocity of injection.

**Eccentricity:** The shape of the orbit is defined by the eccentricity of the ellipse. The mathematical equation for expressing eccentricity is

$$e = \sqrt{1 - \frac{b^2}{a^2}}$$

where  $b$  is the semi-minor axis which in turn is equal to

$$\frac{vr \cos \Theta}{\sqrt{2gn - v^2}}$$

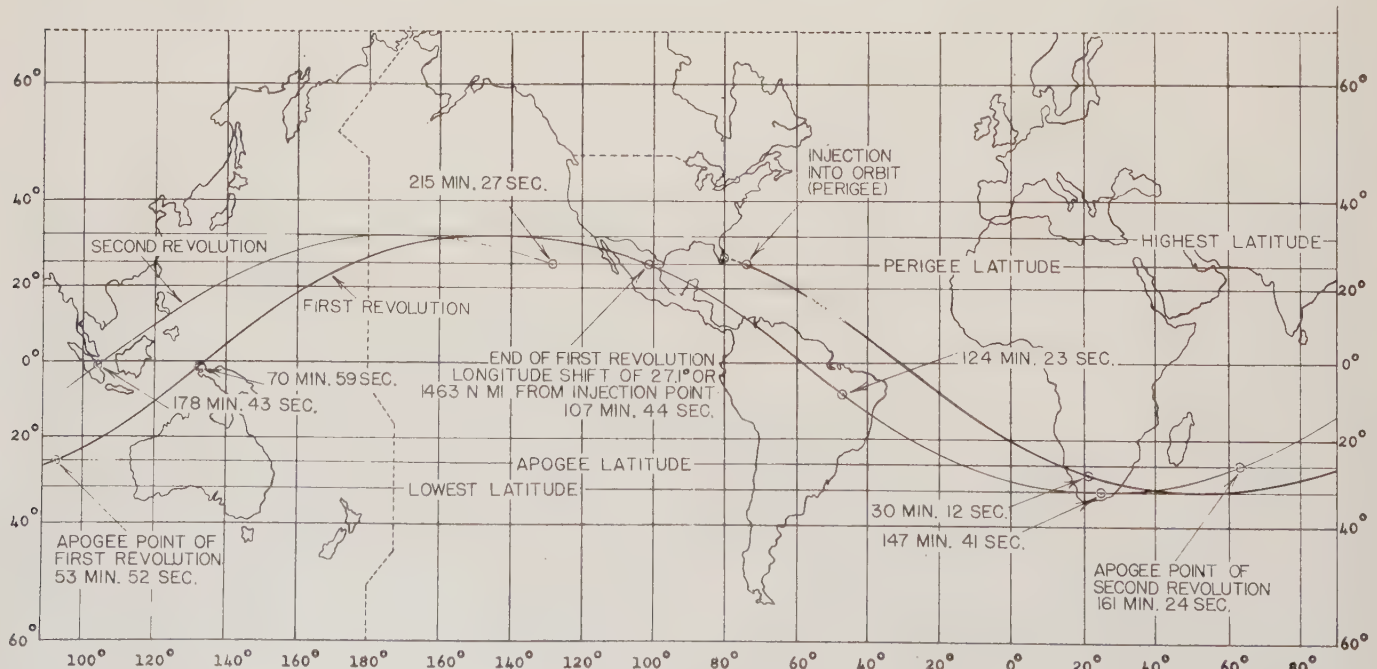


Fig. 2—Projection of orbit on surface of earth. Figures on the orbiter path mark time after injection. Perigee latitude: 25.9 degrees north. Apogee latitude: 25.9 degrees south. Extreme latitude: 34.1 degrees.

$\Theta$  is the angle between the velocity direction at a point on the ellipse and the horizontal to the earth's surface.

The shape of the orbit can range from a circle ( $e = 0$ ) to a parabola ( $e = 1$ ) or hyperbola ( $e > 1$ ) depending on the injection velocity level.

From the eccentricity and semi-major axis, the other dimensions of the ellipse can be computed. The apogee of the ellipse, the point on the ellipse farthest from the center of the earth, is mathematically expressed by  $a(1 + e)$ . Perigee, the closest point to the earth, is equal to  $a(1 - e)$ .

The next step in trajectory preparation is to arrange the propulsion phases so that the prescribed orbital entry conditions can be met.

The first stage trajectory is shaped by initiating a small tilt-over command about 10 seconds after vertical lift-off. The remainder of the first stage trajectory is flown under a no lift condition, allowing only gravity to tilt the missile. After burn-out of the booster, the upper stages are separated and allowed to coast. The stabilization of the coasting stages is done by spin-stabilization. During the coasting period, the cluster configuration is tilted to the attitude which is desired for the upper stages burning period. The final attitude angle of the upper stages is prescribed so that at burn-out of Stage IV the path direction would be horizontal. The upper stages are allowed to coast to near apex of the booster trajectory and are fired to supplement the apsidal velocity. The firing command is given by a pre-set timer.

The following several considerations dictate the choice of injection altitude: the required energy to reach the altitude, errors in velocity magnitude and velocity direction, and satellite lifetime.

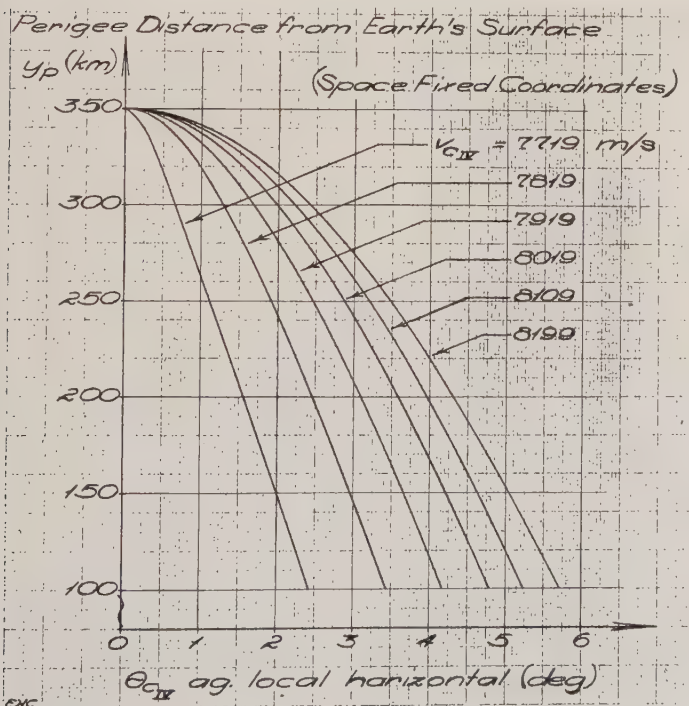


Fig. 3—Perigee altitude as function of injection velocity and injection path angle. Injection altitude 350 km.

The altitude of injection should be high enough so that if an injection path angle error or an error in velocity magnitude should occur, the resulting perigee would be at a sensible altitude, consistent with the desired satellite lifetime.

Fig. 3 shows the effect on perigee of an error in injection path angle for different injection velocities. Fig. 4 shows the effect on apogee of injection errors.

It is interesting to note the sensitivity of perigee to injection path angle errors for near circular velocity ( $v_c = 7695$  meters per second at 350-km altitude).

The trajectories for the Juno I program are laid out with an ample surplus velocity so that in event of either path angle errors or low performance, the satellite would still orbit.

### Explorer I

The trajectory shape for the injection of Explorer I followed the pattern outlined above. The booster was slightly tilted at approximately 10 seconds of flight. The remaining part of first stage tilting was achieved by gravity forces. The booster propellants burned out at approximately 157 seconds. The velocity magnitude was 3210 meters per second measured relative to earth-bound observer and the velocity direction was 51 degrees against the local vertical. The burned out altitude was 100 km above sea level.

During the following free flight period while the missile climbed to an altitude of 350 km, the velocity dropped to 2390 meters per second again measured earth-fixed. A total time period of 394 seconds was spent during first stage burning and coast.

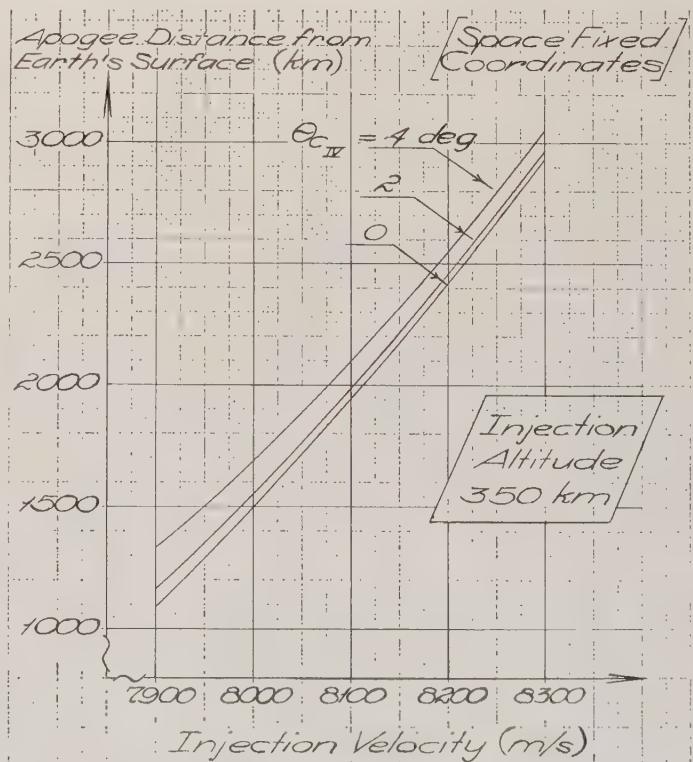
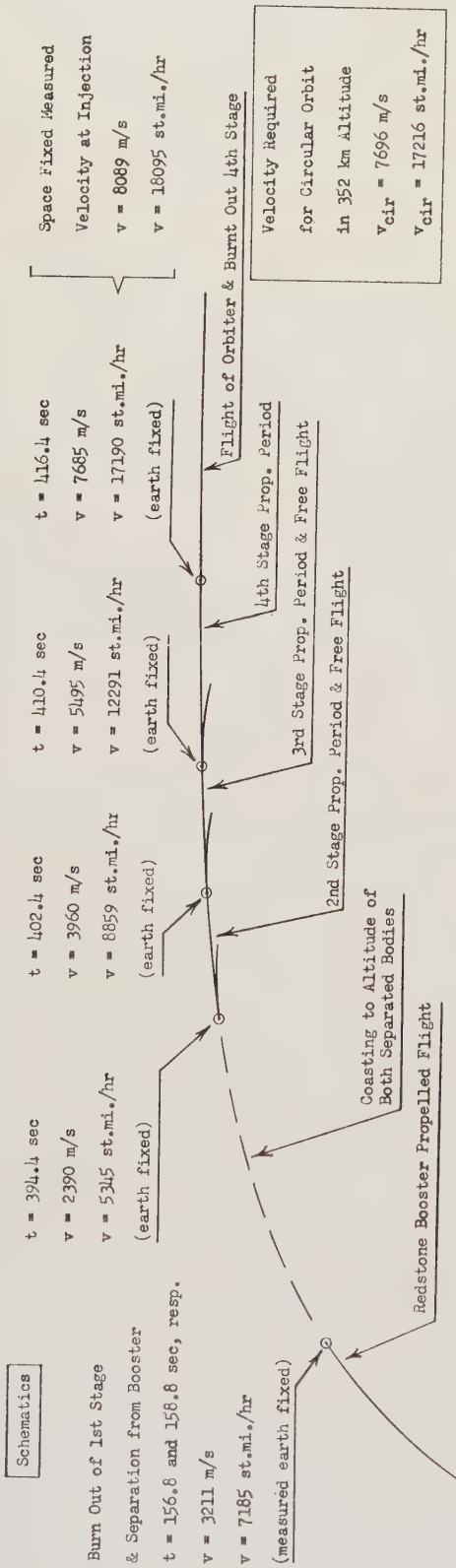


Fig. 4—Apogee altitude as function of injection velocity and injection path angle.





Flight Geometry of Orbiter Injection  
(Altitude and Ground Coverage are at Scale)

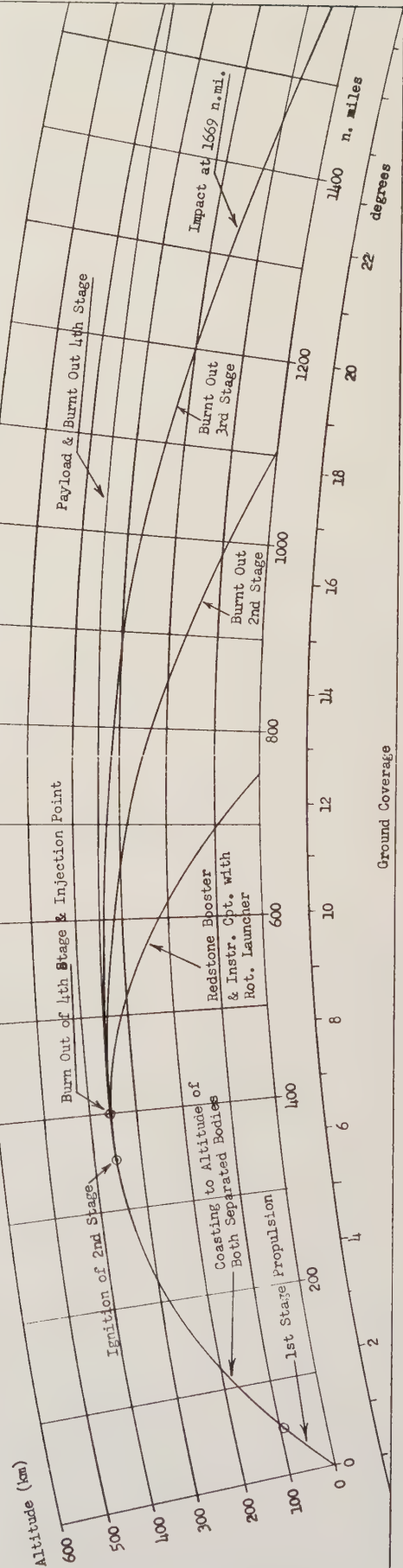


Fig. 5.

At ignition of second stage, the path angle and attitude of the cluster stages was 86.6 and 90.9 degrees respectively against the local vertical. Thus, there was an angle of attack of 4.2 degrees nose down.

During the following burning time of the three solid stages, the path direction approached the space fixed cluster attitude such as to have coincidence of directions at orbit injection, both were there parallel to the horizontal.

The gain in velocity from the three solid stages amounted successively to  $\Delta v_{II} = 1571$  meters per second,  $\Delta v_{III} = 1534$  meters per second,  $\Delta v_{IV} = 2190$  meters per second. The above velocity gains were based on an 18.13 pound payload. The velocity gained by the solid propellant stages plus the initial velocity of 2390 meters per second results in a total velocity at injection of 7685 meters per second understood with respect to earth-fixed coordinates.

The direction of firing of Explorer I was 110 degrees east from north. Adding the earth's rotational component to the earth fixed velocity results in an actual velocity of injection of 8090 meters per second.

As the velocity requirement for a circular orbit at 350-km altitude is 7696 meters per second, the payload enters its orbit with a surplus speed of 393 meters per second. The geometry of flight with respect to earth-fixed coordinates is illustrated in Fig. 5; on the preceding page.

Due to the surplus of 393 meters per second in velocity over local circular velocity, the satellite follows an elliptical flight whose largest distance from the earth's surface is 1900 km (apogee). The perigee is, of course, at the altitude of injection (350 km). The semi-major axis of the ellipse has a length of 75022 km, while the short half axis is 7462-km long, thus, determining the eccentricity to be 0.103. The geometry is presented in Fig. 6.

The period of one revolution is 107.7 minutes.

The inclination of the orbital plane against the equatorial plane is 34 degrees. The path of the orbit over the earth is depicted in Fig. 2.

The trajectory outlay of the remaining Juno II program followed closely the outline above. Table I gives the injection and orbital characteristics of each of the Juno II shots.

Explorer VI

The mission of Explorer VI was to place a 12-foot balloon in orbit. The desired perigee distance was to be at least 750 km. The Jupiter C booster could not launch a satellite into this altitude under the previous described

sequencing. A fifth stage was added to the configuration. The trajectory shape was similar to the previous explorers up to fourth stage cut-off. The fifth stage was not programmed to be fired at this point but it was to coast along the transfer ellipse to apogee and there fired. The resulting perigee altitude of the final orbit would be 750 km.

JUNO II PROGRAM

The Army's Juno II program consisted of earth-circling satellites as well as two lunar probes. Five shots have been attempted to date, two lunar probes and three earth-satellites. Two of the earth satellites shots were unsuccessful and one of the lunar shots was only partially successful.

The booster used in the Juno II program was an elongated Jupiter. The upper stages were again a bundled 11-3-1 arrangement of 6 inch solid propellant rockets.

*Lunar Probe:* To arrange trajectories which terminate at the moon a careful selection of parameters is necessary if one hopes to achieve a collision course. A range of useable parameters can be selected by analyzing the flight geometry that describes the orbit of a lunar probe.

As background knowledge it may be recalled that the ecliptic plane is defined as the plane in which the earth

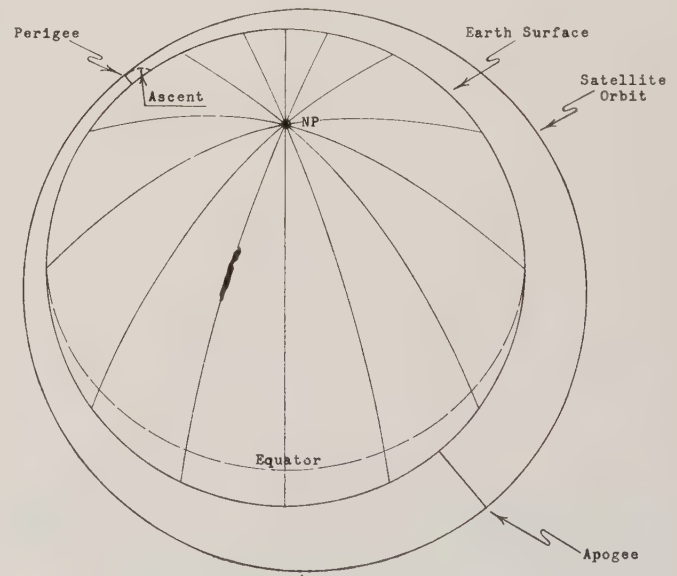


Fig. 6—Geometry of orbital flight. Perigee altitude = 352 km = 218.8 statute miles; perigee velocity = 8089 meters per second = 18,095 statute miles per hour; apogee altitude = 1904 km = 1183 statute miles; apogee velocity = 6573 meters per second = 14,703 statute miles per hour; period of revolution = 107.7 minutes; long-half axis = 7502 km; short-half axis = 7462 km; eccentricity = 0.1034.

TABLE I  
PREDICTED ORBITAL CHARACTERISTICS OF JUNO I SATELLITES

Explorer	Payload Wt. (lb)	Perigee (km)	Apogee (km)	Launch Azimuth	Inclination	Period of Rev. (min)	Eccentricity	Shift In Longitude per Rev.
I & II	18.1	352	1904	110°	34.1°	108	.103	27.1°
III	18.5	352	2043	110°	34°	109	.112	27.4°
IV & V	25.8	287	2984	44°	50.9°	119	.168	29.8°



moves in its orbit about the sun. The earth's equatorial plane shows a nearly constant inclination toward the ecliptic of 23.5 degrees. The earth's polar axis is nearly space-fixed in orientation. The plane of the moon's orbit shows an angle of inclination with the ecliptic of 5 degrees. This celestial system as it appeared at end of 1958 is sketched in Fig. 7.

At the end of 1958, the inclination of the moon's orbital plane to the earth's equatorial plane was 18.5 degrees. The position of the moon above or below the earth equator plane is referred to as declination.

Considering only the Newtonian solution of the two-body problem, neglecting the mass of the moon, the probe flight is planar, with the plane going through the center of the earth. The flight is represented on the celestial sphere by a segment of a great circle, which is determined by the projection on this sphere of the point of injection of the probe into its free flight trajectory and the lunar target.

A series of sketches presented in Fig. 8 show how injection parameters can be bracketed by using the simple Newtonian two-body solution. Launching is assumed to be from Cape Canaveral, latitude 28.5 degrees north while the moon's latitude or declination is the negative 18.5 degrees. The projection of the lunar target location on the earth surface is the "sublunar point." The point diametrically opposite may be called "translunar point." The meridian of the sublunar point is "at noon" with respect to the lunar target; the opposite meridian has "midnight" with

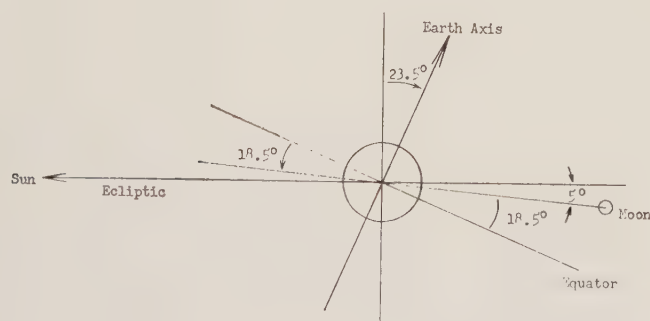
respect to the target location. On the equator we define a scale according to the hours from midnight to noon, which may be coordinated to "hour angles."

Fig. 8 (a) gives the condition of firing from the midnight meridian (the hour angle is zero). The shortest great circle path lies over the north pole, which is indicated by the dashed line, and the flight starts at P (injection point) where the small arrow is attached. The direction of firing is clearly north.

Fig. 8 (b) represents a firing from the same latitude but an hour angle of about 50 degrees from midnight. Here the great circle of the probe flight touches tangentially the latitude of injection which means that the injection occurs with 90 degrees azimuth east from north. Firing at this hour angle consequently gives the largest benefit from the rotation of the earth.

Fig. 8 (c) shows the geometry for a larger hour angle of about 150 degrees (point P). This leads to a much more southerly firing direction. Another situation can also be read from this sketch: The second intersection of the dashed line with the 28.5 degrees latitude circle which is marked by P' is the point at which the azimuth of firing would be as much north from east as at P it is south of east.

Another quantity may be introduced that represents the link between the propelled ascent and the trigonometric



Sketch (b): The Yearly Cycle

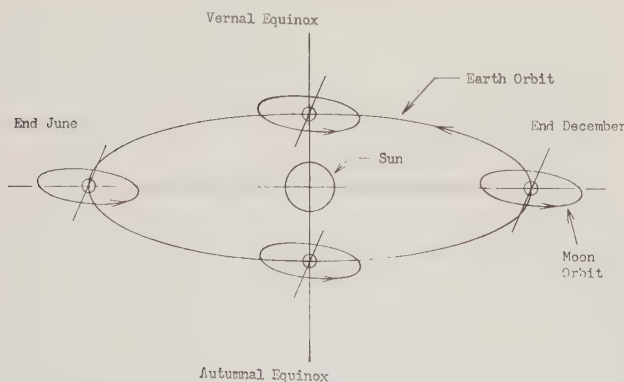


Fig. 7—Sketches of sun-earth-moon system. (a) System at end of 1958. (b) The yearly cycle.

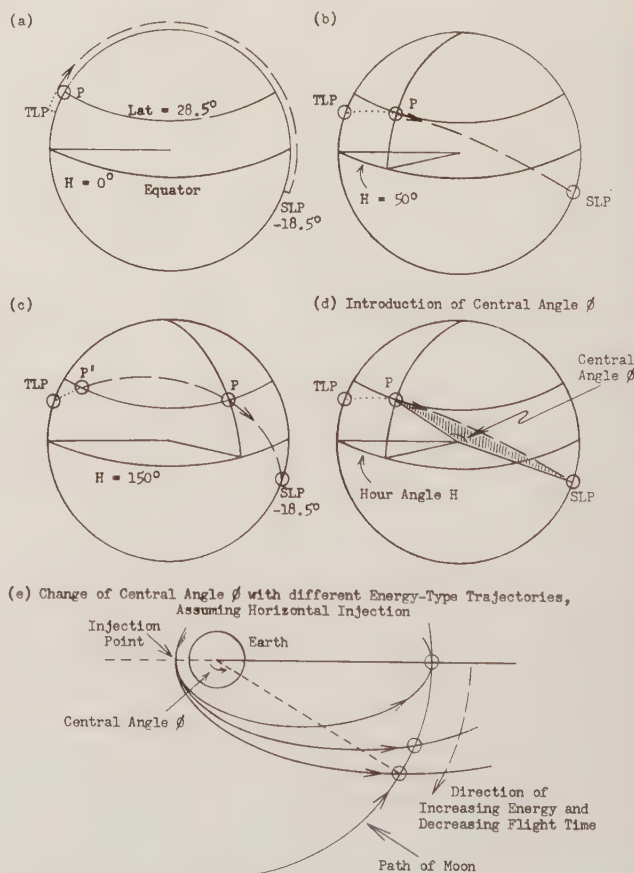


Fig. 8—Firing from PAFB (point P, latitude 28.5 degrees) at moon with declination  $\delta = -18.5$  degrees. (d) Introduction of central angle  $\phi$ . (e) Change of central angle  $\phi$  with different energy-type trajectories, assuming horizontal injection.

relationships of the probe flight. This is the central angle " $\phi$ " defined as the angle subtended at the center of the (space-fixed) celestial sphere between the point  $P$  and sublunar point. It is the angle swept through by the radius vector from center of the sphere to the probe. Fig. 8 (d) clarifies the geometry of  $\phi$ . Fig. 8 (e) indicates how, for horizontal injection, the central angle  $\phi$  decreases with increasing energy of injection, starting with the ellipse whose apogee is at the moon's distance and continuing through the parabolic to hyperbolic velocity injection. With steeper than horizontal injection the central angle moves toward zero, which is reached with vertical injection. This becomes important when referring the geometry to the missile boost phase. The more the path of the boost phase is tilted (to horizontal direction) at final cut-off of the booster, the less work the motor has to expend against the gravity pull. For a three-minute propelled flight path, the difference in impulse requirements between a vertical flight and one that tilts-over smoothly into the horizontal

direction at cut-off is reflected in the difference of gravity losses of about 700 meters per second.

The correlation of the central angle  $\phi$  and lunar declination is shown best in Figs. 9 through 11. The upper part of Fig. 9 shows the latitude circle of Cape Canaveral and the moon in its lowest declination 18.5 degrees below equator. There is only one central angle,  $\phi$ , for which the great circle of the flight plane is tangential to Cape Canaveral latitude and thus offers eastward launching. The geometry resulting in the low lunar declination is favorable in two respects. It offers us the east firing direction together with a central angle  $\phi$  of about 130 degrees.

With increasing lunar declination, the situation gradually gets worse, until the most unfavorable conditions are reached, when the moon is at its highest declination. Figs. 10 and 11 depict the extreme condition of highest declination. Since we now cannot combine the two desired properties of eastward firing and proper large central angle, we would have to make a choice of which condition would

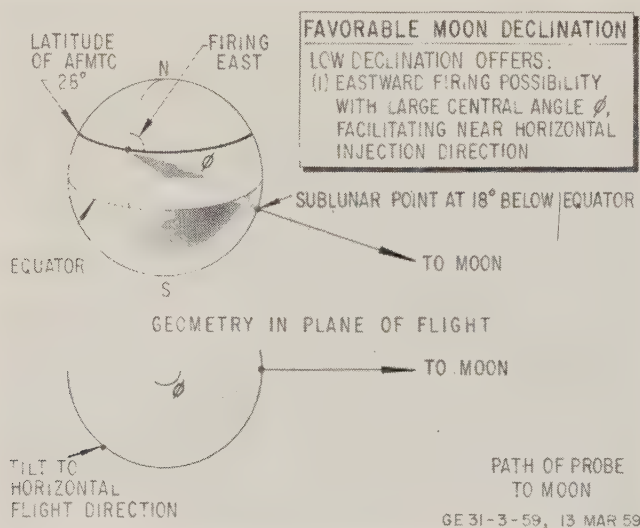


Fig. 9.

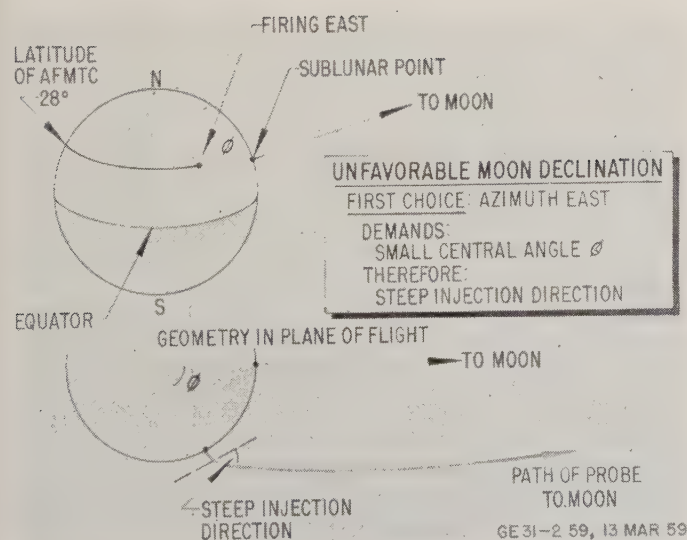


Fig. 10.

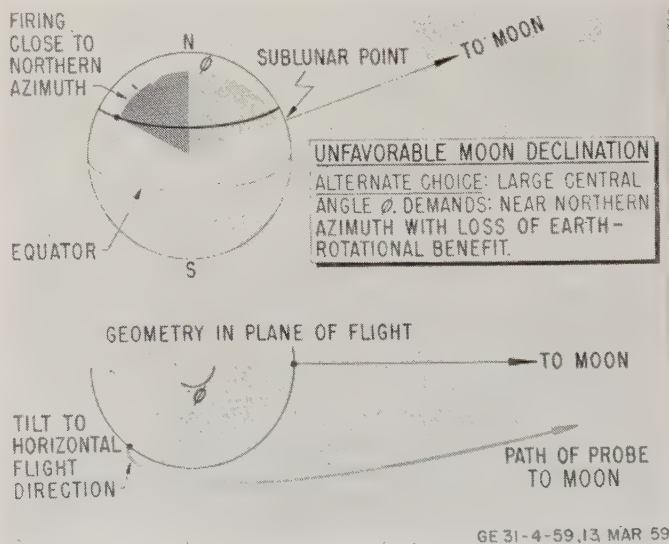


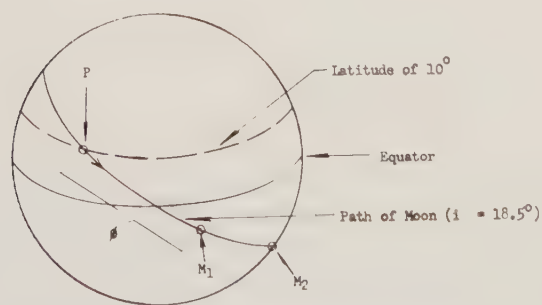
Fig. 11.



be more favorable. Fig. 10 shows the geometry if an eastward azimuth is chosen. The central angle  $\phi$  would be small and consequently the pitch angle would be steep. Fig. 11 shows the other possibility of firing so that the desired central angle condition would be met (thus, horizontal injection), but the azimuth would clearly be in a northern direction which deprives the missile of the earth's rotational component.

Another parameter, the relative inclination, is now introduced. The relative inclination is the angle between the plane of the probe flight and that of the moon's orbit. If the probe is launched in the plane of the moon, we have zero relative inclination which offers a less sensitive trajectory to injection errors. In Fig. 12 the path of the moon is shown extending from plus 18.5 degrees latitude to the negative of this value. Assume that we have a launching site available at plus 10 degrees latitude. In order to have zero relative inclination, the injection point must be exactly in the plane of the moon's orbit. With the daily earth's rotation this happens twice every day. For a given moon's location, however, only one of these crossings is of practical value.

One crossing of the launch site with the lunar plane is indicated in Fig. 12 by point  $P$ . The moon at this time may have the position marked  $M_1$ . In order for the probe to reach the moon, the energy and pitch angle at injection must be calculated so that the central angle  $\phi$ , swept through during flight, is exactly equal to the distance  $PM_1$ . If this combination of velocity and pitch angle is not available, but one corresponding to a larger central angle  $\phi$  is, as that between  $P$  and  $M_2$ , one has to wait some days until the moon has traveled further down in declination. Then



Sketch (b); Firing from Latitude Equal to Moon's Inclination

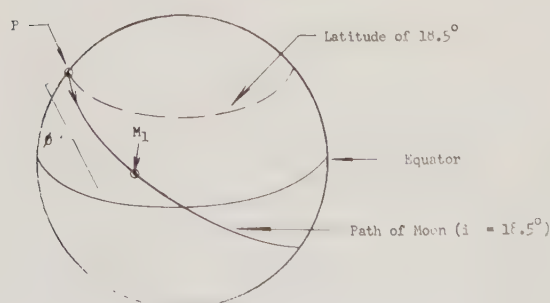


Fig. 12—Geometry developing from firing within the plane of the moon's orbit. (a) Firing from latitude smaller than the moon's orbit inclination. (b) Firing from latitude equal to moon's inclination.

again, only one chance is available during the day for exact coplanar firing. The coplanar firing, however, for our example of 10-degrees latitude can not be arranged so that the azimuth of firing is due east, but only under the azimuth which the moon's path has with the latitude circle of the launch site. Thus, the full advantage of the earth's rotation can not be taken at this latitude.

For the assumed inclination of the moon against the equator of 18.5 degrees, the chance to combine coplanar flight with eastward firing is offered only to launch sites at the latitude of 18.5 degrees. This must be a combination as indicated by point  $P$  in Fig. 12 (b). This chance, however, occurs again only once a day and with each day the moon travels by about 13 degrees on its path, making an adjustment in the injection coordinates necessary to take account of this amount of increasing central angle  $\phi$ .

Since the latitude of Cape Canaveral is 28.5 degrees and inclination of moon's orbital plane to equatorial was 18.5 degrees (1958) coplanar firing was not possible for the lunar probe.

The interconnection of some of the more important parameters is shown in Figs. 13 through 15. It should be emphasized that these results were obtained by the simple Newtonian model. The injection parameters for a lunar hit, if the influence of sun and moon is included, will be slightly different.

In arranging the trajectories for the lunar probes of the Juno II program, certain requirements had to be met.

- 1) The payload weight had to be approximately 15 pounds.
- 2) The probe's arrival at the moon should be observable from the Goldstone (California) tracking antenna.
- 3) The injection velocity should be chosen high enough that the transit time sensitivity to velocity variations at injection is compatible with the observation limitation of the probe from Goldstone.
- 4) The firing azimuths should be between 80 and 102 degrees east from north in order to comply with expected range safety requirements.
- 5) The probe's early hours of flight should be observable from Puerto Rico in order to recover the telemetering data from the cosmic ray experiments.

6) To assure that the probe pass the moon sufficiently closely, the aiming problem at launch (and consequently at injection into the probe orbit) requires either, constantly changing arrangement in pitch, azimuth and velocity, or with these parameters preset, a close tolerance in firing time. The second arrangement was chosen and modified such that several (to a maximum of four) launch trials per day were arranged for a series of days, each trial with fixed settings and firing time tolerances of  $\pm 5$  minutes. The launch trials were to be separated by a minimum of 30 minutes to provide sufficient time for the change of parameter settings.

Taking these requirements and coupling them with the existing geometry and existing vehicle, a feasible trajectory scheme was established.

Considering requirement 1), that lunar or escape veloc-

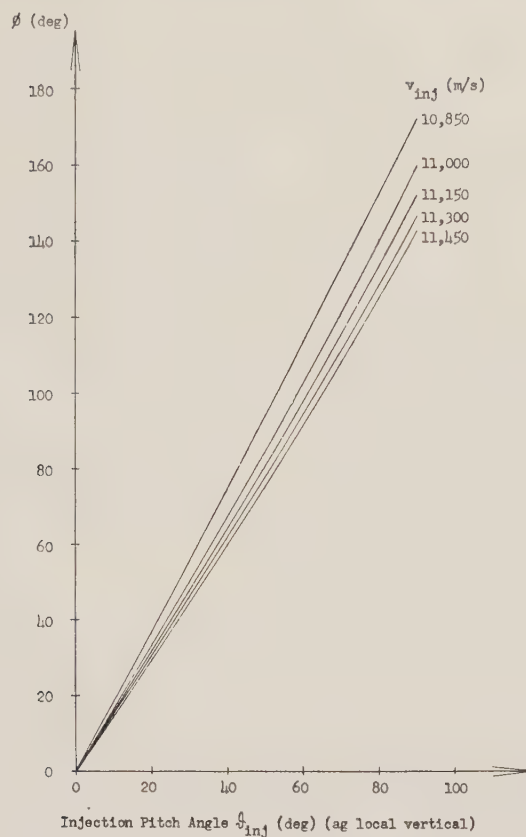


Fig. 13—Central angle  $\phi$  as function of injection velocity  $v_{inj}$  and injection pitch angle  $\theta_{inj}$ . Injection altitude = 300 km. Distance from earth center to moon center = 366,200 km.

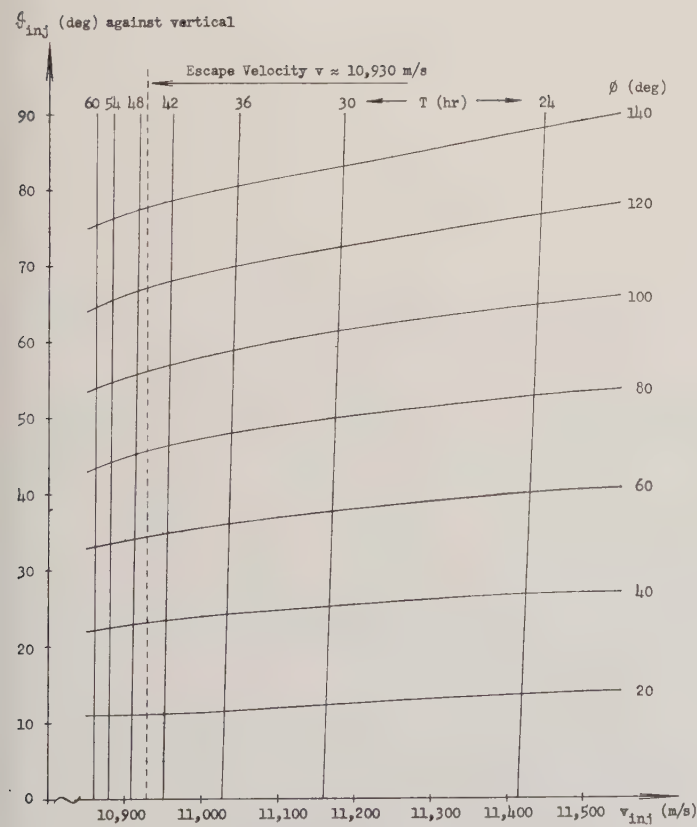


Fig. 14—Transit time  $T$  and central angle  $\phi$  for lunar probe flight plotted over injection velocity  $v_{inj}$  and injection pitch angle  $\theta_{inj}$ . Assumed injection altitude = 300 km. Assumed lunar distance from earth center = 336,200 km.

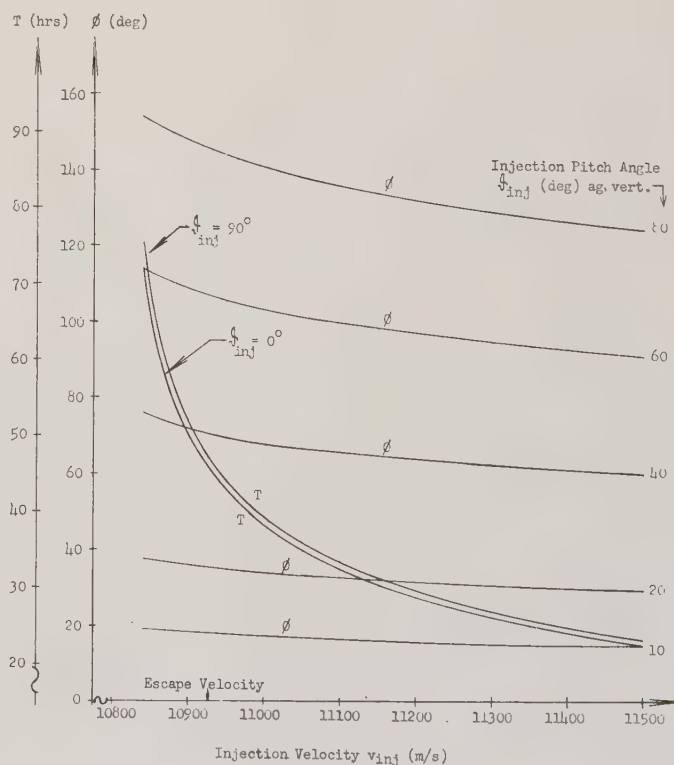


Fig. 15—Central angle  $\phi$  and transit time  $T$  as function of injection velocity  $v_{inj}$  and injection pitch angle  $\theta_{inj}$ . Injection altitude = 300 km. Distance from earth center to moon = 366,200 km.



ity would have to be reached with 15 pound payload, conditions were found where savings in thrust impulse could be realized. Of course, the first means of saving is a near horizontal path direction at booster cut-off. A second means of saving is an eastward firing direction which gives an additional increment of 410 meters per second in injection velocity.

Considering azimuth and pitch direction as described, the velocity at injection is determined by requirement 2) that Goldstone be under the moon at probe arrival. The Goldstone longitude lags behind Cape Canaveral by about 37 degrees in rotational motion of the earth. This implies that the Goldstone station would be in favorable observation position to the moon about half a day after injection time and every full day later. The velocity of injection, consequently, was chosen such that the travel time of the probe was near to either half a day, or one and one half days, or any full day more.

Errors in injection velocity have less effect on miss distance from the moon for high energy than for low energy injection.

Combining the first three requirements resulted in a compromise solution of a 33-34 hour trajectory.

Requirement 4), that the firing azimuth was to be between 80 and 105 degrees east from north coupled with the desired 33- to 34-hour trajectory and with near horizontal injection, limited firings to be near minimum declinations of the moon. This limited the number of days per month that launch attempts could be made.

The requirement of continuous early tracking could be met if the injection into orbit occurred at an altitude sufficiently high for observation from Puerto Rico. Fig. 16 gives the geometry of a trajectory as viewed from Puerto Rico. It can be seen that for low injection altitude, consequently horizontal injection direction, tracking would be lost but regained at a later time. The tracking requirement is not necessarily a contradiction to the performance requirement. A deviation from the full horizontal injection direction is required to alleviate the Juno II vehicle from a large amount of heat protecting material. The flattest trajectory that could be flown by the Jupiter booster, was determined to have a velocity vector direction at cut-off of 71 degrees against the local vertical. This basic booster trajectory was used for all launch dates. Raising the pitch direction at injection as required for succeeding launch trials, was accomplished by changing the angle under which the upper stages were fired. A coasting period of 55 seconds between booster burn-out and cluster ignition was provided in order to damp-out disturbances produced during separation of cluster from booster and nose shroud from the cluster. The necessary tilting of the cluster such that it have proper attitude at ignition of Stage II was also accomplished during this coast period. The tilt program arrangement is shown in Fig. 17.

The aiming problem at launch was solved by arranging a series of firing combinations correlated to a lift-off time. The total scheme of launching dates provided for the

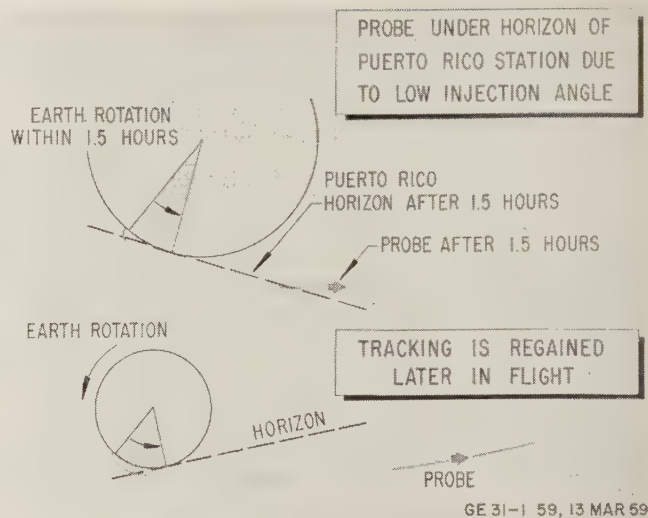


Fig. 16.

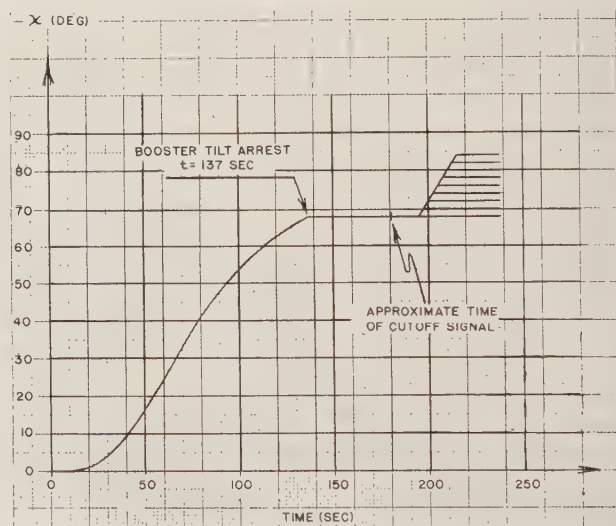


Fig. 17—Gyro tilt program as a function of time. ( $x$  measured space-fixed at vertical from launch.)

lunar probe shots is presented in Fig. 18. Launching was to be attempted in a total of 8 days starting with December 6, 1958. The days nearest to the 10th allowed four trials per day, since the moon was in favorable declination, while the days at the beginning and end of the period allowed a maximum of three trials per day. Two of the provided data on each day, however, were apart by about 20 minutes. Since 30 minutes was determined to be the minimum amount of time for arranging new presettings of the following trial, the 20-minute interval could be utilized only if early indications were found that the time schedule could not be met. Fig. 18 indicates the following data:

1) The optimum time (zero-time) of each launch trial in EST reference. The  $\pm 5$  minute tolerance for firing is symbolized by the box.

2) The pitch angle alignment of the upper stages, measured space-fixed with reference to the launch vertical.

		Schedule of Launch Data (Preliminary)									
		05:00		06:00		07:00		08:00		09:00	
Date Dec	Time of Firing AM; EST										
10	Launch Time Period	<input type="checkbox"/>	<input type="checkbox"/>	<input type="checkbox"/>	<input type="checkbox"/>						
	Optimum Launch Time (hr:min)	4:30	4:50	5:19	5:48						
	Pitch Angle (deg) ag launch vert	84	80	74	68						
	Time of Cutoff Signal (sec)	179.7	179.7	179.9	180.4						
	Azimuth E from N (deg)	86.8	89.5	92.9	96.2						
	Space Fixed Inj Velocity (m/s)	11,142	11,144	11,146	11,147						
11	Launch Time Period			<input type="checkbox"/>	<input type="checkbox"/>	<input type="checkbox"/>	<input type="checkbox"/>				
	Optimum Launch Time (hr:min)			5:27	5:47	6:16	6:45				
	Pitch Angle (deg) ag launch vert			84	80	74	68				
	Time of Cutoff Signal (sec)			179.8	179.8	180.0	180.5				
	Azimuth E from N (deg)			84.8	87.5	91.1	94.5				
	Space Fixed Inj Velocity (m/s)			11,153	11,156	11,157	11,159				
12	Launch Time Period					<input type="checkbox"/>	<input type="checkbox"/>	<input type="checkbox"/>	<input type="checkbox"/>		
	Optimum Launch Time (hr:min)					6:19	6:39	7:08	7:37		
	Pitch Angle (deg) ag launch vert					84	80	74	68		
	Time of Cutoff Signal (sec)					179.9	179.9	180.1	180.6		
	Azimuth E from N (deg)					81.1	83.9	88.1	91.5		
	Space Fixed Inj Velocity (m/s)					11,166	11,169	11,170	11,172		
13	Launch Time Period							<input type="checkbox"/>	<input type="checkbox"/>	<input type="checkbox"/>	
	Optimum Launch Time (hr:min)							7:35	7:55	8:23	
	Pitch Angle (deg) ag launch vert							78	74	68	
	Time of Cutoff Signal (sec)							180.1	180.3	180.7	
	Azimuth E from N (deg)							80.9	83.7	87.5	
	Space Fixed Inj Velocity (m/s)							11,185	11,188	11,190	

Fig. 18.

[illegible]

Fig. 19.



3) The burning time of the first stage has to follow in nominal flight.

4) The launch azimuth alignment measured east from north.

5) The speed of departure of probe at injection (in space-fixed coordinates).

Fig. 19 presents the astronomical data for the time when the probe in nominal flight encounters the moon. These data are presented for each launching trajectory.

A typical trajectory of the series of trajectories prepared may be shortly described. The missile vertically lifts-off and after 10 seconds a small tilt command is given to initiate the gravity tilt program which the missile follows to near cut-off. Cut-off of the booster occurs near 180 seconds of flight. The direction of the velocity vector at cut-off is near 71 degrees measured against the cut-off vertical. Seven seconds after booster cut-off, the instrument compartment and upper stages are separated from the booster. Approximately 7 seconds later the tilt program for aligning the upper stages in proper firing direction is resumed. The total free flight period is 55 seconds from booster cut-off signal. The sequence of operations described is presented in Fig. 20 which gives the geometry of flight for the two extreme pitch angle conditions. After 33 to 34 hours of free flight, the nominal orbit path reaches the altitude of the moon. Though the nominal trajectories are calculated as hit-trajectories, achieving vertical impact on the moon's surface, the experiment was not planned for hit purpose. The optical experiment would not succeed if a hit occurred. The lack of accuracy of the upper stages, however, in velocity as well as attitude alignment made the chance of physical contact of probe and moon extremely slim.

Figs. 21 and 22 illustrate the probe flight geometry. Fig. 21 shows the relationship of the two principal planes, that of the moon's orbit and of the probe's orbit. The two planes intersect at an angle near 22 degrees. Their line of intersection is determined by the center of the earth and encounter point (simplified two-body approach). A third plane that is the equator plane is indicated by a short segment. The earth's north-south axis is cocked to both former principal planes. The probe pierces the equator plane after it has swept through an angle of about 86 degrees from the injection point, measured at the center of the earth. Fig. 22 presents the path of the probe in time scale geometry.

Fig. 23 shows the projection on the earth's surface of the probe's orbit. As can be seen, Goldstone is approximately under the moon at probe encounter.

The requirement for injection accuracy, if moon contact should be achieved, is of interest. The tolerances are as follows:

Time tolerance for launching =  $\pm 1.7$  minutes.

Injection velocity tolerance =  $\pm 36$  meters per second.

Pitch angle tolerance for injection velocity vector =  $\pm 0.24$  degree.

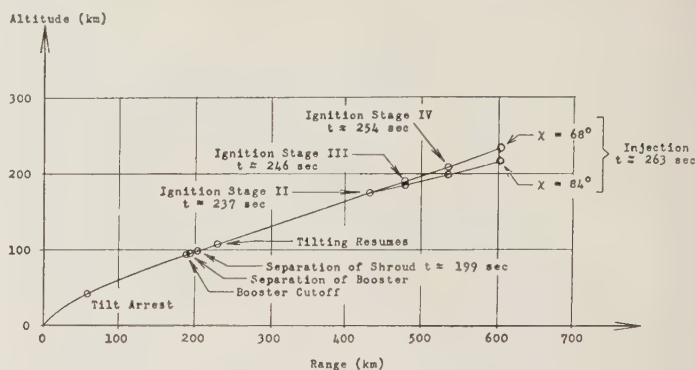


Fig. 20—Trajectory geometry and operational sequence.

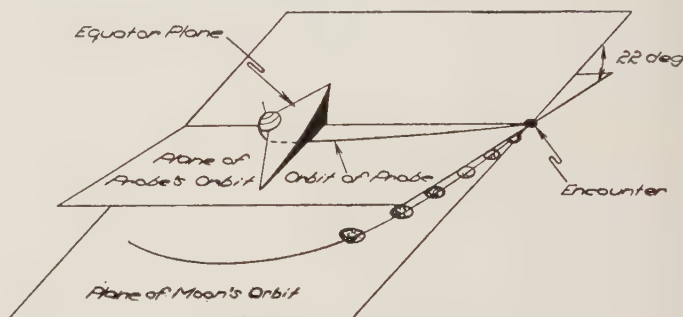


Fig. 21—Relationships of planes in probe flight.

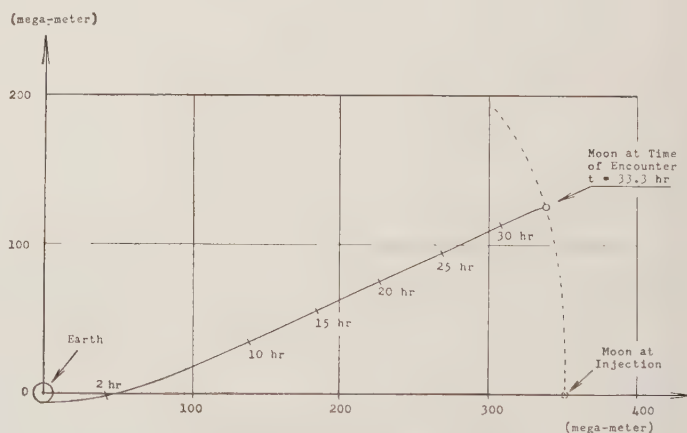


Fig. 22—Orbit of lunar probe.

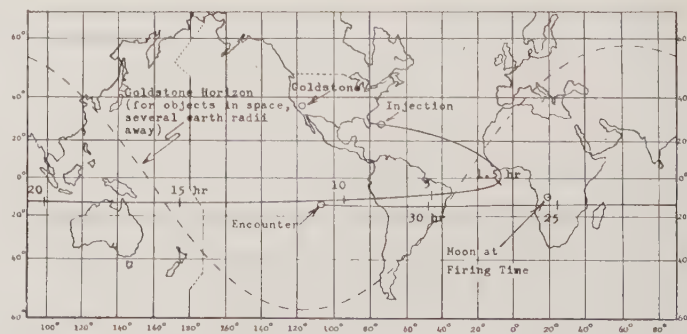


Fig. 23—June 11—lunar probe flight: Moon probe zenith positions. Firing conditions: time of launch = 7 December, 2:19 AM EST; firing azimuth = 88.9 degrees east of north; pitch angle = 72 degrees against local vertical at launch. (Figures on the zenith curve indicate time from probe injection into orbit.)

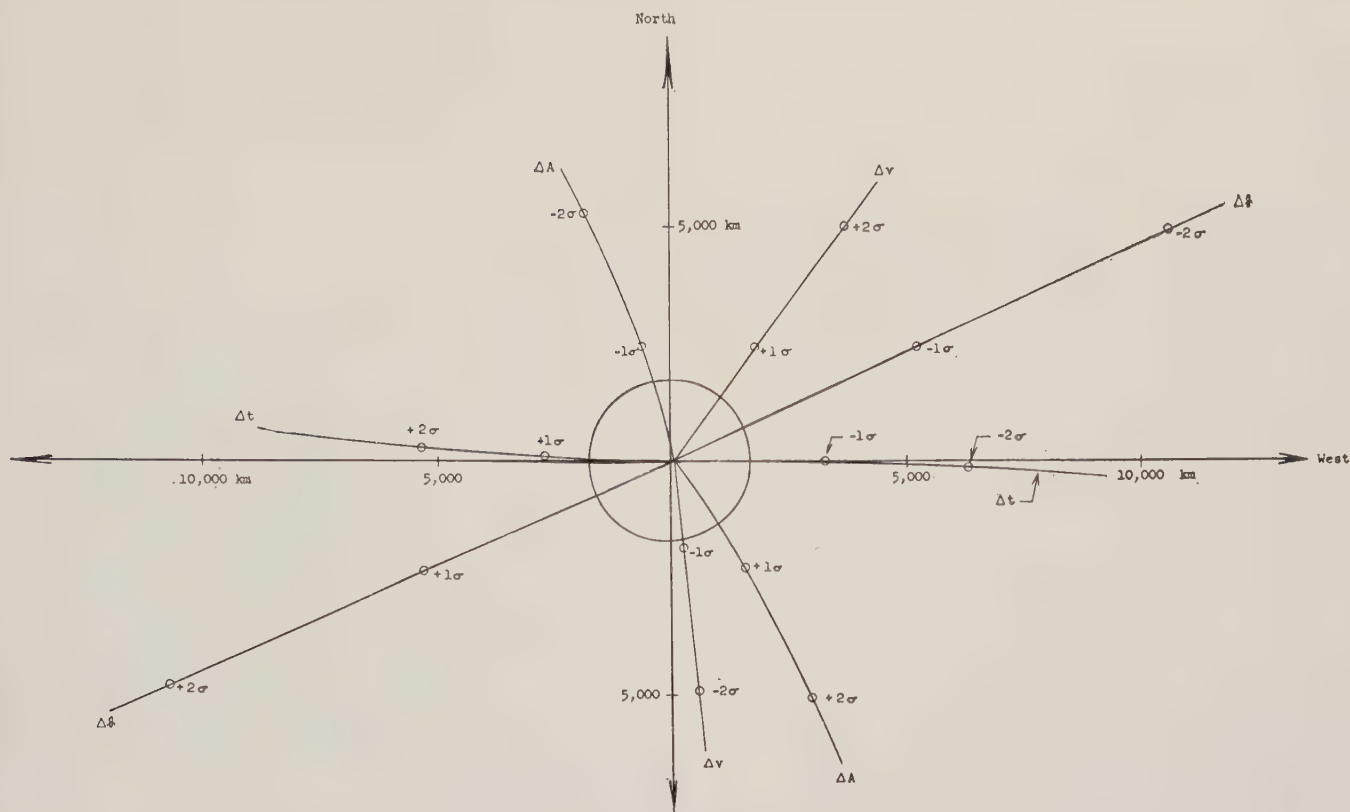


Fig. 24—Pattern of nearest approach of probe to moon.  $2\sigma$  variations: path angle variations ( $\Delta\theta$ ) =  $\pm 1.2$  degrees; injection velocity variations ( $\Delta v$ ) =  $\pm 95$  meters per second; azimuth variations ( $\Delta A$ ) =  $\pm 1.2$  degrees; launch time variations ( $\Delta t$ ) =  $\pm 5$  minutes.

Azimuth tolerance for injection velocity vector =  $\pm 0.44$  degree.

These tolerance values hold for single errors only and assume no error in any of the other listed quantities. The information about the error pattern is shown in Fig. 24.

The plot in Fig. 24 shows at what point the probe under injection errors would pierce a plane, the origin of which is at the center of the moon and which is perpendicular to the line earth center-moon center. The plane is presented as seen by an observer at the sublunar point on the earth looking toward the moon.

#### Earth-Circling Satellites

There have been three earth satellite shots of the Juno II program. The trajectory arrangement followed the pattern outlined in the Juno I program. Of course, the per-

formance capabilities of the Jupiter booster is much greater than the Jupiter C and consequently a much larger payload could be placed into orbit. The nominal trajectory for Explorer VII (the 92 pound payload now in orbit) had the following elliptical characteristics:

Semi-major axis = 7212 km

Semi-minor axis = 7206 km

Eccentricity = 0.041

Inclination of orbital plane to equatorial plane = 50.3 degrees

Longitudinal shift during one revolution = 14.2 degrees

Apogee = 1138 km

Perigee = 546 km.

The actual orbit of Explorer VII was very close to the predicted orbit.



## Deep Space Communications\*

W. D. MERRICK†, E. RECHTIN†, R. STEVENS†, AND W. K. VICTOR†

**Summary**—This paper discusses the various factors that influenced the design of the TRACE deep space communications system, the choice of the operating frequency, and the selection of a suitable ground antenna. The configuration of the three different microwave communications system stations—launch, injection, and deep space—employed in the Pioneer III and IV experiments is given, together with a description of the computing and interstation communications system. A brief description of the performance of the TRACE systems, its proposed development, and its future capabilities is also included.

### I. INTRODUCTION

IN THE SPRING of 1958 the Army was instructed by the Advanced Research Projects Agency to proceed on a lunar program consisting of two firings of a Juno II vehicle, the first firing to be before the end of 1958. The deep space communications for the Army's lunar program was designed, constructed and operated within this time span by the Jet Propulsion Laboratory of the California Institute of Technology with major assistance from the Collins Radio Company and Blaw Knox Company, Equipment Division. The microwave communications system consisted of three different station configurations: launch, injection, and deep space, located at the Atlantic Missile Range, Puerto Rico, and California, respectively. The basic design was code named TRACE (Tracking And Communications, Extraterrestrial). Performance was generally regarded as excellent, permitting good orbit determination and high-quality telemetering to greater-than-lunar distances. The telemetering contributed to the improved description of the inner Van Allen belt, materially contributed to the discovery and description of the outer belt, and for the first time transmitted information from deep space.

### II. DESIGN CONSIDERATIONS

The total time available between initial design and operational status was less than 10 months. An appreciable capital investment was anticipated; consequently, an expendable-equipment philosophy could not be used. Because firing times were closely controlled by orbital considerations, it was important that the communications system be all-weather in order that vehicle firings would not be precluded by poor weather at the tracking and telemetering stations located around the world. Because it was virtually

certain that deep space exploration would continue in the coming years, it was important that the basic design be commensurate with the projected state of the art, specifically with respect to parametric and maser amplifiers, increased power and efficiency in space vehicle transmitters, and future attitude-stabilized spacecraft. In addition, the limited number of firings in the program demanded that the communications system work reliably the first time and be relatively unaffected by large dispersions from the anticipated vehicle trajectory.

These design restrictions pointed toward an extrapolated Microlock system such as had been used in the Explorers, heavily modified by the design techniques used in the Army Corporal and Jupiter radio-guidance systems. It was evident that the Microlock frequency, 108 mc, was undesirable in the long run, that large tracking antennas would be required, that partially coded telemetering would be needed, and that a major effort in real-time computing and interstation communication would be necessary.

### III. CHOICE OF FREQUENCY

The choice of 108 mc for the Explorer Microlock system had been made on the basis of compatibility with the Minitrack network established for the IGY. The Minitrack system had chosen this frequency for a variety of reasons, the principal ones being the availability of efficient and lightweight satellite transmitters, the desirability of using comparatively low-gain ground antennas because of the anticipated satellite orbits, and the desirability of avoiding major ionospheric perturbations of the arriving signals. It was recognized, however, that 108 mc was a comparatively poor choice for deep space communications to be carried out in the 1960–1970 era, for the following reasons. Efficient vehicle transmitters were becoming available at higher frequencies. Large tracking antennas would be required for interplanetary communication. Since the angular motion of a deep space probe relative to a ground station more nearly resembles the motion of a star than a low-altitude satellite, pencil-beam ground antennas would be more practical for a space probe. Perhaps still more important, radio-astronomy evidence had shown that a quiet frequency region existing between approximately 500 and 5000 mc could be exploited using parametric and maser amplification. The final choice of the TRACE communication frequency was based on the practicability of building a particular vehicle transmitter, on finding an appropriate large antenna, and on the availability of certain existing radio-guidance equipment which could be converted easily only to certain selected frequencies. The final choice was 960.05 mc. The vehicle transmitter prob-

\* Manuscript received by the PGMIL, February 1, 1960. Portions of the following report were originated under studies conducted for the Department of Army Ordnance Corps under Contract No. DA-04-495-Ord 18. Such studies are now conducted for the National Aeronautics and Space Administration under Contract No. NASw-6.

† Jet Propulsion Lab., California Inst. Tech., Pasadena, Calif.

lem was solved by L. R. Malling, who designed a transmitter which was completely transistorized with the exception of the final amplifier stage (Fig. 1). The ground receiver system (Fig. 2) was based upon the phase-locked-loop technique of coherent detection. It was constructed by modification of components of a previously proven JPL

radio-guidance system. The original equipment had been fabricated for JPL by Motorola-Phoenix and was modified in part by the Collins Radio Company.

#### IV. CHOICE OF ANTENNAS

The choice of a ground antenna was made after a short but intensive study of the antennas which might be fully operational by the end of 1958, could meet the stringent requirements for a high-quality parabolic surface, and were operable in all-weather conditions, the major weather consideration being high wind. In addition, JPL desired that the resultant capital investment would meet the requirements of the anticipated space communications of the next few years. It was fortunate that a solution to the large-antenna problem existed: an 85-foot-diameter, polar-mounted radio-astronomy antenna designed by Blaw Knox Company was available within 6 months at an established price. The significance of this set of circumstances can perhaps only be appreciated by readers familiar with large antennas. The design, which had been underway for more than five years, was started at the Naval Research Laboratory, developed further at the Carnegie Institute, refined by the Associated Universities, and completed by the Blaw Knox Company just in time for the Army lunar program. On the other hand, although the design was complete, no antennas of this type had actually been con-

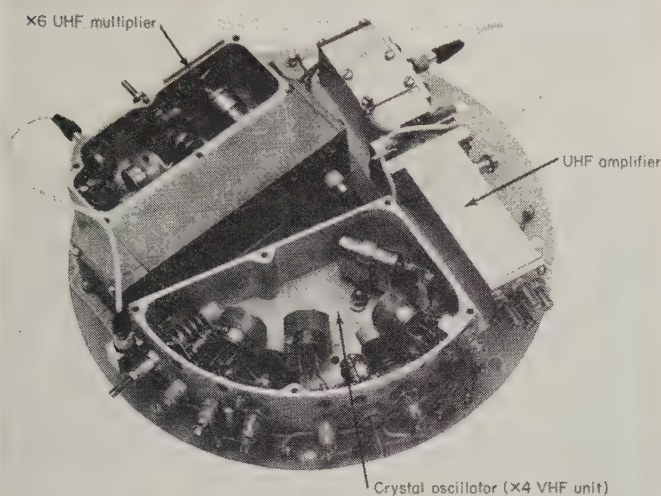


Fig. 1—Lunar probe transmitter, development model.

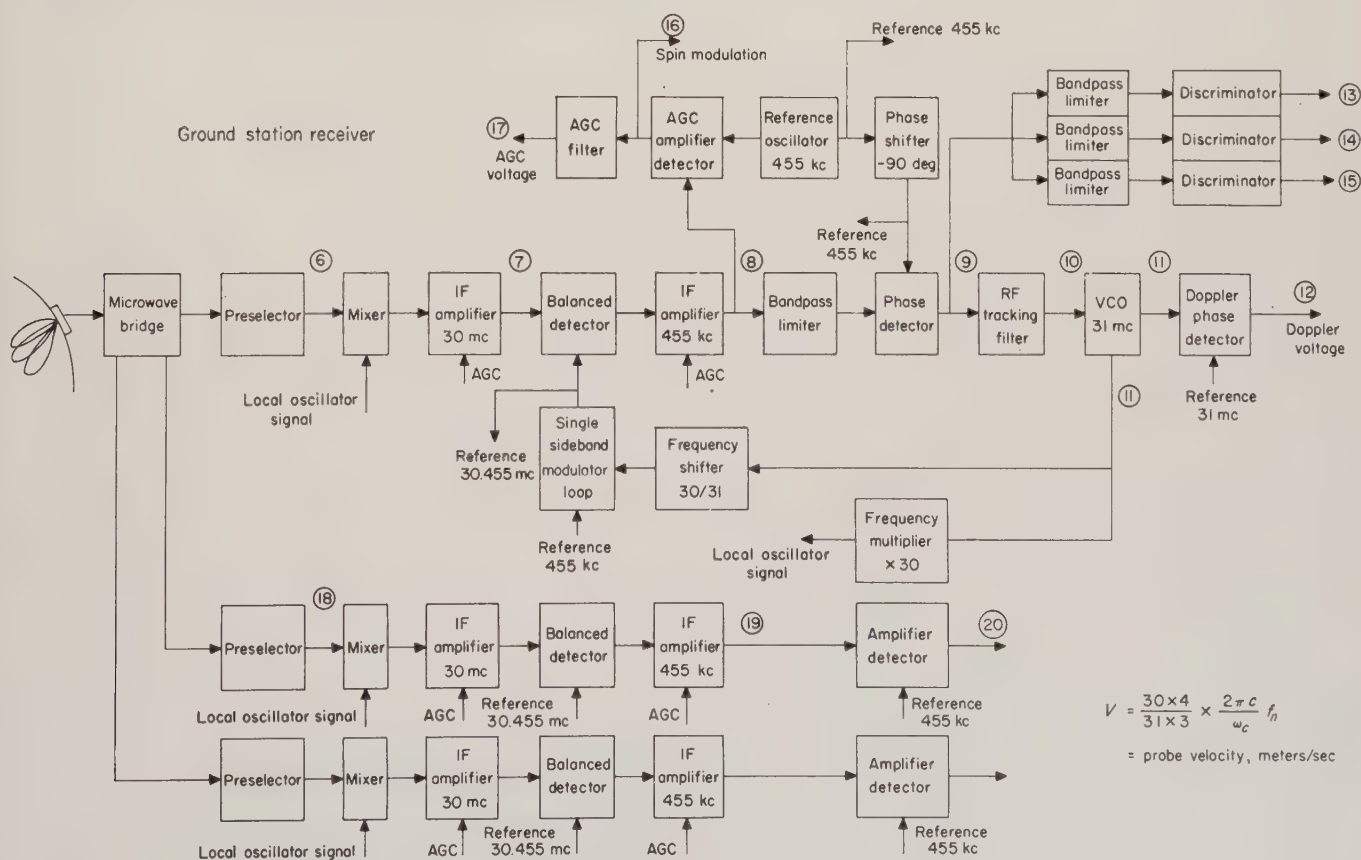


Fig. 2—TRACE system for Goldstone tracking station.



structed in the spring of 1958. In addition, the antenna was designed for a sidereal drive and not for automatic tracking. Fortunately, the areas of deficiency were those in which the considerable experience of JPL in Army radio-guidance systems could be used. The resulting station at Goldstone, Calif., is shown in Fig. 3.

#### V. THE NETWORK

Although the Goldstone deep space station was one of the more dramatic features of the program, it was equalled in importance by a much smaller station at the Atlantic Missile Range and by a mobile station at Puerto Rico (Fig. 4). The station at the Atlantic Missile Range received the signals from the TRACE vehicle transmitter during the very early portion of flight immediately after launch. One-way Doppler information from this station was used to determine whether the launching had been successful. It also provided data to determine the approximate orbit, for use by the subsequent stations in acquiring the TRACE signal on their respective horizons. The Puerto Rico station, from the purely scientific point of view, was the most important station of the three. The Puerto Rico station first received the TRACE signal within five minutes after takeoff from the Atlantic Missile Range and maintained essentially continuous reception of the signal for the next six to eight hours, until the deep space station in California first received the TRACE signal on the local horizon. During this period of time, while the probe was rapidly climbing away from the earth and apparently "circling" the Puerto Rico station, the probe passed through both Van Allen belts and began its journey into deep space.

The AMR station was a simplified version of the deep space station, consisting essentially of only the receiving channel coupled to a manually pointed parabolic antenna. The Puerto Rico station, on the other hand, represented a fully mobile version of the deep space station, with the modifications that its antenna diameter was appreciably less (10 feet instead of 85 feet) and that its servo system was a modified Nike I rather than a JPL deep space design.

#### VI. TELEMETERING SUBSYSTEM

The telemetering subsystem represented the least departure from previous space communications experience. The telemetering, a modulation on the 960.05-mc carrier, can be described as an IRIG/FM modulation system using very small modulation indexes, and detecting by linear phase-locked-loop techniques. This telemetering subsystem design had been previously proven and was particularly applicable under conditions of signal variability due to spinning of the vehicle, unexpected attitude changes of the vehicle, and uncertain propagation conditions.

An interesting variation was used in coding one of the telemetering channels. Previous experience had shown difficulty in achieving sufficient dynamic range of the cosmic-ray measurements. The cosmic-ray instrument pro-



Fig. 3—Goldstone deep space station.



Fig. 4—Puerto Rico tracking station.

duced a series of pulses proportional to the cosmic-ray count. The cosmic-ray count could change over a ratio of 2500 to 1; yet it was important to have data of approximately 10 per cent accuracy, regardless of the absolute count. This problem was solved by taking a series of taps from a scaler, each tap representing successively larger counts per output pulse. The output from each of the taps was set at different voltage levels, and passed through a low-pass filter, and the sum was applied to a subcarrier (Fig. 5). The resultant effect is approximately illustrated in Fig. 6. This particular coding method proved outstandingly successful in the accurate exploration of the Van Allen belts. A short period of Pioneer III telemetering data is shown in Fig. 7. In other respects, the telemetering and recording display system was essentially the same as the JPL FM/FM system originally developed in conjunction with the Army Corporal program.

#### VII. COMPUTING AND INTERSTATION COMMUNICATIONS

The real-time computing and interstation communication system was almost completely new with respect to previous JPL programs, although the general techniques were well within the state of the art. Velocity and angle information from the tracking site was digitalized, converted to a standard teletype format, and relayed to JPL in Pasadena. There it was used in an IBM 704 to calculate the probe's trajectory and to derive pointing informa-

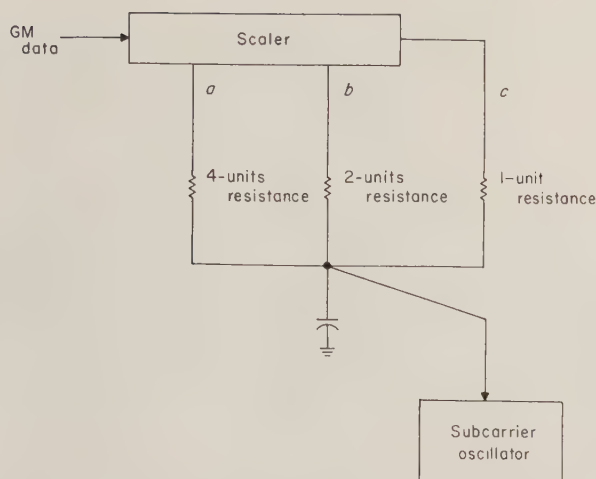


Fig. 5—Weighted mixing circuit planned for soft radiation experiment.

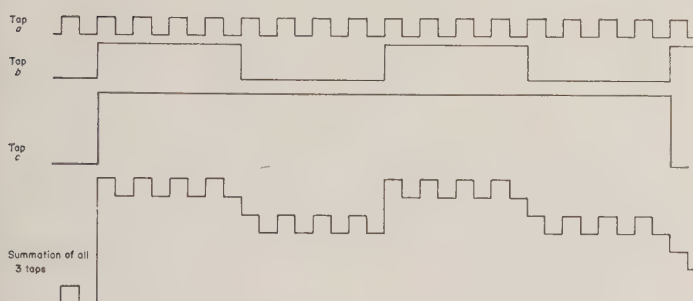


Fig. 6—Individual and mixed wave forms.

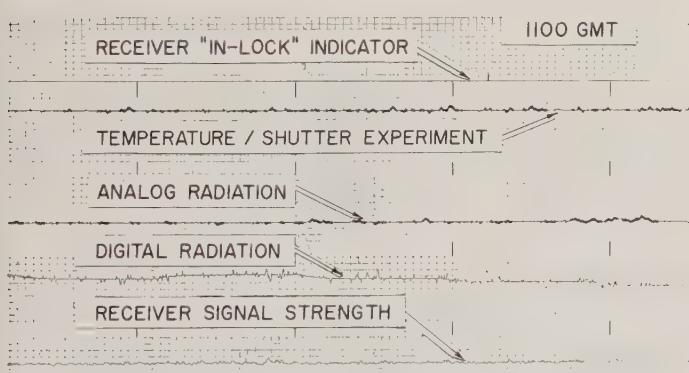


Fig. 7—Pioneer III telemetering data. Sample Puerto Rico Sanborn recording on lunar probe.

tion for signal acquisition by the tracking stations. The computer programming performed a root-mean-square fit of all available tracking data from which best estimates of the injection parameters of the orbit were determined: velocity, position, and angular coordinates of the initial point on the free-flight trajectory. Using these parameters, the complete orbit was calculated, and the acquisition information required by the tracking station was subsequently derived. The success of the technique depended upon the fact that free-flight in the vacuum of space is virtually devoid of unknown disturbances. In this respect, deep space flight is significantly different from satellite

flight in the near vicinity of the earth or missile flight within the sensible atmosphere.

In addition, in the computer programming it was assumed that certain types of errors existed at the various tracking stations: angular bias in the angular tracking system, frequency shifting of the crystal-controlled oscillator in the probe, and frequency shifting in the ground station reference frequencies. As part of the computing operation, the computer solved for these errors at the same time that it computed the orbits. Because of the tremendous amount of tracking data available, it was possible to compute an orbit far more accurately than the instantaneous pointing ability of any one tracking site. The orbit determined by the computing operations could be demonstrated to be better than 0.2 milliradian in accuracy, although the tracking accuracy of Puerto Rico was certainly not better than 8 milliradians and that of Goldstone, 2 milliradians. Given this computed orbit as a standard for comparison, the instantaneous tracking accuracy of the various stations could then be estimated.

## VIII. OTHER STATIONS

Several other stations participated in the Army lunar program on a less formal basis. Several of the Army Microlock stations located on the East Coast of the United States were converted to 960-mc reception to perform an evaluation of the vehicle launching process similar to that performed using the Microlock on the Explorers. These stations, under the direction of the Army Ballistic Missile Agency, closely resemble the JPL launch station in complexity and in recording equipment. The Microlock equipment at Jodrell Bank, installed by the Air Force for its lunar program, was converted by the Air Force to 960 mc to permit reception of signals from the Army probe. The manually positioned Jodrell Bank antenna was most useful at the greater distances when the angular rates were low and the angular position well-known. Various other stations listened to the 960-mc transmission from the probe on a still less formal basis.

## IX. PERFORMANCE

Pioneer III was launched on December 6, 1958, and reached an altitude of 63,500 miles, after which it returned to the earth in the vicinity of Central Africa. During the time of flight the projected point on the earth immediately under the probe traveled from the Atlantic Missile Range to West Central Africa, at which point it "reversed" across the Central Atlantic, South America, the Pacific Ocean, the Indian Ocean, and finally Central Africa. During the flight, approximately 24 hours of radio contact were maintained: 14 hours by Puerto Rico and 10 hours by the Goldstone Deep Space Net Station. The Puerto Rico station showed an ability to obtain usable telemetering to distances in excess of 40,000 miles; the California Deep Space Station, because of its appreciably large antenna, obtained very strong signals throughout its tracking period. The Puerto Rico station obtained ex-



cellent telemetering data on both the rising and falling legs of the flight and consequently was twice able to provide a high-quality description of the Van Allen radiation belts. Operation of all stations and of the vehicle transmitter was well within tolerance. The received signal strength was 3 to 4 db less than expected because the spin axis of the probe had been cocked by a launching vehicle disturbance.

Pioneer IV was launched on March 3, 1959, passed the moon at a distance of 37,300 miles southeast of the moon, and then continued on to become a planet of the solar system. The projected point on the surface of the earth immediately below the probe was similar to that of Pioneer III with the exception that the subprobe point continued circling the earth rather than ending in Central South Africa. Tracking and telemetering performance of the TRACE system for the first 100,000 miles of flight of the probe was closely similar to the first portion of the Pioneer III flight with one exception. A deviation from the standard trajectory caused the probe to dip below the eastern horizon from the Puerto Rico station for a period of 30 minutes; consequently, signal information was lost during that time. Reacquisition by Puerto Rico and all subsequent acquisitions by Goldstone were normal. The Goldstone station first acquired the probe signal 6.5 hours after launch when the Pioneer IV was 60,000 miles from the earth. For 15 minutes, four tracking stations—AMR, Puerto Rico, California, and England—were all locked onto the Pioneer IV transmission. A unique opportunity was thus provided to obtain a four-way fix on the probe to the exact position in space. Goldstone maintained contact for almost 10 hours until the earth's rotation caused the probe to descend below the horizon, and was able to obtain an additional 10 hours of tracking per day for March 4 and 5, 1959. On March 6, Goldstone made its fourth and final acquisition at a range of 399,000 miles. Loss of the signal occurred during this tracking period when the probe's batteries became exhausted. The range at this time was 435,000 miles. Telemetering quality was still high and no difficulty was being experienced in velocity or angle tracking. The TRACE system had therefore met its design goal of providing high-quality space communications to the distance of the moon and beyond. Had more battery life been provided (at a considerable cost in

weight), the TRACE system could have maintained useful contact for about three times as long in both time and distance. The use of parametric amplifiers, excluded from the initial receiver because they had not yet been system proven, would have doubled system performance.

#### X. THE IMMEDIATE FUTURE

The long-term capability of the deep space net is summarized in Table I for the period of 1960 to 1964. The addition of ground transmitters will be noted, to make possible accurate two-way Doppler, accurate ranging, and ground-to-probe command. The increase in spacecraft antenna gain is the result of the use of stabilized vehicles.

TABLE I  
LONG-TERM CAPABILITY OF THE DEEP SPACE NET  
(PREDICTED SCHEDULE)

Characteristic	1960	1962	1964
Transmitter power			
Ground	10 kw	10 kw	10 kw
Spacecraft	10 w	25 w	100 w
Antenna gain			
Ground	46 db	46 db	54 db
Spacecraft	6 db	20 db	30 db
Receiver sensitivity			
Ground	300°K	100°K	40°K
Spacecraft	2000°K	2000°K	400°K
Information bandwidth			
Telemetry (10 db SNR)			
Satellite application	3.5 kc	1 mc	1-10 mc
Lunar application	3.5 kc	1 mc	1-10 mc
Mars application		100 cps, 18 db SNR	10 kc
Venus application		400 cps, 18 db SNR	40 kc
Edge of solar system			10 cps

The decrease in the effective temperature of the ground and spacecraft receiving systems is due to the incorporation of parametric amplifiers. Otherwise, the major elements of the TRACE system—the antennas, tracking equipment, etc.—continue to be used during this period.

Present plans also call for the installation of two more deep space stations spaced at approximately 120° in longitude around the earth. This will permit continuous contact with a deep space probe during its journey to the moon or the planets.

# Lunar Circumnavigation\*

H. O. RUPPE† AND C. L. BARKER, JR.†

**Summary**—A short survey on the mechanics of the free flight part of circumlunar flight is presented. This survey is by no means complete and many refinements have been listed but not explained. Other important fields such as attitude control have been left out completely. It must be stressed that for exact computations of trajectories, special studies covering the astronomical constants and computational methods are mandatory. The launch vehicle, space capsule, environment and its control, onboard power supply, communications, and methods of space navigation and propulsion are but a few of the topics which need treatment if completeness is desired.

Other areas requiring attention are the Earth communications links for both data transmission and vehicle control as well as the major item of payload recovery particularly when that payload is man!

## INTRODUCTION

THIS PAPER presents an introduction to the problems pertaining to circumlunar flight. It is assumed that the reader is sufficiently familiar with the astronomical and astronautical fundamentals such as the structure of the Earth-Moon system, two-body problems, short powered high thrust vehicle propulsion systems, injection, midcourse and terminal phases of flight, atmospheric entry, etc.

The mechanics of circumlunar flight are explained through the discussion of Jacobi's Integral for The Restricted Three Body Problem, of a simple model in which lunar influence is neglected and of an improved model in which a series of two-body problems are solved.

Lunar influence on the circumlunar flight is shown to have three dimensional effects which greatly alter the orbital elements on the return flight. Finally some of the problems associated with re-entry into the Earth atmosphere are presented.

## JACOBI'S INTEGRAL—THE RESTRICTED THREE BODY PROBLEM

A simplified model is assumed for the Earth-Moon system, namely that the Moon moves in a circular orbit around the center of mass of the Earth-Moon system so that the laws of celestial mechanics for a two-body problem are fulfilled. Because of perturbations, the laws cannot be exactly fulfilled for the real constants. The coordinate system for this simple model is chosen such that the Moon remains on the X-axis and the Earth-Moon center of gravity coincides with the origin.

"Jacobi's Integral" can be easily found for a point of very small mass moving under the influence of the described two-body system:

$$\text{Energy } E = \frac{V^2}{2} - \sum_{i=1,2} \frac{\gamma m_i}{|r - r_i|} = \frac{\omega_s^2}{2} (x^2 + y^2) + C \quad (1)$$

where

$V$  = speed of the small mass

Index 1—pertains to Earth

Index 2—pertains to Moon

$r$  = radius vector of small mass

$C$  = constant of integration.

The characters  $|r - r_i|$  represent the distance of the small mass from the center of the Earth or of the Moon.

From (1), we may draw many important conclusions. Consider the small mass moving away from Earth until its velocity becomes zero. The locus of all zero velocity points obtained by starting the small mass from an initial point with the same energy but varied direction is called Hill's Surface. The surface is characterized by the initial condition, which just can reach it, or as is generally done, by the particular nominal value of  $C$  of (1), which just leads to this surface.

The computations are easily made by first using the initial conditions in (1) to obtain  $C$  and then equating the velocity to zero.

$$\sum_{i=1,2} \frac{\gamma m_i}{|r - r_i|} + \frac{\omega_s^2}{2} (x^2 + y^2) = -C. \quad (2)$$

The above equation describes Hill's Surface belonging to a particular value of  $C$ .

Fig. 1 shows a cross section through some of the Hill's Surfaces. If we think of the small mass or vehicle, as it will be called hereafter, starting near to  $m_1$  and that its kinetic energy per unit mass  $\frac{1}{2} V_0^2$ , at the starting point

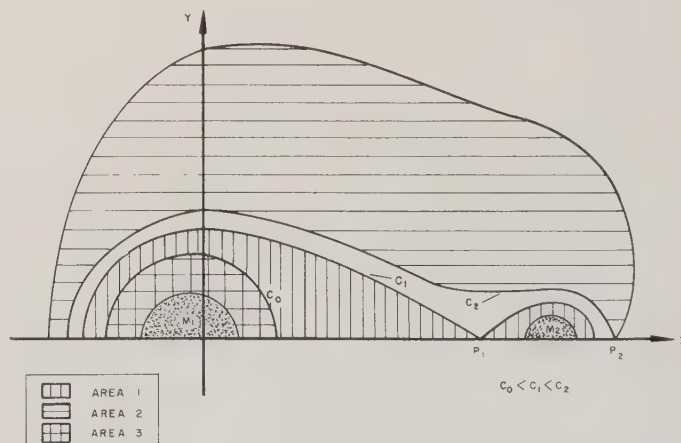


Fig. 1—Scheme of Hill's surfaces.

\* Manuscript received by the PGMIL, February 1, 1960.

† U. S. Army Ballistic Missile Agency, Redstone Arsenal, Huntsville, Ala.



is such that the constant  $C = C_0 < C_1$ , then only Area 3 is accessible to the vehicle. Area 3 is approximately a sphere around earth due to the principal influence of the earth's gravitational field. If the initial  $\frac{1}{2}V_0^2$  is increased so that  $C = C_1$ , the vehicle can "sneak" through  $P_1$  into the general lunar area. By further increasing  $\frac{1}{2}V_0^2$ , the surface is then extended to  $C^2$ . In this last case, the vehicle may leave the Earth-Moon system through  $P_2$  although Area 2 is not accessible.

Let us now consider an example of the above. The starting point is assumed to be 200 km above the Earth's surface. It matters little where on Earth this is. The direction of the initial speed cannot be found from Jacobi's Integral, but if we have a particular velocity  $V_0$  which establishes the surface  $C_0$  for a given  $\frac{1}{2}V_0^2$ , then we know that this surface is a limit beyond which the vehicle cannot pass, but which might not actually be reached.

Measured in the "Jacobian" coordinate system, we have:

$$V_{01} = 10.863 \text{ km/second for } C_1$$

and

$$V_{02} = 10.864 \text{ km/second for } C_2.$$

In the inertial system these values are:

$$V_{01} = 10.893 \text{ km/second and,}$$

$$V_{02} = 10.894 \text{ km/second}$$

while the geocentric speeds are:

$$V_{01}'' = 10.881 \text{ km/second and}$$

$$V_{02}'' = 10.882 \text{ km/second.}$$

Earth escape speed at 200 kms is  $V_{esc}'' = 11.015$  km/second. As seen from the above, we can effect an Earth escape with  $V_{02}''$  being 133 meters per second less than Earth escape speed. This might imply at first glance that the energy law does not hold, as the "escape speed" is derived from the law of conservation of energy.

However in considering the over-all system and not the vehicle alone we find that the energy law still governs. It is shown in (1) that the energy of the vehicle is not constant. Therefore it must pickup or lose energy during the lunar encounter but the total energy of the system is preserved.  $V_0''$  is the minimum cutoff speed to reach the Moon.

Kepler's second law does not hold in this minimum energy case as seen from the inequality of the area constants. At point  $P_1$ , the area constant of the vehicle with respect to Earth is  $\omega_s \times 326800^2 \approx 285 \times 10^3$  (km/second)<sup>2</sup>. At injection this area constant is smaller than or equal to  $V_{01}'' \times r_0 \approx 71.5 \times 10^3$  (km/second)<sup>2</sup>. This change of a factor of 4 can only be accounted for through the inclusion of lunar perturbation effects on the vehicle. Therefore at this minimum speed, it will take a long time before the lunar perturbations enable the vehicle

to cross through point  $P_1$  into the lunar vicinity. This long time may be estimated to be in the order of 5 years making this *minimum* energy transfer to the Moon very impractical.

#### THE SIMPLE MODEL NEGLECTING LUNAR INFLUENCE

A first order approximation of Earth to Moon flights may be made neglecting the lunar influence completely. It can be shown that the results thus obtained are not overly wrong as far as injection velocity, flight time and the major part of the trajectory shape are concerned. The results are unrealistic in the lunar vicinity. If, for example, we neglect the lunar gravitational influence in computing lunar impact velocity then our answer would be quite incorrect.

If we want to throw a vehicle just out to lunar distance from 200-km altitude (injection) above the Earth surface then for minimum speed we would throw it vertically as in trajectory I in Fig. 2. The slender ellipse, trajectory II, results if the vehicle is thrown horizontally from the 200-km altitude. The vehicle has the same potential energy at points  $P_I$  and  $P_{II}$  but has in addition, some kinetic energy at  $P_{II}$ . Therefore the injection speed must be higher for trajectory II. Because the difference is small, only  $\sim 1.6$  meters/second, and as reasons of optimization of the powered phase of the trajectory heavily favor the horizontal injection, standard flight trajectories follow this horizontal or near horizontal injection scheme. From this it is determined that the minimum speed to go out to lunar distance is 10.922 km/second. For a lunar flight, assistance from the Moon is a few centimeters per second which is negligibly small. With this higher speed of 10.922 km/second, the previous argument about the area constant in Kepler's Second Law no longer holds since the vehicle moves as if it were a two-body problem until it is rather close to the Moon.

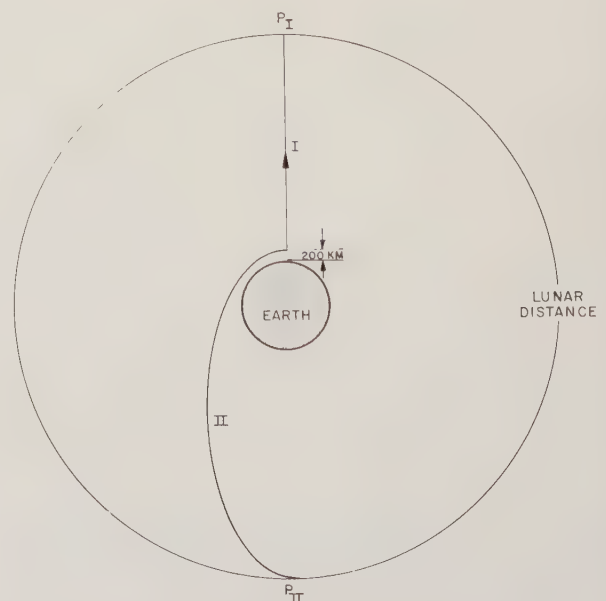


Fig. 2—Possible Earth-to-Moon trajectories.

A flight time of 4.99 days from launch to apocenter is associated with the speed of 10.922 km/second. Lunar influence in the case of a lunar impact reduces this time by approximately 6 hours.

Data for some typical Earth-Moon flights are given in Table I.

TABLE I

Geocentric Launch Speed 200-km altitude horizontal injection		Flight Time	Circumlunar Flight
Absolute Minimum Transfer	10.881 km/second	~ 5 years	Time too long
Minimum Direct	10.922 km/second	~ 4.75 days	Practical
Elliptic	10.965 km/second	~62.5 hours	
Parabolic	11.015 km/second	~51 hours	
Hyperbolic	11.115 km/second	~40 hours	Too fast

### THE IMPROVED MODEL WITH TWO TWO-BODY PROBLEMS

Within the vicinity of a large mass, the vehicle behaves as if it were moving in a two-body problem approximating to a high degree a conic section. "Vicinity" can be interpreted as "sphere-of-action" (Tisserand). Very coarsely the distance from lunar center to  $P_1$  in Fig. 3, is the radius of the lunar sphere in action which we assume to be completely embedded in the Earth's sphere of action.

If a vehicle moving along its trajectory enters the

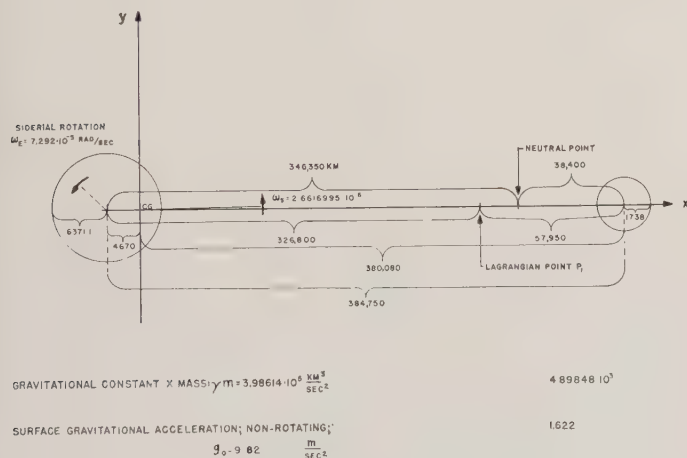


Fig. 3—Scheme of Earth-Moon system.

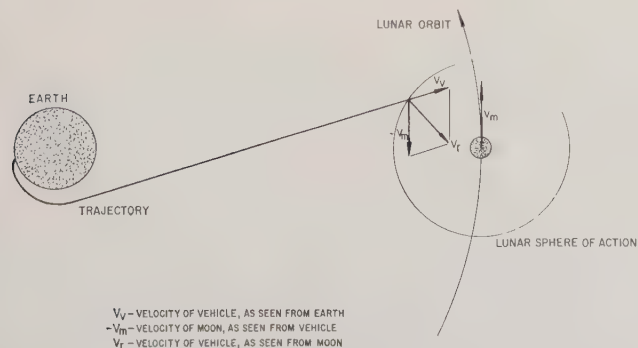


Fig. 4—Entering the lunar sphere of action.

lunar sphere of action, then the motion will occur mainly under the lunar influence. From the vehicle speed  $V_v$ , see Fig. 4, and the lunar speed  $V_m$  (both with respect to Earth) we get the relative speed  $V_r$  between the vehicle and the Moon.  $V_r$  is at least equal to  $V_m$  as can be seen from the diagram. Lunar escape speed  $V_{esc}$  at the border of the lunar sphere of action is about 0.6 km/second. Since  $V_m \approx 1$  km/second,  $V_r > V_{esc}$  and motion within the lunar sphere of action is always hyperbolic. This explains the need for rocket braking when establishing a lunar satellite. As the flight hyperbola can intersect the lunar surface, an impact or rocket braked landing is possible. Allowable errors of very few meters per second in speed and one-fourth of a degree in angle at injection must not be exceeded if a lunar impact is desired. If larger errors are present, then corrections have to be applied either shortly after engine cutoff (vernier) or at some midcourse position or in a terminal phase. Larger errors are allowable for certain trajectories particularly with respect to injection speed. Those trajectories with the more favorable guidance conditions will probably not be used since these require that the vehicle path and lunar motion be coplanar, a condition difficult to realize from our existing launch sites. While the coplanar flight generally eases the guidance problems, azimuth control must be closely maintained to keep the planes in coincidence.

Circumlunar flight which results if the vehicle misses the moon will be discussed next.

### CIRCUMLUNAR FLIGHT

Flight around the Moon is generally classified as strong or weak lunar encounters. Let us consider first the strong encounter or the close lunar miss. In Fig. 5, the vehicle enters the lunar sphere of action at  $P$  with a relative velocity  $V_r$ , which is hyperbolic. It leaves again with  $V_{r2}$  where  $|V_{r2}| = |V_{r1}|$  from the energy law.

As seen from Earth, the speed is now  $V_E > V_A$ . The vehicle has gained energy, and since it was near parabolic velocity before the encounter, it is probably hyperbolic. This diagram explains the mechanics of energy

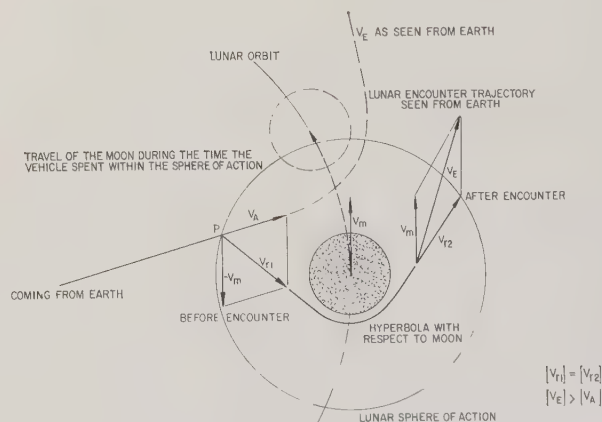


Fig. 5—Motion within the lunar sphere of action.



gain, the possibility of which we have found from Jacobi's Integral.

The Moon in its orbit around Earth has a leading and a trailing portion. It follows from geometrical considerations that energy gains will result when the point of closest approach is over the trailing half as shown in Fig. 5, and that energy losses will result from encounters with the leading half of the Moon. For close circumnavigation with subsequent return to Earth, it is desirable to pass the forward face to prevent an energy gain.

After the lunar encounter, the orbit can be approximated again as an ellipse in the Earth's sphere of action. The closest approach to Earth is given by  $r_{\min} = a(1 - E)$  where  $a$  is the major axis and  $E$  is the eccentricity. If energy has been lost in the encounter,  $a$  becomes smaller. The eccentricity is usually near one before the encounter and decreases in the encounter.

It can easily be seen that for near vertical approaches to the Moon, the area constant  $C_k$  in Keplers Second Law will increase in the encounter because of an increase in the speed component which is vertical upon the radius vector. Any small increase in  $C_k$  causes a decrease in  $E$  for elliptics orbits. Therefore the total change of  $r_{\min}$  cannot be generally stated. It may stay constant, decrease, or increase in the encounter.

If at launch the injection point coincides with  $r_{\min}$ , which would imply horizontal injection, then two possibilities exist:

- 1) To keep the vehicle in orbit for a long time it would be desirable to increase  $r_{\min}$  or at least not to decrease it; or
- 2) to recover the vehicle after one orbit, it would be desirable to maintain or to reduce  $r_{\min}$  to assure impact with the Earth. In the special case for near tangential entry into the Earth's atmosphere  $r_{\min}$  should be kept nearly constant.

Indeed by proper planning of the encounter, either of the two cases can be realized. It is known that for example the Soviet Lunik III increased  $r_{\min}$  so that the lifetime was longer than one revolution in spite of the energy loss due to the leading half encounter.

Following these explanations of the general problems, let us look at the guidance problems. First let us assume that injection conditions have to be nearly correct and that no midcourse or terminal corrections will be made. The margin for error for typical trajectories is of the following order for the coplaner problem. (Table II.)

TABLE II

	Mission	Conditions at Cutoff	
		Speed Margin, Meters/Second	Angular Margin, Deg.
1	Hit the Moon	10	$\frac{1}{4}$
2	Circumlunar trip with return to Earth	10	$\frac{1}{4}$
3	Lunar satellite	1	0.01
4	Circumlunar and return to Earth	0.1	0.001

For the first two missions, the requirements may be met by guidance systems; however, the last two missions require accuracies not possible to realize with injection guidance only. Even were the guidance accuracies sufficient for the last two missions, our knowledge of the physical constants is limited such that the exact value of the ideal injection speed is not known to within 0.1 meters/second. Therefore, midcourse and probably terminal guidance applications will be mandatory.

It is interesting to mention that the trajectory shape will look quite different when plotted in an inertial or the Jacobian coordinate system. Whereas in an inertial system we may have a perturbed ellipse, we may well have the familiar figure eight shape in the Jacobian system. The total flight time for the round trip varies mainly as a function of the maximum distance from Earth. For flights which reach far out in order to avoid close lunar encounters with their strong perturbations, a round trip time of 15 days is typical whereas for strong encounters about 10 days might be typical. In a weak encounter, the vehicle stays outside the lunar sphere of action. This reduces difficulties, as now only minor changes occur in the orbital elements. On the other hand the large distance from the Moon will hinder or prevent some of the desired measurements.

So far only the gravitational influences of Earth and Moon have been considered and these only approximately. There are many refinements necessary for more accurate solutions and these include:

- 1) Exact shape of the lunar orbit and the lunar motion in it.
- 2) Exact gravitational field of the Earth and Moon.
- 3) Solar and planetary gravitational perturbations.
- 4) Radiation pressure, drag, micrometeors, relativistic effects, etc.

In the Earth to Moon flights, the influence of these effects can often be neglected. However, in the circumlunar flights even small deviations of the approach trajectory to the Moon result in a wide deviation of the trajectory after the encounter: The Moon acts as a mechanical amplifier for these small course deviations. Therefore, these small perturbations usually have to be considered. While their influence on the energy requirements is negligible, it does effect the guidance accuracy requirements.

Fuel requirements for corrective actions may be an order of magnitude lower if the deviations are corrected before the lunar encounter rather than after the encounter. The burden of the problem is in the guidance area.

### THE THREE-DIMENSIONAL PROBLEM

The planar case which has been described in the preceding paragraphs is relatively simple. As indicated above, few if any flights to and around the Moon will be coplanar. Doglegging from our present launch sites to place the vehicle in the lunar plane may be accomplished

but only with costly energy losses. It may be expected therefore that an inclination between the lunar plane and that of the vehicle trajectory will exist and that the vehicle's lunar encounter will be in another lunar centered plane with still another Earth centered plane for the return trajectory.

We know that the major axis  $a$  and the eccentricity  $E$  are changed by the encounter. As depicted in Fig. 6, the line of nodes and the inclination will be changed too. The argument of pericenter and epoch are also altered meaning that generally all elements of the approach orbit differ from those of the return orbit. As the changes are quite substantial (see for example inclination in Fig. 6) it is better to consider the approach and return orbits different with some parameters, like energy, being similar.

It is important that the drastic changes induced by the lunar encounter can be explained by the Newtonian gravitational force and in principle by the simple construction seen in Fig. 5, now applied for three dimensional space.

The trajectory, Fig. 6, is not unlike that of Lunik III. It is noted that both the ascent and descent legs of the trajectory occur over the North polar region, a feat which is impossible in the two-body problem. The increased capability of the three-body problem over the two-body provides advantages of judiciously locating tracking and receiving stations in one global area.

Regarding the atmospheric entry point at Earth for the return flight, this point may vary greatly because of the afore described change in inclination.

If the vehicle is at point  $P$  in Fig. 7, it can be shown that there is one trajectory going from  $P$  to  $A$  which is horizontal at  $A$ . This trajectory is connected with a flight time which may not be a desirable one. A new trajectory and flight time is tried and point  $A'$  is reached. If an acceptable trajectory is found then an appropriate correction has to be given at point  $P$ . This correction may be undesirably large or it may even be impossible to transfer at  $P$  to an acceptable trajectory. Therefore it may be that the return flight arrives at a "bad" time. Flight time deviations mean that both the longitude and latitude of the landing spot may vary since the Earth is rotating  $15^\circ$  per hour or 1700 km per hour at the equator. Unless corrections can be effected during the atmospheric portion of the entry flight large deviations of longitude and latitude must be planned for.

Some remarks on the aerodynamic landing phase follow. Rocket braking to any large extent can hardly be considered because of the extremely high energy requirements involved.

#### RE-ENTRY AND RECOVERY

The primary purpose of the circumlunar mission is the recovery of data and/or personnel. Accomplishment of this mission is by one of two basic maneuvers: namely the near miss (of Earth) or the physical recovery.

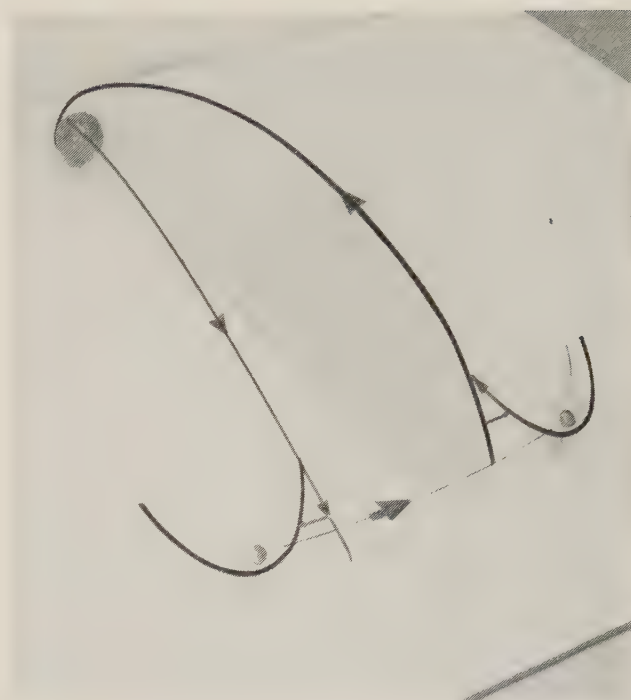


Fig. 6—Three dimensional model of a circumlunar trajectory. In other multibody problems as for example, interplanetary transfer, fundamentally similar considerations prevail.

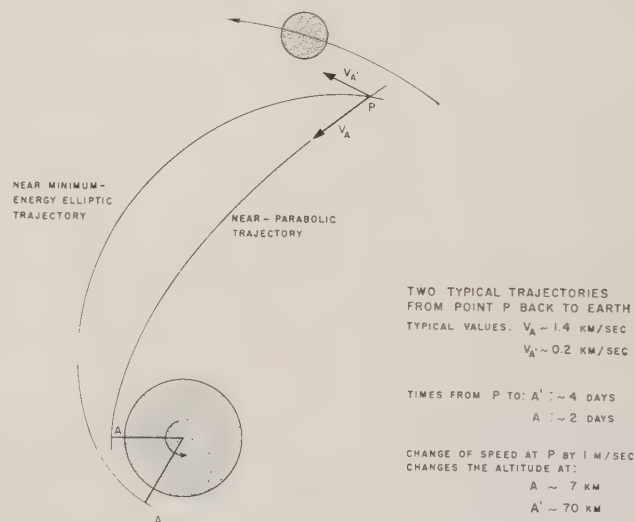


Fig. 7—Return to Earth.

In the case of the near miss, data is recovered by some means of communications such as radio or TV as the vehicle passes near Earth. The  $r_{\min}$  may be such that the vehicle lightly enters or misses completely the Earth's atmosphere on its return flight. Such was the case of the Lunik III. It is the second case, that of re-entry, to which we now direct our attention.

From the preceding sections, it appears that the accuracy of hitting the entry corridor will depend on the available guidance accuracy and available propellant mass for course corrections.

Entry into the earth atmosphere is one of the most critical phases of the circumlunar flight. Maximum entry "g" levels, the method of heat protection, maneuvering requirements within the atmosphere and the accuracy



capability of the trajectory followed prior to entry, all greatly influence the design of the entry body.

Chapman<sup>1</sup> points out that at near parabolic speed the width of the entry corridor for a maximum deceleration of 10 g's is approximately seven miles for a typical ballistic entry body. Chapman also discusses the aerodynamic heating problem showing the effects on both conical ballistic type entry bodies with moderated drag control and the winged entry high lift body.

Excessive "g" levels and/or heating rates above the protective capability of the coating materials will result from entry on the low side of the corridor and a skip and/or excessive total heat transferred will occur if entry is made above the upper limit of the corridor.

Among the factors which influence the ability to hit the corridor, in addition to those described in the previous sections of this paper, is the lack of knowledge of the upper atmosphere. The exact location of the corridor will vary seasonally, with latitude, with wave effect and perhaps even under the influence of local ground disturbances.

The corridor width and location are also changed by the vehicle characteristics. Generally a higher  $L/D$  will widen the corridor and for a given body the altitude of the corridor will shift with a change in ballistic factor. Application of body lift to a conical entry body will give values around  $L/D=0.5$  at hypersonic speed.

The enormity of the problem of obtaining, through trajectory corrections at point  $P$  in Fig. 7, an  $r_{\min}$  which will satisfy all the variables, is now apparent. Midcourse corrections will be required to hit this corridor.

Because of the small width of the corridor and the physical limitations to entering on the low side, it is wise to examine more closely the upper limits of the entry corridor (Fig. 8). As indicated above, entry into the area above the upper limit of the corridor will result in a skip back out of the atmosphere. The passage through the atmosphere results in a loss of velocity but not sufficient to reduce the parabolic velocity to circular velocity or below. If the earth pass is near the "edge" of the atmosphere only a small velocity loss will result and the flight might look like that shown in Fig. 9. If on the other hand, the earth pass is nearer the corridor then a new orbit with a period of perhaps hours may result. In either case, that of an orbit back out to near lunar distance with a period of a week or more or one with a period of an hour and a half or more, control may be maintained through proper short thrust applications at apogee.

The principle reason for more accurate control of the  $r_{\min}$  through apogee corrections (after the first pass) is the fact that the corridor location is now accurately known. Variation of the apogee speed by one meter per second will result in changes of  $r_{\min}$  in the order of 5 to 100 km depending on the orbit of the vehicle.

<sup>1</sup> D. R. Chapman, "An Analysis of the Corridor and Guidance Requirements for Supercircular Entry into Planetary Atmospheres," NASA, Washington, D. C., Tech. Rept. No. TR-55; 1959.

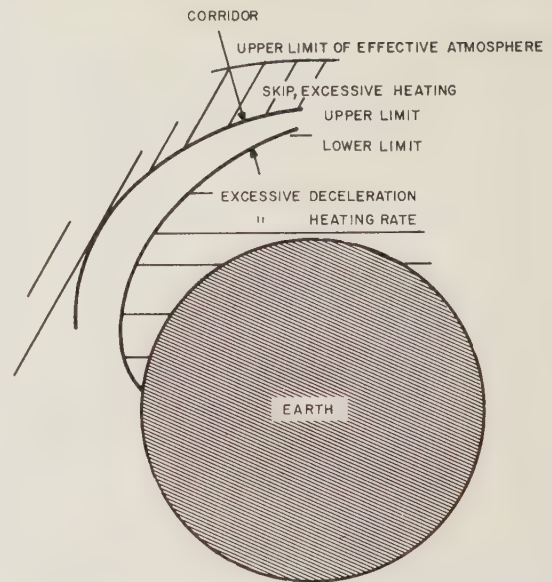


Fig. 8—Earth atmospheric entry corridor.

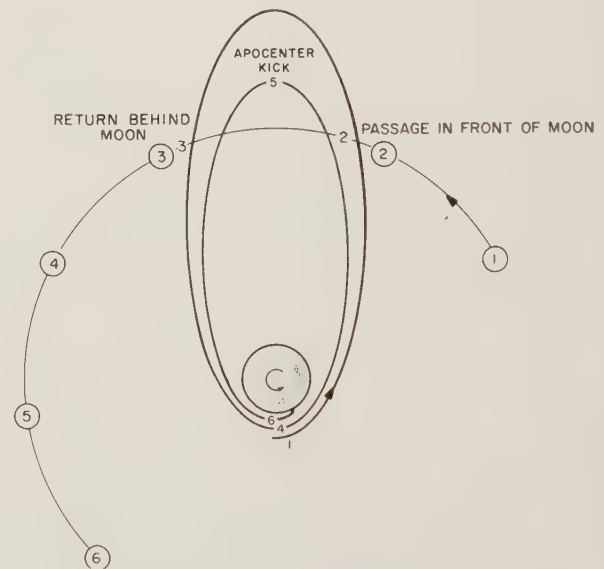


Fig. 9—Orbit and braking ellipse.

Because the skip maneuver has been performed, and sufficient time will elapse between the skip at perigee and the necessary control at apogee, the new orbital elements may be accurately calculated such that a second or third pass may be executed reducing the velocity to more nearly circular or even maintaining that which the vehicle has after the first pass. Addition of a retro kick at apogee will of course cause the vehicle to dip deeper into the atmosphere thus losing velocity at a greater rate.

The use of apogee control to hold off the final entry phase becomes increasingly important for systems where guidance limitations or where unfavorable (from the return stand point) lunar passages make the one pass re-entry unsuitable. It may be highly undesirable to enter on the first pass since the landing point may not be near a recovery area. As discussed above, the

control of entry into the corridor and time of entry and therefore the touchdown location may exceed the capabilities of the guidance and propulsion systems.

The total heating problem may be materially eased by the skip maneuver in spite of an increase in total heat transferred since a radiating type heat sink will cool down during the space portion of the flight picking up only incremental heat loads during each succeeding re-entry pass.

The use of a high drag device such as a balloon or large extendable flaps to slow the vehicle at a much higher altitude should also receive consideration when studying the heating problem. Such a device will generally bring the vehicle to entry on the particular pass during which the device is used.

Design of the re-entry body will influence the maneuver capability of the body. The nonlifting body with flaps may have a very limited flight path variation capability while the high lift body might be capable of up to 2000 miles of corrections. If the atmospheric entry point is so located that the touchdown would occur over one of the polar regions, then even 2000 miles might not be sufficient. All of which indicates that it might be highly desirable to hold off the final entry until a more favorable touchdown position becomes available.

Not only may the vehicle land in the general vicinity

of the poles but since  $\frac{5}{7}$  of the earth is covered by water, water and land landing and recovery must be considered for any vehicle. As the landing might occur on land in remote areas (only  $\frac{1}{6}$  of the land mass may be considered to be suitable) the vehicle must also be capable of rough ground landing. These considerations point out the desirability of control of entry times and location, and stress the necessity for all around survival equipment.

Final descent to the earth surface will involve the use of a parachute for the vehicles with no lift or with very low lift capabilities. Considerations of the winged vehicle of the Dynasoar type will provide limited glide capabilities. It is also conceivable that extendable wings and a small conventional air breathing power plant may be used to further extend the maneuverability of the entry vehicle.

The extension of the time in space through the skip maneuver will increase the requirements for the life essentials carried on the trip in the same manner in which the possible long time from landing to pickup will increase the requirements for those life essentials needed on earth.

Thus we see that a single two body solution of the lunar circumnavigational flight does not introduce the many complicated and interwoven factors which must be considered even for preliminary mission studies.

## Evolution of the Saturn Booster Telemetry System\*

JAMES E. ROREX†

**Summary**—This paper describes the telemetry system to be used on the Saturn booster and, by way of introduction, a brief description of the Redstone and Jupiter telemetry systems is given. The additional requirements for the system caused by the multiple engine booster are pointed out and the design consideration for the system is discussed. A description of the Saturn telemetry equipment is discussed in general block diagram form. No detailed circuit description is given. In conclusion, the physical and electrical characteristics and accuracy requirements are outlined.

### HISTORY AND BACKGROUND

MUCH of the telemetry system developed for the Saturn booster has evolved from systems used in the Redstone and Jupiter missiles. In 1952, the original telemetry system was developed for the early Redstone missiles. This system was constructed of TM components commercially available at that time. Since the telemetry industry was in its infancy, there was not a

great variety of TM components available. The system was a large one-piece chassis with the components plugged in from the front for easy accessibility. Any component that proved unsatisfactory could be easily replaced without removing the chassis from the missile. The system was FM-FM using 16 RDB subcarriers, two of which were commutated (PAM, 10 rps). A five point in-flight calibration was accomplished with a motor driven cam arrangement that actuated calibration relays. This unit weighed about 130 pounds.

The flight records of the early missiles which carried these first systems were very satisfactory from a telemetry standpoint. These units proved to be reliable in operation, serviceable, and capable of accurate data transmission.

Because of the bulkiness of this package, a second unit was designed in 1954 to attempt a reduction in space and weight. Although this end was partially accomplished, the resulting design contained many characteristics considered undesirable. Servicing was difficult and mechanical and electrical design was far from ideal. The choice of TM

\* Manuscript received by the PGMIL, February 1, 1960.

† U. S. Army Ballistic Missile Agency, Redstone Arsenal, Huntsville, Ala.



components at this stage was not considered optimum. This package, called the XO-1, weighed about 110 pounds and occupied 4080 cubic inches.

In 1956, another unit was designed to be used on the early Jupiter missiles. This unit had electrical characteristics similar to the first two units but was a complete redesign so far as the components used and the package layout were concerned. The unit used the latest state-of-the-art components. These components had been sufficiently tested and compared with all other commercially available components to prove specified accuracy and reliability requirements to be realistic. Experience gained with the previous units helped considerably in selecting components and designing the unit. The performance of this unit proved to be very satisfactory. The major objectionable features of the previous units were eliminated. Serviceability and accessibility were greatly improved. Reliability of the components and the unit as a whole was excellent. Three of these units were used on each of the early Jupiters in order to facilitate an average of about 160 measurements. (This figure pertains to the booster and does not include the nose cone.) This unit, called the XO-2, had a volume of approximately 3560 cubic inches and weighed 71 pounds.

Although these units had proved to be excellent from the standpoint of reliability and accuracy, further reduction in size, weight, and power was considered essential. Early in 1958, another telemetry transmitting set was designed. This set was designated the XO-4. Again, the latest state-of-the-art advances available in practical hardware at that time were applied.

Primary considerations of the design in order of the emphasis applied were:

- 1) Reliability,
- 2) Accuracy,
- 3) Minimum size and weight,
- 4) Flexibility,
- 5) Serviceability.

Considerable emphasis was placed on size and weight reduction, since the previous design had been very satisfactory in the other characteristics. No sacrifice of reliability or system accuracy could be tolerated in order to conserve space and weight, although some reduction in serviceability compared to the previous design was necessary. Transistorization was not a primary goal in the design, and transistors were used only in applications where the resulting characteristics of the set would be definitely improved over the use of vacuum tubes.

As in the other designs, commercially available items were utilized wherever practical in order to reduce the cost of development and increase producibility of design. Some modifications were made on several of the components used. In addition, several components were designed in-house because a satisfactory version was not available commercially. Fig. 1 is a bar graph comparison of the size and weight of these units. Fig. 2 is a view of the XO-1, XO-2, and XO-4 packages.

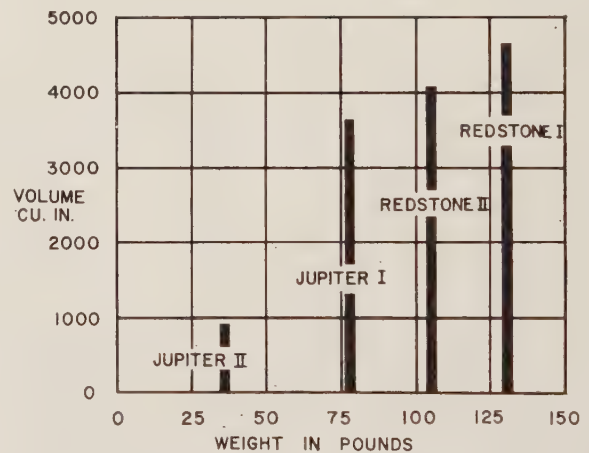


Fig. 1—Bar graph comparison of weight and volume of several Redstone and Jupiter TM systems.

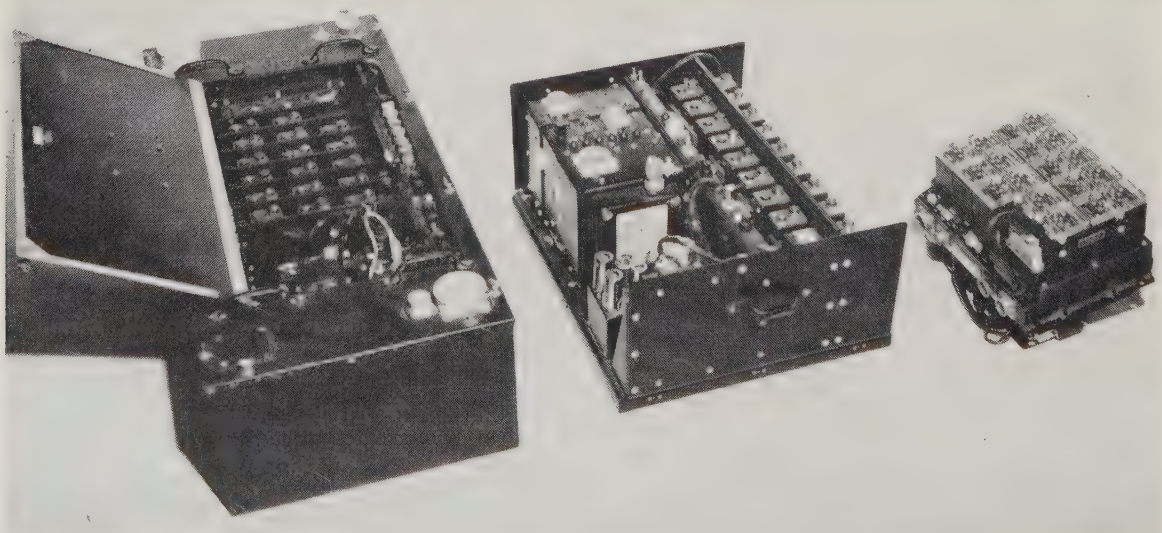


Fig. 2—View of model XO-1, XO-2, and XO-4 TM sets.

## SATURN CONSIDERATIONS

The Saturn booster, now under development at the Army Ballistic Missile Agency (ABMA) contains a cluster of eight Rocketdyne H-1 engines and develops a thrust of 1.5 million pounds. The system is designed in such a manner that failure of any one of the engines will not impair the flight. To accomplish this, it is not only necessary to have independent engine systems, but separate electrical network and measuring systems are required for each engine as well.

The magnitude of the Saturn as compared to the Jupiter increases the requirements for telemetry channels by a comparable magnitude. After the data requirements were compiled and reduced to essentials, the total number of measurements desired is approximately 575. Some of the data are superimposed and time-shared in order to reduce the actual channel requirement to approximately 530. The majority of these are low enough in frequency response to be commutated. However, 21 of the measurements are vibration data that require a frequency response of 1000 cps or more. It is obvious that with the existing FM-FM equipment, the number of TM links would have been excessive and a new approach to the problem was necessary.

In the solution of the problem, the same criteria of previous designs were followed, as well as these additional considerations:

- 1) The system must be, as far as practicable, compatible with existing receiving and recording equipment.
- 2) Existing data reduction equipment must be used to the fullest extent.
- 3) The data must be in such a form that preliminary flight evaluation can be made at the launch site by "quick-look" methods.
- 4) In keeping with the principles of evolution and for reasons of reliability, economy, and familiarity of operational personnel, the system should use, whenever possible, proven components now used on the Jupiter.

## SS-FM SYSTEM

The total data bandwidth capability of an IRIG FM-FM link operating at a subcarrier deviation ratio of 5 is approximately 4 kc. This is a base-band frequency utilization of less than 6 per cent which is obviously inadequate for wide-band data transmission. At this point, it might appear that the best solution for such a problem would be bandwidth reduction by "predigesting" a considerable amount of the data on-board. Although systems are being developed by ABMA that will accomplish this to a large degree, there are several reasons why it is not the best approach for this particular application. The number of test flights for the Saturn are very limited with respect to other programs and therefore all data that are practicable must be obtained. Data "predigestion" is a statistical tool that only reveals certain predetermined statistical data. For R&D flights where it is necessary to reveal the cause of a specific malfunction, statistical data do not supply sufficient information. This is only one of several reasons why on-board data

analysis will not be used extensively on the early Saturn boosters.

Transmission systems utilizing single side-band modulation of an AM subcarrier have been in use for some time in the field of carrier telephony. Such a system for missile-borne telemetry applications has been discussed but has not been seriously considered because of the difficulties in implementing hardware that would meet the requirements of on-missile use. However, recent advances in the development of electronic components, particularly miniature mechanical filters, make it feasible to develop such a system. A subsystem being developed by ABMA for use on the Saturn, utilizing single side-band techniques, will have a base-band utilization efficiency of 60 per cent. Compared to the FM-FM system, this is more than a tenfold increase in efficiency. The system basically consists of fifteen single side-band AM subcarriers on an FM carrier, making the letter designation SS-FM appropriate. Fig. 3 (next page) is a block diagram of the SS-FM subsystem.

The data input of each channel is fed to a balanced modulator and heterodyned with a 455-kc carrier. Neither of the inputs appears at the output of the modulator, only the sum and difference. The output of the modulator is fed to a mechanical band-pass filter which passes only the upper sideband (455-458 kc). A mechanical filter that meets on-missile environmental specifications, and has a shape factor of 1.5, a pass-band peak-to-valley ratio of 1.2 db, and a 5-db insertion loss, has been developed by Collins Radio Company for ABMA. The filter is about 0.4-inch in diameter and about 2.5-inches long. The 455-kc frequency was selected in order to utilize standard tooling in the manufacture of the filters.

To minimize the effects of filter drifts that may attenuate the low frequencies, the carrier has been placed approximately 50 cycles inside the pass band. As a result, data frequencies below 50 cycles are transmitted double side-band, causing phase distortion at these low frequencies. A scheme that will suppress the vestigial sideband by about 40 db is being exploited. If the circuit proves feasible, the low-frequency response will be much less than 50 cycles. The system is presently considered to have a low-frequency response limit of approximately 25 cycles. Where lower-frequency vibration data are necessary, it can be filtered and applied to FM-FM channels.

The second modulator translates the filter output to an assigned base-band frequency. The base-band position is determined by the tone supplied to this modulator from the frequency synthesizer. The output circuitry of the modulator is sufficiently broadband to permit use of the same modulator design for any channel unit. It should be noted that the channel units are identical, thus satisfying the serviceability and flexibility requirements of the design criteria. The output of the channel units are mixed, amplified and fed to a very linear FM transmitter.

The function of the frequency synthesizer is to generate the fifteen carriers for the second modulators and a synchronizing tone for the ground equipment. To accommo-



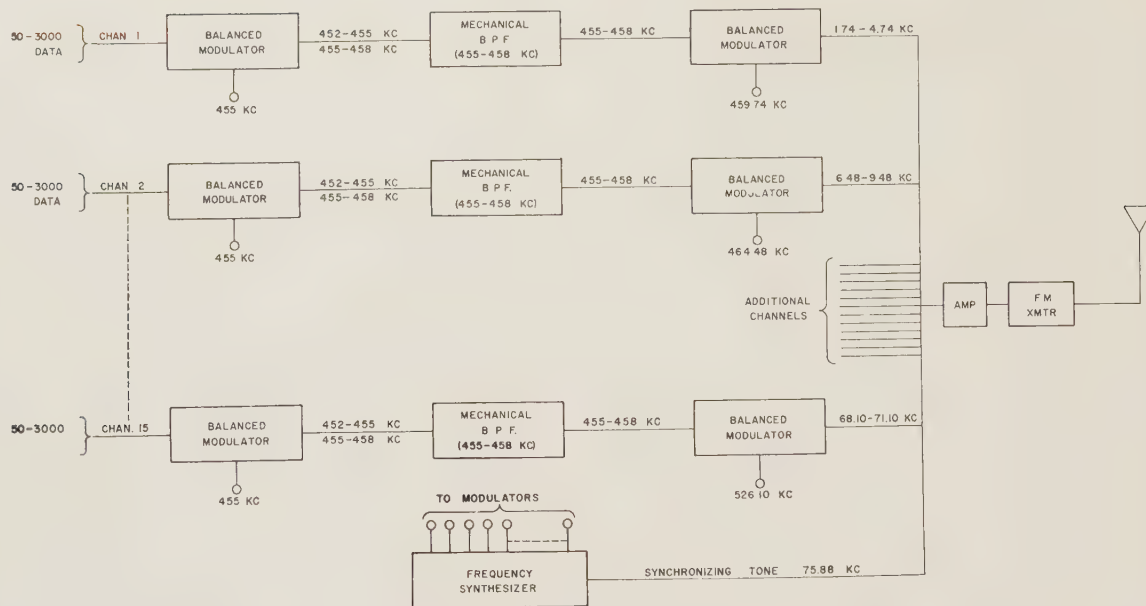


Fig. 3—Block diagram of SS-FM TM subsystem for vibration and other wide-band data.

date a 3-kc information bandwidth and allow sufficient guardband, a channel spacing of from 4.5 to 5-kc was desired. For convenience in designing the frequency synthesizer, 4.74 kc was chosen. This allows an adequate guardband of 1.74 kc. With this spacing, the base-band spectrum extends from 1.74 to 71.10 kc. To facilitate slaving of the ground demodulators to the on-missile reference signals and to simplify on-missile equipment, all the reference signals are derived from one master oscillator. This oscillator is crystal controlled at 910 kc. A selective spectrum generator produces a spectrum of frequencies that are separated precisely by an equal spacing of 4.74 kc. The desired frequency components of the spectrum generator are separated by a set of comb filters. These filters are mechanical filters similar in construction to those used in the channel units. The output of each filter is amplified and fed to the relevant modulator.

The synchronizing tone was chosen to be 75.88 kc since it falls just above the highest base-band frequency and is available in the divider chain from the master oscillator. This tone is used as a reference in reconstructing carrier signals in the demodulation equipment. The tone has other functions, the most important being an AGC reference. Since most instrumentation tape recorders introduce amplitude modulation, AGC is necessary to eliminate this effect. The AGC feature is also used as a scale factor in correcting for on-missile automatic deviation control of the transmitter.

Conventional FM-FM telemetry receivers and tape recorders may be used for recording the data; thus it will not be necessary to purchase additional equipment for receiving stations. At data reduction stations, demodulation equipment is essentially the same as the on-missile hardware. The primary differences are additional output amplifiers and AGC detection and correction circuitry.

Later in the program, this system may be used to carry FM subcarriers, sound intensity measurements, commutation wave trains or voice communication. The flexibility of the system will undoubtedly lead to many diversified uses in the future.

The airborne portion of this system will be packaged in a volume of about 300 cubic inches, weigh about 15 pounds, and consume about 22 watts of power. These figures do not include the power amplifier that may be used for some applications. The amplitude accuracy is about 5 per cent.

#### PAM-FM-FM SYSTEM [2]

The greatest number of data channel requirements for Saturn are for data of low-frequency response. More than 400 such measurements are to be made. In the past, data in this category have been multiplexed by the required number of 27-channel mechanical commutators (PAM). These commutators have been troublesome to maintain but have proven very reliable in flight. Of course, the mechanical switch approaches the ideal in accuracy and, as a result, accuracy requirements have not been difficult to maintain.

A 216-channel PAM-FM-FM subsystem has been designed which will adapt the system to the increased demand of commutated data channels. Fig. 4 is a block diagram of the PAM-FM-FM subsystem.

The heart of this system is a 216-channel transistorized multiplexer. The number of channels was chosen so that existing decommutation equipment could be used for demodulation and, at the same time, achieve a "quick-look" feature for comparing the performance of the eight engines. Each of the submultiplexers will sequentially sample identical measurements for each of the eight engines. For example, submultiplexer number 1 may sample "temperature lox pump bearing" on each engine while submultiplexer number 2 samples "pressures at fuel pump inlet."

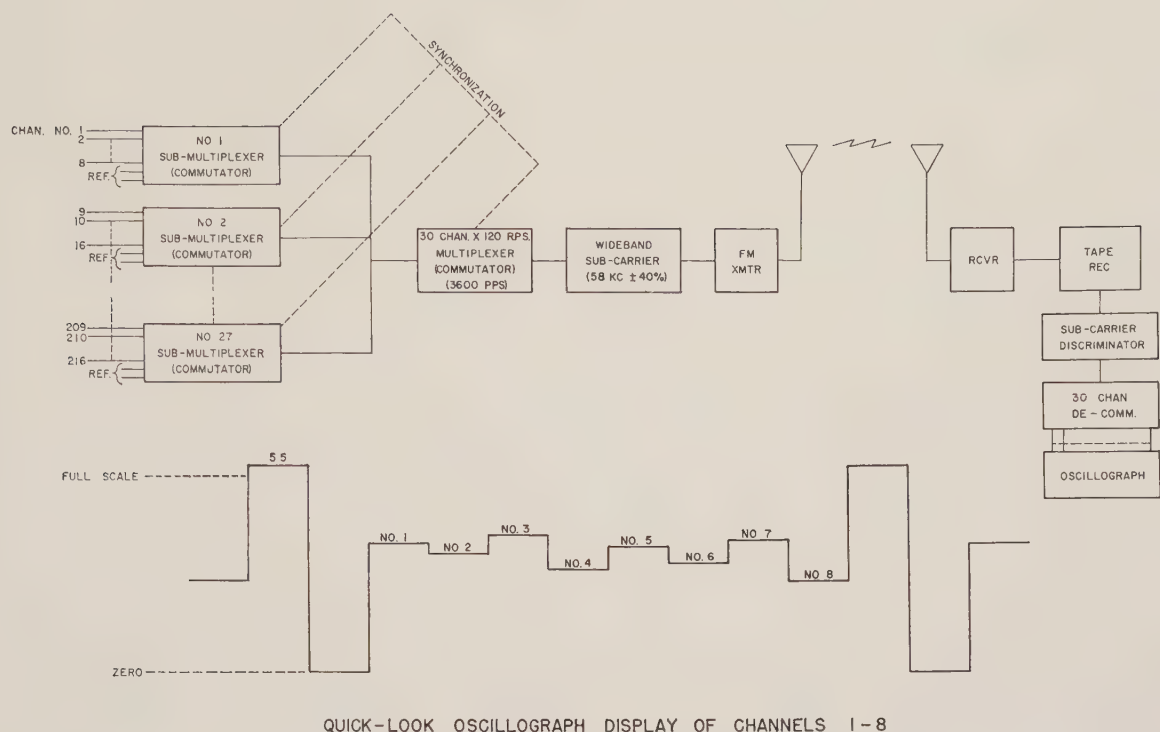


Fig. 4—Block diagram of 216-channel PAM-FM-FM TM subsystem.

Two channels of each submultiplexer are used for frame identification and voltage reference making a total of ten channels. The main multiplexer sequentially samples each of the 27 submultiplexers. Three additional channels are used for voltage reference and master frame synchronization. In order to maintain the accuracy that had been achieved by the mechanical commutators, special attention was given to the design of the transistor gates. As a result, a gate that approaches the characteristics of an ideal switch has been developed. The master frame format is identical to the IRIG-PAM commutation format operating at a rate of 3600 pps. Each data channel is sampled 12 times per second. The data may be handled by the standard IRIG decommutator by playing back the tape recording at 1/4 the recorded speed, resulting in a rate of 900 pps. Some decommutators will handle 3600 pps in real time.

Fig. 4 shows how the output of an oscillograph recording of one decommutated master channel would appear. In order to show the individual subchannels, the channel outputs are shown at different levels. If all engines are functioning properly, the channel outputs will appear practically as a continuous line on the oscillograph, enabling engine malfunctions to be detected at a glance.

If it is desirable to separate the individual data channels, this may be accomplished by feeding the output of each demodulator of the decommutator to a subdecommutator. To facilitate this, the submultiplexer frame identifying pulse is 110 per cent of the master frame synchronizing pulse, allowing amplitude comparison techniques to be used for synchronization of the subdecommutator. Most data reduction centers can handle this format with automatic digitizing equipment with no difficulty.

The output of the multiplexer is fed to a 58-kc wide-band subcarrier. This frequency was chosen in order to use a commercially available oscillator that will accurately carry the 3600-pps wave train and utilize existing demodulation equipment. For 1/4-speed playbacks a 14.5-kc ± 40-per cent discriminator plug-in may be used. For real time or full speed playbacks, a 58-kc ± 40-per cent plug-in is used. The FM transmitter is the same type used on the other links. Transmitter power of 2.5 watts will be adequate for this particular application if no additional SCO's are used. Low frequency SCO's may be added when required.

The total package for this system will weigh about 20 pounds, have a volume of about 400 cubic inches and consume about 20 watts. The system accuracy is better than 3 per cent.

FM-FM SYSTEMS

The additional links necessary to complete the data requirements for the system will be made up of four XO-4B packages. The ABMA model XO-4B telemeter package is an FM-FM system with 15 channels of continuous data plus 54 multiplexed data channels. The multiplexed channels are switched by two 27-channel mechanical commutators and applied to the 22- and 30-kc channels, PAM at 10 rps. All data inputs are 0-5 volts. In-flight calibration is in five steps and is started by on-board program command. A special program plug is incorporated in the system so that calibration may be withheld from channels where required. Preflight calibration is accomplished by command from the checkout console.

The XO-4 consists of components mounted on two chassis. One, the modulator unit, consists of the basic



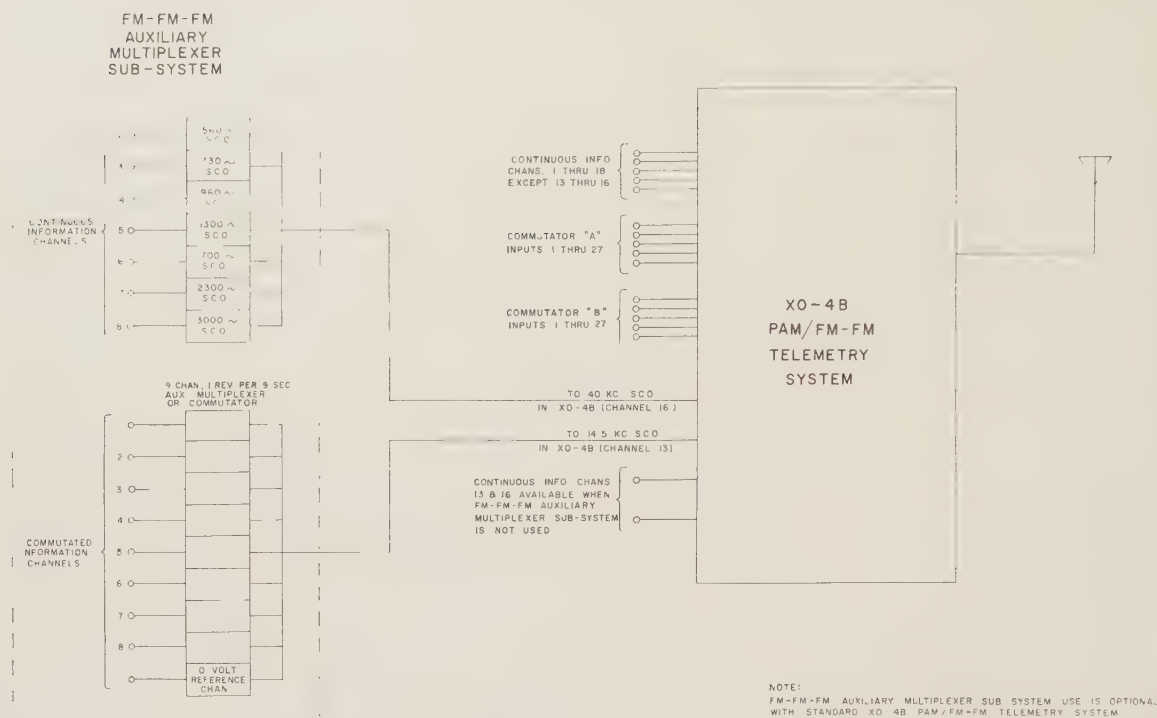


Fig. 5—Block diagram of PAM/FM-FM-FM and/or PAM/FM-FM TM subsystem for Saturn.

chassis on which is mounted the SCO's, mixer amplifier, transmitter, commutator switch, commutator gating unit, blower, calibrator, time delay relays, program plug, 150- and 250-volt power supply, and plugs to receive missile cabling. Weight is about 26 pounds. Most components are mounted independently so they may readily be removed without disturbing other components. The second chassis mounts the RF power amplifier and its associated 350-volt power supply. This unit weighs about 11 pounds. The volume of both units is about 800 cubic inches. Recent tests of the Jupiter missile have carried three of the XO-4 packages and the units have proven, thus far, to be 100 per cent reliable in flight.

#### FM-FM-FM AND FLOWRATE MULTIPLEXER

To increase the number of low-frequency-response continuous-data channels, three of the XO-4B packages will each have seven additional subcarriers modulating the 40-kc channel. Since these triple FM channels are less accurate than FM-FM, the triple FM data will be selected as those having lesser-accuracy requirements. Fig. 5 is a block diagram of this subsystem.

An auxiliary unit that plugs into the XO-4 package will contain the triple FM subcarriers as well as a transistorized nine-channel flowrate multiplexer. The multiplexer sequentially samples the flowmeter output from each engine. Each sample duration is approximately 1 second. The ninth channel is blank and is used for frame identification. To identify gating periods, a reference bias is built into the

multiplexer. The bias alternates on consecutive gates.

Each engine has three flow measurements: "main lox," "main fuel," and "lox flow-to-heat exchanger." For single engine boosters, the bandwidth was available to transmit flowmeter output continuously. In case of the Saturn, this would require 24 continuous channels, each with relatively high response. Accuracy requirements prohibit the use of converters unless a means of accurate calibration can be devised. A flowrate multiplexer may be added to achieve this accurate calibration. The flowmeter outputs are converted to dc and applied to commutated channels. The outputs are also sampled at 9-second intervals by the multiplexer. These samples are used to calibrate the converted data when the data are evaluated.

Each triple FM package adds about 7 pounds and 100 cubic inches to the XO-4 package.

#### CONCLUSION

A block diagram of the Saturn booster telemetry system may be seen in Fig. 6. The system consists of six independent transmission links. The data channel assignment has been based upon data bandwidth and accuracy requirements. Total channel capacity is 546 channels. Some data may be superimposed and time-shared on the same channels, thus increasing the number of available data channels. An effort to miniaturize equipment has been made only in cases where reliability and accuracy would not be sacrificed and costs would not be prohibitive. To achieve accuracy requirements, in-flight calibration is used where applicable.

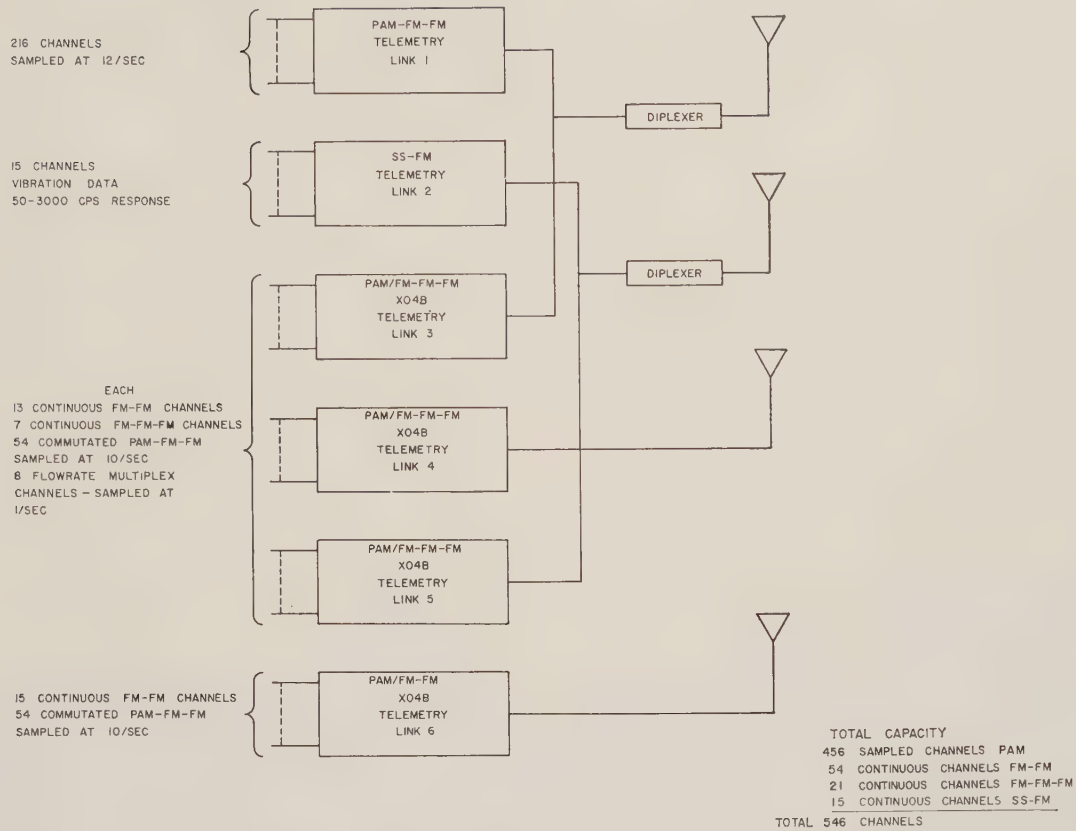


Fig. 6—Block diagram of complete TM system for Saturn booster.

Channel accuracies are as follows:

- 1) 456 sampled channels, PAM, accuracy 3 per cent,
- 2) 54 continuous channels, FM-FM, accuracy 1 per cent,
- 3) 21 continuous channels, FM-FM-FM, accuracy 2 per cent,
- 4) 15 continuous channels, SS-FM, accuracy 5 per cent.

For applications where accuracies of better than 1 per cent are essential, special techniques have been used. In these cases, bandwidth is traded for accuracy.

The complete system will weigh about 220 pounds and the system volume will be less than 3 cubic feet. Total input power is about 1600 watts. It should be noted that these figures include all primary power converters and 35-watt RF power amplifiers for five of the links. Most of the power is consumed by the RF transmitter and power amplifier portions of the system.

More detailed descriptions of the subsystems can be found in the reference material.

#### ACKNOWLEDGMENT

The author gratefully acknowledges the assistance received from his colleagues of the Telemetry Section and Instrumentation Branch.

#### REFERENCES

- [1] W. O. Frost and O. B. King, "SS-FM: a frequency division telemetry system with high data capacity," *Proc. Natl. Symp. on Space Electronics and Telemetry*, San Francisco, Calif., Sec. 7.2; September 20-30, 1959.
- [2] O. B. King, "A high capacity PAM-FM-FM telemetering system for the Saturn booster," *ibid.*, Sec. 7.1.
- [3] W. O. Frost, "An Approach to the Data Transmission Problems of Ballistic Missiles," paper presented at the IRE Region 3 Technical Meeting, Atlanta, Ga.; November 17-18, 1958.
- [4] O. B. King, "A transistorized calibrator for missile telemetry," *Proc. Natl. Symp. on Telemetering*, Miami Beach, Fla., Sec. 2.5; September 22-24, 1958.
- [5] W. O. Frost, "Distortion in FM-FM systems and its effect on system accuracy," *Proc. 1959 Natl. Telemetering Conf.*, Denver, Colo., pp. 45-52; May 24-27, 1959.
- [6] C. T. N. Paludan, "Redstone, Jupiter, Saturn: evolution of a measuring system," *Proc. ARS 14th Annual Meeting*, Washington, D. C., Pub. by ARS, New York, N. Y., reprint #1020-59; November, 1959.
- [7] L. B. Bell, "The army ballistic missile agency method of selection and application of measurements," *Proc. of the Fourth Natl. Flight Test Instrumentation Symp.*, New York, N. Y., ISA, Pittsburgh, Pa., pp. 138-142; May 4-6, 1958.





The President's command of the armed forces is exercised through the Secretary of Defense. The command communications channel extends from the Secretary of Defense through the Joint Chiefs of Staff to the Unified and Specified commands, who exercise direct command control over the operational military forces.

The internal command structures and deployment of the Unified and Specified commands vary widely, depending upon their missions and types of component forces. Fig. 1, which shows the major Unified and Specified commands, illustrates the internal structure of only one—CINCPAC. The Commander-in-Chief Pacific (CINCPAC) directs operational military forces throughout the Pacific Ocean area, consisting of Army, Navy and Air Force components. The Commander-in-Chief Alaska (CINCAL) also exercises command over Army, Navy and Air Force components; however, they are deployed in or near the Alaskan area rather than being spread over a large portion of the globe as in the case of CINCPAC components.

The Strategic Air Command consists solely of an Air Force component. Its nuclear bombers, ballistic missiles, and support elements are deployed throughout the world under the direct operational command of the Commander-in-Chief Strategic Air Command (CINCSAC), whose headquarters are located in central United States.

The Commander-in-Chief North American Air Defense Command (CINCNORAD), located near the Colorado Springs, Colo., area directs the Army, Navy and Air Force elements which are responsible for the air defense of the North American continent. His forces are deployed principally in the Far North along the Arctic Circle, in the continental United States, and in the U. S. coastal waters.

The Commander-in-Chief Atlantic (CINCLANT), while designated as a Unified command, exercises command principally over surface and undersea fleets. These fleet units are deployed in the Atlantic Ocean area.

The Commander-in-Chief Caribbean (CINCCARIB) exercises direction over the land, sea and air units responsible for the defense of the Panama Canal Zone and the U. S. territories in the Caribbean.

All of the commands discussed thus far are located on the North American continent. However, in several cases, elements of the command are widely deployed outside of North America, thus generating long distance command communication needs.

There are currently two major overseas Unified commands: The Commander-in-Chief Europe (CINCEUR) and the Commander-in-Chief Pacific (CINCPAC). Each of these has Army, Navy and Air Force components under the direction of the unified commander; however, the geographical deployment of components of CINCEUR is generally on the European land mass, whereas CINCPAC components are widely deployed in the Pacific, as mentioned above.

This, in general, describes the command aspects of the U. S. military organization and the pattern of supporting communications.

With regard to the Logistics/Administrative structure, the Departments of Army, Navy and Air Force have the responsibility of insuring that their overseas component forces are adequately trained and equipped. This involves an extensive complex of laboratory, depot and training activities within the continental United States. These activities must be interconnected with channels of communications and similarly connected to the military forces supported. As can be seen from Fig. 1, the communications pattern for Logistics/Administrative support is quite different from command support.

Because of the military security problem, it is not possible to present an elaborate discussion of the structure of the intelligence organization in an unclassified paper. The chart, therefore, illustrates an over-simplified concept of intelligence operations. Basically, however, intelligence data are gathered at overseas locations by intelligence activities of the military service and sent to various analysis agencies. This information is then analyzed and distributed as appropriate. The intelligence communication complex thus presents still a *third* pattern of military communications.

With this general picture of the organization, mission and deployment of the U. S. military activities in mind, let us examine this concept from a communications capability viewpoint to determine the adequacy of the worldwide means currently available.

From Fig. 1, it can be seen that a large part of the needed communication support for the military organization can be obtained through lease of commercial facilities. This is true in overseas areas as well as within the continental United States. While such communications are generally characterized by their flexibility, redundancy and reliability, military radio circuits are provided in some cases as an emergency back-up for more critical circuits.

However, this is not the area where the real communication problem lies. The provision of adequate reliable intercontinental long distance communications is the most challenging communications problem facing the military today.

A casual examination of Fig. 1 reveals the extent to which our military forces depend upon such long-distance communications. When the President is traveling outside the United States, his command channel must be extended to lower echelons through long-distance intercontinental communication circuits. CINCSAC's control of his air fleet and CINCLANT's control of his surface fleets are dependent upon such circuits. The command chain to the Unified commands in Europe and the Pacific and the internal command control of CINCPAC are exercised through long-distance circuits.

Intelligence activities and Logistics/Administrative support of overseas forces are geared to ready availability of long-distance intercontinental communication circuits.

Upon examining the importance of these long-distance communications channels in the light of available means for such communications, the potential significance of com-



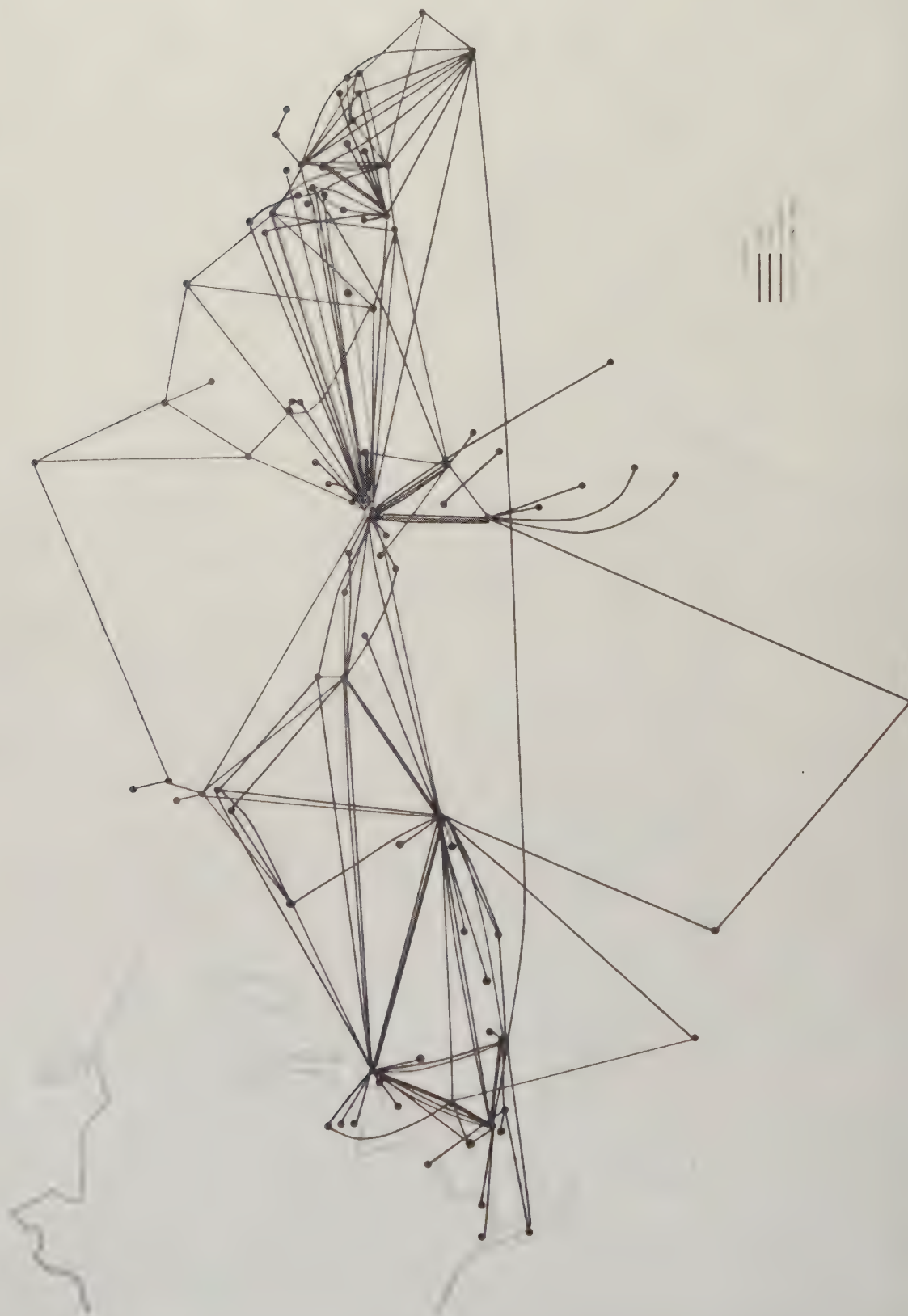


Fig. 2—World wide military communications.

munications satellites becomes evident. Fig. 2 is a composite chart showing the long-distance trunking networks of the Army, Navy and Air Force which are used to meet the needs described above. Generally, four modes are used in these networks: high-frequency radio, low-frequency radio, ionospheric scatter and submarine cable. While each of these modes provides some desirable characteristics, each suffers definite shortcomings for military communications. For example, high-frequency radio is vulnerable to natural ionospheric disturbances, Argus effects and intentional jamming. Unfortunately, it is the only available means of communications to some of our military forces. Low-frequency radio suffers from distance limitations, low information capacity and vulnerability to jamming. Ionospheric scatter suffers from propagation problems and distance limitations. Submarine cable provides virtually no flexibility, requires high installation time and is physically vulnerable. It is customary to provide redundancy in one mode or diverse modes to compensate for these shortcomings.

It is, therefore, easy to visualize the chaotic situation which might result in wartime. Extensive interruption of military radio or cable circuits due to natural or unnatural causes will leave many elements of the military organization without command direction and unable to employ intelligently the weapons provided them. The intelligence input to the Seat of Government will be severely restricted. Logistics and administrative support of overseas component forces will be severely hampered with possible serious consequences.

Because of these factors, military communicators, for many years, have been seeking means whereby excessive dependence upon unreliable means, particularly HF radio, can be eliminated. While some measure of hope was provided by the scatter techniques, limitations imposed by these systems restricted their potential areas of application. Now, however, the possibility of utilizing the communication satellite offers promise of overcoming many of the shortcomings of existing modes.

Communication satellites are potentially capable of meeting virtually all of the communication trunking needs shown in Fig. 2. However, the extent to which they are actually employed will depend upon their capabilities and limitations in relation to other competitive communication means. In this regard, it is not likely that the full theoretical potential of communication satellites will be attainable within the next few years, primarily because of booster limitations and power source problems. The initial operational communication satellites will, therefore, probably be compromise systems which will be used to augment rather than replace more conventional trunking systems.

A principal consideration in the development of military communication satellites is to insure compatibility with present and planned communication systems. As noted above, the area of utilization of communication satellites will most likely be as a trunking system. This trunking system must be responsive to three fundamental types of

communication needs: The first need is for a store-and-forward type service for messages and data which can tolerate a delay in switching and transmission; the second is for real-time communication service wherein minor switching delays can be tolerated but transmission delays are unacceptable; and the third is for full-time service wherein neither switching delays nor transmission delays can be tolerated.

These types of service are being provided today and they form the basis for design of future military communication systems. The Army, for example, is developing the Universal Integrated Communications System, known as UNICOM, the basic concept of which is illustrated in Fig. 3.

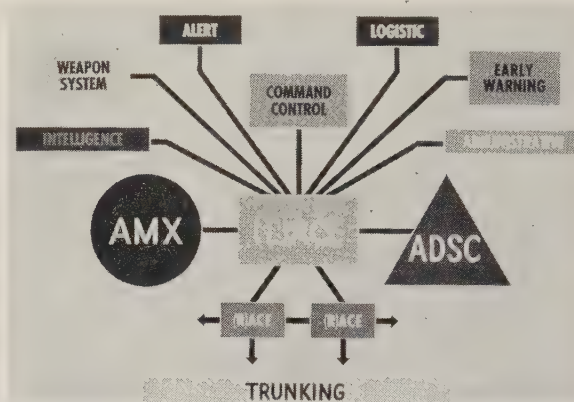


Fig. 3—UNICOM meets operational requirements.

In general, the administrative, logistics and some of the intelligence traffic illustrated in Fig. 3 will be handled by a store-and-forward type service. The remainder of the operational needs illustrated must be met with real time service. However, some categories of real time traffic must be handled on a full-time basis without switching delays, due to their critical nature.

The blocks labeled "LACE" (Local Automatic Circuit Exchange) and "RACE" (Regional Automatic Circuit Exchange) are circuit switching centers which will provide either real time service or full time service with an automatic restoral feature. The block labeled "AMX" (Automatic Message Exchange) is a store-and-forward switching center designed to accommodate messages which can tolerate a delay or which require special processing. The block labeled "ADSC" is an Automatic Data Service Center associated with the UNICOM system. Communication satellites fit into the picture in the bracketed area labeled "Trunking."

The Department of Defense is actively supporting a communication satellite program under the direction of the Advanced Research Projects Agency, intended to meet these trunking requirements. This program is based upon consideration of operational needs, technological limitations, funding limitations and timeliness. The principal efforts which currently comprise this program are known



as Project NOTUS, including Tasks COURIER and ADVENT. Project COURIER will result in a delay repeater satellite in a low-altitude near-equatorial orbit. It will provide a trunking capability for store-and-forward messages handled by the AMX message-switching center described above. Project ADVENT will ultimately provide a number of real time repeater satellites in a synchronous 24-hour equatorial orbit and will provide a number of real time repeater satellites in a synchronous polar orbit. It can be used for real time trunks switched by the ACE type of circuit switching described above.

Because of the technical problems involved in ADVENT, the COURIER communication satellite appears to be the first which can result in an operational capability. In fact, research and development on both ground and satellite components are well advanced and flight tests are planned during the coming year.

Fig. 4 illustrates the fundamental concept of the COURIER system. The satellite will contain a VHF radio transmitter and receiver, magnetic tape recorders and control circuits. It will be placed in a near-equatorial orbit with an orbital period of approximately two hours. Once the satellite is established in orbit, acquisition data, specifying the direction of approach and the time of arrival of the satellite for each orbit, will be stored by each ground station.

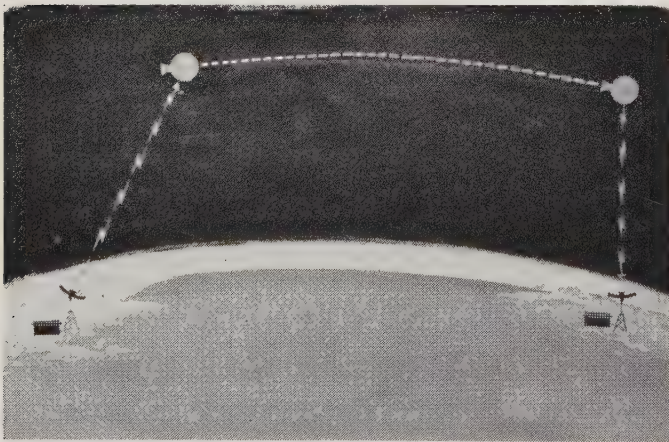


Fig. 4—Delay repeater.

On the basis of these data, at the proper time the ground station will direct the ground antenna toward the horizon in the direction of the approaching satellite. Upon receipt of the satellite beacon signal, the communications antenna of the ground station will lock on and track automatically.

During the period in which the satellite is in view, it will be possible to send and receive information to and from the satellite. Outgoing information will be collected in the ground station in advance and stored magnetically while the arrival of the satellite is awaited. When the satellite passes in view, this information will be transmitted at a rapid rate and stored magnetically in the satellite. Information previously stored in the satellite from

another ground station will be transmitted to the ground, recorded magnetically and distributed to appropriate addressees through the ground communication network. Transmission and reception to and from the satellite will be under the control of a command coding system. To preclude unauthorized use of the system, frequent changes of the command code will be made.

Allowing time for various acquisition and control functions, approximately six minutes will be available for traffic at each ground station currently planned. Initially, it appears likely that the limited access time will result in a satellite capacity of 6 million information bits per orbit between any two ground stations. With improvements in components, such as recorders and power sources, it will be possible to achieve a considerable increase in capacity. However, even on the basis of the present design, one orbiting COURIER satellite will be capable of handling the Army's bulk traffic as projected through 1963.

As a design objective, initially the satellite will have a minimum useful life of at least one year. Planned improvements in component reliability and power sources offer a possibility of an appreciable increase in useful life.

To provide the desired area coverage, a satellite altitude of approximately 2000 miles is required. This is achievable with available boosters. From this altitude, the satellite will have a potential coverage (line of sight) of approximately 3000 miles.

The type of information which initially will be carried by the COURIER satellite will be digital data and teletypewriter messages. However, the satellite will also have the capability of handling analog information since frequency modulated recording techniques will be employed. This capability may be exploited at a later date for voice and facsimile messages.

The COURIER system is scheduled for operation prior to the availability of the UNICOM switching equipment previously described. Consequently, several presently operating Army communications stations must be equipped with interim semi-automatic message handling equipment to utilize the COURIER satellite. The location of these stations will be selected to provide access to the COURIER in areas which are major sources of military communication traffic.

Fig. 5 illustrates a hypothetical system using four ground stations located at Asmara, Philippines, Puerto Rico and Hawaii. These stations will act as gateways to the general areas in which they are located. As gateways they will distribute COURIER messages throughout their respective areas by conventional means and act as area collection points for bulk traffic destined for another area via the satellite.

The communication relay center at those stations equipped with satellite ground facilities will consider the COURIER satellite as just another trunking means. However, special message handling will be necessary for the use of this means since it will be available to a given station for only six minutes out of each orbital period. Prior

to the arrival of the satellite, the communication center must load the ground recorder with outgoing traffic. The communication center must also be equipped to distribute incoming messages from each orbit prior to receipt of additional messages from the following satellite orbit to prevent backlog build-ups.

The initial ground facility shown in Fig. 6 will be made up of two major components: The radio component, consisting of tracking, recording, transmitter-receiver equipment and control devices; and the message processing com-

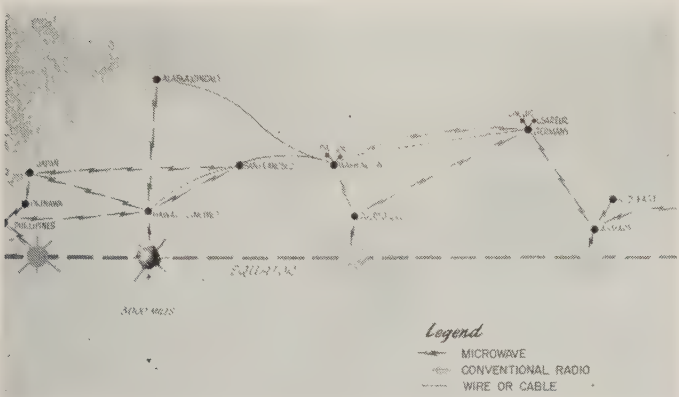


Fig. 5—Integration of the courier system.

ponent, which consists of semi-automatic high speed paper tape equipment. The satellite incorporates radio transmitter, receiver, recorder and control circuits.

Receipt of signals from the beacon transmitter of the satellite will trigger off a sequence of operations whereby the command coder will activate the satellite station, conditioning one recorder to transmit and the others to receive. Messages stored on the ground will then be released to the satellite. Assuming that four ground stations will comprise the COURIER communication satellite system, one satellite recorder will be allocated to each ground station. All messages for any given ground station will be recorded on the recorder designated for that station. A spare recorder may also be carried by the satellite which can be available in case of malfunction, spill-over, or to provide for an additional ground station, if needed. The recorder that is conditioned to transmit will contain all messages destined for the ground station activating the satellite. These messages will be received at the ground station and recorded in the Magnetic Storage device.

Preparation of messages and data for transmission to the COURIER will be accomplished during the two-hour orbital period when the satellite is not accessible. Similarly, all messages received from the satellite will be processed through the communication center within the same two-

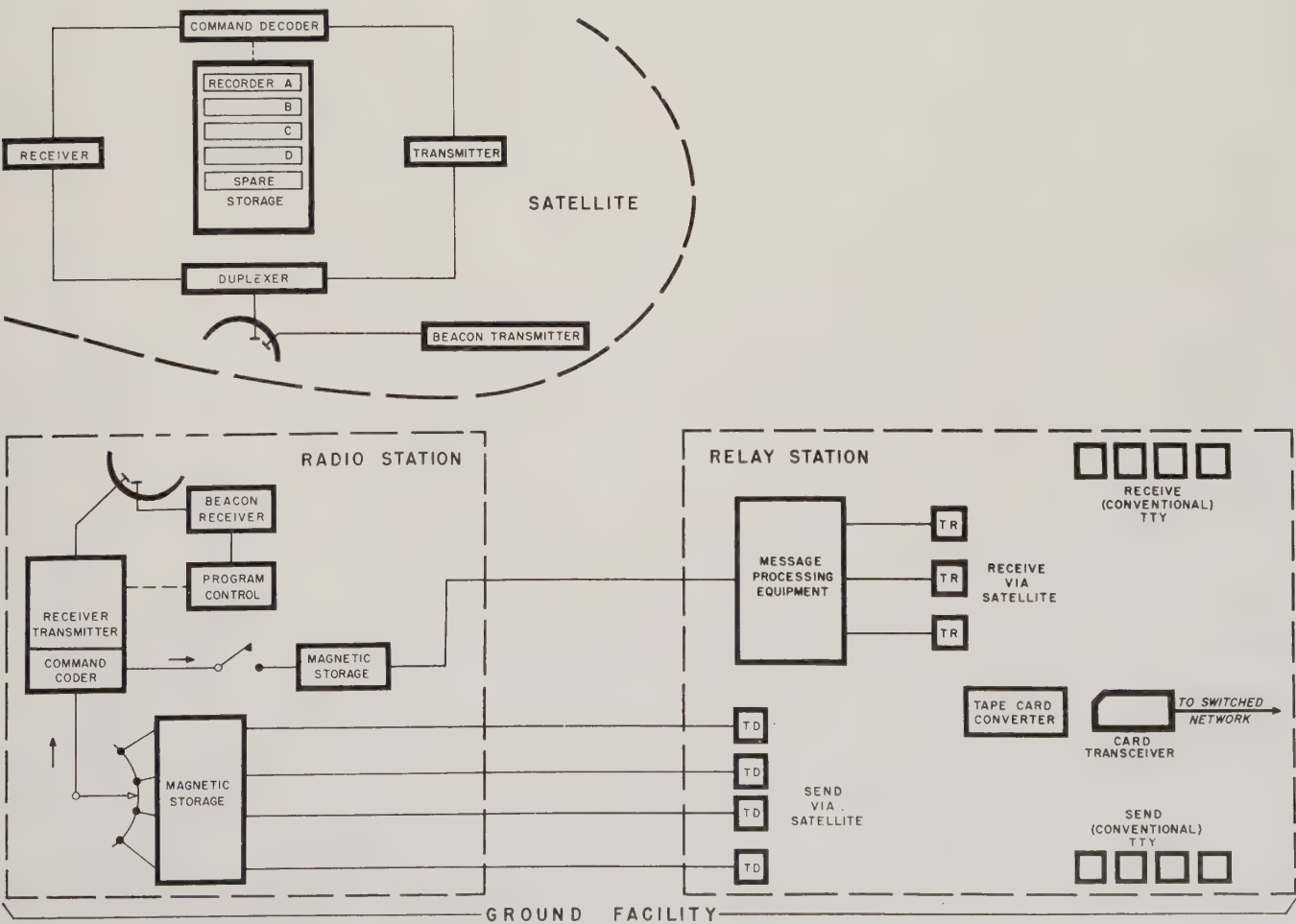


Fig. 6—Operational concept, courier communication satellite system.



hour period. To accomplish this on a compatible basis without changing current station operating procedures, high-speed punched tape equipment will be used at the ground station.

Paper tape transmitter-distributors (TD) operating at 750 WPM will be used to send outgoing messages from a Send-Via-Satellite bank to the Magnetic Storage device. Five or eight hole tape will be accepted by these TD's for teletypewriter messages or data, respectively. These messages will be segregated according to area address by the Magnetic storage device which will consist of a bank of magnetic tapes (one for each addressed ground station) and associated switching and control circuits. The initial operating speeds of the Magnetic Storage device will be 600 bits/sec (record) and 25,000 bits/sec (read). The automatic Program Control will sequentially step through each of the recorders in releasing traffic for transmission to the satellite while at the same time conditioning corresponding recorders in the satellite to receive the traffic for storage.

All message processing and decision functions are performed by the ground equipment to reduce the satellite complexity to a minimum.

The Receive-Via-Satellite bank will consist of 750 WPM typing reperforators (TR) in sufficient quantity to handle the incoming traffic for each station. The Magnetic Storage device which temporarily records the received messages from the satellites will subsequently read the messages into Message Processing Equipment at a rate of 2500 to 6000 bits/sec. The Message Processing Equipment will buffer the messages to a speed of 600 bits/sec (750 WPM) which is the operating speed of each output device. In addition to buffering, the Message Processing Equipment will separate messages having an 8-bit information code from those containing 5-bit information, feeding them to 8 and 5 hole TR's respectively. The 8-hole punched paper tape will be converted to punch cards and retransmitted to the addresses via card transceiver equipment. Teletypewriter messages on 5-hole paper tape will be manually segregated and retransmitted over the conventional teletypewriter message switching system to the addressees.

Automatic cryptographic equipment will be employed "in-line" and be associated with each input TD and TR to assure against unauthorized use of traffic transmitted via the COURIER.

Present planning forecasts operational COURIER satellites as part of the military communication system early in calendar year 1963. While COURIER itself is technically incapable of providing the real-time service for various critical military communication needs, it can improve the over-all capability in this area. For example, use of the COURIER satellite to handle large volumes of bulk traffic will drastically reduce the load on intercontinental high-frequency radio systems. Thus relieved of channel-choking volume, high-frequency radio circuits can be im-

proved in reliability and be used primarily for high-speed demands of intelligence, warning and strategic command control.

The basic concept of the 24-hour instantaneous communication satellite system is illustrated in Fig. 7. To obtain maximum world-wide communications coverage, three of these satellites would be placed in an equatorial orbit at a distance of approximately 22,300 miles from the earth's center. At this altitude the orbital velocity would be such that the satellite would remain in a fixed position with respect to a point on earth and each other. From this altitude virtually the entire surface of the earth can be "seen" by the satellites with the exception of small triangular shaped areas at the poles. To meet the important military communication needs in the polar areas, the 24-hour system would have to be augmented by a system of polar orbiting communication satellites.

The ADVENT satellites will contain active microwave radio repeaters and associated power sources and antennas. Messages transmitted from a ground station to the satellite will be immediately retransmitted to another ground or mobile station in the same manner as a typical ground-based unattended microwave repeater.

While the general concept of the 24-hour system is reasonably firm, the development of a more detailed plan and actual system development must await the solution to several technical problems. Specifically, the problem areas associated with this system which require additional study and work include the following:

- 1) Satellite power sources
- 2) High reliability components
- 3) Satellite stabilization
- 4) Satellite station keeping
- 5) Reduction of susceptibility to unauthorized use
- 6) Reduction of susceptibility to deliberate interference.

On the basis of early estimates of technical feasibility, the operational concept of the 24-hour systems shown in Fig. 8, was evolved. As in the case of COURIER, a basic design objective was to simplify the satellite package to achieve the maximum reliability in the unattended portion of the system. In the system shown in Fig. 8, each satellite is capable of receiving and retransmitting four separate wide-band signals which are separated from each other by a suitable guardband. The types of ground stations are shown: One, an access station labeled "ACE" (the Automatic Circuit Exchange of UNICOM, described previously), and the other, an inter-satellite repeater labeled "Relay Station ACE." Each ACE is allocated one of the four wide-band channels through the satellite to the Relay Station. The wide-band channels are subdivided into several narrower channels, such as telephone channels, which can be de-multiplexed and switched by either the ACE's or the Relay Stations. The ACE's serve as switching centrals and as satellite access stations for subscribers in the local area. The Relay Station ACE serves as a local switching

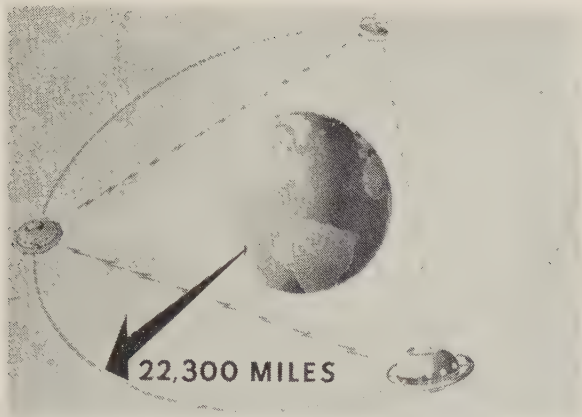


Fig. 7—Concept: real time repeater.



Fig. 8—Operational concept, real time satellite system.

central, as an access station, and as an inter-satellite repeater.

Referring to Fig. 8, the operation of the system may be described as follows: A subscriber call for another local area is switched by the local ACE through the satellite to the Relay Station ACE. At that point, it is switched through one of the satellites to the ACE serving the local

area of the called party. This ACE completes the connection and the circuit is ready for communications. As can be seen, if both of the ACE's involved are in the region served by the same satellite, the satellite repeater is actually carrying the same information twice. While this may seem to be unnecessary duplication, the other alternative would be to perform the switching function in the satellite. However, switching in the satellite would reduce the flexibility and decrease the reliability to an unacceptable level.

Security for all traffic being transmitted over the system will be provided by the use of on-line cryptographic devices associated with the ground stations.

While there is no assurance that the operational system described above will be obtained as a result of the ADVENT project, all of its characteristics appear to be realistically achievable in the time frame established. Development of communication satellite systems providing a greater capability must await the development of improved boosters. Of course, the future will probably see radio repeaters for both military and commercial use incorporated as part of orbiting space stations which serve many functions.

The communication satellite program described is not a futuristic dream of blue sky military planners based on some ill-defined requirements. Quite the contrary, the program is technically sound and has as its basis urgent critical global communication requirements which may have a decided impact on the security of the nation. I have tried to provide an appreciation of these requirements in the early part of this paper. The significance of communication satellites in meeting these requirements can not be overestimated.

Fortunately, the national frame of mind is generally favorable toward space projects. This will assist us in achieving our goals. The ultimate integration of communication satellites in the military network, and the commercial network as well, seems virtually assured. Perhaps some future history will record our feeble pioneering steps in this area, namely, ARPA's Project SCORE, the talking satellite of 1958, as an event ranking in importance with Marconi's first spanning the Atlantic with radio transmissions.



## Concerning Optimum Frequencies for Space Vehicle Communication\*

S. PERLMAN†, W. J. RUSSELL, JR.‡, AND F. H. DICKSON†

**Summary**—In an earlier paper, on the same subject, a number of factors affecting communication with space vehicles were discussed. Among these were receiver signal-to-noise ratio as a function of temperature, cosmic noise, auroral displays, Faraday rotation of the plane of polarization, and gaseous refraction and absorption.

The additional material in this paper treats in a semiquantitative manner and in greater detail the application of elevated heights for earth terminals of space communication systems. This expedient takes advantage of elevated heights to reduce the effects of water vapor and oxygen on limiting the spectrum for radio communication. It is possible to attain some isolation of circuits and extend the range of communication in selected portions of band of 10 to 60 kmc.

THIS paper contains a condensation of a previously published paper, "Concerning Optimum Frequencies for Space Vehicle Communication," which appeared in the IRE TRANSACTIONS ON COMMUNICATION SYSTEMS September, 1959, along with additional information concerning the over-all advantage of utilizing mountain tops for the ground terminal.

The received signal-to-noise ratio determines the optimum frequencies for line-of-sight communication between space vehicles and earth-based stations. The system factors affecting receiver noise, particularly at the mixer and the antenna, are most important. A review of the concepts of receiver noise figure shows that for most receivers it is based on 290°K as the standard IRE reference temperature (see Fig. 1). The contribution to the noise figure,  $F$ , consists of two parts: the noise fed to the receiver input terminals, and  $(F - 1)$  times this noise originating in the receiver.  $F$  has no significance without a reference temperature; for this, it is possible to base computations on an equivalent noise temperature.<sup>1</sup> If the noise source or a receiver input is precooled to less than 290°K, the noise input power is necessarily less, resulting in a different noise figure.

Contributing to the equivalent input noise power of a superheterodyne receiver are the combined noise power of the antenna, the radio frequency preselector stages when used, the mixer circuit, and the intermediate frequency amplifier circuit. In the UHF band of 300 to 3000 mc, replacing the vacuum tube with the crystal diode mixer helps to keep the receiver noise at a minimum. With crystal mixer operation in this band, the antenna noise contribution can be shown to be of secondary importance. The added com-

plexity of vacuum tube preselector circuits at microwave frequencies does not result in worthwhile noise reduction. At these frequencies, broad-band crystal mixers are typically used. The noise contribution<sup>2</sup> to the over-all noise sensitivity in both broad-band and narrow-band mixer operation is a combination of excess mixer noise, excess IF noise, and the normal contribution of noise from the antenna. In a typical broad-band mixer, two-thirds of the equivalent noise temperature arises in the mixer and the IF inputs. (See Fig. 2 for an equivalent circuit of a broad-band crystal mixer).

For minimizing noise, an earth-based receiving antenna should have considerable directive gain. The equivalent noise temperature of an antenna can be described by an integral of the product of the antenna gain in the various directions and the noise temperature distributed in the antenna surroundings. The noise sources contributing to the noise temperature of the antenna are galactic and extragalactic sources, discrete "radio stars," and that resulting from atmospheric absorption and terrestrial absorption. A typical example<sup>3</sup> of a 10-foot diameter parabolic reflector antenna operating at 1000 mc was examined. For a set of assumed conditions, the computed antenna noise temperature is shown as a function of main lobe elevation angle (Fig. 3). At main beam elevation angles of 10° and greater, the above mentioned antenna noise temperature will be reduced asymptotically to 55°K.

Antennas of high resolution will act as radio telescopes and receive cosmic noise. Fig. 4 gives the maximum and minimum cosmic noise<sup>4</sup> as a function of frequency for a receiver of one kilocycle bandwidth. Since terrestrial noises reach the antenna through its minor lobes, reduced minor lobes on a highly directive antenna help to lower its noise temperature.

The sky temperature is dependent on the direction that the antenna is "looking." With increasing frequency more definition is given to the sky noise sources. Fig. 5 gives experimental and theoretical values of radio noise<sup>5</sup> from a quiet sun. The magnitude of solar radio noise is a function of the apparent temperature of the sun. A noisy sun can produce a thousandfold increase in noise input.

\* C. T. McCoy, "Present and future capabilities of microwave crystal receivers," *Proc. IRE*, vol. 46, pp. 61-66; January, 1958.

† Airborne Instr. Lab., "Antenna noise temperature," *Proc. IRE*, vol. 46, p. 2A; May, 1958.

‡ J. D. Kraus and C. H. Ko, "Celestial Radio Radiation," Ohio State University Res. Foundation, Columbus, AF 19(604)1591, pp. 1-45; May, 1957.

§ G. P. Kuiper, ed., "The Sun," The University of Chicago Press, Chicago, Ill., ch. 7; 1953.

\* Manuscript received by the PGMIL, February 1, 1960.

† U. S. Army Radio Propagation Agency, Fort Monmouth, N. J.

‡ Airborne Instr. Lab., "Noise factor and noise temperature," *Proc. IRE*, vol. 46, p. 2A; January, 1958.

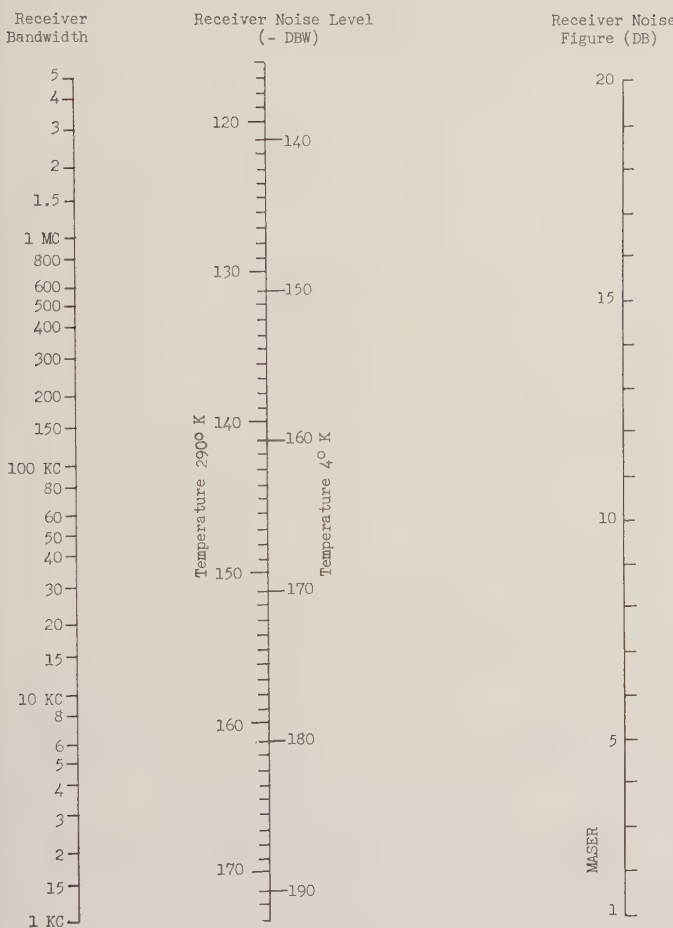


Fig. 1—Nomogram for noise levels in receivers.

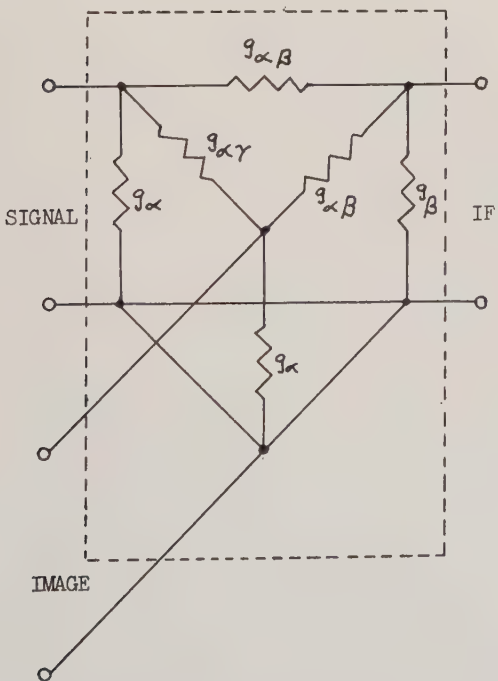


Fig. 2—Equivalent circuit of a broad-band crystal mixer.

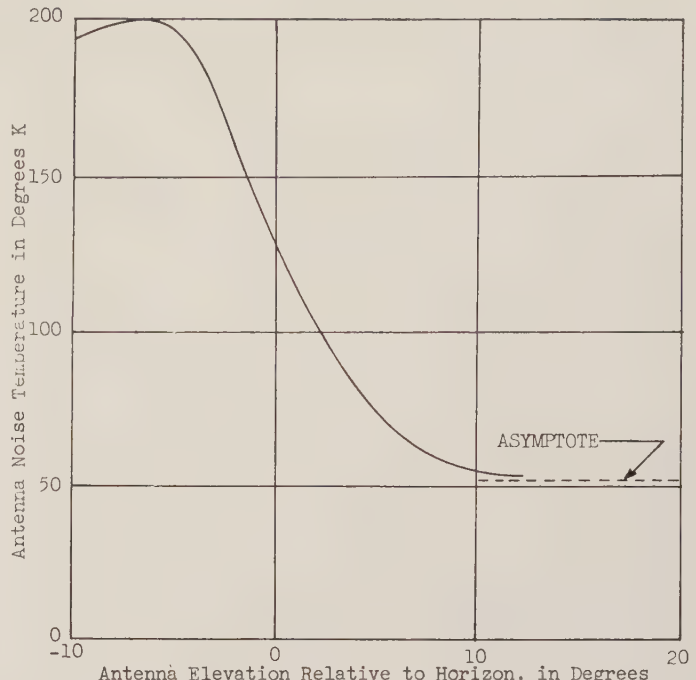


Fig. 3—Antenna noise temperature for a typical 10-foot diameter parabolic reflector operating at 1000 mc.

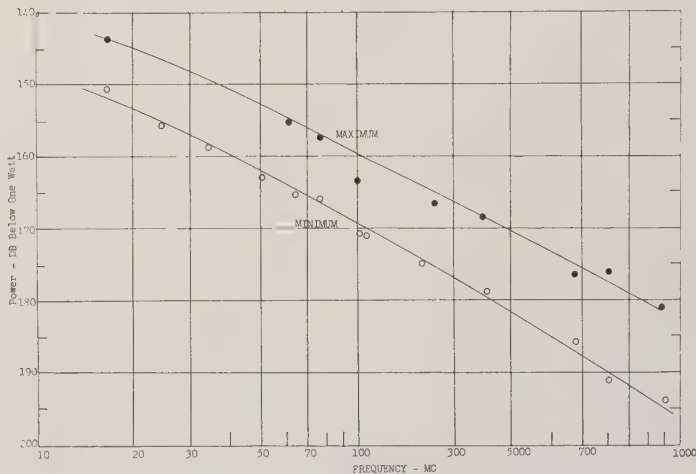


Fig. 4—Maximum and minimum cosmic noise as a function of frequency, 1-kc bandwidth.

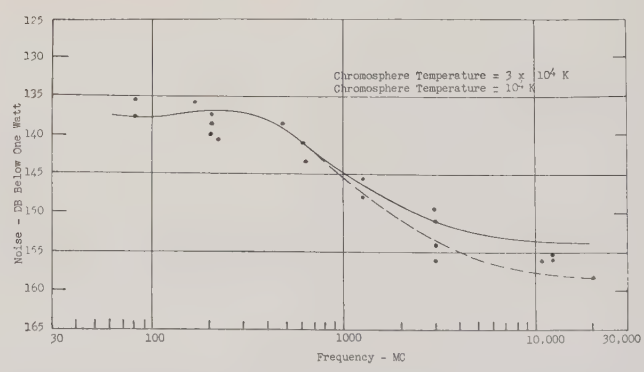


Fig. 5—Experimental and theoretical values of noise from quiet sun. Values observed at the terminals of an antenna having a beam equal to or smaller than the solar disk. Received bandwidth, 1 kc.



The Faraday effect<sup>6</sup> is a slow fading caused by the rotation of the plane of polarization of radio waves as they pass through the ionosphere in the presence of the earth's magnetic field. The Faraday rotation of the plane of polarization changed by a total of ten radians between midnight and dawn, for a two-way 151.11 mc radar signal path from the earth to the moon and return. For a moving space vehicle, the oneway path of Faraday rotation changes with the direction of earth's magnetic field and zenith respectively. The effect of the rotation of the plane of polarization varies inversely with the square of the frequency. This cause of fading is barely detectable as far north as 70° latitude at 108 mc. In tumbling space vehicles, this phenomena is overshadowed by the changing aspect of the antenna. In future stabilized space vehicles with directive antennas, it will be of importance. Circular polarization of a transmitted wave may be necessary to reduce the importance of Faraday rotation.

Since communication with space vehicles can occur from anywhere on earth, the effect of the auroras are of importance. Auroras can occur over a wide range of elevations above the earth and have a wide range of ion densities. Records indicate that extraterrestrial radio waves have been attenuated<sup>7</sup> as high as 17 db in the presence of auroras. Experimental studies<sup>8</sup> seem to indicate auroral attenuation varies inversely with the square of the frequency. Radar echoes<sup>9</sup> were detected at frequencies up to 800 mc. Such echoes are usually Doppler shifted and broadened to adversely effect the usefulness of radar tracking and velocity data. The occurrence both of the aurorae and of ionospheric storms<sup>10</sup> varies with the sunspot cycle.

Above about 200 mc, water vapor begins to absorb radio frequency energy, and oxygen begins to absorb radio energy above about seven kmc.<sup>11</sup> (See Fig. 6.) Radar operation was thus limited to about ten kmc as a ceiling. For space vehicle communication with most earth-based stations, ten kmc could also be considered an approximate ceiling. For oblique ray paths, the equivalent thickness of the atmosphere attenuates signals as shown in Fig. 7. Fig. 8 shows the combined attenuation of water vapor and oxygen between one and 100 kmc.

<sup>6</sup> S. J. Bauer and F. B. Daniels, "Ionospheric Investigations by Means of Lunar Radio Reflections," presented at the URSI Spring Meeting, Washington, D. C., April 24, 1958. Also by private communications; May 1, 1958.

<sup>7</sup> C. G. Little and H. Leinbach, "Some measurements of high-latitude ionospheric absorption using extraterrestrial radio waves," *Proc. IRE*, vol. 46, pp. 334-348; January, 1958.

<sup>8</sup> C. G. Little, W. M. Rayton, and R. B. Roof, "Review of ionospheric effects at VHF and UHF," *Proc. IRE*, vol. 44, pp. 992-1018; August, 1956.

<sup>9</sup> R. L. Leadabrand, Stanford Res. Inst., Stanford, Calif., private communication; July 16, 1958.

<sup>10</sup> L. C. Kelley, "Forecast of Ionospheric Storms and Radio Communications, 1959-1962," Rept. of U. S. Army Signal Radio Propagation Agency, Project 636; June, 1958.

<sup>11</sup> G. H. Millman, "An Analysis of Tropospheric, Ionospheric, and Extra-Terrestrial Effects on VHF and UHF Propagation," Technical Information Series Rpt. No. R56EMH31, pp. 32-35, 40-41, General Electric Co., Syracuse, N. Y.; October, 1956.

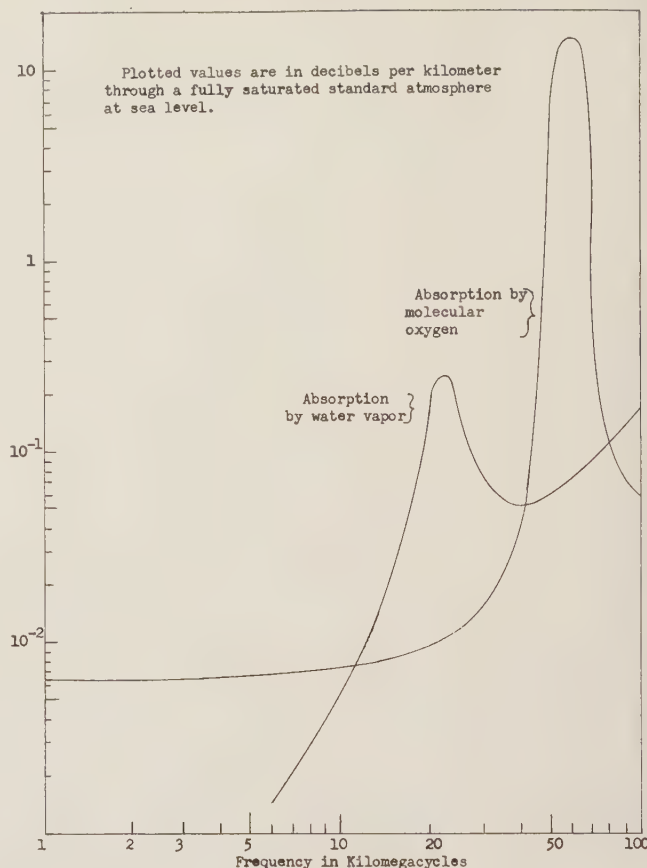


Fig. 6—Absorption of radio energy by oxygen and water vapor in the air. Plotted values are in db/km through a fully saturated standard atmosphere at sea level.

A major breakthrough for increasing receiver sensitivity has come through developments like the maser and the parametric amplifier. The maser, which requires precooling and a focused magnetic field, has been previously discussed. Under laboratory conditions, a noise figure of 0.2 to 0.4 db has been obtained with a maser, which is an improvement of 10-15 db in the obtainable signal-to-noise. The maser can have an equivalent noise temperature of 20° to 25°K in the microwave band.

The parametric amplifier employing the variable capacitance or variable inductance principle is a development of the solid state art that has come into prominence within the past two years. Variable-capacitance diode parametric amplifiers using either "negative-resistance" gain or up-conversion has sufficiently advanced to be applied to working receivers. Such amplifiers obtain the amplified energy from a "pump" oscillator. In general, the parametric amplifier is simpler in construction than the maser and does not require the powerful focusing magnet associated with the maser. Thus the parametric amplifier is more likely to find widespread application where increased receiver sensitivity with a minimum of complexity is a necessity.

In microwave receivers with a noise figure of 8 to 12 db, reductions of 2 to 6 db have been reported, with the addition of parametric amplifiers operating at frequencies

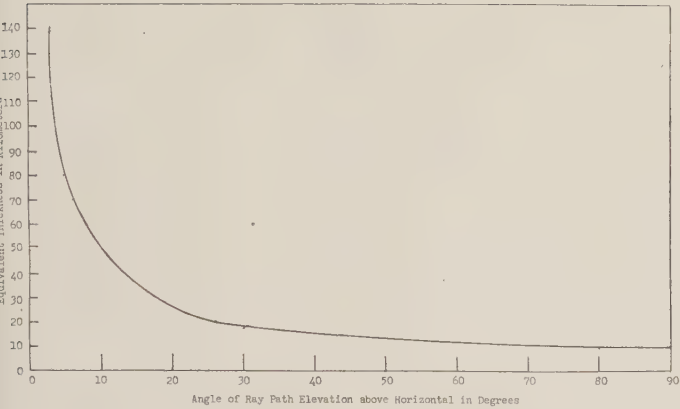


Fig. 7—Equivalent thickness\* of atmosphere for inclined ray paths to outer space.

\* Distance under sea-level conditions yielding the same air density path-length summation as that of inclined ray.

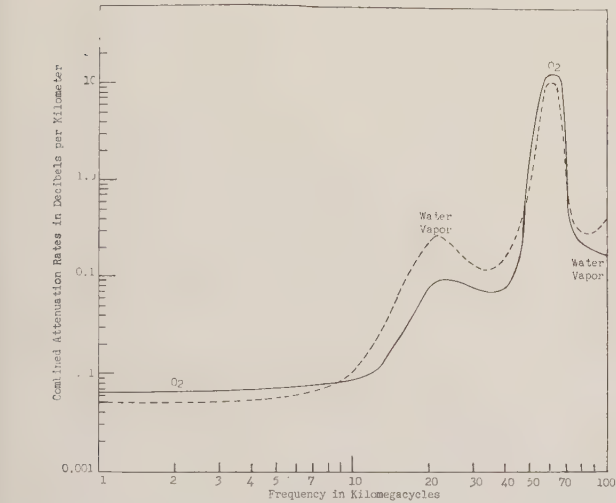


Fig. 8—Combined attenuation rates due to oxygen plus water vapor. Surface conditions in District of Columbia area. Curves labeled in accordance with atmospheric constituent responsible for most of the absorption at the indicated frequencies. Dashed curve—August conditions; solid curve—February conditions.

approaching 10 kmc. Operation of parametric amplifiers at room temperature or precooling with liquid nitrogen to reduce noise still further results in increased receiver sensitivity. One design of a liquid nitrogen cooled parametric amplifier had a noise temperature of 47°K. Such performance is comparable to the noise temperature of a highly-directive antenna aimed skyward.

An over-all picture of the limitations of noise is presented in Fig. 9. This is a composite of all sources of noise, both external and within the receiver.

Signals having frequencies of several thousand megacycles are easily directed into very narrow beams and have found favor in high resolution radar and communications systems demanding highly directive antennas. The recent remarkable progress in the development of very quiet receivers and of high powered sources of radio frequency energy in these bands opens the possibility that the at-

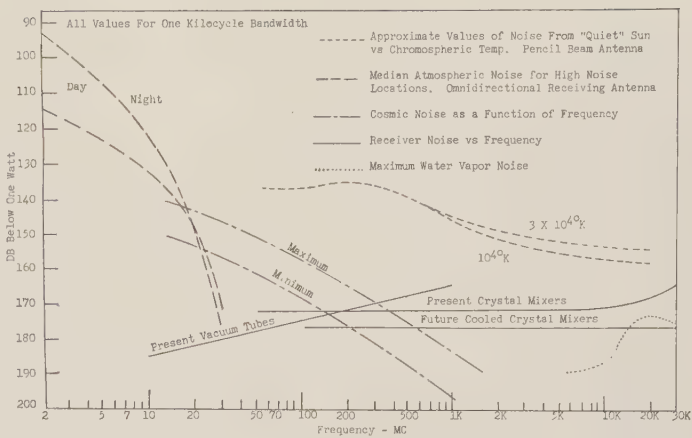


Fig. 9—Noise factors involved in space communication.

mosphere itself may eventually become the significant obstacle to the propagation of radio waves as the frequencies used become ever higher. Furthermore, the atmosphere may set upper limits to frequencies which are practical for particular applications, while yet providing distinct advantages to the operation of other systems at these frequencies. A general consideration of the characteristics of the atmosphere as a radio obstacle is of interest.

The earth's atmosphere is opaque to most frequencies of electromagnetic waves, the energy being either absorbed or being sufficiently refracted to avoid penetration. The parts of the frequency spectrum in which waves can traverse the atmosphere of the earth are commonly called windows. Waves may be absorbed, scattered or refracted by particles, molecules, ions, electrons or dissociated atoms, either by their mere presence or by spatial changes in their distribution. Two important refractive effects are tropospheric ducting and "ionospheric reflection." Refractions disturb the operation of precise systems employing Doppler shifts and phase comparisons.

Most frequencies above 1 kmc are virtually free from absorption, refraction and scattering while passing through regions lying above the troposphere, *i.e.*, above about ten kilometers. However, pronounced refractive effects may occur here at the lower VHF range, consisting mainly of parallax displacements within the ionosphere; ray path curvatures are frequency-sensitive, but are largely self-cancelling in the case of communications to points lying beyond the ionosphere.<sup>12, 13</sup> Tropospheric refraction, on the other hand, is very sensitive to widely varying conditions of humidity and is virtually independent of frequency. The apparent dependence of radio ducting on frequency is a form of wave-guide cutoff rather than a change of tropospheric refraction. Of significance here are the effects of the atmosphere on frequencies exceeding 1 kmc, particularly along paths up through the atmosphere to space

<sup>12</sup> Ibid., pp. 31-36, 121-134.  
<sup>13</sup> G. R. Marner and R. M. Ringoen, "Atmospheric Refraction of 8.7 mm Radiation," IRE CONVENTION RECORD, pt. I, pp. 14-18; 1956.



vehicles. All such frequencies are subject to tropospheric refraction; frequencies in the vicinity of 22 kmc are heavily absorbed by wet air, frequencies in the vicinity of 60 kmc are even more heavily absorbed by molecular oxygen in the air, but none of these frequencies which still lie within the radio frequency spectrum are appreciably affected by the ionosphere. Certain very narrow bands of absorption centered on discrete frequencies of exact molecular resonance may exist in the lower portions of the ionosphere.

Path rays inclined with respect to the surface of the earth have variable curvatures which are introduced by tropospheric refraction that alters the relative fractional portions of the rays as traverse various altitudes. Also, absorption varies widely with altitude, and the absorption accumulated along these rays depends upon the paths taken through the absorbing regions. This influence on the accumulated absorption along paths into space which start with various angles of elevation is the only refractive effect considered here. Of more direct significance to the usefulness of these frequencies for space communications are the absorptions themselves, which are considered as functions of frequency and of humidity for various ray path configurations.

The attenuation per unit distance of SHF radio waves in regions of particular compositions and densities is proportional to the concentrations of the absorbing constituents and is inversely proportional to some power of the absolute temperature.

Absorption rates in db/km by atmospheric oxygen and water vapor under typical sea-level conditions are plotted in Fig. 6 and 8 in separate and in combined form. Note that Fig. 6 indicates that the combined rate of absorption is controlled by the oxygen contribution at all frequencies below 10 kmc, and between 40 and 80 kmc even when the air is very wet, since oxygen is the only significant source of attenuation in dry air. Other published values of absorption by molecular oxygen and water vapor, and values for various conditions of rain and fog, are in the literature.<sup>14</sup> The effects on microwaves of all other constituents and particles are assumed to be negligible.

The attenuations plotted in Figs. 6 and 8 are for sea level conditions. As height is increased, the air and most of its constituents become thinner at an approximately exponential rate. Since the temperature decreases linearly throughout the troposphere and the water vapor concentration is limited by temperature, the humidity decreases rapidly with height under most conditions and must in any case become negligible as freezing stratospheric air is encountered. Most of the atmosphere is seen to lie very near the surface of the earth. Absorption, scattering, and re-

fraction, therefore, become rapidly more severe as the surface is approached. In addition, precipitation and water vapor, which at some frequencies contribute most of attenuation and refraction, are largely confined within the troposphere. All water vapor must maintain an equilibrium with any water particles which may be present. At temperatures characteristic of the stratosphere these vapor pressures are negligible compared to the total atmospheric pressure, causing the cold stratospheric air to act as a vapor trap, and confining virtually all atmospheric moisture to the underlying troposphere. Any moisture entering this freezing belt from either below or above is condensed into ice crystals, thus shielding the warmer air lying above it from the moisture it could otherwise hold. Therefore, above the first subfreezing belt of the stratosphere, all air tends to be as dry as the coldest air below it. In contrast, just above a tropical swamp the air may contain as much as 7 per cent water.

If the concentrations of constituents and temperature of the troposphere are known for each altitude, and if the sea level decibel rates of attenuation are given, the total absorption along any ray path may be accumulated by summing the losses within successive incremental lengths of the path.<sup>15,16</sup> If several such accumulations are computed for angles of elevation, altitudes of radio terminals and tropospheric conditions of interest, the dramatic shielding of the lower terminals is demonstrated. Also shown is the increase in total absorption as the ray path approaches the horizontal.

A concept sometimes employed in calculations of the effects of the atmosphere is called the equivalent thickness.<sup>17</sup> This approximation puts all the atmosphere into a spherical shell, concentric with the earth, having a uniform density equal to that of air at sea level. The resulting thickness is roughly equal to 10 km. At oblique angles, straight line paths through it to outer space are longer, as illustrated in Fig. 7. Absorptions by uniformly diffused constituents are then roughly proportional in decibels to these path lengths. This concept simplifies calculations, but it also introduces inaccuracies.

The ray path is slightly curved by refraction, which must be similarly computed point by point. Changes in humidity distributions change the path curvatures, thereby affecting the absorption accumulated along paths which approach the horizontal. Tropospheric models here employed assume ratios of elevated to surface values of water vapor pressure and of absolute temperature which may be approximated by the sixth power of  $(1 - 0.064Z)$  and by  $(288 - 6.5Z)$ , respectively, where  $Z$  is the altitude in

<sup>15</sup> Ibid., pp. 646-648.

<sup>16</sup> National Defense Res. Committee, OSRD, summary of Tech. Rept. of the Committee on Propagation, vol. 1, pp. 194-220, 203-204; 1946.

<sup>17</sup> G. R. Marner, "Atmospheric Attenuation of Microwave Radiation," IRE CONVENTION RECORD, pt. I, pp. 68-71; 1955.

<sup>14</sup> D. E. Kerr, "Propagation of Short Radio Waves," Rad. Lab. Ser., vol. 13, pp. 12-20, 663-664, 671-692, Mass. Inst. Tech., McGraw-Hill Book Co., Inc.; 1951.

kilometers. These relationships also satisfy accepted standard atmospheres with sufficient accuracy.<sup>18</sup>

Sixteen combinations for absorption by atmospheric oxygen are here treated by approximate means and are presented as plotted decibel accumulations in Fig. 10 for departure angles of 0°, 3°, 30°, and 90°, and for station altitudes of 0, 14,000, 30,000 and 50,000 feet above sea level. Surface temperature is set at 15°C and lapses at a rate of 6.5° per kilometer. The troposphere is assumed to be completely saturated up through the first ten kilometers of altitude, but with no precipitation.

The four heights considered above are typical of possible mountain-top observatory sites, propeller-driven aircraft, and of jet aircraft, respectively. The airborne sites are included because such platforms are now in use to provide seaward extensions of radar. Their use as terminals and relay points for space communications is rendered even more plausible by the consideration that they lend themselves to optical and infra-red techniques for such communication. These nonradio modes are likewise subject to excessive absorption by the lower layers or the troposphere. Their behavior sufficiently resembles that of millimeter radio waves to justify a few approximate examples. Although water vapor absorbs certain portions of the infra-red spectrum, the absorption peaks and "windows" are controlled by the concentrations of carbon dioxide and other more uniformly diffused constituents. At the surface, peak absorption is comparable to that produced at 60 kmc by oxygen, while the two more favorable of the "windows" of lesser absorption provide relatively narrow bands within which the db ratio of attenuation falls to about 1/100 of this peak. Just off the resonant band of frequencies of oxygen absorption, vertically directed rays to outer space may lose, very roughly, about 150, 85, 50, or 20 db of attenuation, depending upon whether they start from sea level or from points elevated by 14,000, 30,000 or 50,000 feet. Rays inclined by 0°, 3°, and 30° above horizontal encounter about 41, 11.5, and 1.8 times as many db of absorption, respectively, as do the corresponding vertical rays. These values may be used as estimates of the peak absorption of infrared rays, and when divided by 100 they approximate the behavior of the two more favorable "windows" of less absorption.

Since oxygen is evenly diffused throughout the troposphere, its contribution to the absorption is proportional to the atmospheric density, with a slight correction for temperature lapse. The partial pressure of water vapor in fully saturated air is a function only of temperature and becomes negligible for this problem at altitudes at which the air first falls below freezing. Furthermore, the total remaining mass of air above these heights is insufficient to support further significant absorption by any constituents other than oxygen and those associated with the

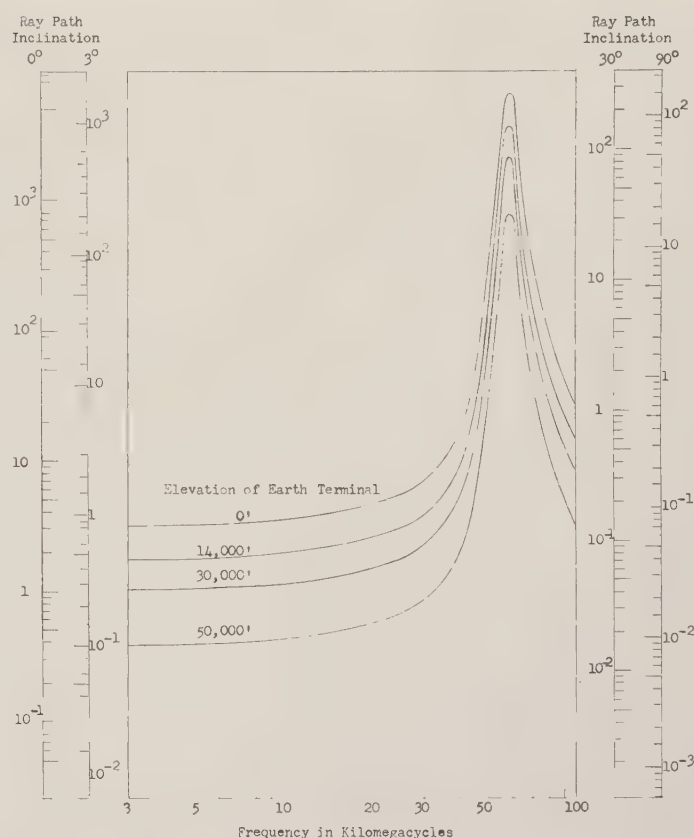


Fig. 10—Earth-to-space absorption by oxygen. NACA standard atmosphere; saturated troposphere. Decibel scales give totalled attenuation by molecular oxygen along paths to space making initial angles above horizontal as indicated on scales, and originating from terminals of elevations indicated on curves.

ionospheric absorption of lower frequency waves.

Absorption by tropospheric water vapor is highly variable, depending upon humidity at various levels or upon the humidity at the surface in a standard atmosphere. Since most humidity lies below heights which are relatively easy to attain with mountain sites or economical aircraft, accumulated decibels of absorption by water vapor along paths inclined at the four angles considered above, which are presented in Fig. 11, (a) through (d), are computed only for sea-level elevations of the lower terminals, and only for altitudes of less than 10 km. Approximate accumulations, starting from moderately elevated sites, may be derived from these curves by geometry and superposition; *i.e.*, the slant range back down to sea level along the rearward extension of the inclined path must be determined and its accumulated absorption removed from the total. Since for a given humidity the absorption rate is a function of frequency, the accumulations in Fig. 11, (a) through (d), are normalized to a basic surface rate of 1 db/km and must be multiplied by typical surface values or by other desired rates.<sup>19</sup> The results of one such conver-

<sup>18</sup> Millman, *op. cit.*, pp. 1-4.

<sup>19</sup> B. R. Bean and R. Abbott, "Oxygen and Water Vapor Absorption of Radio Waves in the Atmosphere," *Geofisica Pura e Applicata*, Milano, Italy, vol. 37, pp. 127-144; 1957.



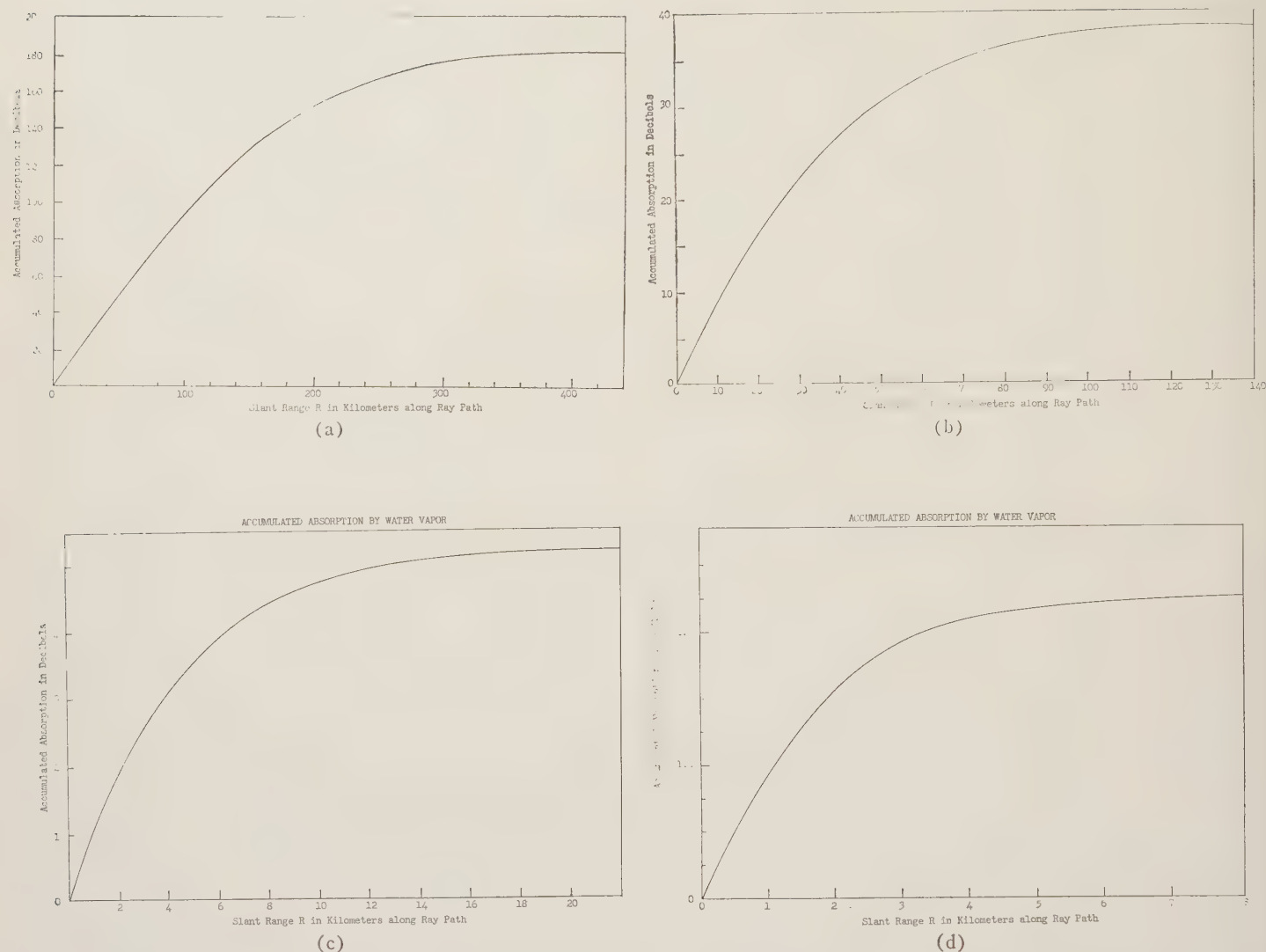


Fig. 11—Accumulated absorption by water vapor. Standard atmosphere, saturated below 10 km. Ordinates normalized to reference absorption rate of 1 db/km at surface, and must be multiplied by actual rates. (a) Ordinate values give absorption by uncondensed water vapor accumulated along path of length  $R$  leaving ground level at elevation angle of  $0^\circ$ . (b) Elevation angle of  $3^\circ$ . (c) Elevation angle of  $30^\circ$ . (d) Elevation angle of  $90^\circ$ .

sion are shown in Fig. 12 (opposite) for the case of a fully saturated troposphere and for paths extending to outer space.

It should be noted that the plotted peak values of loss in db (*i.e.*, those near 22 and 60 kmc) are but rough approximations; all such refinements as spectral line spreading variations with altitude have been ignored, and there is reason to believe that the absorptions at peak and at "window" frequencies do not vary proportionately as the atmosphere thins. As one consequence, the concept of equivalent thickness cannot apply with equal validity to both peak and off-peak absorption levels. These reservations apply to all of the decibel accumulations presented here; however, the decibel errors resulting from such simplification are moderate except at particular peaks of molecular resonance. For instance, recent theoretically derived attenuations at one of the peaks in the 60-kmc band predict nearly four times as many decibels of absorption along

vertically directed rays from sea level to 100 km of altitude as are here assigned to paths all the way out to space.<sup>20</sup> Furthermore, over three quarters of this absorption, as expressed as a db ratio, is accumulated above 33,000 feet, whereas the concept of equivalent thickness predicts that 70 per cent of the loss should be accumulated at lower altitudes. These same theoretical calculations, however, when applied to frequencies which are displaced by only 5/100 of one per cent from true resonance, yield 84 db less total attenuation than at the peak and assign 66 per cent of these to altitudes of less than 33,000 feet. Consequently, these theoretical calculations corroborate the relative advantages of elevated locations for any frequency in the bands of high absorption, unless this frequency should coincide almost exactly with one of the frequencies of molecular

<sup>20</sup> R. J. Schmelzer, "Total Atmospheric Absorption of 60 KMC Radiation" Lockheed Missile Systems Division, Sunnyvale, Calif., LMSD-2793, pp. 11-13; September 19, 1958.

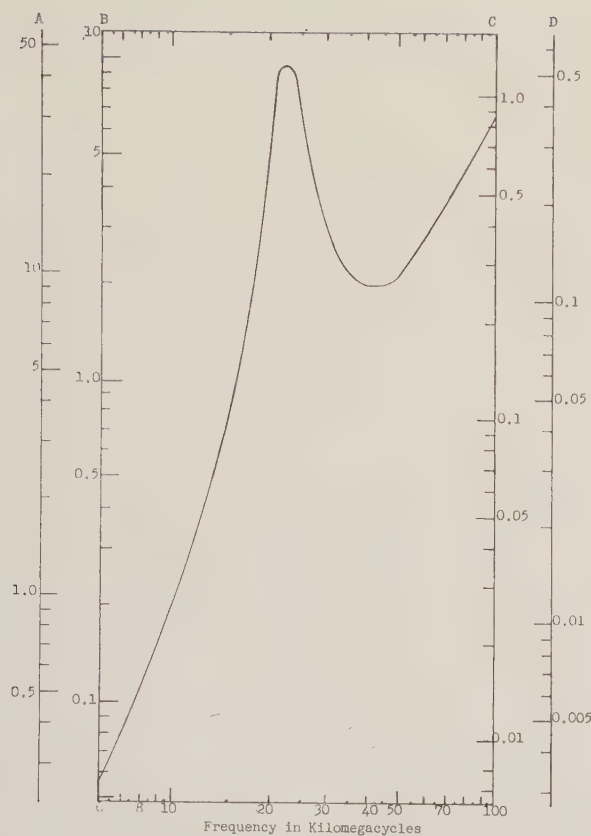


Fig. 12—Totalled absorption along inclined paths to outer space. Scales give db attenuation by uncondensed water vapor from ground to outer space along rays leaving ground at angles: A =  $0^\circ$ , B =  $3^\circ$ , C =  $30^\circ$ , D =  $90^\circ$ . Values computed for fully saturated troposphere. Prorate for less relative humidity.

resonance. Also, these calculations predict the more conventional rates of absorption per km at sea level for all frequencies. Since most of the absorption occurs at the lower levels for frequencies removed from resonance, it is to be expected that these theoretical calculations are not in conflict with the general trend of the rounded or quasi-peak values of absorption by oxygen as presented here. Accurate prediction of absorptions under all practical conditions and at all potentially useful frequencies must await experimentally determined data.

As is demonstrated by the material presented above, elevated locations of the earth-based terminal of radio paths to outer space offer several possible advantages not enjoyed by sea-level sites. First, they permit the use of power levels and frequencies which are unlikely to interfere with lower ground-based receivers and with considerable immunity from ground-based interference. Second, they may enlarge the regions in space into which line-of-sight communications may be extended from the terminal. Third, they extend the upper limit of the frequency range which may be used on highly oblique line-of-sight paths into outer space. Consider first the possibility of reducing mutual interference. Adequate screening of the lower terminal could be achieved by the use of highly directive antennas, but path geometry and limitations on the payload combine to deny to space vehicles this form of circuit isolation. Fortunately, most sites having a potential for mutual interfer-

ence with the circuit to the space vehicle lie far below the elevated earth station and are thus shielded from the desired circuit by the overlying blanket of relatively dense troposphere. The degree of isolation provided by this screen depends on the frequency, on the humidity (particularly if the frequency is near 22 kmc), and on the angle at which the waves traverse the troposphere. For the more steeply inclined ray paths, the use of frequencies differing appreciably from the absorption peaks at 22 kmc (when effective) and at 60 kmc will tend to reduce the degree of possible isolation of the desired circuit and increase the possibility of interference to or from those less elevated locations.

It should be noted that absorptions that were computed are compared in terms of db ratios of power densities before and after absorption takes place. The total accumulations along various paths under various conditions will likewise be proportional when expressed in decibels. Vertical paths to space can scarcely differ by more than  $\frac{1}{2}$  db in their water vapor losses even at 22 kmc, because the loss all the way from sea level up to space is little more than 0.5 db through a fully saturated troposphere (see Fig. 12). A vertical circuit from a high mountain would then have a water vapor loss of about 0.05 db. Fig. 12 also indicates that very oblique paths with the same ten-to-one decibel ratio of loss would provide significantly greater protection against mutual interference. Paths starting upward at elevation angles of  $3^\circ$  encounter totalled water vapor absorption losses varying from 1 to 9 db; the particular value depends upon the altitude of the ground terminal. The use of moderately elevated locations may then provide 8 db of shielding against mutual interference from sea-level locations when the humidity is very high and the ray path is nearly horizontal. An analogous comparison may be drawn concerning absorption by molecular oxygen at frequencies in the vicinity of 60 kmc (see Fig. 10). This curve shows that an elevation of 18,000 feet or more is required to achieve even a two-to-one db ratio of oxygen absorption loss. To obtain from oxygen absorption the same 8 db margin of shielding against interference to and from sea-level locations, this relatively high terminal must accept absorption losses of 8-db on the desired circuit in lieu of 1 db for the case of shielding by water vapor. At more practical heights even greater losses must be taken to provide this 8-db margin of shielding. Unlike the case of the absorption by water vapor, even vertical paths can develop any desired degree of loss from absorption by molecular oxygen in the atmosphere if the frequency is properly adjusted along the steep slope of the absorption peak, as plotted in Fig. 10. However, should a path become more oblique, a similar readjustment of frequency is required to prevent the absorption along the desired path from becoming excessive.

It appears that partial reduction of interference to or from relatively close but lower locations may accrue to any well-engineered circuit to outer space employing an elevated terminal and the highest practical frequency below 60 kmc.



However, it also appears that continuous and automatic control of both frequency and power output are required to insure such protection unless communications are limited to vehicles lying almost directly overhead, such as a satellite in an equatorial orbit with a twenty-four-hour period. Very oblique paths and very wet air may provide barely adequate shielding at relatively slight cost in terms of absorption loss along the desired circuit path. This protection, however, is against mutual interference with lower locations which have ray paths to the space vehicle which are at least as oblique as is the ray path for the elevated terminal. Interference remains a problem with respect to locations lying more directly beneath the vehicle, regardless of whether water vapor or oxygen is providing the attenuation. Conversely, if a vertical path is to be protected from mutual interference by the use of a frequency as close to the 60-kmc absorption peak as can be tolerated by the system gain, most locations with a potential for mutual interference will have oblique ray paths to the vehicle, which will result in some additional protection.

Considering the possible extension of range, previously mentioned, arising from the use of elevated locations, it need only be mentioned that the extension of line of sight limitations may be achieved only by the use of ray paths depressed below the horizontal. Some portion of such rays must pass twice through the same atmospheric layers below the elevated terminal in order to regain the terminal's altitude on their way back up towards space. Only moderate extensions of range are possible even with the higher elevations, and then only at the cost of using grazing ray paths which compound twice over all the high absorptions and uncertain refractive curvatures of highly oblique paths from the ground to space. Thus, the apparent increase in distance range based on the geometrical considerations is still subject to the limitations due to atmospheric absorption.

Inspection of Fig. 6 suggests that the virtual removal of all significant absorption by water vapor would raise the upper limiting frequency for space communication from some value between 10 and 20 kmc up to rather over 40 kmc. However, note the steep slope and very high peak of

the oxygen absorption curve, plus the obvious difficulty of achieving sufficient altitudes to put large fractions of the atmosphere beneath the elevated station. These circumstances suggest that the use of such a location offers little advantage with respect to producing any further upward extension of the range of useful frequencies as limited by absorption by molecular oxygen.

A satellite with a period of one sidereal day placed in an equatorial orbit directly over a suitably elevated earth station equipped with highly directive antennas could provide the stable geometry needed for carefully controlled communication through the shielding layers of troposphere and ionosphere. Given sufficient transmitter power and a frequency suitably absorbed by oxygen, such a circuit would be highly unlikely to interfere with other receivers, whether located in space or on the ground, or to be interfered with by transmissions from such locations. Pending the development of equipment capable of operating in such a fashion at frequencies in the 60-kmc range, optical and infrared communication may be utilized. It has been previously stated that these exhibit very similar behavior when they are properly filtered. Any frequency to which the atmosphere as a whole is either opaque or reflective could then be used for further communication between this satellite and other space vehicles, providing relayed circuits between the ground and these vehicles which would in their entirety be free from mutual interference with facilities lying below the atmosphere.

As was shown, it is possible to communicate on a line-of-sight between a space vehicle and an earth-based station at any frequency for particular directions of looking that will penetrate the ionosphere. To obtain a signal path with a minimum of attenuation at the receiver, the effects of noise and absorption loss due to cosmic and solar noise, Faraday rotation of the plane of polarization, auroral absorption and scattering, water vapor, and oxygen absorption must be reduced or even eliminated. The recommended band of frequencies that will do this extends from about 1000 to 10,000 mc. There is, however, no sharp demarcation at these limits. Elevated earth-locations, if sufficiently high, will permit extending the upper limiting frequency.

# Project SCORE: Signal Communication by Orbiting Relay Equipment\*

SAMUEL P. BROWN†

**Summary**—The development program which led to the successful launching and demonstration of the first satellite communication is described in this summary paper. A brief description of the system is included, the results obtained during the operational phase are described, and the impact of the results on future satellite programs discussed.

**PROJECT SCORE:** "Signal Communication by Orbiting Relay Equipment," was designed primarily as an experiment to demonstrate the feasibility of communicating between two or more ground stations separated by intercontinental distances using a satellite as an active repeater. A secondary objective of the experiment was the definition of possible problem areas that would be encountered in the ultimate development of a practical operational satellite communication system for military and/or civilian use.

The Advanced Research Projects Agency, in conjunction with the U. S. Army and the U. S. Air Force, undertook this project in mid-1958 with a dual objective in mind; this was to demonstrate the unique capability of the Atlas missile to be guided into orbit as an actual satellite and once that orbit was achieved, to demonstrate how a delayed repeater, or "store and forward," satellite communication system might be applied. The U. S. Army Signal Research and Development Laboratories was assigned the responsibility for the communication system, including spaceborne and ground complex equipment in July, 1958 with a target launching date of early November, 1958. With such a short deadline, little sophistication was permitted in the design, but the basic elements for the eventual operational type system were included. The development of SCORE and the characteristics of the system which dramatically demonstrated the feasibility of this new communication concept are outlined below.

Initial requirements analysis indicated that the short time frame would restrict the location of ground interrogation and command stations to areas within the continental United States. Within these limitations, optimum sites were chosen in California, Arizona, Texas, and Georgia. These locations permitted a variety of tests of both the delayed-repeater and real-time category. In the delayed-repeater mode, messages were sent from a particular ground station to the orbiting satellite equipment, where they were recorded and stored on magnetic tape. Upon suitable command at a later time from a different ground station, the stored message was transmitted from the satellite to the interrogating ground station, completing the message transfer. In the real-time mode, messages were sent from a particular ground station, but the recorder in the satellite was bypassed and the message retransmitted in a

radio-relay mode by the satellite transmitter back to other ground stations within range. The locations chosen permitted testing of the real-time mode at varying ground distances from about 700 to 3000 miles.

Naturally, a major factor which governed the final selection of ground sites was the expected orbital conditions. Preliminary calculations indicated an elliptical orbit with a perigee of approximately 100 miles and an apogee of 500 to 800 miles. The launching was to be from the Atlantic Missile Range at Cape Canaveral with an inclined orbit of approximately  $30^\circ$ . With a variation in latitude extending to  $30^\circ$  North, the ground sites were clearly limited to the southern extremes of the United States. Fig. 1 illustrates the orbit geometry and the location of the four operating ground stations.

The expected altitude limitations of the satellite indicated that a slant range of approximately 1000 miles would be adequate for system planning purposes. Other considerations, such as the capability of available electronic equipment and the existence of a potentially suitable missile antenna, dictated the choice of frequencies in the VHF range. The system parameters finally selected are indicated in Table I, with the margins applicable to the above-mentioned slant range of 1000 miles.

The establishment of the basic system parameters in

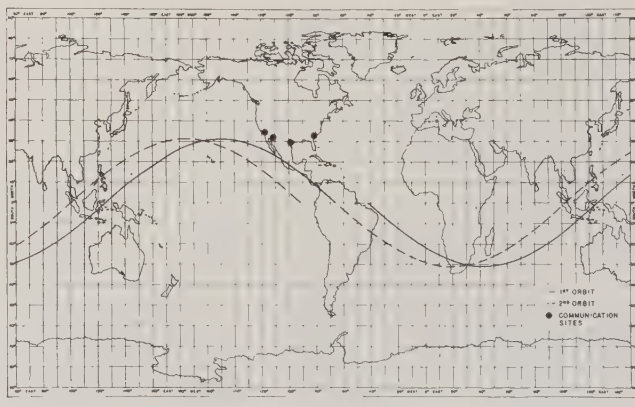


Fig. 1—SCORE satellite orbit.

TABLE I  
SCORE SYSTEM PARAMETERS

	Satellite	Ground
Transmit frequency	132 mc	150 mc
Receive frequency	150 mc	132 mc
RF power output	8 watts	1000 watts
Noise figure	10 db	6 db
IF bandwidth	40 kc	40 kc
Audio bandwidth	0.3-5.0 kc	0.3-5.0 kc
Antenna gain	-1 db	16 db @ 150 mc
FM threshold	10 db	10 db
Fade margin	39 db	19 db

\* Manuscript received by the PGMIL, February 1, 1960.

† U. S. Army Signal Res. and Dev. Lab., Fort Monmouth, N. J.



advance of the program schedule permitted the early initiation of the accelerated development phase. While, as previously noted, the total time frame restricted the development work to primarily an application engineering type of work utilizing available equipment, many problems of a system and environment nature still had to be solved. Typical of these problems was the development of a thermal design to maintain the satellite electronic components within tolerable temperature limits while in orbit, and a mechanical design to insure the satisfactory operation of the same components following the initial powered flight. A detailed description of the elements of both the spaceborne and ground elements of the system are contained in previously published information<sup>1-4</sup> and will not be repeated in this summary paper. However, Fig. 2 indicates the major elements of the satellite components which were mounted in the Atlas missile, while Fig. 3 is an interior view of the mobile ground stations which were designed and constructed.

With the successful launching of Atlas missile 10B on December 18, 1958, the first objective of the program was achieved and on the following day, the now famous Christmas message from President Eisenhower to the world was transmitted from the satellite system to the Cape Canaveral installation team. During the ensuing planned life of the experiment, until battery exhaustion occurred on December 30, 1958, the system demonstrated conclusively the practical operation of a satellite radio-relay system capable of spanning intercontinental distances. For example, voice as well as single and six-channel frequency division multiplexed teletype traffic was transmitted to the satellite system, recorded, stored, and relayed individually to the ground stations at their command. The equivalent of over 140,000 words was successfully transmitted during this period in the delayed-repeater mode, while eleven real-time relays were accomplished between California and Georgia.

This system, which was developed into an actual operating network in record time, demonstrated the complete feasibility of using store and forward type communica-

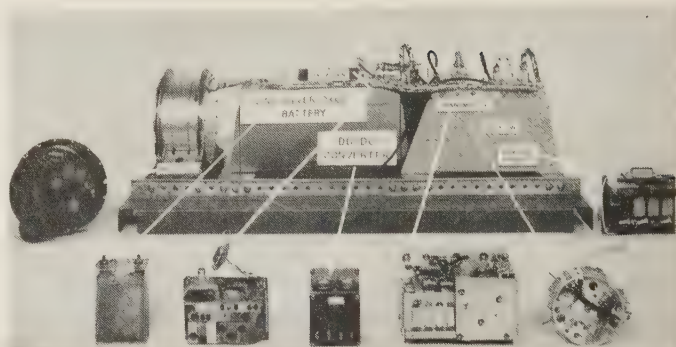


Fig. 2—Communication components for Project SCORE satellite.

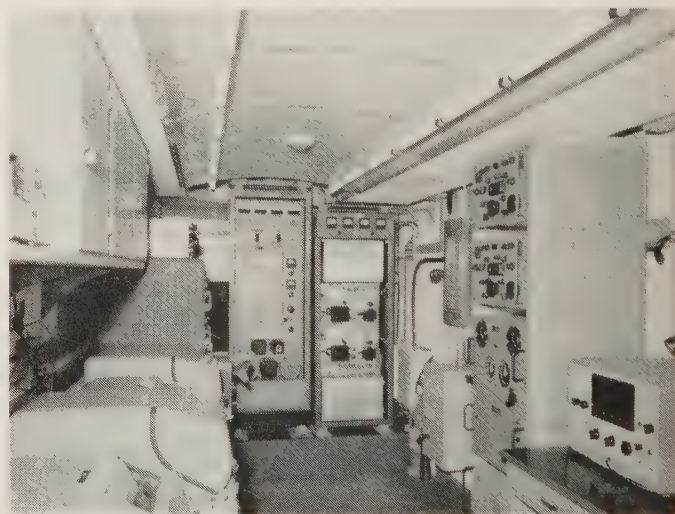


Fig. 3—Interior of SCORE communication system ground station.

tion satellites over intercontinental distances. In addition, the timing of this dramatic experiment was most significant, both from a world-wide political standpoint and from consideration of the rapidly approaching saturation point in existing global communications facilities. The expansion of this demonstrated technique to an economically practical, operational world-wide communication system involves system parameters that are within the present state of the art and engineering capabilities already available. A specific discussion of the parameters that appear practical of attainment is included in a companion paper in this publication.<sup>5</sup>

<sup>1</sup> S. P. Brown, M. I. Davis, H. C. Hawkins, R. C. Riehs, and G. P. Senn, "Project SCORE," U. S. Army Signal Res. and Dev. Lab., Fort Monmouth, N. J.; April 15, 1959.

<sup>2</sup> M. I. Davis and G. N. Krassner, "SCORE—first communication satellite," *J. Amer. Rocket Soc.*, vol. 4, p. 37; May, 1959.

<sup>3</sup> S. P. Brown, M. I. Davis, H. C. Hawkins, and G. P. Senn, "The ATLAS—SCORE communication system," *Proc. Natl. Conv. on Military Electronics*, Washington, D. C., June, 1959, pp. 401-406.

<sup>4</sup> S. P. Brown and G. P. Senn, "Project SCORE," *Proc. IRE*, vol. 48, pp. 624-630; April, 1960.

<sup>5</sup> T. P. Mottley, D. H. Marx, and W. P. Teetsel, "A delayed-repeater satellite communication system of advanced design," this issue, p. 195.

# A Delayed-Repeater Satellite Communication System of Advanced Design\*

T. P. MOTTLEY†, D. H. MARX‡, AND W. P. TEETSEL‡

**Summary**—This paper describes a delayed-repeater satellite communications system consisting of an orbiting delayed-repeater radio-relay station which passes over terminal ground stations located within the viewing area of the satellite.

Messages are exchanged between the satellite and a ground station operating in the 2-kmc band utilizing both polarization and frequency diversity techniques to provide a continuous transmission circuit regardless of the satellite attitude.

Data storage in the satellite is accomplished by the use of newly-developed magnetic tape recorders.

Signals in the band near 108 mc provide telemetry and command control functions. The telemetry used is a modified standard FM/FM system, while the command control circuit enables selection of satellite control functions. Power for the satellite electronics is derived from solar energy using solar cells which charge nickel-cadmium batteries.

Each of the ground stations consists of radio transmitting and receiving equipment and an automatic-tracking 28-foot-diameter parabolic antenna. Each station will acquire the satellite and track it during a pass over a station. Data from the satellite are transmitted (tape loading) to the ground station upon command. Simultaneously, data for the other two stations are transmitted to the satellite (tape unloading) from the ground station. Message sorting in the satellite is accomplished by use of the appropriate tape recorders, which in turn are activated by ground commands.

In the ground stations, teletype messages on paper tape are converted to a serial pulse train at a 50-kilobit-per-second rate by a paper-tape reader and a magnetic recorder-reproducer. This message-train frequency modulates a 1-kw UHF transmitter and is transmitted to the satellite where the information is deposited.

A quadruple-diversity UHF receiving system using low-noise parametric preamplifiers is used to receive the down-traffic from the satellite. The 100-watt VHF ground transmitter provides for the transmission of initial commands to the satellite and a phase lock VHF receiver on the ground provides for beacon acquisition and telemetry reception.

## I. INTRODUCTION

ON December 18, 1958, a new era of radio communication began with the Atlas launching of the U. S. Army Signal Research and Development Laboratory Project SCORE<sup>1</sup> satellite payload. For the following two-week period, teletype and voice traffic were transmitted by ground stations to the satellite, stored there, and later retransmitted to earth. Through the use of a rudimentary satellite-borne radio relay station employing tape-recorder memory and four companion ground stations, communication was begun by means of delayed-repeater satellite intermediaries. This project represented

the first step of an evolutionary program to develop communication satellite systems for use by the military services. This paper describes the form that one type of an advanced design of satellite communication system might take, using the delayed-repeater technique.

## II. SYSTEM CONCEPT AND PARAMETERS

The use of earth-orbiting satellites as delayed-repeater radio stations which receive, store, and retransmit messages has been the subject of considerable study by various groups and individuals, since the operational application of these devices offers attractive means of overcoming present-day circuit congestion on existing world communication networks. One needs only to review present and projected traffic growth patterns of current systems to appreciate fully the impact of satellite communication systems on future communication net planning and the promise held forth by future satellite-supplemented global communication networks.

The interrelation of the ground-station locations, communication service areas, and duration and frequency of service is illustrated by the following discussion.<sup>2</sup> An equatorial radio-relay station orbiting at 300 miles above the earth provides 11 minutes of possible communication to ground stations located on the equator once every 95 minutes. Service can also be provided to stations less than 1500 miles north or south of the equator with the same frequency but with diminished communication time. The same satellite orbiting in a plane which intersects the equatorial plane at an angle of 50° can provide communication over a much larger global surface. However, the frequency of service between the equatorial stations is reduced to approximately two or three satellite "passes" every twelve hours.

Considering any probable deployment of ground stations and choice of orbit altitude, a variation in slant range from 100 to 3300 statute miles between a ground station and the satellite has been used as a criterion for system design. The satellite would accommodate five ground stations and not require attitude stabilization. Table I summarizes the salient system parameters prescribed for the purposes of this paper; carrier-to-noise ratio calculations follow, based on these parameters and on others mentioned below for all of the radio links required in such a system. These computations do not include allowances for fading but do allow for equipment degradation over an assumed one-year period of operation.

\* Manuscript received by the PGMIL, February 1, 1960.

† Astro-Electronics Div., Communications Dept., U. S. Army Signal Res. and Dev. Lab., Fort Monmouth, N. J.

‡ S. P. Brown, M. I. Davis, H. C. Hawkins, and G. P. Senn, "The ATLAS-SCORE communication system," *Proc. Natl. Conv. on Military Electronics*, Washington, D. C., June, 1959, pp. 401-409.

<sup>2</sup> For a more comprehensive discussion, see, for example, J. R. Pierce and R. Kompfner, "Transoceanic communication by means of satellites," *Proc. IRE*, vol. 47, pp. 372-380; March, 1959.



## A. List of Symbols and Units

$C/N$  = carrier-to-noise ratio at receiver in db

$B$  = bandwidth in mc

$d$  = slant range in statute miles = 3300 miles maximum

$f$  = frequency in mc = 130 and 1800 mc for calculations shown below

$G_r$  = receiving antenna gain in db

$G_t$  = transmitting antenna gain in db

$L_a$  = antenna polarization loss in db

$L_{du}$  = duplexer loss in db

$L_{di}$  = diplexer loss in db

$L_t$  = tracking loss in db

$L_T$  = total RF plumbing loss between antenna and parametric-amplifier terminals

$L_x$  = cable and rotary joint loss in db

$NF$  = noise figure in db

$P_n$  = noise power in dbw

$P_r$  = received carrier power in dbw

$P_t$  = transmitted carrier power in dbw

$T_a$  = antenna temperature in °K

$T_e$  = effective receiving system temperature in °K

$T_r$  = effective receiver temperature in °K

$K$  = Boltzmann's Constant =  $1.38 \times 10^{-23}$  watt-second/°K

## B. Ground-to-Satellite VHF Link

$$P_r = P_t + G_t + G_r - 37 - 20 \log f - L_{di} - L_a - 20 \log d$$

$$P_r = 18.5 + 19 - 4 - 37 - 70 - 42 - 0.5 - 3 = -119 \text{ dbw}$$

$$P_n = -144 + 10 \log B + NF$$

$$P_n = -144 - 15 + 8 = -151 \text{ dbw}$$

$$C/N = -119 + 151 = 32 \text{ db}$$

C. Satellite-to-Ground VHF Link—Beacon Mode<sup>3</sup>

$$P_r = P_t + G_t + G_r - 37 - 20 \log d - 20 \log f - L_x - L_{du} - L_a$$

$$P_r = -13 - 4 + 19 - 37 - 70 - 42 - 1.5 - 0.2 - 3 = -152 \text{ dbw}$$

$$P_n = -144 + 10 \log B + NF$$

$$P_n = -144 - 30 + 4 = -170 \text{ dbw}$$

$$C/N = -152 + 170 = 18 \text{ db}$$

D. Satellite-to-Ground VHF Link—Active Mode<sup>3</sup>

$$P_r = P_t + G_t + G_r - 37 - 20 \log d - 20 \log f - L_x - L_{du} - L_a$$

$$P_r = 1.8 - 4 + 19 - 37 - 70 - 42 - 1.5 - 0.2 - 3 = -137 \text{ dbw}$$

$$P_n = -144 + 10 \log B + NF$$

$$P_n = -144 - 22.2 + 4 = -162 \text{ dbw}$$

$$C/N = -138 + 162 = 25 \text{ db}$$

## E. Satellite-to-Ground UHF Link

$$P_r = P_t + G_t + G_r - 37 - 20 \log d - 20 \log f - L_x - L_{du} - L_t$$

$$P_r = 9 - 4 + 41 - 37 - 70 - 65 - 1.5 - 0.2 - 0.5 - 1 = -129 \text{ dbw}$$

$$P_n = KT_e B$$

$$\text{where } T_e = T_a + (L_t - 1) 290 + L_t T_r$$

$$T_e = 130 + (1.74 - 1) 290 + 1.74(170) = 640^\circ \text{K}$$

$$P_n = -168.6 + 28.1 - 10 = -151 \text{ dbw}$$

$$C/N = -129 + 151 = 22 \text{ db}$$

## F. Ground-to-Satellite UHF Link

$$P_r = P_t + G_t + G_r - 37 - 20 \log d - 20 \log f - L_{di} - L_t - L_a$$

$$P_r = 28.5 + 41 - 4 - 37 - 70 - 65 - 1 - 1 - 3 = -112 \text{ dbw}$$

$$P_n = -144 + 10 \log B + NF$$

$$P_n = -144 - 3 + 14 = -133 \text{ dbw}$$

$$C/N = -112 + 133 = 21 \text{ db}$$

TABLE I  
SYSTEM PARAMETERS

Frequencies:	1.7-2.3 kmc and 108-150 mc	
Effective message transmission rate:	50,000 bits/second	
Satellite storage:	15,000,000 bits/station	
Stations accommodated:	5 maximum	
UHF CIRCUITS		
	Satellite	Ground Station
Power output	8 watts	850 watts
Noise figure	14 db	—
Noise temperature	—	640°K
IF bandwidth	550 kc	100, 200 or 500 kc
Antenna gain	-4 db	41 db
Antenna polarization	linear	circular transmission, diversity reception
VHF CIRCUITS		
	Satellite	Ground Station
Standby power output	50 mw	—
Active power output	1.5 watts	85 watts
Noise figure	8 db	4 db
Standby IF bandwidth	30 kc	1 kc
Active IF bandwidth	30 kc	6 kc
Antenna gain	-4 db	19 db
Antenna polarization	circular	linear transmission, diversity reception

These calculations indicate reasonably strong signal paths at the worst case of 3300 miles slant range.

The system includes ground-station complexes which simultaneously perform the tracking, data-exchange, and telemetry functions in conjunction with the space-borne radio relay station. The tape recorders aboard the satellite store messages from the ground stations, and (upon command) the satellite retransmits the messages to provide communication to another ground station once acquisition is accomplished and the UHF and VHF links are established. In an exchange of messages between the satellite and a ground station, the data stored on magnetic tapes are transmitted to the satellite serially at an effective 50 kilobit-per-second rate and stored by the satellite tape recorders assigned to other ground stations. Readout of data from the satellite is accomplished (upon command) simultaneously with the transmission of data to the satellite. A combination of frequency-diversity transmission

<sup>3</sup> This calculation assumes a satellite attitude in which polarization is 45° displaced between antennas.

from the satellite and polarization-diversity reception by the ground station is used to reduce errors in delivered messages caused by signal fading. A combined output of both diversity systems is derived to feed the ground-station message-recovery equipment. Tracking and acquisition of the satellite are accomplished by the 28-foot dual-feed tracking antenna. Concentric beams at approximately 130 and 1800 mc are generated by the antenna system in such a manner as to provide E and H plane outputs for both of these bands.

The 18° VHF beam of the antenna is used for beacon acquisition. The "up" and "down" circuits as well as automatic tracking are established via the one-degree microwave beam. During a typical satellite "pass" over a ground station, initial contact is made by the reception of signals transmitted from the beacon operating in its "standby" mode of operation. The ground station then commands the satellite to become active. Sector scanning of the antenna is initiated upon reception of a command acknowledgement that the satellite has switched to the "active" mode during which the satellite's microwave transmitters are activated. As the satellite rises through the plane formed by sector scanning the one-degree ground antenna beam, the antenna automatically locks on the satellite signal when the received signal exceeds the threshold level. This signal is received at the ground station by low-noise high-gain parametric front-end receivers which provide the sensing signals for the automatic tracking antenna servo-drive system. The conical scan system used to derive the azimuth and elevation error signals is provided by a rotating RF lens ahead of the microwave feed. Automatic coast features are built into the antenna tracking circuits to minimize the problems of re-acquisition should this be required during a message exchange with a ground station. Establishment of the up and down microwave circuits, as well as the telemetry VHF link, is required to accomplish properly a message exchange during a "pass." If both ground-to-satellite links are disrupted after acquisition for a period greater than 20 seconds, the satellite will revert to its "standby," low-power mode of operation, and the re-acquisition of the satellite is required. Approximately, three minutes are expended for acquisition, equipment-warmup time, and operational dead time.

The condition of the satellite batteries, which are charged by solar cells, is an essential parameter which must be determined after acquisition and prior to a message exchange. This is available over the telemetry link, and the possibility of a data exchange is dependent on this parameter. Further solar charging is required before a message exchange can be accomplished if the battery charge is too low. The solar charging cycle is dependent on orbit considerations. This system requires charging during approximately 60 per cent of the total orbit time to provide 44 watts of instantaneous power from a 19,000-cell solar generator aboard the satellite. The satellite power supply furnishes approximately 600 watt-hours of energy per day, based on 10 per cent losses

caused by micro-meteorite erosion after one year and 15 per cent by solar cell mismatch to batteries, 80 per cent battery efficiency, and solar cell illumination 60 per cent of orbit time. For a duty cycle of 10 per cent (2.4 hours per day), an average of 250 watts are available from the power supply during active periods. Peak loads during a data-exchange cycle plus the power required during standby and acquisition time are estimated to average only 225 watts over the active periods.

Fig. 1 shows the sequence of events during a typical satellite acquisition. Initial acquisition of the satellite is achieved by manual tracking of the signal received by a ground station from the VHF beacon transmitter operating at a 50-mw level. Messages at a ground station are stored on magnetic tapes which have sufficient capacity for a five-minute transmission to the satellite. During this period, data are transmitted over the UHF up circuit at a rate of 55 kilobits per second. A total of 16.5 megabits is capable of being transmitted during this period, but dead time in data processing reduces the total to approximately 15 megabits. In order to exchange this data on sequential orbit passes, the ground tape recorders must be reloaded between "passes." The message-processing equipment that would be required at a ground station would depend upon the communication service to be provided. This would be more or less conventional equipment and is not particularly pertinent to the satellite relay system design.

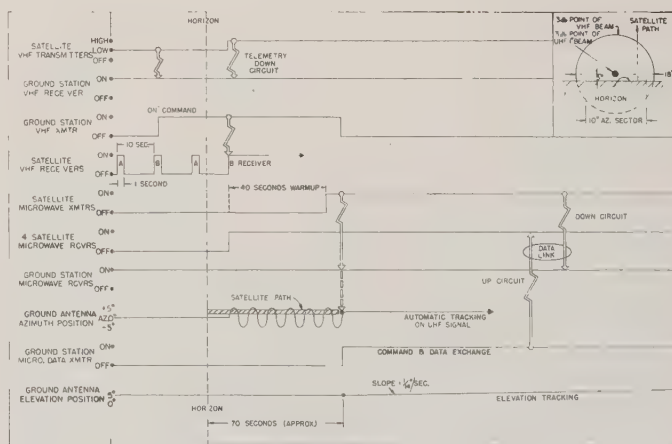


Fig. 1—Satellite acquisition sequence chart.

Telemetry of satellite parameters to the ground station prior to and during message exchange is accomplished over the VHF down circuit. Seven subcarriers are used in an FM/FM System. Commutation on the subcarriers is required to accommodate all telemetry data. Each channel is time-sequenced to provide three seconds for positive calibration, one second for negative calibration, and two seconds for each of five parameters.

Data received from the ground station are stored in the satellite on magnetic-tape recorder reproducers. A storage unit is assigned to each ground station with provision for



switching in either of two spare storage units. A simultaneous recording and reproducing capability during a pass is possible because of this manner of assignment of storage units and the fact that only one ground station is in contact with the satellite at one time.

To provide a continuous circuit on the microwave data link, a tracking capability is required in the ground antenna system. The satellite elevation velocity on a zenith pass is in the order of  $0.06^\circ$  per second at the horizon. For a five-degree screening angle, the elevation velocity increases to approximately  $0.08^\circ$  per second, as it comes into line-of-sight with a ground station. This elevation rate is compatible with the automatic acquisition features of the antenna system, since the  $3^\circ$  per second sector scan rate provides approximately six opportunities to intercept and lock on the transmitted satellite signal. Angular error data for the servo drive system are derived from the conical scan modulation on the UHF down signal which is preserved in the ground station receiver and phase-referenced with a reference source. Severe tracking accuracy requirements are not imposed, except for restriction of off-target limits of the tracking beam to minimize the "down" circuit amplitude variations caused by tracking errors to 1 db or less.

The above paragraphs have given a description of an advanced delayed repeater satellite communication concept. However, the reader has probably noticed the minimizing of "art-advancing" techniques within this concept.

The operational parameters chosen for the system, particularly satellite parameters, were selected with ease of attainment and an evolutionary advance over the SCORE experimental system as key considerations. A short discussion of some of the more challenging system-design aspects follows.

A collateral choice of operating frequency and satellite size places severe limitations on methods of establishing message circuit continuity regardless of satellite attitude. The operating frequency was selected in the 2-kmc region because of noise, propagation, and component considerations. Since the satellite is a sphere limited in size by assumed vehicle considerations, this combination of conditions rules out any known method of getting the required omnidirectional coverage from a single antenna array. The solution to the problem is the use of antenna apertures capable of providing hemispherical coverage when mounted on the sphere, and the non-phase-coherent use of these apertures. This arrangement provides a satellite radiation pattern which is linearly polarized in random orientations, depending upon the particular satellite orientation existing at any instant. Described more fully in subsequent paragraphs, this method is employed in conjunction with ground-station circular-polarization transmission and quadruple-diversity reception. The frequency and polarization diversity techniques used in the ground receiver, which employs low-noise parametric amplifier front ends, ensure the continuity of the message circuit and minimize the message-error rate.

Use of a 28-foot diameter parabolic antenna at frequencies in the 2-kmc region results in a beamwidth of one degree. Acquisition of the satellite with an antenna beam of this size requires accurate ephemeris data or some other mode of assistance. The evolved acquisition technique permits the system to operate independent of externally-supplied tracking data. Frequencies in the 108-150-mc band were chosen for the VHF links based on the availability of completely transistorized satellite receivers and transmitters in that band. The VHF ground antenna beamwidth of approximately  $19^\circ$  is more than adequate for implementing the acquisition procedure.

Frequency modulation is used throughout the system because it appears to offer the best compromise among equipment simplicity, reliability, and circuit performance. Modulation indexes approximating unity are used in all circuits. The use of FM techniques minimizes the satellite power needed to produce a baseband signal-to-noise ratio of approximately 20 db in the ground stations and allows the use of existing equipment and techniques. Ground station receivers incorporate AFC circuitry; and, accordingly, IF bandwidths are predicated only on the anticipated received signal spectrum and AFC signal centering characteristics. Satellite receivers do not employ afc circuitry and; hence, the IF bandwidths of these receivers include allowances for receiver and ground transmitter drift, Doppler shift, and the anticipated received signal spectrum.

### III. SATELLITE DESIGN

To accomplish its primary mission, the satellite must be capable of transmitting, receiving, and storing ground-originated messages. In support of this mission, the satellite transmits a beacon signal, telemeters internal data to the ground station, implements valid commands, and acknowledges commands. Fig. 2 is a simplified block diagram of the satellite system.

Physically, the satellite would be spherical with a solar-cell surface density of approximately 70 per cent. The solar cells, which are shingled together with a special ad-

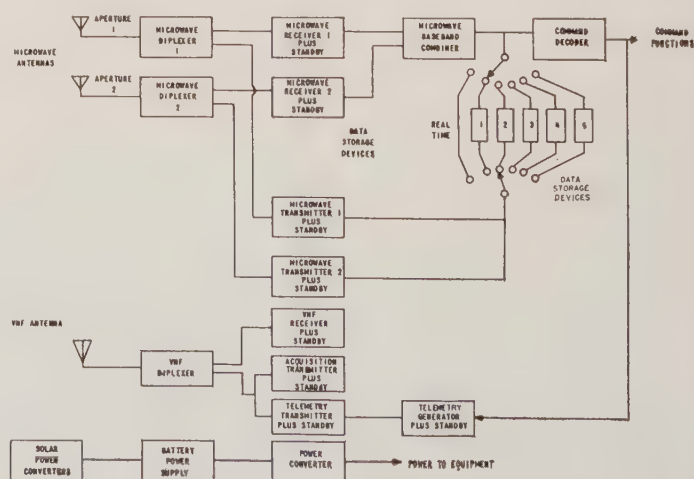


Fig. 2—Satellite, block diagram.

hesive and mounted on the satellite in modules, number about 19,000. Four VHF antenna assemblies are equally spaced around the satellite's equator. Each assembly consists of a probe extending beyond the outer surface of the satellite and containing a flexible section to permit folding when the satellite is placed in its shroud. Two UHF slot antennas, both of which are mounted to ground planes fabricated in a single structure from sheet magnesium alloy, are located at antipodean points on the satellite equator. To provide a uniform reflective area, all solar cells are mounted outside the reflective ground plane areas. Shell material consists of honeycomb fiberglass sandwiched between two thin fiberglass layers, with a conducting metal surface sprayed on the fiberglass but covered with another fiberglass layer. The inner structure, composed of platforms mounted on aluminum-tubing truss members, supports the various components in the satellite. The platforms are also made of the above-mentioned sandwich material to effect an over-all weight reduction without reducing the strength of the structure.

The UHF antenna apertures, one of which is shown in Fig. 3, provide continuous coverage through a solid angle exceeding a hemisphere. At no point within the hemisphere is the response poorer than 4 db below an isotropic radiator. The method of achieving spherical coverage is through a non-phase-coherent employment of the aperture pair. Separate UHF receivers detect signals present at each aperture, while separate transmitters operating on frequencies spaced approximately one per cent apart broadcast from each aperture. Received intelligence is combined at baseband, and transmitted intelligence is fed jointly to both transmitter modulators.

Each UHF slot antenna is fed by a coaxial-line probe which bridges the gap formed by the walls of the notch. As a transmission-line element, the antenna may be regarded as a tapped quarter-wave line used to transform the radiation resistance appearing at the apex of the fin to that of the coaxial line. From the standpoint of the radiation pattern, the antenna is a half-wave slot cut in a

ground screen which is then folded up into a fin with the E-plane center line of the slot becoming the apex of the fin. This results in broadening the H-plane pattern without affecting the already sufficiently broad coverage of the E-plane pattern.

Simultaneous use of the antenna apertures with companion transmitting and receiving apparatus is accomplished through the use of a pair of microwave duplexers. These duplexers provide antenna-to-receiver and antenna-to-transmitter insertion losses of under 1 db, decoupling loss between the transmitter and receiver of greater than 50 db, and transmitter-to-antenna isolation at the receiver frequency of approximately 20 db.

The primary and standby UHF receivers indicated in Fig. 2 are operated simultaneously during the satellite's active intervals. This method of operation sacrifices 3 db of received RF signal when contrasted to a system capable of switching between the primary and standby units. However, it enhances the reliability of the satellite design. Each UHF receiver is a single-conversion superheterodyne receiver employing a three-pole passive preselector, second harmonic mixing, and 30-mc IF amplification. These completely transistorized receivers have the following characteristics:

Noise figure	14 db
IF bandwidth	550 kc
Frequency stability	0.002 per cent
Spurious rejection	> 50 db
Power consumption	1.5 watts
Volume	200 cubic inches

Baseband combination of the four microwave receiver outputs is accomplished in a separate completely transistorized unit. Through the use of circuitry that senses out-of-band noise power, each receiver's contribution to the composite output is varied to optimize the baseband signal-to-noise ratio. Since the use of out-of-band noise as a combining criterion does not permit distinction between receiving a very strong signal and a defective receiver, a ground-originated pilot tone is employed as a fail-safe feature. Any receiver that produces an unacceptable pilot-tone output is automatically removed from the combining circuit. In addition to serving its prime mission, the baseband combiner implements other functions within the satellite. These include providing an analog voltage for a telemetry sensor which is used to allow the monitoring of received-signal strength, and output potentials used to control automatic operation of the command decoder.

The combiner message output is routed to the data-storage devices or the real-time circuit as commanded from the ground station. A portion of this output is also used in the command decoder. Message storage is accomplished through the use of five miniature magnetic tape recorder-reproducer machines. Each machine is capable of recording and reproducing up to five minutes of analog data. A shuttle transport design with a tape speed of 30 inches per second provides opposite-direction recording and play-

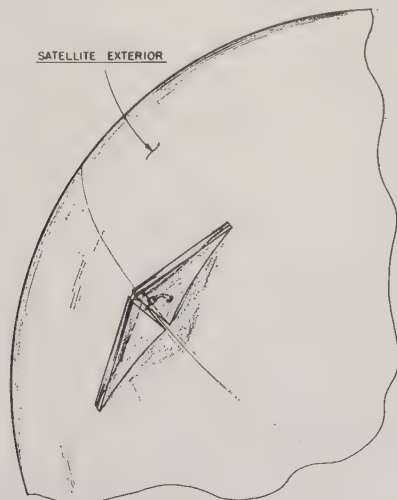


Fig. 3—Linearly polarized antenna.



back. While this causes traffic to be read out backwards, it does enable some equalization of phase distortions produced by the recording and playback heads. Erasure of old traffic is accomplished by an erase oscillator circuit that functions during the recording cycle with sufficient effectiveness to assure a 35-db signal-to-noise ratio. Life tests of the magnetic tape employed indicate a high confidence factor for one year of trouble-free operation at duty cycles up to ten per cent. To enhance further the reliability and to minimize driving power, the transport construction employs a constant-tension spring system between the play-out and the take-up reels.

Real-time operation bypasses the tape-recorder data-storage units with a circuit that couples the baseband combiner output to the UHF transmitter modulators. A special circuit designed to suppress the rebroadcasting of commands is placed in this circuit. The purpose of including a real-time capability is to facilitate propagation tests and checkout of the communication link prior to data transmission. It is also used to effect a form of fail-safe satellite operation. Command decoder logic places the satellite in its real-time operational mode upon acquisition. Therefore, if the satellite has not failed in a manner that precludes acquisition, the probability of achieving at least real-time operation is extremely high.

Four microwave transmitters, two primary units, and two backup units generate RF signal outputs for the satellite-to-ground data link. Used in pairs, these units are depended upon for at least 8 watts of output power and are selected by ground station command. In this transmitter design, microwave power is generated by a cavity oscillator equipped with a quick-heating planar power triode. Anode cooling is accomplished through the use of a wax-filled, hermetically-sealed reservoir. The reservoir is thermally connected to the anode of the tube but electrically insulated from it. This cooling system depends upon the intermittent nature of system operation. It provides a heat reservoir of great capacity during the relatively short transmitting periods and effects cooling by conduction and radiation during the off period. The large energy storage provided by this device results from the change of state of the wax from solid to liquid when it is heated. The cathode and grid seals of the tube are cooled by conduction through metal collets so that the cavity becomes the short-period heat sink, which is cooled by the conduction of heat to its surroundings during the off periods. Two tuned cavities are used in this grid isolation oscillator, one for the plate circuit and the other for the cathode circuit. The plate cavity is of radial design, operating in the  $TM_{0,1}$  mode. It is tuned by means of two threaded plugs introduced through the cylindrical cavity wall  $180^\circ$  apart. Power is coupled to the load by means of a pickup loop capable of being adjusted to obtain optimum loading of the oscillator. The cavity design includes a plate bypass capacitor, which permits the dc power to be shunt-fed to the plate. The cathode circuit is tuned by a  $\frac{3}{4}$ -wavelength coaxial-line type cavity operating in the

TEM mode. The grid-isolation circuit is inherently stable and will not oscillate unless feedback is deliberately introduced between plate and cathode circuits. In this transmitter, the feedback is obtained by means of four loops in the cathode cavity, equispaced around the wall common to both cavities. The free ends of these inductive loops pass through individual holes in the common partition, and project into the plate cavity where they act as capacitive probes.

Frequency modulation of the oscillator is obtained by coupling a reactance into the cathode cavity whose magnitude varies with the modulating voltage. This is accomplished by utilizing the changes in characteristics of a reverse-biased crystal diode when the bias voltage is modulated. This modulator is connected to the cavity through an adjustable length of tuned coaxial transmission line, and an adjustable coupling probe inserted into the cavity opposite the high-voltage point on the center conductor of the cavity.

The frequency drift present in the self-excited oscillator is compensated for by an automatic frequency control system. A crystal-controlled 50- to 70-mc oscillator is used as a frequency standard. A multiplier chain provides a local oscillator signal at the eighth harmonic of the crystal. A filter inserted between the multiplier chain and the crystal mixer eliminates unwanted responses. In the crystal mixer, a sample signal from the transmitter beats against the fourth harmonic of the local oscillator signal, translating the sample signal to an intermediate frequency in the above 50- to 70-mc range. The IF signal is then passed to an electronic switch controlled by a 400-cps square-wave oscillator. A signal from the crystal oscillator is also fed to the switch so that the switch output consists alternately of the transmitter sample and the crystal oscillator signal, commutated at the 400-cycle rate. The commutated output of the switch is then fed to a limiter-discriminator, which delivers a square-wave output whose amplitude depends upon the frequency difference existing between the transmitter sample and the reference signal. The phase of the square wave depends upon which of the two signals is higher in frequency. The output signal from the discriminator is ac-coupled to an audio amplifier, which is used to drive one phase of a two-phase motor. The motor, with its second phase powered by the 400-cycle source, is used to vary a tuning screw mounted in the cathode resonator. The UHF transmitter, with its automatic frequency control (AFC) disabled, has an initial drift of from 6 to 14 mc, depending upon the planar triode selected. The frequency stabilizes to within one megacycle of the operating point after approximately two and one half minutes. With AFC, the transmitter can be locked into frequency in 40 seconds and the frequency can be maintained to within 0.005 per cent over a temperature range of 0 to  $130^\circ\text{F}$ .

VHF satellite circuitry supports system requirements for a tracking beacon, telemetry, command acknowledgment, and initial satellite acquisition. The major units supporting these requirements are shown in Fig. 2. The VHF

antenna consists of four quarter-wave whips spaced and electrically fed in quadrature. This configuration gives an antenna pattern that is circularly polarized along an axis normal to the plane of the whips, and elliptically polarized over most of the remaining sector. Since the satellite diameter is approximately one half wavelength in the operating frequency band, nulls would be experienced in the coverage.

A VHF diplexer, consisting of complementary filters with distributed inductances and lumped capacitances, permits simultaneous receiver and transmitter operation. Salient characteristics of this unit follow:

Reception insertion loss	0.5 maximum
Transmission insertion loss	0.2 db maximum
Transmitter/receiver isolation	60 db minimum
VSWR	1.25 maximum
Transmitter decoupling	30 db minimum

The VHF receiving system consists of primary and standby receivers that alternately search for an RF signal from the ground station. A battery-saver circuit causes the receiver pair to operate in the following cyclic fashion. First, one receiver is on for one second; next, both receivers are off for nine seconds; then, the other receiver is on for one second; and lastly, both receivers are again off for nine seconds. This operation reduces standby satellite power without unduly compromising reliability because of fail-safe features incorporated in the system. While the satellite is active, the VHF receiver first intercepting a signal is locked on and used to effect automatic functions within the command decoder circuitry.

Each receiver is a single-conversion superheterodyne unit including a transistor RF amplifier. By use of the inherent capabilities of the diplexer, a 50-db image rejection is attained. Noise figures of 8 db have been measured. The local oscillator is crystal controlled and provides a mixing signal higher in frequency than the operating frequency with a stability of  $\pm 0.002$  per cent over the anticipated temperature range. The IF amplifier frequency is 10.7 mc with a 3-db bandwidth of 30 kc. The narrow bandwidth is achieved through the use of a crystal filter following the first stage of amplification. Six stages of IF amplification are used, providing nominal gain of 15 db per stage. The first five stages provide enough gain to raise a threshold signal of  $-112$  dbw to the limiting level in the last stage. All IF amplifier stages following the narrow-band filter include diodes for limiting. Limiting occurs in the last IF stage on threshold signal levels, and, as the signal level increases, additional stages reach the limiting level. Following the last IF amplifier stage, a discriminator driver stage and a crystal discriminator are used. A video amplifier which follows the discriminator uses two stages of voltage amplification, followed by an emitter follower for impedance matching. The voltage amplifiers use two transistors connected in the compound Darlington configuration to provide very stable gain characteristics over a wide range of temperature. Degenera-

tive feedback from the second-stage collector to the first-stage emitter is employed for added stability and a convenient gain control. The outputs of both VHF receivers, the active unit and the standby unit, are connected in parallel to the input of the decoder. The output of the emitter follower stage is designed to present a high impedance when the transistor is not active. In this way, no appreciable power is lost and switching of the two outputs is avoided.

The functions of providing RF energy to serve as a beacon signal and to convey telemetry data are divided among an acquisition transmitter, a telemetry transmitter, and their respective backups. All are completely transistorized, the former delivering 50 mw from its output stage and the latter delivering 1.5 watts. Frequency is maintained to within  $\pm 0.002$  per cent through the use of crystal-controlled oscillators. The acquisition transmitter emits a cw signal during satellite standby periods, and the telemetry transmitter is frequency modulated by subcarrier oscillators to provide data when the satellite is active.

The first seven channels of the I.R.I.G. FM/FM telemetry standards<sup>4</sup> are employed as subcarriers. These subcarriers are 400, 560, 730, 960, 1300, 1700, and 2300 cps respectively. Channels 2 through 7 are commutated to provide a positive and negative calibration level and five data samples. The positive calibration consists of three seconds during which the subcarrier oscillators, deviated a positive 7.5 per cent, are at their maximum frequencies. A one-second negative calibration period places each subcarrier oscillator frequency at its minimum due to a negative 7.5 per cent deviation. Mid-range calibration is not believed to be required on a regular basis. However, it is available to the operator, through selective commanding of the satellite and observance of the command acknowledgement signals. Data are modulated on the commutated channels during five two-second intervals. These data consist of the following:

- Battery voltages
- Solar charging currents
- Load current
- Temperatures
- Magnetic-tape positions
- Transmitter power outputs
- Receiver signal strength levels

Primary satellite power is derived from approximately 19,000,  $2 \times 1$  centimeter, nine per cent efficiency solar cells. These cells are individually optically coated, assembled in shingles on metal skins curved to fit the satellite, and distributed about the surface. To prevent shaded cells from loading the power circuit, each group of shingles is diode blocked from other shingles. A pair of diode-blocked 28-volt nickel-cadmium batteries is used for power storage. The combination of diode-blocked solar-cell shingles operating with dual battery supplies is used to en-

<sup>4</sup>"Telemetry Standards for Guided Missiles," Inter-Range Instrumentation Group, White Sands Missile Range, N. M., Document #103-56; October, 1956.



hance power supply reliability. Fig. 4 illustrates the important features of the power-supply arrangement. Each battery complement, charged by the solar power converters to which it is connected, is capable of supporting the 220-watt active and 4.5-watt standby power consumption of the satellite for approximately a 10 per cent duty cycle. In order to minimize interference and voltage breakdown problems associated with launching, the satellite is not activated until it is injected into orbit. The activating switches are microswitches that sense the presence of the upper stage of the missile. Upon injection, these switches close, thereby providing redundant turn-on. The umbilical circuit provides launch-site control of the payload. Through the wiring provided, it is possible to charge and discharge remotely each battery supply and to operate the satellite electronics with both internal and external power.

One of the major satellite design problems is that of ensuring that the payload can withstand the thermal environment in which it must operate. In order to control the internal temperature of the satellite, it is necessary to consider two distinct environments. The first is encountered during the launch phase when the satellite will be subjected to the thermal environments resulting from the aerodynamic heating of the missile nose cone; a maximum skin temperature of approximately 300°F may be experienced for less than four minutes during this period. Hence, satellite skin materials and solar cells capable of withstanding this temperature are used, and thermal isolation is provided between the outer surface of the satellite and internal components to effect a time lag which prevents damage to internal components for that amount of time. The second phase is during its life in orbit when the satellite is subjected to the extremes of intense heat and cold of space. The degree of heating to which the satellite components are subjected during the launch phase depends on the trajectory of the launch vehicle through the earth's atmosphere, selection of satellite materials, and structure of the nose cone, as well as the internal conducting paths, and radiation geometry between the nose cone and the satellite.

#### IV. GROUND EQUIPMENT DESIGN

Each ground station is comprised of three semi-trailers of operating equipment, test equipment, and maintenance parts, in addition to a 28-foot parabolic dish-type tracking-antenna system. The control semi-trailer houses complete operating facilities for the entire ground station, including a control console, command generator, message-processing equipment, master timing unit, and telemetering data-processing and display equipment. The radio semi-trailer contains all the required VHF and UHF transmitting and receiving equipment. All maintenance parts and test equipment required for the equipment in the other semi-trailers are included in the maintenance semi-trailer. The antenna system consists of a 28-foot dish mounted on a 40-foot tower with both VHF and UHF feeds and associated RF hardware. A shelter enclosed within the tower

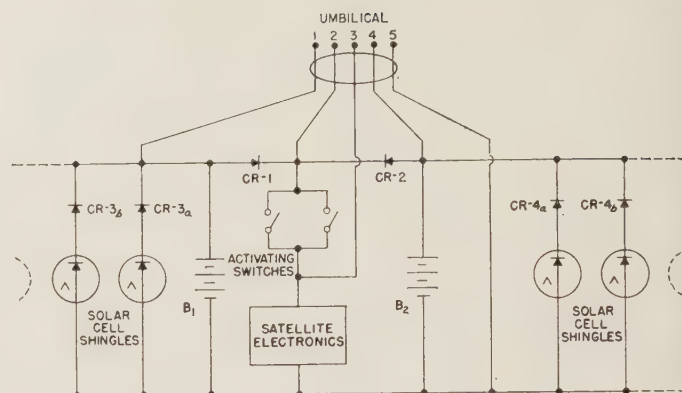


Fig. 4—Satellite power supply, simplified diagram.

contains the servosystem and antenna control equipment.

A layout diagram for a ground station is shown in Fig. 5. All equipment is contained within a 100 × 200-foot area with the exception of the antenna boresight tower, which is located outside the fenced-in area at an appropriate site. Three-phase four-wire wye-connected, ac power is used. This 120/208 volt 60-cps power will be supplied by a commercial concern, and four 45-kva engine generators are provided as backup to ensure uninterrupted power for the installation. A control box facilitates changeover between commercial and backup power. All power lines within the area shown are buried. An "00" isolated ground wire used throughout the ground station reduces ground currents. The antenna is mounted on a reinforced concrete pad and is designed to withstand wind velocities up to 150 mph. The ground station is a semi-fixed installation which may be transported and reassembled at another properly prepared location.

A simplified block diagram for the entire ground station is shown in Fig. 6. Teletype messages on perforated paper tape are read out by the paper-tape reader prior to recording on magnetic tape at a slow speed. The magnetic tape is then played back at a faster rate by the magnetic tape reproducer. This output signal is used to frequency modulate a UHF carrier which is transmitted to the satellite. Repeated messages from the satellite are received by the quadruple-diversity receiving system. The received signals are recorded on magnetic tape at a fast rate and played back by the magnetic-tape reproducer at a slower speed. The paper-tape perforator then punches a paper tape usable by the teletype receivers. A combined agc signal from the UHF receiving system, retaining the amplitude-modulated tracking signal obtained from conical scanning with the ground antenna, is demodulated and compared with the reference generator signal to obtain error signals for automatic tracking and positioning of synchros, controls, and indicators. The VHF system provides for the transmission of initial commands to the satellite and for the reception of beacon and telemetry signals from the satellite. Telemetry data processing, a master timing system, and recording equipment are integrated as shown. Coarse positioning of the relatively wide VHF beam from

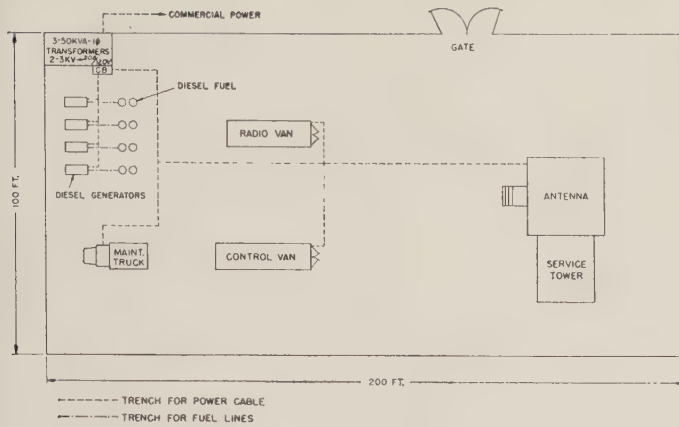


Fig. 5—Power layout of ground station.

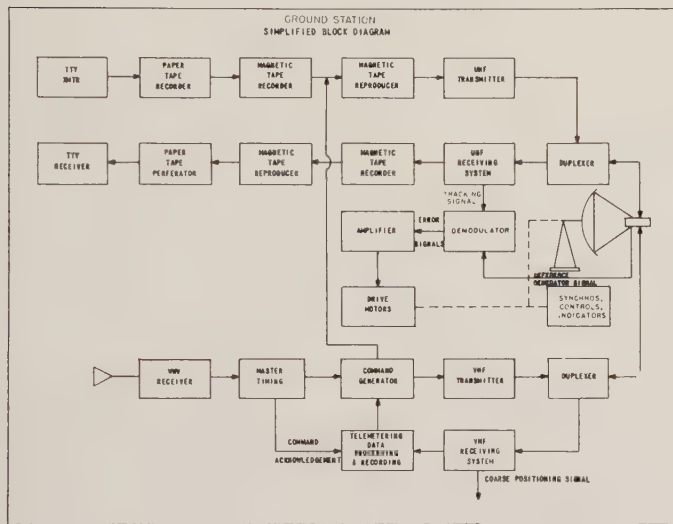


Fig. 6—Ground station, simplified block diagram.

the antenna is accomplished by peaking a meter indication of the AGC signal from the dual-diversity VHF receiver.

The ground station may logically be divided into three major subsystems as follows: the control center, the radio system, and the antenna system. A simplified block diagram for the control center equipment is shown in Fig. 7. Four AN/FGC-25X and two AN/TGC-5X teletypewriter sets provide for simultaneous transmission and reception of teletype messages. The AN/TGC-5X, a torn-tape relay, is capable of operating in conjunction with two AN/FGC-25X machines. Messages may be initiated with the AN/FGC-25X from a keyboard, electrical signals, or a standard punched tape; but the AN/TGC-5X requires punched tape or electrical signals and does not have a keyboard. Various combinations of the six teletypewriter sets are obtained through the patch panel, thus providing a suitable message generating and receiving capability for an experimental system. Connected for 60-wpm operation, the teletypewriters employ the standard five-unit start-stop Baudot code.

Teletype tapes, manually transferred to the photoelectric paper-tape reader, are read out at a speed of 200 characters per second. A 10 per cent guard space is allowed be-

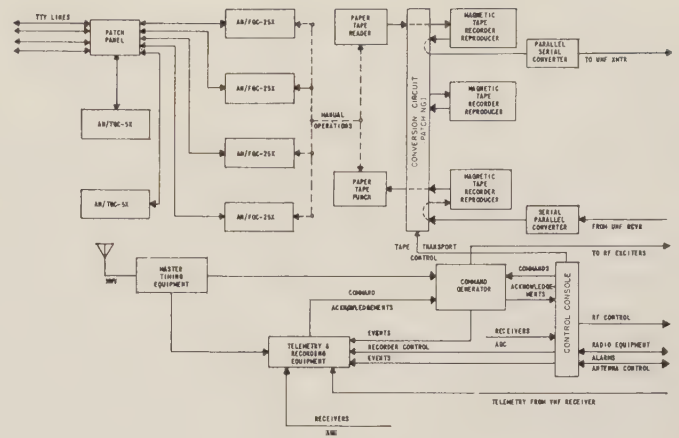


Fig. 7—Control center, block diagram.

tween characters to accommodate deterioration in the speed control of the electromechanical teletype machines and tape reader for a one-year period of time. The reader output consists of parallel pulse trains which are fed to any of three identical tape machines. These machines are used for both speed-up and slow-down of the message rate. Each transport has six speeds: 60, 30, 15, 3.36, 1.68, and 0.84 inches per second. However, in normal operation, the 1.68 and 60 inches per second speeds are used to speed up to and slow down from 55 kilobits per second. Maintained to an accuracy of  $\pm 0.5$  per cent, the tape speed has a maximum cumulative peak-to-peak flutter of 0.1 per cent from 2 to 500 cps at 30 inches per second.

Each character of the message is recorded in parallel on six tracks of the magnetic tape which are played back at a faster rate to the parallel-to-serial converter. The seventh or stop bit of the character is inserted in the parallel-to-serial converter. The parallel method of message-rate conversion is used to allow operation of the paper-tape reader and magnetic-tape machines at speeds sufficiently slow to minimize excessive mechanical wear caused by high speeds. The converter stores the five code bits of a character in a buffer flip-flop store which holds them until a pulse from a diode-matrix output gate causes a transfer of the character to the diode matrix. These five bits, plus the start and stop bits of the character, are then read out as a serial pulse train from the diode matrix by a count-of-seven counter and are amplified and routed to the UHF transmitter.

Incoming traffic from the UHF receiver is converted to parallel form by the serial-to-parallel converter. The signals received by the radio equipment in the form of gaussian pulses are first shaped by the serial-to-parallel converter to obtain full-bauded rectangular pulses. Since the bit rate of the messages received from the satellite is affected by the speed variation of satellite tape machines and, to a lesser extent, ground station tape machines, a local clock is operated at a frequency corresponding to the bit rate of the incoming messages. To accomplish this, a local oscillator is frequency controlled by an error signal developed by comparing the incoming-message signal fre-



quency with the local-oscillator frequency. The local oscillator in conjunction with a start-stop pulse synchronization circuit controls a binary matrix which provides six outputs to be stored serially in a buffer. These outputs correspond to five teletype code bits and a control bit. All six bits go through pulse generators to obtain signals within the bandwidth of the magnetic-tape machines, and they are then read out in parallel for recording on the selected machine. A more than adequate frequency response of 100 to 100,000 cps is obtained by recording at 60 inches per second. The magnetic tape is then played back, at a rate of 1.68 inches per second, to the paper tape punch which operates at a rate of 200 characters per second. The output paper tape is then converted by the teletypewriters to teletype tapes and/or printed pages.

The control console contains the necessary equipment for the operation of a ground station from one point. Front panel controls are provided for magnetic-tape machines, antenna positioning, selection of commands, events recording, and radio equipment control. Teletypewriter sets and paper-tape equipment are operated manually in an off-line manner and are not controlled from the console. The console also displays UHF and VHF receiver AGC signals, command acknowledgements, transmitter alarms, and other critical signals. Commands selected by the console are generated by the command generator and transmitted to the satellite by the radio equipment. The FM/FM telemetry signal from the satellite is recorded on magnetic tape and also separated into its seven channels by subcarrier filters. Discriminators with a linearity of approximately 0.2 per cent are used to obtain dc voltages representing the telemetered data. These data are suitable for strip-chart real-time recording. The chart recorders are also used to record time and events and AGC voltages from the UHF and VHF receivers, which are FM/FM telemetered from the radio equipment semi-trailer. A master timing system provides a time base for the telemetry recording and command generator equipment. The master timer counts down from a 1-mc crystal frequency to obtain the pulse time base required for the ground station, and is stable to within one part in  $10^8$  per day. The timing unit can be synchronized with signals received from WWV if required.

The radio equipment includes the UHF and VHF transmitting and receiving systems and the necessary duplexers, diplexers, and harmonic filters. The UHF equipment (see Fig. 8) receives the serial pulse train from the message-processing equipment, and the signal spectrum is limited to 50 kc by an approximately Gaussian-shaped filter having a low pass cutoff of 300 cps. After amplification, the pulse train frequency modulates a stabilized 70-mc carrier frequency. A tuned discriminator is used in the modulator AFC circuit. The modulator signal output is then mixed with a crystal-controlled local-oscillator frequency of 1700 to 2230 mc to obtain the desired carrier frequency to be transmitted. The mixer-amplifier output is at the 5-watt level with a carrier frequency stability of 0.0005 per

cent per day. The power amplifier uses a CW four-cavity tuneable klystron to amplify the power level to approximately 1100 watts. A harmonic filter in conjunction with the duplexer reduces transmitted harmonics to 80 db below the carrier signal level. The transmitter output signal is then divided into two paths which are used to provide the horizontally and vertically polarized antenna outputs. A phase shifter in one path provides the  $90^\circ$  phase shift necessary to effect circularly-polarized radiation from the ground antenna.

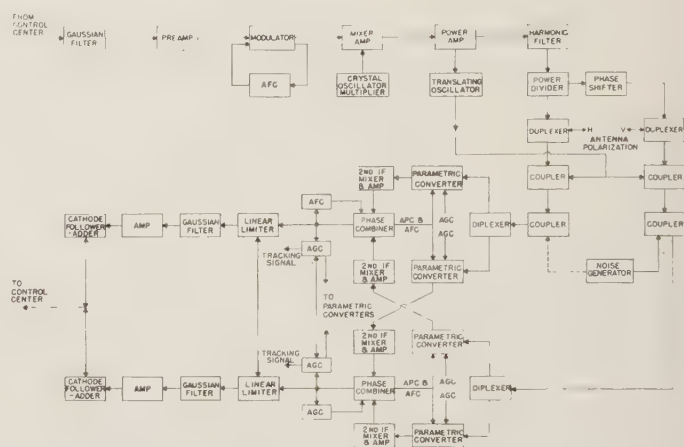


Fig. 8—UHF radio equipment, block diagram.

The two UHF power duplexers permit both circularly polarized transmission and polarization diversity reception. Each duplexer handles 500 watts at present but is capable of handling the full transmitter output to allow linearly polarized transmission, if desired. The pass-band insertion loss for each duplexer is approximately 0.2 db. A translating oscillator and mixer, which shifts the transmitted signal frequency to the expected received signal frequency, facilitates checking of the UHF system for maintenance purposes without receiving a signal from the satellite. When using this self-checking feature, the derived signals are coupled to the received signal paths as shown in the diagram, and a noise generator is coupled to either signal path to simulate a noisy received signal.

A quadruple diversity UHF receiving system is necessary to prevent losing the signal transmitted from the satellite due to nulls and variations in polarization of this signal caused by the nonisotropic satellite antenna. Both predetection and postdetection combining are used since separate noncoherent transmitter modulators are used in the frequency diversity satellite transmission. A predetection phase combiner is not used to combine all four IF signals since the signals to be combined must be approximately phase coherent.<sup>5</sup> Two diplexers with insertion losses of approximately 0.5 db are used and in conjunction with the

<sup>5</sup> For comprehensive discussions of diversity combining techniques, see D. G. Brennan, "Linear diversity combining techniques," *Proc. IRE*, vol. 47, pp. 1075-1102; June, 1959, or numerous other articles.

parametric converters provide a spurious response of 80 db below the input signal level.

The receiving system is a double conversion superheterodyne system with a dynamic range of  $-140$  to  $-100$  dbw. Received signals of either linear polarization are separated on a frequency basis by the duplexer filters and are accepted by the four parametric converters. These lower-sideband up-conversion units employ hermetically sealed variable-capacitance silicon diodes and an X-band klystron pump generator to obtain a 2-db noise figure with a gain of approximately 20 db and a 5-mc bandwidth. Each parametric converter is a dual unit with one path for the received signals and the second, containing a tunable local oscillator, for accommodating a wide variation of input frequencies. Both the signal and the local-oscillator converters are pumped by the klystron, and the converter outputs are mixed in a conventional X-band balanced mixer to provide the 70-mc IF signals. Summed automatic phase and frequency control voltages from the phase combiner control the local-oscillator frequency. The AGC signals derived from the phase combiner outputs are used in the 70-mc IF amplifiers following the mixers. The first IF signals are then routed to the second IF strips, as shown in Fig. 8, to allow polarization diversity phase combining of the intelligence on each of the received carrier frequencies. The second mixer heterodynes the 60.2-mc local-oscillator frequency with the first IF frequency to obtain a 9.8-mc frequency. Replaceable Gaussian-type bandpass filters allow selection of detection bandwidths of 100, 200, or 500 kc. The amplified second IF signals are then combined in pairs in two phase combiners.

Automatic phase control (APC) voltages, derived by comparing the signals from the 9.8-mc amplifiers to the common combiner output in respective phase discriminator circuits, are added to AFC signals derived from separate discriminators, and the sum is applied to the respective first local oscillators to maintain a constant phase relation. The second IF signals are added in pairs in the combiner hybrids, and since they are in phase and the noise is random, an improvement in signal-to-noise ratio is effected. The AFC signals are used to allow frequency tracking of incoming signals to an accuracy of  $\pm 0.001$  per cent of the carrier frequency which may vary in frequency as much as  $\pm 150$  kc because of Doppler shift, satellite transmitter frequency shift, and receiver local-oscillator drift. The phase combined outputs are then fed to the linear limiters and also to AGC circuitry. The AGC signals are combined to obtain the tracking signal for the antenna servo system and are used to maintain constant amplitude signals in all four receiver channels. The AGC combining is effected by cross-coupled detectors with emitter followers outputs.

Baseband frequency diversity combining is accomplished by the linear limiters and cathode follower-adders. The baseband combiner linearly controls the amplitudes of the respective limiter outputs in accordance with the ratio of the input signal levels and maintains the sum of the amplitudes approximately constant. Controlled bias voltages for

conventional diode limiters are used to vary the limit level. The control voltages are obtained by detecting and amplifying the input signal levels to the limiters. By the use of diode cross-coupling between the linear limiter outputs, the signals are limited to a fixed amplitude, but the ratio of the outputs may still vary. Gaussian-shaped 50-kc low-pass filters reject frequencies outside of the baseband. The baseband signals are then amplified to the level needed by the message processing equipment and added prior to cathode follower output circuits. As indicated in Fig. 8, the receiving system output signal may be taken from either of the cathode follower-adder circuits as selected by relays not shown. This allows the receiving system to be operated on a two-channel polarization diversity basis if only one frequency is transmitted from the satellite.

The VHF radio equipment, which receives signals from the command generator in the control center, is shown in Fig. 9. These signals are amplified and used to phase modulate a crystal-controlled oscillator frequency of approximately 4.5 mc. This modulated signal is then frequency multiplied to the final VHF carrier frequency resulting in a carrier frequency stability of better than 0.001 per cent per day. The power level is amplified from 5 to approximately 110 watts by the power amplifier. A harmonic filter in conjunction with the duplexer attenuate transmitted harmonics to 80 db below the carrier frequency power level. Two duplexers are used to allow switching the transmitter output from one linear antenna polarization to the other and still allow polarization diversity reception. Two tunable band-pass filters joined to the common antenna cable by a tee are used in each duplexer, and an insertion loss of 0.2 db is realized in each duplexer. A translating oscillator and mixer provide a self-checking capability in the same manner as described for the UHF radio equipment.

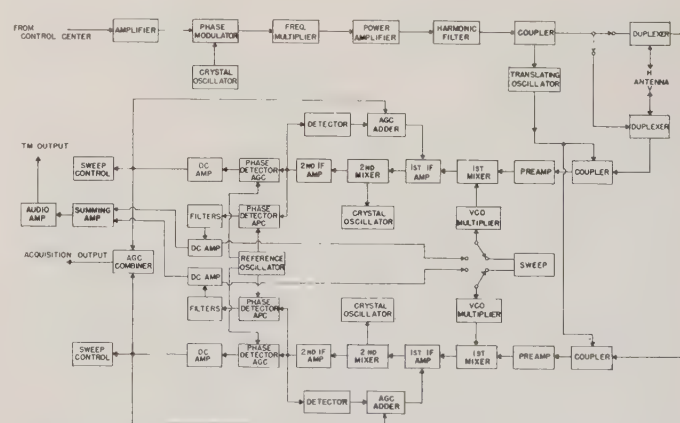


Fig. 9—VHF radio equipment, block diagram.

The VHF receiving system is a double superheterodyne polarization diversity system with a dynamic range of  $-155$  to  $-110$  dbw for beacon signals and  $-145$  to  $-90$  dbw for telemetered signals. Appropriate filters are automatically selected for optimum beacon or telemetry reception. Phase-lock techniques allow the use of relatively



narrow detection bandwidths of 1000 to 6000 cps for beacon and telemetry reception, respectively. The system noise figure is reduced to 4 db by the preamplifiers, and spurious response is maintained better than 80 db down by the selectivity of the duplexers and receiving system. The amplified signals are mixed with signals from frequency multiplied voltage controlled oscillators, which are independently swept at a rate of one cycle per second until phase lock is accomplished on both channels. The resulting 21.4-mc IF signals are amplified and mixed with 16.9-mc crystal-controlled oscillator signals in the second mixers. The 4.5-mc IF signals obtained are then amplified and detected. A noise amplitude detected signal is obtained in each receiver channel and added to a phase-detected combined AGC signal to maintain effectively equal gain in both receiver channels for telemetry operation. During beacon operation, the AGC signals for the first IF amplifiers are derived independently. A common 4.5-mc crystal controlled reference oscillator is used for both AGC phase detectors and also for both APC detectors. The 4.5-mc IF output signals go through buffer amplifiers as shown in Fig. 9. The AGC phase-detector outputs go through low-pass filters and then dc amplifiers, prior to combining. The dc-amplifier outputs also operate the sweep control circuits which disable the 1-cps voltage-controlled oscillator sweeps when a phase lock has been accomplished in that particular channel. The combined AGC output is displayed at the control console in order to facilitate manual positioning of the antenna as indicated by obtaining a peak reading on the meter. The buffer amplifiers in the APC phase-detector circuits also shift the signal phases by  $90^\circ$  so that the phase-detector outputs may be used to maintain the two channels in phase for summing.

These APC phase-detected signals are spectrum-limited by the beacon or telemetry filters, which are automatically selected when a 15-db change of received-power level is sensed at the audio output after the satellite switches from the beacon to the telemetry transmitter. The filtered signals are then amplified and summed to provide an audio telemetry output. The dc amplifier outputs are also used to provide a dc signal to the voltage controlled oscillators for use in automatically tracking the carrier frequencies in both channels. The sweep control circuits, therefore, select either the dc-amplifier outputs or the sweep outputs for frequency control of the voltage-controlled oscillators.

The antenna system includes the UHF and VHF feeds, the parabolic reflector, the drive mechanism, the rotary joints, and the tracking system. The UHF feed system is comprised of waveguide and a waveguide feed, a lens, a lens drive motor, a radome and the reference generator. The horizontal and vertical RG-105/U aluminum waveguide lines are joined to a length of circular waveguide at the feed, which is supported such that its center is at the reflector focal point. A four-element ridged waveguide antenna is mounted within the circular waveguide. The elements are fed independently in pairs by coaxial lines from the horizontal and vertical waveguides to pro-

vide two linear orthogonal fields of the  $TE_{1,1}$  mode. The ridged-waveguide elements are arranged in space quadrature around the circumference of the drive shaft for the rotating lens, and each element is continuously tapered from the circular-waveguide surface at the input end to the shaft at the lens end. An isolation of better than 20 db is maintained between the two polarizations. Then lens, rotated by its drive motor to effect conical scanning at a 30-cps rate, is an artificially-loaded dielectric hemisphere whose dielectric constant is tapered across the waveguide aperture to provide the required phase shift for the transmitted and received signals. The reference generator is driven by the lens drive motor and supplies the phase reference signal for the automatic tracking loop. The VHF feed system is comprised of a crossed dipole antenna with a disk-type reflector. Since the UHF feed system is more critical, the VHF feed center is slightly displaced from the reflector focal point, thus defocussing the VHF antenna system. However, the resulting  $45^\circ$  phase error and  $\frac{1}{4}$ -db gain decrease are not large enough to affect significantly ground system operation.

A 28-foot parabolic reflector with an F/D ratio of approximately 0.4 is used. The reflector surface is perforated to reduce wind loading. Four steel spars support the feeds. The UHF signals between the antenna system and the radio equipment are propagated in a horizontal and a vertical waveguide with flexible sections used at the radio equipment junctions to allow for slight misalignments. Ridged waveguide sections provide the required transitions between waveguide and coaxial lines to allow coaxial rotary joints. Both the horizontal and vertical lines entering the antenna system go through two quadruple-rotary joints before reaching the feed. Coaxial lines are used throughout the VHF system which employs the other two channels of the azimuth and elevational rotary joints. Both the UHF and VHF systems have total transmission-line and rotary-joint losses of 1.5 db or better. The maximum VSWR presented to the radio equipment is 1.5.

An electromechanical servosystem (see Fig. 10) automatically points the high-gain, narrow-beam antenna system and tracks the satellite. The antenna is driven in azimuth and elevation by dc generators which control the servo drive motors. One prime mover is employed for both generators. The error signals, power amplified by the magnetic amplifiers, are derived from the combined agc voltage from the UHF receiving system. This AGC signal has a dc component which varies in amplitude with the received signal strength from the satellite and an amplitude-modulated ac signal resulting from the conical scanning of the antenna. The dc component is used to operate relays in both angle control loops to switch from the sector scan to the automatic tracking mode of operation when the signal level exceeds the threshold value. The ac signal goes through a low-pass filter to reduce 60-cps interference with the 30-cps AM signal. The filtered signal is then compared with the 30-cps reference generator signal and separated into azimuth and elevation error signals in the phase demodu-

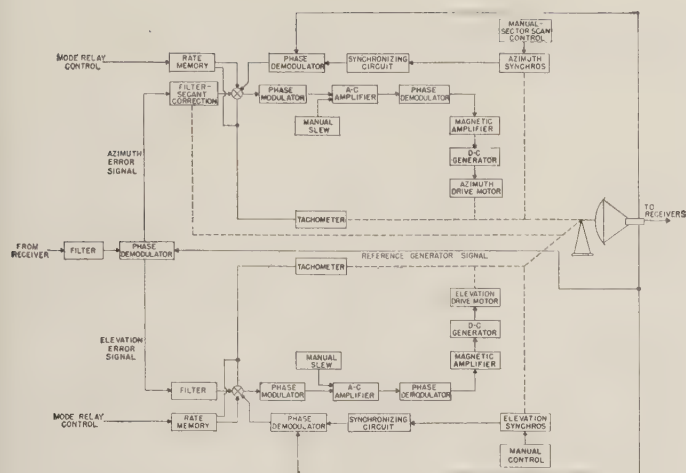


Fig. 10—Ground antenna servosystem, block diagram.

lator. The error signals are both filtered to remove 30-cps components and used as inputs for the servo control loops. A correction voltage proportional to the secant of the elevation angle is used to increase the azimuth-loop gain as the elevation is increased up to  $85^\circ$ , in order to compensate for the fact that a given angular error at high elevation angles is primarily azimuth error. Consequently, the azimuth servo response will lag if its loop gain is not increased. The  $85^\circ$  limit is set by practical limitations which preclude increasing the gain to infinity in accordance with the secant function.

The error signals are summed with tachometer feedback signals at the servo inputs. Rate-memory voltages are applied to the servo loops in lieu of the error signals, during automatic tracking, when the mode relay control is caused to operate by the falling of the dc-signal level below its threshold value. At that time, the rate memories cause the servo loops to drive the antenna at the angular rates at which it was operating prior to the reduction of received-signal level. During the manual mode of operation, the azimuth and elevation handwheels position two-speed synchro systems. The synchro voltages as selected in the synchronizing circuits are compared with the reference voltage in demodulators, whose output voltages are then used as error signals for the servo loops. The synchronizing circuits choose either the 36:1 or 1:1 speed synchro voltage depending on whether angular error is small or large, respec-

tively. An azimuth-sector scan mode is used after the antenna has been positioned manually, during the acquisition phase of operation. An azimuth sector of  $\pm 5^\circ$  can be scanned at a rate of  $30^\circ$  per second, and the position control error signals in the sector scan mode are derived from the synchro voltages as described above. When the dc component of the AGC signal exceeds its threshold value, the mode relay control causes the elevation channel to go immediately into automatic tracking mode. The azimuth channel, however, does not go into the automatic mode immediately because of its considerable inertia from sector scanning. The azimuth motion is decelerated at its maximum of  $12^\circ$ /second/second subsequent to the shorting to ground of the azimuth servo amplifier by the mode-relay control. When the rate, sensed by comparing the tachometer output with a reference voltage in a coincidence circuit, is  $\frac{1}{4}^\circ$  per second, the azimuth channel switches into the automatic tracking mode.

The dc error-signal sums are modulated and demodulated to allow using high-gain ac amplifiers. A lead-lag compensation network is used at the input to the magnetic amplifiers, and the resulting velocity constant for both channels is approximately  $30 \text{ second}^{-1}$ . Manual slew capability is provided in both channels by applying variable ac voltages to the ac amplifiers to drive the antenna at faster than normal tracking rates. Maximum tracking and slewing rates are both  $15^\circ$  per second.

#### CONCLUSION

Communication satellites, operating in the microwave region, possess the capability to handle reliably a large portion of the world's ever increasing communication requirements. Many systems are being designed in an attempt to harness this capability; employing delayed repeater, real-time repeater, and passive reflector techniques. This paper has given a broad view of an advanced delayed repeater satellite communication system concept.

#### ACKNOWLEDGMENT

The authors wish to acknowledge the assistance provided by other members of the engineering staffs of the U. S. Army Signal Research and Development Laboratory and by members of the engineering staffs of various industry companies that have made proposals, suggestions and presentations, or discussed the subject with the authors.



# Progressive Communication Satellite Systems Design\*

J. E. BARTOW†, D. L. JACOBY†, AND G. N. KRASSNER†

**Summary**—This paper describes the progressive design, on a phased basis, of a typical communication satellite system capable of meeting a variety of military and civilian applications. The system philosophy stresses reliability and flexibility of operation, with provision for both point-to-point and area coverage, to serve both fixed and mobile ground terminals, and to operate in either a military or nonmilitary environment. Considerations leading to choice of basic system parameters are presented. Major subsystems comprising the satellite payload are described and illustrated. The achievement of maximum reliability and long life is recognized as having the highest priority in satellite design and recommended approaches to the problem are indicated. The equipment required at a communication ground station is described as a function of the quantity and type of communications provided and the desired degree of mobility. Some typical configurations are described. Finally, some conclusions are presented regarding the merits of this type of system and its relation to the over-all space program and global communication requirements.

## INTRODUCTION

THE design of communication satellite systems is influenced to a large extent by the technology of the launching vehicles. The great cost of placing a satellite in orbit dictates the design of a long-life system so as to provide an equitable return on the investment. The limited payload of present boosters and the increase in payload capabilities in future years, with the development of powerful boosters such as the Saturn, permit a gradual transition from limited-capacity simple designs to high-capacity sophisticated designs.

Communication satellites will see wide application in both military and civilian systems. The ever expanding requirement for world-wide communication dictates the utilization of this medium for the transmission of teletype, voice, data, television, etc. Considering comparative costs of HF radio, ionospheric and tropospheric scatter, microwave radio relay, and submarine cable systems required to provide flexible and reliable long-range communication, the utilization of satellites for this purpose appears inevitable.

The following discussions will be limited to the 24-hour equatorial "synchronized" satellite systems. The design of these systems will be preceded by the development of lower-altitude communication satellite systems.

## SYSTEM CONCEPTS

A satellite located 22,300 statute miles above the equator, rotating in the direction of the earth's rotation, will maintain a fixed position with respect to the earth. In general, active control of the satellite by means of ground tracking and command control of jets mounted on the satellite will

be required to minimize the satellite drift over long periods. The 24-hour satellite is visible to about one third of the earth's surface. A satellite antenna with a beamwidth of  $20^\circ$  will illuminate this entire area. Three or four such satellites equally spaced can illuminate all the earth except a small part of the polar regions, although equally spaced satellites may not be the most practical for operational considerations.

Because of the great cost of launching, it is desirable that one satellite serve many ground stations. Fig. 1 shows a possible location of three satellites and the area of coverage of each. The satellite located at  $100^\circ$  west longitude will cover both North and South America. An alternate system comprising two satellites at  $40^\circ$  and  $170^\circ$  west longitude also is depicted in Fig. 1, covering the continents bordering the Atlantic and Pacific areas, respectively. A more advanced system will consist of many satellites in the 24-hour circular equatorial orbit, probably unequally spaced in orbit to provide greater communication capability for those areas of the world anticipating a greater traffic handling requirement.

Each station within one area could transmit to any other within the same area by means of a satellite repeater. In order to transmit to stations in either of the other two areas, inter-area repeaters are required. The inter-area repeaters receive signals from one satellite and transmit them to another. In this way, all stations within the three areas have the ability to communicate with all others.

It has been indicated previously that the 1000-to-10,000-mc range appears most promising for space communication.<sup>1</sup> In this range, wide transmission bandwidths are available. The useful bandwidth of early systems will be limited, however, by the available power output of the satellite. An increase in power output is accompanied by both an increase in amplifier weight and an increase in primary power requirements, which again increases weight. The capacity of early systems, therefore, will be limited by the performance (carrier-to-noise ratio) of the satellite-to-ground path.

Since the satellite must receive and transmit signals from many ground stations, the question arises as to whether many narrow-bandwidth channels or one wide-band channel should be employed. The advantage of the many narrow channels is that the output stages can be operated at relatively high efficiency (assuming FM transmissions) while the single wide-band channel must have sufficient linearity to pass all signals without mutual interference. In addition, if one of the narrow-bandwidth chan-

\* Manuscript received by the PGML, February 1, 1960.

† U. S. Army Signal Res. and Dev. Lab., Fort Monmouth, N. J.

<sup>1</sup> J. E. Bartow, G. N. Krassner and R. C. Rihs, "Design considerations for space communication," 1959 IRE NATIONAL CONVENTION RECORD, pt. 8, pp. 154-167.



Fig. 1—Areas of coverage of three 24-hour satellites.

nels were to fail, the remaining channels would still provide useful, if reduced, service. Failure of the single wide-band channel would be catastrophic, unless redundant components were available.

The satellite will receive, translate in frequency and re-transmit each signal. The satellite transmission frequencies are chosen to be different than the receive frequencies to avoid severe transmitter-to-receiver isolation requirements. No modulation detection is provided in the satellite since it would neither improve performance nor simplify circuitry. The low-level satellite stages will have low amplitude as well as low phase distortion. The output amplifier will, however, be operated at maximum efficiency in order to minimize the input power requirements. Therefore, FM modulation will be used. The basic information may be in the form of frequency division multiplex, pulse code time division multiplex, or binary data signals.

Early systems must be designed with minimum payload weights and primary power requirements. By adding "building blocks" to these systems, increased capacity and reliability can be obtained. The parameters for the first system described are given in Table I.

TABLE I

Satellite	
Bandwidth	1 mc per channel
Number of channels	10
Power output per channel	1 watt
Frequency range	1700–2400 mc
Antenna gain	18 db
Antenna diameter	20 inches
Stabilization	
Attitude	$\pm 2^\circ$
Position	$\pm 2^\circ$
Primary power	300 watts
Total payload	1000 pounds
Ground Station	
Bandwidth	1 mc
Power output	1 kw
Antenna gain	43 db
Antenna diameter	28 feet
Receiver noise temperature	100°K
Carrier-to-noise ratio	22 db



Ten 1-mc satellite channels will provide five full duplex circuits. Each ground station can employ a 12-voice channel PCM multiplex equipment or FDM equipment with an increased number of channels.

If each ground station is equipped to receive the transmissions from all other stations, an alternate mode of operation is possible. Individual voice channels destined for various stations then could be multiplexed and transmitted over one RF channel. For instance, at station A, three channels could be assigned for transmission to station B, two to station C, and one channel each to stations D through J, as shown in Fig. 2. In addition, these channels can be re-assigned at any time. If desired, the voice channels can be unassigned and either manually or automatically switched upon demand. In this mode of operation, both the send and receive channels must be cleared before the conversation can begin.

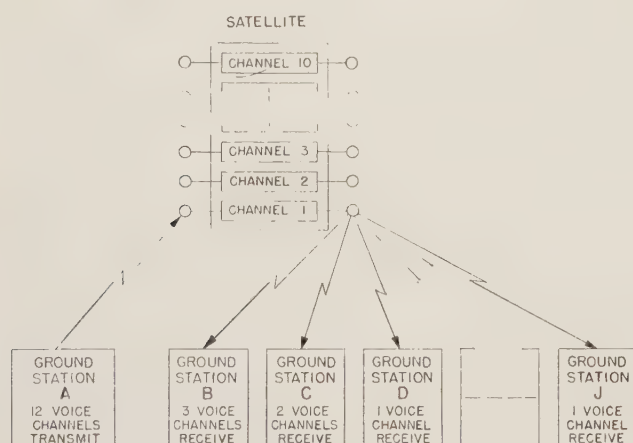


Fig. 2—Voice channel allocation.

As launching capabilities increase and stabilization techniques improve, we may consider more advanced systems. With greatly increased payloads, communication satellite systems can be designed to transmit wide-band signals between many stations throughout the world. The number of RF channels in the satellite may be increased to 20, 30 or perhaps 50. However, the number of users is less likely to increase this greatly than is the requirement for increased capacity for each user. Therefore, the individual RF channel bandwidths must be increased and the satellite power output and/or antenna gain increased to maintain an adequate carrier-to-noise ratio. Increasing the antenna gain would reduce the area of coverage and require a multiple antenna system to cover all stations. The complexity of this scheme must be evaluated in relation to the alternate choice of increasing the satellite power output.

The use of high-gain (35-db) satellite antennas and 5-watt power output is chosen in the more advanced system. Inflatable paraboloidal antennas appear most promising since they can be stored in a small volume during launch and expanded after the proper orbit is attained. These antennas must maintain the correct orientation towards the ground stations. Either very accurate satellite attitude and

position control or antenna tracking circuits must be provided in the satellite since the antenna beams may be narrow (one degree or less). Fig. 3 shows the diameter of the area of illumination of the earth's surface as a function of the beamwidth of the antenna.

In order to transmit signals from a part of the earth visible to one satellite to a part visible to another, satellite-to-satellite relay may be employed. The use of high gain antennas is required to overcome the increased free space loss (path length 45,600 statute miles for satellites spaced  $120^\circ$  apart) and greater receiver noise of this path compared with the satellite-to-ground path.

The following parameters, given in Table II, describe a communication satellite system capable of transmitting television or other wide-bandwidth signals among many points throughout the world.

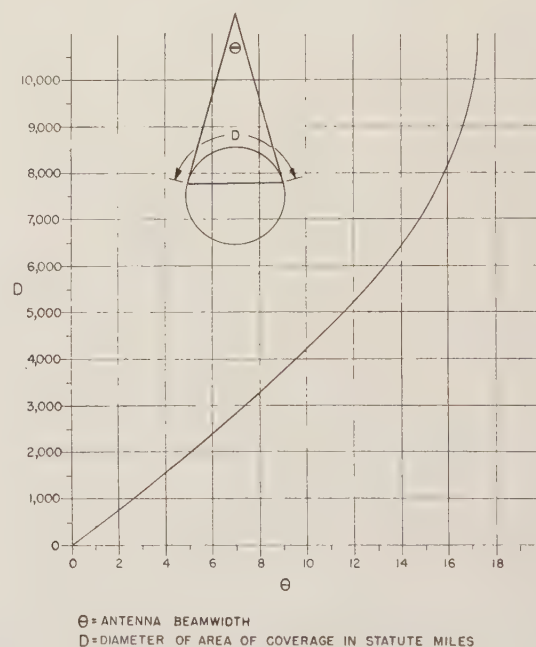


Fig. 3.

TABLE II

Satellite	
Bandwidth	100 mc per channel
Number of channels	6
Power output per channel	5 watts
Frequency range	4400-5000 mc
Antenna gain	35 db
Antenna diameter	5 feet
Antenna beamwidth	$2.8^\circ$
Stabilization	
Attitude	$\pm 0.5^\circ$
Position	$\pm 0.5^\circ$
Primary power	1000 watts
Total payload	3000 pounds
Ground Station	
Bandwidth	100 mc
Power output	10 kw
Antenna gain	56 db
Antenna diameter	60 feet
Receiver noise temperature	$100^\circ\text{K}$
Carrier-to-noise ratio	24 db

## SATELLITE PAYLOAD DESIGN

The design of the spaceborne communications payload should stress long-term reliability, economy of size, weight and power drain which, of course, implies maximum use of transistors. The volume and weight saved by the use of transistors may be used to gain greater over-all reliability by employing redundancy of those components with a short mean-time-to-failure.

An initial ten-channel system is postulated using the parameters listed in Table I.

The satellite also will provide a means for relaying command, attitude, position and reliability (component switching) data, and for transmitting various telemetry data to the ground sites. Progressive design of the system would include intersatellite transmissions, higher microwave frequencies, greater information capacity (bandwidth), steerable satellite antennas, and more accurate position and attitude stabilization.

The weight distribution for two typical systems is tabulated in Table III below. System *A* is a 1000-pound package; System *B* weighs 3000 pounds. The systems include a solar energy conversion system plus chemical storage batteries to provide continuous power of 300 watts and 1000 watts, respectively.

TABLE III  
WEIGHT DISTRIBUTION

	System <i>A</i>	System <i>B</i>
Communications Electronic Equipment (including telemetry, beacons, command)	250	1100
Antenna System (including supports, drives)	30	350
Power Supply (solar deck, batteries, structure)	250	500
Guidance and Control (attitude and position)	200	450
Shell and Structure	200	400
Unassigned and Safety Factor	70	200
Total	1000 pounds	3000 pounds

These weights do not include the aerodynamic shroud, thermal canopy, and supporting interface structure. If the injection guidance and control system and the final stage are not separated, this represents additional, but not useful, weight in orbit.

In the initial design, a multiple narrow-channel system is employed for maximum reliability. Failure of a component in any repeater chain, therefore, does not cause total satellite failure. Microwave triodes, such as the ruggedized 2C39B, have proven long-term reliability, particularly under de-rated operating conditions. One watt output per tube is a conservative design at fixed frequency; some fifteen watts have been obtained at 2000 mc. Each signal (channel) is amplified in an individual IF amplifier. The output power of one watt per RF signal is applied to a common antenna and radiated to the ground stations. A twenty-inch diameter parabolic antenna, with a beamwidth of approximately 20° and a gain of 18 db over an iso-

tropic radiator, is proposed for maximum coverage and simplicity. The microwave antenna is fixed to the satellite body and depends on the satellite stabilization equipment for proper orientation. A VHF whip or turnstile array with reflector is used for the telemetry system.

As payload capabilities increase, satellite stabilization and position control will become more refined, and parallel advances will be made in the state-of-the-art of electronic components and devices. The design of a highly linear satellite repeater will allow the simultaneous transmission of several signals through each repeater.

Flexible design is desirable so that the system may be employed efficiently as either a high-performance (high carrier-to-noise ratio) system or a high-capacity system. Since civilian and military requirements for voice channels, data transmission and television vary greatly with geographical location, a "building block" system design is recommended. It would be possible, therefore, to achieve higher capacity, more ground stations, and longer life by redundant use of subsystems.

The later design of a satellite communication system will make extensive use of TWT's as wide-band low noise receiving devices, power amplifiers, and as synchrodrines, wherein frequency translation and amplification occur in one device. Since payload weight is at a premium, the perfection of depressed collector techniques will produce higher-efficiency TWT's, thereby reducing power supply requirements correspondingly.

The preamplifier stage primarily determines the sensitivity of the satellite repeater. Therefore, it must have a low noise figure, wide bandwidth, and sufficient gain to override the noise of the next stage. The RF amplifier stage requires high gain and wide bandwidth. The requirements of both stages can be satisfied with a TWT. A ferrite isolator between the first and second stage will prevent oscillation due to the reverse gain characteristics of the TWT. Mu-metal shields or equivalent are required to prevent interaction of the magnetic fields. Use of TWT's with their inherently high gain permit omitting conversion to intermediate frequency. Frequency translation allows for ease of transmission without desensitization or regeneration in the associated receivers, *i.e.*, to avoid excessive gain at one frequency. A technique such as the synchrodyne, where the mixing and amplifying function are combined, is proposed. The local oscillator signal voltage is applied between the cavity-coupled cathode and helix of the TWT causing phase modulation of the incoming signal. The signal is amplified as it passes through the helix. A typical gain for this stage is 35 to 40 db.

Separate highly-stable transistorized oscillator-frequency multipliers will be used for each repeater to provide additional reliability and reduce filtering requirements.

In order to maintain system linearity, the excess gain will be compensated for by use of AGC circuits or fixed attenuators inserted by ground command. The output of each final power amplifier will be fed through a combiner-filter to a duplexer to the antenna. This combiner-filter,



possibly stripline to minimize size and weight, will match the PA and the microwave beacon to the duplexer, and filter out the sidebands produced by overloading or harmonics incurred in the final amplification.

An initial system will not include a ground-to-satellite command link except for control of impulse nozzles for stabilization. Such a link will be required as the system design progresses; and, as the complexity and functions required of the satellite repeater increase, the number of commands needed for proper operation will increase. These will include switching of antenna mode (scan, track, etc.) or of operational mode (point-to-point or "broadcast" transmission), switching of redundant components, and position and orbit correcting commands. The use of transistor logic circuitry rather than conventional relays may increase over-all reliability. One must consider also the alternative of performing these switching functions in the satellite on a command basis rather than relying upon automatic circuitry in the payload, at least in early systems.

For maximum reliability, the command control receiver will be entirely transistorized except, perhaps, for the first local oscillator frequency multiplier string. Later systems might employ diodes or transistor frequency multipliers to further increase reliability.

Considering now the design of the telemetry equipment, the initial system will use a PAM-FM-FM type transistorized VHF telemetry system, which can accommodate a high channel capacity without excessive bandwidth, transmitter power, weight and size. Later systems will employ PCM telemetry for its greater signal-to-noise capability. Some 75 data channels is typical of early requirements and perhaps double that figure for the next phase. The telemetry would be used both to monitor equipment performance and to send command acknowledgements. Parameters to be measured include internal and external (skin) temperatures, micrometeorite hits, radiation intensity, power supply levels, solar cell operation, received and transmitted levels, critical circuit and component parameters, and satellite stabilization information. For command acknowledgement, a typical reply consists of a 9-bit binary digital signal, 2 bits for synchronization and 7 for the reply (128 replies possible). Slow commutation rates, 5 cps or less, are adequate for slowly varying information functions.

It appears advantageous to include in the design of the system a UHF or SHF low-power CW beacon to permit acquisition and tracking, as required, by the ground site. The VHF telemetering signal is unsatisfactory for this function because of the broad beamwidth of the ground VHF antenna. Later systems employing intersatellite antennas also will use beacon receivers to control antenna orientation.

A high-efficiency transistorized dc/dc converter will be used to convert the low battery dc voltages to the proper

plate and screen voltages for the tubes. These converters, which have better than 85 per cent efficiency, are basically transistorized relaxation oscillators with excellent reliability and no moving parts. Later designs will have conversion efficiencies of 90 per cent or even better.

In the near future, for primary power requirements up to one kilowatt, solar conversion systems are generally the most satisfactory power supply. Solar cell platforms will be controlled and programmed to face the sun continually. The present 10 per cent group efficiency of solar cells may increase to 15 per cent in several years. Perhaps a greater potential weight saving is possible by eliminating the silicon cell covers and their attendant 20 per cent reduction of incoming solar energy. Progress in system design will include spectral coatings to improve temperature characteristics of the solar cells, which suffer a power loss of 0.35 per cent per °C above 25°C. Optical coatings will be developed to spectrally filter (reflect) the portions of the spectrum not utilized by the solar cell, and will reduce its equilibrium temperature and increase emissivity of the active surface. Thin film coatings will also serve as protection against erosion by micrometeorite dust.

Assuming that continuous operation of the communication system is mandatory, a power storage supply is required for the time during which the earth shadows the satellite from the sun. Initial systems will use sealed nickel cadmium storage cells to supply peak power to the system. These cells will be recharged by the solar supply during sunlight periods. For future systems of 2000 watts or more a solar (fuel cell) regenerative system of the  $H_2$ - $O_2$  or metal hydride type could result in considerable weight savings over a solar cell-nickel cadmium supply.

In order to maintain satisfactory system performance (at least a 20-db carrier-to-noise) of higher-capacity systems, high-gain steerable satellite antennas must be used, and continuously oriented toward the ground stations, including mobile ground stations such as aircraft and ships. Perhaps the 20°-beamwidth antenna previously used will be retained for broadcast coverage or emergency use.

Initially, antenna steering will be by mechanical means to provide the satellite with a tracking capability. Electronic steering has attractive future potential, however, to serve many users at random orientation to the satellite, and to simplify the vehicle stabilization. The weight of this type of system is much less than several large reflectors. Electronically steered antennas have the wide slew angle, high gain qualities desirable for use with mobile receiving and transmitting stations, and the lack of moving parts avoids interference with the stabilization design. An inflatable Luneberg lens with multiple feeds is another possible antenna design. Size and weight of such a device are prohibitive at the present time, however.

The vehicle stabilization system represents a major design area. The satellite position (range, elevation and azimuth) can be determined from the ground stations and

position-correction signals transmitted from the ground to the satellite's command receiver. These commands are translated by a control computer to actuate specific pairs of impulse nozzles to maintain the correct position. There are many methods to sense the satellite attitude, including a Polaris star tracker, a sun-seeking photo cell, an inertial platform, an infrared horizon scanner, a radio interferometer receiver, and satellite antenna position sensors. Attitude may be determined primarily by the use of two body-fixed sensors, an infrared horizon seeker providing a reference perpendicular to north, and a Polaris star seeker, compensated for its apparent motion,  $1^\circ$  from true north. Steps must be taken to insure that the horizon seeker does not follow the sun when it appears behind the earth at and near the equinoxes. The same nozzle system would be used for both attitude and vernier position control. An auxiliary inertial spherical flywheel will compensate for motion of the antennas and solar deck.

In more advanced systems, the satellite attitude stabilization will be refined to a sufficient degree that the frequency can be raised from 5 to 10 kmc or higher, and the rigid satellite antenna increased at least fourfold in diameter to an inflatable type 20 feet in diameter, and possibly with multiple antenna feeds. In addition, the position control system will be so precise that fixed orientated ground reflectors may be used.

Fig. 4 illustrates a functional diagram of a typical integrated satellite payload.

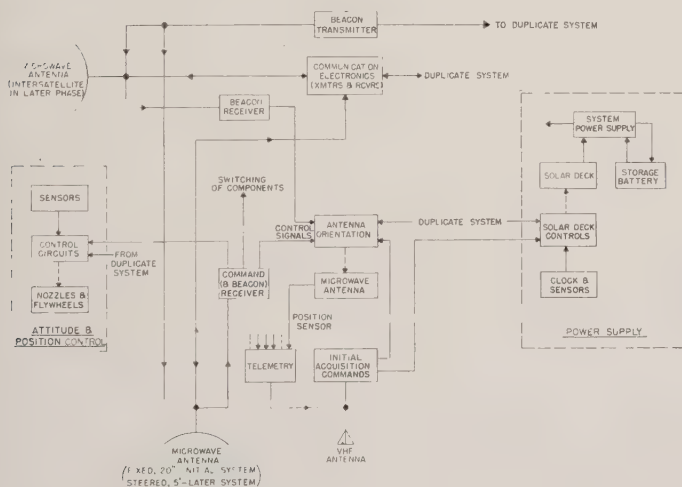


Fig. 4—Satellite payload functional diagram.

The design of the satellite structure is affected by stringent and often conflicting requirements. The structure must be compatible with thermal design, launch and orbital environment, and stabilization requirements. The design must accommodate the communications electronics, guidance and control equipment, and must support sun-oriented solar cell decks and large highly-directional antenna systems with a maximum strength-to-weight ratio. Finally,

the complete package must be mounted in the satellite shell in a manner which allows simple separation from the last stage of the vehicle. These design characteristics must be considered both individually and then as an integrated design group, to achieve an optimum working system.

Packaging considerations must take into account the effects of the environment both during launch and in orbit, for the complete satellite. Microwave reflectors and large solar decks should be retracted into the shell container during launch and ascent. In early systems, ambient temperature ranges in orbit of  $0$  to  $50^\circ\text{C}$  may be expected. Passive coatings with proper absorptivity to emissivity ratio and active thermostatic controls will limit temperature variations of more sophisticated satellites to perhaps  $20^\circ$ – $30^\circ\text{C}$ , greatly simplifying the problems related to temperature-sensitive components and devices, as described below.

A typical over-all packaging for the "second generation" satellite will include a sun-oriented (except for a possible  $\pm 23^\circ$  inclination to the ecliptic plane) solar deck which rotates with respect to the main satellite body. The satellite body rotates once about its axis for each rotation about the earth so that one side always faces the earth. Several microwave antennas, mounted on extensions and adjustable in orientation will automatically "search and lock on."

During the brief period between separation of the final stage and the activation of the solar deck and microwave antennas, a transistorized VHF receiver will serve as the interim command receiver.

The satellite will be in full sunlight most of the time. There will be two periods per year when eclipses will occur. These periods are each of 44 days duration. The time spent in the shadow is important both to the power supply design (solar energy converters) and to the thermal design of the satellite. The maximum time in the earth's shadow is 67 minutes.

The thermal design must compensate for transient cooling when passing through the shadow, as well as the high skin temperature due to incident radiation when in the sunlight. As system design progresses, special coatings will be used to reflect the nonusable solar energy. The surface materials of the parabolic reflector must be carefully selected and distortion due to thermal gradients minimized, particularly as the dimensional tolerances decrease. Later systems, as we have noted, tend towards higher RF frequencies, shorter wavelengths, and therefore tighter dimensional stability limits, making this problem more acute. These systems may very likely use active thermostatic temperature control systems at some sacrifice of over-all system complexity.

Manufacturing techniques, shipping and handling, storage, etc., influence reliability but are not amenable to quantitative evaluation. For this reason and because of the inconclusive life data, it is difficult to calculate precise reliability factors.



In keeping with progressive design philosophy, later systems would be expected to operate for longer lifetimes with greater reliability in order to be economically worthwhile. Tube aging for a period of several months will stabilize tube characteristics and eliminate those tubes subject to premature failure. Exhaustive inspection and testing during development and fabrication are mandatory, of course. Operation at reduced filament voltage and plate dissipation power will result in increased life expectancy.

The use of redundancy to extend operating life must be balanced against the cost of added weight and volume, and the possible failure of sensing and switching circuits. The more sophisticated design of the future will provide detection and automatic switching of redundant spares within the satellite. However, nothing can replace fail-safe methods and conservative design which employs de-rated components.

The application of redundant components, the use of more fully proven components and techniques, and the experience gained in earlier systems should increase satellite operational life expectancy from an initial  $\frac{1}{2}$ -1 year to 2 years or more.

Many component improvements will affect the progressive system design. Crystals will have greater stability at higher frequencies, using overtone crystal units. Crystal oven power consumption will be reduced to milliwatts by reducing thermal losses. Long-term developments may produce solar energy converters with superior high-temperature performance and compound semiconductor types with 30 per cent efficiency. Higher power requirements suggest the use of regenerative fuel cells and nuclear power sup-

Economic considerations dictate that ground stations will be located near major communication centers so that they will have an operational capability at the conclusion of research and development and engineering evaluation phases. For similar reasons, during the early phase, major equipment parameters will be selected where feasible to satisfy the requirements of more advanced operational type systems as well. For example, large tracking antennas will require higher power, lower noise, and wider bandwidth than may be indicated as initial system goals.

Because of the inherently high cost of a communication satellite system, it is imperative that the system satisfy the greatest number of potential customers. These include both military and commercial users, and both fixed and mobile type installations. While the great majority of stations will undoubtedly be landbased, one cannot overlook the possibility that shipborne or airborne stations will require access to the system. There will be large variations also in the types and volume of communications required at individual stations. All these factors dictate a flexible approach to the planning of communication satellite stations.

Table IV lists some equipment parameters and communication capacities which appear technically feasible for the various types of service under consideration. Mobility is, of course, a relative term but as used here implies the ability of a complete station to be transferred and made operational at a new location in the order of 24 hours. Mobility can only be provided at a sacrifice in power output, antenna gain and noise figure and consequent reduction in communication capacity as compared to a fixed installation.

TABLE IV  
EQUIPMENT PARAMETERS

Type of Service	Power	Antenna Gain	Receiver Bandwidth	Receiver Noise Temperature	Capacity	
					Commercial	Military
Fixed	10 kw	56 db	100 mc	100°K	1000 voice plus TV	100 voice or TV
Mobile	1 kw	44 db	10 mc	300°K	100 voice	10 voice
Airborne	1 kw	20 db	10 kc	300°K	1 voice	

plies. The application of higher-frequency, higher-power output transistors is obvious. New cathode materials and cathode processing techniques will increase tube life. Open tube structures are a possibility.

#### GROUND STATION CONSIDERATIONS

The previous discussion has indicated that during the next 5 to 10 years communication satellites can be developed of steadily increasing size and capacity to match increasing capabilities of launching vehicles. This has led to the philosophy of a progressive system design. In keeping with this approach, the ground stations must be designed with a high degree of flexibility and growth potential in order to minimize obsolescence.

Military systems inherently must provide a higher degree of security, reliability and freedom from interference than their commercial counterpart. It has been assumed in Table IV that these more severe requirements can be met if the capacity of the system is reduced by a factor of 10.

Despite the apparent diversity of requirements, there is no need to develop completely different equipments for each type of service. Rather, the building block approach, as shown in Table V, will be applied, resulting in maximum use of common equipment. The actual building blocks employed at a given location will, of course, be a function of the amount of communication to be provided as well as the type of service.

TABLE V  
EQUIPMENT BUILDING BLOCKS

	Commercial			Military	
	Fixed	Mobile	Airborne	Fixed	Mobile
Antennas					
60-foot Fixed	x			x	
14-foot Mobile		x			x
1-foot Airborne			x		
Transmitters					
10 kw PA	x			x	
1 kw PA		x	x		x
Exciter	x	x	x	x	x
Receivers					
Maser	x			x	
Parametric		x	x		x
Basic	x	x	x	x	x
Terminal Equipment					
Multiplex	x	x		x	x
Military Applique				x	x
TV	x			x	
Telephone			x		

In addition to providing communications, the ground station will serve other important functions. Being equipped with an accurate tracking antenna, it will provide continuous angular tracking data of the satellite. These data, together with similar data from other stations, provide a fix on the satellite position. With the aid of a computer, deviations from the desired 24-hour orbit can be readily determined as well as the timing and direction of corrective thrusts to be applied to the satellite. Orbit correcting is initiated by coded commands transmitted from the ground station to the satellite.

The communication ground station also will be furnished with equipment for receiving, recording, and ana-

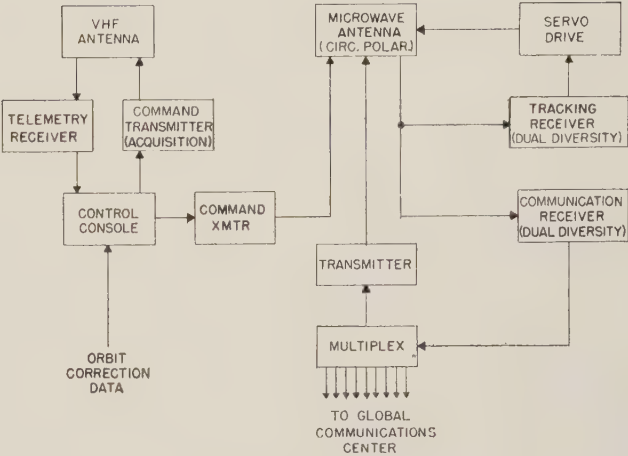


Fig. 5—Ground station functional diagram.

lyzing telemetering data from the satellites and, through the command system, provide for control of the satellite communication equipment and power supply. Fig. 5 is a function diagram of a typical ground station.

CONCLUSION

The communication satellite systems discussed appear to be attainable in the not too distant future. The realization of these systems is dependent on the development of more advanced missile technology and highly reliable electronic components. Early evaluation of a limited capacity system will be followed by higher-capacity more advanced systems suitable for operational use employing satellites launched by powerful boosters such as the Saturn. Timely consideration of the actual military and commercial requirements will result in an effective development program and an optimum system design.



# USASRDL Upper-Air Research with Rockets\*

H. J. AUFM KAMPE† AND J. R. WALSH†

**Summary**—The evolution of the velocity-of-sound rocket experiment to measure temperatures, wind speed and direction, and densities at elevations 30 to 80 kilometers is described. Rocket soundings of the atmosphere were made at three locations: White Sands Missile Range, New Mexico; Fort Churchill, Canada; and Guam. Results from White Sands and Fort Churchill are presented.

Miniaturization of the equipment and changes in techniques resulted in an all-weather capability which is enabling meteorological agencies to formulate plans to carry out synoptic meteorological and other interesting investigations, using for the first time in the history of meteorology the rocket as a routine instrument carrier.

The tracking of X or S band by radars to determine high-elevation winds is described briefly.

## EVOLUTION OF USASRDL ROCKET RESEARCH PROGRAM

WITH the advent of rockets as a tactical weapon in modern warfare, scientists engaged in the development of guided missiles were curious to know the state of the atmosphere above 100,000 feet. Little or no data were available to indicate the temperature and density structure of the atmosphere, the pressure variations, the composition, and the wind speed and direction.

In 1945, at the close of World War II, the Army, Navy, and Air Force initiated an extensive program to investigate the properties of the upper atmosphere. A test area located at White Sands Proving Ground, near Las Cruces, New Mexico, was activated, and plans were made to launch captured V-2 rockets and smaller American-made rockets. A panel of engineers and scientists was formed to provide a common ground for the discussion of results and future plans. This group was later known as the Upper Atmosphere Rocket Research Panel. The Signal Corps, through the U. S. Army Signal Research and Development Laboratory (USASRDL), which is responsible for developing meteorological equipment for the Army, entered this new field of endeavor and assigned personnel to investigate upper-air parameters such as wind velocity, composition, pressure, and temperature. Instruments with a high rate of response and capable of withstanding the vibrations and accelerations of a rocket in flight had to be developed. Furthermore, a research and development program, sponsored by USASRDL, was started at the University of Michigan, Ann Arbor, in June, 1946. This program undertook the development of instruments which would be flown in the V-2's and the smaller American-made Aerobees.

## EARLY EXPERIMENTS

### WAC Corporal

The Jet Propulsion Laboratory (JPL), California Institute of Technology, was engaged in 1945 in the development of the WAC Corporal—a small, American-made rocket with a ceiling of some 150,000 feet. USASRDL had the opportunity to participate in these early experiments, and efforts were made to measure atmospheric parameters (temperature, pressure, wind speed and direction) by ejecting equipments from the rocket at apogee. Preparations were rushed, the experiments were crude, and as a result little or no data were obtained. However, much experience and “know how” were gained which were applied in the experiments which followed.

### Methods to Measure Pressure, Density, and Temperature

The University of Michigan, through a research contract sponsored by USASRDL, developed four methods to measure pressure, density, and temperature. In one method the pressures at the tip and at four points on the side of the nose cone were measured. From these the Mach number may be calculated by a theory due to Taylor and Maccoll (1933) and Stone (1948). By measuring the Mach number and the velocity of the rocket, the velocity of sound and ambient temperature may be directly calculated. In the second method, the angle of the shock wave formed by a wedge at the front of the rocket was to have been measured by taking shadowgraph pictures with an optical apparatus. The Mach number is a function of the shock-wave angle. In the third method, the angle of a shock wave formed by a cone was measured by an array of moving probes containing pressure gages, the gages giving signals on passing through the shock wave.

With the first three methods used in five flights in which the missile performance was satisfactory, temperature measurements of useful precision were obtained with one method, the moving probes. An analysis of the difficulties encountered showed that equipment complexity was a major cause of failure, and errors in measuring the angle of attack and velocity of the missile were larger than anticipated.

In the fourth method,<sup>1</sup> a four-foot-in-diameter sphere, when inflated, was dropped from rockets on three flights at White Sands Missile Range. The velocity and acceleration trajectories were measured by Doppler radar and the

\* Manuscript received by the PG MIL, February 1, 1960.

† U. S. Army Signal Res. and Dev. Lab., Fort Monmouth, N. J.

<sup>1</sup> F. L. Bartman, “Falling sphere method for upper air density and temperature,” *J. Atmos. Terr. Phys.*, Special Suppl., vol. 1, pp. 98-107; 1954.

ambient air density was calculated from the drag equation and the ambient temperature from the hydrostatic equation and the equation of state of a perfect gas. All of the flights were only partially successful.

### *Diffusive Separation in the Upper Atmosphere*

The University of Michigan developed an experimental technique of collecting samples of the upper atmosphere in steel bottles carried aloft in rockets.<sup>2</sup> The samples collected were analyzed primarily for helium, neon, argon, and nitrogen. Samples to 100 km were obtained. The analyses of the samples showed no separation to 60 km; in samples taken above 60 km, separation increasing with the mass difference and with altitude was detected. However, small amounts of separation detected in ground air-control bottles associated with these latter samples threw some doubt on the results. Therefore the experiment was repeated with the result that diffusive separation seem to begin between 60 and 90 km.

### *The Rocket-Grenade Experiment*

Parallel with the efforts progressing at the University of Michigan, USASRD scientists developed another method capable of measuring temperature and wind simultaneously. Earlier efforts to measure the wind speed and direction at high altitudes were based on the optical tracking of visible man-made trails of talc or chemical smoke ejected from a rocket in flight. The high rate of diffusion of the trails quickly resulted in a lack of contrast between the trail and its surroundings, which caused the experiment to be impractical. With the new method, temperature and wind were determined from acoustical propagation measurements using grenades ejected from an Aerobee rocket as sources of sound. Either 7 or 9 grenades were ejected and exploded at regular intervals as the missile traveled the upward leg of a nearly vertical trajectory. The times of the explosions and their positions in space were accurately determined. The times of arrival at the ground of the sound waves from the grenades were measured by means of a sound-ranging array which lay almost directly below the exploding grenades. These times allowed the calculation of the elevation and azimuth angles of arrival of the sound waves. Because the grenade flashes must be photographed against the star field by the ballistic cameras, all firings were made at night.<sup>3,4</sup>

In principle, the velocity of sound in the layer defined by

two grenades, and thus the temperature, may be found by dividing the thickness of the layer by the time the sound wave spends in the layer. In practice, however, the problem is severely complicated by the facts (1) that one must deal with a three-dimensional problem and (2) that the atmospheric winds are also effective in propagating a sound wave. The basic equations are

$$C = kT^{1/2},$$

$$V = C + W,$$

where  $C$  is the velocity of sound caused by the elastic properties of the medium,  $k$  is a constant of the medium,  $T$  is the absolute temperature,  $V$  is the velocity of propagation of the sound wave, and  $W$  is the velocity of the wind. The method can be applied to altitudes to which the composition of the atmosphere stays constant and the wavelength of sound waves is large compared to the mean free path length of the molecules. Another limit of the experiment is established by the fact that the attenuation of the sound about 90 km is beginning to become prohibitively large.

The results of 12 firings at White Sands Missile Range are plotted in Figs. 1 and 2. Fig. 2 illustrates the clear-cut seasonal effects and the presence of maximum wind speeds between 50- and 60-km altitude.

### AEROBEE FIRINGS AT FORT CHURCHILL, CANADA

Although these data obtained at White Sands Missile Range probably give a fairly complete picture of the temperature and wind structures in the region between 30 and 80 km at a specific latitude (32° north), it was felt that the lack of similar data at other, especially higher, latitudes precluded any reasonable attempt to create a model of the general circulation in the atmosphere. In addition to the lack of data, there seemed to be the possibility that 32° north is more or less a nodal point in the seasonal variations at high altitudes because of the fact that there was no observed seasonal variation in the temperature, but there was a strong seasonal variation in the wind. Therefore it was decided to carry out more firings at a higher latitude.

The International Geophysical Year (IGY) offered a very good opportunity for accomplishing this at Fort Churchill, Canada. However, in carrying out the rocket-grenade experiment in Canada, a problem arose which did not exist at White Sands Missile Range; this had to do with the widely different cloud-cover conditions at the two places. Up to that time the rocket-grenade experiment was a clear-weather, nighttime experiment and was designed as such, as the use of ballistic cameras for the grenade burst locations indicates. This method of determining the grenade-burst locations had to be abandoned if one wanted to adopt this very powerful method for determining simultaneously wind and temperatures up to 90 km at any other location than those situated in the subtropical high-pressure belt, particularly if firings were to be carried out at predetermined times. The solution to this problem was found by

<sup>2</sup> "Diffusive Separation in the Upper Atmosphere," University of Michigan, Ann Arbor, Engrg. Res. Inst. Rept., presented at the Oxford Conference on Upper Atmospheric Rocket Exploration, Eng.; August, 1953.

<sup>3</sup> M. Ference, W. G. Stroud, J. R. Walsh, and A. G. Weisner, "Measurement of temperatures at elevations of 30 to 80 kilometers by the rocket-grenade experiment," *J. Meteorology*, vol. 13, pp. 5-12; 1956.

<sup>4</sup> W. G. Stroud, W. Nordberg, and J. R. Walsh, "Atmospheric temperatures and winds between 30 and 80 km," *J. Geophys. Res.*, vol. 61, pp. 45-56; March, 1956.



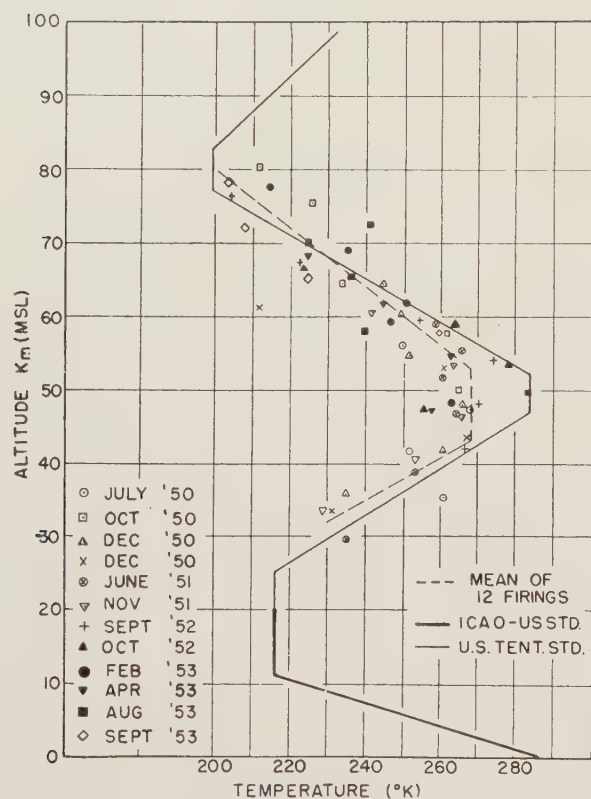


Fig. 1—Temperature in upper atmosphere measured by the rocket-grenade experiment at White Sands Missile Range, N. M. (the dashed curve is the mean curve through the data, while the solid curve is the most recent standard atmosphere).<sup>5</sup>

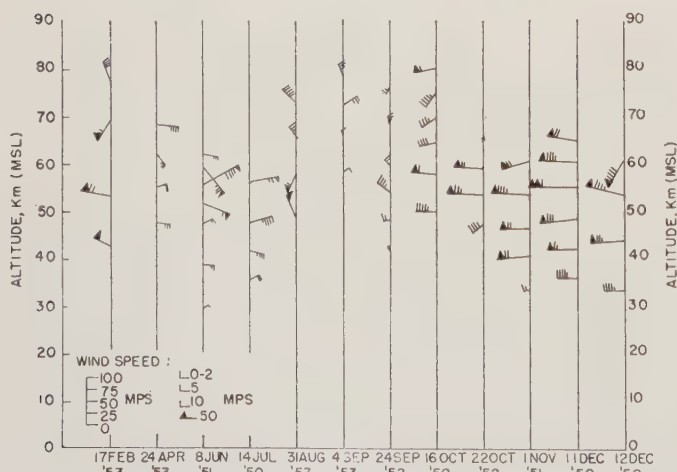


Fig. 2—Winds in the upper atmosphere measured by the rocket-grenade experiment at White Sands Missile Range, N. M. The wind speed is demonstrated by both the number of flags and by the length of the flagpole, as pointed out in the figure. If the end carrying the flags points upwards, the wind is from the north; if it points to the left, the wind is from the west.

using the DOVAP system for determining the location of the rocket.<sup>5</sup>

The DOVAP system is a continuous wave Doppler tracking system which makes a continuous comparison between two signals transmitted between two stations. One signal is transmitted directly between the stations, the other via the missile being tracked. The frequency of the signal sent to the rocket is doubled there and retransmitted to at least three ground stations. In order to know the location of the grenade burst with respect to the rocket, the grenades were detonated at a known position in front of the rocket by means of a lanyard. The times of the grenade explosions were determined (weather permitting) by infrared ground flash detectors, infrared-sensitive devices installed near the front end of the rocket, and by the DOVAP system. The latter was used in all but the first flights because it was noted that when the explosion of the grenades occurs, the electromagnetic radiation of the DOVAP is temporarily modified by the ionized hot gases from the explosion. This disturbance is documented on the DOVAP record. With this modification and with making the microphone array at the ground less wind-sensitive, the rocket-grenade experiment was made an all-weather experiment able to be carried out at any time.

With financial help from the National Science Foundation and with close cooperation of the before-mentioned University of Michigan group under the direction of L. M. Jones which, under contract, developed and constructed the payload, personnel of USASRD under the supervision of W. G. Stroud carried out ten (5 in the summer and 5 in the winter) very successful rocket-grenade firings at Fort Churchill, Canada, starting on November 12, 1956, and ending on January 27, 1958.<sup>6</sup> This time, instead of the 7 or 9 grenades as carried in the White Sands firings, 19 grenades (see Fig. 3) were carried aloft on board each Aerobee rocket as shown in Fig. 4. Fig. 5 is a composite of all summer temperatures, and Fig. 6 is one of all winter temperatures. The dissimilarity between the two is striking. Very low temperatures were found at 80 km in the summer, and a high temperature prevailed above 60 km in the winter. The data also indicate the incorrectness of the "NACA standard atmosphere" which, until a few years ago was usually used as a standard by aircraft and missile designers. Using the hydrostatic equation and balloon data which agree within  $\pm 2^\circ$  at the overlapping region around 30 km, density and pressure were calculated. Fig. 7 shows a composite of the summer and winter densities; here, also, the difference between summer and winter density in the region of about 40 to 80 km is striking and very significant. Fig. 8 (p. 220) shows the winds with altitude on various days.

<sup>5</sup> At that time it was felt that the available radar equipment was less accurate than the DOVAP system.

<sup>6</sup> W. G. Stroud, W. Nordberg, W. B. Bandeen and P. A. Titus, "Rocket Grenade Measurements of Temperature and Winds in the Mesosphere over Churchill, Canada," IAS; No. 60-47.

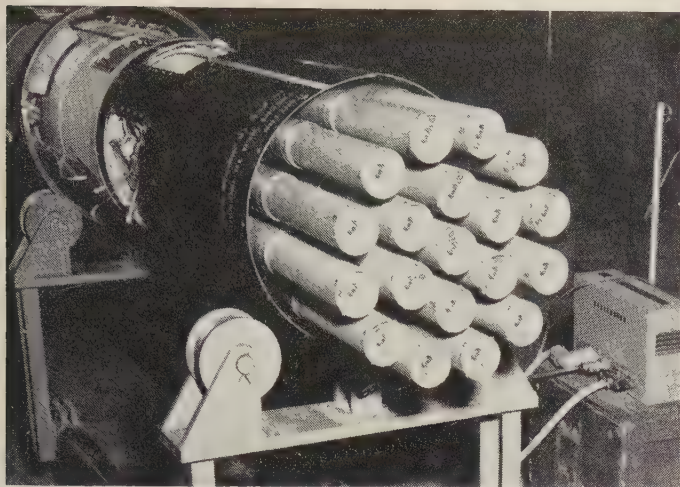


Fig. 3—The grenade section with front cone and sides removed showing the 19 grenades. Each grenade is about 2.1 inches in diameter.

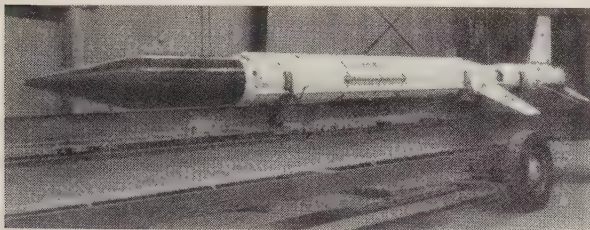


Fig. 4—Photograph of Aerobee Type AJ-10-34 with booster carrying the grenade instrumentation (dark section of rocket). The DOVAP antennas may be seen banded to the rocket tankage about halfway back.

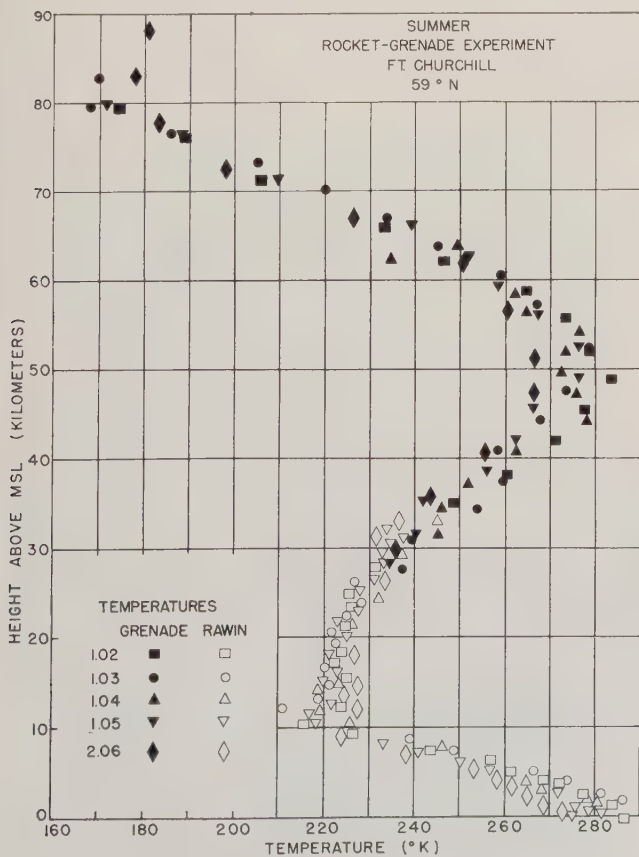


Fig. 5—Composite of summer temperatures.

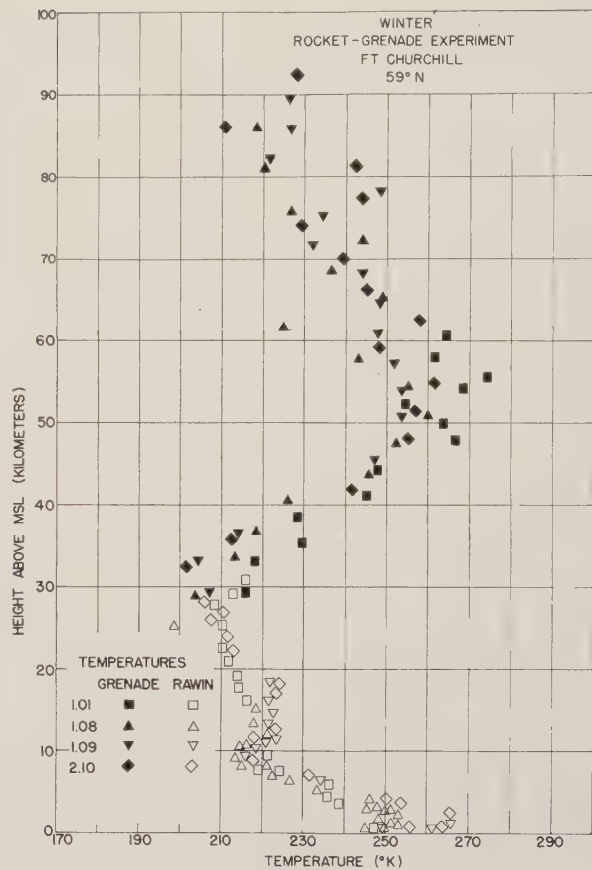


Fig. 6—Composite of winter temperatures.

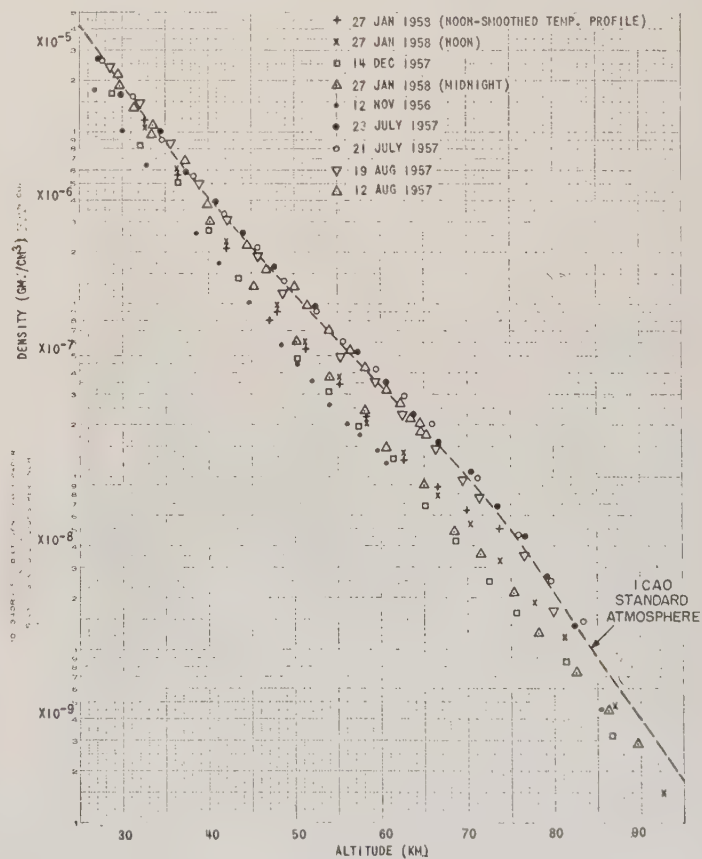
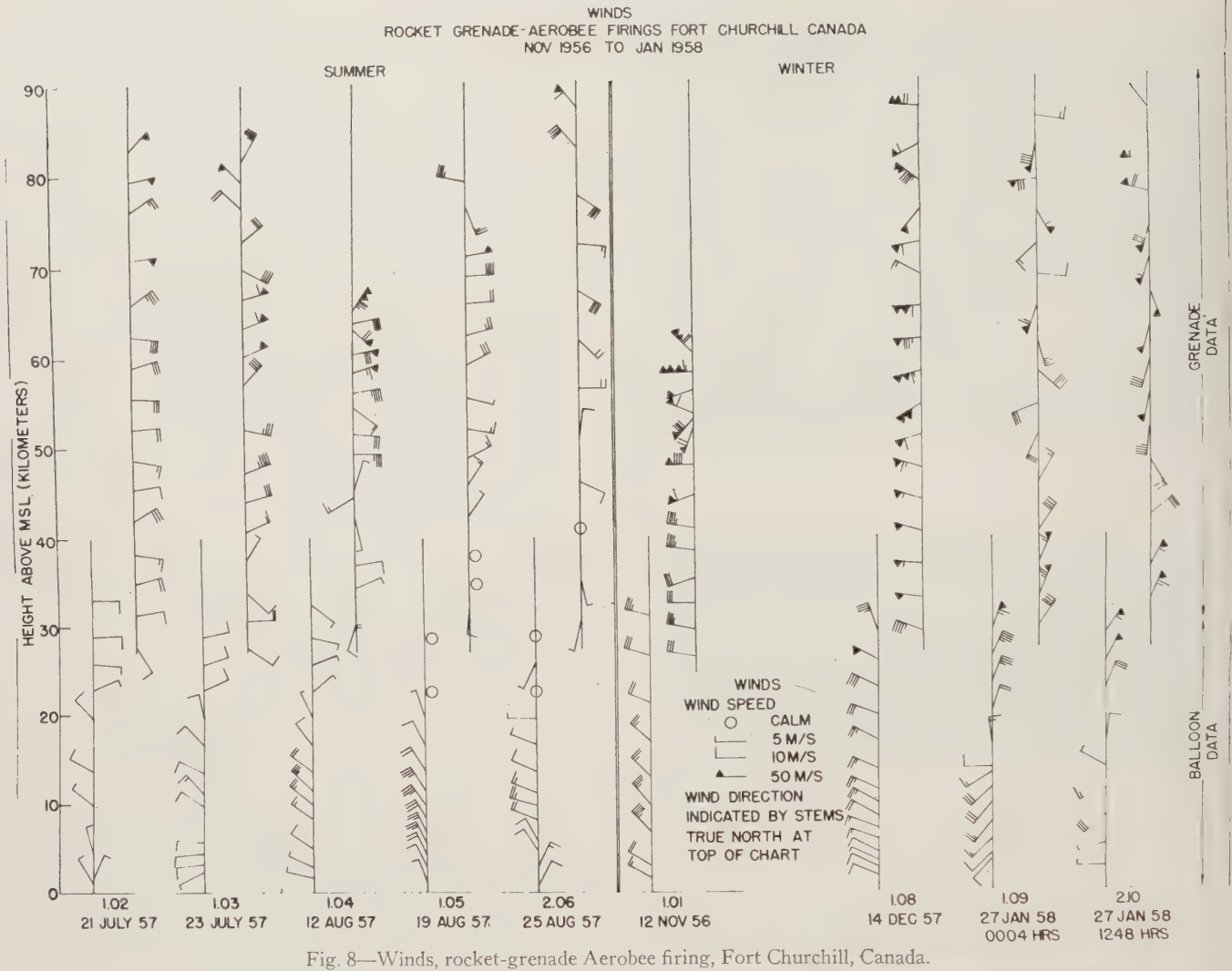


Fig. 7—Density data, as computed from the rocket-grenade experiment carried out at Fort Churchill, Canada.





#### NIKE-CAJUN FIRINGS AT GUAM

While the Aerobee firings were proceeding at Fort Churchill, the rocket-grenade experiment was miniaturized at USASRDL, using a Nike-Cajun combination as the vehicle (Fig. 9). This step was taken to reduce the rather high costs of the Aerobee experiment. Thus a grenade section carrying ten grenades of 1- and 2-pound weight was designed to fit the Cajun. The Cajun is a 6½-inch-diameter rocket of 107-inch length, less nose cone, and a weight, less payload, of roughly 250 pounds. The Nike-Cajun carries a payload of 100 pounds to approximately 100 km. With this equipment and again with financial help from the National Science Foundation and technical support from the Michigan group, firings at Guam were carried out in the Fall of 1958. This location was chosen since practically no data existed on the upper atmosphere over the Pacific Ocean. Nine rockets were fired with good success. The data are presently being evaluated.

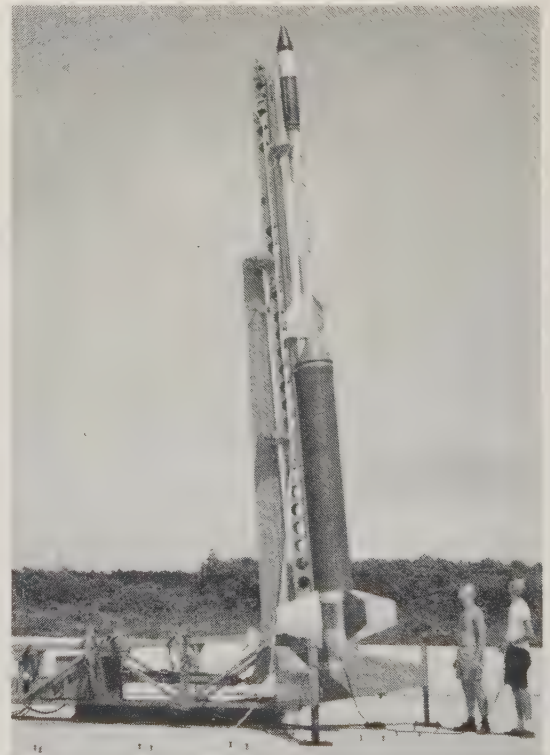


Fig. 9—The Nike-Cajun with rocket-grenade experiment in the head.

# SYNOPTIC ROUTINE MEASUREMENT OF UPPER ATMOSPHERE PARAMETERS WITH SMALL METEOROLOGICAL ROCKETS

Simultaneously with the exploration of the upper atmosphere by means of the above-mentioned limited number of rocket firings, USASRDL, in close cooperation with the Air Weather Service and the U. S. Weather Bureau, had set up a network of 11 stations distributed over the United States, Canada, Greenland, and Panama. At these stations, routine daily flights using special high-altitude balloons and equipment were made during one month of each season for five years. The results of these flights pointed out two facts: 1) in order to obtain a really good thermodynamic and dynamic picture of the upper atmosphere, synoptic measurements of a network of stations must be carried out, and 2) data from altitudes higher than those reached by balloons should be collected. While the second fact can be realized by using rockets, these rockets must be relatively small, easy to launch and, especially, inexpensive in order to fulfill the requirements stated in the first fact.

At the time of the first plans to use small rockets for meteorological routine measurements, only the Loki Type I and II rockets were available. The Loki is a small, relatively inexpensive vehicle which can easily be launched by two or even only one person (Fig. 10). The Loki dart has a diameter of  $1\frac{3}{8}$  inches and a length of 40 inches. Its booster has a diameter of 3 inches and a length of 63 inches, and the total weight is 29 pounds. While the Loki I rocket does not reach altitudes much higher than those reached by balloons, the Loki II is able to carry a payload of one pound to between 70 and 85 km, depending on the altitude of the launch site. The payload section of the standard dart has a volume of only about 22 cubic inches. Because of this limitation and because the wind is one of the most important atmospheric parameters desired by the missile designer and meteorologist, the first payload for the Loki II was one pound of X- or S-band chaff to be tracked by radar. Depending on the wind structure and turbulence, the chaff cloud disperses more or less during its descent, and there-

fore the quality of the data deteriorates somewhat with decreasing altitude. However, many valuable data have already resulted in wind profile measurements from 85 km to approximately 30 km. The advantage is that these profiles are continuous in contrast to the wind values of the rocket-grenade experiment which are averages over approximately 3-km layers. Investigations are being made on the use of payloads such as parachutes, chaff dipoles joined in long filaments to prevent dispersion, and others.

In the meantime, another small rocket suitable for meteorological use was developed by Atlantic Research Corporation, Alexandria, Virginia, under the sponsorship of the Navy and Air Force. It is the Arcas (Fig. 11, next page) with a diameter of 4.5 inches, a length of about 92 inches, and a total weight, less payload, of 65 pounds. A payload of 12 pounds is carried to approximately 60 km from sea level. USASRDL developed the meteorological radiosonde for this rocket (Fig. 12) which, at the present time, measures temperature only. However, space is provided for a pressure-measuring instrument. In the future, other sensors which measure density, ozone, etc., will be added or exchanged.

The instrument package is ejected from the rocket at peak altitude and carried to the ground on a 16-foot metallized parachute. The radiosonde is tracked by the AN/GMD-2 rawinsonde equipment which, by a phase-comparison method, can determine the distance of the package very accurately. The elevation angle is also determined. The parachute is metallized and can therefore also be tracked by radar. While the Arcas rocket has already yielded excellent results, its development phase is not yet finished.

With the Loki and Arcas progressing satisfactorily, it was decided that the time had come for making plans for a synoptic meteorological network. Since this had to be a cooperative undertaking, the Air Force, Navy, NASA, and U. S. Weather Bureau were invited to participate. These agencies responded to this invitation, and an informal but very enthusiastic group composed of upper-air meteorologists and instrument designers of the above-named agencies and USASRDL, as well as of meteorologists of the various missile ranges, was formed to plan and carry out synoptic meteorological and other interesting investigations, using for the first time in the history of meteorology the rocket as a routine instrument carrier. At the beginning a 6- to 8-station network is planned which will be expanded in the future. Daily flights in one month of all four seasons, and on special days several flights per day, will be carried out. With this meteorological rocket network, a new era in meteorology will commence.

Parallel with these routine measurements, USASRDL will continue to carry out special investigations, not necessarily only of meteorological nature, to enhance our knowledge of the upper atmosphere. With the beginning of the satellite era, the subsatellite regions were threatened with neglect, although the knowledge about them is of utmost importance in the field of guided missiles, meteorology, electromagnetic wave propagation, and others.

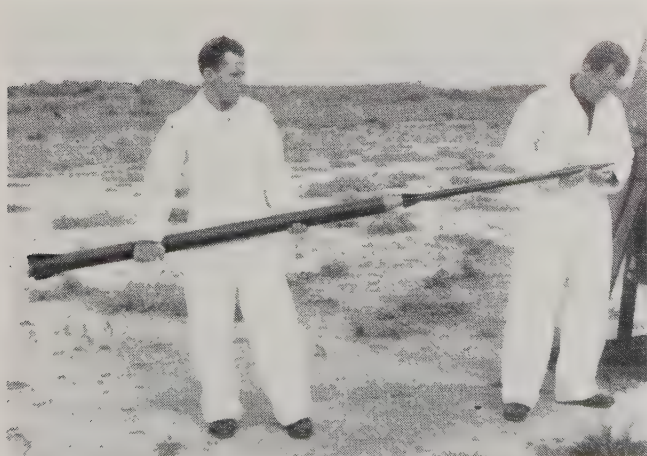


Fig. 10—The Loki rocket.





Fig. 11—The Arcas rocket.

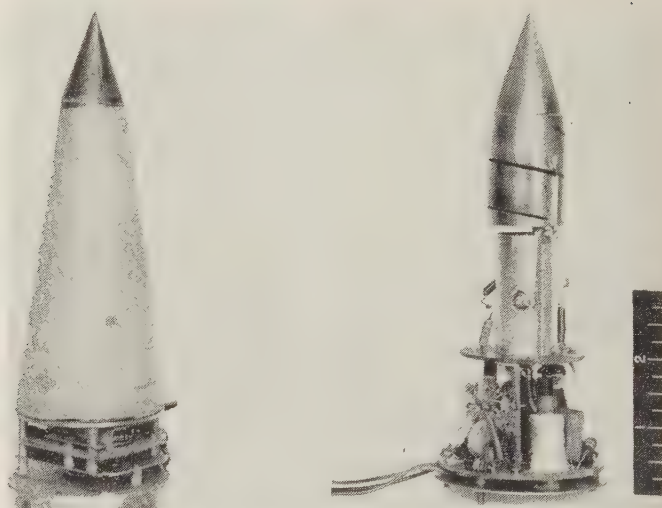


Fig. 12—Radiosonde set AN/DMQ-6, part of Arcas rocket, used with Rawin set AN/GMD-2. (a) 1660-1700-mc transmitter and 403-mc superregenerative receiver mounted and encapsulated in plastic form. (b) Before encapsulation.

## Upper Atmospheric Research at the Ballistic Research Laboratories\*

JOHN C. MESTER†

**Summary**—A summary of BRL activities in upper atmosphere research is presented. From a quite modest beginning, the International Geophysical Year gave impetus to a considerable program. Results of electron content measurements in the ionosphere employing rocket borne transmitters are reported. Studies of the water vapor content of the atmosphere and the optical properties of the earth's horizon using balloon borne and rocket borne instrumentation are being made. Some comments on the use of catalytic surfaces to study recombination rates in the atmosphere are given.

### INTRODUCTION

**H**ISTORICALLY the Ballistic Research Laboratories' interest in upper air research grew from its responsibility for tracking instrumentation.

In 1945 the BRL was requested by the Office, Chief of Ordnance, to design, install and operate the ballistic range instrumentation at the newly organized White Sands Missile Range. In line with this request, range tracking systems including tracking telescopes, cinetheodolites, fixed position cameras and radio-doppler receivers were ready for operation when the first V-2 was fired at White Sands in April, 1946. The fortunate inclusion of upper atmosphere research experiments in the early V-2 firings at White Sands and the needs of the research agencies for trajectory and missile flight characteristics led quite naturally to the BRL cooperation in the upper atmosphere research program. Indeed, the results from a number of the research experiments depended on precision measurements of trajectory speeds and certain events associated with the experiments.

As the development and improvement of the DOVAP

\* Manuscript received by the PGMIL, February 1, 1960.

† Ballistic Res. Labs., Aberdeen Proving Ground, Md.

(Doppler Velocity and Position) system progressed, intensive studies were made as to the possible limitations of the system. Partially as a result of these studies, Berning<sup>1</sup> in 1950, devised a method to utilize the DOVAP system in the measurement of electron densities in the ionosphere. In like manner the employment of optical tracking devices and cameras gave rise to concern with the problem of image jitter caused by atmospheric motions and variations. One experiment resulting was the study of the earth's optical horizon by means of photographs taken from balloons.

With the advent of serious detailed planning in 1953 for the International Geophysical Year, the BRL broadened its upper air research program: First as a member of the Special Committee for IGY responsible for planning the U. S. rocket research program, next as a member of the Technical Panel on Rocketry of the National Academy and finally, as a scientific agency participating in the IGY. In addition to its participation as a scientific agency, the BRL was assigned the further responsibility of furnishing and operating ballistic tracking instrumentation at the Fort Churchill IGY rocket facility. Some of the scientific experiments undertaken by BRL during the IGY and continuing today are discussed below.

#### ELECTRON DENSITY MEASUREMENTS

The DOVAP system,<sup>2</sup> developed by BRL, employs two CW signals, one sent directly from the ground transmitter to the ground receivers, the other transmitted by way of the rocket in flight. The signal received by the rocket is doubled in frequency and retransmitted to the receiver. This rebroadcast signal is picked up by the receivers on the ground and beat against the suitably doubled frequency arriving at the receivers directly from the ground transmitter. The beat frequency between the two signals is the Doppler Frequency due to the missile motion in the transmitter-missile-receiver path. Integration of the Doppler frequency as a function of time from some known initial point gives when multiplied by the wave length of the carrier, the distance from transmitter to missile to receiver. This distance defines an ellipsoid of revolution, the foci of which are the transmitter and the receiver. Three receivers then define three ellipsoids, the intersection of which gives the position of the missile. If the propagation were taking place in vacuum where the phase velocity of propagation is constant, the DOVAP solution would give the true trajectory of the rocket, but, due to presence of the ionosphere, the phase velocity is not constant and errors are introduced. If one had an accurate reference trajectory one could by comparing it to the DOVAP trajectory deduce the index of refraction and hence, the electron density of the medium. This reference trajectory can be obtained by computing a vacuum trajectory using as initial conditions the DOVAP

data above the appreciable atmosphere but below the ionosphere.

Of the approximately sixty rockets fired at Fort Churchill which carried DOVAP, some twenty-five are being used to obtain electron density. In addition, a number of rounds at White Sands Missile Range have been reduced. These rockets were fired nearly vertically, so that by neglecting horizontal motion and the earth's magnetic field one obtains for the electron density at the rocket, assuming the electron content below the rocket to be time invariant during the flight

$$N(e/cc) = k \left( 1 - \frac{\dot{Z}_d}{\dot{Z}_v} \right)$$

where  $\dot{Z}_d$ ,  $\dot{Z}_v$  are the vertical components of velocity from the DOVAP and vacuum trajectories respectively and  $k$  is a constant dependent on carrier frequency. (For the frequencies used with DOVAP,  $k = 5.89 \times 10^7$ .)

In Fig. 1 is shown the electron density profile obtained from pre-IGY, BRL Nike-Cajun rocket fired at White Sands. The agreement between the up and down leg of the trajectory is considered to be excellent. For comparison purposes, the electron density calculated from an ionogram taken during the flight is shown.

Fig. 2 shows the profile obtained from the first IGY flight at Fort Churchill, a Naval Research Laboratory Aerobee hi. The scatter in the data precluded using the down leg of the flight. Some of the fine structure of the ionosphere is quite evident for this flight.

Of particular interest is the profile obtained from IGY flight ABM 10,200, an Aerobee-300 rocket jointly sponsored by the Air Force Cambridge Research Center, BRL and the University of Michigan. This rocket appears to have reached the F-2 maximum as evidenced by the decrease in electron density near peak. Two curves of electron density from the ionogram are plotted; the two values arise from the difficulty in determining the altitude of the first reflection from the photograph. Above 200 km either curve is in good agreement with the values obtained from DOVAP, while below that altitude the interpretation of first reflection at 155 km gives considerably better agreement. The up leg data clearly indicated a relatively constant electron density in the 160–180-km region. Unfortunately, data was not available from the down portion of the flight for comparison.

#### FARADAY MEASUREMENTS

When an electromagnetic wave traverses a birefringent medium such as the ionosphere, its plane of polarization undergoes a rotation referred to as Faraday rotation. For frequencies much higher than the gyromagnetic and collision frequencies, the rate of Faraday rotation with respect to the ray path of a linearly polarized wave propagated along the earth's magnetic field may be expressed as

$$\frac{d\Omega}{dr} = -k \frac{H \cos \phi N}{(2\pi f)^2}$$

<sup>1</sup> W. W. Berning, "Ionospheric charge densities from radio Doppler records," *J. Meteorology*, vol. 8, pp. 175–181; June, 1951.

<sup>2</sup> A. L. G. deBey and E. D. Hoffleit, "DOVAP—Instrumentation and an Analysis of Results," Ballistic Res. Labs., Aberdeen Proving Ground, Md., Tech. Rept. No. 677; November, 1948.



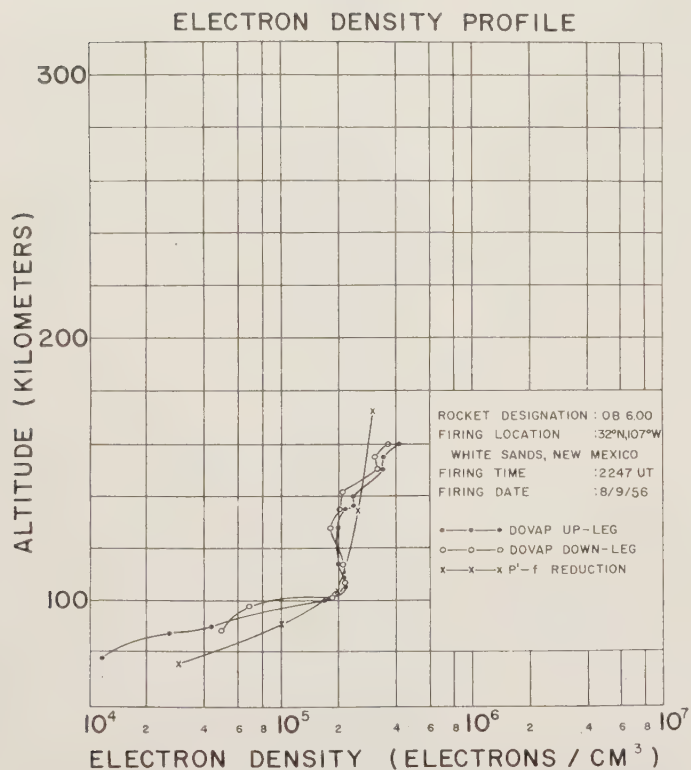


Fig. 1—Electron density obtained by DOVAP trajectory comparison method for Nike-Cajun rocket OB6.00.

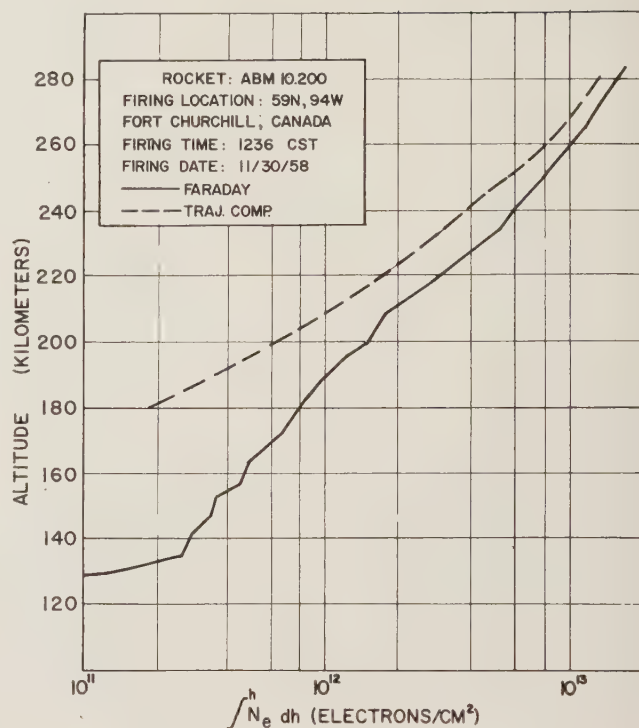


Fig. 3—Total electron content from Faraday measurement on Aerobee 300 ABM10.200.

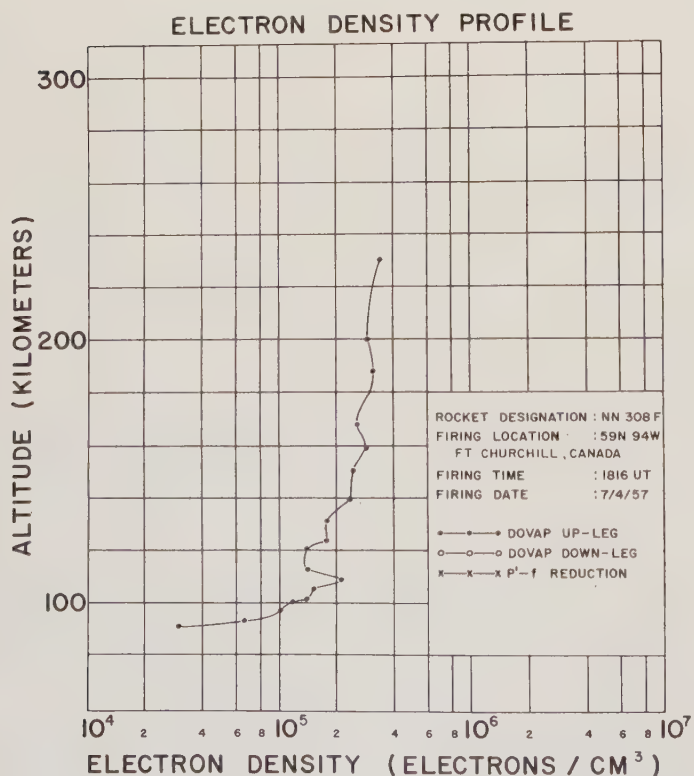


Fig. 2—Electron density obtained by DOVAP trajectory comparison method for Aerobee hi NN3.08.

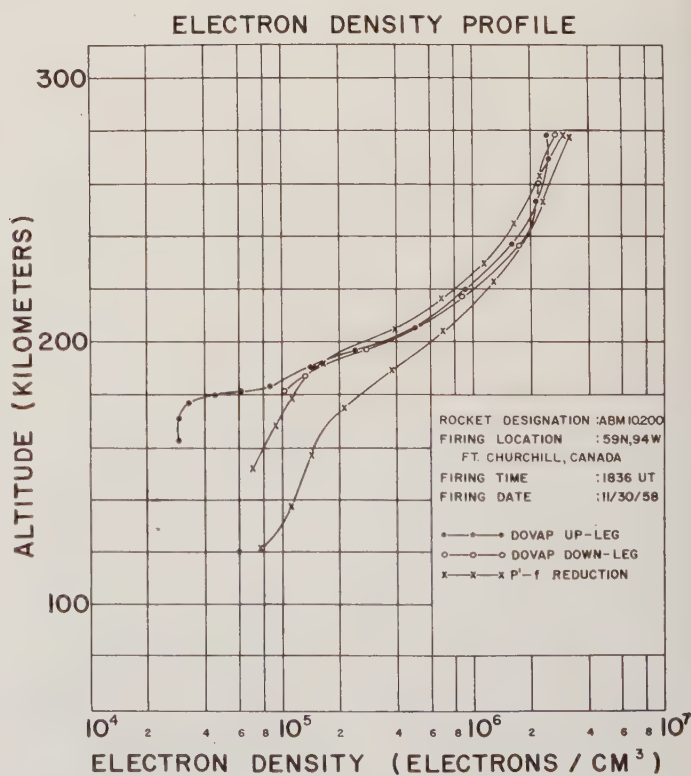


Fig. 4—Electron density obtained by DOVAP trajectory comparison method for Aerobee 300 AMB10.200.

where

$\Omega$  = Faraday rotation in radians.

$dr$  = incremental distance along the ray path, assuming flat earth

$$dr = \frac{dh}{\cos \theta}$$

where  $h$  is altitude,  $\theta$  is angle between the ray path and the vertical.

$H$  = earth's magnetic field intensity in ampere turns per meter.

$\phi$  = angle between the magnetic field and the ray path.

$f$  = frequency of the signal.

$N$  = electron density of the medium in electrons/cm.<sup>3</sup>

$k$  = a constant involving the charge and mass of the electron, the permittivity and permeability of free space and the velocity of light in vacuum.

Using for  $H$ , a mean value  $\bar{H}$ , and assuming that  $\phi$  and  $\theta$  are constant, which for rockets fired at Fort Churchill is reasonably so, upon integrating one obtains for the total Faraday rotation

$$\Omega = \frac{k\bar{H} \cos \phi \sec \theta}{(2\pi f)^2} \int_{h_1}^{h_2} N dh.$$

The DOVAP system can be used to determine the total Faraday rotation in the following manner. The Faraday appears in the data in the same manner as rocket spin. By means of right and left hand antennas, one can separate this spin plus Faraday from the normal Doppler cycles. Above the effective atmosphere but below the ionosphere, this data represents the true spin of the rocket and for a stable rocket remains effectively constant. Upon entering the ionosphere the Faraday rotation begins and the DOVAP data give rocket spin plus Faraday. By differencing the DOVAP data from the true spin, one obtains Faraday rotation versus altitude. Prenatt<sup>3</sup> has applied this method to a number of rocket rounds at Fort Churchill. In Fig. 3 is shown the integrated electron content from 122 km to the altitude shown obtained from the upward flight of ABM 10.200 at Fort Churchill. The down leg is not shown since it virtually falls on top of the up curve except for a slight spread at the lower altitudes. Also shown is the integral of the electron density curve obtained by the DOVAP-trajectory comparison method as given in Fig. 4. The two curves differ considerably at the lower altitudes with the trajectory comparison technique giving lower electron content. However, as the altitude increases the curves tend together and near peak the agreement is quite acceptable.

#### MAGNETIC FIELD MEASUREMENTS

Short term variations in the Earth's magnetic field have been attributed, for many years, to the existence of tidally induced motions of charged particles in the lower ionosphere. The nature of the resulting currents, particularly in auroral regions, is of great geophysical interest.

<sup>3</sup>R. E. Prenatt, "Faraday rotation measurements at Fort Churchill," *J. Geophys. Res.*, vol. 64, pp. 1340-1341; September, 1959.

During the IGY, three Nike-Cajuns instrumented with proton precession magnetometers were fired by BRL at Fort Churchill to study variations in the Earth's magnetic field, with simultaneous measurements of ionospheric electron densities by the DOVAP trajectory technique. One of these flights occurred on a particularly quiet day, magnetically, and should serve as an excellent calibration round for the earth's field above Fort Churchill. Data from these flights are being reduced and the magnetic field measurements are to be published shortly in the *Journal of Geophysical Research*.

#### HORIZON STUDIES

Early photographs of the horizon obtained from high altitude rockets launched at White Sands Missile Range<sup>4</sup> had shown well defined atmospheric haze bands. The upper boundary of the haze generally appeared so sharp, in contrast to the ground horizon which is often obscured by the dense haze that it seemed desirable to investigate the feasibility of adopting this "photometric horizon" as a precise reference system for the determination of the orientation of missiles in flight.<sup>5</sup> To carry out this investigation, special photographic equipment was prepared by BRL and flown in high altitude balloons in the White Sands area. The photographs obtained indicated that the height of the photometric horizon corresponded well with the presumed height of the tropopause. Since the tropopause is neither rigidly fixed nor necessarily smooth within the atmosphere and since secondary striations are often observed, the photographs proved to be of great interest for studying the structure of the atmosphere.

At high latitudes the height of the polar tropopause is between 8 and 13 km, while at low latitudes the tropical tropopause height is between 13 and 18 km. The complexity of photographs obtained at White Sands indicate that in the midlatitude, one has the simultaneous appearance of both the tropic and polar tropopause. This can be seen from Fig. 5. This photograph was taken by a balloon borne camera from an altitude of approximately 25 km above White Sands. The over exposed portion is the earth. Examination of the haze portion shows alternately dark and bright bands peculiar to the midlatitudes.

To verify that the striations observed in the White Sands photographs were due to simultaneous presence of the polar and tropical tropopauses, it was decided to take photographs at Fort Churchill where only the polar tropopause was to be expected. Seven Nike-Cajun rockets equipped with either two or three cameras were fired by BRL at Fort Churchill during the IGY. Approximately 27 seconds after launch the cameras started operating at two frames per second until the peak of the trajectory at ap-

<sup>4</sup>T. A. Bergstrahl, "Photography from the V-2 Rocket at Altitude Ranging up to 160 Kilometers," U. S. Naval Res. Lab., Washington, D. C., Tech. Rept. No. R-3083; 1957.

<sup>5</sup>D. Reuyl, D. J. Davis and L. Ewalt, "Notes on the Optical Horizon for the Determination of the Vertical for Guided Missiles," Ballistic Res. Labs., Aberdeen Proving Ground, Md., Tech. Rept. No. 512 (C); 1950.



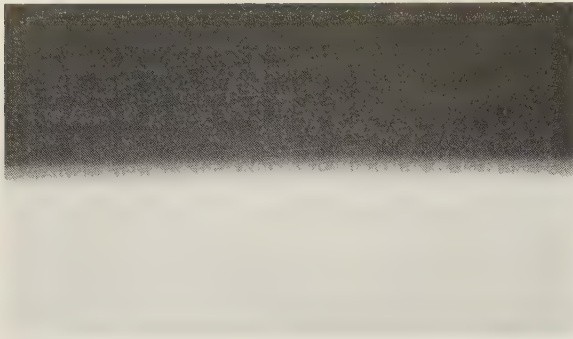


Fig. 5—Horizon photographed from balloon borne camera at White Sands missile range.

proximately 110 km. After peak the nose cone was separated from the rocket and drag brakes were used to slow down and stabilize the nose cone. At about 10 km a parachute was deployed for the final descent, and a beacon was turned on to be used for radio direction finding. Recovery of the cameras was accomplished on four of the seven shots. In two instances the beacon failed to operate and in the third, nose cone separation did not occur. In those cases where the nose cone was recovered, the camera instrumentation was in such good condition that, with only moderate refurbishing, it could be reflown as was done with two of the packages.

Examples of the photographs obtained are shown in Fig. 6. The left hand portion is of two frames, one-half second apart with the rocket at approximately 70 km. The rocket was still quite stable at this point as can be seen from the small motion of the horizon from frame to frame. The right hand sequence, also of two frames a half second apart, is from the same flight but with the rocket at 88 km. The considerable yawing and precession motion of the rocket at this point is evident.

While the measurement of the haze thickness shown by the Fort Churchill photographs gave considerable scatter on a frame to frame basis, the abundance of material yielded a statistically significant mean value of the height of the photometric horizon of  $11.0 \pm 0.4$  km. This mean value gives evidence that the photometric horizon represents the polar tropopause.<sup>6</sup>

#### WATER VAPOR MEASUREMENTS

Water vapor concentrations to altitudes of 80 km are quite important in the meteorology of the higher atmospheric levels. The horizontal as well as the vertical distribution of this important constituent can serve as an excellent tool in the study of transport and mixing processes. Further, the chemical properties of water vapor, if this constituent is sufficiently present, plays an important role in heat exchange phenomena in the atmosphere. To

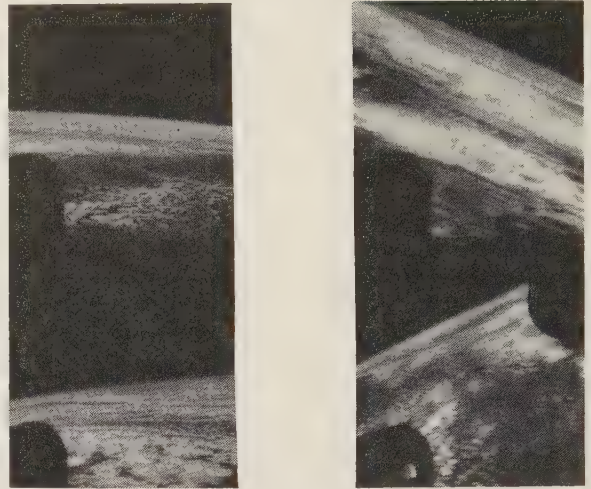


Fig. 6—Horizon photographed from rocket borne camera at Fort Churchill.

quantitatively measure the water vapor content, BRL undertook the development of an infrared hygrometer to be flown in a Nike-Cajun rocket. At the same time balloon borne dew point hygrometers were to be flown to give independent measurements up to 30 km. The one rocket flight so far attempted, yielded no water vapor measurements due to telemetry failure. However, the flight did indicate the need for the redesign and repackaging of the rocket borne infrared hygrometer instrumentation. This redesign has been accomplished and a Nike-Cajun flight of the hygrometer is scheduled for April, 1960.

A number of balloon flights carrying a dew point hygrometer have been made by BRL.<sup>7</sup> The flight package weighs 8-1/2 pounds. The principle in the hygrometer is the dew point determination by measurement of the temperature at the time of dew spot or frost spot (if the dew point is below freezing) deposition. In Fig. 7 is shown the results of two of the flights. The dew point data have been transformed into mixing ratio, that is grams of water per kilogram of dry air, in order to gain better insight into the variability of humidity in the stratosphere. Of greatest interest in Fig. 7 is the definite increase shown in water vapor with altitude in the stratosphere where the prevalent view has been that water vapor is practically nonexistent at these altitudes.

#### RECOMBINATION STUDIES

Using balloons, the investigation of the recombination of free radicals and atomic particles in the lower stratosphere are being carried out by means of specifically coated thermistors used as catalytic surfaces.<sup>8</sup> At the same

<sup>6</sup> D. Hoffleit and T. R. Bechtol, "Photographic Studies of the Horizon Patterns from High Altitude," presented to Amer. Rocket Soc., November, 1959.

<sup>7</sup> J. A. Brown and E. J. Pybus, "Stratosphere Water Vapor Measurements by Means of a Dew Point Hygrometer," presented to the Conference on Stratospheric Meteorology of the Amer. Meteorology Soc., Minneapolis, Minn.; September, 1959.

<sup>8</sup> J. A. Brown and G. I. Lavin, "Preliminary Results Obtained with Catalytic Surfaces in the Upper Atmosphere During Balloon Flight," Ballistic Res. Labs., Aberdeen Proving Ground, Md., Tech. Rept. No. 1230; December, 1958.

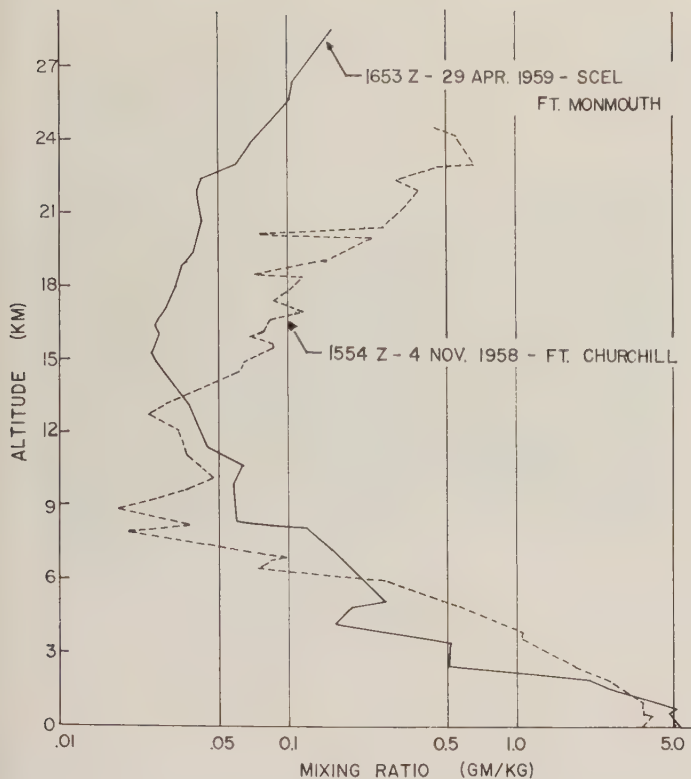


Fig. 7—Mixing ratio of water measured with DEW point hygrometer.

time laboratory investigation of specific coatings are being carried out. Flight data to 38 km have been obtained. Using a silver coating, a temperature spike separated from the ambient temperature by 26° Centigrade was obtained. It is believed that this was due to the recombination of atomic oxygen or possibly the formation of ozone from molecular and atomic oxygen with the subsequent values of recombination of 117,000 and 170,000 calories per mole respectively. On another flight, using a nickel coated thermistor particle concentrations of  $1 \times 10^{11}$  atomic oxygen particles per cubic centimeter were obtained at 38 km. This is in close agreement with the theoretical model of Miller.<sup>9</sup>

#### STRONGARM

At 7:00 A.M., November 10, 1959, BRL in conjunction with the University of Michigan launched a five stage vehicle from the NASA Wallops Island station to measure electron densities. The vehicle consisted of an Honest John, two Nike-Ajax boosters, a slow burning Recruit (Yardbird) and a scaled Sergeant especially prepared by the Jet Propulsion Laboratory. The five-stage vehicle, which for the first time flight tested the Yardbird, was code named

Strongarm. The nose was instrumented with a very stable dual frequency transmitter broadcasting on two coherent frequencies of 37 and 148 mc. Since the index of refraction varies inversely with the square of the frequency, by differencing the Doppler frequency at 148 mc with four times the Doppler at 37 mc, one can obtain a measure of the electron density in the ionosphere. Similarly by observing the difference in the Faraday rotation at the two frequencies one can measure the total electron content. The ground station, which employed tracking filters to follow the signal at long distances, used right and left hand helices at both frequencies to eliminate missile spin. The ground station automatically recorded the differential Doppler and Faraday rotation. The missile attained an altitude in excess of 1750 km and was successfully tracked in excess of 25 minutes both from Wallops Island, Virginia, and from Spesutie Island, Aberdeen Proving Ground, Md. Reduction of the data is in process and preliminary results indicate that successful measurements of electron density and total electron content to peak were accomplished. The experiment was originally designed for a day and night shot to measure the variation of the ionosphere with time of day. However, the second shot on November 18 failed when the third stage did not ignite.

#### CONCLUSION

The foregone has been but the briefest of summaries of the BRL activities in upper air research. As is obvious this work is of a continuing nature, with facts accumulated today indicating the way to new experiments of tomorrow. The increase of knowledge of our environment is of importance not only from the scientific aspect but is necessary to the Army in its role in national defense in the proper design and evaluation of systems which must operate in this environment. The BRL shall endeavor to pursue research in this field.

Already planned for late summer 1960 is another day-night Strongarm experiment to measure electron density up to and above the F-2 maximum. Work in recombination rates and in water vapor measurements will continue with an extension beyond balloon altitude by employing the small meteorological rocket ARCAS. As was previously mentioned the rocket borne infrared hygrometer is to be flown in April, 1960 at Fort Churchill. Coordinated with the rocket flight, balloon borne dew point hygrometers will be flown at a number of sites to attempt to map water vapor content over a large area at the same time. The obvious extension of horizon photography to the tropical region needs to be undertaken. The design of new experiments and new measurement devices such as the rocket born Langmuir probe to measure electron and ion densities being developed by the University of Michigan with BRL support is of prime importance to our understanding of the upper atmosphere. Much remains to be done.

<sup>9</sup>L. E. Miller, *J. Geophys. Res.*, vol. 62, p. 363; September, 1957.



# The Radar Beacon Comes Into Its Own\*

PERRY L. WHITE†

**Summary**—This article tells the missile radar-beacon story from the beginning of V-2 missile firing in America until today. It compares the weight, dimensions, characteristics, and uses of former beacons with those used today. It also describes briefly new beacons under development, and tells how some of the future missiles and satellites may use these beacons.

## INTRODUCTION

THE value of the radar beacon as a means to extend normal radar tracking range and to perform auxiliary functions of command and telemetry is well recognized by most groups associated with missile range instrumentation and missile development. The ever increasing demands placed upon the radar beacon and the continuing acceptance of its usefulness as a radar aid have stimulated continuing development and improvement, resulting in the intricate, though compact and versatile, device it is today.

## THE FIRST MISSILE BEACON

The first German-made V-2 missile fired at White Sands Missile Range in 1946 carried a AN/APN-55 Beacon, a very limited performance beacon of moderate size which was developed by the Signal Corps as an interim unit. The success of the AN/APN-55 led to the development of the higher-performance large-size AN/DPW-1 beacon, shown in Fig. 1. The total AN/DPW-1 beacon assembly weighed approximately 43 pounds installed, and at first there were no command channels available.

The effectiveness of these first radar-beacon combinations influenced the design of guidance systems for early American missiles. Several of these first missiles carried either the AN/APN-55 or the AN/DPW-1, with up to six command channels added. This served as a guidance package and was used for the ejection of parachutes carrying cameras, upper-atmosphere sampling capsules, and other research tools. The AN/DPW-1 Beacon was later used as the guidance link for the Viking Missile. Many of the missiles flying in 1960 and years to come, requiring radar commands, will be carrying the AN/DPN-50 Beacon shown in Fig. 2. This beacon represents significant improvement over previous designs, in terms of increased reliability, higher ratio of performance to weight, and greater operational versatility. The receiver-transmitter (RT) assembly is  $3\frac{3}{4}$  inches high,  $7\frac{1}{2}$  inches wide,  $10\frac{5}{8}$  inches long, and weighs approximately 15 pounds. The secondary power supply is approximately one half the size



Fig. 1—Radar beacon AN/DPW-1 (XE-2). Left to right: battery box, dynamotor, radar beacon.

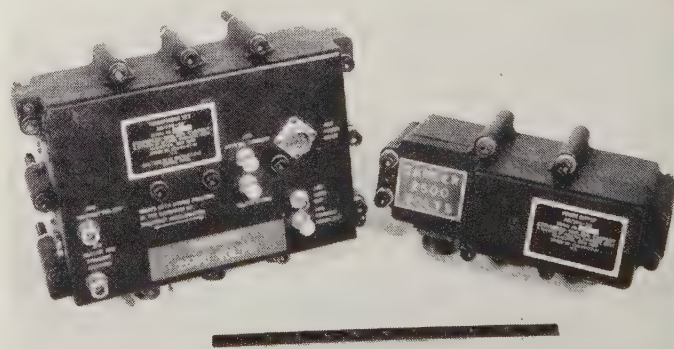


Fig. 2—Radar beacon AN/DPN-50.

of the RT, weighs about nine pounds and operates from a power input of either 115 volts 400 cycles or 26.5 volts dc. The beacon contains the facility for receiving command inputs, and it will deliver audio tones for further processing by an external command-control selector not a part of this beacon assembly, with a capability of up to 12 command channels. This beacon is also capable of accepting telemetering input from an external device such as telemetry unit AN/DKT-9 and of radiating telemeter data along with the pulse used as a tracking source by the radar.

The AN/DPN-43 Beacon, shown on the right in Fig. 3, is the modern beacon comparable to the AN/APN-55. It is  $2\frac{1}{2}$  inches in diameter,  $6\frac{1}{2}$  inches long, and weighs approximately 3 pounds, with its own internal power supply. It will do almost the same job the AN/APN-55 beacon would do, with more reliable operation because

\* Manuscript received by the PGMIL, February 1, 1960.

† U. S. Army Signal Missile Support Agency, White Sands Missile Range, White Sands, N. M.

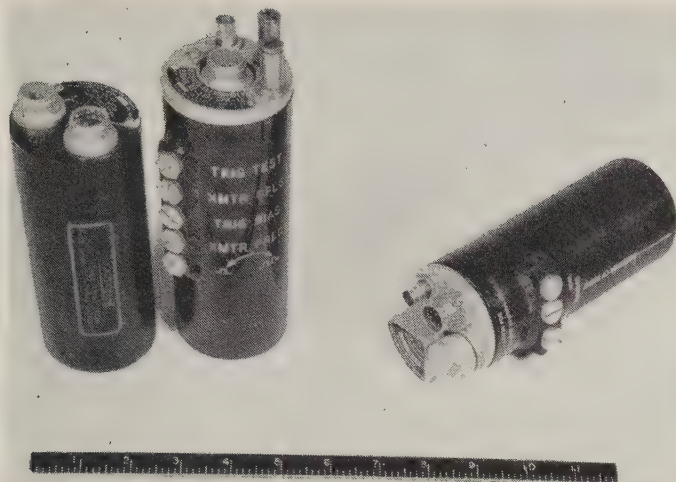


Fig. 3—Left: radar beacon with power supply AN/DPN-19. Right: radar beacon (transistorized) AN/DPN-43.

of a more rugged design, and with only a fraction of the AN/APN-55 size and weight. This beacon, developed in 1958, is completely transistorized except for the use of a pencil tube as the transmitter.

The AN/DPN-19 Beacon and power supply are shown on the left in Fig. 3, to indicate the contrast in size between a transistorized and a nontransistorized beacon. The beacons are essentially equal in performance, except that the AN/DPN-19 has a 50-watt transmitter while the AN/DPN-43 has a transmitter with a nominal 2-watt peak power output, with some units producing as much as 10 watts.

The above discussion has described some of the missile beacons developed by the Signal Corps. There are many others, as evidenced by the chart on Fig. 4.

In addition to the beacons listed previously, the U. S. Army Signal Missile Support Agency has sponsored another development which is being carried out by the U. S.

Specification Number	Nomenclature	Frequency Band	Size	Total Weight Lbs With P.S.	Receiver		Transmitter Peak Power Watts	Environmental	
					Trig Sensitivity Dem	Coding		Longi-tude G's	Transverse G's
SCL-2468 19 Nov 51	AN/DPW-1 (XE-2B)	S	6"D 12"L	43	-65	3 Pulse	2000	50	25
SCL-2468 1 Apr 51	AN/DPN-14	S	6"D 12"L	22.5	-65	3 Pulse	500	50	25
SCL-2421 3 Jan 51	AN/DPN-19	S	2.5"D 7"L	5	-40	1 Pulse (No Code) 2 Pulse	50	100	25
SCL-2665 23 Dec 52	AN/DPN-30	S	2.5"D 6"L	3.5	-40	2 Pulse	2	100	25
SCL-2666 22 Dec 52	AN/DPN-31	S, C, S	4 $\frac{1}{4}$ " $\times$ 8 $\frac{1}{8}$ " $\times$ 11 $\frac{1}{4}$ "	11	-40	3 Pulse	50	50	25
SCL-2721 5 Jul 54	AN/DPN-32	X	2.5"D 7 $\frac{1}{2}$ "L	5	-44	2 Pulse	50	100	25
SCL-5067 15 Dec 54 AMM#1, 3 Jun 55	AN/DPN-41	S	2.5"D 9.5"L	5	-42	1 Pulse (No Code) 2 Pulse	50	200	25
SCL-2993 2 Aug 54 AMM #3, 27 Mar 58	AN/DPN-42	C	2.5"D 8"L	6	-41	1 Pulse (No Code) 2 Pulse	50	200	25
SCL-5008 4 Oct 54 AMM#1, 1 Apr 56	AN/DPN-43	S	2.5"D 6.5"L	3	-38	2 Pulse	2.0	100	25
SCL-5564 Mar 58	AN/DPN-48 (XE-2)	S, C	7 $\frac{7}{16}$ "H 9"W 16"L incl MTG	29	-60	1 Pulse	S-200 C-100	100	25
SCL-5351 Oct 56 SCL-5351A 2 Apr 58	AN/DPN-50	C	3 $\frac{3}{4}$ "H 7.5"W 10 $\frac{5}{8}$ "L	24	-65	1 Pulse 2 Pulse 3 Pulse (OPT)	500C 1000C	100	25
SCL-5568 3 Mar 58 AMM#1, 29 Jul 58	AN/DPN-55 (XE-1)	C	9 $\frac{1}{8}$ "L 7 $\frac{1}{8}$ "W 4 $\frac{3}{8}$ "W	19	-65	1 Pulse	400	100	25

Fig. 4—Status of U. S. Signal Corps Transponders (radar beacons) as of May, 1959.



Army Signal Research and Development Laboratory. Resulting from this development will be such items as missile beacons nomenclatured AN/DPN-57 and AN/DPN-58, to be completed during 1960. These units are of the crystal video receiver type, transistorized to the fullest practical extent, and will provide a command capability and operation in the C and X bands, respectively. Also, there are under development a 40-kw beacon magnetron and suitable companion modulator tube, which will make possible the design of radar beacons of considerably greater range than the typical 1-kw beacons used in the longest-range missiles. A 40-kw beacon when used in conjunction with radars such as the AN/FPS-16 will permit target tracking ranges of up to 15,000 miles, and when used with modified radars could prove useful in space-probe work.

Radar beacons will find a greater use on missiles, satellites, and space probes as these craft become more refined

and as the problems of payload and power limitations on these vehicles are solved. For instance, the Project Mercury capsules will each carry two types of radar beacons for radar tracking aid. These serve to extend the radar range and thus to furnish more data for position prediction purposes. There are many other future uses of radar beacons; some are discussed below.

Manned space ships may require radar on board to prevent collision with other craft, as well as with natural and artificial satellites. Should radar be carried for this purpose, it would then be essential that the radar be used to its full capability. The radar-beacon combination could provide an economical communication link between craft in space, as well as between craft and operating bases, thereby facilitating such functions as landing, navigation and rendezvous, through the employment of suitable command and guidance techniques.

## Preliminary Radar Performance Data on Passive Rocket-Borne Wind Sensors\*

NORMAN J. BEYERS†

**Summary**—Rocket vehicles are being used to expel passive wind sensors in the altitude range of 100,000 to 300,000 feet. The sensors are tracked with S-band and X-band radars to determine wind direction and velocity. Both chaff and metalized parachutes serve as wind sensors and AGC voltage recordings made on both X-band and S-band radars during tracking periods are presented. The recordings are calibrated in decibels above the radar minimum discernible signal and plotted vs slant range. A short discussion of the effects of chaff dispersion is included. Although chaff dispersion deteriorates the effectiveness of the target at a rate of about 20 db/hour, it is concluded that the effective radar target size of the sensors and the slant ranges over which they are employed are quite compatible when AN/MPQ-12 and AN/MPQ-18 radars are utilized.

### INTRODUCTION

AIR movement has been a primary concern to meteorologists and atmospheric physicists for many years. Equipment and techniques to measure horizontal surface winds were the first to be developed and applied and have been generally adequate. Included in these methods are: wind vanes, anemometers, aerovanes, strain gauges, and others. Winds above the surface are not so readily measured. Balloons have been the chief source of wind measurements between the surface and the maximum meteorological balloon altitude (about 100,000 feet). Generally, the balloon carries a target (active or pas-

sive) and is tracked by radiosonde or radar ground equipment. For wind measurements above balloon altitudes, rocket vehicles are being utilized, and both direct and indirect measuring techniques applied. Some of the rocket techniques involving grenades, smoke clouds, chaff, and parachutes are used to over 100 miles above the earth's surface. Optical, acoustic, and radar ground equipment provide the parameter recordings.

A particular type of meteorological rocket wind sensor system currently being utilized by this agency measures wind between 75,000 and 270,000 feet. Small meteorological rockets expel passive radar targets at desired altitudes and the wind velocity and direction are determined by tracking the targets with radar as they descend.

### TARGET TYPES

Several types of targets have been used in meteorological rockets in an effort to determine an optimum system. There are two parameters to be considered when choosing a target: radar reflectivity and response to wind flow. In this discussion two general target types, parachutes and chaff, will be considered and the interest will be limited to radar reflectivity. The fall rates of the sensors affect the response to the wind flow and are determinants for assignment of the altitude range over which they are used. Generally, parachutes are applied from 175,000 feet to the surface and the chaff is used from 270,000 to about 150,000 feet.

\* Manuscript received by the PGMIL, February 1, 1960.

† U. S. Army Signal Missile Support Agency, White Sands Missile Range, White Sands, N. M.

The chaff vehicle is the Loki II rocket which attains a maximum altitude of about 250,000 feet when fired from sea level and approximately 270,000 feet when fired from White Sands Missile Range, N. M. (4000 feet MSL). The Loki I carries an eight-foot parachute and is capable of 120,000 feet for sea-level launches and 140,000 feet when fired from WSMR. The ARCAS rocket has been developed to carry additional meteorological sensing equipment suspended on a fifteen-foot parachute to approximately 250,000 feet. The fall rate of the parachute at altitudes above 175,000 feet is excessive and corrections must be applied to determine accurate wind measurements.

Several types of chaff are available and have been used by this agency, including: ribbons of brass, copper, and aluminum foil, and Suchy chaff consisting of cylindrical dipoles of metalized nylon, varying in diameter from 0.0035 to 0.012 inch. All chaff was cut to half wavelength for S or X-band radar. The two-pound payload contains

between 1.5 and 2 million dipoles. Fig. 1 contains examples of both foil and Suchy chaff cut for S-band radar (10 cm). The scale is in inches. The eight and fifteen-foot parachutes have been of the canopy type and constructed of mylar or metalized silk or nylon for optimum radar reflectivity. The fifteen-foot ribbon-type mylar parachute pictured in Fig. 2 will be used in future instrumentation.

#### RADAR INSTRUMENTATION

The radar available during firings at WSMR have included both X-band and S-band tracking radars. In addition, the AN/FPS-16 instrumentation radar recently installed at WSMR is available and will be used for future tracking operations. Some of the general characteristics of the radars are listed in Table I. The Signal Missile Support Agency radar tracking facilities at "C" station are pictured in Figs. 3 and 4. There are five S-band and two X-band radars at the "C" station facility.

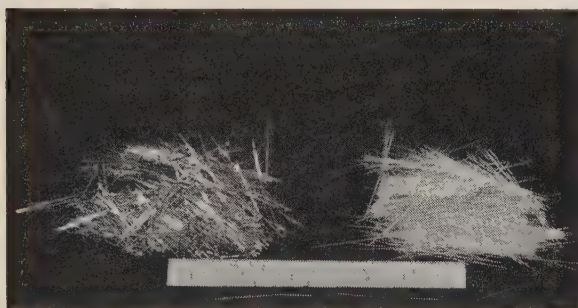


Fig. 1—Foil chaff (left) and Suchy chaff (right). Scale in inches.



Fig. 3—"C" station, White Sands Missile Range, N. M.

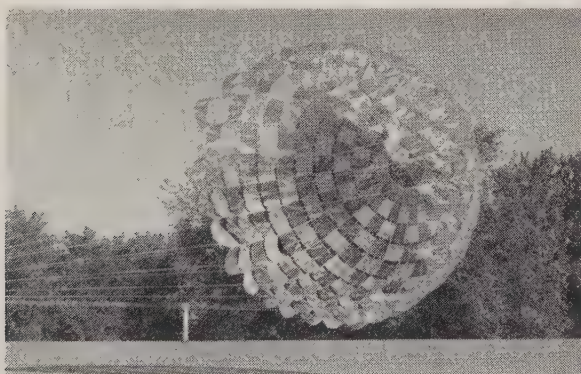


Fig. 2—Fifteen-foot-diameter ribbon-type mylar chute.



Fig. 4—AN/FPS-16 at White Sands Missile Range, N. M.

TABLE I  
WSMR RADAR CHARACTERISTICS

	X-Band System (9000 mc)	S-Band System (2700 mc)	C-Band System (5500 mc)
Type	AN/MPQ-12	AN/MPQ-12 & 18	AN/FPS-16
Antenna	8-foot parabolic	10-foot parabolic	12-foot parabolic
Beam width	0.9 degrees	2.5 degrees	1.1 degrees
Polarization	Vertical, horizontal and circular	Linear rotating and circular	Vertical, horizontal and circular
Peak power	200 kw	250-300 kw	1000 kw
Maximum range	400,000 yards	400,000 yards	400,000 yards
Tracking precision	Approx. $\pm 2$ mils and $\pm 40$ yards	Approx. $\pm 2$ mils and $\pm 40$ yards	$\pm 0.14$ mils and $\pm 15$ yards
PRF	Variable	Variable	Variable
Over-all sensitivity incl. antenna gain	-140 dbm	-140 dbm	-158 dbm



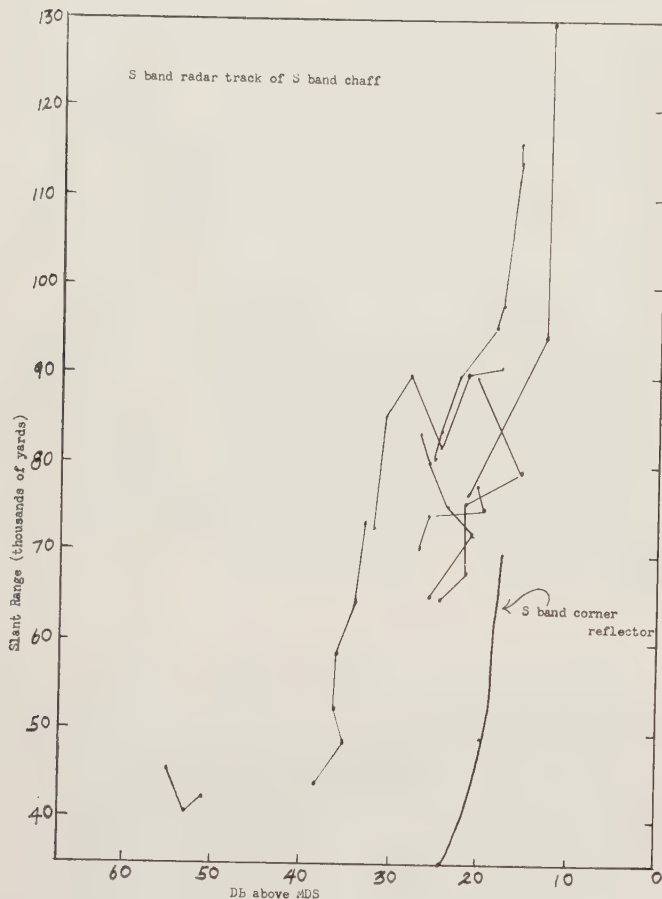


Fig. 5—Signal strength above MDS vs slant range of S-band chaff.

#### DISCUSSION AND CONCLUSIONS

Signal strength recordings have been obtained during chaff and parachute tracks in about 20 cases at WSMR. The recordings were in the form of continuous AGC voltages calibrated to decibels above the minimum discernible signal (MDS) and recorded simultaneously with the slant range in thousands of yards.

Eight cases are presented in Fig. 5. A plot based on a track of a corner reflector is included in Fig. 5 for comparative purposes. The corner reflector was a standard ML 307/ap aluminum foil reflector carried aloft by a 1200-gram balloon. The results of the dispersion of the chaff are apparent. Signal return is undoubtedly a function of the additional parameters, time and wind structure, as well as slant range. In order to approximate the effects of time and wind structure, the variation due to slant range was removed. This was accomplished by removing the variation with slant range attributable to a solid spherical target. It would be supposed that the signal level would always decrease with time, however in Fig. 6 some plots contain instances of the reverse. This phenomenon is attributed to a probable shift of the radar to a different "patch" of chaff in the target area, that is, one with a stronger return. Another possible explanation is a redistribution of the chaff so that a greater signal return was evidenced for a time. However, both of the above mechanisms which serve to enhance signal return should

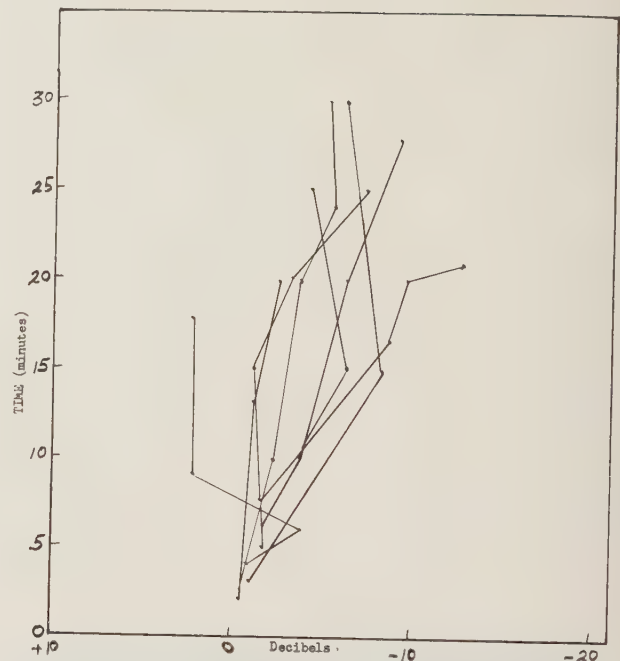


Fig. 6—Signal strength vs time after expulsion of chaff.

provide only temporary stimulus and generally the signal should and does deteriorate with time (range being constant).

The results of 4 X-band chaff tracks are presented in Fig. 7. For comparison an X-band track of a six-inch sphere carried aloft by balloon is included. The chaff in this figure was deployed by Loki I's in special tests. The chaff fall rate at Loki I altitudes (140,000 feet) is only about 300 feet/min, consequently, although the chaff tracks in Fig. 7 average about 25 minutes (the same as in Fig. 5), the total slant range variation is considerably less than shown in Fig. 5.

Parachute tracks are presented in graph form in Fig. 8. Four eight-foot chutes are included with a single fifteen-foot ARCAS parachute. All tracks were made with S-band radars. Again the corner reflector is presented for comparison.

Before drawing any conclusions from the data presented above, it might be well to point out some important factors. All of the data were gathered with standard radar under normal operating conditions. Hence, some variation in performance characteristics are to be expected and are evidenced in the data. Signal strength recordings were made of only one radar during an operation.

The first consideration is the effective target size presented by the wind sensor to the radar. From the results in Fig. 5 for chaff and the radar range equation [1] it appears that the chaff carried in a Loki provides an effective target of approximate 45 meters<sup>2</sup>. Similar results are evidenced for the X-band chaff in Fig. 7.

Of considerable interest is the variation in signal return with wavelength and polarization. Unfortunately there were no presentable recordings made, but there is definite evidence from observed signal return at the radar, that it is not necessary to match dipole and radar wavelength

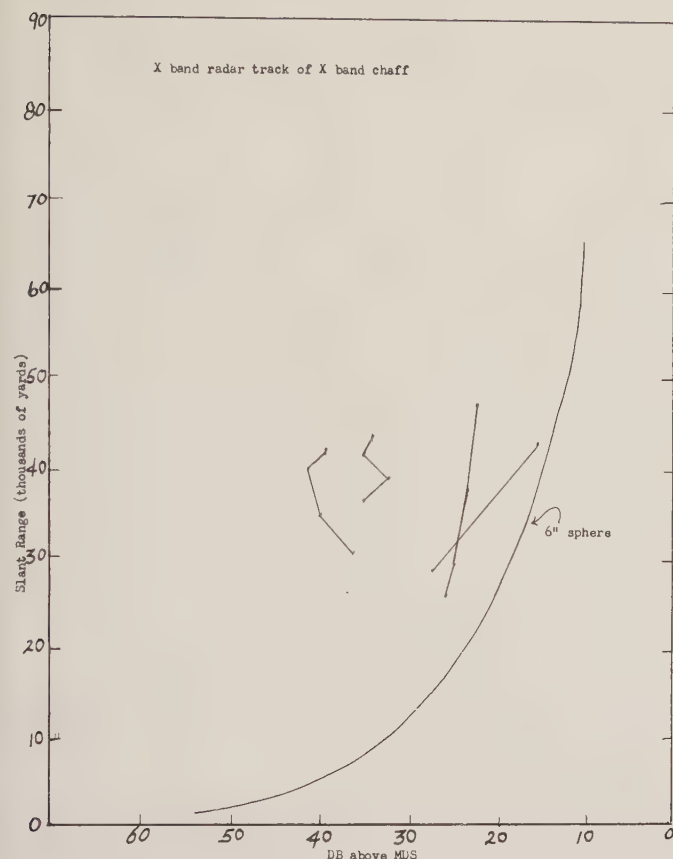


Fig. 7—Signal strength above MDS vs slant range of X-band chaff.

exactly. That is, X-band chaff can be tracked with S-band radar with only about a 10 per cent loss in signal return compared with S-band chaff signal return. Similar results were obtained with X-band radar and S-band chaff. Also, polarization appears interchangeable as similar signal strengths were observed on a single parcel of chaff whether circular, horizontal or vertical polarization was applied. It might be inferred then, that as it falls, the chaff is randomly oriented with respect to the radar.

An additional conclusion might be drawn about chaff targets from Fig. 6. Although a goodly variation exists, it appears that there is an average deterioration of target effectiveness at a rate of about 20 db/hour due to chaff dispersion.

The eight-foot parachutes in Fig. 8 indicate an effective target size of about 9 meters<sup>2</sup> and can be tracked to more than 100,000 yards slant range with the above radar. The single fifteen-foot ARCAS chute recording is approximately equivalent to the 45 meters<sup>2</sup> target size of the two-pound chaff target which gives adequate signal return to be tracked in excess of 150,000 yards.

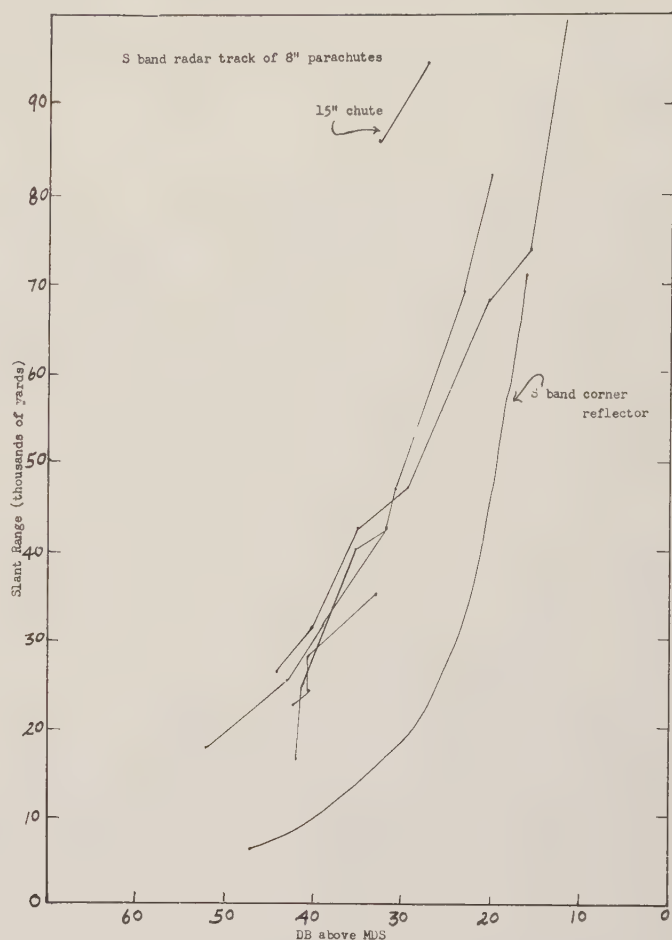


Fig. 8—Signal strength above MDS vs slant range of parachutes.

#### BIBLIOGRAPHY

- [1] D. E. Kerr, "Propagation of Short Radio Waves," McGraw-Hill Book Co., Inc., New York, N. Y., 1st ed., p. 470; 1951.
- [2] H. J. aufm Kampe, "Upper air-wind measurements with small rockets," *J. Meteorol.*, vol. 13, pp. 601-602; December, 1956.
- [3] W. W. Vaughn, "Use of Chaff to Determine Wind Velocity at Aircraft Altitudes," Air Force Armament Center, Eglin Air Force Base, Fla.; July, 1957.
- [4] D. E. Cline, "Rocket Beacon Wind-Sensing System," U. S. Army Signal Res. and Dev. Lab., Fort Monmouth, N. J., Engrg. Rept. E-1205; 1957.
- [5] K. R. Jenkins and W. L. Webb, "Rocket Wind Measurements," U. S. Army Signal Missile Support Agency, White Sands Missile Range, N. M., Tech. Memo 531; May, 1958.
- [6] K. R. Jenkins and W. L. Webb, "High-altitude wind measurements," *J. Meteorol.*, vol. 16, pp. 511-515; October, 1959.
- [7] W. L. Webb, and K. R. Jenkins, "Flight Testing of the ARCAS," U. S. Army Signal Missile Support Agency, White Sands Missile Range, N. M., Tech. Memo 544; June, 1958.
- [8] K. R. Jenkins, "Measurement of High Altitude Winds with Loki," U. S. Army Signal Missile Support Agency, White Sands Missile Range, N. M., Tech. Memo 544; June, 1958.
- [9] W. L. Webb and K. R. Jenkins, "Application of meteorological rocket systems," *J. Geophys. Res.*, vol. 11; November, 1955.



# Automatic Meteorological Data Collecting System\*

R. THOMAS† AND M. McLARDIE‡

**Summary**—The automatic data collecting system, as designed, permits automatic sensing and logging of 64 meteorological parameters measured on a 220-foot tower. The design permits simultaneous measurements of all parameters at all levels, with response of the instruments on the order of a few seconds. There is a resultant increase in data accuracy and acquisition, flexibility of observation periods, ease of maintenance and simplicity of operation. With those capabilities, studies requiring large volumes of data on a continuing basis are feasible with existing manpower.

## METEOROLOGICAL REQUIREMENTS FOR AUTOMATIC METEOROLOGICAL DATA COLLECTING SYSTEM

METEOROLOGICAL data are gathered at the Signal Missile Support Agency Missile Geophysics Research Tower, for research and development studies which are designed to improve missile impact prediction techniques and which support investigations of the microwave and infrared index of refraction. In addition, direct support of tactical missile firings and meteorological sounding rockets is furnished contractors and users on the Range. In many of the investigations an appreciable amount of accurate data must be collected in a form that permits ease of reduction, to attain results having statistical significance.

Conventional recording methods on chart systems introduce variable reading and recording errors and require considerable time and manpower to reduce the data. This report describes a system designed to sense and log automatically sixty-five different meteorological parameters as measured on a 220-foot steel tower.

The fundamental requirement was to design a system capable of simultaneous measurements of various meteorological data from high resolution instruments mounted on a 220-foot tower at White Sands Missile Range. Measurements of wind velocity in both the horizontal and vertical plane, differential temperatures, and relative humidity are taken from ten levels while pressure measurements are taken at the base, midpoint and top of the tower.

It was felt that simultaneous sampling of all parameters at all levels with boom spacing of 20 feet or less would provide more complete information about the micro changes taking place in the first several hundred feet of the atmosphere than would a step-sampling approach or logarithmic spacing. With this detailed a knowledge of the atmospheric structure, forces such as the horizontal wind affecting an unguided missile along the initial portion of its trajectory, can be determined more accurately.

With the automation of the SMSA Missile Geophysics Research Tower, it will be possible to collect 500,000–700,000 observations annually as compared with a meager 1040 from the old method of recording on chart systems. Data will be automatically recorded on tape for processing on a high-speed computer. Elimination of the time-consuming process of chart evaluation and manual tape punching reflects an approximate saving of 3900 manhours annually. (Manhour saving is based upon 1040 observations per annum.)

## A BLOCK DIAGRAM OF THE SYSTEM DESIGNED TO SOLVE THE RESEARCH PROBLEMS IS GIVEN IN FIG. 1

Sampled signals flow from the sensing elements in various forms to analog/digital converters. The converter outputs are in either minimum error binary coded decimal or ten-line decimal. The codes are routed by the digit and storage control to the proper translator, on a schedule determined by the program control panel. This schedule includes the insertion of computer program information between the data points, as required. The translator outputs are ultimately applied to a typewriter and tape punch in the code required by the computer. When the record is made an advance signal is generated, which allows the system to proceed to the next datum. Since the system is not clocked, it proceeds at the speed of the slowest element in the loop, which corresponds at present to about ten decimal digits per second.

The system accuracy and resolution are given for each parameter in Table I. Although not given quantitatively, the dynamic errors in the sensors are required to be as small as possible, consistent with a 98 per cent reliability figure. Insofar as possible, standards of calibration are certified by the National Bureau of Standards, and gauge makers tolerance is observed in the actual instrument calibrations.

## System and Component Response

The design of a system which converts continuous functions into digital form involves consideration of the sampling and quantizing theorems. Both theorems are essentially satisfied in the system as designed.

**System Sampling Rates:** System speed as related to rate of change of the variables is considered. The program control is capable of varying both the frequency of observations and the number of observations taken at any time. Hence, individual variables may be examined for high- and low-frequency components by proper setting of the sampling frequency, the number of samples to be taken at each observation, and the number of parameters to be sampled. Present sampling cycles are: continuous, 1 min-

\* Manuscript received by the PGMIL, February 1, 1960.

† Bendix Pacific Div. of Bendix Aviation Corp., Hollywood, Calif.

‡ U. S. Army Signal Missile Support Agency, White Sands Missile Range, N. M.

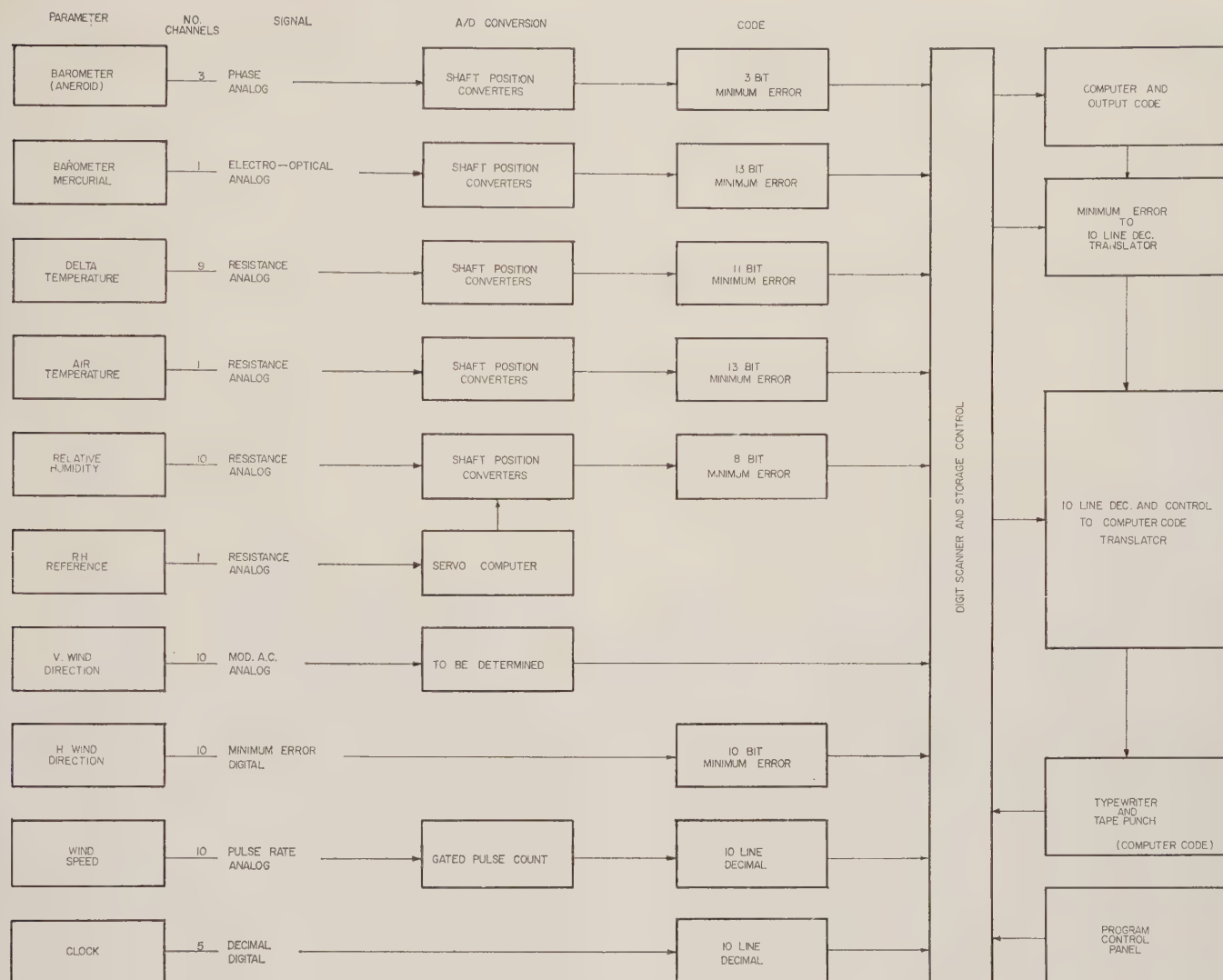


Fig. 1—Automatic data collecting system for the SMSA-MG research tower.

TABLE I

Function	Range	System Print Out	Sensor Standard Error of Measurement	Quantizing Error	Other Errors	Least Accuracy	RS Accuracy	Notes
Wind speed	0 to 99.9 mph	0.1 mph	0.14 mph	0.005 mph	0.02 mph	0.165 mph	0.14 mph	Assumes 0.005 second gate time error at approximately 75 mph
Wind direction	0°-360°	1°	1.5° max <sup>2</sup> 0° min	0.5° max	0	2° max 0° min	1.6° max 0° min	
Air temperature	-20°C to +55°C	0.2°C	0.04°C max	0.1°C	0.06°C	0.18°C	0.115°C	Is servo error
Differential temperature	-20°C to +20°C	0.2°C	0.02°C	0.1°C	0.02°C	0.14°C	0.102°C	Is servo error
Barometers reference	830 mb to 930 mb	0.1 mb	0.1 mb*	0.05 mb	0.003 mb*			
Tower	830 mb to 930 mb	0.2 mb	0.2 mb*	0.1 mb	0.07 mb*			Is servo error
Relative humidity				0.5 per cent				
15 per cent to 99 per cent	00 per cent to 99 per cent	1 per cent	1.5 per cent	0.5 per cent	0.1 per cent*	2.1 per cent	1.58 per cent	
4 per cent to 15 per cent			0.9 per cent <sup>1</sup>	0.5 per cent	0.1 per cent*	1.5 per cent	1.03 per cent	

\* Estimated pending final check.

<sup>1</sup> Mean of 0.4 per cent to 1.5 per cent.<sup>2</sup> Sensor and analog measurement equipment normally rated as 3°. Absence of analog equipment allows estimated 1.5° max. Sensor error, and 0° min.

ute, 5, 10, 30, or 60 minutes. Present recording periods are: 30 seconds, 2.5, 7.5, 15, or 30 minutes. Data frames may vary in length between 11 or 12 parameters and one.

**Sensing Element Sampling:** In general, the sensing elements are effectively sampled at rates considerably in excess of two times their highest frequency response. Hence no distortion of information occurs as a result of the ana-

log to digital conversion process. As an example, the temperature sensors have a standard frequency response of approximately 3 cycles per second, and are sampled at a rate of 120 per second.

**Wind instruments:** A difficulty arises in the case of the wind direction instruments since they have no defined fixed response "time."



The "response time" varies with the wind speed and magnitude of change, and, in general, becomes shorter as wind speed increases; therefore a "sampling rate," however defined, must be related to both wind speed and rate of change of direction. The digital converter used on the vane operates at the speed of the vane, regardless of speed, and hence meets the requirement of "sampling rate" and is related to both magnitudes. However, until a valid definition of "response time" becomes available, it will be difficult to apply conventional sampling theory to instruments of this type.

The wind speed instrument generates quanta at a rate which varies with wind speed. However, a "time constant" is defined which relates the time required to reach a new equilibrium value to the amount of change, and this can be evaluated at its highest frequency, *i.e.*, shortest period. The period is approximately 0.1 second with a step change from 0 to 30 mph. Under test conditions, this implies a rate of change in output frequency from 0 to 867.8 cps, or 8678 cps. The pulse count to digital converter can respond to a rate of 10 kc, and therefore can "sample" at a rate in excess of the highest frequency present in the sensor. The average "period" under all conditions is 0.5 second, which implies an average "frequency response" of less than 1000 cps, and the "sampling rate" of the digital converter is thus approximately 10 times that rate.

It is realized that the above application of the sampling theorem may be somewhat arbitrary, hence the terms "sample," "period," "frequency response," etc., have been enclosed in quotes.

*Rest of instruments:* The rest of the sensing elements are more conventional in characteristics, and are listed in Table II, with frequency response ( $f_0$ ) and sampling rates employed.

TABLE II

Sensor	$f_0$	Sampling Rate
Wind direction	No standard definition	Equal to speed of sensor response under all conditions
Wind speed	No standard definition, nominal 1000 cps	10,000 cps
Temperature (differential and absolute)	3 cps	120 cps
Barometric pressure	5 cps	120 cps
Relative humidity	3 cps	120 cps

*Quantizing:* The quantizing theorem is adequately considered. In general, quantizing width is not more than 0.01 of the range, and is usually less. The barometric unit, for example, quantizes to 0.0001. In effect, quantizing to a fineness represented by a minimum of seven binary digits and a maximum of thirteen digits is accomplished. Therefore statistical moments may be recovered with little or no error where the variables have an approximately normal

distribution, particularly if Sheppard's corrections are applied.

### Component and Subsystem Problems

*Relative Humidity:* The relative humidity measurements were required to be recorded directly as "RH" in the per cent. Plumbing was prohibited, so psychrometric methods were not usable. Electric sensing elements were considered on the basis of long-term stability, reproducibility, and sensitivity at values of 5 per cent RH. The instrument possessing these qualities is made with a partially hydrolyzed polyvinyl acetate film containing a small percentage of lithium chloride, and has a response characteristic which curves with absolute humidity and ambient temperature. In normal use, its output would be read by an observer, who would then look up correction factors in charts relating the ambient temperature, indicated value, and RH. In order to use the inherent accuracy and resolution of the sensing element, the digital system had to perform equivalent corrections.

The true digital nature of the system made several approaches possible, including a digital tabular "look up" system. However, the method selected consists of an essentially analog computation of the corrective values, and automatic application of the corrective values to the RH analog/digital converters. The resulting digital outputs are then per cent RH with all corrections included. Corrections for radiation errors are made unnecessary by special shielding.

The temperature correction data for the RH unit are derived from a radiation shielded Bendix-Pacific resistance thermometer. A standard error of 0.01°C and a maximum error of 0.03°C as determined by comparison with a certified standard are characteristic of these units. The temperature sensor was constructed to have a time constant equal to the RH sensors, and was extensively tested to confirm the design.

The actual curvature of the RH element response is derived from a separate element by a differential transformer servomechanism with a resolution of approximately 2 per cent or better.

The rotation of the output shafts of the servomechanisms, which are proportional to temperature and RH curvature, is used to drive a characterized potentiometer which generates the correction value for the RH sensor outputs. The net result is a direct indication of per cent RH at the output of analog/digital converters in the RH subsystem.

*Temperature and Pressure:* Temperature and pressure measurement problems were largely those of precision. Except for extreme refinement, construction is conventional and requires very little discussion.

*Radiation shielding:* Of interest is the use of radiation shielding in all cases where radiation might generate spurious temperature effects. The radiation shield consists of two concentric shields around the sensing element, a hat-shaped shield positioned above it, and a double shield

below which serves to protect against induced ground reflection and radiation. There are two precisely balanced forced aspiration paths, one through the sensor and the other between the thermally balanced primary shield and the first secondary shield. The shield has been tested under solar radiation intensity equivalent to twice that found on the Great Salt Lake Desert, and has been found to be very efficient. Under the test conditions, no measurable radiation error was observed in the temperature sensor output.

### Coding Methods

Analog-to-digital conversion is accomplished in two general ways: 1) shaft position converters are used to generate minimum error binary codes, and 2) pulse-count-to-digital converters are used to generate 10-line decimal codes. In order to avoid conversion between codes with different radix numbers, the binary codes are all radix 10, and are thus compatible with the decimal outputs.

*Shaft Position Encoders:* The binary code system used for encoding data is known as minimum error binary coded decimal. Each decimal character is coded by a combination of five binary digits in such arrangement that adjacent decimal numbers differ by only one binary digit. This code arrangement eliminates large "crossover" errors when the coder is advanced from one increment to the next.

An illustration of the natural "additive" binary code compared with a minimum error code shows that the largest coding error which can occur with the use of the minimum error code is plus or minus one number position. The natural binary code can have larger errors. (See Table III.) A well-known example of minimum error coding is known as the Gray Code.

TABLE III

Decimal Number	Natural Binary Code	Minimum Error Code
0	0 0 0 0	0 0 0 0
1	0 0 0 1	0 0 0 1
2	0 0 1 0	0 0 1 1
3	0 0 1 1	0 0 1 0
4	0 1 0 0	0 1 1 0
5	0 1 0 1	0 1 1 1
6	0 1 1 0	0 1 0 1
7	0 1 1 1	0 1 0 0
8	1 0 0 0	1 1 0 0
9	1 0 0 1	1 1 0 1
10	1 0 1 0	1 1 1 1
11	1 0 1 1	1 1 1 0
12	1 1 0 0	1 0 1 0
13	1 1 0 1	1 0 1 1
14	1 1 1 0	1 0 0 1
15	1 1 1 1	1 0 0 0

A typical error of this type can occur when moving from 7 to 8 in the natural code, where the decimal value 7 may be interpreted as a 15 simply by slight mechanical imperfection changing the left digit to a 1 before the other digits change. Notice that the left digit of the minimum error code is the only one which changes, and so no error can occur. This idea can be extended to the minimum error

binary coded decimal in such a way that no errors occur even on changing several digits of the decimal number such as from 19 to 20. An illustration of this code is shown (Table IV) in comparison to a typical natural code used in digital computers. It is seen that even when changing from 0.09 to 10 or from 19 to 20 that only one digit of the minimum error code system changes and no gross errors occur.

TABLE IV  
XS3 TO MINIMUM ERROR CODE COMPARISON

Decimal Number	Typical Binary Code (excess three)		Minimum Error Code	
	Tens Digit	Units Digit	Tens Digit	Units Digit
0 0	0 0 1 1	0 0 1 1	0 0 1 1	0 0 1 1
0 1	0 0 1 1	0 1 0 0	0 0 1 1	0 0 0 1
0 2	0 0 1 1	0 1 0 1	0 0 1 1	0 1 0 1
0 3	0 0 1 1	0 1 1 0	0 0 1 1	0 1 1 1
0 4	0 0 1 1	1 0 0 0	0 0 1 1	0 1 1 0
0 5	0 0 1 1	1 0 0 1	0 0 1 1	1 1 1 0
0 6	0 0 1 1	1 0 1 0	0 0 1 1	1 1 1 1
0 7	0 0 1 1	1 0 1 1	0 0 1 1	1 1 0 1
0 8	0 0 1 1	1 1 0 0	0 0 1 1	1 0 0 1
0 9	0 0 1 1	1 1 0 1	0 0 1 1	1 0 1 1
1 0	0 1 0 0	0 0 1 1	0 0 0 1	1 0 1 1
1 1	0 1 0 0	0 1 0 0	0 0 0 1	1 0 0 1
1 2	0 1 0 0	0 1 0 1	0 0 0 1	1 1 0 1
1 3	0 1 0 0	0 1 1 0	0 0 0 1	1 1 1 1
1 4	0 1 0 0	1 0 0 0	0 0 0 1	1 1 1 0
1 5	0 1 0 0	1 0 0 1	0 0 0 1	0 1 1 0
1 6	0 1 0 0	1 0 1 0	0 0 0 1	0 1 1 1
1 7	0 1 0 0	1 0 1 1	0 0 0 1	0 1 0 1
1 8	0 1 0 0	1 1 0 0	0 0 0 1	0 0 0 1
1 9	0 1 0 0	1 1 0 1	0 0 0 1	0 0 1 1
2 0	0 1 0 1	0 0 1 1	0 1 0 1	0 0 1 1
2 1	0 1 0 1	0 1 0 0	0 1 0 1	0 0 0 1

*Pulse Counters:* The wind speed and time coders are both pulse-count-to-digital converters, but different in their mode of operation.

*Time coder:* The clock time pulses are derived from the 60-cycle power line, in order to keep a correspondence between the system record time and other electrical clocks in the same area.

One-second pulses are generated by counting cycles with a synchronous motor. Each of the one-second pulses is applied to a decade scaler, which transfers a count to a quinary scaler every ten seconds. On the sixtieth decade scaler count, a one-minute counter is pulsed. This process is carried through, and a complete record in military notation of month, day, hour, minute and second is continuously available as a ten-line decimal code. This "calendar clock" is a variation of the standard Bendix-Pacific clock which is used with digital computers and other digital system.

When a record is to be made, the time code is stored and held until recorded, at which time the storage is cleared.

*Wind speed coder:* The wind speed coder is a gated pulse-count-to-digital converter.

The wind speed three-cup anemometer instrument generates pulses with a repetition rate linearly proportional to



wind speed, with a best straight line characteristic represented by

$$Vi = 0.627 + \frac{F}{29.547} \quad (1)$$

where

$Vi$  = indicated wind speed in miles per hour,  
 $F$  = repetition rate of output pulses, and  $F$  is gated for a time  $tg$ , where

$$\frac{q}{F} = tg, \quad (2)$$

in which

$q$  = number of quantum units required to indicate wind speed to one part in 10,000, which is

$Vi \times 100$ ; i.e.,  $q = Vi \times 100$ ,

$tg$  = time in seconds required to sum  $q$ .

The computer requires a calibration factor; therefore the system must maintain a simple, constant relationship between true wind speed  $Vt$  and indicated wind speed  $Vi$ .  $tg$  is calculated to provide the factor as follows:

$$Vt - Vi = K. \quad (3)$$

$K$ , evaluated at  $Vi = 0$ , is 0.627 and, therefore,

$$Vi = Vt - 0.627. \quad (4)$$

Substituting (4) in (2),

$$tg = \frac{100Vt - 62.7}{F}. \quad (5)$$

Eq. (5) gives a time gate value of 3.385 seconds, for a constant difference of 0.627 mph between  $Vi$  and  $Vt$  over the full range of the instrument.

The time gate control is derived from a 10-kc crystal-controlled source, and is adjustable in increments of 0.01 second. This implies an error of 0.005 second, which is equivalent approximately to 0.1 per cent of calibrated wind speed.

The value so obtained is available to the system as a ten-line decimal code. When a record is to be made, it is stored until read-out is accomplished.

**Code Translation:** The minimum error code exists in three forms in the system depending upon required resolutions, mechanical limitations, etc. In addition, ten-line decimal is generated. These codes must be converted to the specific computer or transmission system.

The translation is accomplished by providing a degenerate matrix which converts from 12 lines to a 6-bit binary code. Ten of the lines represent decimal values from 0 to 9 and the remaining lines are used to generate mechanical codes.

The minimum error codes are passed through a matrix which possesses a one-bit memory and which has a 12-line output. The output lines correspond to decimal values 0 to 9 plus control line. Codes of the variety described are inserted into the matrix at either the binary input terminals or the decimal input and the output is fed to the tape punch and typewriter.

## Rocket Sounding of High Atmosphere Meteorological Parameters\*

K. R. JENKINS†, W. L. WEBB†, AND G. Q. CLARK†

**Summary**—The need for systematic data collection pertaining to meteorological parameters in the high atmosphere has led to the development of several relatively economical meteorological rocket vehicles and uncomplicated rocket payloads. The progress toward an optimum system has been encouraging during the past two years, but the over-all state of the sensor development has lagged behind rocket performance. The complexity of the atmosphere in the area of interest indicates a need for extensive theoretical study in the application of sensors and corrective techniques applied to empirical data obtained during rocket flights.

The Signal Corps has been active in the development and testing of rocket vehicles and sensors as well as telemetry systems for recovery of the measured data. Over one hundred and fifty rounds have been fired at White Sands Missile Range in testing of hardware and techniques and in training personnel and perfecting launching techniques for application in a more comprehensive observations system.

The Loki meteorological sounding rocket has proven to be the first reliable vehicle to be used in large numbers. It can be fired under almost all conditions, but is restricted in payload to the simplest sensors. So far, only wind measurements have been made, using a small parachute below 150,000 feet and chaff above that level to 280,000 feet. The Arcas has considerably increased the capability of the system by providing telemetry for other sensors as payload on a 15-foot diameter parachute.

An effort toward the installation of a permanent synoptic meteorological rocket sounding network has been made with the initiation of a one-year series of soundings in October, 1959, and a planned schedule of daily firings for one month of each season during 1960. Rocket payloads compatible with the monetary and physical limitations of the initial series of soundings are discussed.

### INTRODUCTION

DURING the International Geophysical Year the dimensions of the earth's atmosphere were sounded on a scale which was made possible only by the advent of high-performance rocket vehicles. Earlier peri-

\* Manuscript received by the PGMIL, February 1, 1960.

† U. S. Army Signal Missile Support Agency, White Sands Missile Range, N. M.

odic soundings had been made at White Sands Missile Range, N.M., utilizing captured V-2 rockets and other modifications of tactical missiles. This led the way to the greater application of rockets to high-altitude soundings during the world-wide geophysical experiments of 1957 and 1958. With the launching of artificial earth satellites, a gigantic step was made in the technique of evaluating the gaseous envelope that encircles the planet Earth; but in achieving this feat, a significant portion of the atmosphere was by-passed. Balloon techniques and telemetry links have been successfully applied to sounding the atmosphere to nearly twenty miles altitude, but only very expensive and complicated balloon soundings have furnished data at altitudes approaching thirty miles above the earth's surface. The lowest efficient orbital threshold for artificial satellites is approximately 200 miles above the earth's surface, and atmospheric density at that altitude, while insignificant to earthbound man, dooms the satellite to a short existence. Limitations imposed on the balloon sounding techniques by the thin air of the high atmosphere and by the intolerable drag exerted by the same atmosphere on satellite vehicles have outlined a zone which can be sounded only by indirect methods or by the application of rocket vehicles equipped with fast-response sensors. The zone can be stated, roughly, as extending from twenty miles to two hundred miles above the earth's surface.

World War II provided impetus to the advancement of the meteorological science in the form of a great influx of talented scientific personnel and in the tremendous impact of demands for data to higher altitudes. The period since World War II has been marked by several major advances in technical areas involving the earth's atmosphere. Nuclear explosions at high altitudes, radioactive fallout, atmospheric re-entry and exit problems on long-range ballistic missiles, wind effects on ballistic trajectories within the atmosphere, artificial satellite orbits, high-performance aircraft, electromagnetic and acoustic propagation, and other major demands for geophysical data have established a requirement for an extensive exploration of the entire gaseous envelope of the earth's atmosphere.

Preliminary soundings have indicated significant spatial and time variability. Atmospheric tides, wind speeds measured in hundreds of miles per hour, severe ionospheric disturbances, magnetic field perturbations, and many other geophysical phenomena already detected have served to point out the instability of the tenuous outer reaches of the atmosphere.

The classical technique of measurement is to expose a sensor in the medium to be measured for an adequate period of time to obtain approximate equilibrium with the medium. The nature of the high atmosphere presents a great challenge because stable platforms for measurement cannot be employed. More elegant approaches involving the use of fast response sensors are currently under development and may serve to overcome the low density problem. In general, these sensors measure quali-

ties of the atmosphere which will provide an indirect method of obtaining the more commonly sought parameters, such as temperature and density. In the region below fifty miles above the earth's surface, very light sensors, such as chaff, provide an indication of wind speed and direction and direction and density values. The use of parachutes or inflated spheres seems limited to the atmosphere below forty miles altitude, because of rate of fall and problems of deployment.

The nature of the atmosphere changes markedly with altitude, and limits and definitions applicable at sea level no longer apply. Extensive research will be required to evolve proper corrective values for measurement made in the atmosphere where the mean free path of molecules is greater than the sensor dimensions. Radiational and isolation problems are significant and cannot be resolved without application of much theoretical work to the empirical data currently being obtained.

#### U. S. ARMY SIGNAL CORPS PARTICIPATION IN ROCKET EXPLORATION

The U. S. Army Signal Corps has the responsibility for furnishing meteorological research and development support to U. S. Army Research and Development projects. The Signal Corps history in meteorology goes back to the pretelegraph days and the period of the opening of the Western United States. The weather has long been recognized as a significant factor in military strategy, and since man has shed his earthbound existence the nature of the atmosphere has been accorded its rightful place in the military planning.

The Signal Corps participation in sounding rocket research ties in the application of electronic telemetry components and ground recording systems, the effect of the atmosphere on ballistic trajectories, the use of the rocket as a vehicle for sounding atmospheric parameters which are needed for proper evaluation of electromagnetic and acoustic propagation, for the furtherance of the science of military meteorology, and for an understanding of the energy transfer processes which provide for the flow of heat to the earth and make life possible.

The role of the Signal Corps in International Geophysical Year [1] proceedings and in the instrumentation of many of the artificial satellites has been recognized, but recently a more extensive use of the rocket vehicle technique has been promulgated and set in motion. Dr. Hans aufm Kampe [2] of Signal Research and Development Laboratory, Fort Monmouth, N.J., was an early pioneer in the application of chaff and the Loki rocket to meteorological research. In 1957, the Signal Missile Support Agency at White Sands Missile Range, N.M., embarked on an extensive program of developing a meteorological rocket capability which could be of extreme value to all the military services. The work consisted of training crewmen in rocket launching techniques, ballistic studies, rocket payload development and testing, application of



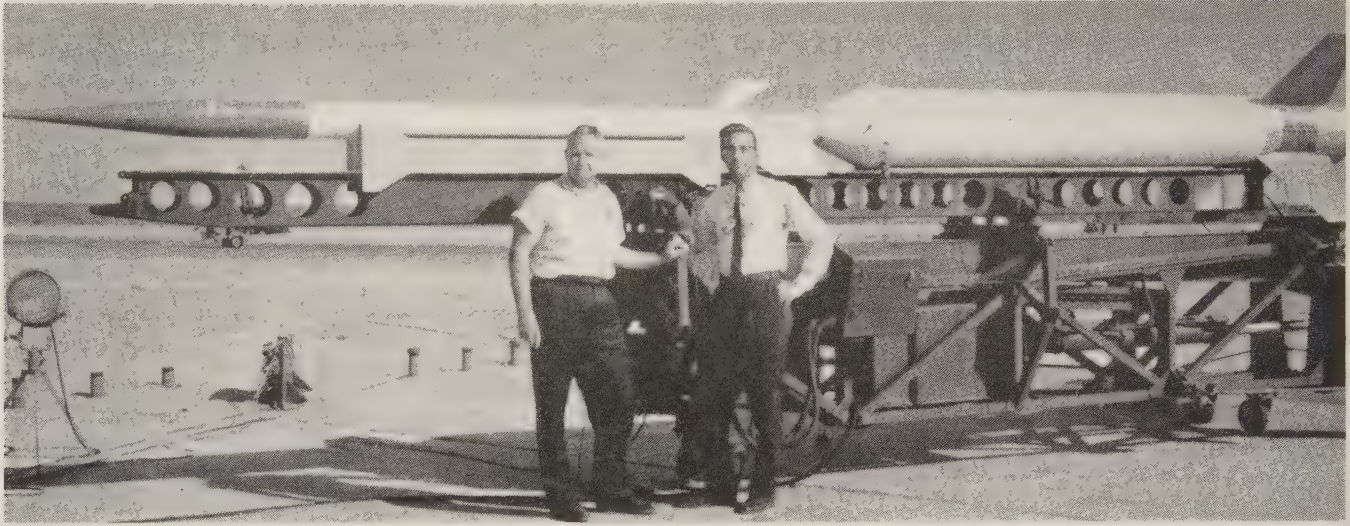


Fig. 1—Nike Cajun research rocket which reached an altitude of 121 miles.

existing meteorological vehicles[3], research in new sensor techniques, and planning rocket launching facilities. By mid-1959, the White Sands Missile Range Agency had launched more than one hundred and fifty sounding rockets consisting of seven types of vehicles and had attained data to 121 miles above the earth's surface (Fig. 1). Many tactical rockets of relatively long range had been provided direct support by the furnishing of wind speed and direction data to fifty miles altitude[4].

#### THE METEOROLOGICAL ROCKET SOUNDING NETWORK

For several years, the need for a synoptic meteorological rocket network has been stated by military and civilian scientists. The results of International Geophysical Year firings and subsequent sounding rocket experiments by the military services verified the need for an extensive program of soundings at several launch sites. Selection of launch sites for a six-station meteorological rocket network has been made, governed by availability of ground support equipment. The launch sites selected for the initial network consist of Fort Churchill, Canada; Fort Greely, Alaska; Point Mugu, Calif.; Wallops Island, Va.; Eglin Air Force Base, Fla.; and Cape Canaveral, Fla. The operating agencies consist of the U. S. Army Signal Corps, U. S. Air Force, U. S. Navy, and the National Aeronautics and Space Agency. A test program currently underway calls for daily firings at each of the sites for one month during each of the seasons.

A major portion of the data will be obtained by use of the Loki and the Arcas meteorological rockets. The Loki has been in use for several years and has proved to be quite reliable and is relatively easy to fire. It is particularly useful because it is insensitive to meteorological conditions, and can be fired under almost all situations. The Loki is limited in payload space and weight and has thus far been limited to measurement of wind. The Arcas has only recently been applied operationally and its reliability is not yet established. It has an adequate payload weight and

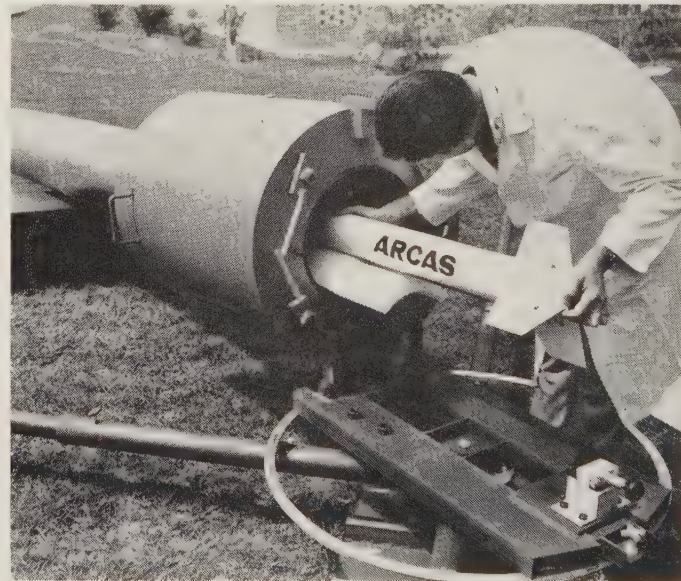


Fig. 2—An Arcas rocket and its launcher.

volume for most meteorological experiments, but is limited in the wind conditions under which it can be fired. Fig. 2 is a photograph of an Arcas rocket and its launcher.

#### SENSING SYSTEMS

##### *Active Telemetry Techniques*

The requirement for economical rocket payload components resulted in various modifications of the AN/AMT-4 transmitter, which is the standard balloon-borne radiosonde telemetry link utilized in routine weather observations. The AN/AMT-4 operates nominally at 1680 megacycles in its normal modulating mode. The use of the AN/AMT-4 makes possible the use of existing GMD-1 ground support equipment for tracking the payload and recording meteorological data. The most common modification to the transmitter lies in the replacement of the standard temperature-sensing resistor with a tiny bead

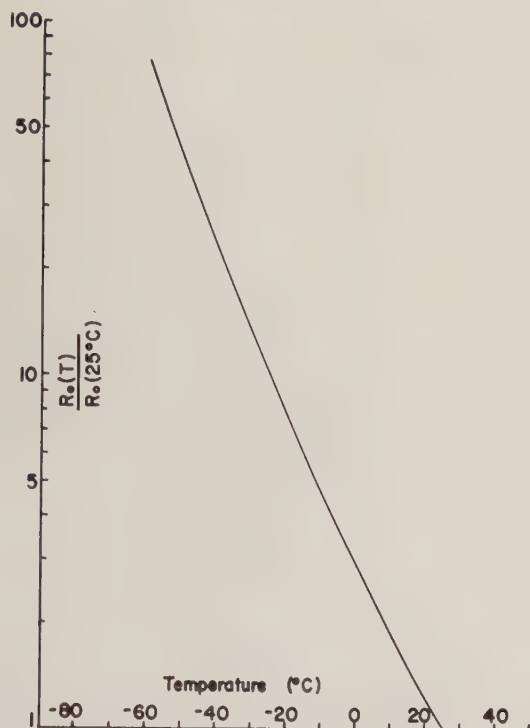


Fig. 3—Temperature resistance characteristics of the VECO 43A6 thermistor.

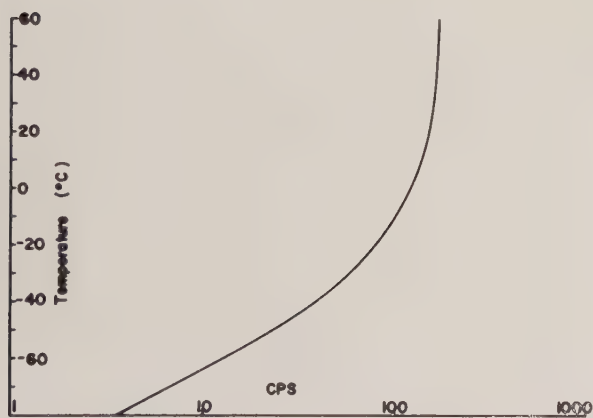


Fig. 4—Ambient temperature modulation repetition rate for the AN/AMT-4 with the VECO 43A6 thermistor.

thermistor to provide fast response to temperature changes at the high fall rates experienced above 20 miles altitude. One application of the temperature sensor consists of a VECO model 43A6 bead thermistor. It has a nominal resistance of 30,000 ohms at 25°C and is characterized by a negative temperature coefficient (Fig. 3) of 4.1 per cent/°C at 25°C. The leads of the thermistor are composed of  $\frac{1}{4}$ -inch lengths of one mil platinum-iridium wire which extend from opposite sides of a 10-mil bead composed of a ceramic-like semiconductor coated with glass on which is deposited a thin aluminum film. A dissipation constant of 0.09 milliwatt/°C at 25°C is obtained on application of a sensing current, and a thermal time constant of 0.5 second is available at sea level. A plot

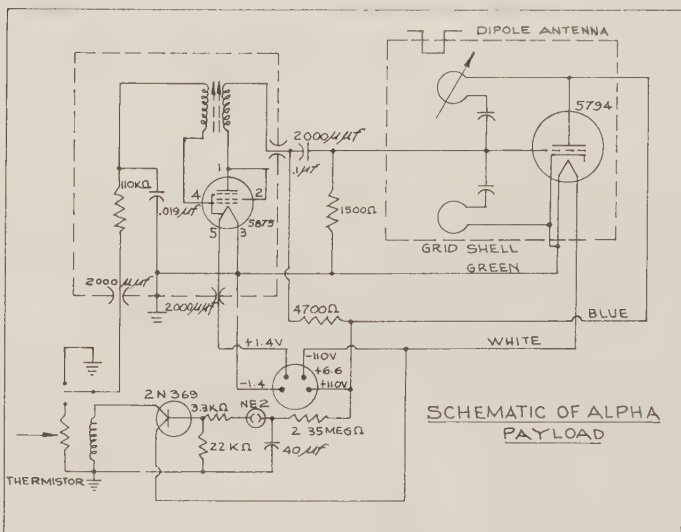


Fig. 5—Circuit diagram of the AN/AMT-4 with the thermistor and reference switching circuit.

of ambient temperature vs modulation repetition rate of the AN/AMT-4 is presented in Fig. 4. The power supply must be compatible with weight and space limitations, and must be relatively economical and long-lived to provide adequate power for the two-hour period of descent by parachute.

Fig. 5 is a schematic diagram of one of the circuits used to determine temperature. The 5794 and 5875 tubes and their associated components comprise the standard AN/AMT-4 transmitter which consists of a blocking oscillator which amplitude modulates the cavity-tuned 5794. In this case, the AM is in excess of 100 per cent since the negative going pulses from the blocking oscillator are of a magnitude great enough to cut off the 5794 when coupled to the grid. The intelligence to be transmitted is then imposed upon the repetition rate of the blocking oscillator. The repetition rate of the blocking oscillator may be described by the following equation:

$$t = \tau + RC \ln \frac{E}{-E_0} \quad (1)$$

where

$t$  = time between pulses

$\tau$  = time of conduction of B. O.

$R$  = resistance in grid circuit of B. O.

$C$  = capacitance in grid circuit of B. O.

$E$  = potential across the capacitor at instant of blocking

$E_0$  = potential across the capacitor at instant B. O. tube begins conduction.

For a given circuit  $\tau$  is a constant and is predominantly determined by the characteristics of the B. O. transformer.

From (1) it can be seen that the most direct method of varying the pulse repetition rate of the B. O. is by varying either  $R$  or  $C$ . Since

$$\frac{\partial t}{\partial R} = C \ln \frac{E}{-E_0} \quad (2)$$



and if  $E$ ,  $E_0$ , and  $C$  are constants, then the period will be a linear function of  $R$ . It is a relatively simple matter to make  $R$  a function of temperature; therefore, the repetition rate of the blocking oscillator becomes a function of temperature. This purpose is accomplished by inserting a thermistor of suitable characteristics into the grid circuit of the blocking oscillator. The thermistor used is a VECO 43A6. This thermistor has a negative temperature coefficient of resistance, as can be seen in Fig. 3. It is also apparent, from the same figure, that

$$\ln \frac{R_T}{R_0} \approx K \quad \text{where} \quad R_0 = R_{25^\circ\text{C}}. \quad (3)$$

If equality is assumed, then:

$$R_T = R_0 e^{-KT} \quad (4)$$

and

$$\left( \frac{\partial t}{\partial R} \right) \left( \frac{\partial R}{\partial T} \right) = -KC \ln \frac{E}{-E_0} e^{-KT} R_0. \quad (5)$$

Again, if  $C$ ,  $E$ , and  $E_0$  are constants, it follows that where

$$\frac{\partial t}{\partial T} = A e^{-KT},$$

$$A = -KR_0 C \ln \frac{E}{-E_0}.$$

As the temperature decreases,

$$\frac{\partial t}{\partial T} \rightarrow \text{constant}.$$

The thermistor used is chosen so that resultant plots are essentially linear in the range of temperatures of most interest.

In order to ascertain any change of circuit parameters which might be reflected in a change of repetition rate, a switching circuit has been added which periodically short-circuits across the thermistor to ground. This switching is accomplished by placing a relay in the emitter-collector circuit of a  $p-n-p$  transistor. The transistor is normally conducting, thereby maintaining the relay in the activated condition. The base circuit is connected through a neon bulb to a capacitor which is charged towards  $B+$  potential through a resistor. When the capacitor reaches a high enough potential, the neon bulb fires and applies the potential of the capacitor, less the voltage drop across the bulb, to the base of the transistor. This back bias is sufficient to terminate current flow in the collector circuit, thereby causing the relay to switch. As soon as enough charge has leaked from the capacitor to extinguish the neon bulb, the transistor resumes conduction, and the relay is again in the activated condition. The repetition rate of the switching cycle may be controlled by the value of the resistor through which the capacitor is charged.

The receiving system is the standard GMD-1 which consists of an automatic tracking antenna system, receiver,

pulse discriminator, and chart recorder. The received pulses are discriminated and the resulting dc level drives the recorder. When properly calibrated, the recorder yields a plot of temperatures vs time. This plot may be correlated with predicted trajectory, azimuth and elevation information from the GMD-1 tracking equipment, or radar trajectory data, to yield a plot of temperature vs altitude.

### Passive Sensing Systems

The application of passive tracking of radar reflective materials transported to high altitudes by rocket vehicles has proven to be a reliable technique for obtaining wind speed and direction at altitudes in excess of those obtainable by balloon methods. The targets may consist of millions of dipoles which present optimum radar reflectivity in the S-band, X-band, or L-band ranges. This payload is classic in its simplicity, but dispersion with time is a distinct disadvantage. A second technique consists of an inflatable sphere bearing a corner reflector within the balloon envelope. This system presents a point source radar target, but the chemically induced inflation technique is complex.

A third application in use consists of a metallic coated mylar or nylon parachute. The parachute method presents an excellent radar target, but parachute deployment problems increase drastically with altitude. Above fifty miles the atmospheric density results in excessive fall rates[5] which render wind speed and direction data obtained by any of these techniques doubtful (Fig. 6).

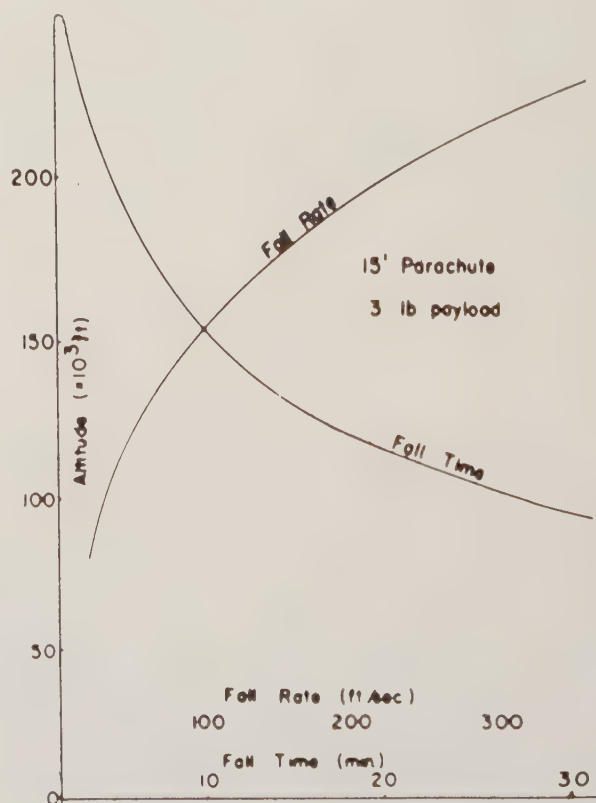


Fig. 6—Fall rate of the Arcas 15-foot parachute with a 3-pound payload.

## CONCLUSION

Techniques and rocket vehicles capable of attaining fairly accurate and economical meteorological measurements to altitudes up to fifty miles above the earth's surface are currently in existence. The use of standard balloon-borne electronic telemetry systems with only minor modifications has proved feasible in the new meteorological rockets. Certain special requirements, such as space and weight minimization, have led to experimentation with new telemetry and sensing techniques. Measurements made at higher altitudes require a more elegant approach. Many parameters must await the development of adequate sensors. The need for extensive exploration of the high atmosphere has been more clearly defined with the launching

of long-range ballistic missiles and artificial satellites, and the increased recognition of the effects of the earth's atmosphere on the progress of mankind.

## BIBLIOGRAPHY

- [1] W. G. Stroud, "Meteorological rocket soundings in the Arctic," *Jet Propulsion*, vol. 28, pp. 817-822; December, 1958.
- [2] H. J. aufm Kampe, "Upper air wind measurements with small rockets," *J. Meteorol.*, vol. 13, pp. 601-602; December, 1956.
- [3] W. L. Webb, K. R. Jenkins, and G. Q. Clark, "Flight Testing of the Arcas," U. S. Army Signal Missile Support Agency, White Sands Missile Range, N. M., Tech. Memo. 623; 1959.
- [4] K. R. Jenkins and W. L. Webb, "Rocket Wind Measurements," U. S. Army Signal Missile Support Agency, White Sands Missile Range, N. M., Tech. Memo. 531; 1958.
- [5] D. E. Cline, "Rocket Beacon Wind Sensing System," U. S. Army Signal Res. and Dev. Lab., Ft. Monmouth, N. J., Engrg. Rept. E-1205; 1957.

## Automatic Rocket Impact Predictor\*

LOUIS D. DUNCAN†

**Summary**—The ARIP was designed to improve rocket impact predictions. Previous procedures involved lag time in wind measuring which could not be fully accounted for in an x-time firing decision. This lag time assumes an importance in direct proportion to the magnitude of the wind weighting factors, which with some free flight rockets could be as large as 50 per cent of the total wind effect.

Five Aerovane anemometer sensors distributed in the first 100-foot layer provide the data via mechanical and electronic coupling to a computer which has been preset for the ballistic values of a particular rocket. The computer output then activates an X-Y plotter which has been previously zeroed for all other cumulative displacement effects.

## INTRODUCTION

UNGUIDED sounding rockets such as the Arcas, Asp, and Aerobee are used to carry instrumentation to high altitudes for atmospheric research. The trajectory and impact of such a rocket are functions of the wind encountered during flight and the launcher positioning.

Wind weighting factors and launcher tilt displacement are determined from theoretical calculations. Wind measurements are made periodically before the launching to establish a trend for the basis of an impact prediction. Pilot balloon ascents are made at frequent intervals to provide timely wind data for the first 1500 to 2000 feet. Radiosonde balloons are used to provide wind data above this level. There are several reasons why this method is unsatisfactory: 1) the time required to compute wind displacement from balloon data; 2) the time variability of the lower winds; and 3) range safety requirements, etc.

Rockets such as the Arcas and Asp experience approximately 40 to 50 per cent of their total wind effect in the first 100 feet of the trajectory. A large error in the impact prediction can occur since it is difficult to predict winds in this layer.<sup>1</sup> The Automatic Rocket Impact Predictor was designed to compute continuously the displacement caused by winds in the first 100 feet of the trajectory, thereby reducing the impact prediction error.

## DEVELOPMENT

During the theoretical evaluation and flight testing of the Arcas,<sup>2</sup> it was found that the rocket experienced 47 per cent of its total wind effect during the first 100 feet of flight. It was felt that a method should be developed to determine the displacement of the rocket due to the wind in this layer which would consider the wind variability.

A method was developed which consisted of a protractor, a wind weighting scale, and chart recordings of wind speed and direction from an anemometer positioned near the launch site. To determine the indicated change in the impact point due to a change in the wind vector, the impact

<sup>1</sup>R. Helvey, L. Traylor, and M. McLardie, "Low Level Wind Profiles," Missile Geophysics Division, U. S. Army Signal Missile Support Agency, White Sands Missile Range, N. M., Progress Rept. No. 1; June, 1959.

<sup>2</sup>W. L. Webb, K. R. Jenkins, and G. Q. Clark, "Flight Test of the Arcas," Missile Geophysics Division, U. S. Army Signal Missile Support Agency, White Sands Missile Range, N. M., Tech. Memo. 623; May, 1959.

\* Manuscript received by the PGMIL, February 1, 1960.

† U. S. Army Signal Missile Support Agency, White Sands Missile Range, N. M.



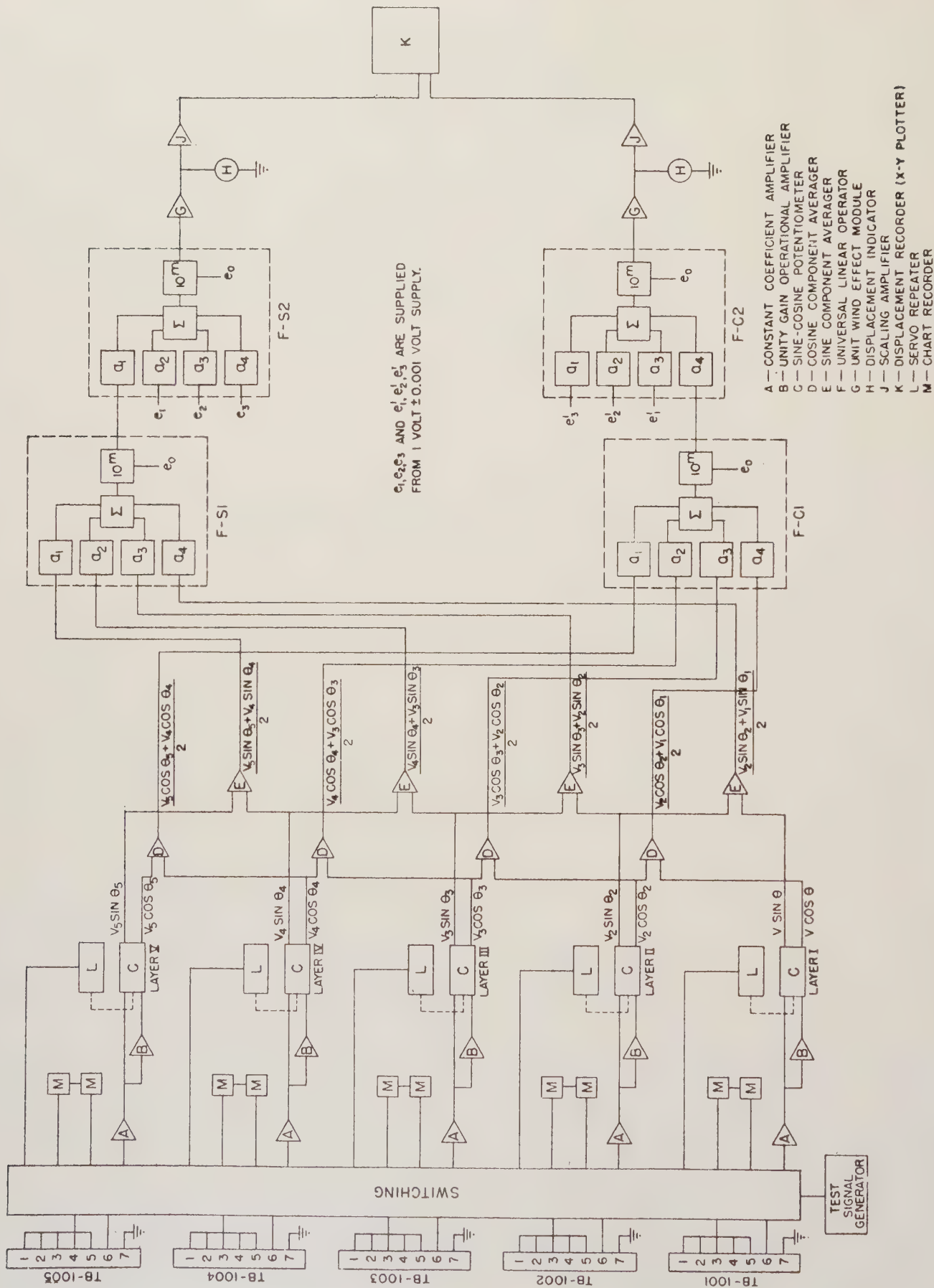


Fig. 1.

predictor (a meteorologist or ballistician) took a visual observation of the record charts and applied this change on a range map by using the protractor and wind weighting scale. This method proved inadequate because of the human factor and the limiting accuracy of the equipment. It was decided that a special-purpose analog computer would perform this function more reliably.

#### CONSTRUCTION AND FUNCTION

The present ARIP consists of five Aerovane anemometers mounted at specific points on a 100-foot tower positioned near the launch site, a special-purpose analog computer, and an X-Y plotter which is capable of writing on a range map. The computer is a purely electromechanical system which consists primarily of sine-cosine potentiometers positioned by servo transmitters in each wind-sensing instrument (anemometer) and universal linear operators.

The ARIP acquires wind data or simulation thereof in the form of wind speed (dc voltage analog) and direction (servo shaft rotation position) from Bendix-Friez Aerovanes. These wind data are also recorded on Esterline-Angus twin flush graphic wind speed and wind direction recorders having synchronous and electric phantom chart drives.

Through appropriate electronic circuitry (Fig. 1) the wind data are converted into wind components. Corresponding wind components for each two successive levels are then averaged and multiplied by predetermined wind weighting factors which have been set into the computer by appropriate electronic voltage dividing circuitry. These displacement values are indicated both on visual meters and on the X-Y plotter. The plotter has been zero positioned for displacement caused by all factors other than the wind in this layer; hence, the impact of the rocket is indicated instantaneously on the range map.

## The Satellite Vanguard II: Cloud Cover Experiment\*

R. A. HANEL<sup>†</sup>, J. LICHT<sup>†</sup>, W. NORDBERG<sup>†</sup>,  
R. A. STAMPFL<sup>†</sup>, AND W. G. STROUD<sup>†</sup>

**Summary**—This paper contains a summary of the launch and performance of the first meteorological satellite, Vanguard II. A brief description of its instrumentation is given.

#### INTRODUCTION

A SATELLITE vehicle is ideally suited for visual observation of the earth and the detection of its radiation. Meteorology depends on a world-wide station and reporting network which is incomplete over large ocean areas and inaccessible land masses. A recent publication [1] states, *e.g.*, that no weather reports are received from an 800-mile-diameter area north of Hawaii and also from similar regions in the Atlantic, Arctic and Antarctic. Over quite extensive areas of the globe, the station density is so low that only the most cryptic weather information is available. This state of affairs had been recognized at an early time in the U. S. IGY satellite planning and it was decided to conduct the Cloud Cover Experiment within the Vanguard program as a forerunner to

more sophisticated meteorological satellites. The instrumentation for the standard sphere-type Vanguard satellite was designed by a team of physicists and engineers at the U. S. Army Signal R & D Laboratory.

#### SATELLITE ORBIT

Similar to the Nipkow principle of the early days of television, the satellite spin was supposed to provide the time sweep and its continuous flight path to produce advancement of the individual lines. Mounted on the satellite sphere were two optics whose axis made a 45-degree angle with the spin axis. At times when the spin axis pointed to the earth's center one optic would sweep a circle of the earth's surface, and when the spin axis was parallel to the earth's surface the two optics would alternately sweep a figure determined by the intersection of a cone and a sphere. In intermediate positions, a continuous transition from the circle to the latter pattern were to occur. Immediately following launch the spin axis was supposed to lie in the orbital plane. Due to the equatorial bulge of the earth, this plane slowly drifts causing the spin axis to move out of the orbital plane. Bandwidth considerations demanded that the satellite had spun at approximately 30 rpm.

\* Manuscript received by the PG MIL, February 1, 1960.

<sup>†</sup> National Aeronautics and Space Administration, Washington, D. C.



## INSTRUMENTATION

Lead-sulfide detectors in the one-degree field of view optic converted the reflected sunlight which was allowed to pass through a 0.7 to 0.8 micron filter into electrical signals. The detectors were excited by a 290-cps oscillator in an unbalanced bridge network. Circuitry and levels were designed so that equal intensities on both optics generated half of the maximum subcarrier signal; illumination on one optic increased this signal, while illumination on the other one decreased it.

The geometry of the optics on the satellite was such that at no time did both optics view the earth simultaneously. The composite signal was then recorded on a small endless-loop tape recorder. The record circuitry and 0.3-ips tape speed were chosen consistent with the low oscillator frequency.

Light intensities on the un-illuminated side of the earth are too small to be detected by this instrument, and for this reason all unnecessary power consumption was turned off when solar cells imbedded in the optics detected insufficient light levels. The recorder could record for 50 minutes. When the satellite passed over a readout station, a coded signal was transmitted and the interrogation receiver turned on a playback motor and a 108-mc 1-watt transmitter.

The playback speed was 50 times faster so that the message from one orbit could be read out in one minute. The subcarrier whose spectrum was shaped for vestigial side-band operation in the playback amplifier modulated the plate of the output tube to approximately 50 per cent of the crystal-controlled transmitter.

A separate 10-milliwatt tracking oscillator provided the necessary position information. The use of a temperature-sensitive crystal permitted the measurement of the satellite's temperature. These RF sources and the command receiver input were connected through suitable wave traps and a hybrid to a common turnstile antenna.

Although the complete satellite weighed 21.5 pounds, the instruments including batteries was only 8 pounds. Weight limitation did not permit the addition of precession dampers. The moments of inertia were approximately equal in the direction of the symmetry axis and the antenna plane. A photograph of the satellite (Fig. 1) shows the top shell removed. The upper optic is visible pointing towards the operator. The instrument and batteries are located in the cylindrical portion. The antennas are not shown in this picture.

The tape recorder with the endless-loop cartridge located underneath the three horizontal rollers is shown in Fig. 2. Record and playback motor are the two vertical cylinders, drive-capstan, record- and playback-head can be recognized also. Two electronic boards containing low-frequency electronics and the transmitter are depicted in Figs. 3 and 4.

The ground stations were equipped with 22-db gain antennas trainable over 60 degrees. These antennas drove

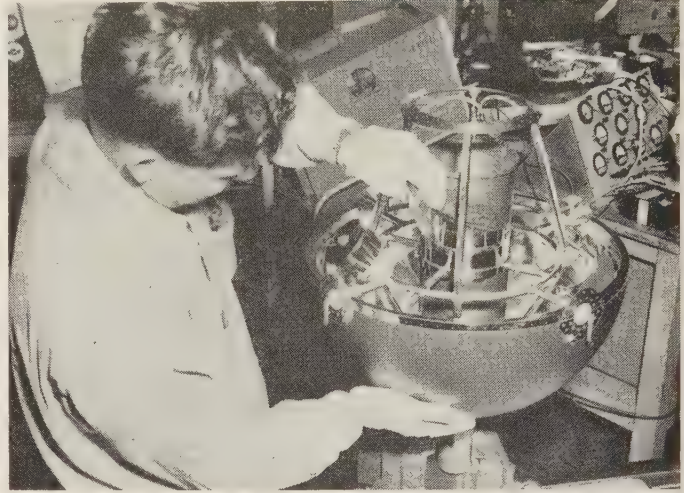


Fig. 1—Cloud cover satellite top shell removed.



Fig. 2—Vanguard II endless-loop tape recorder.

3-db noise-figure receivers whose output was recorded on instrumentation-quality magnetic tape recorders.

## LAUNCH SEQUENCE AND OPERATION

On February 17, 1959, the Vanguard rocket SLV-4 placed this instrument in an elliptic orbit (perigee approximately 350 miles; apogee 2000 miles). The satellite was mounted on the solid-propellant third stage through a low-friction bearing. Thus, the high spin of the rocket was transmitted to the sphere. During the long burning and coast period, too much spin was transferred to the satellite so that compressed air was released through nozzles to counter-rotate the sphere for correct spin prior to its separation from the third stage.

On SLV-4 the third-stage burning was very rough, presumably causing initial precession of the spinning third-stage satellite combination. Spin reduction by counter-rotating the satellite with the third stage still attached

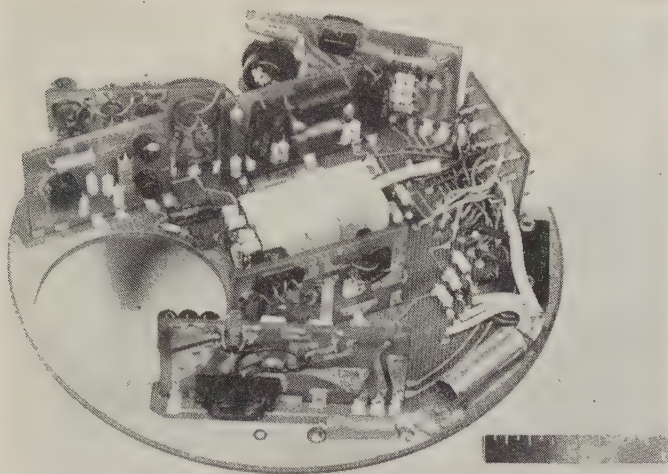


Fig. 3—Electronics board with subcarrier oscillator, record and playback amplifier, day-night switch and relays.

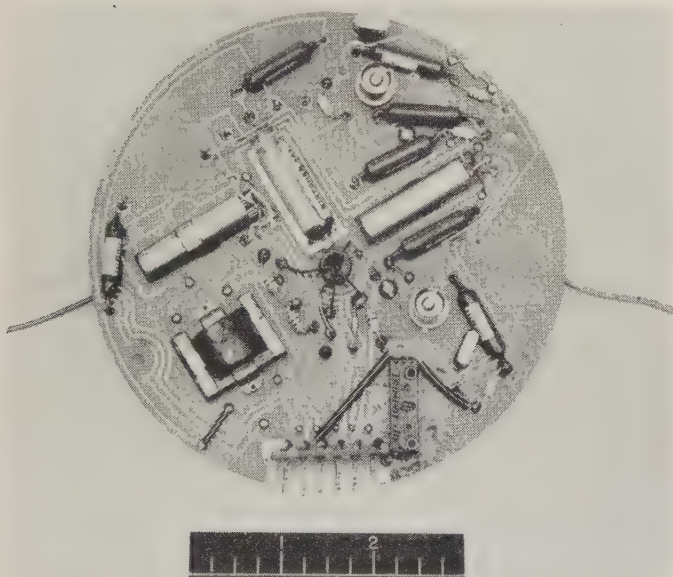


Fig. 4—Transmitter board.

increased the precession angle so that when the satellite separated it was tossed off with an unpredictable motion.

Operationally, the satellite was interrogated over its life of 210 orbits with a reliability of 85 per cent. Causes for noninterrogation were such difficulties as ground instrumentation trouble or operator errors. Whenever the satellite was closer than 1000 miles, the data received could be used for analysis. The satellite temperature designed for 35°C was 34°C shortly after launch and increased gradually because the orbit drifted into longer sun illumination periods.

Determination of the satellite motion is still under active investigation. Measurements of the fading pattern performed during its operation can be related to the antenna pattern of the turnstile antenna and its motion [2]. Also, the influence of the tape-recorder flywheel and its start and stop on the satellite motion is being investigated since the unpredicted motion resulted in the "spin" axis not being parallel to the axis of the flywheel.

This first "meteorological" satellite has had the following results: A complex, advanced electronic instrumentation was successfully operated for three weeks in a satellite. This entire satellite met all design requirements placed on it except that of being injected smoothly with the intended spin axis. It is anticipated that rudimentary albedo data may be obtained from it. Certainly, a wealth of information and experience in the creation and operation of such instruments have been collected.

#### BIBLIOGRAPHY

- [1] S. Fritz, "On observing the atmosphere from satellites—I," *Cloud Observations Weatherwise*, vol. 12, no. 4; August, 1959.
- [2] F. O. Vonbun, "Analysis of satellite motion from radio reception," this issue, p. 359.
- [3] W. G. Stroud, R. Hanel, W. Nordberg, and R. A. Stampfl, "Meteorological measurements from earth satellite," *Annals of the IGY*, vol. 6, pt. 2, pp. 340-345; 1958.
- [4] R. Hanel and R. A. Stampfl, "An earth satellite instrumentation for cloud measurements," 1958 IRE NATIONAL CONVENTION RECORD, pt. 5, pp. 136-141.
- [5] R. Hanel, R. A. Stampfl, J. Cressey, J. Licht, and E. Rich, "Tracking Earth's weather with cloud cover satellite," *Electronics*, vol. 32, pp. 44-49; May, 1959.



# TIROS—The System and Its Evolution\*

H. I. BUTLER† AND S. STERNBERG‡



Fig. 1—Picture taken with wide-angle camera of TIROS (frame no. 5, orbit 76, April, 1960) showing the Florida Peninsula and the extending coastline up to the Carolinas on the right, and a major portion of the Gulf of Mexico on the left.

**Summary**—At 6:40 A.M. on April 1, 1960, the TIROS I satellite was launched, went into its planned orbit, and demonstrated full capability of operation. The cloud pictures returned to earth not only fulfilled all the expectations of the satellite designers from a technical standpoint, but also proved to be informative and of practical value to meteorologists. The effects of the space environment on the satellite itself remained well

within the design extremes. Ground operations also went according to plan, with the highly-automated equipment successfully programming the satellite, and then reconstructing the received pictures and their identification coding for photographic reproduction. One of the photographs taken by the wide-angle camera is shown in Fig. 1.

The following paper, prepared before the date of launch, describes the satellite and ground data-acquisition system. A brief history tracing the evolution of the project from its earliest concepts is included, as well as a discussion of the major factors, both technical and managerial which affected the final design.

\* Manuscript received by the PGMIL, March 28, 1960.

† Astro-Instrumentation Branch, Astro-Electronics Division, USASRDL, Fort Monmouth, N. J.

‡ Astro-Electronics Products Division, RCA, Princeton, N. J.

## INTRODUCTION

TIROS is the name given to the meteorological satellite program of the National Aeronautics and Space Administration (NASA). TIROS I is the first U. S. satellite to carry a television camera on board. The initials stand for Television and Infra-Red Observation Satellite, since both types of sensors are employed. The objective of this satellite program is to give the meteorologist a pictorial view of the weather from a vantage point well above the weather.

The basic system consists of 1) the satellite with sensors, recorders, transmitters, receivers, attitude indicator, solar cell power supply, and control circuitry; and 2) the primary command and data acquisition stations. The supporting elements of the system are the tracking network (for orbit determination as contrasted to data acquisition), the data analysis center, the control center, the communications network to tie these elements into a coherent operational system, and the pre-launch check-out facilities.

It is the intent of this paper to give an indication, from a management point of view, of some of the problems and factors which vitally affect the course of a development program—particularly a highly-complicated program such as a satellite system. Since a satellite system is such a complex mechanism, a sufficient amount of design and operational information is given so that the workings of the TIROS system and its main elements can be well understood.

## EVOLUTION AND HISTORY OF THE TIROS PROJECT

A brief history of the TIROS project is included primarily to help place in proper perspective the design considerations and changes which took place in the satellite configurations. This history was shaped by a series of management decisions based on timing, equipment priorities, economics, and assignment of organizational responsibilities.

TIROS evolved from a relatively modest start in life as a first try at the problem of viewing the earth's surface by means of a TV camera installed in a satellite. It had its roots in a study conducted by the Radio Corporation of America for the Rand Corporation under an Air Force contract initiated in 1951. The objective at this stage was to evaluate the general reconnaissance potential of a TV satellite. The results of the study were generally quite favorable, and several projects evolved leading toward the development of flight-type equipment.

As a result of an unsolicited proposal, the Army Ballistic Missile Agency (ABMA) in 1956 awarded a contract to RCA to reduce to practice an early feasibility television satellite, using the Army's Jupiter C missile system with a Redstone booster. This missile system later placed into orbit Explorer I, the United States' first artificial earth satellite. The program was later expanded, upon decision of the Department of Defense and the Army Ballistic Missile Division, and redirected toward a more specific mission, that of target acquisition and location.

A contract again was awarded to RCA covering the initial phases of a program which included the design and construction of a satellite to be launched by a Juno II missile system using the Army's Jupiter IRBM ballistic missile as the booster. Included in the contract was the requirement for a complete system design of the satellite structure, power supply, stabilization, environmental control, orbital dynamics, and electronic instrumentation. In addition, the contract required development of the associated ground systems equipment necessary for the proper operation of the satellite system. Responsibility for the vehicle system remained with ABMA; responsibility for the payload and ground complex was subsequently assigned to the Signal Corps.

In mid-1958, it was determined that this project came within the purview of the Advanced Research Projects Agency (ARPA). This agency, after reviewing the existing program, decided that it was well suited to meet a very high priority and urgent requirement for a meteorological satellite; as a result, work on the television satellite was directed toward the development of a meteorological system. An Ad Hoc Committee on Meteorology was created by ARPA to help formulate the design objectives for a satellite program with particular emphasis on the initial payload which was to be of an exploratory nature. This committee included representation from ARPA, ABMA, Office of Naval Research, National Advisory Committee for Aeronautics, Air Force Cambridge Research Center, U. S. Weather Bureau, University of Wisconsin, Rand Corporation, U. S. Army Signal Research and Development Laboratory, and the Astro-Electronic Products Division of RCA. The Committee recommended the inclusion of a number of design objectives (described later in this paper) which in addition to TV cloud-cover observation using high-, medium-, and low-resolution cameras, proposed a series of measurements in the infrared and in the ultraviolet and X-ray regions. It was possible to include most of these in the specifications for TIROS.

At about this time, further work on the Juno II missile program was discontinued and the available vehicles were reassigned to the Explorer series for satellite cosmic ray exploration. As a result of this decision and of others related to the over-all problems of missile advancement, the Juno IV program was conceived and initiated by ABMA. This program consisted of the Jupiter booster plus new liquid-fuel upper stages. The physical design characteristics of size, form factor, and weight of the TIROS satellite were based on the Juno IV system. However, as a result of a realignment of the national space program, it was necessary to shift the TIROS project from the Jupiter to the Thor, and with this, the responsibility for the vehicle system was transferred from ABMA to the Air Force Ballistic Missile Division and its subcontractors, Space Technology Laboratories and the Douglas Aircraft Corporation.

In April, 1959, as a result of the apportioning of project responsibilities between ARPA and the newly-formed ci-



vilian space administration, the TIROS project was transferred from ARPA to the National Aeronautics and Space Administration (NASA). In its role as over-all system manager, NASA is coordinating the efforts of the Ballistic Missile Division of the Air Force and those of the Signal Corps with the NASA Goddard Space Flight Center, the Minitrack network, the NASA Computing Center and the U. S. Weather Bureau Meteorological Satellite Center.

#### DESIGN OF THE TIROS SYSTEM

The TIROS system evolved as a result of a series of management decisions and their historical results. The earliest feasibility television satellite (Project Janus) weight of 20 pounds was specified by the capability of the Jupiter C missile system. The payload consisted of a television camera (using a  $\frac{1}{2}$ -inch vidicon) with a frame rate of 1 per second, powered from chemical batteries. The slow-speed scan rate produced a video bandwidth of 125 kc which could be transmitted through the standard existing telemetry band at 240 mc. The receiving stations were those that existed "down range" at Cape Canaveral for receiving missile test data. A dove prism optically immobilized the image within the 750-rpm spinning frame.

Stabilization of the optical axis in space was accomplished by using the spin momentum generated during the launch phase. The Jupiter C satellite was required to be a rod-shaped body with a diameter of approximately 5 inches. In a spinning, picture-taking satellite, it is extremely important for successful operation that the optical axis remain parallel to the spin axis. Such alignment is difficult to maintain when it is necessary to point the optical axis along the longitudinal axis of a rod-shaped body. A disk-shaped body has its maximum moment of inertia around the figure axis, and will spin stably around that axis. However, a rod-shaped body prefers to spin about a stable axis which is perpendicular to the (longitudinal) figure axis of the rod, since that is the line around which the mass of the body has its maximum moment of inertia.

During the launching process, the Jupiter C satellite received a spin rate of 750 rpm around its longitudinal axis for stabilization. Due to unbalance impulses (which are impossible to avoid), the vehicle precesses. This oscillation builds up if there is any energy dissipated (such as heat due to mechanical bending) in phase with the precession oscillation. The system finally ends up spinning about its axis of maximum moment of inertia, and appears to be tumbling. This was recognized by RCA early in the Janus program and was later proven by Explorer I, which actually did tumble due to the whipping of the crossed dipole antennas which were used for the 108-mc beacon. To counteract this problem, an "active" damping system was invented (Fig. 2) to produce mechanical friction out of phase with the precession oscillation. This required that there be a net power gain by the system, derived, in this case, from the chemical batteries. With such a device, the system would spin true about its longitudinal (rod) axis.

The laboratory model of the 20-pound system (shown in Fig. 3) was demonstrated immediately after Sputnik I, and was scheduled for launching in the spring of 1958.

The expansion of the program in early spring of 1958 changed the design of the TV satellite in order to meet the requirements of a reconnaissance mission and a different missile system, Janus II. A new optical system (shown in Fig. 4) was required to meet the specifications for increased picture resolution. Perkin-Elmer Corporation, under subcontract to RCA, designed a cassegranian-type optical system with an 8-inch aperture and an 8-inch focal length. A dove prism for image immobilization could no longer be used; the spinning satellite had to be slowed down from an initial 450-rpm speed to as slow a speed as would still maintain enough angular momentum for stabilization—about 7 rpm. Although an increase in weight to 85 pounds was possible in the new system, it was still impossible, due to limitation of form factor, to achieve a ratio of moments of inertia which would provide a disk-shaped system. A design was conceived, however, which would solve both problems of speed slow-down and conversion from rod to disk characteristics while the satellite was in orbit. Weights at the ends of four wires would be slowly paid out to a distance of six feet. In the process of increasing the moment of inertia, this would (in a

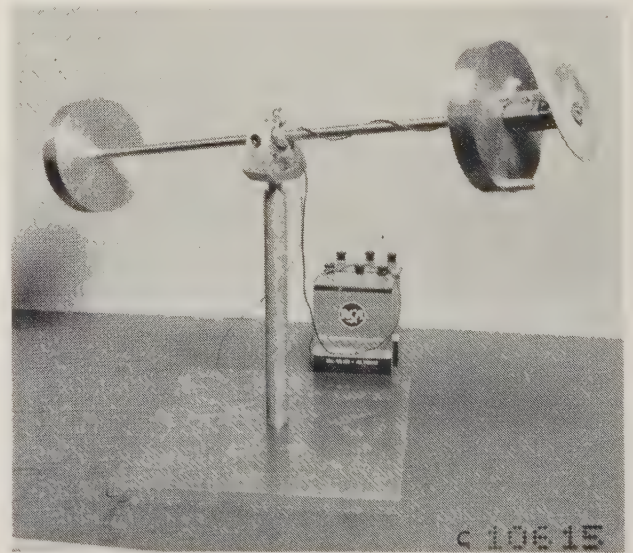


Fig. 2—"Active" precession damping device (on test fixture).

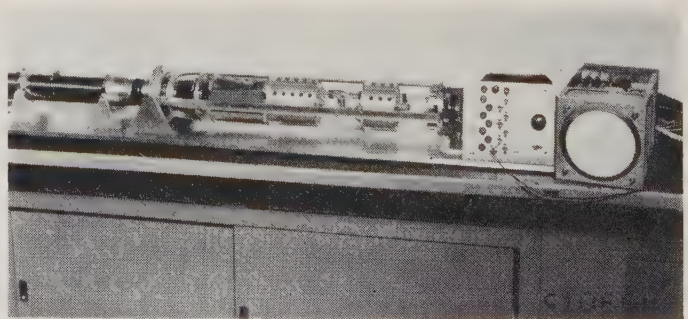


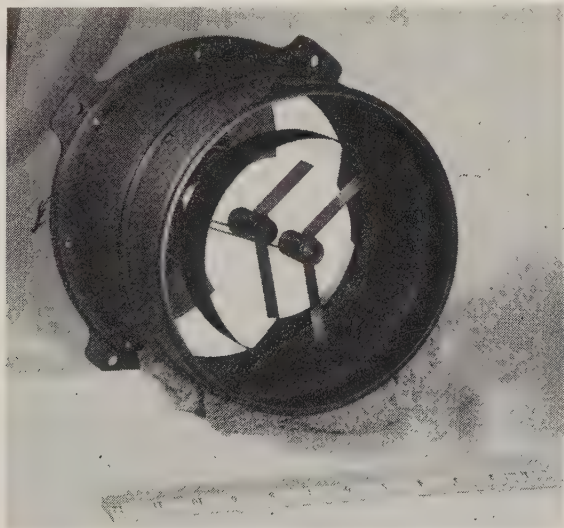
Fig. 3—Model of 20-pound Janus satellite.



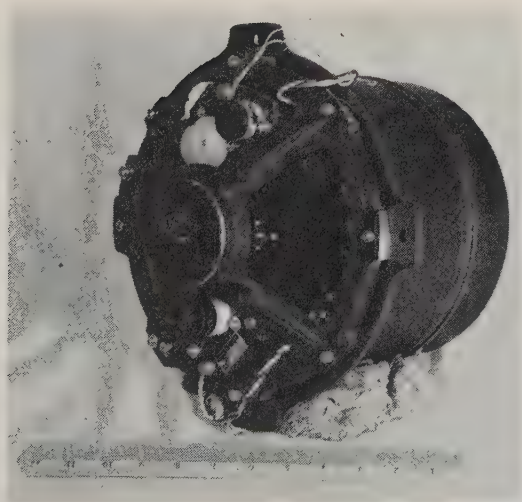
momentum conservation system) slow down the angular speed. By keeping the extended weights and wires, now under tension from centrifugal force, as part of the overall mechanical system, the total satellite system would effectively be converted from a rod to a disk-shaped body. The dissipation of energy released from the flexing of the wires due to any precession would cause the oscillation to damp out, as in a stable disk-shaped system, keeping the figure axis, spin axis, and optical axis properly aligned. This system was demonstrated on a tester built at RCA and shown in Fig. 5.

Development of a lightweight, rugged, low-power drain magnetic tape recorder was initiated in order to store pictures taken at remote locations in the orbit. Video bandwidth of 125 kc compatible with the vidicon scan rate was provided. Nickel-cadmium storage batteries with a solar-cell (charging) power supply were substituted for the limited-life chemical batteries. A picture of a full-size model of this satellite is shown in Fig. 6.

The initiation of the new Juno IV missile system replaced the Juno II for the TV reconnaissance satellite.



(a)



(b)

Fig. 4—Optical system for reconnaissance satellite.

Now, a third stage that would accommodate a disk-shaped satellite was available. A housing 42 inches in diameter and 17 inches in height was designed. Since the upper stage was liquid and equipped with guidance control, no spin was needed for stabilization during the launch phase. Consequently, the satellite could be placed into orbit at the spin rate needed for orbital attitude stabilization, consistent with picture-taking requirements (*i.e.*, 7 rpm). The despin weights and wires were thereby eliminated, resulting in a

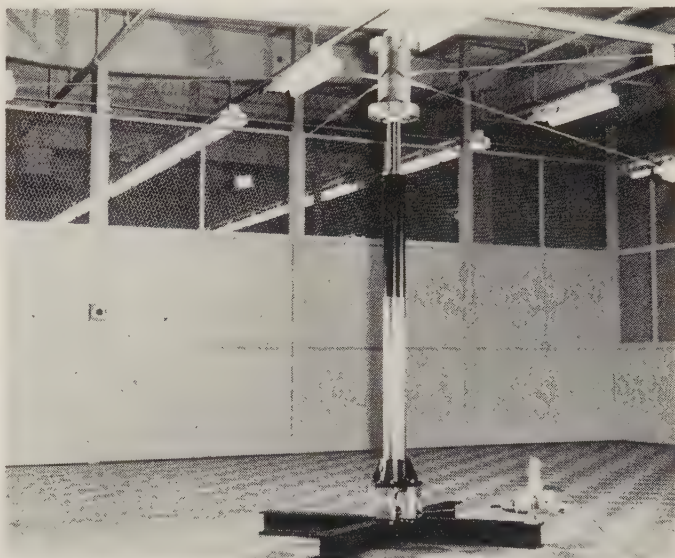


Fig. 5—Weight and cable spin-rate reduction device (on test fixture).

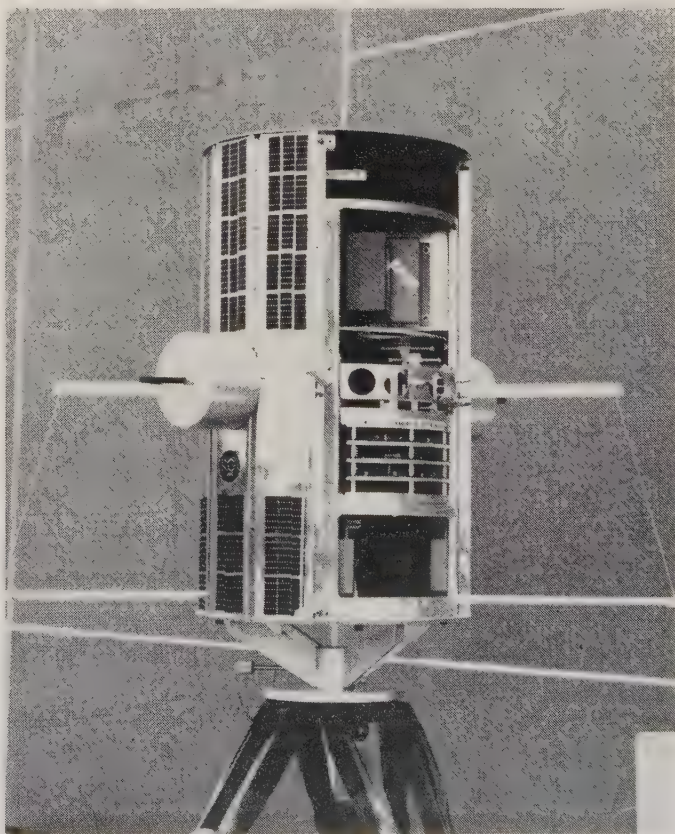


Fig. 6—Full-size model of Juno 85-pound satellite.



much simpler system. Reliability was served by the new simplicity and the redundancy now possible due to the increased orbital lifting weight capability of the Juno IV.

As previously mentioned, in mid-1958 it was determined that the project came within the purview of the Advanced Research Projects Agency (ARPA). At the same time, the mission requirement was directed toward meteorology and away from reconnaissance. The new requirement permitted a drastic change in optics. Rather simple off-the-shelf refractive optical systems were found adequate to fulfill the much coarser resolution specification for cloud observation. The heavier and more complicated cassagranian optics was abandoned. Three complete and independent TV camera and magnetic recording systems were to be provided for three steps of resolution and coverage. A two-second frame was selected for picture readout, reducing the video bandwidth requirements to 62.5 kc.

A "scanning" infrared observation system covering five selected bands in the infrared spectrum was added. This subsystem was assigned to U. S. Army Signal Corps (later transferred to NASA) for development, and was to be installed in the satellite by RCA. The introduction of this new system required that an increase in spin speed (to 12 rpm) be provided and maintained during orbit. Since the infrared sensor system tied to the spinning vehicle provided for a spot scan of the earth, a specific scanning speed was necessary to assure overlapping lines as well as full utilization of the resolution capability of the system. It was realized that without some on-board power for control of spin speed, the magnetic field would slow down the satellite in a relatively short period of time, rendering the infrared scanning useless. A number of small "spin-up" rockets, whose firing was controlled from the ground, were equispaced around the periphery of the satellite to compensate for spin slowdown. In order to power the increase in payload, additional solar cells were required, finally reaching a total of 9300 individual silicon  $1 \times 2$  cm cells.

At this point in its genealogy, the TIROS satellite was very close to its final system design. The shift from the Jupiter-Juno IV missile system to the Thor involved the transfer of missile system responsibility to the Ballistic Missile Division of the Air Force. A former problem was again introduced: the final stage of the missile system used solid fuel, and was spin-stabilized (at 120 rpm). Thus, it would be necessary to slow down the spin rate of the satellite in orbit from 120 rpm to 12 rpm. Again, the weight and cable despin system was considered, but this time, the complication of maintaining the extended weights as part of the satellite system was found unnecessary, since no conversion of the ratio of moments of inertia from rod to disk was required. A simpler system was installed, in which weights and cables wrapped around the satellite are allowed to fly out under the influence of centrifugal force at the initial angular velocity, and then are released to continue into space, carrying with them sufficient momentum to slow down the spin rate to 12 rpm.

The final shift in management responsibility from ARPA to NASA in April, 1959, did not entail any major redesign in the TIROS system. The policy rather was to endeavor to assure that no further changes or additions be made in the TIROS satellite. The final form of the satellite structure (and antennas) is shown in Fig. 7. The component layout in the anterior is shown in Fig. 8.

The above discussion has attempted to point out the very strong influence of management decisions on the design configuration of the TIROS satellite.

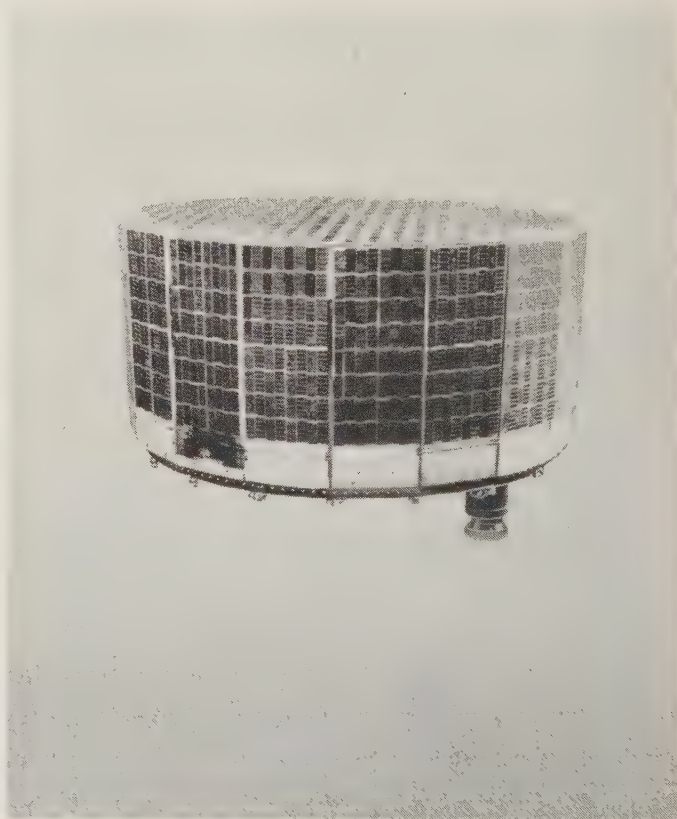


Fig. 7—The TIROS satellite.

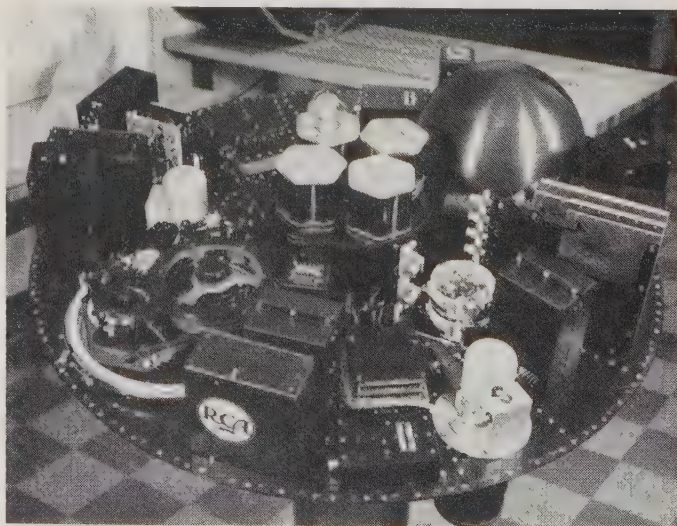


Fig. 8—The TIROS satellite (payload) electronic components.

It should not go unnoticed that, as changes were necessitated in the satellite, complementary and equally important changes had to be made in the ground equipment. However, these are not covered in the present paper.

#### DESCRIPTION OF THE TIROS SATELLITE

The main elements of interest of the TIROS satellite are the television and infrared sensor subsystems, the ground station command and control system, the data acquisition system and the pre-launch check-out system.

In the television subsystem, two cameras are employed. One, equipped with a wide-angle lens, will provide coarse, large-area coverage; the other, equipped with a longer focal-length lens, will provide relatively fine information on cloud structure. The cameras are miniaturized units, designed around a ruggedized  $\frac{1}{2}$ -inch vidicon picture tube. The "sticky" (high-persistence) characteristics of the vidicon make it possible to achieve appreciable bandwidth compression by using a low read-out rate. Exposure is set for approximately 2 msec and readout has been extended to approximately two seconds. Although several modes of operation are possible, the principal mode will be one in which a series of "coarse" pictures which overlap approximately 50 per cent are taken simultaneously with a series of high-resolution pictures, one of which falls in the center of each coarse picture.

The area on the surface of the earth which can be observed by the cameras is limited mainly by two factors, presence of sunlight and orientation of the satellite. Since the satellite is spin stabilized (that is, the spin axis is fixed in inertial space), the surface bearing the cameras faces the earth for only part of each orbit. At the point where proper camera orientation and adequate sunlight coincide, a series of exposures is made. Each picture taken by the cameras is read out and stored on magnetic tape, and then is subsequently read out when the satellite passes over a primary ground-data station. At those times when the orientation and sunlight coincide and the satellite is within range of one of the ground stations, it is possible to read out the cameras in "real time"; that is, to bypass the tape recorders and transmit the picture information directly. If the satellite is passing overhead, the ground station is photographing itself!

With the importance of reliability constantly in mind, it was decided to make the two camera systems completely independent of each other, except for the synchronization of exposures previously mentioned. Each camera feeds into its own recorder, recorder electronics, and picture transmitter. To carry this philosophy through to its logical conclusion, independent function-control "clock" assemblies and command receivers were provided in the satellite as well.

The design of the system provides for two types of infrared observation. One of these, identified as the Scanning Infrared subsystem, is an expanded version of the Vanguard Cloud Cover experiment wherein the rotation or spin of the satellite provided the equivalent of the horizon-

tal scan of a raster, and the orbital motion of the satellite provided the equivalent of the vertical scan. Actually, the raster pattern is much more complex, since the infrared sensors "look" simultaneously "up" and "down" at  $45^\circ$  to the spin axis. The shape of the scan line varies as a function of changing attitude of the scanning cone as it intersects with the spherical earth. This technique results in a much broader coverage over the surface of the earth than the TV system, and takes advantage of the fact that infrared observation is not restricted to sunlit areas.

The spectrum ranges selected for the scanning infrared subsystem are:

- 1) 0.2 to 5.0 microns (to provide a measurement of the earth's albedo or reflected energy from the sun),
- 2) 7.0 to 30 microns (to measure the total radiated energy of the earth and its atmosphere),
- 3) 8.0 to 11 microns (to measure, through a "window" in the atmosphere, the temperature of the earth's surface, or the "bottom" of the atmosphere),
- 4) 5.9 to 7.0 microns (to measure, in effect, the temperature of the "top" of the atmosphere. This is the wavelength range at which the water vapor in the atmosphere absorbs the radiated energy from the earth),
- 5) 0.55 to 0.74 micron (the visible spectrum) (to provide a reference for the preceding four measurements, and for comparison with the TV pictures).

The second infrared subsystem utilizes two relatively simple nonscanning sensors with approximately the same response as 1) and 2) above. These are aimed parallel to the TV cameras, and cover approximately the same area as the coarse resolution camera. These measurements will permit an estimate to be made of the heat budget of each area observed, and to correlate this with the cloud cover.

The recording and transmitting equipment for the infrared subsystems are contained in a common package which is independent of the TV equipment. The scanning system is designed for continuous operation and makes use of a magnetic tape recorder with an endless loop of tape. Sufficient tape is provided for a nominal orbit of 100 minutes duration and, upon interrogation by one of the ground stations, the tape speed is increased by approximately 30:1 for playback. A different transmission frequency is used by the infrared transmitter, permitting both the infrared and the TV information to be telemetered simultaneously. While the tape is playing back the recorded data, the output of the sensors modulates a separate channel of the transmitter to provide direct data readout in "real time," bypassing the tape recorder.

It is reasonable to assume that the spin axis of the satellite is not likely to lie in the plane of the orbit. Any one of several effects, such as uneven burning of the third carrier-rocket stage, precession, or even slight tip-off upon separation from the third stage, can shift the axis by an appreciable amount. Since both of the sensors (TV and infrared)



are aimed with respect to the spin axis, it was necessary to include a system for determining the attitude of the spin axis in space. This system employs a separate infrared sensor which scans the earth as the satellite rotates and detects, essentially, the horizons. The data is telemetered continuously through 108-mc beacon transmitters to the ground stations, from which it is relayed to the computing center, where it is processed with the orbit elements to give the spin-axis attitude. In addition to the primary stations, attitude-axis data recorders will be installed in Minitrack stations at Lima, Peru; Santiago, Chile; the Ascension Islands; and Goldstone, California.

The purpose of the primary command and data-acquisition stations is to transmit instructions to the satellite and to receive observed-information from the satellite. The primary ground stations are equipped with a 60-foot-diameter, self-tracking parabolic antenna and the electronic equipment for programming, transmitting, receiving and data recording.

A programming console at each primary ground station is designed to permit a considerable flexibility in control of the satellite functions. Control may be exercised manually or by automatic sequence, and the satellite may be programmed for remote operation or direct response. The automatic mode requires less time and reduces the likelihood of operator error. The total time that the satellite is in range varies from pass to pass (from approximately 6 to 14 minutes), and this period must be divided among the three functions, stored data read-out, direct data read-out, and the transmission of instructions for remote camera operation. Hence, preprogramming permits most efficient use to be made of the time that the satellite is within range, thus retaining the maximum time for direct camera read-out.

It should be noted that programming is complicated by the problem that, with only two primary stations, there are several passes in a 24-hour day that are not within range of either station. However, the satellite can be programmed in advance (as far ahead as 3 passes) for read-out on a subsequent pass. In all likelihood, the meteorologists will require this more complicated mode of operation.

The receiving and recording equipment consists of independent subsystems for handling the TV and infrared data. To preclude the possibility of having "holes" or nulls in the received signal as the satellite rotates, the satellite was equipped with a circular polarized transmitting array. On the 60-foot receiving antenna, both horizontal and vertical dipoles are employed, and these feed separate receivers connected to diversity combiners. Two high-quality multitrack tape recorders are employed. The basic TV and infrared outputs are recorded on both machines to provide backup, and the remaining channels are used for reference data such as sun angle, synchronization pulses, indexing, time, etc. The handling of the TV picture is illustrated in Fig. 9.

The TV picture signal, in addition to being recorded

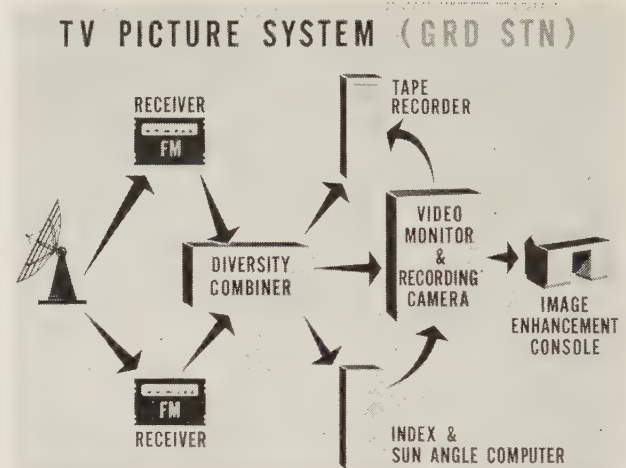


Fig. 9—The ground-based TV picture subsystem.

on tape, is displayed on a video monitor. Since the scan rate is the same low rate at which the picture was recorded in the satellite, a picture can be seen only when a high-persistence cathode-ray tube is employed. However, good photographic copy can be obtained from a short persistence, high-ultraviolet cathode-ray tube. The picture is built up line by line and is photographed by a 35-mm camera, mounted opposite the CRT screen. The camera is automatically advanced frame by frame until playback from the satellite is completed. To provide additional film strips quickly, the signal recorded on the ground station tape recorder can be played back through the monitor as many times as is needed. Each frame is indexed and contains a coded reference of the position of the satellite with respect to the sun, from which the relation to North can be determined.

For use in the check-out of the satellite through all of the many pre-launch operations at Cape Canaveral [see Fig. 10], a compressed (rather than simplified) version of a command control and data acquisition station was devised. This equipment permitted rapid interrogation of the satellite in all of its modes and reduced the evaluation of performance to GO, NO-GO type of criteria.

The entire operational phase of the program is directed from the Space Operations Control Center of NASA, at which location the actual sequence of operations for each satellite orbit is prepared, and specific instructions are transmitted to the primary ground stations at Kaena Point (operated by Lockheed Missile and Space Division for the Ballistic Missile Division of the Air Forces) and at Fort Monmouth (operated by the U. S. Signal Corps). These instructions are primarily from three sources of information, the NASA Computing Center, the Weather Bureau Meteorology Satellite Center, and the primary ground stations themselves. The computing center, in turn, bases its calculations on tracking data and attitude axis data received from the Minitrack network and also from the primary ground stations. The satellite tracking complex is illustrated in Fig. 11. The meteorology center ana-

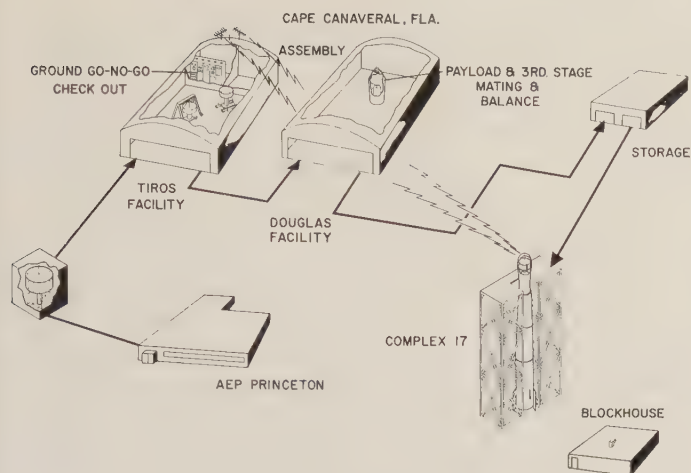


Fig. 10—Pre-launch handling of the TIROS satellite.

lyzes all data, and when a choice exists as to where data may be acquired by the satellite, recommends those areas which are of greater meteorological significance. This control complex is illustrated in Fig. 12.

At both Kaena Point and Fort Monmouth, teams of meteorologists will be stationed with representation from the Weather Bureau, Air Force Cambridge Research Center, Air Weather Service, Navy Research Weather Facility, and the U. S. Army Signal Corps Research and Development Laboratory to conduct real-time analysis of the data. The results of the picture interpretation will be transmitted to the Meteorology Satellite Center for use in planning subsequent instructions to the satellite and for correlation with weather data from other sources. In support of this operation, weather radars and sky cameras will be employed to provide data "looking up" which may be correlated with data of the satellite "looking down."

In order to extract the maximum amount of information from the pictures, one untouched set of film exposures from each satellite pass will be forwarded to the Naval Photo Interpretation Center for precision development and photogrammetric processing.

The integration of the satellite payload with a Thor Able rocket vehicle presented many problems requiring coordinated effort for their solution, and many compromises had to be worked out between the contractors and government agencies involved (the Air Force Ballistic Missile Division, Space Technology Laboratories, Douglas Aircraft Corporation, the RCA Astro-Electronic Products Division and the Signal Corps). A scientific payload such as TIROS imposes many restrictions on the vehicle system, and the vehicle, of course imposes many restrictions on the payload.

TIROS presented a number of problems during the course of its development. Some of the more interesting are discussed below.

In order to have the "bottom" of the satellite face the earth in the northern hemisphere under good lighting conditions for the longest period of time, it was desirable to

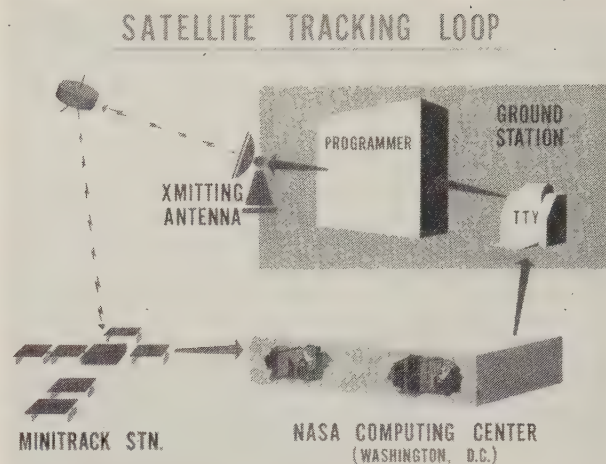


Fig. 11—The TIROS satellite tracking complex.

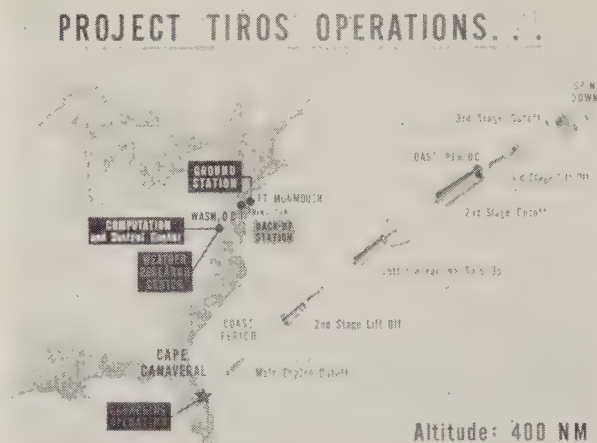


Fig. 12—The TIROS satellite system launch and control operations.

fix the time of launch with a tolerance of  $\pm 15$  minutes. To prevent sunlight from entering the infrared optics during the launch trajectory, the payload and vehicle had to be properly oriented on the stand. A fairing or "shroud" protects the payload and third stage until it was jettisoned after the second stage burnout. This was not an unmixed blessing. Fortunately, it was of molded fiberglass construction, transparent to radio frequencies, so that the satellite could be interrogated during pre-launch check-out. However, it was only translucent to sunlight, and consequently the solar cells could not keep the storage batteries charged. It was necessary, therefore, to bring power through the umbilical cord and third rocket stage to an interface contact between the third stage and the payload.

An opaque fairing also made it necessary to introduce artificial illumination for sensor check-out. However, the fairing made it possible to air-condition the payload while it was on the stand, which eliminated moisture condensation and reduced the effects of thermal shock, particularly on the optics.



## CONCLUSION

It is interesting to note that Project TIROS had its beginning before Sputnik I, lived through a period of sudden national awareness of the Space Age, and finally emerged as a completed design (somewhat changed in form). During this time, many government management decisions changed both the mission and technological requirements of the system. Many of these decisions resulted in a change of the launching missile system. This, in turn, was reflected in design changes in the TIROS satellite and ground system.

The ability of the over-all space system designer to substitute missile systems and still retain the capability of a working satellite and ground system is of special interest. Missiles may be considered as "space trucks" for the launching of satellites, and any missile system that conforms to a given payload weight vs orbital altitude dependency and a known accuracy of guidance can be used.

Small changes in these missile specifications will not appreciably modify the mission or resulting output of the total system.

However, changes in specific missile systems during the equipment design phase of the program can result in non-optimum solutions to design problems and difficulty in maintaining funding and time schedules.

If one were to look for forces which acted to smooth out the gyrations and perturbation in the program, two factors would predominate. First there was a strong requirement for a system such as TIROS. Second, continuity was maintained by having at least one organization with sufficient over-all technical system responsibility stay with the program throughout its history. The authors recognize the broad national effort involved in the TIROS program, the successful conclusion of which depended on the flexibility, determination, and skill of many people and many organizations.

## Surveying and Mapping from Space\*

CHARLES S. SPOONER, JR.†

**Summary**—Artificial satellites promise means of completing precise surveys of the world and of acquiring world-wide photographic coverage for the production of topographic maps. The applicability of satellites to the field of geodesy is covered, and problem areas associated with map compilation serve to emphasize a critical research area.

THE advent of artificial satellites, and their relation to the acquisition of mapping data, is roughly comparable to the relation of aircraft to the same problem 50 years ago. Prior to that, we were primarily obliged to accomplish our control surveys and our mapping by occupying stations on the ground. Technical revolution resulted with the appearance of the aircraft and the aerial camera, for, by leaving the ground, we could literally and figuratively see a bigger picture. Then followed four decades wherein the elaborate camera and stereoscopic plotting instrument systems and the effective airborne electronic surveying systems, in use today, were perfected.

A second technical revolution is about to be interposed as man gains the vantage point offered by artificial satellites. Within a short period of time, reliable sensors operating from stations in space will "dump," in some form, imagery from an appreciable percentage of the earth's surface every 90–120 minutes! The processing of such a

deluge of information presents insurmountable problems, if one thinks in terms of our present procedures and capabilities.

But our problem is not restricted to perfecting means of rapidly reducing voluminous raw data into meaningful end products, such as topographic maps. There is the matter of completing our precise surveys of the world; surveys which are prerequisite to the preparation of accurate maps.

Present satellites, that is, the ones currently overhead and ones to be launched in the near future, are, for our purposes, useful only for obtaining geodetic data. These are equipped with instruments to acquire various types of scientific data in support of other physical sciences, but none of these relate directly to mapping. Except for the fact that a radio transmitter within the satellite helps fix its location, present satellites participate no more actively in the acquisition of mapping data than the moon itself. Ground observation, either electronic or optical, is a necessary adjunct. Thus, for mapping problems, present satellites may be considered passive rather than active instruments. The only information we acquire thereby is positional, which is useful just for geodesy and not for map compilation. This in itself, however, is sufficiently important to justify considerable effort. The Army Map Service has been studying and actively carrying out pro-

\* Manuscript received by the PGMIL, February 1, 1960.

† Army Map Service, Washington, D. C.

grams involving geodetic applications of artificial satellites for over three years. What are some of these applications? The main ones are:

- 1) more precise distance measurements;
- 2) more accurate knowledge of the size and shape of the earth;
- 3) increased knowledge of the earth's gravitational field.

In the first application, *i.e.*, more precise distance measurements, careful observations or tracking of artificial satellites can give distance and azimuth between points where these quantities are now imperfectly known. The requirement here is the tying together of unconnected or imperfectly connected datums of the islands and continents. For example, points can be located accurately within Western Europe and points can be located accurately within North America. However, a point in Western Europe cannot be positioned accurately with respect to a point in North America since different datums are used for the two continents which have not been accurately connected. This requirement for the connection of various datums is being actively worked on, and in many instances, present connection values will suffice. There are many areas in the world, however, as yet poorly surveyed. It is hoped that the application of artificial satellites will reduce, in some instances, current positional discrepancies by a factor of 20. In this regard, there is an operational project being conducted by the Army Map Service called Project BETTY. This effort employs electronic tracking stations established in various Pacific islands for the purpose of observing artificial satellites. Many data have been collected and when they are finally reduced, we should have much more accurate positional data connecting these islands to both the Asian and American mainlands.

The second application, *i.e.*, more precise information on the size and shape of the earth, is closely tied with the first. Fundamental to the conversion of one datum to another is the determination of the size and shape of the Earth, since one of the defining elements in any datum is the identity of the spheroid upon which the coordinates of the position are to be expressed. The United States is now using the Clarke 1866 Spheroid in North America; the International Spheroid in Europe, the USSR and China; the Bessel Spheroid in Japan; the Clarke 1880 Spheroid in most of Africa; and the Everest Spheroid in India, Burma and most of Southeast Asia. The uncertainties in the dimensions of these are such that a redetermination of the size and shape of the earth is desirable. Two parameters are involved: the flattening of the earth, and the equatorial radius of the earth. At present, the flattening is known to an uncertainty of about one part in 100,000, and the equatorial radius to an uncertainty of one part in 60,000. It is desired to reduce these uncertainties by a factor of 10 or better. In seeking the assistance of

artificial satellites in resolving these problems, there is the difficulty of obtaining the requisite satellite orbital theory so that causes for orbital perturbations can be separated out. The requirement for improving the flattening lies in refining orbital theory and in obtaining a satellite whose orbit is more amenable to precise analysis. With respect to the equatorial radius, present methods do not seem to offer an immediate improvement. Here more precise orbital information and a near circular orbit would be of great help.

Incidentally, results have already been obtained in improving the value of the flattening. The value generally accepted up to now by the Western world, based mainly on the work of John Hayford of the U. S. Coast and Geodetic Survey in the early 1900's, was that the flattening of the earth at the poles was one part in 297. This has not been a universally accepted value, however, since the Russians arrived at a value of one part in 298.3, based on their own large-scale triangulation adjustments. Preliminary computations of the flattening, from analysis of satellite orbits, indicate closer agreement with the Russian figure. We cannot blame this on the fact that they may have secretly trained their satellites to yield this result, since our own satellites confirm this also.

The third application mentioned is in regard to the gravitational field of the earth. Here there have already been fruitful results. The reader may recall that a few months ago, the newspapers carried a story stating that observations on the Vanguard satellite, 1958 B, showed that the earth was pear-shaped. This effect was discovered by Dr. John A. O'Keefe, presently with the National Aeronautics and Space Agency, Washington, D. C. This pear-shapedness is actually an irregularity in the earth's gravitational field. Such irregularities will produce corresponding irregularities in the orbital path of the satellite. Although the latter might be due in part to the effects of atmospheric drag, Dr. O'Keefe was able to determine that there is a bulge of about 50 feet in the earth's equipotential surface at the North Pole and a corresponding depression of 50 feet at the South Pole. Irregularities in the earth's gravitational field will, in general, cause a satellite to be off its predicted path at any time. From the previous discussion on distance measurements and the figure of the earth, one can see that it is of considerable importance to determine most precisely the orbital path of a satellite. Thus, the causes of all discrepancies must be discovered, including those due to the earth's gravitational field, and those due to air drag. One way to accomplish this is to launch the satellite to a sufficiently high altitude, say, at least 600 miles. There, most of the effect of atmospheric resistance will have disappeared, and the resulting orbital discrepancies can be attributed to variations in the earth's gravitational field, which can be accounted for by refining suitably the orbital equations.

The present satellites are providing much data toward



meeting our geodetic requirements, but they are far from entirely satisfactory for these purposes. Three features would increase their usefulness for geodesy: 1) a near polar orbit so that geodetic observations could be made at all latitudes; 2) an orbital height as high as possible so that the earth's atmosphere will have negligible interference on the orbit; and 3) the incorporation of instrumentation, such as a flashing light, so that observations could be more frequent and precise, which would, in turn, enable us to calculate the orbit more exactly.

Let us now turn our attention to the problem of the acquisition of data in support of map compilation. In this case, the satellite must be an active participant in acquiring these data. There are three main problems to be considered here: 1) what type of sensor should be used by the satellite to acquire these data? 2) how should the information be passed to the ground? and 3) how can this information be transformed into usable end products? These are all highly technical questions to which many a solution has been advanced, but the feasibility of most of them remains uncertain. The two all-important qualities required for mapping photography are a favorable geometrical arrangement and an adequate level of information content. In photography taken from extreme altitudes, the two requirements are in conflict. Geometrical considerations call for a large angular coverage, produced by comparatively short-focus lenses. Information content is improved by the employment of lenses of greater focal length. When the size of the photograph format is limited by the camera weight that can be carried aloft, the angular coverage decreases with increasing focal length. As to the sensor, it would seem that it must be designed to obtain photographic data if mapping is contemplated. Television-type imagery and radar photography are, of course, useful for intelligence purposes, but image degradation of the former and geometric infidelity of the latter negate their usefulness for preparing topographic maps. With conventional photography, resolution is an important consideration. Currently, conventional mapping photography is taken from planes flying 20,000 to 30,000 feet using 6-inch focal

length cameras. Resulting photographic scales run from 1/40,000 and 1/60,000. The scales of photographs taken from artificial satellites will be much smaller, of the order of 1/3,000,000! Of course, such small-scale imagery can be enlarged to bring out detail, but very soon resolution quality becomes severely taxed. The second problem, of how the information would be passed to the ground, involves the advantages and disadvantages of transmitting the imagery to ground stations electronically or by recovering the nose-cone containing the exposed photographic film. Image degradation will plague the transmitting method until finer TV rasters are perfected, and nose-cone recovery will remain an expensive and uncertain technique until re-entry and other landing procedures are developed. The third problem, of how data obtained from the satellite can be transformed expeditiously into usable form, is in many ways the most difficult of all. The data obtained will be highly variable in quality due to atmospheric conditions and orbital observations. Moreover, the continuity of data will doubtless be broken up by clouds, darkness, oceans, etc. Thus, aerial triangulation or the extension of horizontal control will be difficult. Furthermore, because of the great heights from which camera exposures are to be taken, it will be extremely difficult to secure accurate vertical control data. The winnowing out of useful data from the deluge of material provided from space stations is another question. These considerations are mentioned to emphasize the fact that the use of artificial satellites for obtaining map compilation data is a much more difficult problem than their use for obtaining geodetic data. Moreover, the geodesists have precise tools, in the form of large-scale electronic computers, tracking radars and optical telescopes already on hand to acquire and process satellite data. The map compiler has little or no instrumentation with which to handle imagery once gained from artificial satellites; very little of the present photogrammetric instrumentation is applicable. This serves to identify a critical research area which must receive expert attention, if the advantages offered by space vehicles are to be exploited for the purpose of surveying and mapping the world.

# Radio Interferometry Applied to Geodesy\*

WERNER D. KAHN†

**Summary**—Mark II Minitrack, a basic type of radio interferometer, is used to obtain observational data from artificial earth satellites. It is assumed that the antenna field pattern can be approximated by a family of coaxial cones whose common apex is the electrical center of the system. The mathematical theory of calibrating the system with stellar radio sources and the reduction of satellite observational data is given, with an error analysis of the system.

## THE MARK II MINITRACK SYSTEM

THE Mark II Minitrack system is a basic type of radio interferometer. The simplest form of this system consists of two antennas which are separated by a baseline of length  $d$ . They are joined together by a transmission line which at the center is connected to a receiver. The receiver is then connected to a recorder.

Since a radio signal source such as an artificial satellite is at a great distance compared to the separation of the two antennas, two rays from the signal source arriving at the two antennas may be considered to be parallel (Fig. 1). By simple geometry the path difference  $S = d \sin \theta$ ; the corresponding difference in phase angle  $\vartheta$  between the signals induced at  $A_1$  and  $A_2$  is

$$\vartheta = \frac{2\pi d \sin \theta}{\lambda}, \quad \text{since} \quad S = \frac{\vartheta}{2\pi} \lambda,$$

where  $\lambda$  is the wavelength in air at the signal frequency. As the direction angle  $\theta$  of the signal source changes relative to the baseline, the value of  $\vartheta$  will vary and the signals produced at the receiver by the two antennas will be alternately in and out of phase. When  $\vartheta = (2j-1)\pi$ ,  $j=1, 2, 3$ , the signals will cancel and there will be no signal output from the receiver, but when  $\vartheta = 2(j-1)\pi$ , the signals will add and there will be maximum signal output from the receiver. By accurately timing the change in phase  $\vartheta$ , the direction of the radio source, *e.g.*, satellite, with respect to the baseline can then be measured.

A typical Mark II Minitrack station has three antenna baselines, each 1000 feet in length. A baseline is formed by two antenna arrays, each made up of sixteen colinear dipoles, spaced one wavelength apart. All three baselines have as a common midpoint the electric center of the station. The three baseline azimuths measured from local north are  $30^\circ$ ,  $90^\circ$ , and  $330^\circ$ . The corresponding azimuths of any radio signal source in the center of the field pattern of any one of the three baselines will be  $300^\circ$ ,  $0^\circ$  and  $60^\circ$ .

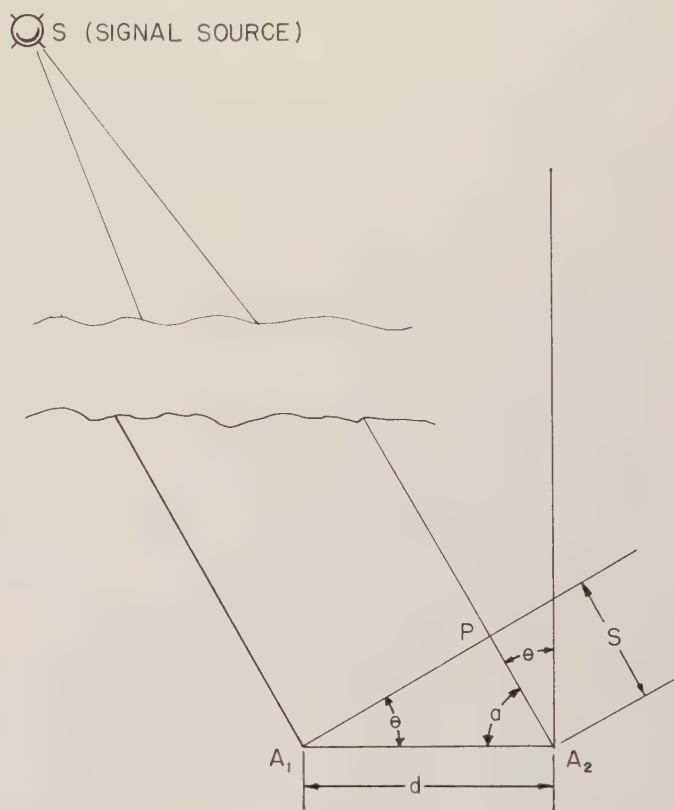


Fig. 1—Geometry of Mark II Minitrack phase angle tracking system.

In the Mark II Minitrack system the signals from two antenna arrays are combined in a hybrid junction which has two outputs. The combined signal from one output is connected to the input terminals of a double superheterodyne receiver, while the other output is connected to a separate but identical unit. Two local oscillators which are common to both receivers produce phase coherence of the signal at the output terminals of the receivers. The 108-mc input signal frequency is translated to 11.295 mc in the first mixer converter, after which it is amplified by the first IF amplifier. The second mixer converter translates the 11.295-mc signal to 470 kc after which the remaining required amplification is supplied.

The 470-kc signals at the outputs of the receivers are fed to three circuits: 1) null detector, 2) combined AGC detector, 3) product detector. The envelopes of the 470-kc signals existing at the outputs of the receivers are virtually identical except for a 180-degree phase shift. When one is in a null the other is maximum. As the first approaches a maximum envelope amplitude, the second approaches a minimum amplitude.

The AGC detector obtains its output from the input with the highest amplitude. The AGC is therefore alternately controlled by first one and then the other chan-

\* Manuscript received by the PGMIL, February 1, 1960.

† Army Map Service, Washington, D. C.



nel, although it controls the gain of both continuously. The independent receiver outputs are detected in the null detectors, the outputs of which, coupled with the time, produce the necessary tracking data. The product detector, which combines the null outputs from the null detectors, provides tracking data with improved signal-to-noise characteristics.

#### CALIBRATION OF MARK II MINITRACK

Before data obtained with Mark II Minitrack can be used, however, the field pattern of the interferometer must be studied. Two principal methods have been proposed: 1) exploration of the pattern by means of a signal transmitted from an aircraft which in turn is tracked optically, and 2) exploration of the pattern by means of radio star tracking. To date, only 2) has been used by the Army Map Service; this method will therefore be discussed.

It is assumed that the antenna field pattern can be approximated by a family of coaxial cones, whose common apex is at the electric center of the Minitrack station. The equation of such a family of cones in inertial space coordinates is

$$\begin{aligned} \pm \sin c = & -\cos b \cos (A + a) \cos \delta \sin (\lambda + \theta_G - \alpha) \\ & - \cos b \sin (A + a) [\cos \varphi \sin \delta \\ & - \sin \varphi \cos \delta \cos (\lambda + \theta_G - \alpha)] \\ & + \sin b [\cos \varphi \cos \delta \cos (\theta_G + \lambda - \alpha) \\ & + \sin \varphi \sin \delta], \quad (1) \end{aligned}$$

where

- $\Delta a$  = the error in azimuth of the antenna baseline,
- $\Delta b$  = the error produced by departure of the antenna baseline from horizontal,
- $\Delta c$  = the error resulting from a difference of length in the transmission lines from the two antenna arrays to the receiver (this error is interpreted geometrically as the complement of the semi-apex angle of the cone),
- $\alpha, \delta$  = right ascension and declination of radio star,
- $\varphi, \lambda$  = latitude and longitude of Minitrack station,
- $A$  = assumed azimuth of the radio signal source when it is in the center of the field pattern,
- $\theta_G$  = Greenwich sidereal time,
- $\theta_{G_0}$  = Greenwich sidereal time at 0<sup>h</sup> UT,
- $\tau$  = the time corresponding to a phase difference  $\vartheta = (j-1)\pi$ ,  $j=1, 2, 3, \dots$ ,
- $\theta_{G_0} = \theta_{G_0} + 15^\circ 04' 10.6864/\text{hr } \tau$ .

Because  $(a, b) \ll 1^\circ$ , and  $A$  is constant, the calibration will consist of differential corrections obtained from a least square solution of the differential form of (1). That is,

$$\begin{aligned} \Delta(\lambda + \theta_G - \alpha) \\ = \left[ \frac{U \sin \varphi - \cos \varphi \tan \delta}{U} \right] \frac{\sec^2 A}{V} \Delta a \end{aligned}$$

$$\begin{aligned} & + \left[ \frac{U \cos \varphi + \sin \varphi \tan \delta \sec^2 A}{U} \right] \frac{\sec A}{V} \Delta b \\ & + \frac{\sec \delta \sec A}{U} \cos c \Delta c, \quad (2) \end{aligned}$$

where

$$\begin{aligned} U &= [V - \cos^2 \varphi \tan^2 \delta \tan^2 A]^{1/2}, \\ V &= 1 + \sin^2 \varphi \tan^2 A, \\ c &= \sin^{-1} S/d, \end{aligned}$$

and

$$\begin{aligned} \sin (\theta_G + \lambda - \alpha) &= \frac{-\tan \delta \tan A \cos \varphi + U \sin \varphi \tan A}{V}, \\ \cos (\theta_G + \lambda - \alpha) &= \frac{U + \tan^2 A \tan \delta \sin \varphi \cos \varphi}{V}. \end{aligned}$$

$\Delta(\lambda + \theta_G - \alpha)$  is interpreted as being  $\Delta\tau$  or  $(\tau_{\text{obs}} - \tau_{\text{comp}})$ .

For a solution to be possible, many transits, by a minimum of three radio stars through the antenna field pattern, are needed.

The computed transit time  $\tau_{\text{comp}}$ , must be obtained for every  $\tau$  corresponding to  $\vartheta = (j-1)\pi$ , for it is required to calibrate each member cone of the family of coaxial cones.

A simple approach is first to determine when the star's azimuth nearly corresponds with the azimuth the star will have if it is in the center of the interference pattern. Since the  $(\alpha, \delta)$  coordinates are fixed for the star, and the  $(\varphi, \lambda)$  are fixed for the station, the time  $\tau_{\text{comp}}$  when  $|A - A_c|$  = minimum, is computed from the following set of equations. To make this computation the two following cases are considered:

a)  $A = 0^\circ$

$$\tau_c = \frac{\alpha - \lambda - \theta_{G_0}}{15^\circ 04' 10.6864/\text{hr}} \quad 0^\circ \leq (\alpha - \lambda - \theta_{G_0}) < 360^\circ,$$

b)  $A \neq 0^\circ$

$$\begin{aligned} \tau_c &= \frac{1}{15^\circ 04' 10.6864/\text{hr}} \left[ (\alpha - \lambda - \theta_{G_0}) \right. \\ & \left. + \sin^{-1} \left\{ \frac{-\tan A \tan \delta \cos \varphi + \sin \varphi \tan A U}{V} \right\} \right]. \quad (3) \end{aligned}$$

When

$$\tau_{\text{obs}} \approx \tau_{\text{comp}}$$

then

$$|A - A_c| = \text{minimum.}$$

Letting this  $\tau_{\text{comp}}$  correspond to the null number  $N$  when  $N=0$ , all times preceding  $N=0$  corresponding to  $N=-1, -2, -3$ , etc., and succeeding times from  $N=0$  corresponding to  $N=1, 2, 3, \dots$ . The times  $\tau_c$  corresponding to each  $\vartheta = \pi(j-1)$ ,  $j=1, 2, 3, \dots$  are then obtained from the relation

$$\tau_{cN_+} \equiv \tau_{c0} + \Delta\tau,$$

$$\tau_{cN_-} \equiv \tau_{c0} - \Delta\tau,$$

$$N_+ \equiv N > 0,$$

$$N_- \equiv N < 0,$$

$$\Delta\tau = \frac{\sec \delta}{15^{\circ}04'10.6864/\text{hr}} \cos^{-1} \left\{ \frac{R \sin \delta}{S} + \cos \eta_N \left[ \left( 1 - \frac{R^2}{S \cos^2 \eta_N} \right) \left( 1 - \frac{\sin^2 \delta}{S} \right) \right]^{1/2} \right\},$$

$$R \equiv \sin \delta + \sin \eta_N \sin A \cos \varphi,$$

$$S \equiv 1 - \cos^2 \varphi \sin^2 A,$$

$$\sin \eta_N \equiv N \sin \eta_1,$$

$$\sin \eta_1 \equiv \frac{1}{2} \left[ \frac{v}{1.000333 f \times d} \right], \quad (4)$$

with

$v \equiv$  velocity of light taken as  $299.7929 \times 10^6$  meters per second,

$f \equiv$  frequency received from radio signal source, taken for the present as  $108 \times 10^6$  cps,

$d \equiv$  separation between antenna arrays, taken for AMS Minitrack as 1000 feet.

The computed transit times  $\tau_c$  corresponding to  $\vartheta = (j-1)\pi$ ,  $j=1, 2, 3 \dots$  for a given transit by a radio star are now related to the observed transit times  $\tau_0$  of the same star, and  $\tau_0 - \tau_c = \Delta\tau$  is formed. By making many such observations from a minimum of three radio stars,  $\Delta a$ ,  $\Delta b$ ,  $\Delta c$  can then be determined for every null  $N$ . The observation equations are formed by relating  $\Delta\tau$  to (2) thus forming a set of observation equations for every  $N$ ; hence by the method of least squares the calibration constants are obtained.

Calibration of Mark II Minitrack in this manner constitutes a mapping of the antenna field pattern. Results obtained using this method indicate that for  $N=0$  the calibration is most accurate, *e.g.*, for Clark Air Force Base, P.I., the RMSE of calibration is well within  $\pm 24''$ . As we depart from  $N=0$  the RMSE increases.

This is to be expected, since as the sensitivity of the instrument decreases (which is what happens for  $N \neq 0$ ,  $-k \leq N \leq k$ ,  $k=1, 2, 3 \dots$ ), the random errors inherent in each observation increase.

Table I gives the stellar radio sources used for calibration of Mark II Minitrack. It is also seen that part of the RMSE of calibration is due to the uncertainty in the radio star position. Errors also arise from the non-stratified characteristic of the ionosphere called the wedge effect (see Smith [1]). This effect can introduce a random error of about 15 inches and a systematic shift of as much as 1 foot.

TABLE I

Star Name	Position (1950)	Change Due to Precession/Year
Cassiopeia-A	$\alpha: 23^{\text{h}} 21^{\text{m}} 12^{\text{s}} \pm 1^{\text{s}}$ $\delta: 58^{\circ} 32' 06'' \pm 0.7'$	$2^{\text{s}}705$ $19^{\circ}756$
Cygnus-A	$\alpha: 19^{\text{h}} 57^{\text{m}} 45^{\text{s}}.3 \pm 1^{\text{s}}$ $\delta: 40^{\circ} 35' 00'' \pm 1'$	$2^{\text{s}}076$ $9^{\circ}851$
Taurus-A	$\alpha: 05^{\text{h}} 31^{\text{m}} 29^{\text{s}} \pm 2^{\text{s}}.5$ $\delta: 22^{\circ} 00' 00'' \pm 3'.0$	$3^{\text{s}}609$ $2^{\circ}487$
Virgo-A	$\alpha: 12^{\text{h}} 28^{\text{m}} 10^{\text{s}}.5 \pm 2^{\text{s}}.5$ $\delta: 12^{\circ} 44' 00'' \pm 6'.0$	$3^{\text{s}}036$ $-19^{\circ}890$
Centaurus	$\alpha: 13^{\text{h}} 22^{\text{m}} 30^{\text{s}}.0 \pm 4^{\text{s}}$ $\delta: 42^{\circ} 46' 00'' \pm 2'.0$	$3^{\text{s}}509$ $-18^{\circ}758$

#### DETERMINATION OF MARK II MINITRACK STATION COORDINATE CORRECTIONS FROM SATELLITE OBSERVATIONS

Let  $\bar{u}_i$  ( $i=1, 2, 3$ ) be a right-hand Cartesian coordinate system with its origin at the observer, let the  $\bar{u}_3$  axis be parallel to the earth's axis of rotation and positive to the north, and let the  $\bar{u}_1$  axis be parallel to the meridian of Greenwich and positive in the direction of Greenwich. The equation of the cone in this coordinate system is then

$$F = [\bar{u}_i]^T [p_{ij}] [\bar{u}_j] = 0,$$

where

$$p_{ij} = p_{ji},$$

$$p_{ij} = RSR^T,$$

$$R \equiv \begin{bmatrix} -\sin \lambda & -\sin \varphi \cos \lambda & \cos \varphi \cos \lambda \\ \cos \lambda & -\sin \varphi \sin \lambda & \cos \varphi \sin \lambda \\ 0 & \cos \varphi & \sin \varphi \end{bmatrix},$$

$$\times \begin{bmatrix} \cos (A + \Delta a) \cos \Delta b & \sin (A + \Delta a) & -\cos (A + \Delta a) \sin \Delta b \\ -\sin (A + \Delta a) \cos \Delta b & \cos (A + \Delta a) & \sin (A + \Delta a) \sin \Delta b \\ \sin \Delta b & 0 & \cos \Delta b \end{bmatrix},$$

$$S \equiv \begin{bmatrix} 1 & 0 & 0 \\ 0 & -\tan^2 (c + \Delta c) & 0 \\ 0 & 0 & -\tan^2 (c + \Delta c) \end{bmatrix}.$$

(5)



If from an accurate ephemeris of the satellite we obtain the satellite coordinates  $\bar{u}_i$  ( $i=1, 2, 3$ ) at the time  $\tau$  corresponding to  $\vartheta = (j-1)\pi$ ,  $j=1, 2, 3, \dots$ , then the satellite will be on the surface  $F=0$  if and only if the station position is correct. To determine when the satellite lies on a particular member of the family of cones, the following procedure is to be used. If  $A_0$  = assumed azimuth of satellite at the time  $\tau$  when the satellite transits the center of interference pattern, and  $A_c$  = computed azimuth of satellite at the time  $\tau$  when the satellite transits center of interference pattern.

$$A_c = \tan^{-1} \left[ \frac{\bar{u}_1 \sin \lambda - \bar{u}_2 \cos \lambda}{\bar{u}_1 \sin \varphi \cos \lambda + \bar{u}_2 \sin \varphi \sin \lambda - \bar{u}_3 \cos \varphi} \right], \quad (6)$$

and

$$\Delta A \equiv A_0 - A_c,$$

then  $|\Delta A| = \min$  at the time, when the satellite will be closest to the center of the interference pattern. This is the reference instance from which by simple extrapolation the position of the satellite can be related to each member of the family of cones for every time  $\tau$  corresponding to  $\vartheta = (j-1)\pi$ .

The position of the satellite is given by the ephemeris in  $x_i$  ( $i=1, 2, 3$ ) coordinate system with origin at the gravitational center of the earth, the  $x_3$  axis coinciding with the rotational axis of the earth, the  $x_1$  axis pointing to the vernal equinox.

The observer's position, on the other hand, is known only in relation to the center of the reference ellipsoid used in geodetic datum. It can be expressed as

$$\begin{bmatrix} u_1 \\ u_2 \\ u_3 \end{bmatrix} \equiv \begin{bmatrix} (N+h) \cos \varphi \cos \lambda \\ (N+h) \cos \varphi \sin \lambda \\ [N(1-e^2) + h] \sin \varphi \end{bmatrix}, \quad (7)$$

where

$N$  = radius of curvature in the prime vertical,  
 $h$  = height of the Minitrack station above the ellipsoid,  
 $e$  = eccentricity of the ellipsoid.

To refer the satellite to the observer's topocentric coordinate system  $[\bar{u}_i]$ , in which the antenna field pattern (5) is observed, a rotation and two translations are needed to give the relationship

$$\begin{bmatrix} \bar{u}_1 \\ \bar{u}_2 \\ \bar{u}_3 \end{bmatrix} \equiv \begin{bmatrix} \cos \theta_G & \sin \theta_G & 0 \\ -\sin \theta_G & \cos \theta_G & 0 \\ 0 & 0 & 1 \end{bmatrix} \begin{bmatrix} x_1 - x_{c1} \\ x_2 - x_{c2} \\ x_3 - x_{c3} \end{bmatrix} - \begin{bmatrix} u_1 \\ u_2 \\ u_3 \end{bmatrix}, \quad (8)$$

where

$x_i - x_{c_i}$  = the unknown coordinate difference between the center of the earth and the ellipsoid,  
 $\theta_G$  = Greenwich sidereal time at  $\tau$ ,  
 $\theta_G \equiv \theta_{G_0} + 15^\circ 04' 10.6864 / \text{hr } \tau$ .

Suppose now that the station coordinates  $u_i$  are incorrect by the amount  $\Delta u_i$ . Then the change in the function  $F$  in (5) is

$$\Delta F = -2[\bar{u}_i]^T [P_{ij}] [\Delta u_j], \quad (9)$$

because

$$[\Delta \bar{u}_j] = \begin{bmatrix} \sin \\ \cos \end{bmatrix} (\theta_G)_{ij} [\Delta x_j] - [\Delta u_j] = -[\Delta u_j] \quad (10)$$

(since  $[\Delta x_j] = 0$  if an accurate orbit is assumed).

Eq. (5) becomes

$$0 = [f(\bar{u}_j(u_j^1))]$$

for the corrected position  $u_j^1 = u_j + \Delta u_j$ , and

$$F = [f(\bar{u}_j(u_j))] \neq 0$$

for the uncorrected position. Therefore

$$\Delta F = [f(\bar{u}_j(u_j^1)) - f(\bar{u}_j(u_j))], \quad (11)$$

or

$$\Delta F = 0 - F = -F.$$

On the other hand, the Mark II Minitrack station is assumed to be at a height  $h$  above the surface of the spheroid,

$$\frac{u_1^2}{(R_e + h)^2} + \frac{u_2^2}{(R_e + h)^2} + \frac{u_3^2}{[R_e(1 - e^2)^{1/2} + h]^2} = 1. \quad (12)$$

Differentiating this equation for the possible error in position, we get

$$\sum_{j=1}^3 m_j \Delta u_j = 0, \quad (13)$$

where

$$[m_j] \equiv \left[ \frac{u_1}{(R_e + h)^2}, \frac{u_2}{(R_e + h)^2}, \frac{u_3}{[R_e(1 - e^2)^{1/2} + h]^2} \right].$$

For the three antenna baselines of the Mark II Minitrack system,  $A = A_k$  with  $k=1, 2, 3$ ; thus three sets of families of cones are defined by the subscript  $k$ .

If we let

$$\gamma_{kj} \equiv -2[\bar{u}_i]^T [P_{ij}^k],$$

then (9) can be written in the form

$$\Delta F_k = \sum_{j=1}^3 \gamma_{kj} \Delta u_j. \quad (14)$$

Then  $[\Delta u_j]$  is determined by the method of least squares, the observation equations being

$$\begin{aligned}\Delta F_1 &= \sum_{j=1}^3 \gamma_{1j} \Delta u_j, \\ \Delta F_2 &= \sum_{j=1}^3 \gamma_{2j} \Delta u_j, \\ \Delta F_3 &= \sum_{j=1}^3 \gamma_{3j} \Delta u_j, \\ 0 &= \sum_{j=1}^3 m_j \Delta u_j.\end{aligned}\quad (15)$$

and

#### ERROR ANALYSIS

When the Mark II Minitrack instrument is calibrated by using radio star observations, the rms error expected for the solution of the above equations is of the order of  $\pm 200$  seconds of arc. A separation of the rms error into its component parts is given below.

source of rms error	rms error
radio star position	$\pm 170$ seconds of arc
calibration	$\pm 24$ seconds of arc
orbit	$\pm 100$ seconds of arc.
observation	$\pm 20$ seconds of arc.

It is seen that the largest contribution to the error comes from the radio star positions and from the orbit.

In terms of the corrected station coordinates, an overall error of 200 seconds of arc, evaluated at satellite alti-

tudes ranging from 200 km to 1000 km, means the following uncertainty:

satellite altitude	rms error
200 km	$\pm 200$ meters
800 km	$\pm 800$ meters
1000 km	$\pm 1000$ meters.

#### CONCLUSION

Corrections to Mark II Minitrack station coordinates can be improved by 1) calibration with aircraft, which will cut in half the rms error in the correction to the station coordinates, and 2) availability of a satellite orbit which will fit the observations used for its determination to  $\pm 20$  seconds of arc. This means that the error in the corrected station coordinates will be 20 per cent less than what is now obtained.

#### ACKNOWLEDGMENT

The author is greatly indebted to W. M. Kaula and S. W. Henriksen for their invaluable suggestions.

#### BIBLIOGRAPHY

- [1] V. R. Simas and C. A. Bartholomew, "Mark II Minitrack tional Analysis," U. S. Naval Res. Lab., Washington, D. C.; February 2, 1960. (Unpublished report.)
- [2] W. D. Kahn, "Calibration of Minitrack Mark II," *J. Astron.*, vol. 62, pp. 396-399; December, 1957.
- [3] J. L. Pawsey, "A catalogue of reliably known discrete sources of cosmic radio waves," *Astrophys. J.*, vol. 121, pp. 1-5; January, 1955.
- [4] F. G. Smith, "Ionospheric refraction of 81.5 mc/s radio waves from radio stars," *J. Atmos. Terr. Phys.*, vol. 2, pp. 330-355; 1952.

## Application of Electronic Distance Measuring Equipment in Surveying\*

THELMA A. ROBINSON†

**Summary**—Recent improvements in electronic distance-measuring equipment have made it possible to obtain higher degrees of accuracy in surveys for mapping. Electronic equipment has therefore become a far-reaching and powerful tool when used for establishing geodetic control in remote areas, between distant triangulation stations, over impassable terrain, and through intervening vegetation, where it is impossible to connect stations by visual methods. As a result of this broader coverage made possible by electronic measurements, more extensive geodetic connections are provided for the determination of the size and shape of the earth and consequent mapping of paths of missiles and of satellites.

This paper gives an up-to-date account of these geodetic applications of HIRAN, LORAC, tellurometers, geodimeters, as well as flares, and includes a brief description of the systems.

Some of the limitations and problems encountered with these instruments are described and the accuracies which have been obtained from specific field surveys are noted.

RECENT developments and improvements in electronic distance-measuring equipment utilizing the time of propagation of radio waves have made it possible to obtain higher degrees of accuracy in surveys for mapping. Since distances can be measured more rapidly electronically than by tapes, the recent improvements have provided a great stimulus to surveying by trilateration, that is, by the solution of networks of triangles from the measurement of the lengths of their sides. This is in sharp contrast to the conventional method of solution by triangulation, that is, through optical observation of the directions of the sides.

\* Manuscript received by the PGMIL, February 1, 1960.

† Army Map Service, Washington, D. C.



Trilateration by electronic equipment has the following advantages over triangulation:

- 1) It is possible to survey over impassable terrain such as dense jungles and steep mountains, over broad bodies of water, through intervening vegetation or underbrush, through smoke and fog, and in remote undeveloped areas.
- 2) Distances ranging from a few miles up to as much as 500 miles may be measured.
- 3) Working time can be substantially reduced.
- 4) Daytime as well as nighttime operation is possible.

Since longer distance measurements can be obtained, it is possible to connect continents and thereby determine a better over-all spheroid as a mathematical approximation to the figure of the earth and its orientation. This, in turn, will help us to predict better the paths of satellites and missiles around the earth.

Whether by trilateration or triangulation, the ultimate product is the computed intersection at the vertices expressed in latitude and longitude. The positions may be mapped, and distances between them or between places referred to them can be determined.

The accuracy of the measurements is dependent on the type of electronic equipment used and on the length of the line measured. The accuracy has ranged up to that of first-order, which is good to within one part in one hundred thousand and possibly one part in two hundred thousand.

A short description of some of the electronic distance-measuring equipment and of its operation is given below. Information and accuracies gained from specific field tests conducted by government agencies and private industry are noted.

### SHORAN-HIRAN

The basic SHORAN system consists of an airborne set (a transmitter, receiver and electronic timing unit) and a stationary, but portable, ground transponder at each end of the line to be measured. The aircraft proceeds in level flight across the line in the neighborhood of its midpoint, transmitting a series of discrete pulses to the two ground stations at separate frequencies. The pulses received at the ground stations actuate the respective transponders and return pulses are transmitted to the aircraft receiver. The time elapsed for each pulse's "round-trip" is measured by the airborne unit by means of a frequency-controlled time-scale generated for each outgoing-incoming pulse. The minimum combined path time to both stations can then be determined by inspection but, more rigorously in practice, by the mathematical method of least squares.

This minimum air path is then reduced to sea-level distance by applying length and curvature corrections to the SHORAN ray. The length corrections allow for the variations in the speed of light for different atmospheres at various altitudes of the SHORAN ray and for the time delay in the electronic equipment which is not part of the actual distance. The curvature correction takes into account the effect of the variation of the index of refraction

on the ray path at various altitudes. The corrected length and curvature, combined with the height of the airplane, determine the intersection of the ray path with the spheroid, and therefore give the projected spheroidal distance.

Since SHORAN's high-frequency transmission is line-of-sight, the altitude of the aircraft and of the ground antenna must be increased to obtain longer ranges. Distances of up to five hundred miles between stations have thus been measured. SHORAN has been used extensively by Canada to map its vast and undeveloped northern areas, including the Arctic islands. The final distances have been assessed as accurate to 1 part in 56,000 and confirmed by a limited number of SHORAN stations since incorporated in the conventional triangulation to the south.<sup>1</sup> A detailed description of the SHORAN system is given by Aslakson.<sup>2</sup>

HIRAN, on the other hand, is a modified and improved SHORAN system employing special operating techniques (such as amplitude control and finer calibration) whereas SHORAN was essentially a makeshift application of United States bombing equipment. HIRAN, a contraction taken from the initial and terminal letters in High-Precision SHORAN, therefore permits distance measurements to accuracies which are close to first order. The U. S. Air Force 1370th Photo-Mapping Group has used HIRAN extensively in various parts of the earth, including a 2300-mile undertaking which has connected Europe to North America through Iceland and Greenland.<sup>3</sup>

In order to assure uniform accuracy of the trilateration survey, the pattern of the network is analyzed for strength of figure by appropriate mathematical formulas.<sup>4</sup> Thus, if the predicted uncertainty in, say, the longitude of a specific position appears excessive, the addition of east-west lines terminating in that point is required. Actually, an equal excess of lines is used at all stations and the discrepancies are averaged out by least-squares adjustment.

HIRAN is also used extensively in conjunction with aerial photography, when there are not sufficient known ground positions within the field of view of the camera for proper referencing of the land features. In HIRAN-controlled photography, the position of the aircraft camera, and therefore the center of the photograph, can be determined by recording the HIRAN distances of two known distant ground stations.

### LORAC

The word LORAC, a contraction taken from the initial letters in Long Range Accuracy, is a phase comparison

<sup>1</sup>J. E. R. Ross, "Canadian SHORAN Project," paper presented at the Internatl. Assoc. of Geodesy Symp., Washington, D. C., May 5-12, 1959; unpublished.

<sup>2</sup>C. Aslakson, "Principles of SHORAN Mapping," (Report written for Aero Service Corp.), Philadelphia, Pa.; 1956.

<sup>3</sup>Final Rept. of Results, Phase III, Project 53 AFS-1, Greenland-Icecap Tie, 1370th Photo-Mapping Group, Air Photographic and Charting Service (MATS); November, 1956.

<sup>4</sup>S. D. Owen, "Evaluation of HIRAN Networks," paper presented at the Internatl. Assoc. of Geodesy Symp., Washington, D. C., May 5-12, 1959; unpublished.

radio-location and distance-measurement system developed by the LORAC Service Corporation originally for oil prospecting and other surveys. The comparatively small weight and size of its airborne units (144 pounds and 4.7 cubic feet, respectively) in contrast to those of HIRAN made LORAC an ideal system for survey applications by the U. S. Army, in view of the limited size of its aircraft.

The U. S. Army Engineer Research and Development Laboratories contracted for LORAC field tests in 1956 and 1956-1957 in Louisiana and in Arizona, respectively. In Louisiana, the distance-measurement capability of LORAC was tested for lines ranging between 40 and 260 miles over sea water, various types of terrain, and combinations of water and land. In Arizona, radio-location as well as distance-measurement capabilities were tested over desert and mountainous terrain. The accuracies obtained were within 1 part in 100,000 or better (that is, first-order), for entirely sea-water paths, but for extreme nonhomogeneous land paths consisting of complex mountain and desert terrain, the accuracies were only to within 1 part in 25,000. Terrain of intermediate homogeneity gave intermediate accuracies. Further tests, this time for lines up to 500 miles in length, were scheduled for April, 1960, in Florida. By using medium frequencies which follow the earth's curvature, the aircraft need not fly higher for these longer lines.<sup>5,6</sup>

The determination of distance or position by means of phase comparison of radio waves depends on the principle that waves arriving from two different sources give rise to a phase discrepancy caused by the difference in the lengths of the two paths. In the LORAC system, the two ground transmitters (which may be several hundred miles apart) are not phase-synchronized with each other, and therefore a stationary distant receiving station would be measuring a constant phase difference in addition to that caused by the path length differences. Furthermore, since the two CW transmissions differ by an audio frequency, the stationary receiving station would detect recurring  $0^\circ$  through  $360^\circ$  shifts of phase.

At any specific instant, the phase interaction of each wave cycle from the first transmitter with those from the second forms a family of hyperbolas with the transmitters as foci. Along each hyperbola the phase difference is constant, but it varies through the successive hyperbolas from  $0^\circ$  through  $360^\circ$ , recurrently.

Imposition of the dynamic phase change caused by the difference of CW frequencies mentioned earlier, then, simply causes the identical pattern of family of hyperbolas to re-establish itself everywhere at the end of every  $0^\circ$ -to- $360^\circ$ -phase cycle.

<sup>5</sup> Final Rept. of Field Tests of the Application of a Phase Comparison Radio Location System to Distance Measurement, Engineer Res. and Dev. Lab., Fort Belvoir, Va.; February-May, 1956.

<sup>6</sup> Final Rept. of Field Tests of the Application of a Phase Comparison Radio Location System to Distance and Position Measurement Over Mountainous and Desert Terrain, Engineer Res. and Dev. Lab., Fort Belvoir, Va.; May-July, 1957.

If a second independent receiver were now placed at the site of the stationary receiving station, the phase difference would, of course, be the same and therefore, subtracting one from the other, would give zero phase difference. However, if one of the two receivers were then moved along from there to another position, the amount of phase difference caused by its distances from the transmitters would vary, but the phase difference caused by the lack of transmitter phase synchronization would remain constant and the phase variation caused by the difference of CW frequencies would be at the same rate as at the stationary receiver. Therefore, by transmitting the phase difference of the stationary station to the mobile receiver and subtracting the two, the net phase difference caused by the new position alone is obtained.

Actually, the mobile receiver would record zero-net-phase difference no matter where it might intersect the hyperbola that passes through the "reference" station and has the transmitters as foci. The hyperbolas corresponding to the successive positions of the mobile receiver are determined by recording the number of complete and fractional phase cycles traversed with respect to the reference station. The corresponding distance between the hyperbolas of the reference and mobile (airborne) stations (along the line of the two continuous wave transmitters) is computed approximately from one-half the product of one of the CW wavelengths and the number of cycles counted.

Since it requires the intersection of two hyperbolas to determine the position of the mobile unit, a second family of hyperbolas is generated by means of a third CW transmitter used in conjunction with the second, and a similar reduction as above is made.

The above system is used, for example, to position the camera during aerial photography. A variation of the system is used to determine distance between two ground transmitter positions. This is accomplished by flying the mobile unit in an arbitrary path around the two ground positions. In this manner, the hyperbolas are traversed in opposite directions for each half of the circuit, and therefore negative as well as positive, phase cycles are recorded. This gives a minimum accumulated total when crossing the extension of the line joining the ground transmitters.

Since the total number of hyperbolas traversed is the same along the straight line between the CW transmitters as along any other route, the number of phase cycles recorded for half the circuit can be translated to the required distance by the formula given above. Further details may be found in the "Survey Officer's Manual."<sup>7</sup>

#### LIGHT-CROSSINGS AND FLARES

Although surveys by light-crossings and flares do not use electronic equipment exclusively or measure distances,

<sup>7</sup> "Survey Officer's Manual (The Application of LORAC to Precision Terrestrial Line-Length Measurement and Position Fixing)," LORAC Service Corp. under contract from U. S. Army Engineer Res. and Dev. Lab., Fort Belvoir, Va.; (undated).



they have been developed for close support of the HIRAN and LORAC systems just described. Their prime purpose is to provide more accurate orientation of long survey lines used in electronic trilateration networks.

The light-crossing system may be likened to HIRAN, in that an airplane flies across the line of two non-intervisible distant ground stations in the neighborhood of its midpoint. However, instead of obtaining the minimum distance sum, it determines the direction of the station line by means of the pair of station-to-aircraft directions that are  $180^\circ$  of each other, modified by an appropriate correction caused by the convergence of the meridians toward the poles.

The aircraft, flying at night and carrying an intense electric light, is guided across the station line in a straight path which is determined optically from an auxiliary third ground station by means of a telescope clamped in the prescribed direction. The light is also continuously tracked optically by an observer at each of the two end stations, and successive pairs of direction readings to the aircraft light are recorded by cameras which are triggered simultaneously by pulses emanating from the airplane. All observed directions are referred to celestial north as a common reference, but small corrections are applied to these horizontal directions because of the discrepancy between the actual direction of gravity and the perpendicular to the approximating spheroid assumed for the earth. The pair that differs by  $180^\circ$ , modified by the convergence of the meridians, is determined by least squares to obtain the direction between stations.

Direction surveys by the flare method, on the other hand, employ three non-intervisible ground stations forming a large triangle such as in HIRAN networks. Parachute flares are dropped in the general area of three or more predetermined locations within this triangle, each flare in turn being optically tracked simultaneously from the three ground stations until extinguished. From the geometrical relations existing between the directions observed, the directions of the sides of the ground triangle can be computed.

Both of the above direction methods were tested by the Army Map Service (supported by private and other government organizations) in 1957 in Arizona for lines up to 85 miles long. The light-crossing has subsequently been applied operationally. In all cases, the direction accuracies have generally been within less than one second, which is equivalent to good first-order triangulation.

It is interesting that, no matter how scalene the ground station triangle may be, its strength of figure is identical to that of an equilateral triangle; that is, for any chosen flare position in an equilateral triangle, there always exists a corresponding position of equal strength in the scalene triangle. Furthermore, for the light-crossing as well as the flare method, the strength of figure is independent of the orientation of the station lines and of the flight direction.

The theory, application, field results and strength of figure derivations are given in Sodano<sup>8</sup> and Sodano and Robinson.<sup>9</sup>

#### TELLUROMETER

The tellurometer is a portable electronic phase-comparison instrument designed to measure relatively short distances with high accuracy. It is fairly rugged in the field under the rigors of transportation and weather. Each of the two main units weighs only 38 pounds, and is generally capable of ranges up to 60 km. Unlike conventional optical survey instruments, it can measure through underbrush and even small trees, and operate by day as well as night.

The manufacturer has estimated the accuracy to be within 1 part in 330,000 of the distance measured, plus or minus 5 cm. This means that the net proportional accuracy will be lower for shorter lines; thus for lines less than 15 km, the 5 cm would be the limiting accuracy, while on lines over 15 km, the 1 part in 330,000 would begin to contribute to the limiting accuracy. Tellurometer tests and operations by many nations in various countries have borne out its capabilities for first-order accuracy. Modifications and additions (a few of which are now being incorporated by the manufacturer) give promise of consistent accuracies of 1 part in 200,000, or better.

Since the tellurometer is designed to measure short line-of-sight distances, its phase-comparison system is simpler than that used on long non-intervisible lines by LORAC. The distance between two ground positions requires transmitters only at those two sights, since phase synchronization can be accomplished by direct linkage rather than by cancellation from a reference station. The mobile unit for traversing and keeping a record of the number of phase cycles between the ends of the line is also eliminated. Instead, to resolve the ambiguity of how many whole cycles precede the fractional cycle which is measured by phase comparison of the returning and outgoing signal, the carrier is modulated by four different frequencies to allow four separate phase comparison readings. The distance must, of course, be known in advance within one wavelength of the lowest modulating frequency, and the successively more refined readings are obtained from the three higher modulating frequencies.

Basically, the equipment consists of a master unit which transmits the modulated carrier from one end of the line to the remote unit at the other. The units focus the signal with parabolic antennas. The remote unit receives, amplifies and retransmits the modulated wave back to the master with only infinitesimal internal delay. The returning signal

<sup>8</sup> E. M. Sodano, "Determination of Laplace azimuth between non-intervisible distant stations by parachuted-flares and light-crossings," *Bull. Géodésique*, no. 49, pp. 16-32; September, 1958.

<sup>9</sup> E. M. Sodano and T. A. Robinson, supplementary study to Sodano, *ibid.*, presented at the Internatl. Assoc. of Geodesy Symp., Washington, D. C., May 5-12, 1959; unpublished.

is then compared in phase to the outgoing at the master. As in other electronic systems, corrections to the theoretical velocity of light must be applied in accordance with meteorological conditions not only at the end sites, but also in between, if possible. Most important, the ground characteristics cannot be overlooked, since flat bare ground as well as smooth water surfaces are likely to produce strong reflected waves which give longer apparent distances at first, the error cyclically reducing to zero and increasing again as longer lines are measured, as noted in the "Tellurometer Handbook."<sup>10</sup>

At present, an airborne tellurometer is contemplated to measure longer lines, to serve as an intermediary in the positioning of distant ground stations relative to known ones, and to perform aerial photography while positioning the airborne instrument itself.

#### GEODIMETER

The geodimeter is a distance-measuring instrument based on electronic-optical principles and therefore it must be used generally at night. It is portable, though appreciably heavier than the tellurometer. The very high accuracy of the geodimeter, however, provides an extremely useful means of measuring starting base lines of triangulation networks, thus eliminating laborious measurements with tapes suspended over ground stakes. Since it can measure base lines up to 50 miles during good visibility, there is no need (as in the much shorter taped ones) to expand the base line by means of a network of triangles.

The geodimeter is a phase-intensity comparer. Essentially, it transmits pulses of light at a rate which is synchronous with the sensitive-insensitive periods of a receiving photo tube. The transmitted pulses of light travel from the geodimeter to a mirror at the opposite end of the line to be measured and are reflected back to the receiving photo tube. Depending on the round distance traveled, the pulses of light will return during the sensitive, intermediate or insensitive phase of the photo tube. The amount of

electrical current resulting indicates the proportion of one sensitive-insensitive period that the light pulses required over and above an integral number of periods. The measurement is then repeated with a lower frequency (as in the case of the tellurometer) to determine more easily the number of integral periods.

The geodimeter generates the light pulses by means of a so-called Kerr cell, preceded and followed by a light polarizer. Since the two polarizers are rotated 90° to each other, no light can pass through. However, by applying a voltage to the Kerr cell (which contains highly purified nitrobenzene) the angle of polarization of the light changes, thus allowing it to pass through both polarizers. By applying an alternating voltage to the Kerr cell, pulses of light are effectively generated. This same alternating voltage, which is actually a high-modulating frequency from a radio transmitter, is also synchronously applied to the receiving photo tube as noted earlier.

Various models of geodimeters have been developed, depending on the specifications of accuracy, size, weight, length of lines to be measured and special applications. The accuracy of the more precise models is within 1 part in 300,000, or better, which is probably as accurate as the best conventional triangulation itself.<sup>11,12</sup> Thus this, as well as the various other electronic distance measuring systems described herein, has made significant contributions to surveying, mapping, determination of the best approximation for the figure of the earth and of its influence on the motion of satellites or missiles.

#### ACKNOWLEDGMENT

The author wishes to express her gratitude to E. M. Sodano of the Army Maps Service for his invaluable assistance, especially concerning the electronics of the systems.

<sup>11</sup> "Geodimeter, For Measuring Distances by Light Waves, Types I and II," Engineer Res. and Dev. Lab., Fort Belvoir, Va.; December, 1955.

<sup>12</sup> E. Bergstrand, "The Geodimeter System," paper presented at the Internatl. Assoc. of Geodesy Symp., Washington, D.C., May 5-12; unpublished.

<sup>10</sup> "Tellurometer Handbook, Technical Instructions No. 1," Corps of Engineers, U. S. Army Map Service, Far East, 1st ed.; March, 1959.



# Semi-Active Correlation Radar Employing Satellite-Borne Illumination\*

O. E. RITTENBACH† AND W. FISHBEIN†

**Summary**—This paper describes a semi-active radar system in which the transmitter is carried in a satellite. The satellite transmits a randomly modulated signal. On the ground the radar has two antennas and receivers. One antenna points at the satellite, the other at the target. The signal from the satellite-oriented receiver is delayed and correlated with the satellite signal reflected from the target. The delay corresponding to the peak of the correlation function is used to determine range. It is planned to test this system with various communications satellites.

## WHY CORRELATION RADAR?

CONVENTIONAL radar transmits one short radio-frequency pulse every repetition period. The pulse duration is determined by the required range resolution, the pulse repetition time by the round trip time for a target at maximum range. For a given peak power, the ratio of pulse duration to repetition time (duty cycle) limits the average power transmitted. Correlation radar permits a higher duty cycle by transmitting several pulses every repetition period. To avoid range ambiguities, the transmitted pulses must be coded. In the receiver, a correlator is needed for decoding.

For example, assume, instead of transmitting one pulse every repetition time we transmit seven closely spaced pulses, coded  $+ - + + - - -$ . (+ means a pulse of peak power and unit pulse time in phase with a local oscillator, — means a pulse of peak power and unit pulse time  $180^\circ$  out of phase with a local oscillator.) In order to obtain a correlation function, one requires a variable delay line, a multiplier, and an indicator with a low-pass frequency characteristic, *i.e.*, an integrator (Fig. 1). If only one fixed target is present, the indicator will read between  $-1$  and  $0$ , except for one setting of the delay line. At this position, the time delay of the signal from code generator to transmitter to target to receiver to multiplier is equal to the time delay of the reference signal from code generator through delay line to multiplier. At this delay setting, the output of the multiplier is always positive, despite the fact that the code changes randomly between positive and negative [Fig. 2(a)]. This is so because the input signals to the multiplier are of the same polarity at any one instant and the product of the two signals of the same polarity is always positive. The indicator rejects the high-frequency components out of the multiplier and shows only the algebraic sum, that is, seven.

In all other positions of the delay line, all combinations of plus and minus randomly appear at the two inputs of the multiplier [Fig. 2(b)]. The product at the output can then be both plus and minus. The value shown on the indicator tends to zero.

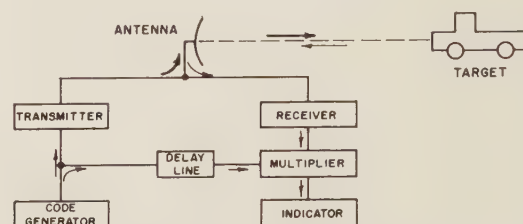


Fig. 1—Correlation radar.

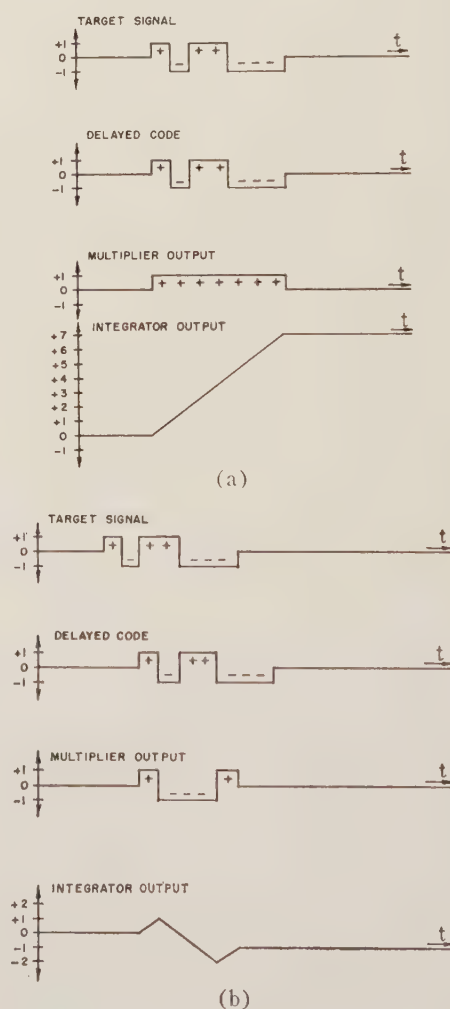


Fig. 2—Correlation process. (a) Signal round trip time equal to code delay time. (b) Signal round trip time not equal to code delay time.

\* Manuscript received by the PGMIL, February 1, 1960.

† U. S. Army Signal Res. and Dev. Lab., Fort Monmouth, N.J.

If a moving target is present, then, at the corresponding position of the delay line, the output voltage at the multiplier is modulated with the Doppler frequency. The frequencies present at the output of the multiplier are combinations of the Doppler frequency  $f_d$  and multiples of the repetition frequency  $f_r$ , *i.e.*,  $f_d$ ,  $f_r - f_d$ ,  $f_r + f_d$ ,  $2f_r - f_d$ ,  $2f_r + f_d$ , . . . . . Thus, if targets can have Doppler frequencies which are higher than  $f_r/2$ , their true Doppler frequency cannot be determined. The resulting Doppler frequency ambiguity can be minimized by making the pulse long enough to encompass several cycles of the Doppler frequency. In the limit, the ambiguity can be entirely avoided by increasing the duty cycle to 100 per cent. In addition, a greater average power thereby can be transmitted. The code generator could then be, for example, a noise generator.

### SEMI-ACTIVE RADAR

If the transmitter is on continuously and one antenna is used for transmitting and receiving, it is only possible to obtain the necessary isolation between transmitter and receiver at very low transmitter power levels. In most cases, saturation of the receiver can only be avoided through the use of widely-separated transmitting and receiving antennas. (See Fig 3.) Here the reference is sent to the receiver through a suitable communications link. The setting of the delay is a function of the geometry of the triangle formed by the transmitter, receiver and target. Knowing the delay setting, the angle  $\theta$ , and the distance between transmitter and receiver, the distance from target to receiver can be determined.

### SATELLITE-BORNE TRANSMITTER

In the semi-active radar system, the transmitter should be highly elevated in order to illuminate a large target area with a minimum of shadow. A captive balloon is one possibility. Another possibility is to make use of radiation from a satellite which is stationary with respect to the earth, *i.e.*, one which has an orbit of 52,000 miles diameter.

The system is shown in Fig. 4. The receiver station requires two antennas, one looking at the target and the other at the satellite, in order to obtain a reference. To reduce the necessary search time, a tapped delay line can be used instead of the variable line of Fig. 1. Each tap supplies one input of a multiplier. The second input of each multiplier is fed with the target signal. Every multiplier output is connected to an indicator representing a discrete target distance. For target to receiver distances, which are very small compared to the distance from satellite to receiver, the range of the satellite does not measurably influence the delay corresponding to target distance. The target range is then given by

$$R = \frac{\tau c}{1 - \cos \theta},$$

where  $\tau$  is the tap delay and  $c$  is the velocity of light.

To get an indication of the detection range possible, we assume a transmitted power of 100 watts, illuminating an area 7000 miles in diameter. A one square meter target is then illuminated with  $10^{-12}$  watts. If the target scatters this power equally in all directions, an antenna of one square meter area at a distance of 1000 yards will receive  $10^{-19}$  watts. With a receiver noise figure of 4 db and an indicator bandwidth of one cycle, the signal-to-noise ratio will be about ten to one. Since the radiation on every point of the illuminated area is nearly constant, the signal received by the antenna will vary inversely as the square of the distance to the target. Therefore, the same equipment will again give a ten-to-one signal-to-noise ratio on a 100 square meter target at a range of 10,000 yards.

The satellite radiation can be used in this manner for target location over an area of about 40,000,000 square miles. Thousands of receiving systems can operate with a single satellite transmitter. Since the receivers are passive, there is no danger of mutual interference.

### EXPERIMENTAL PROGRAM

An experimental semi-active correlation radar system is under development at U. S. Army Signal Research and Development Laboratories. Future experiments are planned in which the radiation will come from communications satellites.

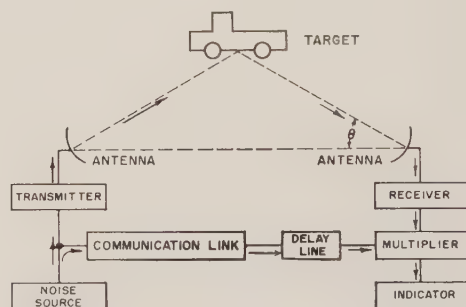


Fig. 3—Semi-active correlation radar.

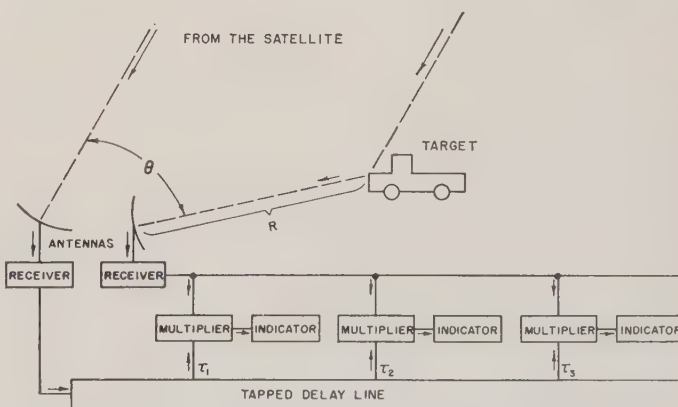


Fig. 4—Semi-active correlation radar using satellite-borne illumination.



# Artificial Ionospheres for Communications\*

F. F. MARMO† AND A. ENGELMAN†

**Summary**—This paper suggests the utilization of an artificial ionosphere (artificial electron cloud) for RF communication. For convenience the presentation is given in two major parts. The first part is concerned with the general considerations associated with the generation, dynamics and other physical characteristics of the artificial ionospheres. It presents a general survey of the data and analysis from several experiments designed and performed expressly for obtaining critical engineering parameters required for the systematic development of these clouds as a propagation medium. These parameters include 1) chemical yield of contaminant, 2) thermal ionization efficiency, 3) upper atmosphere wind velocities, 4) wind shear, 5) ambipolar diffusion, 6) neutral diffusion, 7) solar photoionization probabilities, and 8) several decay processes including mutual neutralization, chemical consumption, electron attachment, recombination, etc. The effect of these processes upon the propagation capabilities of electron clouds is emphasized. Finally, some suggested improvements are offered for optimizing the artificial ionosphere propagation capability.

The analytical model for cloud reflection, which is discussed in detail, is the spherically symmetric Gaussian electron distribution cloud. Cross-sectional cloud values as a function of time, including the maximum case, are discussed for this model. Calculations of cloud effectiveness for other reflective cases assuming various distribution functions, as well as one refractive case, are also presented. For the model discussed, the RF communications capability of the artificially generated ionosphere is presented. Since it is of first-order importance, the geometrical limitation of cloud generation altitude as a function of system communications range is considered. The altitude requirements for the limiting case of world-wide communications will be noted. In addition, the electronic system parameters, e.g., antenna gains, transmitter power, carrier frequency, bandwidth, etc., that are required to perform certain communications functions are presented in detail. Finally, the utility of existing UHF troposcatter communications equipment for optimum electron cloud communications will be demonstrated.

## INTRODUCTION

THE feasibility of utilizing artificial electron clouds (artificial ionospheres) for communication purposes has been demonstrated by Marmo, *et al.*<sup>1-7</sup>

\* Manuscript received by the PGMIL, February 1, 1960. The work performed for this paper has been partially supported by the U. S. Army Signal Corps, Fort Monmouth, N. J., under Contract No. DA36-039-SC-78971.

† Geophysics Corporation of America, Boston, Mass.

<sup>1</sup> F. F. Marmo, J. Pressman, L. M. Aschenbrand, A. S. Jursa and M. Zelikoff, "Formation of an artificial ion cloud; photoionization of NO by solar lyman alpha at 95 km," *J. Chem. Phys.*, vol. 25, p. 187; July, 1956.

<sup>2</sup> F. F. Marmo, L. M. Aschenbrand and J. Pressman, "Artificial electron clouds—I: Summary report on the creation of artificial electron clouds in the upper atmosphere," *Planet. Spa. Sci.*, vol. 1, pp. 227-237; August, 1959.

<sup>3</sup> F. F. Marmo, J. Pressman and L. M. Aschenbrand, "Artificial electron clouds—II: General considerations," *Planet. Spa. Sci.*, vol. 1, pp. 291-305; December, 1959.

<sup>4</sup> F. F. Marmo, L. M. Aschenbrand and J. Pressman, "Artificial electron clouds—III: Release of atomic potassium at 121 km," *Planet. Spa. Sci.*, vol. 1, pp. 306-318; December, 1959.

<sup>5</sup> J. Pressman, F. F. Marmo and L. M. Aschenbrand, "Artificial electron clouds—IV: Thermal ionization study, nighttime release of cesium at 101 km," *Planet. Spa. Sci.*, vol. 2, pp. 17-25; October, 1959.

<sup>6</sup> F. F. Marmo, J. Pressman, E. R. Manning and L. M. Aschenbrand, "Artificial electron clouds—V: Morning twilight study, release of cesium and sodium at 128 and 116 km," submitted to *Planet. Spa. Sci.*

<sup>7</sup> J. Pressman, F. F. Marmo and L. M. Aschenbrand, "Artificial electron clouds—VI: Low altitude study, release of cesium at 69, 82 and 91 km," *Planet. Spa. Sci.*, vol. 2, pp. 166-178; June, 1960.

In the initial series of papers dealing with electron cloud physics the emphasis was directed toward establishing the foundation of this new technique for studying the several physical and chemical processes associated with the earth's upper atmosphere. Here, the emphasis is directed more toward the practical utilization of artificial electron clouds for RF propagation, and for this purpose the name artificial ionosphere is employed as more descriptive. However, throughout the text electron clouds and artificial ionospheres are used interchangeably.

The format adopted here is as follows. First, a brief summary report is given of the chronological history of several initial rocket experiments performed for the express purpose of creating artificial ionospheres. Second, there is presented a brief review of some methods derived for the determination of several important engineering parameters associated with the generation of reproducible effective artificial ionospheres at pre-selected altitudes and with predetermined RF scatter capability. These parameters include chemical yield, chemical consumption, thermal ionization efficiencies, solar photoionization probabilities, wind velocity, wind shear, diffusion (both ambipolar and neutral) microscopic cross-section values (electron attachment, ion-electron recombination, photodetachment, mutual neutralization, chemical reactivity, etc.), to name several. Finally, there is discussed the applicability of the artificial ionosphere to the general communication problem in an analytical manner. For this, neither the physics of the artificial ionosphere nor its generation will be considered as *a priori* inputs to the problem. Instead, simplified generalized solutions are given which relate such basic parameters as communications effectiveness of the cloud as a function of wavelength, time, capacity, bandwidth, reliability, range, etc.

## BACKGROUND AND EVOLUTION

The first of the artificial ionosphere experiments was conducted during March, 1956, in which 18 pounds (275 moles) of nitric oxide gas was released from high-pressure containers at an altitude of 95 km; this has been previously reported.<sup>1</sup> The success of this experiment (an artificial electron cloud with an initial average density of about  $4 \times 10^6$  electrons per  $\text{cm}^3$  was radar detected for more than 10 minutes) indicated that it would be feasible to use other more effective contaminants to create artificial electron clouds at various altitudes with a wide range of electron densities, time durations, sizes, shapes and other parameters. Logically, a systematically planned series of rocket experiments was initiated and performed by Marmo, *et al.* at AFCRC in order to study the basic characteristics and effects of electron clouds with certain predetermined characteristics.

TABLE I  
SUMMARY OF UPPER ATMOSPHERIC ARTIFICIAL IONIZATION EXPERIMENTS CONDUCTED AT HOLLOMAN AIR FORCE BASE, N. M.

No.	Date	Study Constituent	Moles	Approx. Release Time (MST)	Release Altitude (km)	Vehicle
1	November 19, 1957	Potassium	153	0932	121	Aerobee
2	May 20, 1958	Cesium + 10 per cent Sodium	Cs-43	0245	101	Nike-Cajun
3	May 21, 1958	Cesium + 2 per cent Sodium	Cs-46	0434	128	Nike-Cajun
4	May 22, 1958	Sodium	61	0432	116	Nike-Cajun
5	September 15, 1958	Cesium	27	0934	82	Nike-Cajun
6	September 16, 1958	Cesium	28	0933	69	Nike-Cajun
7	September 18, 1958	Cesium	30	0953	91	Nike-Cajun

The following experiment was performed but was unsuccessful due to mechanical failure:

A	September 19, 1957	Cesium	110	0930	—	Aerobee
---	--------------------	--------	-----	------	---	---------

The following was the initial experiment previously reported:

B	March 12, 1956	Nitric Oxide	275	1415	95	Aerobee
---	----------------	--------------	-----	------	----	---------

Examination of the solar photoionization probabilities, thermal ionization efficiencies and other physical parameters of various considered contaminants indicated that the family of alkali metal elements offered a particularly high potential for obtaining high density, long-lived electron clouds at altitudes between 70 and 200 km with presently available experimental techniques. In addition, it was felt advantageous to keep this systematic study confined to one given chemical family; this affords several advantages. Therefore, it was decided to utilize only the alkali metals (Cs, K and Na) throughout these initial experiments. Of these, it was felt that Cs afforded the best potential for obtaining a maximum-type artificial ionosphere. Thus, a series of rocket experiments designed for these purposes was initiated on September 19, 1957. This report deals with those experiments performed up to September 18, 1958. The several experiments of this initial series are summarized in Table I. A brief summary of the pertinent features of the several flights is included in the Table.

Since Cs afforded an optimum probability for success, the first Aerobee rocket experiment of the series was performed in September, 1957, whereby 110 moles was scheduled to be released at an altitude of about 120 km. The experiment was unsuccessful because the material was not released due to mechanical failure of both the primary and back-up release mechanisms.

Previous scheduling had called for a release of potassium vapor during the month of November, 1957. There was no opportunity to reschedule the unsuccessful cesium experiment due to relatively difficult delivery problems; therefore, it was decided to continue the original schedule. A successful release of a payload containing 153 moles of potassium was accomplished from an Aerobee at 121 km. This flight occurred at about 0932 MST on November 9, 1957; it is represented by entry 1 in Table I. The electron cloud formed from this experiment was readily detected by conventional radar techniques. Fig. 1 depicts one of the more interesting representative pieces of data. This result is an ionogram obtained from a C-3 vertical ionosonde located at White Sands Proving Grounds, N. M., and clearly shows the

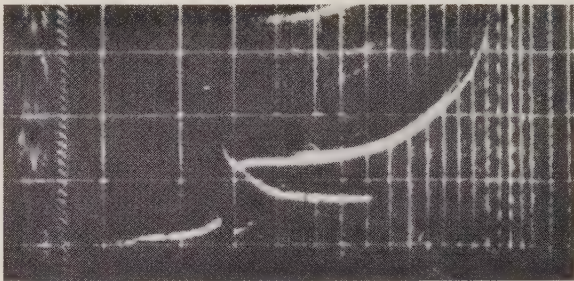


Fig. 1—Ionogram obtained 30 minutes after chemical release as recorded by C-3 vertical ionosonde located at White Sands Proving Ground, N. M., for experiment conducted in November, 1957. This display depicts the slant range vs maximum frequency. Each altitude marker represents 100 km; the frequency scale goes from 1 to 25 mc. The artificial cloud is shown between the normal E and F regions at about 170-km slant range. The maximum frequency return is about 8 mc.

detection of the man-made cloud lying between the normal E and F layer (at about 170 km slant range) at 30 minutes after the release of the contaminant.

The interpretation<sup>4</sup> of the results pertinent to the ionized cloud which was formed in this experiment suggested that some process in addition to photoionization was responsible for the initial electron production. The chemical nature of the experimental method indicated that the effect was probably due to thermal ionization. In addition, the data analysis also indicated that subsequent experiments could utilize the smaller, less expensive and more reliable solid fuel two-stage Nike-Cajun vehicle. The results of experiment 2, Table I, supported the correctness of both of these conclusions. For example, the nighttime (not solar illuminated) Nike-Cajun release of Cs at 101 km resulted in the thermal generation of a radar detectable artificial ionosphere.<sup>5</sup> In addition, a method of “doping” (with a Na compound) was employed for making visible the artificial cloud.

Experiments 3 and 4, Table I, were designed primarily for obtaining correlation of both optical and radar data from the artificial ionospheres. This afforded a new dimension for experimental investigation of radar propagation physics. This capability was accomplished by rendering the released contaminant visible by utiliz-



ing the twilight detectability of sodium resonance radiation against a morning twilight sky background.<sup>8</sup> Two experiments were performed: 1) a Nike-Cajun release of a mixture of cesium and sodium (2 per cent) was conducted at 128 km on May 21, 1958, and 2) a payload which included only the sodium compound was released by a Nike-Cajun at 116 km on May 22, 1958. Both experiments were successful in that they afforded the opportunity of providing good photographic and spectral coverage for over 8 minutes. Fig. 2 shows a series of three pictures obtained on the May 21 experiment using a light amplifying unit (Lumicon) capable of obtaining series photographs. The first picture was obtained 2 seconds after release time and the latter two show the cloud development after 1 and 2 minutes, respectively.

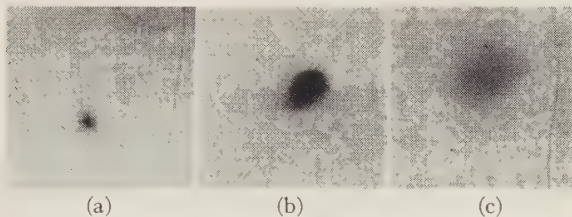


Fig. 2—Photographs taken from television screen of Lumicon depicting the dynamics of cloud formation for experiment conducted May 21, 1958. Picture (a) was obtained 2 seconds after chemical release, (b) and (c) after 1 minute and 2 minutes, respectively.

The diffusive expansion and wind shear characteristics are clearly indicated, and the utilization for data of this type is illustrated later.

The last series of experiments briefly discussed here is indicated by items 5, 6 and 7 of Table I. These releases were performed to investigate and determine the practical altitude below which long-lived, usable, high density artificial ionospheres cannot be generated by these techniques employed here. The results have indicated that a tentative lower limit is set at about 70 km. For example, the time durations for the 40.7-mc backscatter echoes were found to be only 70 seconds, 4.3 seconds and 1.5 seconds for the 91-km, 82-km, and 69-km releases, respectively.

The detailed analyses of these several experiments are presented elsewhere.<sup>7</sup> However, for completeness, a very brief review of some extracted pertinent results is given in the next section.

#### ENGINEERING PARAMETERS AND THEIR DETERMINATIONS

The optimum utilization of artificial ionospheres for communications requires information on several varied parameters. These can include 1) chemical yields, 2) chemical consumption, 3) thermal ionization efficiency, 4) solar photoionization probabilities, 5) ion-electron recombination coefficients, 6) electron attachment probability, 7) solar photodetachment probability, 8) collisional detachment, 9) mutual neutralization, 10) wind

velocity, 11) wind shear, 12) diffusion (both ambipolar and neutral), to name several. Fortunately, analysis of the previously mentioned experiments has resulted in the development of methods for acquiring information on most of these parameters. These methods and results are discussed below.

#### A. Chemical Yield and Thermal Ionization Efficiency: Analysis of Thermal Nighttime Release

A sodium-doped Cs payload was released at 101 km during a nighttime experiment to determine the magnitude of thermochemical effects upon the production of artificial electron clouds. Subsequent analysis of radio-radar and optical data pointed toward the fact that it was indeed possible to ascribe to thermal processes the generation of an ample number of electrons to account for the observed electron cloud. A thermochemical treatment of these data with application of the Saha relationship suggested that the value for the total number of thermally generated electrons,  $N_e$ , should be placed at about  $3 \times 10^{21}$  and that the thermal ionization probability,  $c$ , for cesium for this system is about  $10^{-8}$ . These results were compatible with experimental conditions in which the temperature of the canister chemical reaction was taken to be in the vicinity of 3000° Kelvin and with the canister-bursting pressure range occurring between 300 to 500 atmospheres. In addition, an alkali metal chemical yield of less than 10 per cent was indicated. These facts were further substantiated by optical and radar data from subsequent experiments in the series in which yields of between 2 to 5 per cent have been determined in an independent manner; in addition, thermal efficiencies of about  $10^{-8}$  and  $5 \times 10^{-4}$  were ascribed to Cs and K, respectively. These are discussed later.

Independent of the previous theoretical findings, an initial cloud optical radius of about 250 meters and an initial electron density of the order of  $10^7 \text{ cm}^{-3}$  were determined from an analysis of optical (visible cloud) and radar data, respectively. From these determinations it was experimentally concluded that the total electron content of the cloud,  $N_e$ , was indeed of the order of  $3 \times 10^{21}$  in agreement with the thermochemical theoretical treatment employed. Additional independent determinations of about  $10^{21}$  for  $N_e$  are discussed in another section of this report. Thus an average  $N_e$  value of between 1 to  $3 \times 10^{21}$  was ascribed to this specific system for other applications.

#### B. Diffusion, Chemical Yield, Ionization Efficiency: Analysis of C-3 Radar Data

This section will outline some of the analysis methods which were employed for radar data, the results of which yielded values for several important engineering parameters. Of all the radar data obtained, the C-3 ionosonde data were considered the most compatible to analysis. The analysis presented in this section is restricted to experiments 1 and 3 in Table I, namely the K and Cs releases at 121 and 128 km, respectively. It

<sup>8</sup> J. F. Bedinger, E. R. Manring and S. N. Ghosh, "Study of sodium vapor ejected into the upper atmosphere," *J. Geophys. Res.*, vol. 63, pp. 19-29; March, 1958.

has previously been demonstrated<sup>3,4,6</sup> that for these cases the dominant factor causing a decrease in the elec- The solution for the center-point density of (1) and (2) is given below; details are found elsewhere.<sup>6</sup>

$$n_e(0, t') = n_{e0} \frac{r_0^3}{m^{3/2}} + \frac{\sigma_p N \exp(-\sigma_p t_1)}{2\pi^{3/2}(D_n - D_a)} \left[ \frac{1}{m^{1/2}} - \frac{\exp(-\sigma_p t')}{p^{1/2}} \right]$$
$$+ \frac{N}{4\pi} \left( \frac{\sigma_p}{D_n - D_a} \right)^{3/2} \exp \left[ \frac{\sigma_p m}{4(D_n - D_a)} \right] \left\{ \operatorname{erf} \left[ \frac{\sigma_p p}{4(D_n - D_a)} \right]^{1/2} - \operatorname{erf} \left[ \frac{\sigma_p m}{4(D_n - D_a)} \right]^{1/2} \right\} \quad (3)$$

tron concentration is diffusion. Electron decay processes such as attachment, recombination, and others are not sufficiently fast to account for the time constants of the effects to be discussed. Thus, ascribing the observed electron density decrease to diffusion only results in considerable simplification in the mathematical model employed. In particular, the governing equations are given by the following coupled differential equations:

$$\frac{dn_c}{dt} = D_n \nabla^2 n_c - \sigma_p n_c \quad (1)$$
$$\frac{dn_e}{dt} = D_a \nabla^2 n_e + \sigma_p n_c \quad (2)$$

where

- $n_c$  = concentration of neutrals/cm<sup>3</sup>
- $n_e$  = concentration of electrons/cm<sup>3</sup>
- $D_n$  = neutral diffusion coefficient cm<sup>2</sup>/sec
- $D_a$  = ambipolar diffusion coefficient cm<sup>2</sup>/sec
- $\sigma_p$  = photoionization probability, sec<sup>-1</sup>.

where

$$m = (r_0^2 + 4D_a t')$$
$$p = (r_0^2 + 4D_n t')$$
$$n'_e = \frac{N[1 - \exp(-\sigma_p t_1)] + Q}{\pi^{3/2} r_0^3}$$

and  $t'=0$  when  $t=t_1$ . Other terms are defined as follows:

- $r_0$  = Gaussian half-width
- $N$  = total number of atoms at  $t'=0$
- $Q$  = total number of electrons at  $t'=0$ .

A detailed analysis has been presented elsewhere<sup>6</sup> in which sufficient discussion is included concerning the best fit of the experimental C-3 data to (3) for both experiments. The several parametric values obtained from the analysis are summarized in Table II. The degree of agreement between the theory and experimental results is illustrated in Figs. 3 and 4 where the C-3 data from both the K and Cs releases are indicated by the open circles. The two closely spaced sets of  $D_a$  and  $D_n$  values are shown to illustrate the sensitivity of the technique.

TABLE II  
VALUES USED FOR OBTAINING BEST FIT TO EXPERIMENTAL C-3 RADAR DATA

Constituent	Altitude of Release (km)	Photoionization Probability $\sigma_p$ (sec <sup>-1</sup> )	Thermal Efficiency (c)	Total Number Particles in Cloud ( $N$ )	Initial Release $r_0$ (m)	Neutral Diffusion Coefficient $D_n$ (cm <sup>2</sup> /sec)	Ambipolar Diffusion Coefficient $D_a$ (cm <sup>2</sup> /sec)
Cesium	128	$6.5 \times 10^{-4}$	$10^{-3}$	$1.0 \times 10^{24}$	300	$2.5 \times 10^8$	$4.2 \times 10^7$
Potassium	121	$1.9 \times 10^{-5}$	$5 \times 10^{-4}$	$3.0 \times 10^{24}$	200	$6.2 \times 10^7$	$9.2 \times 10^6$

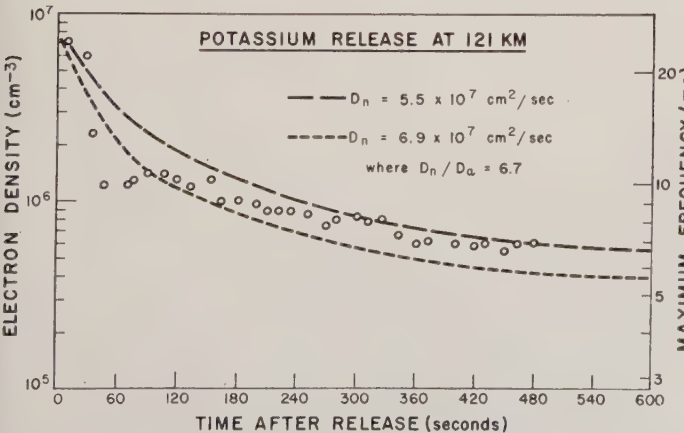


Fig. 3—The best fit values of  $D_n$  and  $D_a$  to the experimental C-3 data obtained from the experiment in which potassium was released at 121 km.

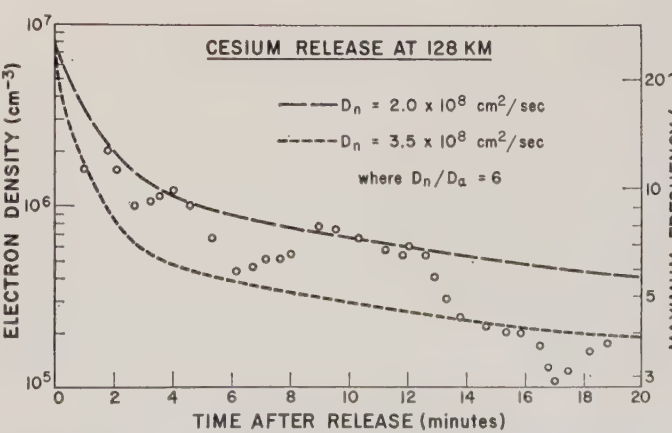


Fig. 4—Plot of the C-3 experimental data for the release of cesium at 128 kilometers depicting the best fit values of  $D_n$  and  $D_a$  and illustrating the sensitivity of the technique.



### C. Optical Data: Diffusion and Chemical Yield

For obtaining diffusion and chemical yield determinations it is assumed that the initial, very rapid, explosive expansion occurring at release leads to a Gaussian cloud of half-width  $r_0$ . It is at this point that we set  $t=0$ . Subsequently, the density is expected to vary with time and position in accordance with

$$n_e(r, t) = \frac{N}{\pi^{3/2}(4Dt + r_0^2)^{3/2}} \exp\left(-\frac{r^2}{4Dt + r_0^2}\right) \quad (4)$$

where

$n_e(r, t)$  = number of particles/cm<sup>3</sup> at distance,  $r$ , from the center at time,  $t$ .

$N$  = total number of particles in cloud

$r_0$  = half-width of Gaussian  $1/e$  value at  $t=0$  (cms)

$D_n$  = diffusion coefficient for neutral species at cloud height (cm<sup>2</sup>/sec).

The total number of particles in the line of sight ( $\tau$ ) at distance,  $d$ , (cms) from center is given by

$$\tau = \frac{N}{\pi(4Dt + r_0^2)} \exp\left(-\frac{r^2}{4Dt + r_0^2}\right) \quad (5)$$

If  $\sigma_t$  is the absorption cross section, and it is assumed that the optical size of the cloud is determined by the distance from the center of that isophote for which  $\tau = 1/\sigma_t$  (since the intensity drops rapidly for  $\tau > \sigma_t$ ), we have

$$d^2 = -(4Dt + r_0^2) \ln \frac{\pi}{\sigma_t N} (4Dt + r_0^2) \quad (6)$$

$$d_{\max}^2 = \frac{N\sigma_t}{e\pi} \quad (7)$$

$$t_{d\max} = \frac{1}{4D} \left( \frac{N\sigma_t}{e\pi} - r_0^2 \right) \quad (8)$$

$$t_{d=0} = \frac{1}{4D} \left( \frac{N\sigma_t}{\pi} - r_0^2 \right) \quad (9)$$

where

$d_{\max}$  = maximum radius of optical radius,

$t_{d\max}$  = time to achieve this maximum radius, and

$t_{d=0}$  = time for cloud to disappear.

In Fig. 5 the experimental values from some Beattie-Coleman camera data for the May 21 flight are plotted. Application of the above theory yields a good fit for the values of  $D_n = 7 \times 10^7$  cm<sup>2</sup>/sec and  $N = 1.5 \times 10^{22}$  sodium atoms. This suggests a chemical yield of approximately 3 per cent. The value of  $D_n$  is consistent with the theoretically determined values of  $D_n$  at the altitude in question.<sup>9</sup> It should be noted that since  $t_{\max} = 1/D$ , small

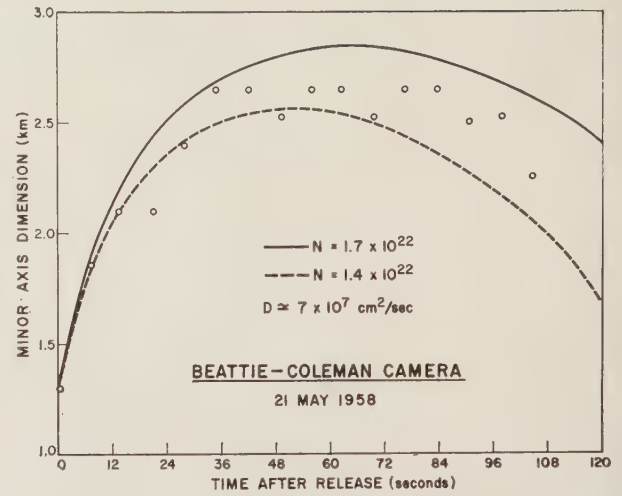


Fig. 5—The time variation of the minor axis optical diameter is indicated by the circles. The dashed and solid curves are theoretical curves for two different yields but the same diffusion coefficient.

changes in  $D$  shift the maximum and the curve along the  $t$  axis in an extremely sensitive fashion.

Eq. (9) for the disappearance of the contour line defining the optically dense cloud and the observed neutral diffusion coefficient,  $D_n$ , was used to determine the yield of the Cs vapor itself for the May 21, 1958 flight. For this purpose, the cloud photographed in the second resonance line at 4557 Å was used and noted to last for about 130 seconds. If the ratio of optical cross sections for the first and second resonance lines of Cs is taken to be about 100 to 1, then the recorded contour line corresponds to about  $3 \times 10^{13}$  atoms/cm<sup>2</sup>-column. Thus, this suggests that the total number of Cs atoms released is about  $10^{24}$  or about 3 per cent, in agreement with the deduced sodium (doping agent) yield above.

### D. Wind Determination: Velocity and Shear Data

The formation of a small, visible, photographable cloud at altitude can yield wind velocity data by means of simple optical triangulation techniques. A method of obtaining shear information from optical data is given below. In addition, a geometric method of extracting accurate horizontal wind velocity values from C-3 radar data is also included.

The pertinent radar data for obtaining horizontal wind velocities is the change in the electron cloud slant range vs time. The data from the C-3 ionosonde are shown as circles in Fig. 6. The range points represent averages of the four soundings taken during each minute at 15-second intervals and over a 20-minute period. The smooth variation of the range with time for this 20-minute period is strong support for the presence of a newly-generated small electron cloud. The initial slant range is about 150 km; the subsequent change in slant range in time is presumably due to constant velocity horizontal ionospheric winds. The character of the curve with a shallow minimum indicates the geometry depicted in Fig. 7 in which the positions of cloud release

<sup>9</sup> A. Dalgarno, private communication, Queen's University, Belfast, Ireland.

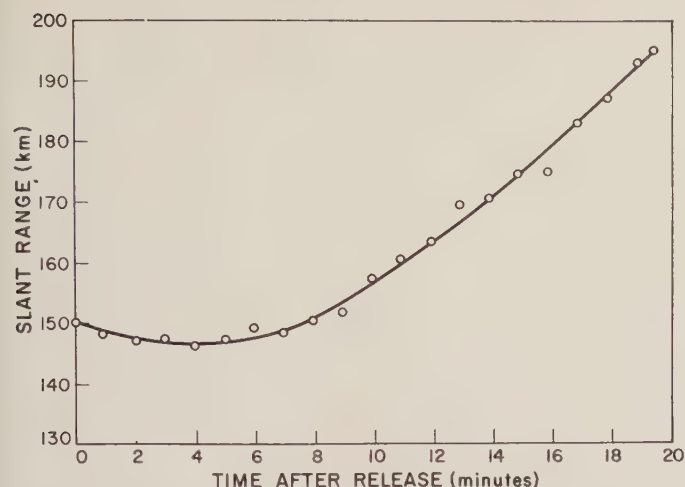


Fig. 6—The circles represent the C-3 radar slant range vs time for the May 21 experiment. The solid line is a best fit from (10) and a constant, horizontal wind velocity of 140 m/sec.



Fig. 7—Schematic representation of geometrical determination of winds from C-3 slant range vs time plot.

and C-3 stations are included. Further, this situation can be described mathematically by the expression

$$S = [S_0^2 + Wt(Wt - 2S_0 \cos \theta_0)]^{1/2} \quad (10)$$

where

$S_0$  = initial slant range

$S$  = slant range between cloud trajectory and C-3 line of sight

$\theta$  = initial angle

$W$  = wind velocity.

The best fit to the data was obtained for a  $W$  value of 140 m/sec; the theoretical curve is shown as the solid line in Fig. 6. The excellent fit between the experimental points and the theoretical curve appeared to corroborate the notion of horizontal winds with a constant velocity of about 140 m/sec. This (140 m/sec) velocity is considerably greater than those previously determined in a similar manner, namely, 60 m/sec and 78 m/sec at 95 km<sup>1</sup> and 121 km,<sup>4</sup> respectively. Concerning wind direction, it was clear from Fig. 7 that an ambiguity existed on the basis of these data alone. However, in this instance, visual observations dictated the choice of direc-

tion as 87° rather than 293°. This case suffices to illustrate the geometric method of obtaining wind information via these and similar data.

Wind shear in the upper atmosphere has recently been measured by a technique in which a long sodium filament is ejected into the upper atmosphere between 70 and 200 km<sup>10</sup>. Careful analysis of the optical data leads to accurate shear data. Clearly, in a similar manner a point release can be utilized to determine the wind shear at the release altitude. For example, photographs of the contaminant cloud indicated an initially spherical cloud becoming ellipsoidal with time because of the prevailing wind shear at the cloud position (see Fig. 2).

The shear effect may be described by the following equation:

$$\frac{dn_c}{dt} = D\nabla^2 n_c - W \left( \frac{dn_c}{dx} \right) \quad (11)$$

$n_c$  = number of particles/cm<sup>3</sup>

$D$  = diffusion coefficient, cm<sup>2</sup>/sec

$W$  = wind velocity, taken parallel to  $x$  axis, cm/sec.

The treatment of this equation will not be included in this discussion since it does not fall within the scope of this work. The present treatment is restricted to a more crude model, which however, gives a good qualitative fit to the data.

If it is assumed that 1) the rate of diffusion is independent of the cloud shape, 2) shear does not affect the growth of the minor axis and 3) the minor axis remains small compared to the elongation, it can be shown<sup>6</sup> that for shear-produced elongation

$$L = Y(at + \frac{1}{2}bt^2) + \text{constant}. \quad (12)$$

Plotted in Fig. 8 are the variation with time of the minor axis on the left-hand graph and on the right-hand graph, the variation with time of the major axis together with the plot of (12). From these, a shear value of  $Y = 1.1 \times 10^{-2} \text{ sec}^{-1}$  was obtained. The data pertain to camera data of May 22.

Similar plots have been applied to optical data for both the May 22 and 21 experiments as obtained from other optical instrumentation. Corresponding data from the May 22 flight yielded a shear constant of  $1 \times 10^{-2} \text{ sec}^{-1}$  in agreement with the above. The value obtained for May 21 in each case was  $6 \times 10^{-3} \text{ sec}^{-1}$ . These values were consistent with those obtained by sodium streamer experiments.<sup>10</sup>

#### *E. Low Altitude Data Analysis: Chemical Consumption, Mutual Neutralization and Other Electron Decay Processes*

Discussed in this section will be the series of three experiments which were undertaken for the two-fold purpose of studying the effect of low altitudes (below

<sup>10</sup> E. R. Manring, J. F. Bedinger, H. B. Pettit and C. B. Moore, "Some wind determinations in the upper atmosphere using artificially generated sodium clouds," *J. Geophys. Res.*, vol. 64, pp. 587-592; July, 1959.



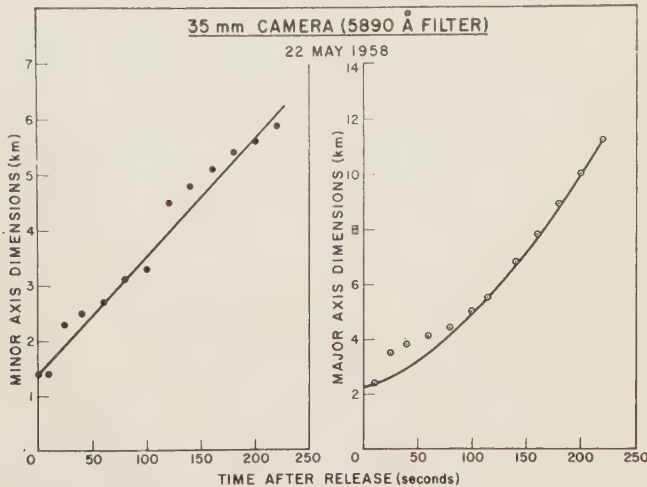


Fig. 8—The solid dots and circles represent the time variation minor and major axes optical diameters, respectively. The two curves show the best theoretical fit and indicate a wind shear of  $1 \times 10^{-2} \text{ sec}^{-1}$ .

100 km) upon the formation of artificial ionospheres and the roles of a number of electron decay processes after the generation of these clouds. It was found that several decay processes (*e.g.*, chemical consumption, recombination, electron attachment, mutual neutralization, etc.) predominate at low altitudes in contradistinction to other processes which exert maximum influence above the 100 km region.

From these experiments, information was obtained concerning some of these processes. Of particular importance was the derivation of coefficients for chemical consumption and mutual recombination.<sup>7</sup>

Of the several radio-radar probes utilized in the Cs releases at 91, 82, and 69 km, a 40.7 pulsed radar located 15 miles east of the launch site yielded the most consistent—and therefore usable—data. The analysis applied to these data indicated a total cloud duration of about 70 seconds at 91 km, 4.3 seconds at 82 km and 1.5 seconds at 69 km.

The short lifetimes observed for the low-altitude generated clouds are due to at least two important effects: 1) the rapid destruction of Cs atoms by chemical consumption which prevents subsequent photoionization, and 2) rapid electron destruction through attachment followed by mutual neutralization. It was found, for the types of releases discussed in this paper, that the diffusion rate of the charged particles is much too slow to account for the observed cloud history. Also, the photoionization production term remained relatively uninfluenced by diffusion of the neutrals except at about 90 km.

Therefore, it is felt that the results of these experiments have established 70 km as an approximate lower altitude limit for effective duration for artificial ionospheres generated by these techniques. Detailed analysis is presented elsewhere<sup>7</sup> and is not reviewed here since the results are of a negative nature for our present discussion.

## SUMMARY OF DATA ANALYSIS

The foregoing is intended as a review of some of the main points in the systematic study of the physics of artificial ionospheres. The study has revealed that the theoretical photoionization cross sections are consistent with the data contained, and that cesium is the most effective of the alkali metals used for this purpose. It has been shown that the chemical yields have been disappointingly small, namely, of the order of 2 to 3 per cent. Thermal ionization has been shown to be an effective process in the generation of artificial ionospheres, but here again, efficiencies of only about 0.1 per cent of the released number of atoms have been achieved. Thus an over-all electron yield of only about  $3 \times 10^{-5}$  has been achieved.

An optical method has been devised for the successful determination of the cloud initial half-width, chemical yield, wind shear and neutral diffusion coefficients. A simple method has been used for determining (with one degree of ambiguity) the wind velocity from radar slant range data. A mathematical model has been applied to those experimental releases above 120 km in order to describe the observed electron decay history. The analysis gives measures of neutral and ambipolar diffusion, chemical yield, degree of thermal ionization and initial half-width. Reasonable correlation of radar data with the optical techniques employed has been demonstrated.

Another mathematical model has been devised and employed for the lower altitude (below 90 km) range which accounts for the dominant processes at these altitudes. These techniques also yield useful information on neutral and ambipolar diffusion, photoionization cross sections, mutual neutralization, thermal ionization and chemical consumption of the alkali contaminant by atmospheric oxygen. Information on electron attachment rates should be easily available by application of similar techniques.

Finally, the foregoing summary has made obvious the possible usage of artificial electron clouds for radar propagation purposes. In particular, a significant potential for this application is indicated by the small chemical yields and thermal efficiencies experienced with the methods employed here. Clearly, these are capable of substantial increase. Specifically,  $Q$  values<sup>11</sup> of more than  $3 \times 10^{22}$  should be easy to achieve with minimum effort. A systematic chemical engineering study is being currently pursued to this end and should yield substantial improvement towards realizing the full potential of the utilization of artificial ionospheres for radio-radar propagation. In fact, in the following sections, a  $Q$  value of about  $3 \times 10^{22}$  is considered as a realistic parameter. Full utilization of upper atmospheric wind shear, filament releases, other geometric release patterns, etc., are being investigated. Indeed, a systematic study is being

<sup>11</sup> For discussion of the propagation aspects the more familiar symbol,  $Q$ , is used for total electron content. Thus, the  $Q$  value is synonymous to the previously discussed  $N_e$ -value.

pursued in order to realize the full potential and optimum conditions for the proper utilization of artificial ionospheres for RF propagation.

### ELECTROMAGNETIC MODELS

The following discussion is devoted to an analytical description of the characteristics of the electron cloud or artificial ionosphere, as a reflector of incident RF energy. Many theoretical cloud shapes, electron density distribution models and reflection efficiencies have been analyzed, but due to space limitations only selected ones indicative of the types of calculation will be presented here. It should be noted that throughout this discussion the simplifying assumption of diffusion controlled processes has been invoked so that the complicated differential expressions become more amenable to analytical solution. It is clear that this also restricts the applicability of the following to high altitude releases, *i.e.*, to releases above about 120 km.

The analysis discusses the propagation path provided by an artificial ionosphere in the absence of the normal ionosphere. Therefore, some care must be exercised in interpreting the results in the presence of the ambient electron density field. It has been shown earlier that it is not difficult to achieve electron densities exceeding normal *F*-layer values by about  $10^2$  for significant periods of time. Thus, maximum usable frequencies are greater than normally existing MUF values by about an order-of-magnitude; this is substantiated by the experimental observations reported here.

For a detonation-type release of contaminant in a non-sunlit environment, the dominant production process for electrons is thermal ionization. In a relatively quiescent atmosphere, under these conditions, the electron cloud has been observed to exhibit spherical symmetry for protracted periods of time. The functional dependence of the initial electron density,  $N_e'(r, 0)$  is assumed to be Gaussian. The particular selection offers the advantage of mathematical simplicity while preserving a good approximation to the physical situation.

The well-known partial differential equation of diffusion in free space, with point symmetry is

$$\frac{\partial n_e'}{\partial t} = D_a \nabla^2 n_e' \quad \text{for } r \geq 0, t > 0 \quad (13)$$

where  $n_e'$  is the electron density and  $D_a$  is the ambipolar diffusion coefficient. It is assumed that the initial electron density,  $N_e'(r, 0)$  at any point ( $r \geq 0$ ) is defined by a Gaussian distribution where

$$n_e'(r, 0) = \frac{Q}{\pi^{3/2} r_g^3} \exp\left(-\frac{r^2}{r_g^2}\right), \quad (14)$$

where  $r_g$  represents the value of  $r$  at which the density is  $1/e$  of the initial center-point density. The function  $n_e'(r, t)$  which satisfies the diffusion equation (13) and the initial condition (14) as well as the following boundary conditions:

$$\frac{\partial n_e'}{\partial r} = 0 \text{ at } r = 0, \quad t \geq 0$$

$$n_e'(r, t) < M; \quad \text{where } M \text{ is an arbitrary constant,} \quad (15)$$

is

$$n_e'(r, t) = \frac{Q}{(\pi r_g^2 + 4\pi D_a t)^{3/2}} \exp\left(-\frac{r^2}{r_g^2 + 4D_a t}\right) \quad (16)$$

where  $Q$  is defined as the total number of electrons.

Since the model assumes neither electron production nor dissipation after  $t_0$ ,  $Q$  may be defined in terms of the electron density and the differential element of volume,  $n_e'(r, t) dV$ . To demonstrate the consistency of definitions, the integral expression for  $Q$  is given by

$$\begin{aligned} & \iint_V n_e'(r, t) dV \\ &= 4\pi \int_0^\infty \frac{Q r^2}{(\pi r_g^2 + 4\pi D_a t)^{3/2}} \exp\left(-\frac{r^2}{r_g^2 + 4D_a t}\right) dr. \end{aligned} \quad (17)$$

Eq. (17) can be integrated by introducing the change in variable

$$y = \frac{r}{(r_g^2 + 4D_a t)^{1/2}} \quad (18)$$

so that (17) can be rewritten as

$$\iiint_V n_e' dV = \frac{4Q}{(\pi)^{1/2}} \int_0^\infty y^2 e^{-y^2} dy \equiv Q. \quad (19)$$

It should be noted that the Gaussian distribution is completely defined by the choice of two of the three parameters  $r_g(t)$ ,  $n_e'(0, t)$  and  $Q$ , so that  $r_g$  may now be eliminated. By setting the value of  $r_g$  to zero, the function  $n_e'(r, t)$ , from (16) becomes

$$n_e'(r, t) = \frac{Q}{(4\pi D_a t)^{3/2}} \exp(-r^2/4D_a t). \quad (20)$$

This simpler form of the electron density distribution function still satisfies the basic diffusion equation and accompanying boundary and initial conditions. If the time dependent value of the radius,  $r$ , in (20), for which the electron density is  $1/e$  of the center density, is defined by

$$a = (4D_a t)^{1/2} \quad (21)$$

then the center density can be rewritten as

$$n_e(0, t) = \frac{Q}{(4\pi D_a t)^{3/2}} = \frac{Q}{\pi^{3/2} a^3}. \quad (22)$$

If the radius,  $r_c$ , is defined as that effective radial distance at which reflection occurs at the wavelength,  $\lambda$ , then  $n_e(r, t)$  can be expressed<sup>12</sup> by

$$n_c(r_c, t) = \frac{\epsilon_0 m \omega^2}{e^2} = \frac{\pi}{\lambda^2 r_0} \quad (23)$$

<sup>12</sup> U. S. Dept. of Commerce, "Ionospheric Radio Propagation," NBS Circular 462, pp. 4-14; June, 1948.



where

$\omega$  = angular frequency

$\lambda$  = wavelength

$\epsilon_0$  = dielectric constant of free space

$m, e, r_0$  = mass, charge and classical radius of the electron.

The parameter  $t_c$  represents the duration of time for which the electron density is greater than or equal to the critical electron density at  $r_c$ . With respect to the RF system,  $t_c$  is a measure of the time during which the cloud may act as a suitable RF reflector for the wavelength  $\lambda$ . From (20)  $r_c$  is defined (for times  $t < t_c$ ) as

$$r_c = a \left[ -\log_e \left( \frac{\pi^{5/2} a^3}{\lambda^2 r_0 Q} \right) \right]^{1/2}. \quad (24)$$

For the case of the perfectly reflecting sphere, the scattered radiation can be considered isotropic (cloud gain,  $G_c=1$ ), and the total cross section available for use as an RF energy reflector is  $\sigma = \pi r_c^2$ , or

$$\sigma = \pi a^2 \log_e \left( \frac{\lambda^2 r_0 Q}{\pi^{3/2} a^3} \right). \quad (25)$$

By introducing the parameter

$$X = \frac{\pi^{5/3} a^2}{\lambda^{4/3} r_0^{2/3}}, \quad (26)$$

(26) can be written as

$$\frac{\sigma}{\lambda^{4/3}} = (2.14) \cdot 10^{-10} X \left[ \log_{10} Q - \frac{3}{2} \log_{10} X \right]. \quad (27)$$

This expression is used for graphical representation in Fig. 9. For fixed wavelength, this figure demonstrates the variation of cross section with time (or the parameter  $X$ ). Curves are drawn for five representative values of  $Q$  between  $10^{20}$  and  $10^{24}$ , where again  $Q$  is considered constant with time.

A dimensionless parameter

$$\gamma = \frac{n_e(r_c, t)}{n_e(0, t)} = \exp(-r_c^2/a^2) \quad (28)$$

may be used to define the attainable cross section at some critical electron density as a function of its fractional center-point value at any  $t < t_c$ . In Fig. 9, the results are plotted for  $\gamma=0.25$  (point B), 0.49 (C), 0.81 (D) at the appropriate  $X=(\gamma Q)^{2/3}$  positions on the curves. The results show that maximum cross section, for a given value of  $Q$ , lies between points B and C. After reaching the maximum value, as  $\gamma$  gets larger or as the critical electron density approaches the center-point value, the critical radius begins shrinking, so the effective cloud cross section decreases. If the maximum value for  $\sigma$  is given by

$$\sigma_{\max} = \frac{3}{2} X_m \left( \frac{r_0}{\pi} \right)^{2/3} \lambda^{4/3} \quad (29)$$

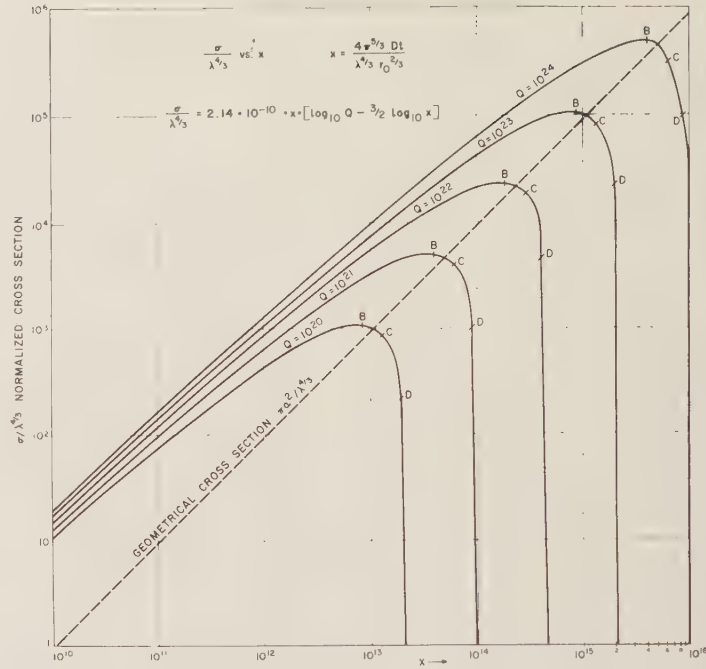


Fig. 9—Spherical Gaussian diffusing cloud.

then the corresponding value of  $X(X_m)$  is given by

$$X_m = \frac{Q^{2/3}}{e}. \quad (30)$$

Fig. 10 is a plot of (29).

The time  $t_c$ , required for the center-point electron density to equal the critical value,  $\pi/\lambda^2 r_0$ , is

$$t_c = \frac{a_c^2}{4D_a} \quad (31)$$

$$a_c = \left( \frac{r_0 \lambda^2 Q}{\pi^{5/2}} \right)^{1/3}. \quad (32)$$

In the spherically symmetrical, Gaussian distribution model proposed above, refraction of the propagated energy has been neglected. Similar treatments are available elsewhere,<sup>13</sup> for the parabolic and homogeneous distributions. In the latter cases, the tendency is toward increasing the value of the cross section,  $\sigma$ , and to shifting the directional factor,  $G_c$ , from uniformity toward favoring forward over backward scattering.

For an artificial ionosphere generated at an altitude of 120 km and placed midcourse between receiver and transmitter, the ground range is about 2470 km and the incidence angle,  $i$ , of propagated energy at the cloud is  $78^\circ 58'$ . Fig. 11 compares the resultant cross sections as functions of time for several simple electron density distribution functions which have been assumed for the thermal ionization model. The geometrical cross section

$$\pi a^2 = 4\pi D_a t' \quad (33)$$

<sup>13</sup> V. R. Eshleman, "Theory of radio reflections from electron-ion clouds," IRE TRANS. ON ANTENNAS AND PROPAGATION, vol. AP-3, pp. 32-39; January, 1955.

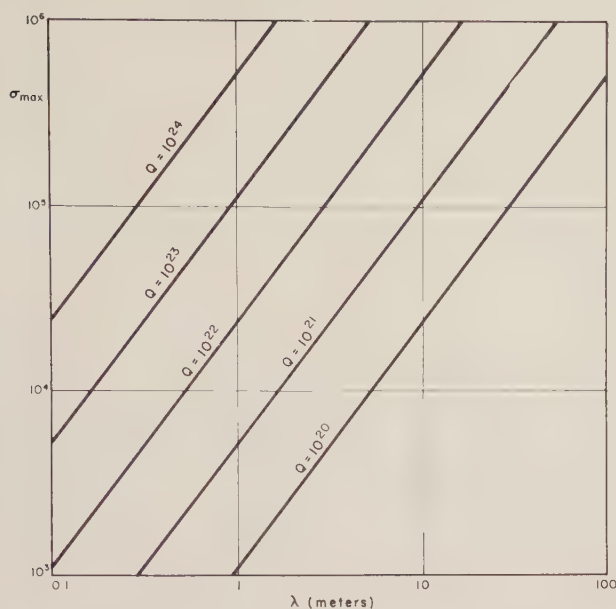
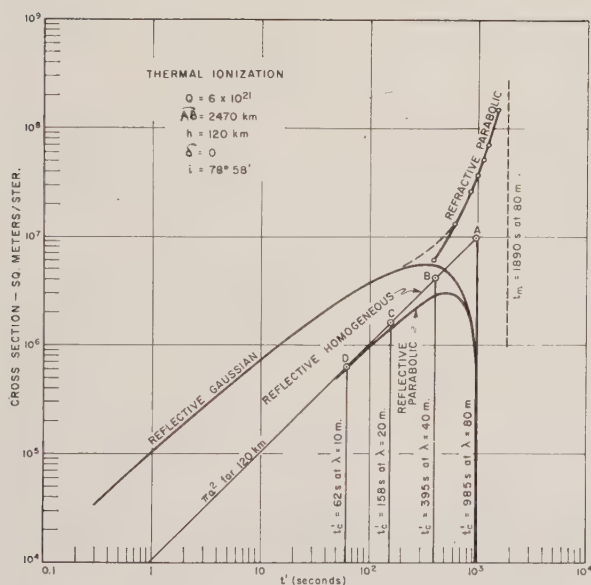
Fig. 10— $\sigma_{\max}$  vs  $\lambda$ .

Fig. 11—Cross section vs time (night release).

is constructed first, where  $t'$  is a normalized time referring to a point source diffusion model so that  $\pi a^2$  becomes a straight line on the log-log presentation. The time scale  $t'$  then represents time commencing at the termination of the initial explosive phase, after which the expansion process is diffusion controlled. As noted in Table II, the value of the ambipolar diffusion constant at this altitude was experimentally determined to be  $9 \times 10^6 \text{ cm}^2/\text{sec}$ . In addition, it was shown earlier that a  $Q$  value of about  $2 \times 10^{21}$  was experimentally achieved. Here, in order to place the parameterization on a mole basis, a convenient value of  $Q = 6 \times 10^{21}$  (0.01 mole) has been assumed as representative for employment in this discussion. Normalized critical times ( $t'_c$ ) have been

calculated from (31) and (32) for the four wavelengths, 10, 20, 40 and 80 m. These  $t'_c$  values are shown on the  $\pi a^2$  line as points, A, B, C, and D, respectively. The radio cross sections as functions of time for the models considered have only been constructed on the figure for  $\lambda = 80$  meters, but the corresponding curves for the other three cases can be imagined by translating the curve down the  $\pi a^2$  line by the appropriate distance AB, AC, or AD, respectively. This invariance of shape is an advantage gained in using the adopted model and the log-log plot.

Use of the term "reflective" in describing any of the three models so termed, infers replacement of the cloud by a totally reflecting surface defined by the critical radius at the frequency of interest. The three reflective models neglect the bending or refraction of the rays by the electrons lying in front of the critical surface. This effect is taken into account in the case of the refractive parabolic model, which is the geometric optics treatment of the problem. This demonstrates a very real practical effect: the extension of time and frequency for directions other than backscattering to longer times and higher frequencies the nearer the forward direction is approached. Physically, this effect results directly from the slight refractive bending of rays through the under dense electron concentrations. This leads to an MUF value, higher than the critical frequency corresponding to the density at the center of the cloud. Conversely, at fixed frequency, a "maximum usable time" may be defined which is longer for the more forward directions. This effect is also range dependent through the relation of range to cloud angle of incidence for the same terminal antenna elevation angles.

It should be noted that throughout this analysis only thermal ionization has been considered. There is available, under certain conditions, the additional generative process of photoionization, whereby a greater total number of electrons are formed simply by releasing the neutral contaminant into a sunlit environment. This has been demonstrated in an earlier part of this paper. However, since the application of the artificial ionosphere is a reflector of incident RF energy for routine communications system use, it is preferable to demonstrate the cloud effectiveness without the benefit of photoionization. In any event, the added photoelectrons may be regarded as a bonus effect for daytime releases.

#### GEOMETRY OF THE SITUATION

The degree of success of a communications system using an artificial ionospheric reflector at altitude is measured here by the received signal-to-noise ratio during the information transmission interval. The factors which influence the received signal are the previously discussed product of cloud cross section and gain ( $\sigma G_c$ ), the electronic system parameters, and the geometry of the situation. With respect to the latter, Fig. 12 illustrates the interdependence of the four basic parameters of



interest:  $h$  = cloud altitude,  $\alpha$  and  $\beta$  = antenna elevation angles,  $\theta$  = angular range between terminals given by

$$\theta = \widehat{AB}/d \quad (34)$$

where

$d$  = radius of the earth = 6371 km

$\widehat{AB}$  = ground range between terminals.

From simple trigonometric relationships it can be shown that the angular range is given by

$$\theta = \cos^{-1} \left[ \left( \frac{d}{d+h} \right) \cos \alpha \right] + \cos^{-1} \left[ \left( \frac{d}{d+h} \right) \cos \beta \right] - [\alpha + \beta]. \quad (35)$$

The slant ranges ( $R_1$  and  $R_2$ ), which are required in the radar range equation, are similarly obtained and given by

$$R_1 = (d+h) \sin \alpha_h - d \sin \alpha \quad (36)$$

$$R_2 = (d+h) \sin \beta_h - d \sin \beta. \quad (37)$$

where  $\alpha_h, \beta_h$  are the elevation angles at altitude described in Fig. 12. Solutions to the general ( $\alpha \neq \beta \neq 0$ ) (35) have been calculated and plotted<sup>14</sup> for various altitudes of interest. The generalized solution for the cloud altitude of 130 km is presented in Fig. 13 for illustrative purposes.

There are several interesting special geometric cases which, because of their special logistic configurations, give them a high probability of being employed in actual system operation. The first case is described by placing the cloud directly over one of the terminals ( $\beta = \pi/2$ ) and setting the antenna of the other terminal on the horizon ( $\alpha = 0$ ). In this case

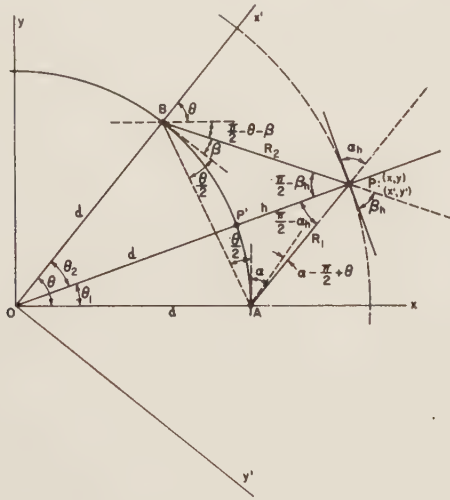


Fig. 12—Details and parameters of geometry.

<sup>14</sup> Geophysics Corp. of America, "A Study of an Advanced Electromagnetic Communications System," Boston, Mass., Final Tech. Rept., prepared under U. S. Signal Corps Contract No. DA-36-029-SC-78971; December, 1959.

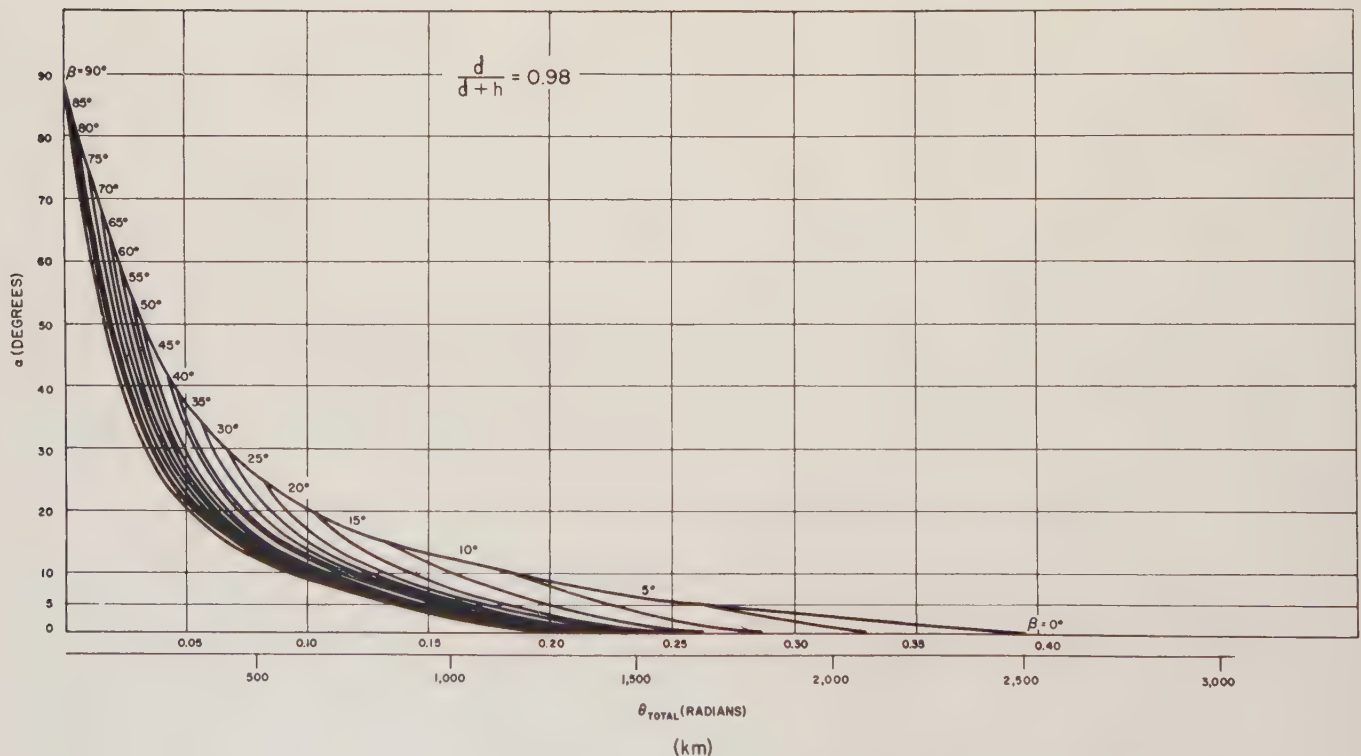


Fig. 13—Total range between stations ( $\theta$ , radians or  $\widehat{AB}$ , km), as a function of terminal angles ( $\alpha$  and  $\beta$ ) for  $d/d+h=0.98$ .

$$h = d(\sec \theta - 1) \tag{38}$$

describes the angular range as a function of altitude. The maximum achievable range at any altitude is realized when the cloud is placed midway between the terminals at altitude and both antennas are placed on the horizon. Then

$$h = d\left(\sec \frac{\theta}{2} - 1\right) \tag{39}$$

describes the geometry. In order to determine the geometry which would permit around-the-earth communications, the parameter  $\theta$  in (39) is set equal to  $2\pi$  radians/ $n$ , where  $n$  is the number of clouds required. The governing equation is then given by

$$h = d\left(\sec \frac{\pi}{n} - 1\right) \tag{40}$$

which is plotted in Fig. 14. It should be noted that the solution blows up at  $n=2$  and that an altitude of one earth radius requires three clouds. For the current state of the art of effective cloud generation altitudes (100 to 150 km), only about fifteen electron clouds are required to satisfy the geometric requirements for around-the-globe communications.

### ELECTRONIC PARAMETERS

As indicated in the previous discussion on the cloud cross section models, transmission in the HF region presents no serious difficulties because the reflection characteristics and duration of the cloud are maximized at the lower frequencies as demonstrated by several experiments. Applications of the cloud to systems in the HF band are important during times of minimum natural ionospheric activity or when transmission of a high reliability message is sought, where the reliability required is greater than that intrinsically supplied by the ambient ionosphere. It is of interest at this point to demonstrate the applicability of the cloud to higher frequency, short burst, greater bandwidth (or information capacity), high reliability (or signal-to-noise ratio) communications.

It has been shown<sup>15</sup> that for a pulse code modulated (PCM) system, a signal-to-noise ratio of about 17 db is equivalent to a reliability or error rate of the transmitted message of one per megabit ( $10^{-6}$ ). If the assumption of an available information bandwidth (in bits/sec) equal to  $10^{-4}$  of the carrier frequency in the UHF band is made, then, for example, at 100 mc, a cloud duration of 10 seconds would be required to transmit  $10^5$

bits of information (100 sec for  $10^6$  bits, etc.). The UHF region from about 100 to 300 mc represents an excellent choice of wavelength band since even the earliest experimental evidence indicated successful signal propagation at these frequencies.<sup>2</sup> It simultaneously presents the communications engineer with the opportunity of transmitting information at these frequencies over extended ranges by a new and unique mode.

As indicated earlier, it is presently feasible to generate  $Q$  values of greater than  $3 \times 10^{22}$ . With this assumed value and a cloud generation altitude of 120 km (where the ambipolar diffusion coefficient is about  $9 \times 10^6$  cm<sup>2</sup>/sec), use of (31) predicts the duration of the cloud as a function of frequency. Table III contains the total information content transmitted over the cloud duration for the assumptions which have been made. The frequencies chosen in this band then are capable of supporting the transmission of about  $3 \times 10^5$  bits of total information over time intervals of between 8 and 33 seconds.

An analytical expression associated with this model for the cloud cross section, as a function of frequency,

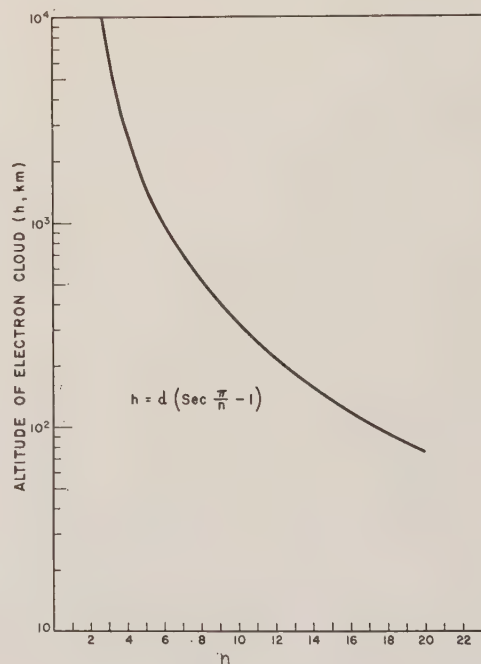


Fig. 14—Variation of height of cloud with number required to provide communications around the earth.

TABLE III  
CRITICAL TIMES AND INFORMATION CONTENT FOR  $\lambda=1, 2, 3$  m

Wave-length (m)	Fre-quency (mc)	Information Bandwidth = $10^{-4}$ f (bps)	Critical Time (sec) ( $Q=3 \times 10^{22}$ ) ( $D_a=9 \times 10^6$ cm <sup>2</sup> /sec)	Total Infor-mation Con-tent (bits)
1	300	$3 \times 10^4$	8	$2.4 \times 10^5$
2	150	$1.5 \times 10^4$	20	$3.0 \times 10^5$
3	100	$10^4$	33	$3.3 \times 10^5$

<sup>15</sup> F. E. Terman, "Electronic and Radio Engineering," McGraw-Hill Book Co., Inc., New York, N. Y., p. 972; 1955.



which is assumed constant over the transmission time, is obtained by substituting  $3 \times 10^{22}$  electrons for  $Q$  in (29) such that

$$\sigma = 5 \times 10^4 \lambda^{4/3}. \tag{41}$$

Use of (29) to obtain this average estimate of  $\sigma$  requires some further justification since the derivation was based on a maximum value for the spherically symmetric Gaussian model. As indicated previously, an enhanced signal level is theoretically available through the use of the more physically representative refractive approximation model. This is borne out by the fact that, experimentally, the reflective model underestimates the cloud cross section. As such, although (41) represents the maximum cross section for the reflective case it will be assumed as the relationship representative of constant cross section for the refractive model assumed here.

The general form of the radar range equation is expressed as

$$P_R = \frac{P_T G^2 \sigma \lambda^2}{(4\pi)^3 R_1^2 R_2^2} = SMkT\Delta f \tag{42}$$

where

$P_R$  = received power

$P_T$  = transmitted power

$G$  = antenna gain

$R_{1,2}$  = slant ranges

$S$  = signal to noise ratio

$M$  = receiver noise figure (assumed constant = 8 over the frequency band)

$k$  = Boltzmann's constant =  $1.371 \times 10^{-23}$  watt-sec/deg

$T$  = ambient receiver temperature =  $300^\circ\text{K}$

$\Delta f$  = receiver bandwidth.

This equation has assumed identical receiver and transmitter antennas so that the gains are equal. To determine the system effectiveness over a minimum slant range  $R_2$  of about 1400 km (850 miles) for a generation altitude of 140 km, two geometries are considered: 1)  $\alpha=0, \beta=\pi/2$  (minimum terminal separation) and 2)  $\alpha=0, \beta=0$  (maximum separation). Further, the gain of a parabolic antenna is given by

$$G = \frac{4\pi^2 K a_i^2}{\lambda^2} \tag{43}$$

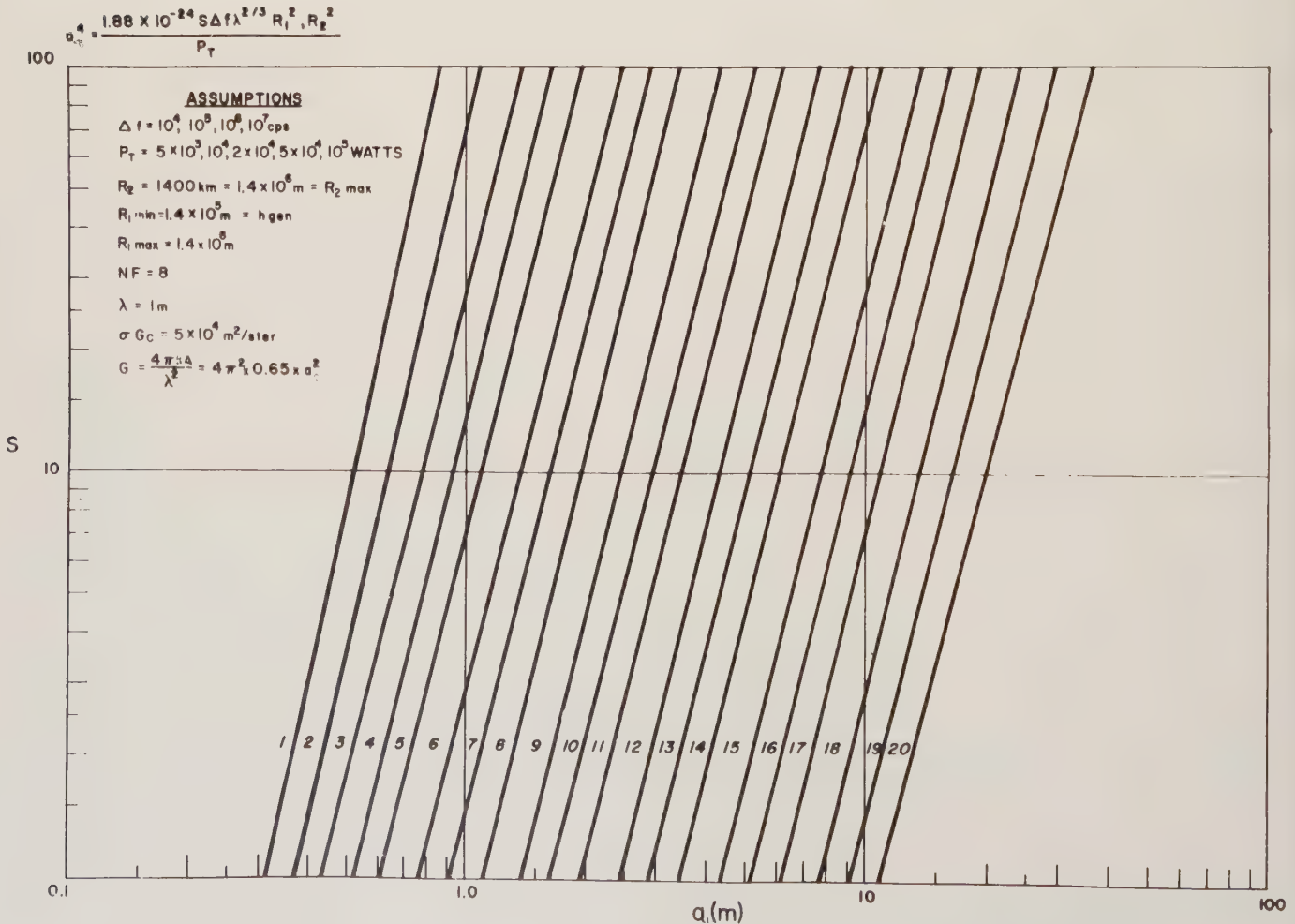


Fig. 15—Signal-to-noise ratios as a function of antenna size for selected ranges, bandwidths and transmitter powers.

where

$K$  = antenna efficiency factor = 0.65  
 $a_t$  = radius of antenna.

It is interesting to observe how great a price in antenna size is incurred as a function of signal-to-noise level. Substituting (41) and (43) into (42) the following expression is obtained:

$$a_t^4 = 2.35 \times 10^{-25} \frac{SM\Delta f \lambda^{2/3} R^4}{P_T}, \tag{44}$$

which has been graphed in Fig. 15, where for simplification, only one frequency,  $\lambda = 1\text{m}$ , has been considered. Interpretations of other wavelengths are made simply by noting the  $\frac{2}{3}$  power relationship in (44). Several power levels ( $5\text{ kw} < P_T < 100\text{ kw}$ ) and various values of bandwidths ( $10\text{ kc} < \Delta f < 10\text{ mc}$ ) have been assumed. The two previously discussed geometries, overhead ( $R_1\text{ min}$ ) and midcourse ( $R_1\text{ max}$ ) clouds have been assumed, leading to two corresponding slant ranges, 140 and 1400 km, respectively. The resultant antenna size functions are then plotted vs signal-to-noise ratio. Tabulation of the assumptions made for each of the curves in Fig. 15 is included in Table IV. Consider the signal-to-noise level of 17 db for the cases of 50 kw transmitted power and a 1-mc bandwidth for the minimum geometric case, and the same power, but 10-kc bandwidth of maximum range, or the midcourse cloud case. It is observed that the 17-db level (error rate =  $10^{-6}$ ) is realizable in both cases when use is made of an eighteen-foot-diameter parabolic antenna.

This preliminary analysis suggests that very modest UHF systems, in terms of power, antenna size, etc., can communicate high information content messages with extremely low error rates, at least in principle.

In order to demonstrate the feasibility of conducting routine UHF communications in the high information burst, low error rate mode, using the artificial electron cloud as the reflector, a specific United States Army Signal Corps communications system will be discussed in some detail. The electronic system parameters, which will be alluded to in the following discussion are enumerated in Table V.<sup>16</sup>

It has been assumed that  $R = 800\text{ km}$  in (44) so that when  $\alpha = \beta = 0$  in the altitude domain between 100–150 km, link ground ranges of about a thousand miles can be achieved. Substituting the values of Table V into the radar range equation it is seen that

$$P_R = 6.9 \times 10^{-20} \sigma. \tag{45}$$

Since the 0-db level is given by the rated receiver sensitivity of  $-120\text{ dbm}$ , the cloud cross section  $\sigma$  only

TABLE IV

Curve	Equation	$\Delta f$	$P_T$	$R_I$
①	$\alpha^4 = 7.2 \times 10^{-3}\text{ S}$	$10^4$	$10^6$	Min.
②	$1.44 \times 10^{-2}\text{ S}$	$10^4$	$5 \times 10^4$	Min.
③	$3.6 \times 10^{-2}\text{ S}$	$10^4$	$2 \times 10^4$	Min.
④	$7.2 \times 10^{-2}\text{ S}$	$10^4$ $10^5$	$10^4$ $10^5$	Min. Min.
⑤	$1.44 \times 10^{-1}\text{ S}$	$10^4$ $10^5$	$5 \times 10^3$ $5 \times 10^4$	Min. Min.
⑥	$3.6 \times 10^{-1}\text{ S}$	$10^5$	$2 \times 10^4$	Min.
⑦	$7.2 \times 10^{-1}\text{ S}$	$10^5$ $10^4$ $10^6$	$10^4$ $10^6$ $10^5$	Min. Max. Min.
⑧	$1.44\text{ S}$	$10^5$ $10^6$ $10^4$	$5 \times 10^3$ $5 \times 10^4$ $5 \times 10^4$	Min. Min. Max.
⑨	$3.6\text{ S}$	$10^6$ $10^4$	$2 \times 10^4$ $2 \times 10^4$	Min. Max.
⑩	$7.2\text{ S}$	$10^6$ $10^4$ $10^7$ $10^5$	$10^4$ $10^4$ $10^5$ $10^5$	Min. Max. Min. Max.
⑪	$1.44 \times 10^1\text{ S}$	$10^6$ $10^4$ $10^7$ $10^5$	$5 \times 10^3$ $5 \times 10^3$ $5 \times 10^4$ $5 \times 10^4$	Min. Max. Min. Max.
⑫	$3.6 \times 10^1\text{ S}$	$10^7$ $10^5$	$2 \times 10^4$ $2 \times 10^4$	Min. Max.
⑬	$7.2 \times 10^1\text{ S}$	$10^7$ $10^5$ $10^6$	$10^4$ $10^4$ $10^5$	Min. Max. Max.
⑭	$1.44 \times 10^2\text{ S}$	$10^7$ $10^5$ $10^6$	$5 \times 10^3$ $5 \times 10^3$ $5 \times 10^4$	Min. Max. Max.
⑮	$3.6 \times 10^2\text{ S}$	$10^6$	$2 \times 10^4$	Max.
⑯	$7.2 \times 10^2\text{ S}$	$10^6$ $10^7$	$10^4$ $10^5$	Max. Max.
⑰	$1.44 \times 10^3\text{ S}$	$10^6$ $10^7$	$5 \times 10^3$ $5 \times 10^4$	Max. Max.
⑱	$3.6 \times 10^3\text{ S}$	$10^7$	$2 \times 10^4$	Max.
⑲	$7.2 \times 10^3\text{ S}$	$10^7$	$10^4$	Max.
⑳	$1.44 \times 10^4\text{ S}$	$10^7$	$5 \times 10^3$	Max.

TABLE V  
ELECTRONIC SYSTEM PARAMETERS OF UHF SYSTEM  
TERMS AS RELATED TO FIG. 15

Parameter	Symbol	Value	Remarks
Transmitter Power	$P_T$	1 kw	
Frequency	$f$	400 mc	$\lambda = 0.75\text{ meter}$
Antenna Gain	$G$	25 db	15-foot parabola same for transmitter and receiver
Bandwidth	$\Delta f$	120 kc	
Receiver Sensitivity	$P_R/P_N$	$-120\text{ dbm}$	At 0-db level, $P_R = P_N = 10^{-15}\text{ w}$

<sup>16</sup> C. E. Sharp, private communication, U. S. Army Signal Corps, Fort Monmouth, N. J.



needs to be  $1.4 \times 10^4$  to produce a 0-db signal at the thousand-mile range. From the model postulated previously, the theoretically available value of  $\sigma$ , however, at 400 mc is  $3.4 \times 10^4$ . This infers a 3.5-db signal propagated by the cloud for the example considered. Since routine communications will require on the order of 10 to 15 additional db of signal-to-noise ratio to accomplish its mission, it is appropriate here to examine the overall situation for sources to acquire additional capability.

Certainly one obvious means is in raising the rated transmitter power level from its 1-kw value. Increases of 5–10 db appear quite possible from slight equipment modifications in this direction. Increasing the number  $Q$  of electrons in the cross section equations by either increased payloads or greater ionization efficiency of the contaminant (or both) appears realizable and some additional 10 db of signal from this source appears feasible.

It has been demonstrated, therefore, that a 3.5-db signal can be transmitted over a thousand-mile range using existing U. S. Army Signal Corps UHF communications equipment. By appropriate transmitter power level increases and also by increasing the number of contaminant electrons, both of which appear to be achievable, it is felt that short burst, high information rate, low error probability communications could be initiated within the very near future on a routine, systematic basis by proper utilization of artificial ionospheres.

#### ACKNOWLEDGMENT

The authors wish to acknowledge the significant scientific input from the following personnel of the Geophysics Corporation of America: Leonard M. Aschenbrand, Dr. Herbert K. Brown, Dr. Robert O'B. Carpenter, and Jerome Pressman.

## Basic Research Efforts in Astrobiology\*

R. S. YOUNG† AND J. L. JOHNSON†

**Summary**—The special problems involved in performing basic biological experiments in space vehicles are described, emphasizing the need for unique types of instrumentation. Some of the techniques used in preliminary experiments in recoverable nose cones of Army ballistic missiles are explained in detail. The reasons for doing this type of research in these vehicles are included.

#### INTRODUCTION

THE PURPOSE of this paper is to acquaint the instrumentation expert with some of the special problems which arise under atypical experimental circumstances, and to describe some of the special devices which have been used to date in performing biological experiments in space.

Space on recoverable Jupiter nose cones has been utilized on a noninterference basis in order to conduct NASA-sponsored basic biological experiments. These experiments were designed in an attempt to answer questions pertaining to the effects of various flight parameters (for example, weightlessness, cosmic radiation, increased gravity-load) on cellular systems and intact organisms. This simple type of experiment was not expected to solve any

momentous problems. The desired result was to gain some insight into the problems (if any) ultimately to be studied in space biology, using these missiles as experimental tools. Only when the state of the art reaches such a point as to permit refined experimentation in a controlled satellite or probe environment will it be possible to expect results from which firmly based conclusions may be drawn.

Obviously, a space vehicle (rocket or satellite) presents an environment which is not usually encountered in the biological laboratory. It is this environment which makes biological experimentation necessary and of interest, while at the same time offering a stern challenge to the instrument designer. The instrument designed for laboratory study of biological systems is no longer of use except perhaps as a prototype. All instruments must now be able to withstand high  $G$ -loads (perhaps as high as 40  $G$ 's or higher), vibrations, and must be capable of functioning in the desired fashion under zero-gravity. At the same time the instrument must be capable of sustaining a living system without toxic effects and remaining as sensitive or possibly more sensitive than it was in the laboratory. Weight and size become of paramount importance; miniaturization of instruments is essential. The biological system being studied must be afforded a constant and normal environment during flight, except for the parameter to be studied, so that the results obtained may be interpreted in terms of control experiments.

\* Manuscript received by the PGMIL, February 1, 1960. This paper was presented under the title of "Design Criteria for Instrumentation to Investigate Biological Space Flight Effects" at the meeting of the Instrument Society of America on September 23, 1959 in Chicago, Ill.

† U. S. Army Ballistic Missile Agency, Huntsville, Ala.



There are two general reasons for doing biological experimentation in space vehicles: 1) to gain evidence pertaining directly to "Man in Space"—that is, research directed toward evaluating safety factors in future manned flights, and 2) to obtain data of a basic nature—that is, to study the effects on living systems of those space flight conditions which are not reproducible in the laboratory, and which do not necessarily have immediate application to space flight. The choice of organism is largely dependent on what is to be studied.

For example, the effect of zero-gravity on biological systems at the cellular level is of great interest; that is, will cells (of any organism) function properly under weightless conditions? We know from the flight and recovery of monkeys in a Jupiter nose cone that monkeys will survive such flights (including short periods of weightlessness) in apparently good condition. However, this does not really answer the question of what actually happens at the functional or cellular level in the animal. It is conceivable that there may be a profound effect on the metabolism of the individual cells. Perhaps cell division or the permeability of cell membranes is affected, which would not be apparent in gross observations of recovered intact animals. In other words, the flight and recovery of animals does not necessarily mean that we have answered all questions of biological significance in space flight. The question as to whether or not cell division is affected by zero-G can best be answered by flying unicellular organisms and exposing them to weightlessness for as long a period of time as is necessary to get the required data.

The problem, then, is to fly a living system instrumented so that the maximum amount of basic information is obtained. This problem has been complicated by the fact that these missiles are not designed for this type of experimentation. We have been able to put experiments in Army Jupiter nose cones which were recovered. This has been done on a noninterference basis in whatever space has been available in the nose cone. We have had almost no telemetering available and almost no power. Presumably these conditions will not always be the rule. We are designing experiments which include both electrical power and telemetering capabilities. These will be briefly discussed later.

#### RESULTS AND CONCLUSIONS

In May, 1959, experiments were designed and flown in a recoverable Army Jupiter nose cone. Most of these experiments were passive; that is, they consisted simply of flying material (yeast, bacteria, mold, seeds, etc.) and studying that material upon recovery for radiation or other damage. However, included in this payload was an experiment designed to determine the effect of weightlessness on two basic cellular phenomena—cell division and fertilization. Since neither telemetering nor electrical power was available, and space was restricted to a few cubic inches, the experimental design was quite simple. Eggs and sperm of the marine invertebrate, the sea urchin,

were used. The object was to mix the sperm and eggs in sea water during the 3–4 minute zero-gravity phase of the flight (after booster cutoff) so that the fertilization reaction could take place in the absence of gravity, if possible. Fig. 1 shows the 5 inch  $\times$  1½ inch aluminum cylinders which were used to house the experiments. These cylinders were oriented in the direction indicated. Inside the cylinders was the experimental package (Fig. 2), consisting of an insulating sheath and three small capsules (Fig. 3) each with an internal volume of about 5 ml. These were

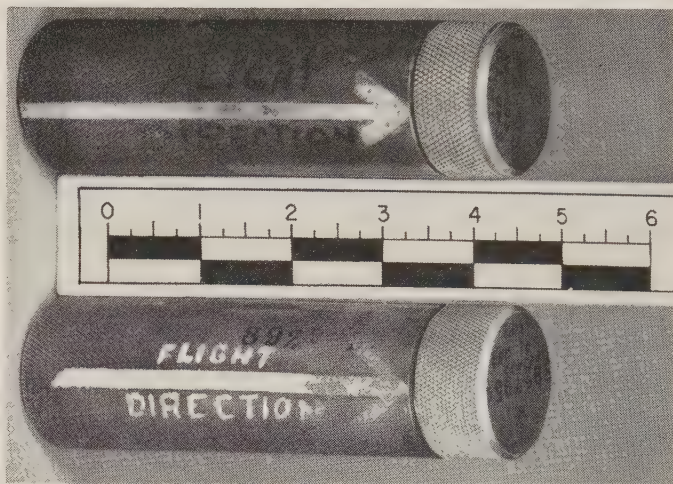


Fig. 1.

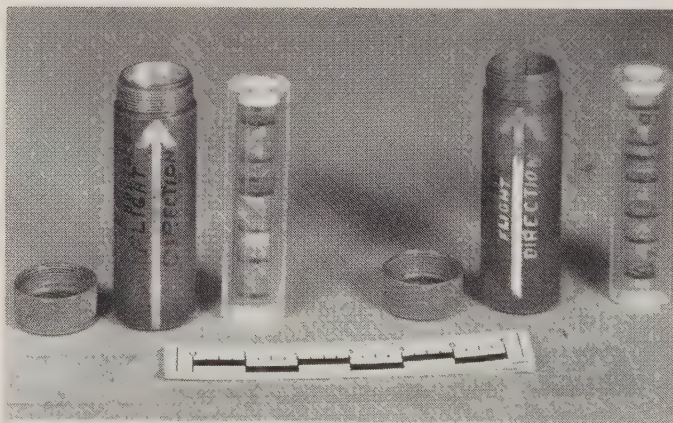


Fig. 2.

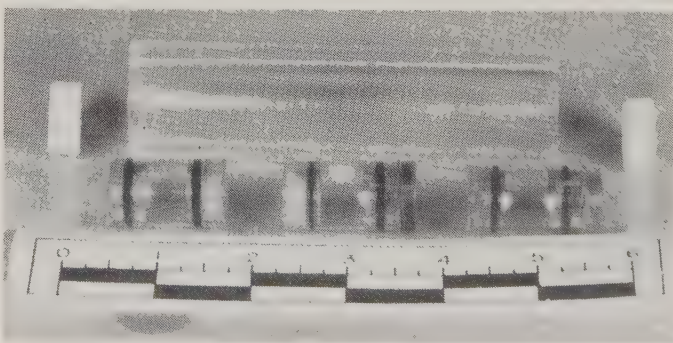


Fig. 3.



the experimental units. Fig. 4 shows one of the units disassembled with the two steel balls and magnet (far left) used to seal the small chambers at each end of the cylinders. Fig. 5 shows the method of placing one of the steel balls into its socket in the lid, and Fig. 6 demonstrates the technique of sealing the capsule by using a hypodermic needle to bleed off the air which is being compressed as the lids are forced into place. The rubber O-rings provide an

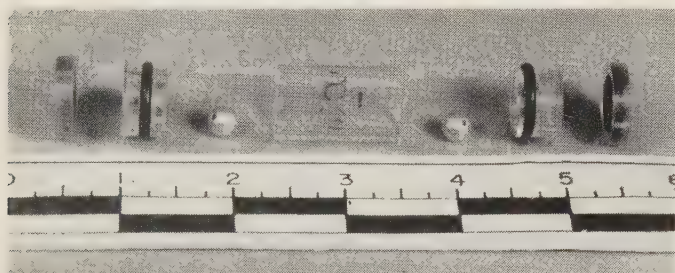


Fig. 4.

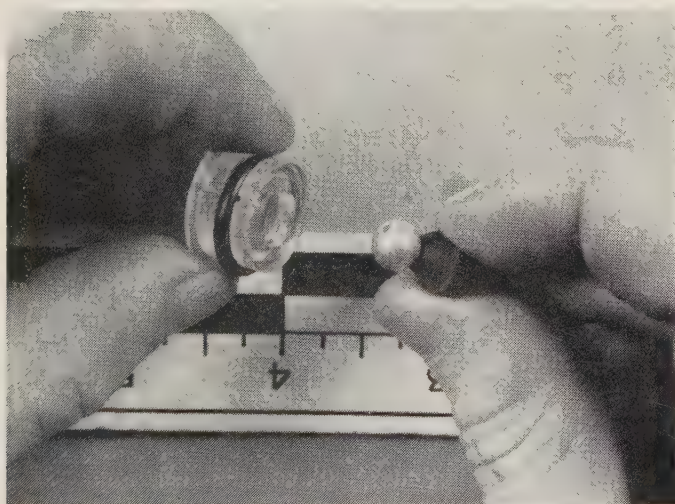


Fig. 5.

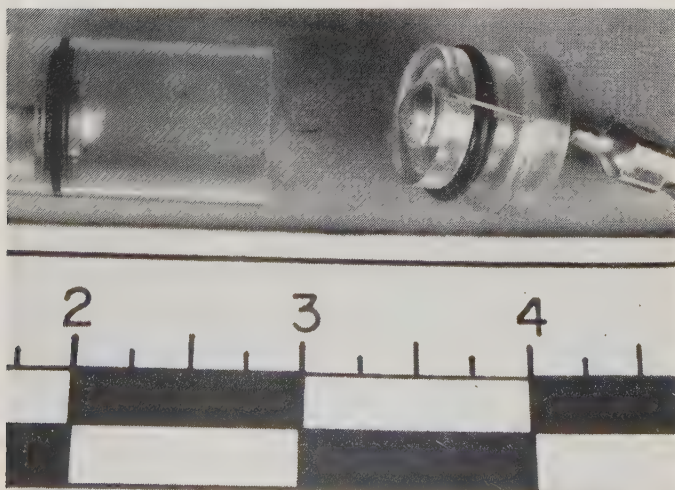


Fig. 6.

air- and water-tight seal for the container. Fig. 7 shows the two lids with adjustable screws projecting into the small chambers inside them.

With these devices (6 capsules) the experiment was set up in the following way. A small drop of sperm was placed behind one of the balls and a predetermined volume of fixative solution behind the other. The balls were then placed in position, sealed with a thin film of silicone grease, and held in place by the small wafer-shaped magnet on the outside of the lid. The magnetic field was adjusted by the screw in the lid. Thus, the intact capsule contained 3 to 4 ml of sea water with a few hundred sea urchin eggs in the barrel of the capsule. The depression in the lid contained fixative at one end and sperm at the other. The steel balls sealing the depressions in the lids were held in place by an adjustable magnetic field. The capsules were oriented in the cylinder so that the sperm end was forward in the direction of takeoff. The Jupiter missile will reach a peak acceleration of over 10  $G$ 's, so that the balls at the sperm ends of the capsules are calibrated, by adjusting the screws, to pull out at 10  $G$ 's. This in effect released the sperm into the sea water immediately preceding booster cutoff, so that fertilization would take place during weightlessness. During re-entry, the  $G$ -load was applied in the opposite direction and was sufficient to pull the ball out of the other end and to release the fixative which killed the eggs and preserved them for laboratory study upon recovery. In some of the capsules there was no fixative, so that the eggs, if fertilized during weightlessness, would continue to develop and would be active larvae upon recovery. In other capsules the eggs were fertilized before installation in the nose cone.

In the first series of such experiments, several difficulties were discovered. The cadmium plate used on the balls proved toxic over long periods of time, and the fixative used was not adequate. However, the device was satisfactory mechanically, and it serves as a useful experimental instrument under these very special circumstances. The



Fig. 7.



device has been modified subsequently, so that we now have a similar instrument (Fig. 8) which is electrically triggered. On signal, an electrical pulse which burns out the wire holding the plunger in place is sent through the system, thus injecting sperm, and later fixative, into the medium. This makes timing of the reaction more accurate and permits the initiation of the fertilization reaction on the launching pad (previously impossible) at such a time that the egg will be in the process of cell division during the weightlessness phase of the flight. This allows us to study the effect of zero-*G* on the process of mitosis and cell division. As the payload and power capabilities increase, the experimental and instrument design can be refined considerably. In performing biological experiments it is necessary to have very accurate temperature control, since biological systems respond to slight changes in temperature. It may be desirable to control temperature to less than  $\pm 0.1$  degree. This presents a problem in the nose cone of a rocket, where the ambient temperatures may vary by many degrees. To date it has been possible only to insulate the cylinders, which gives some protection, but

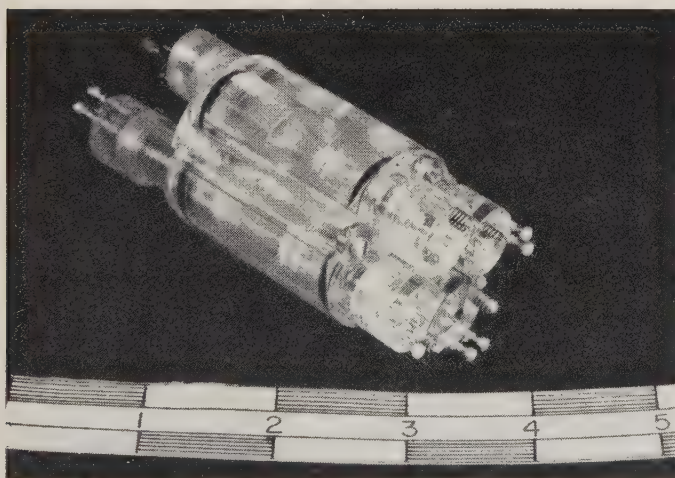


Fig. 8.

still inadequate temperature control. Space does not permit the installation of the usual sort of temperature control equipment. We have developed a system which will offer sufficiently accurate temperature control within an adjustable range, providing this range is below ambient temperature. This device consists of a well-insulated inner capsule surrounded by a low boiling point liquid and an adjustable relief valve. The choice of liquid depends on the temperature desired, and the evaporation rate (thus the cooling rate) is controlled by the valve. There are no power or sensor requirements necessary for its operation. Of course such a device has some limits in its application, but under the special and limiting environment of a nose cone, it may be very useful.

There are many other experiments the biologist would like to perform, in rockets and in satellites with and without telemetering. Some experiments require recovery of the material, some do not. All require special instrumentation. It would be helpful to know how cells respire (use oxygen and liberate carbon dioxide) under weightless conditions and while being bombarded by cosmic radiation. Attempts have been made (by ONR and others) to develop a respirometer, small in size, capable of accurately measuring and telemetering gas volume changes of 100 cubic milliliters or less per hour in a rocket or satellite. This device should be flexible enough to make possible the use of a wide variety of cellular systems (yeast, bacteria, algae, eggs, etc.). It must be able to withstand acceleration environment, and be able to operate in a vacuum, and during zero-*G*.

Obviously the problems involved are many and varied, and each experiment has its own special requirements. Each vehicle has its own requirements, which are in turn impressed on the instruments. In this new area of instrumentation, there is need for a great deal of thought and work by people interested in this very specialized technology. This paper is an attempt to make clear some of the problems and methods of approach.



# Bio-Telemetry in the Nose Cones of U. S. Army Jupiter Missiles\*

S. J. GERATHEWOHL†, S. W. DOWNS, JR.‡, G. A. CHAMPLIN‡,  
AND E. S. WILBARGER, JR.¶

**Summary**—On December 1, 1958, a South American squirrel monkey, and on May 28, 1959, a rhesus and a squirrel monkey, were launched in the nose cones of two U. S. Army Jupiter missiles. The experiments were done by scientists of the Army and Navy medical departments, and personnel of the Army Ballistic Missile Agency. They were done on a noninterference basis with the main mission of the missile.

The primary objective of the bio-flights was to demonstrate that animals can survive ballistic flights unharmed, if an adequate life support is provided. The secondary aim was to design, construct and test such a system, to develop countdown and launching procedures, and to recover the specimen after flight. Moreover, technical and scientific information on the physiologic and behavior status of the animal was to be gained through telemetry.

Although the first animal was lost, valuable data were obtained on the functioning of the bio-package during flight. They served to improve the second experiment, which added substantially to the understanding of the biomedical requirements for space flight. Moreover, Able and Baker were the first primates recovered unharmed from an operational IRBM nose cone after re-entering the earth's atmosphere.

## INTRODUCTION

AFTER the successful recovery of several U.S.A. Jupiter (SM-78) nose cones during the previous years, the Surgeon General of the Department of the Army, in the summer of 1958, suggested to the Commanding General of the U. S. Army Ordnance Missile Command, that space not otherwise used in rockets be made available for biomedical research. About four months later, a South American squirrel monkey, and in the spring of 1959, a rhesus monkey and a squirrel monkey, were launched at Cape Canaveral, Fla. Scientists from the U. S. Army Medical Research and Development Command and from the U. S. Naval School of Aviation Medicine shared the bulk of the work in a common effort. The Army Ballistic Missile Agency was in charge of the technical side of the project, particularly of hardware design and construction, transportation, and telemetry. The second of these bio-flights was sponsored by the National Aeronautics and Space Administration. The experiments were accomplished under "noninterference" conditions with the technical mission of the missiles.

Experiments of this sort demand the cooperative work of a large number of persons and various organizations furnishing elaborate equipment, specialists, test facilities, training and conditioning of the animals, and ingenious

ways of improvisation. Although the difference in objectives, the specification of the biomedical requirements, the realization of plans and ideas, and the administrative and organizational difficulties were serious obstacles for the accomplishment of the mission, the cooperation between biologists and engineers, medics and missile men, scientists and administrators in an entirely new field of endeavor proved to be gratifying and successful. This also holds for the interservice cooperation and the assistance provided by the many specialists from universities and supporting agencies.

Man cannot venture into space unless the human factor requirements for his health and survival have been met by the engineer. Traditionally, the experiment with animals paves the way that leads into the unknown. It carries on where the mechanical payload fails to yield the necessary information. Contrary to the unmanned research vehicle situation, the animal payload can register the effects of the space environment upon the living organism, can perceive, perform, and act as an organic multichannel recorder. However, the return for a high investment is extremely small, if the specimen dies on the launching pad or the missile fails in the initial part of its flight. Hence, this type of studies requires greater care in preparation and involves much higher risks than almost any other type of biomedical experimentation.

## MISSION OBJECTIVES

The primary objective of the two bio-flights was to demonstrate that primates can survive ballistic missile flights unharmed, if an adequate and efficient life support system is provided.

Secondary objectives were to design, construct and test such systems, to develop countdown and launch procedures; to obtain technical and scientific information on the physiologic and behavior status of the animals during launch, flight, and recovery; and thus to establish further parameters for the advancement of manned space flight.

## MISSION PROFILE

The Jupiter missiles were launched from Cape Canaveral, and reached the target area located approximately 1500 nautical miles east in the Atlantic Ocean after a flight of about 15 minutes. The nose cone traveled at a speed of about 10,000 mph reaching a peak altitude of about 300 nautical miles. The Jupiter has a maximum acceleration of about 12 *g* during liftoff, and a maximum deceleration in excess of 30 *g* during re-entry. There are also short jerks

\* Manuscript received by the PGMIL, February 2, 1960.

† U. S. Army Ballistic Missile Agency, Redstone Arsenal, Huntsville, Ala.

‡ Aviation Medical Officer, Hq. U.S.A.E., Heidelberg, Germany.

¶ Nuclear Power Div., Office of the Chief Engr., Dept. of the Army, Washington 25, D.C.

and vibrations producing accelerative forces in the order of 10 G. The free-flight period after burnout, separation of the nose cone from the booster, and second tilt lasts until spin-up; and this was about 7.8 minutes in Bio-Flight 1, and about 4.2 minutes in Bio-Flight 2. This involved weightlessness and various amounts of subgravity. Impact forces were in the range of 9 to 10 G. A schematic picture of the flight trajectory of the Jupiter IRBM is given in Fig. 1.

On the other hand, they are very sensitive indicators of stressful situations.

The rhesus monkey (*Macaca mulatta*) was selected because of the amount of information available on the physiology and training ability of this species. It is rather aggressive in the untamed state; but capable of tolerating relatively high functional stresses that would make it an almost ideal animal to manually perform in a nose cone. This part of the experiment was intended to investigate how high ac-

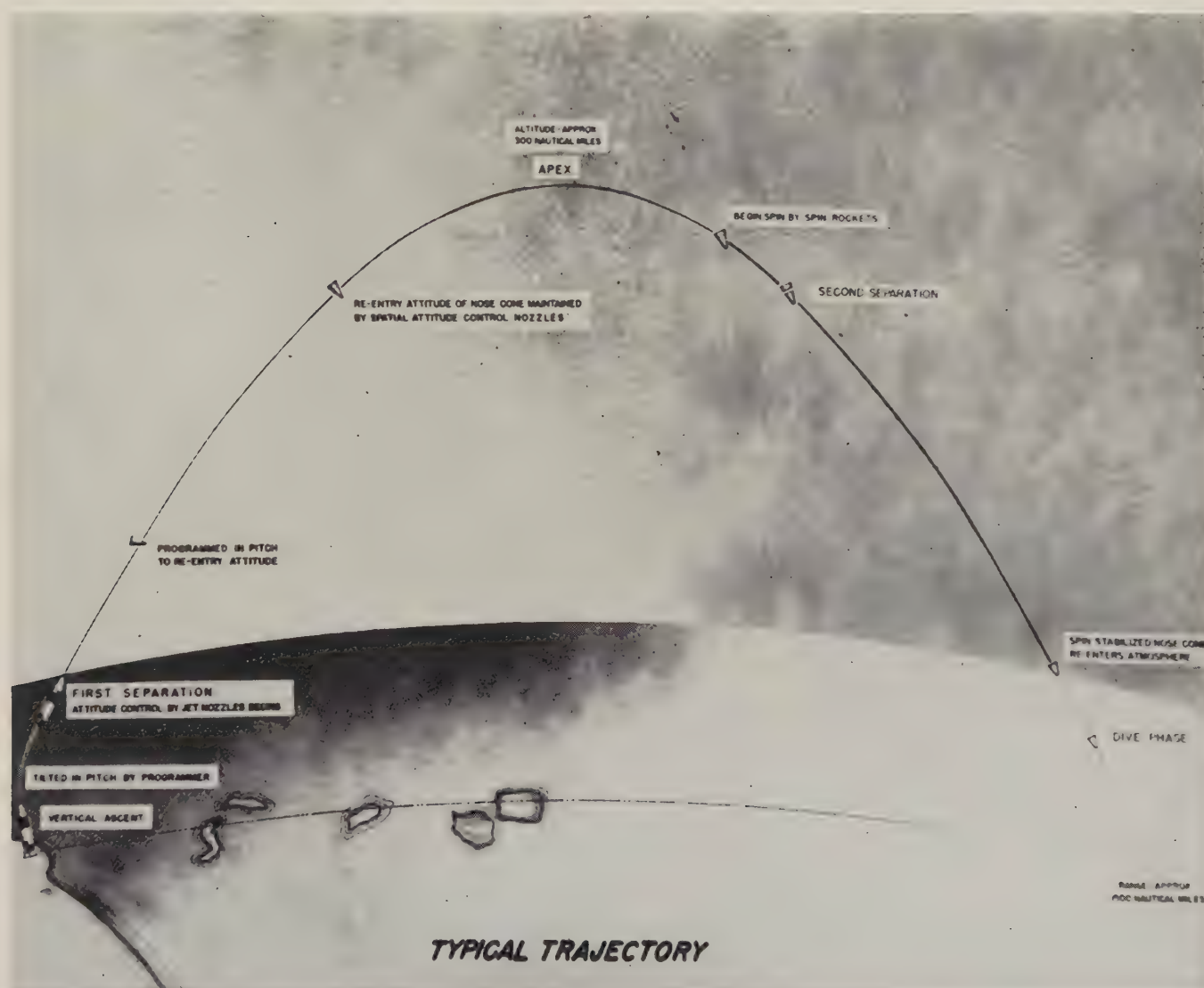


Fig. 1—Typical flight trajectory of U. S. Army Jupiter IRBM.

## BIOMEDICAL PREPARATIONS

### The Animals

The squirrel monkey (*Saimiri sciurea*) was chosen primarily because of its small size and weight. The two animals used weighed about 300 grams each. However, members of this species are easily excited and show wide fluctuations in respiration, heart rate, and body temperature.

celerations and weightlessness effect learned coordinated action. Because of a last-minute decision, however, the Indian-born, avoidance trained monkey had to be substituted by an American-born rhesus which could not be trained in time to perform properly.

### Effects of Restraint and Confinement

Countdown and checkout procedures required that the



squirrel monkeys would have to stay in their capsule for a maximum of about 24 hours. If search and recovery were difficult, this period could be longer. Since the large capsule was to be installed below the recovery package, the rhesus monkey might have to stay incarcerated for as long as 90 hours.

The squirrel monkeys were gradually conditioned to their restraint and confinement up to 24 hours and longer. Body temperature, respiration, and motility served as criteria for their final selection. Continuous struggling and temperatures over 103°F disqualified the animals from further training. The heart rate of the restraint squirrel monkey varied from 120 to 375 beats per minute; respiration ranged from 50 to 150 breaths per minute.

In preliminary studies at the Walter Reed Army Institute of Research and the Army Medical Research Laboratory, the rhesus monkeys were fully restrained in plaster casts for 72 hours and longer. The heart rates were found to be in between 130 to 200 beats during restraining, and breathing ranged from 18 to 40 movements per minute.

The rhesus monkeys were kept immobilized at an ambient temperature averaging 68°F. They were hand fed; some received no food at all. Monkeys that were firmly restrained showed virtually no struggling, but animals with loose casts struggled continuously. Several animals, previously infected with pneumonia and septicemia, died within 24 hours. However, no deleterious effects were found upon responsiveness, heart rate, hematocrit, and general well-being in healthy animals. Thus, it was suggested to keep the second-best animal in reserve to be packaged and substituted for the best one, in case it should die during the first 24-hour period on the pad.

#### *Conditioning to G Forces*

Training runs on the ABMA centrifuge served to adapt the rhesus monkeys to the acceleration pattern during lift-off. The animals were gradually brought up to about 10 *G* within 160 seconds while bar-pressing responses and the electrocardiogram (EKG) were registered. Essentially, increments in acceleration were associated with increases in response rate; but the animal stopped performing at high rates of change and at high *G* forces. The animals responded properly during periods of constant angular acceleration and up to 8 *g* with little or no impairment of performance. By and large, performance improved through learning and conditioning.

Essentially, the effect of acceleration on avoidance behavior in the rhesus was found to be quite similar to the effect of presenting an additional or extraneous punishing stimulus. Since experiments involving extremely high *G* forces can also cause injury and trauma, no attempts were made to condition the experimental animals to acceleration stresses similar to that expected to occur during re-entry.

#### *Pre-Launch Facilities*

Provisions were made for adequate animal housing, colony isolation in case of an epidemic disease, physiological base line studies, behavioral response training, and other pre-launch activities at Cape Canaveral. Two medical trailer vans were constructed containing animal compartments, operation rooms, laboratory and checkout facilities. They were equipped with air conditioning, refrigeration, water and power supply, measuring devices, and sewage disposal. A K-9 military vehicle housed one of the rhesus colonies. Complete facilities for clinical studies including hematology, parasitology, and microbiology, were also available. The health status of the animals was daily checked by a veterinarian on duty from the Redstone Arsenal Post Hospital. The medical launching team including technicians and animal handlers, who set up shop at the Cape about two weeks before the launching date, numbered about 20 individuals for Bio-Flights 2A and 2B. An identical bio-pack was prepared for each experiment as a back-up. The spare and a third animal were used as controls during the actual flight.

#### THE BIO-PACKAGE

##### *Biomedical Capsules*

The small capsule for the squirrel monkey was made of aluminum sheet material and well insulated. An access port on both ends of the capsule facilitated the placement of equipment into the box. A gas sampling port permitted the checking of the cabin atmosphere after the capsule was hermetically sealed by an O-ring at the circular door plate. The weight of the small bio-pack was about 30 pounds. The capsule is shown on the left side in Fig. 2.

The six-pound rhesus monkey was housed in a cylindrical capsule of 0.19-inch aluminum alloy. It measured about 18 inches in diameter, 41 inches in length, and had a free volume of about 10,000 inches<sup>3</sup>. The door on one end was circular and sealed by an O-ring. One-inch fiber-glass wool provided inside insulation. Flanges and cross braces were welded to the outside wall for strength and attachment of the capsule to the nose cone. Two oxygen bottles, several tubes, the CO<sub>2</sub>-absorber unit, the electronics package, batteries, and a 16-mm motion picture camera (B. B. Milliken Co., Mod. DBN-4 with 25-mm Wollensack Raptor lens) were mounted on the framework. Pressure-tight seals closed the connections to the inside. The whole package weighed about 250 pounds. The large capsule is shown in Figs. 3 and 4. The capsules and the entire bio-packs were pressure, vibration, temperature, and acceleration tested. To meet the water integrity requirement, the capsules were also submerged and tested at 3 atmospheres differential pressure. All capsules were designed and—with the exception of the one used for Bio-Flight 1—built in ABMA workshops.





Life Support Equipment

The schematic layout of the environmental package in the nose cone is shown in Fig. 5. The characteristics of the 24-hour sustaining equipment for the small bio-pack are listed in Table I. 365 grams of Baralyme, and later 200 grams of lithium hydroxide, kept the CO<sub>2</sub> concentration below 1 per cent. The HiOH was tightly packed in a wall pocket to prevent dust formation during periods of vibration. 100 grams of Mobilbead (silica gel) and 20 grams of activated carbon were used as water and urine neutralizers.

Baralyme (4060 grams) and Mobilbead (3216 grams) were also employed to remove CO<sub>2</sub> and H<sub>2</sub>O from the atmosphere of the larger capsule. Two blower fans circulated the air through the CO<sub>2</sub> absorption unit. The protective cover, which conserved the capacity of the Mobilbead during the long countdown period, was removed by means of a rip cord shortly before the flight.

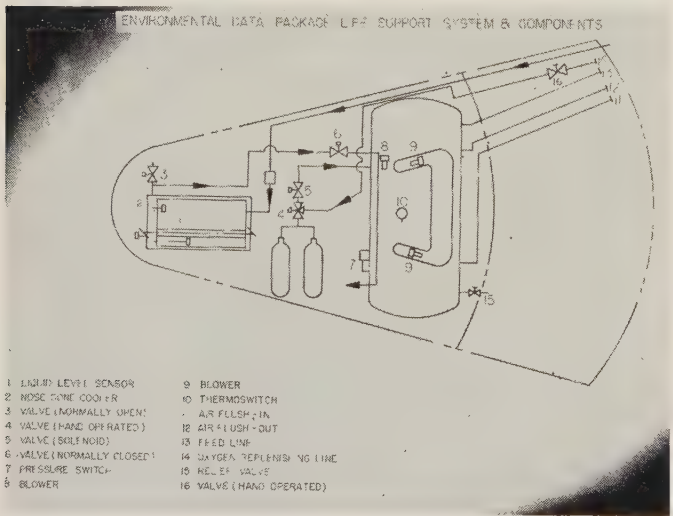


Fig. 5—Schematic layout of the environmental package in the nose cone of Jupiter missile AM-18 (Bio-Flight 2B).

TABLE I

NOSE CONE EXPERIMENT	
BIO-FLIGHT NO. 2A	
TOTAL VOLUME	670 CU. INCHES
TOTAL WEIGHT	29.5 POUNDS
OVERALL DIMENSIONS	9.75 X 12.5 X 6.75 INCHES
VOLUME OF MOBILBEAD	12.5 CU. INCHES
VOLUME OF BARALYME	35 CU. INCHES
OXYGEN SUPPLY	22 CU. INCHES AT 1800 PSI
VOLUME OF OXYGEN (STD. COND.)	44.15 LITERS
INSULATION	5 IN. FIBERGLASS & .5 IN. RUBBER
HEAT SOURCE	8.5 WATTS
TEMPERATURE CONTROL	THERMOSTAT 55° TO 65°
CIRCULATION	CONVECTION
MISSILE CONNECTION	ONE 13 PIN ELECT. CONNECTOR
TIME OF INSTALLATION	6 HOURS PRIOR TO LIFTOFF
ELECTRICAL REQUIREMENTS	1.5 WATTS (ELECTRONICS ONLY)
ELECTRICAL SOURCE	28 VOLT NOSE CONE BATTERIES

In the small capsule, compressed O<sub>2</sub> from a 22-inch<sup>3</sup> bailout bottle maintained normal O<sub>2</sub> pressure for about 60 hours at a consumption rate of 0.7 liter/hour. The storage pressure (1700 psig) was reduced to 70 psig by a reduction valve, and a needle-type bleeder secured the necessary O<sub>2</sub> flow. Another tube served as a relief in case of over-pressurization.

An air-flushing unit and an independent O<sub>2</sub> supply system maintained a tolerable atmosphere within the large capsule. It was flushed during all ground operations. After the nose cone was inaccessible, the two O<sub>2</sub> bottles, charged at 1500 psig, started operating by demand, keeping the cabin pressure between 14.6 and 15 psia. In addition, a mechanical demand regulator served as a back-up in the event of failure of the electric system. A pressure-relief tube was also installed to secure a safe upper limit.

The temperature in the small capsule was determined by an 8-watt inside resistor-type heater, set to maintain about 51°F, and the nitrogen cooling of the nose cone. This proved to be too low and the animal shivered.

In the large capsule, the temperature was controlled by a heat exchanger thermostatically operated at 68.4°F. A blower fan circulated the air within the cabin. The exchanger was supplied with cold N<sub>2</sub> gas from the nose cone. The missile power source was used to operate the system.

The squirrel monkeys received no liquids shortly before, and no food during the experiment. Thus, the amount of bodily waste products was minimal. Diapers filled with Mobilbead were used to neutralize the moisture of urine and feces.

The rhesus monkey, on the other hand, received intraperitoneal infusions of 5 per cent dextrose at the rate of 5 cc per hour because of the long countdown period on the pad. The feeding procedure was discontinued upon sealing of the nose cone, when the thin polyethylene tube was cut. Although marginal, this dose was sufficient to sustain life. Body wastes accumulated in diapers. Specifications of Bio-Flight 2A are given in Table II.

TABLE II

NOSE CONE EXPERIMENT	
BIO-FLIGHT NO. 2A	
MEASUREMENTS - TELEMETERED*	FREQUENCY RESPONSE
ELECTROCARDIOGRAM - 1-2 MILLIVOLTS INPUT	180 CPS
RESPIRATION THERMISTOR	10/SECOND
BODY TEMPERATURE THERMISTOR (30°-100°F)	10/SECOND
AMBIENT TEMPERATURE THERMISTOR (15°-40°C)	10/SECOND
AMBIENT PRESSURE (10-18 PSI)	10/SECOND
*THESE WILL BE RECORDED ON ELECTROMAGNETIC TAPE THROUGH RE-ENTRY.	
MEASUREMENTS - PHYSICAL	METHOD
HEAVY NUCLEI COSMIC RAYS	NUCLEAR TRACK PLATES
ATMOSPHERIC COMPOSITION	CHEMICAL ANALYSIS OF ABSORBENTS & AIR
MEASUREMENTS - PRE AND POST-LAUNCH	
PSYCHOLOGICAL	PHYSICAL & LABORATORY EVALUATION
PSYCHOLOGICAL	LONG TERM COMPARATIVE PERFORMANCE STUDIES

### Specimen Support and Protection

The squirrel monkey was supported by flexible polyurethane padding and a perforated silicone rubber bed. A chest plate and wide nylon straps kept it in place. The bed and the protective helmet were molded after the animal. The animal, ready to be inserted into the capsule, is also shown in Fig. 2.

The protective couch suggested for Project Mercury served as a prototype for the rhesus support system. It consisted of an aluminum frame and a fiber-glass mold in accord with the body contours of the specimen. The legs, slightly bent, were held by nylon straps. A fiber-glass chest plate pressed the animal gently into the bed of lined polyurethane foam. The fiber-glass helmet, also lined and split for adjustment, protected the head against shocks and served to fasten it to the couch. The wiring for the physiological transducers was placed on the underside of the couch and cabled to quick-disconnect plugs. The couch was installed in the capsule so that the *G* forces during re-entry were directed from chest to back, thus providing maximum protection.

### BIOMEDICAL INSTRUMENTATION

Bio-Flight 1 and the Baker part of the second flight required a much simpler electronics system than the Able part of Bio-Flight 2.

The measurements made on the squirrel monkey (Old Reliable) were EKG, respiration rate, heart sound, body temperature, capsule temperature and capsule pressure. In the second nose-cone experiment, the heart sound of the squirrel monkey was omitted because of insufficient telemeter channels.

A somewhat more elaborate program was planned for Able. This consisted of the above measurements and also two electromyograms, pulse velocity, humidity, and per cent CO<sub>2</sub>. In-flight photography and a behavioral response study system were included. A schematic representation of the program for the nose-cone experiment Bio-Flight 2B is given in Table III.

### Electrocardiogram

One of the most important measurements was the EKG. Implanted electrodes were used which gave a peak-to-peak signal of approximately 1 to 6 mv. This required an amplifier gain of 1000 to 5000 to fully utilize the subcarrier which was a 0-5-volt dc voltage-controlled subcarrier oscillator. A single-ended amplifier was found to be satisfactory for use with the squirrel monkeys. This amplifier operates from 28 volts dc, a readily available missile voltage, has a gain of 5000, and an input impedance of 50 K ohms. The frequency response is 3 db down at 1 cps and 750 cps. No attempt was made to have a dc amplifier, since it was desirable to eliminate dc shift generated by movement of the subject.

On the rhesus monkey, a balanced input amplifier was

used with circuit as shown in Fig. 6. This amplifier has an input impedance of 50 K ohms each side to the ground. An adjustment is provided to equalize gain in order to have maximum common mode rejection. The amplifier was operated at a gain of 5000 but had a maximum gain of 10,000. The signal-to-noise ratio was approximately 25 to 1 for a 1-mv peak-to-peak input signal.

In both amplifiers, some components had to be selected, and some "tailoring" of the individual amplifiers was necessary. Since only a small quantity was built, this was not objectionable. Both amplifiers utilized printed circuits in packaging.

In both flights, the amplifiers used with the squirrel monkeys functioned properly and the desired information was obtained. However, a short time before take-off, the EKG amplifier used with Able began erratic oscillations. After recovery, it was determined that one of the wire leads had become detached from the embedded electrode. Good data were obtained from the control animal held in the hanger.

TABLE III

NOSE CONE EXPERIMENT BIO-FLIGHT PROJECT 2B	
TOTAL VOLUME 310,000 CU IN	ELECTRONIC MEASUREMENTS
TOTAL WEIGHT 225 LBS	F. ELECTROCARDIOGRAM
OVER-ALL DIMENSIONS 18" DIA X 41" LONG	ELECTROMYOGRAM (FLEXOR)
VOLUME OF MOBILEHEAD 264 LITERS	ELECTROMYOGRAM (EXTENSOR)
VOLUME OF PARALYME 122 LITERS	HEART SOUNDS (REINFORCED)
HEAT SOURCE 40% N <sub>2</sub> O <sub>2</sub>	PULSE VELOCITY (CAROTID)
COOKING SOURCE GASEOUS NITROGEN	PULSE VELOCITY (FEMORAL)
O <sub>2</sub> SUPPLY 234 CU IN AT 1500 PSI	RESPIRATION RATE
VOLUME OF O <sub>2</sub> STO CONDENSED LITERS	BODY TEMPERATURE (90°-110°F)
INSULATION 1 IN POLYURETHANE	BEHAVIORAL RESPONSE
CIRCULATION 0.28 GPM AT 0 PSI 28V	BEHAVIORAL STIMULUS (VISUAL-AUDITORY)
GROUND SERVICE 0.45 GPM AT 0 PSI 6V	ELECTRIC SHOCK
AIR FLUSHING 2 AIR CHANGES MIN	AMBIENT TEMPERATURE (15°-40°C)
FEED LINE INTRAPERITONEAL	AMBIENT PRESSURE (0-8 PSI)
O <sub>2</sub> TOPPING LINE	AMBIENT RELATIVE HUMIDITY (30-100%)
CAMERA RUNNING TIME 15 MIN	AMBIENT CO <sub>2</sub> (0-7%)
POWER SUPPLY	PHYSICAL MEASUREMENTS
ELECTRONICS 15 WATTS	HEAVY MIDDLE COSMIC RAYS NUCLEAR TRACK PLATE
CAMERA 56 WATTS	IRRADIATION SURVEY FILM BADGE
CAMERA LIGHTS 40 WATTS	TOTAL BODY COUNT
LIGHT STIMULUS 10 WATTS	INTERNAL ENVIRONMENT ANALYSIS OF ABSORB
tone stimulus 85 DECIBELS	PSYCHOPHYSIOLOGICAL MEASUREMENT
SHOCK 28V 1 SEC PULSES	MOVIE 16MM ANSCO-CHROME
	16 FPM

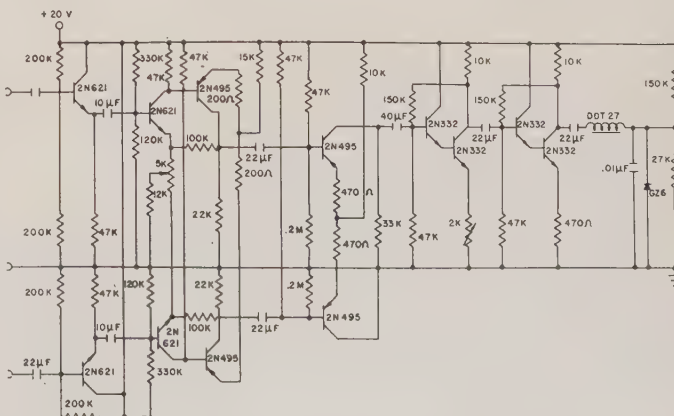


Fig. 6—Amplifier circuit for measurement No. 12A26.









The bridge was excited with dc; and a chopper amplifier and demodulator were used. The solid-state chopper was operated at 10 kc. This frequency was selected in order to avoid possible interference with other measurements. Circuit diagram is seen in Fig. 10.

#### Ambient Pressure

In both flights, the ambient pressure was measured with a bourdon tube gauge with potentiometer pickoff. The potentiometer was supplied with a 5 dc and the output applied to telemeter.

#### Behavioral Response

A behavioral response system was designed for use during flight. The animal was to be trained to press a bar switch to avoid a mild electrical shock. The timer circuit as shown in Fig. 11 applies a mild shock voltage to the animal once every two seconds unless the bar switch is pressed at less than two second intervals. It can be seen that continuous holding of the switch in the closed position will not withhold the shock. The animal was to be trained to press the bar switch when a stimulus of a red light and

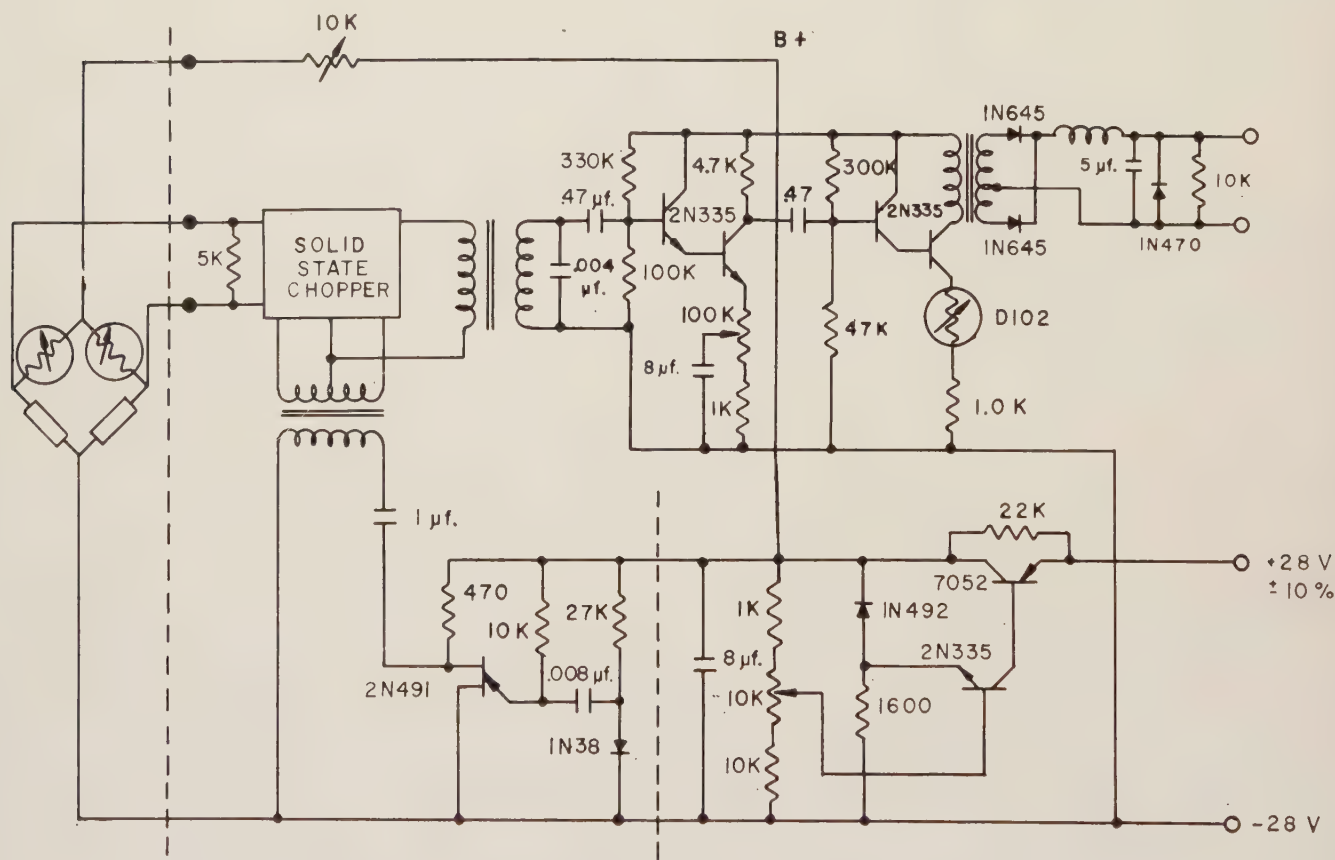


Fig. 10—Circuit diagram used for measurement No. 12A22.

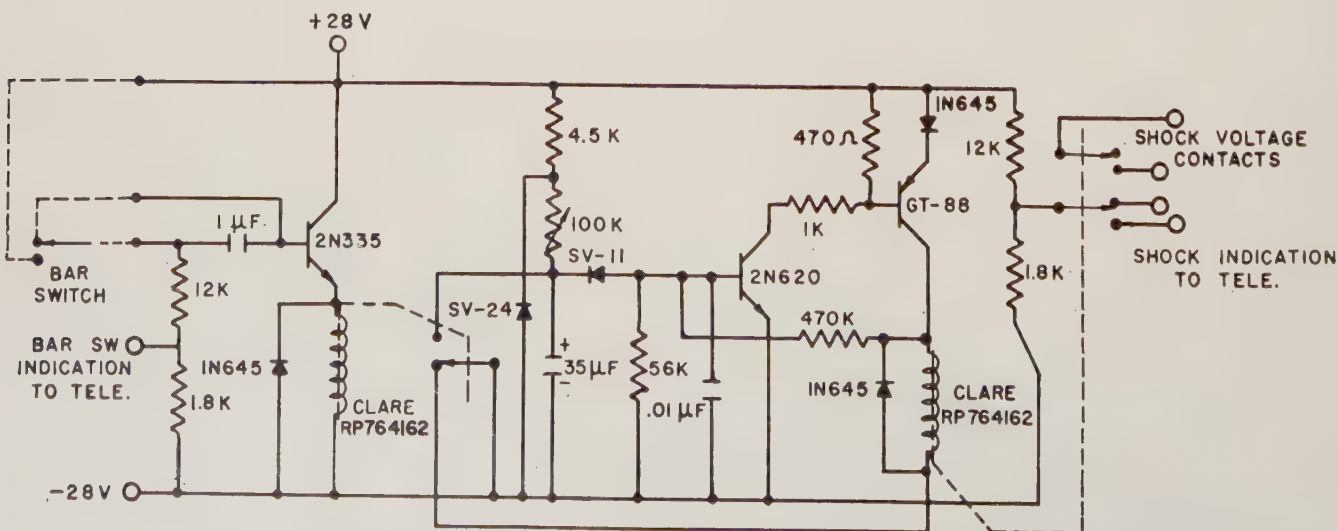


Fig. 11—Wiring diagram of timer circuit as used for measurement Nos. 12A27 and 12A28.

a 1-kc audible sawtooth tone was given. Animals trained this way will perform in this manner for long periods of time, even under conditions of severe distraction. However, this behavioral response experiment was not used during the flight since Able had not received sufficient training. It was decided not to attempt this experiment during flight because the animal might not remember to press the bar switch intermittently and thus be subjected to a continuous shock, which would cause stress on the animal and interference with the other measurements.

Packaging

Two types of packaging were used for the biomedical flights. The package used for the squirrel monkeys is seen in Fig. 12. The electronic circuits are on printed circuit cords and are stacked. The pressure gauge was mounted on the package and also the thermistor for ambient temperature measurement. The signals from the animal were brought in through the small connector near the center of the package. All power and the telemetered signals were through the connector at the left of the figure. This en-

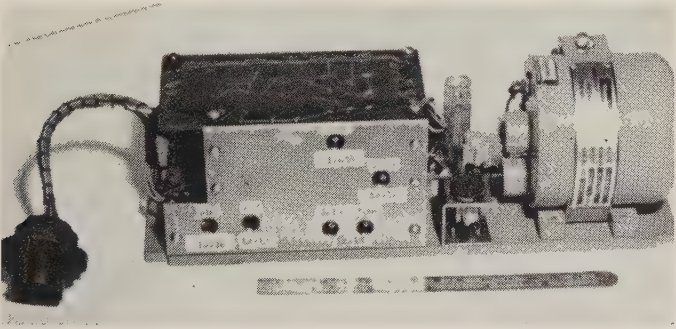


Fig. 12—Electronics package for small bio-pack.

tire package was placed inside the container with the animal.

A somewhat different method was used on the rhesus monkey. All the electronics were packaged on plug-in printed circuit cards. A typical card is seen in Fig. 13. This particular one was used for pulse velocity. Fig. 14 shows the package used with some cards in place. The power and telemeter signals were through the connector at the left and the signals from the capsule containing the animal are at the right. The plug-in cards were used to allow individual measurements to be removed for service or modification without affecting the rest of the circuits. A cover, containing guide rails to secure the cards, was placed over the unit and fastened with screws.

The biomedical and telemetry parameters Bio-Flight 2A and 2B are given in Table IV. The information to be gained during the last phase of the flight was recorded on tape in the nose cone.

LAUNCH PREPARATIONS AND PRE-LAUNCH DATA

At about 70 hours prior to launch, the rhesus monkeys were readied for the experiment. The EKG electrodes

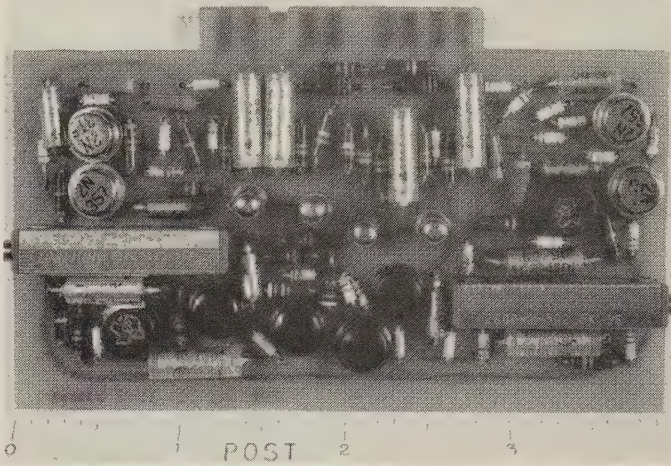


Fig. 13—Plug-in printed circuit card used for Bio-Flight 2.

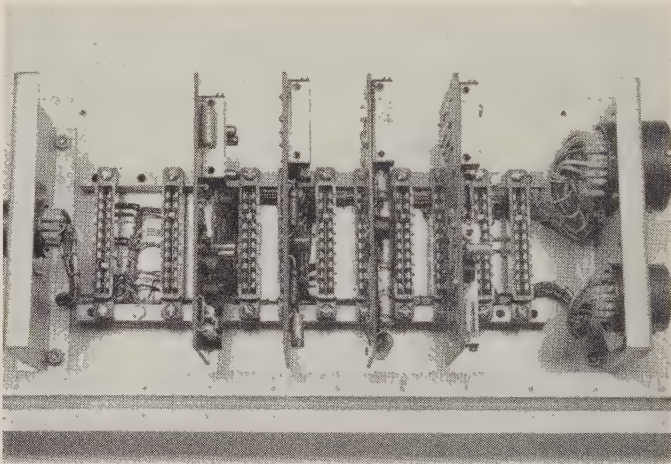


Fig. 14—Electronics package assembled for Bio-Flight 2.

TABLE IV  
BIOMEDICAL AND TELEMETRY PARAMETERS OF BIO-FLIGHT  
NUMBERS 2A AND B

Measure Number	Variable	RDB Chan-nel	RDB Response	Sub-carrier* Fre-quency
12A12	EKG A	5 -14	330 cps	22 kc
12A13	Respiration A	5A- 1	10 per second	30 kc
12A15	Body Temperature A	5A- 2	10 per second	30 kc
12A16	Ambient Temperature A	5A- 3	10 per second	30 kc
12A17	Ambient Pressure A	5A- 4	10 per second	30 kc
12A18	Ambient Temperature B	5A- 5	10 per second	30 kc
12A19	Ambient Pressure B	5A- 6	10 per second	30 kc
12A20	Relative Humidity B	5A- 7	10 per second	30 kc
12A21	Pulse Velocity B <sub>1</sub>	5 - 6	25 cps	1.7 kc
12A22	Percentage CO <sub>2</sub> B	5A- 9	10 per second	30 kc
12A23	Pulse Velocity B <sub>2</sub>	5 - 6	25 cps	1.7 kc
12A24	Respiration B	5A-13	10 per second	30 kc
12A25	Body Temperature B	5A-14	10 per second	30 kc
12A26	EKG B	5 -13	220 cps	14.5 kc
12A27	Behavioral Response B	5A-15	10 per second	30 kc
12A28	Reinforcement Shock B	5A-16	10 per second	30 kc
12A29	EMG <sub>1</sub> B	5 -17	790 cps	52.5 kc
12A30	EMG <sub>2</sub> B	5 -16	600 cps	40 kc
12A31	Heart Sound B	5 -18	1050 cps	70 kc

\* FM/FM: Carrier Frequency 239.5 mc.



were implanted, the respiration and body thermistors were attached, the infusion tube inserted, and Able was restrained in her couch and secured in the capsule. The electronics package was checked, the capsule sealed and pressure tested. It was then turned over to personnel from the Missile Firing Laboratory, ABMA, for installation into the nose cone and transferred to the launching pad. The control animal was identically prepared, placed in the spare capsule, and kept in an air conditioned room with the capsule door open for direct observation. A third animal was merely restrained and held as a substitute for Able. Feeding and measurements were then started on Able and the control animal; the alternate was merely fed orange juice during the period of restraint.

Fig. 15 shows the body (colonic) temperature, capsule temperature, and heart and respiration rates of Able on the pad, and also those of the control monkey (No. 1111) in the spare capsule. Information received on Baker during the countdown period is given in Table V. Able's

capsule atmosphere was maintained through air flushing; and the capsule was moved considerably during checkout and mating of the nose cone to the missile. Able and her control were prepared about 70 hours, Baker about 10 hours, prior to launch. Fig. 15 and Table V show that the preparation of the flight was tolerated quite well by the animals.

During the countdown period, the biomedical data were displayed in two blockhouses and in the telemetry room at Cape Canaveral. Two ten-man teams composed of biomedical and biotechnical specialists alternated in the around-the-clock monitoring of the two large bio-packs. Ten hours before liftoff, Able's body temperature suddenly dropped. This was soon compensated by increasing the capsule temperature. At X -5 hours, her EKG was lost; and heart rate was then determined from the heart sound data.

#### FLIGHT DATA REPORT

##### Temperature and Capsule Pressure

Curves for body temperature, capsule temperature, and capsule pressure of the two bio-flights are given in Fig. 16. While body temperature and capsule pressure stayed almost constant in Bio-Flight 1, the capsule temperature increased gradually during the flight period.

In Bio-Flight 2A (Baker), the capsule pressure remained at an almost constant level of 17.7 psia.

In Bio-Flight 2B, Able's body temperature rose slightly during the first 500 seconds and averaged about 100.3°F for the rest of the flight. Her capsule (ambient) temperature varied slightly but within the tolerance range of the animal. Fig. 16 also shows a sudden fall of Baker's ambient temperature in conjunction with a sharp rise in pressure at spin-up, while within Able's capsule both temperature and pressure increased at that instance. This cannot be entirely explained by the environmental control system parameters.

##### Heart Functions and Breathing Rate

The time courses of heart and breathing rates of the two squirrel monkeys are shown in Fig. 17. While Old Reliable's heart rate fluctuated considerably and decreased gradually throughout the entire experiment, Baker's curve proved to be more stable. Engine noise at ignition produced an increase in heart rates. Breathing also quickened, but the changes in respiration always lagged behind the cardiac effects. With the increment in acceleration, the heart rates became faster, but dropped at peak acceleration shortly before burnout. Respiration during powered flight followed a different pattern. The breathing rates of the animals decreased with increasing accelerative forces, and respiration became very shallow at or about engine cutoff. Baker manifested a short period of pronounced hyperapnea at peak acceleration. As the state of weightlessness was approached, there was a slow return of the heart and breathing rates to their basic levels.

The period of free-flight and weightlessness was generally quiet and undramatic. In Bio-Flight 1, the vehicle

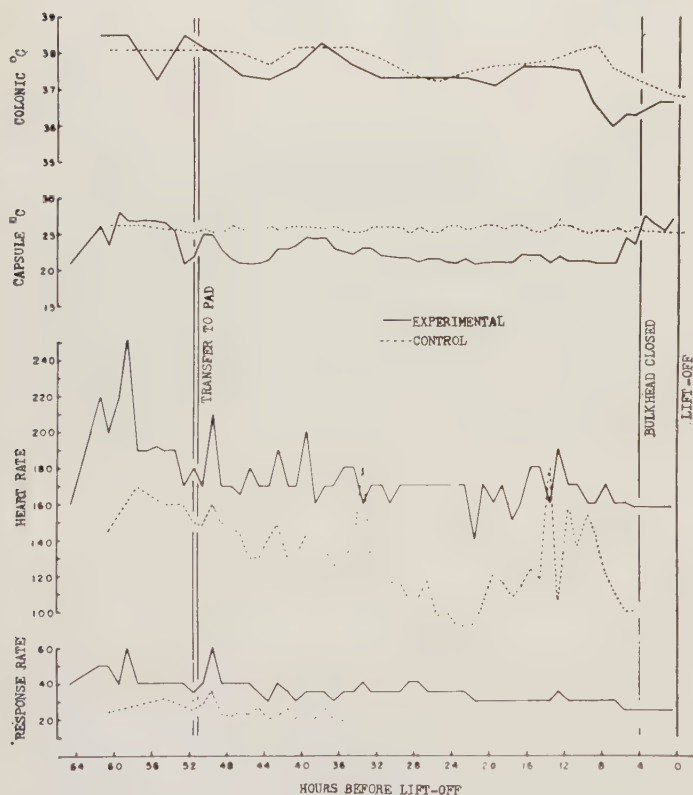
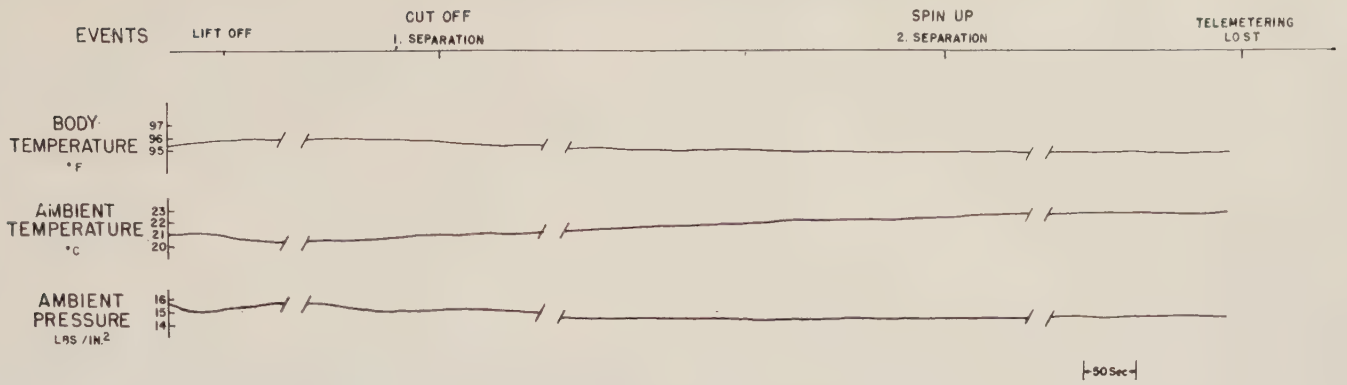


Fig. 15—Pre-launch data from Bio-Flight 2B: Able and control animal No. 1111.

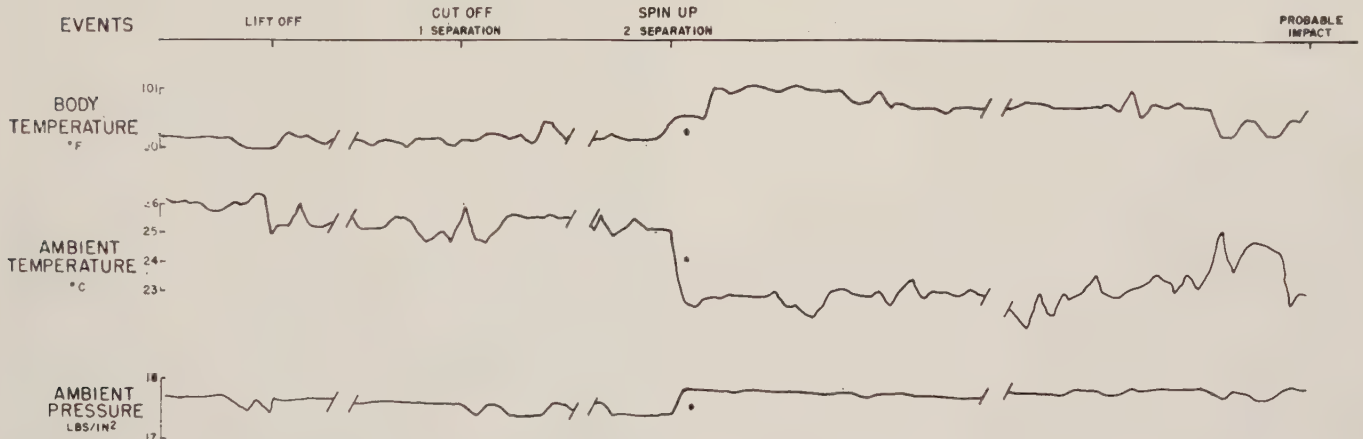
TABLE V  
PRE-LAUNCH DATA FROM BIO-FLIGHT 2A (BAKER)

Local Time EST	Breathing Rate (per minute)	Heart Rate (per minute)	Body Temperature °F	Capsule Temperature °C	Capsule Pressure psia
1935	—	280	96.0	26.5	—
2030	96	265	99.0	29	15.2
2130	80	270	99.0	29	15.7
2230	80	270	99.0	29	15.7
2330	85	280	99.0	29	15.8
0030	90	290	99.6	28	16.2
0130	85	290	99.0	27.5	16.8
0230	—	300	—	—	—

## BIOFLIGHT 1 (OLD RELIABLE)



## BIOFLIGHT 2 (BAKER)



## BIOFLIGHT 2 (ABLE)

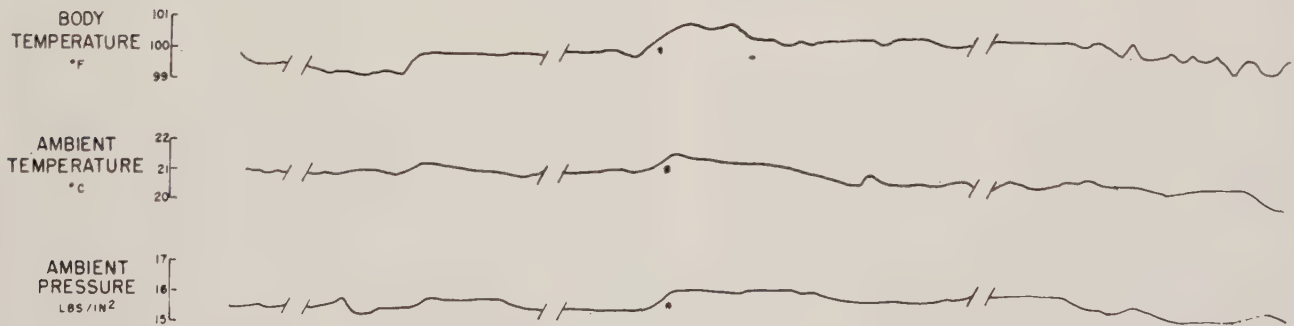
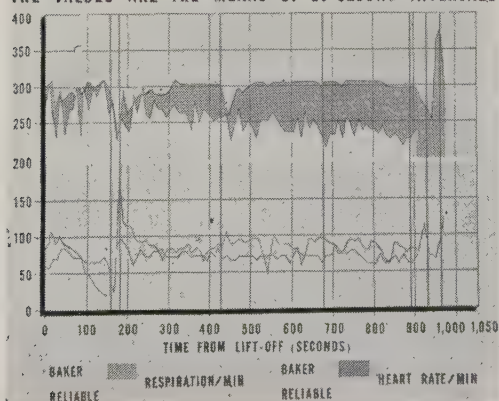


Fig. 16—Telemetered flight data obtained in Bio-Flight No. 1 and No. 2: Temperature and pressure readings.

HEART RATE AND RESPIRATION OF TWO SQUIRREL MONKEYS (RELIABLE AND BAKER) DURING FLIGHTS IN JUPITER MISSILES AM-13 AND AM-18. THE VALUES ARE THE MEANS OF 10 SECOND INTERVALS



HEART RATE AND RESPIRATION OF A RESUS MONKEY 'ABLE' DURING FLIGHT IN JUPITER MISSILE AM-18 THE VALUES ARE MEANS OF 10 SECOND INTERVALS

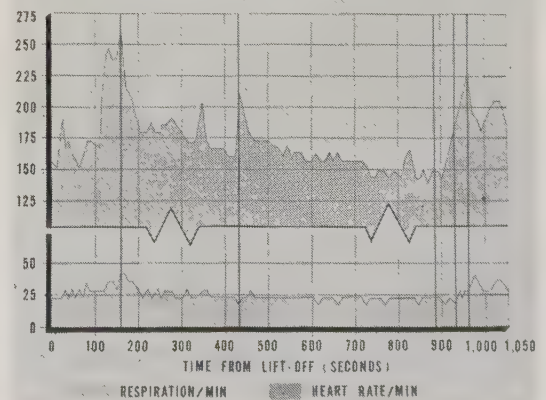


Fig. 17—Telemetered flight data obtained in Bio-Flight 1 and 2A.

Fig. 18—Telemetered flight data obtained in Bio-Flight 2B.



tumbled very slowly, imposing 0.03 *G* upon Old Reliable. Baker, on the other hand, was completely weightless for about 4½ minutes. His heart rate was regular at a rate just under 300 beats per minute. Respiration was also stable at or about base-line values. Spin-up and second separation caused a sudden appearance of high-frequency artifacts in the EKG and a transient quickening of the heart beat.

During re-entry, Baker developed premature beats and a temporary decline in cardiac rate. Thereafter, it rose abruptly, reaching an absolute maximum of 378 beats per minute, and showing pronounced irregularities during the last 30 seconds of flight. His respiration rate, which had increased with increasing deceleration forces, fell rapidly, but increased again at impact.

Able's heart and breathing rates are displayed in Fig. 18. It also showed a cardiac reaction to engine ignition, and a steep increase with a maximum rate of 258 beats per minute during peak acceleration. The return to base level was merely interrupted by spin-up and other missile events. Breathing increased during liftoff but showed a decrease and stabilization course similar to that of heart rate. The free-flight period was generally uneventful with the exception of an abrupt head movement, struggling, and a temporary increase in cardiac activity. Weightlessness was terminated by spin-up, which produced an acceleration of about 0.01 *g*. The response to this is clearly visible in Fig. 18. Thereafter, there was little variation until the beginning of the re-entry phase. As the nose cone was decelerated by the atmosphere, Able's head and back were forced deeply into the couch. This is clearly noticeable on the film, which also shows the animal in distress at this point. The sharp rise and fall in deceleration was depicted only by a rise in the cardiac and respiration curves; the peak of the first one coincided with impact, while that of the second one lagged behind. From impact to the end of telemetry, both functions quickened and respiration was shallow.

#### *In-Flight Photography*

The field of view on the film was about 5 × 8 inches, so that Able's head and the upper portion of her chest plate were visible. Since the helmet had been prepared for a larger animal, Able withdrew into it for protection against the bright light. Hence, her face was visible only a small part of the time, particularly during in-flight events. Table VI is the evaluation of the in-flight film obtained.

#### *Miscellaneous*

The attempted measurements of *pulse velocity* were not obtained because of difficulties in fitting the microphone to the femoral artery of the small animal after it was restrained.

The transducer for *relative humidity* measurements was found not to work already during pre-launch and checkout procedures.

Cursory examination of the *electromyogram* has indi-

TABLE VI  
ABLE'S REACTION DURING FLIGHT (AN IN-FLIGHT  
FILM EVALUATION)

Event	Movement
Acceleration	Head back in helmet. Intermittent swallowing. Head movement. Intermittent swallowing. Head pushed far back in helmet. Swallowing. Gulped, appeared to cry out. Moved head out of helmet so that eyes showed. Blinking, swallowing. Opened mouth, closed mouth. Moved head, rolled eyes.
Free-Flight	Started moving head back in helmet. Completed moving head back in helmet. Swallowing. Started moving head out of helmet. Completed moving head out of helmet. Blinked, rolled eyes. Started moving head back in helmet. Completed moving head back in helmet. Pushed head far back in helmet. Pulled head partially out. Pushed head far back in helmet, then pulled head out. Blinked intermittently. Gradually pushed head back in helmet. Swallowing. Moved head further back in helmet.
Spin	Abruptly pulled head out of helmet; eyes visible. Started moving head back in helmet, completed moving head back in helmet. Head far back, intermittent swallowing. Rapid swallowing.
Re-Entry	Head far back, intermittent swallowing. Pulled head out of helmet, head vibrating in rapid nod-like motion. Pursed lips in characteristic manner as if hooting; being forced far into polyurethane foam. End of film.

cated that there were no observable changes in the EMG records that show deviations from normal control values.

#### RECOVERY AND POST-FLIGHT EVENTS

The nose cone of missile AM-18 was recovered by the U.S.S. *Kiowa*. The small capsule was removed first, and Baker's EKG registered at a rate of 280 beats per minute. About one hour later, electronic measurements of Able's physiology and environment yielded a heart rate of 144, a body temperature of 92°F, a CO<sub>2</sub> concentration of less than 1 per cent, a capsule temperature of 63.3°F, and a capsule pressure of 14.5 psia. These values are relatively low, probably representing an error due to faulty calibration or salt water spray. Upon opening, the capsules seemed to be slightly over-pressured. Both animals appeared tired, though somewhat aggressive; but they readily accepted food and water. Baker became very tame and has remained well ever since.

A picture of Able shortly after her recovery is given in Fig. 19. She showed minor abrasions on the temples from the ill-fit of her helmet. Following examinations, radiation counts, and TV debut, she died an anesthetic death during the removal of the electrodes. Autopsy did not reveal any evidence of injury.



## DISCUSSION

It is rather interesting to speculate on the stability of the primate organism and the adaptability of its physiological functions. Retrospectively, it appears that the stresses involved in the experiments were unusual and high. The animals were immobilized, isolated, ill-fed, and in a state of marked psychophysiological strain. The highest  $G$  loadings had to be tolerated at about the end of the

experiment and in a state of apparent exhaustion. Although the periods of high- $G$  forces and weightlessness were short, the extremes were considerable and the changes from one state to the next rapid. In spite of this, the cardiovascular and electric phenomena of the heart were remarkably well maintained.

Fig. 20 displays samples of the telemetered in-flight data revealing the excellence of quality. They were recorded during the weightless state. The EKG is of good quality and shows that the time courses of depolarization and repolarization occurred in a normal and orderly fashion. Comparison with the recordings prior to launch showed that weightlessness did not alter these processes and, therefore, hemodynamic phenomena were adequate and insured good coronary circulation. For this to have been true, arterial blood pressure must have been maintained.

Any conjecturing concerning the mechanisms for the fluctuations in heart and breathing rates or the cardiac irregularities at this time would accomplish nothing. The variables were plentiful and most, if not all of them, are quantitatively unknown. That emotional effects entered into the physiological phenomena is clearly evident from the startled reactions to the noise of the engine, and also from the cinematographic records of the facial expression of Able. Nevertheless, the entire integrated responses resulted in animals whose physiological functions remained sufficiently stable and intact to insure a safe flight.

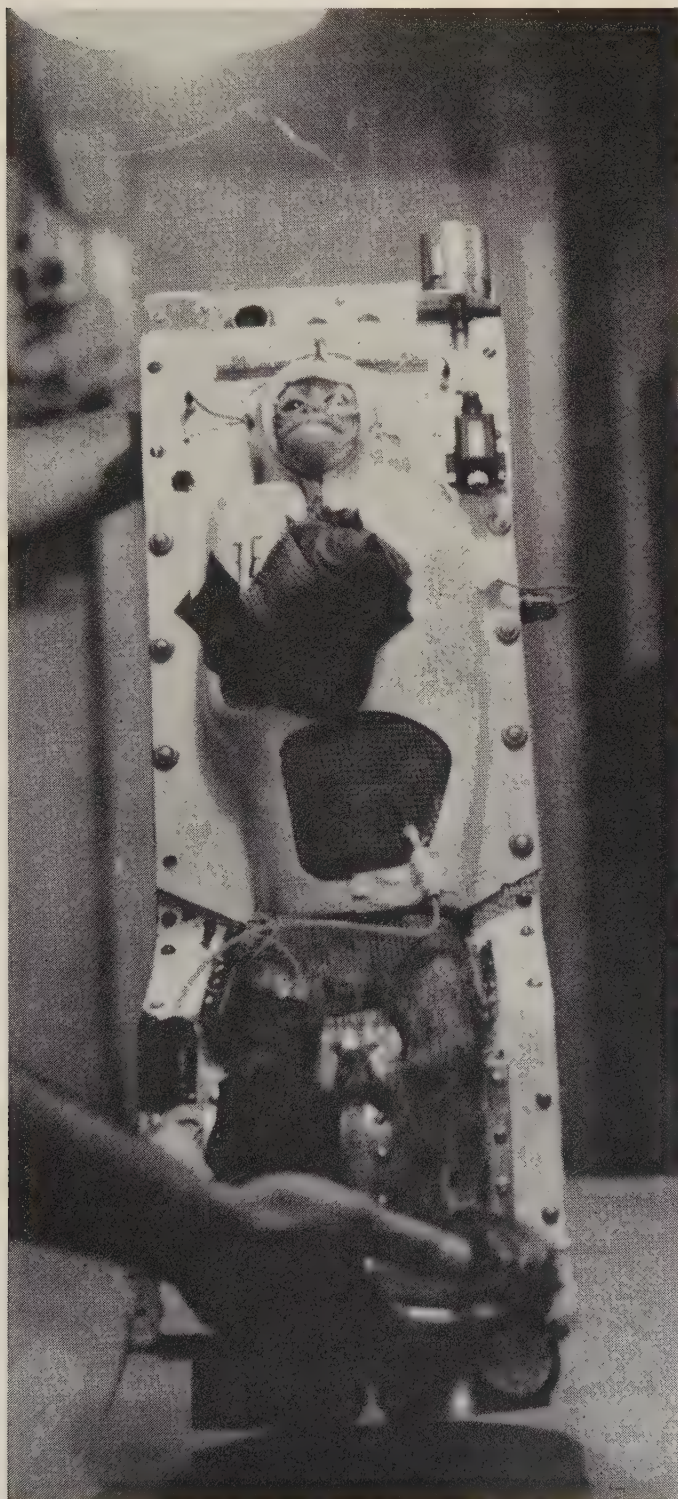


Fig. 19—Rhesus monkey Able shortly after recovery.

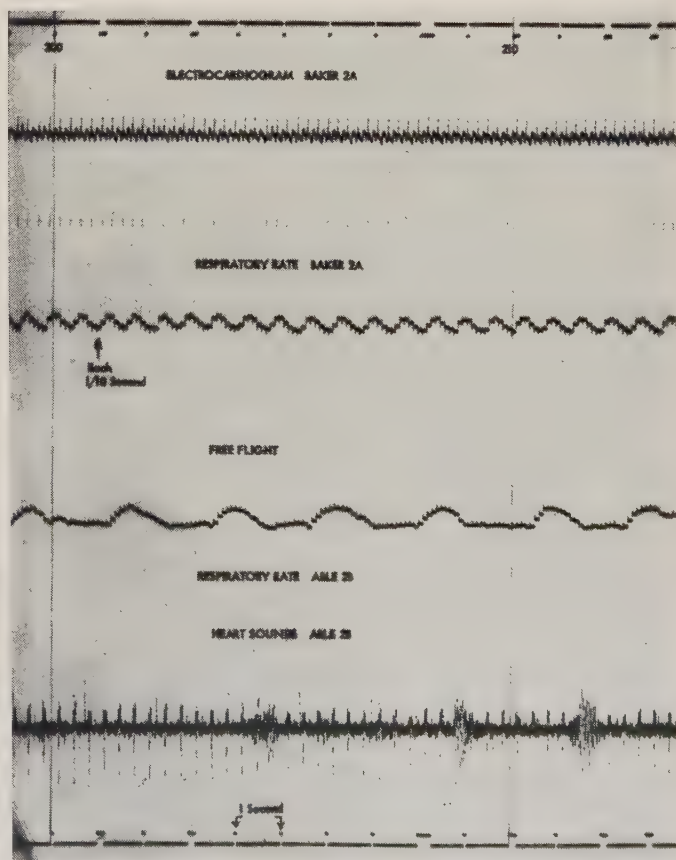


Fig. 20—Telemetered flight data obtained in Bio-Flight 2A and 2B: oscillogram.



## CONCLUSIONS

The results obtained from the two experiments satisfy our early objectives. On both the basic and applied levels of the problem they yielded significant data which provide a better understanding of the reactions of the primate organism to the stresses involved in rocket flights. The engineering parameters, which in particular determine the final integration of biomedical and technical requirements, were designed in detail and employed for the fabrication of a life support system which proved efficient for the viability of the animals. Thus, Able and Baker were the first primates recovered unharmed from an operational IRBM nose cone after re-entering the earth's atmosphere on a long ballistic trajectory.

By extrapolation and application of our data it can be said that the results also point toward safe human travel in a space vehicle. The essential results can now be summarized as follows:

1) It has been demonstrated that primates can be launched in IRBM's and safely recovered in a selected target area, alive, alert, and unharmed by their frightful experience.

2) Life support systems fully capable of monitoring small primates have been developed and actually tested under rocket flight conditions.

3) Sensing devices, amplifiers, and signal monitoring electronic equipment have been actually applied for measuring and controlling biomedical and environmental parameters, while their small size, weight, power consumption, and efficacy were properly maintained.

4) Scientific information has been obtained which will contribute to the realization of manned space flight.

## ACKNOWLEDGMENT

Dr. G. E. Burch, Professor of Medicine, Tulane University, evaluated and interpreted the electrocardiographic results. His contribution to this article is highly appreciated.

## BIBLIOGRAPHY

- [1] G. E. Burch and S. J. Gerathewohl, "Some Observations on Heart Rate and Cardiodynamics During Weightlessness," presented at the 2nd World and 4th European Congress on Aviation and Space Medicine, Rome, Italy; October 27-31, 1959.
- [2] G. A. Champlin and S. J. Gerathewohl, "Bio-Flight Project 2 (U)," Bioastronautics Research Unit of the U. S. Army Med. Res. and Dev. Command, AOMC, Redstone Arsenal, Huntsville, Ala., Rept. Contr. Symbol CSCRD-16 (Secret); June 21, 1959.
- [3] G. A. Champlin and E. S. Wilbarger, Jr., "Bio-Flight Project 2B (Revision I)," Bioastronautics Research Unit of the AOMC, Rept. Contr. Symbol CSCRD-16, Redstone Arsenal, Huntsville, Ala.; July 10, 1959.
- [4] G. R. Emanuel, "Jupiter Missile AM-18, Thermal Environment Analysis Unit. Systems Report of Temperature and Pressure Control Systems, Environment Temperatures, Pressures, and Special Measurements (U)," Evaluation Section, Propulsion and Mechanics Branch, Structures and Mechanics Lab., DOD, ABMA, Redstone Arsenal, Huntsville, Ala., Rept. No. DSD-TR-27-59 (Secret); July 17, 1959.
- [5] D. Flickinger, "Results of Animal Investigation in Space Vehicles to Date," presented at the 30th Annual Meeting of the Aeromedical Assoc., Los Angeles, Calif.; April 27-29, 1959.
- [6] C. R. Fullmer, "Actual Trajectory of Jupiter Flight Test AM-13 (U)," Flight Evaluation Branch, Aeroballistics Lab., DOD, ABMA, Redstone Arsenal, Huntsville, Ala., Rept. No. DA-TN-52-59 (Secret); May 22, 1959.
- [7] C. R. Fullmer and J. P. Lindberg, "Aeroballistics Evaluation of Jupiter Test Flight AM-13 (U)," Flight Evaluation Branch, Aeroballistics Lab., DOD, ABMA, Redstone Arsenal, Huntsville, Ala., Rept. No. DA-TM-69-59 (Secret); May 27, 1959.
- [8] A. Graybiel, J. H. McNinch, and R. H. Holmes, "Observations on Small Primates in Space Flight," presented at the 10th Congress of the International Astronautical Federation, London, England; August 31-September 5, 1959.
- [9] A. Graybiel, *et al.*, "An account of experiments in which two monkeys were recovered unharmed after ballistic space flight," *J. Aviation Med.*, vol. 30, pp. 871-931; 1959.
- [10] "Army Biological Experiment 2B on Jupiter IRBM AM-18 (U)," Missile System Engineering Branch, Structures and Mechanics Lab., DOD, ABMA, Redstone Arsenal, Huntsville, Ala., Rept. No. DSL-TN-16-59 (Secret); May 11, 1959.
- [11] M. Uherka and W. Kistler, "Army Medical Service Research and Development Command Special Experiment for Jupiter Missile AM-13 (U)," Missile Systems Engineering Branch, Structures and Mechanics Lab., DOD, ABMA, Redstone Arsenal, Huntsville, Ala., Rept. No. DSL-TN-28-58 (Secret); October 27, 1958.
- [12] A. C. Weisler and C. C. Haygood, "Biological Experimental Acceleration Environment Jupiter Missile AM-18 (U)," Flight Evaluation Branch, Aeroballistics Lab., DOD, ABMA, Redstone Arsenal, Huntsville, Ala., Rept. No. DA-TM-87-59 (Secret); July 10, 1959.
- [13] E. S. Wilbarger, "Biomedical Measurement in Ballistic Missiles," U. S. Army Med. Res. and Dev. Command, Bioastronautic Res. Office, AOMC, Huntsville, Ala., Special Rept. CSCRD-16-3; September 20, 1959.

# Recovery System Development\*

R. M. BARRAZA† AND W. G. HUBER†

**Summary**—The design and development of a recovery system involves extensive studies and tests to determine the best configuration for each specific application. Thought should be given to using off-the-shelf, well proven components where applicable in any new recovery system design. This will reduce the development cost and yield higher system reliability. In discussing the design and development of recovery systems, the over-all problem can be broken down to include considerations of structural integrity of the vehicle; *i.e.*, deceleration loads it can safely withstand, re-entry heating, practical end conditions of velocity and altitude at which recovery system sequence can be initiated with reliable operation, efficiency of system; *i.e.*, weight and space requirements of the system for the amount of braking force developed, flotation equipment if required, and locating devices.

This paper discusses these considerations in detail and their application to present and future booster and payload recovery systems being developed by the U. S. Army Ballistic Missile Agency.

## LIST OF SYMBOLS

$C_D$  = drag coefficient.  
 $E$  = energy, foot pounds.  
 $F$  = force, pounds.  
 $g$  = acceleration of gravity, feet/second<sup>2</sup>.  
 $h$  = distance, feet.  
 $L$  = wetted length, feet.  
 $S$  = reference area of parachutes, feet<sup>2</sup>.  
 $t$  = time, seconds.  
 $V$  = velocity, feet/second.  
 $W$  = weight, pounds.  
 $X$  = multiplying factor.  
 $\rho$  = air density.

## RECOVERY SYSTEM DEVELOPMENT

### *Re-Entry Into the Atmosphere*

IN ORDER TO accomplish recovery of a re-entry body, it must have the structural strength and heating protection to re-enter the atmosphere. Studies must be made to determine whether the recoverable unit has sufficient stability to keep re-entry loads and heating within tolerable limits. If not, the use of kick rockets, stabilization balloons, retractable stabilizing fins or other means for alignment of proper attitude at time of re-entry must be employed.

In the case of the Jupiter nose cone, the body was sufficiently stable so that no external forces were required to maintain an approximate zero angle of attack on re-entry. Here the nose cone was positioned, prior to second separation, by a tilt program in the missile to the calculated re-entry angle of the particular flight. Such effects as nose cone configuration, velocity, altitude and time

of deployment influenced the parameters the tilt program injected into the nose cone to govern re-entry attitude and to minimize aerodynamic loading and thermal affects.

Stability must also be studied when the recovery of rocket boosters is considered. Aerodynamic loading and thermal effects must be minimized. The problem of excess fuel must be studied carefully and a system chosen that takes into account its effect on booster dynamics and possible necessity to dump it before or after re-entry.

As an example, the Mercury-Redstone booster can adequately withstand the re-entry loads and heating; therefore, its recovery system does not function until after the re-entry phase of the flight. On the other hand the SATURN booster cannot withstand the re-entry conditions and, therefore, uses an attitude control system and an inflatable drag and stabilization device before re-entry to elevate loads and heating.

In order for a missile or space vehicle to perform its assigned mission at maximum efficiency, the missile designers must obtain the minimum structural weight to fuel weight ratio. In taking such an approach, it is of utmost importance to investigate every conceivable means for reducing the weight of the structure. As a result, it is probable that the deceleration loads and re-entry heating imposed on the structure will pose a major requirement in the design and application of recovery techniques.

To control the energy of the vehicle during re-entry, so that it will not prove disastrous to the structure, is one of the important problems. Deceleration during re-entry is due to aerodynamic drag which varies with the ambient air density and the square of the vehicle velocity. The gas dynamic heating rate varies approximately with the air density and the cube of the velocity. Deceleration as well as heating rates depends strongly on the vehicle shape and trajectory. Therefore, both parameters have to be studied carefully before selecting the method of recovery.

### *Deceleration Phase*

When a booster does not lend itself to a favorable attitude, auxiliary forces may be needed to guarantee the desired type of re-entry. This brings in a problem that most recovery design engineers are faced with. Missile designers seldom think of the recovery system at the early stages of the missile development program; not until all other requirements are fulfilled and all components properly placed is the recovery engineer given a small area in which to place his system. Ex-

\* Manuscript received by the PGMIL, February 1, 1960.

† U. S. Army Ballistic Missile Agency, Redstone Arsenal, Ala.



tensive studies must be performed in most cases on the recovery system to insure proper functioning because the primary mission of the booster must not be interfered with by structure modifications designed primarily to aid recovery. This in turn makes the recovery system more complicated because of the unknown attitude the booster may have at the time of deployment. The method of initiating the recovery sequence has to also be able to sense the proper deployment time no matter what the booster attitude may be. The deployment of the initial deceleration and stabilizing parachute must not exceed the bending moments the booster can tolerate.

An investigation is necessary to determine the most favorable method of decelerating the vehicle after it has been through the portion of flight (controlled or uncontrolled depending on the requirements) outside the sensible atmosphere and has made its re-entry. To date, most of the experience in accomplishing this has been through parachutes or retro-rockets. Since reliability is of great importance, the system should not incorporate too many new developments, however it should not suffer from obsolescence. Detail requirements for each subsystem should be thoroughly investigated so that impractical requirements will not be made in one area to simplify the design in another. The design should be such that every individual component in the entire recovery subsystem is as simplified as possible. Built-in reliability should be considered in the selection of every part, component, and subassembly. The use of techniques and/or components which would require extensive developmental work should be avoided.

With the above in mind, the recovery system design requires the use of components which offer high drag at low weight and stowage volume. Having gone through the extreme re-entry conditions, conventional materials may now be used. Parachutes have several characteristics which make them suitable for this deceleration phase. Among these features are the ability to produce very large drag areas with very small stowage weights and volumes, controlled drag areas in prescribed steps as system dictates and fairly low production costs.

Parachutes are designed to fulfill specific performance requirements. The factors normally outlining the performance requirements are: recovery weight, rate of descent, stability, acceleration load limits, package weight and volume. Types of parachute canopies most frequently used today are flat circular, extended skirt, guide surface, ribbon and ringslot, as illustrated in Fig. 1. A brief description of each type follows.

1) Solid flat circular canopy: This canopy is often employed where a high opening shock and high oscillation may be tolerated and where the cost must be held to a minimum.

2) Extended skirt canopy: This canopy has good stability and low opening shock characteristics, and it requires relatively long filling time compared to the flat

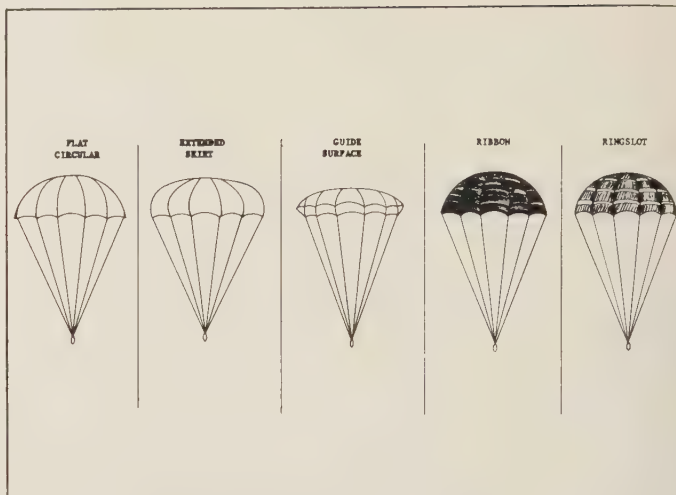


Fig. 1—Schematic illustration of various types of canopies.

circular canopy. It is generally used for final stage recovery.

3) Guide surface canopy: The ribless type guide surface canopy exhibits good opening and stability characteristics and is generally used for high-speed recovery and first stage deceleration applications.

4) Ribbon canopy: This canopy is being used at present for deceleration of aircraft and for bringing down heavy airborne loads. It exhibits good stability and low opening shock characteristics. The stability is controlled by varying the ribbon spacing which automatically controls the geometric porosity.

5) Ring slot canopy: The performance of the ring slot canopy is very similar to the ribbon canopy, and is also used for aircraft deceleration and for load extraction purposes when the velocity and force are within tolerable limits. The cost and bulk of this canopy are considerably less than the ribbon canopy.

These basic types of parachutes are often modified to meet specific requirements or improve their general function. Clusters of two or more parachutes are used if large drag areas are required. When large drag areas are required, stowage, deployment, or manufacturing problems may dictate the use of clusters. Experience has shown that clustering of large size parachutes requires reefing for short periods, even at rather low deployment speeds, in order to insure an even inflation and stress distribution on all canopies.

The Jupiter nose cone recovery system uses ribbon type parachutes exclusively, whereas the ABMA booster systems employ both ribbon and solid flat circular canopies.

Parachutes, in principle, follow aerodynamic laws.<sup>1</sup> Mathematical equations to describe their performance sometimes become complicated due to their complexity and sometimes changing shape, therefore mathemati-

<sup>1</sup> "Re-Entry and Recovery Investigation and Study," Space Recovery Systems, Inc., El Segundo, Calif.; December, 1959.

cal and empirical relations are used to calculate and design parachutes. The rate of descent ( $V$ ) for a parachute is dependent on vehicle weight ( $W$ ), parachute drag area ( $C_D S$ ), and the altitude at which the parachute is descending ( $h$ ). The function for rate of descent is shown in graphical form in Figs. 2 and 3.

$$V = \left( \frac{W}{C_D S \rho / 2} \right)^{1/2}$$

Loads on parachutes consist of two types: dynamic pressure caused by relative velocity and acceleration caused by the relative velocity between the parts of the parachute. These forces may be referred to as air loads and inertial loads, respectively, and are related as follows:

$$F = C_D S \cdot \frac{\rho}{2} \cdot V_S \cdot X_1 \cdot X_2$$

where  $C_D S$  is the parachute drag area and  $V_S$  the initial velocity of parachute prior to start of inflation.  $X_1$  is a factor which takes into account the velocity decay of the parachute during the inflation process. When recovery weight is very large compared to the air loads, the  $X_1$  factor approaches 1.0. Under such conditions almost no velocity decay occurs. This is known as an infinite mass case and occurs frequently where deceleration with reefed parachute is used. When the parachute canopy loading  $W/C_D S$  is low enough to allow a velocity decay during parachute inflation, the  $X_1$  factor becomes less than 1.0 to account for the lower velocity at full parachute inflation. "The USAF Parachute Handbook"<sup>2</sup> presents a method for the determination of the  $X_1$  factor. The  $X_2$  factor takes into account the inertial forces developed in the parachute and the elasticity of the system. This factor also varies with the type parachute. Because of its complex nature it is best expressed as a simple empirical factor. (See Table I.)

The time in which this inertial force rise occurs is very short, and remains constant for a given type of parachute. Since the inertial force rate is a function of the elasticity in the parachute, the force rise time is characteristic of the parachute material elastic constant. The elasticity of the system will also set up oscillations, but these are quickly damped out.

With the assumption of constant gravity, air density and drag coefficient the equation of motion can be integrated, either in a closed form or step by step calculation. The velocity and parachute force can then be established as function of altitude and time. This is necessary to determine parachute disreefing times and to avoid excessive parachute loads.

A vehicle re-entering the atmosphere at high supersonic speeds must be decelerated to a comparatively slow velocity before the final stage recovery system can

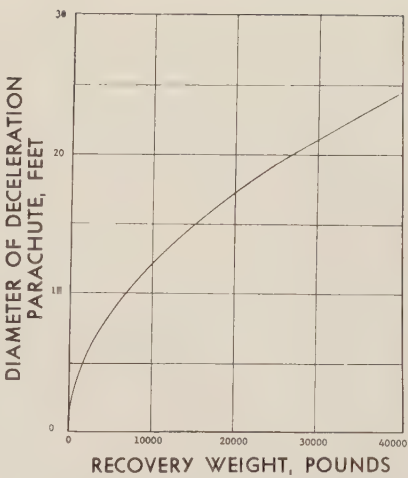


Fig. 2—Diameter of deceleration parachute as function of recovery weight equilibrium velocity 200 kias.

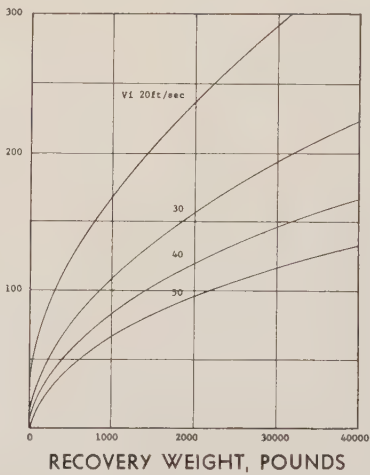


Fig. 3—Diameter of single main parachute as function of recovery weight and impact velocity  $v_i$ .

TABLE I

Type Parachute	$X_2$ (Shock Factor)
Flat circular	2.0
Extended skirt	1.4
Guide surface	1.2
Ribbon	1.05
Ring slot	1.10

be deployed. Deployment of the deceleration parachute is tolerable at high subsonic speeds. Reefing of the parachutes is often necessary in order to prevent excessive deceleration loads to the recovery vehicle. For this reason, most recoveries are accomplished in a series of steps with progressive increases in drag area, thereby lowering the velocity while staying within safe load limits.

The deceleration parachute is usually of a ribbon type since it is capable of high velocity deployment and has a low shock factor. It is often deployed in a reefed condition and disreefed after a suitable time delay. The main recovery parachute is deployed when the deceleration parachute no longer has the ability to reduce the vehicle velocity.

<sup>2</sup> "United States Air Force Parachute Handbook," Wright Air Dev. Center, Wright-Patterson AFB, Ohio, Tech. Rept. No. 55-265; December, 1956.



The main recovery parachute is chosen for its low rate of descent and stability characteristics. The extended skirt-type parachute modified with a conical canopy is often used to meet these needs. Deployment of the main parachute is usually done with a pilot parachute. Once again reefing is employed in order to keep opening loads to a minimum.

#### *Terminal Landing Phase*

The equilibrium velocity determined by the final recovery system may still be high enough to cause severe damage at impact. This velocity or energy, therefore, has to be destroyed by a shock absorbing system. Such a system has either to produce work to slow the vehicle down (retro-rockets) or must be able to absorb work by converting the vehicle's energy into a harmless form.

A vehicle with the weight  $W$  may descend with a velocity  $V_i$ . If  $h$  is the distance above the ground at which shock absorption will be initiated, the vehicle then has the total energy.

$$\begin{aligned} E_t &= E_{pot} + E_{kin} \\ &= h \cdot W + \frac{W}{g} \frac{V_i^2}{2} \end{aligned}$$

$X$  is the number of  $g$ 's deceleration the vehicle can withstand during final impact; the maximum force which can be applied is:

$$F = X \cdot W.$$

Assuming that this decelerating force is constant during the "stroke"  $h$ , the work ( $F \cdot h$ ) is done. If the velocity of the vehicle at the end of the stroke is zero, this work has to equal the energy of the vehicle at the beginning of the stroke:

$$F \cdot h = W \cdot X \cdot h = Wh + \frac{W}{g} \frac{V_i^2}{2}.$$

Solving this equation for the stroke  $h$  gives:

$$h = \frac{V_i^2}{2g(X - 1)}.$$

The shock absorption systems most commonly used today to convert the energy of the vehicle into some other energy form at impact are nose spikes, airbags and crushable materials.

Nose spikes have been used successfully as shock absorbers for test vehicles with high allowable peak decelerations. Disadvantages are high rate of descent necessary to overcome drift angles produced by side winds and prevent penetration of nose spike, and they must be used on soft soil.

Airbags have been used quite successfully in connection with aerial delivery of platforms, drones and missiles. An airbag essentially consists of inflatable fabric coated balloons. These bags are stored in the deflated

condition, deployed and inflated after the final recovery parachute (s) has (have) opened and the vehicle is in the vertical descent. The bags are provided with pressure sensitive diaphragms placed over orifices that rupture and control bag pressure decay upon ground contact. Because of low weight and stowage volume requirements airbags are very frequently used for ground shock absorption.

Crushable materials are often used for shock absorption. Materials used are of low density and weight which have high shock absorption characteristics. The allowable deceleration rates and space available for these materials make the above systems unfavorable for use in large missile boosters.

Retro-rockets may be used in conjunction with last stage parachutes for final deceleration at impact. If retro-rockets are used to decelerate a descending vehicle, thrust  $F$  has to conform with the requirements of maximum allowable deceleration. If thrust is constant, the deceleration will be constant and the required rocket burning time can be calculated  $t = V_i/X \cdot g$ , with  $V_i$  being initial velocity of vehicle. The altitude at which retro-rocket system is ignited is  $h = \frac{1}{2}X \cdot g \cdot t^2$ . Solid propellant rockets are best suited for this final retarding because of their simplicity and reliability. The Saturn booster recovery system employs eight solid propellant rockets to reduce the final impact velocity.

Sensing systems to determine altitude, velocity, dynamic pressure, deceleration or time are needed to accurately and reliably initiate deployment of the recovery system. Sensing instruments must sense proper conditions and provide signals for initiation of the recovery sequence. The accuracy of the sensing device can determine the quality of the recovery system and the reliability of the sensing device will determine the success or failure of the recovery sequence. Various systems are available and some are outlined below:

1) Timer—The timer can be set prior to firing of the missile and initiated on take-off. Based on predetermined flight time, the timer releases a switch or mechanically actuates parachute deployment.

2) Aneroid—The aneroid senses air pressure. It normally is set to a certain altitude and operates at descent. A time block must be provided to prevent operation while in the lower altitudes during ascent. Time lag, temperature compensation, and proper manifolding of the pick-up heads must be resolved to insure operation.

3) Inertia switches—The inertia switch ( $G$  switch) functions whenever there is an acceleration of a given magnitude. There are a number of inertia switches available that may function on a deflection principle, magnetic principles, crystal pressure, etc. The switches are used to sense ground impact or deceleration during re-entry.

4) " $q$ " sensor—The  $q$  sensor is similar to the aneroid except that pitot pressure (dynamic) is used to activate a switch or deflect a diaphragm (with strain element) and thus closes an electric circuit.

5) Proximity fuse—The proximity fuse is generally used to sense the surface distance at relatively low altitudes. The reliability of the fuse is very high but present designs are limited to altitudes below 5000 feet.

Parachute deployment systems fall into two main categories. One is by the use of a pilot parachute, the other is by developing a high pressure gas beneath the parachute pack to cause ejection by direct thrust on the pack while it is in the compartment. Fig. 4 illustrates three sealing methods using gas build-up beneath the pack.<sup>3</sup> Fig. 4(a) shows operation of a "piston bag." Fig. 4(b) employs a blast bag, fastened to the bottom of the compartment, which contains the gases and extends as gas expands. Fig. 4(c) employs a blast bag fastened to the top of the compartment and inverts as gas expands.

Both methods have several subdivisions, including pyrotechnic methods for deploying the pilot parachute.

Parachute disconnects are devices that separate the parachute from the load at predetermined conditions. The two most common uses of disconnects are when switching from one stage to the next during descent, and after impact to avoid dragging of load due to high surface winds.

The water recovery phase will be discussed since all of ABMA's recoveries have been confined to water impact areas.

After the vehicle has landed safely and undamaged in the water, it must be kept floating either by its own buoyancy or by special flotation equipment. Two commonly used methods for flotation are the use of foam materials and flotation bags. The foam materials can either be incorporated into the structure or produced shortly before impact. After full deployment of the main parachute, the flotation bags can be ejected from their containers in order to be fully inflated prior to water impact.

After the vehicle is safely floating, a means of locating the unit must be considered as part of the recovery cycle. Several forms of radio frequency modulation are available. The pulse modulation system is the most desirable as it is capable of giving the highest radiated signal output with the smallest power supply. The Sarah (Search and Rescue and Homing) beacon transmitter was the unit used in the ABMA nose cone recoveries.

<sup>3</sup> "Proposal for a Recovery System for the JUNO V Booster," Cook Res. Labs., Morton Grove, Ill.; December, 1958.

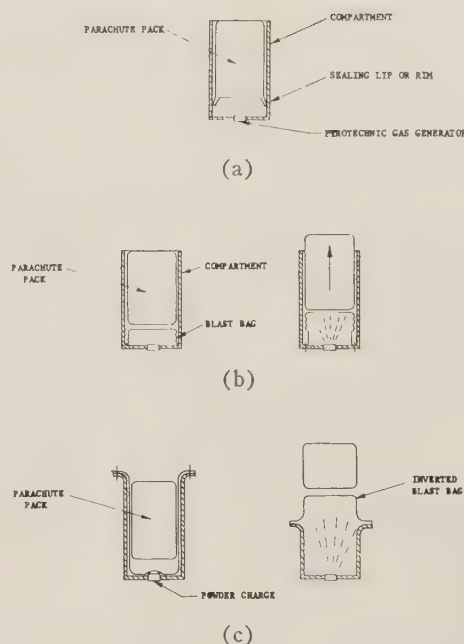


Fig. 4—Parachute deployment systems. (a) Piston bag deployment system. (b) Blast bag deployment system. (c) Blast bag deployment system.

The transmitter, antenna, and power supply were mounted on the flotation balloon assembly. The balloon assembly contained dye markers which were used to aid visually in locating the nose cone from the air. A continuous light was incorporated into the battery package.

Sofar (Sound, Fixing and Ranging) bombs were ejected from the nose cones prior to impact to provide means to locate the impact area by the underwater explosion. An additional Sofar remained with the nose cone which would give an additional explosion signal if the recovery system failed and the nose cone sank. The Sofar bombs are simple devices that are pressure actuated and have a high reliability rating.

As has been pointed out, the development of a recovery system is a complex process. The system is made up of many subsystems which must be selected to meet the individual requirements and integrated into a complete recovery system within the recovery body. All problem areas must be carefully studied and analyzed both singly and jointly with all other problems so that the final selected system represents the best possible compromise.



# Electronic Components for Space Instrumentation\*

JAMES P. McNAUL†

**Summary**—The advent of the space age has placed unique requirements on the design and application of electronic components. Not only has a rigorous environment been imposed on components, but the system demands have often exceeded the state of the art of component development. From all indications these system demands will greatly increase over the next few years.

This paper briefly describes some of the Research and Development programs which have been accomplished at USASRD in meeting the space age system and environmental requirements. Based on future system requirements, some programs now in existence, as well as some which are planned, are discussed, and some general conclusions are presented on the work that must be done if the proper electronic components are to be available when needed.

## INTRODUCTION

AS THE dynamic expansion of scientific technology has occurred over the past decade, electronic know-how in research, development, and production has been hard pressed, in many areas, to keep up with it. Nowhere have the requirements placed on electronics been more severe than in the area of space instrumentation. The demands for size, weight, and power requirement reductions, the need for increased RF power output, and, above all, the requirement for extreme reliability under the exacting environmental demands of space have resulted, in many areas, in a complete reorientation of our Research and Development programs. In other areas, the only change necessary in existing programs was to impose new and stringent reliability and environment conditions. While the imposition of such requirements may not seem very profound, it can have considerable effect on a particular program. For example, to modify a particular electron tube development program designed for field equipment where tubes can be replaced if they burn out after 1000 hours, to one suitable for a communications satellite where 10,000 hours minimum life must be a design goal, requires a complete change in design criteria, production techniques and testing procedures. And yet, a whole satellite program can be delayed or even made impossible because such a tube is not available. As always (and even more urgently in space electronics), the scientists and engineers working in the field of electronic components must anticipate the equipment engineer by several years in order to give him the tools he needs to put his equipment idea into effect. The equipment engineer cannot be content to hope that the steadily advancing state of the art will give the tools he needs *when* he needs them. It is only through vigorous attack on every technical barrier, every reliability weakness, and every size and weight limitation that the art will move ahead at the necessary pace.

\* Manuscript received by the PGMIL, February 1, 1960.

† U. S. Army Signal Res. & Dev. Lab., Fort Monmouth, N. J.

## COMPONENT ACCOMPLISHMENTS

In order to show a logical progression of research and development leading to today's and tomorrow's components, it is best to discuss some accomplishments of programs started prior to and shortly after the arrival of the space age in October, 1957. It should be pointed out that many techniques now widely in use for space instrumentation actually resulted from programs which were initiated for other types of equipments or for general state-of-the-art improvements. These techniques were then taken, improved upon, and adapted to our space needs.

An example of this is the use of ferrite devices and printed circuit techniques for microwave applications. The development of new microwave techniques was a necessity before these frequencies could be used in space applications. For example, Fig. 1 shows a mixer package de-



Fig. 1—A microwave mixer designed and built at USASRD for an internally developed missile-borne ammonia beam maser for very stable frequency control.

signed and built at USASRD for an internally developed missile-borne ammonia beam maser (Microwave Amplification by Stimulated Emission of Radiation) for very stable frequency control. The entire mixing package includes two balanced mixers, three cavity filters, two polarization converters, a ferrite load isolator, a short shot hybrid, a dummy load, a harmonic generator, and a klystron. This entire package, occupying less than 1/20 cubic foot, and weighing approximately three pounds, provides the tie between the accurately controlled maser frequency and the transmitter frequency, with greater than 130 db isolation. Also, the development and design of strip-line type components affords a means of packaging functional microwave parts in light, compact assemblies where power requirements are low. As an example, a microwave receiver front end, including a high-pass filter, a band-pass filter, an impedance matching transformer, and two directional couplers with loads, was designed on a plate 10 inches  $\times$  4 inches.



Another area which has been rapidly pushed to increased capability is that of passive parts. The capacitor, resistor, and inductor represent the elemental building blocks of electronic circuitry and, as such, have received intensive work. Many notable developments in this field have been initiated, advanced and exploited so that their timely use in the latest satellite and missile developments has been possible. In the field of capacitors and resistors, a major reduction in size, increased stability, and greatly increased reliability have been achieved through Signal Corps sponsored research and development effort. Extensive reliability programs have been carried out on these parts with objective failure rates of 0.01 per cent per thousand hours. Such capacitors and resistors have been successfully developed and are now being used extensively in missile and satellite packages. For example, the glass, tantalum, and ceramic capacitors and precision resistors which were widely used in the Explorer series became available through USASRDL efforts. Also, the cloud cover satellite of Project Vanguard makes use of essentially these same parts, as shown in Fig. 2.<sup>1</sup>

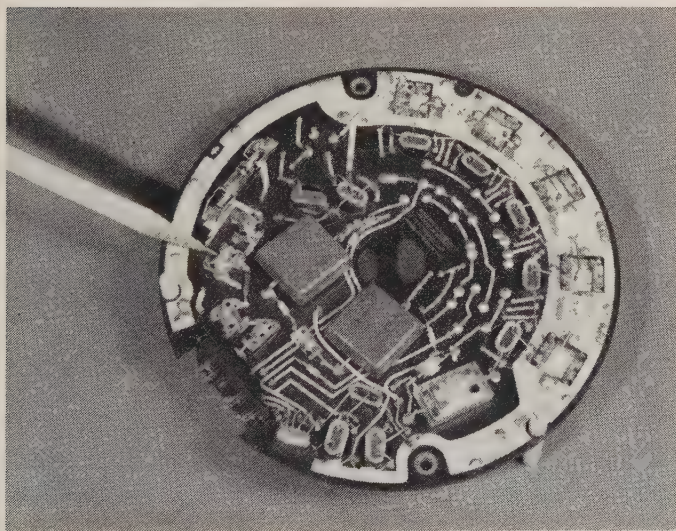


Fig. 2—A receiver deck from the Project Vanguard satellite series using passive parts resulting from Signal Corps Research and Development.

These are just several examples of how the output of existent programs have been adapted and put to good use in the space program. Many others could be cited; for instance, the development and fabrication of high stability quartz crystals for missile and satellite programs, the development of the mesa-type transistor and the Varactor diode under Signal Corps programs, and the first application of solar cells to a U. S. satellite program.<sup>2</sup>

One particularly obstinate problem has been that of developing a crystal unit which would maintain a high de-

gree of frequency stability during launching and flight of a space vehicle. Concentrated effort, however, has resulted in a crystal, designed and fabricated within USASRDL, which was used in the earlier missiles and later in the Explorer satellites. Since there are rigorous demands upon performance of this delicate component, it has been necessary to hand-tailor each with meticulous care by personnel long familiar with the problems involved. This fact, together with the special equipment for final testing, makes USASRDL one of the few areas in the world where this capability exists.

While the detailed accomplishments of various Signal Corps sponsored programs have been extensively reported over the past several years, a general listing of some of the components used in various U. S. space programs is shown in Table I (next page). Although this is only a partial listing and does not show the large number of programs involved, it does illustrate the dependence of our space program to date on many component programs which were not specifically tailored to space needs.

#### CURRENT PROGRAMS

While much has been accomplished, much more remains to be done. Many USASRDL programs now in existence are tailored specifically for various space applications and many more are advancing the state of the art along lines required by space activities. Included in the latter are almost the entire solid-state Research and Development program and a good portion of the electron tube program. The tube program is of particular interest, since many people have been counting the tube out of space applications.

However, aside from the fact that the associated ground complex cannot be separated from the space vehicle in considering a program, tubes are going to continue to play an important part in many space applications. Increasing our communication capability to the millimeter wave region, reducing heater power requirements, increasing tube reliability, and increasing our RF power output capabilities at all frequencies all play an important part in the increased application of electron tubes to space programs. The last point is of particular significance. It is important to increase ground transmitter power for many reasons—both for communication and surveillance purposes—and many programs of both a general nature (such as tube structures, cathode construction, etc.) and specific tube developments for space applications are in process.

However, of increasing importance to surveillance systems where increasing transmitter power is not always possible due to other component and system limitations, as well as space-oriented transmitters, and where it is impossible to pay the price of increased dc power for increased RF power output, are the various low noise amplifier developments which can result in a considerable increase in receiver sensitivity. There are many approaches to the problem of reducing noise, involving both electron beam and solid-state devices. Among these are the solid-

<sup>1</sup> R. A. Hanel, *et al.*, "The satellite Vanguard II: cloud cover experiment," this issue, p. 245.

<sup>2</sup> W. Shorr, D. Linden, and A. F. Daniel, "Power sources designed for space," this issue, p. 313.



TABLE I  
AREAS WHERE SIGNAL CORPS COMPONENT R&D HAS CONTRIBUTED TO ARMY SPACE EFFORTS

Signal Corps Components Contributions	1958 $\alpha$ Explorer I	1958 $\beta$ Vanguard I	1958 $\gamma$ Explorer III	1958 $\epsilon$ Explorer IV	1958 $\zeta$ Score	1959 $\alpha$ Vanguard II	1959 $\iota$ Explorer VII	Pioneer II	Pioneer III	Pioneer IV
Transistors	X	X	X		X	X	X		X	X
Diodes	X		X		X	X	X		X	X
Frequency Control Crystals	X	X	X	X	X	X	X		X	X
Tubes					X	X				
Relays					X	X				
Stable Capacitors	X	X	X	X	X	X	X			
Solar Batteries		X					X			
Chemical Batteries	X		X	X	X	X	X		X	X
Power Converters	X		X		X					
Printed Wiring	X	X	X	X	X	X	X		X	X
Packaging					X	X	X			
Beacons	X		X	X					X	X

state maser, diode parametric amplifier, low noise traveling-wave tube, and the beam-type parametric amplifier. This is an area of considerable research and development activity.<sup>3</sup>

Figs. 3-5 show some of the theoretical and achieved results of various programs in this area. On the left, in each case, is shown the maximum and minimum cosmic noise for a receiver of one-kc bandwidth. In the higher frequency range is plotted atmospheric noise in terms of oxygen and water vapor absorption. Ionospheric effects, as such, are not shown on this chart. In each figure the curves indicate theoretical predictions while the points show actual results achieved. In Fig. 5 on the traveling-wave tube, the X shown just below 1 kmc illustrates the achievement on a particular beam-type parametric amplifier. This area illustrates the complexities of the components picture which faces the system designer today. In each space application the parameters of operation must be weighed against the system requirements and, in most cases, a specific development undertaken to achieve a device with the proper capability.

Of equal importance as the noise reduction in increased communications capability is the reduction in bandwidth in order to conserve power and increase range.<sup>4</sup> The necessary high stability and precision for this application is available in the world of atoms and molecules. Atomic beam frequency standards and molecular beam oscillators (masers) provide exceptional, long-term stabilities, far exceeding those possible with crystal oscillators. Recog-

nized authorities in the field of microwave physics working under Signal Corps contracts, and members of the USASRDL team of scientists have developed these equipments to a point where the atomic beam frequency standard is ready for such ground military applications as satellite tracking and position locating. Each, being a self-contained standard, requires no external source for calibration, thus permitting extremely close netting of frequencies throughout a system.<sup>5</sup>

This particular technical area also shows the interaction between tubes and solid-state devices occurring in many applications. The state of the art in semiconductor devices is constantly and rapidly being pushed forward. As this capability increases, more and more use will be made of these devices. The inherent high efficiency, long life, and small size of the solid-state transistor and diode have actually made the space age possible. As the power and frequency limits are raised, these devices are bound to find even more application. In fact, it can be said that many possible systems are being held back because of the lack of availability of semiconductor and electron beam devices with the proper capabilities.

Another problem area in which much work is being done is that of microminiaturization. Present space attempts have, at best, used the latest subminiature techniques using transistors and printed circuits wherever possible. This simply is not going to be good enough as space systems become more complex—even considering that some applications, such as a satellite devoted completely to communications using microwave components, do not lend themselves to microminiaturization. The requirements for equipments such as sophisticated computers and naviga-

<sup>3</sup> J. P. McNaul, "Low Noise Devices as Systems Elements," presented at the Fifth Conf. on Radio Interference Reduction, Armour Res. Found., Chicago, Ill.; October, 1959.

<sup>4</sup> W. Victor, "A communications requirement for the space age," *Proc. 13th Annual Frequency Control Symp.*, USASRDL, Fort Monmouth, N. J., pp. 248-260; May, 1959.

<sup>5</sup> F. H. Reder and G. M. R. Winkler, "World-wide clock synchronization," this issue, p. 364.

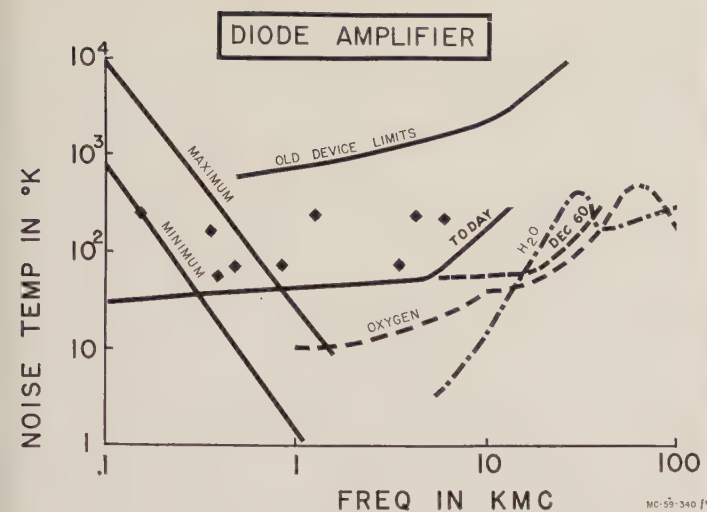


Fig. 3—Present and predicted diode parametric amplifier capabilities shown with cosmic noise on the left and atmospheric noise on the right.

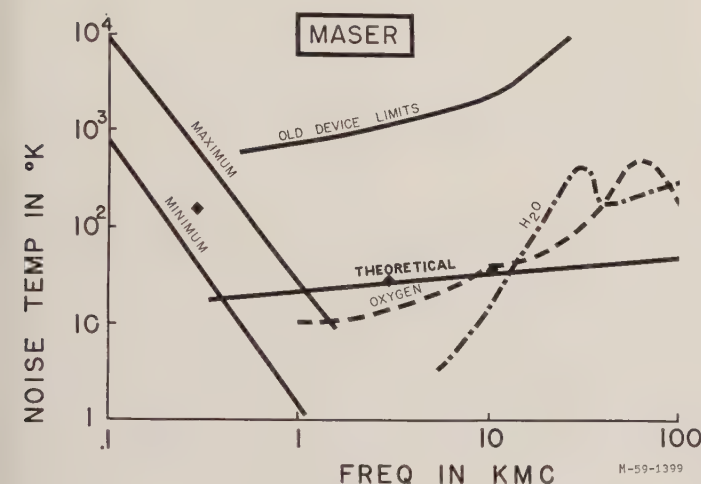


Fig. 4—Solid-state maser capability shown as a theoretical curve and several spotted achievements.

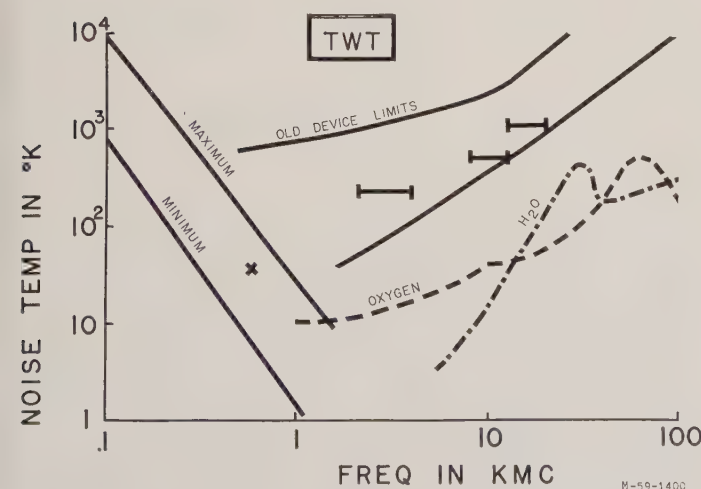


Fig. 5—Traveling-wave tube noise capabilities shown as a predicted curve and three achievements over specific bandwidths. The X on the left indicates a specific development in an electron beam parametric amplifier.

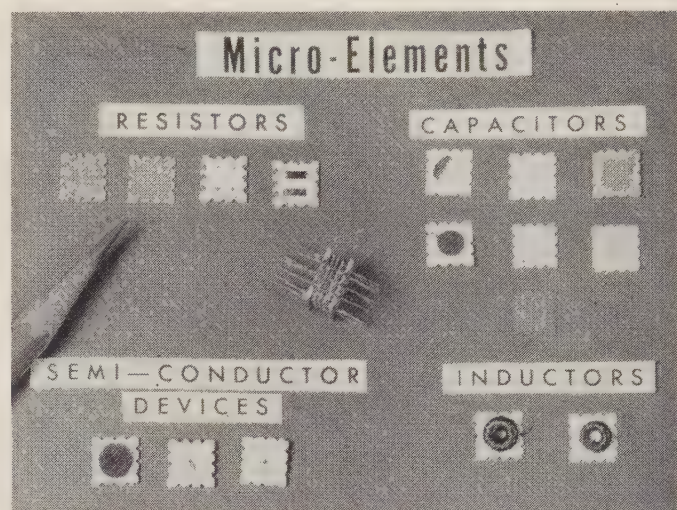


Fig. 6—The basic micro-elements of the Signal Corps micro-module program. In the center is shown a micro-module subassembly having a given circuit function.

tional systems in manned space crafts, complicated switching mechanisms in multi-user communication satellites, and complex encoding, decoding, and command equipments used in any military communication or surveillance satellite dictate at least a 10:1 or preferably a 100:1 reduction in size over the best present techniques.

In order to achieve the goal of a 10:1 reduction in size the Signal Corps has undertaken a program to develop the techniques and basic components for a new concept in packaging—the micro-module concept.<sup>6</sup> As can be seen from Fig. 6, the micro-module concept consists of conventional miniaturized components repackaged around a basic  $3/10 \times 3/10$  inch ceramic wafer. These wafers may then be stacked together and interconnected in the proper sequence by riser wires proceeding up the side of the assembly as shown in the center of Fig. 6. This entire micro-module assembly, having a given circuit function, is encapsulated and then interconnected by the most appropriate technique with other assemblies into an operating equipment. The operating parameters for the concept, a one- to two-watt power dissipation per micro-module, working frequencies up to 100 mc, 75-volt maximum levels, and the applicability to general circuitry (IF, RF, audio, filter, oscillator, and computer logic circuits) will permit its application to many of the most necessary space equipments which are not now possible because of their size, weight, and complexity problems.

The micro-module concept does not stop there. Because of its standardized configuration, it will serve as the logical vehicle for the solid-state circuitry now evolving from Signal Corps Research and Development programs. This will make feasible the extensive space exploration which is bound to come in the 1965–1975 period.

<sup>6</sup> S. F. Danko, W. L. Doxey, and J. P. McNaul, "The micro-module: a logical approach to microminiaturization," *Proc. IRE*, vol. 47, pp. 894–903; May, 1959.



Again, these are just the highlights of existent Signal Corps programs which are tailored to the present and future needs of the space age. The same story could be told for almost every component area from the development of very low drift crystal oscillators for long life communication satellite applications to the investigation of the effects of outer space environments on the electrical and physical properties of representative dielectric materials.

#### FUTURE PROBLEMS AND PROGRAMS

Although the component engineer may feel content that many problem areas are well under control, new requirements are constantly arising which leave no room for complacency. One of the most fundamental and difficult problems is that of the extreme reliability, in a stringent environment, which is required for any space application. Whether a life is involved in a manned space probe or millions of dollars worth of equipment are risked in a satellite attempt, a component failure cannot be allowed to cause ultimate program failure. In many areas, component reliability problems have been solved to the extent necessary. However, in many more areas, hardly a start has been made.

Faced with the fact that for many years (perhaps indefinitely) electron beam devices will be used for many long life space applications because of power, frequency or bandwidth, the Signal Corps is now attempting to determine methods of greatly increasing the operating life of various tube types. Success in this general area by Bell Telephone Laboratories and some European companies have shown that there is no inherent reason why vacuum tubes should not be capable of very long life. However, it is not possible at this time to predict with any degree of confidence whether or not a given tube will have the required lifetime. In fact, most of today's microwave tubes have rather short lifetimes, in the order of 1000 hours, for two reasons.

- 1) In order to keep the cost per tube low, no attention has been paid to expensive production methods required for long life tubes.
- 2) In order to push the tube performance (and, hence, the system performance) to a maximum, the cathode loading and other device parameters are frequently operated in excess of more conservative designs.

By exploiting appropriate methods of tube design and testing, considerable improvement is feasible.

By maintaining careful control of cathode loading and temperature, high vacuum (better than  $10^{-7}$  mm Hg), careful selection of materials, and the establishment of ultraclean tube processing facilities, it should be possible to design tubes that have a minimum life of well beyond 10,000 hours. However, even after tubes have been designed with the proper parameters and processing techniques have been worked out, an extensive testing program will have to be undertaken to develop a degree of confi-

dence in any design predictions. Unless reliable means are found to shorten life testing or to reduce sample quantities, as many as several hundred tubes may have to be placed on life test for extended periods of a year or more to meet some of the stringent requirements for operational satellite systems.

These programs are time-consuming and costly, but they must be started and started soon if we are to realize the full implication of satellite potentials. Besides initiating work as outlined above, USASRDL is pursuing a vigorous program of basic research in cathode materials, tube structures, and processing techniques, all of which will increase its ability to consistently design and fabricate highly reliable tubes.

The tube area is not the only one where reliability problems exist. All electromechanical parts, such as relays or servomechanisms, are immediately suspect when failure occurs. Again, much work is being done in these areas. For example, work is being conducted on the development of solid-state switching devices which will provide direct replacements for relays from the application viewpoint. Such devices will provide less than millisecond switching speeds, imperviousness to mechanical environment, considerable weight and size reduction, and life expectancies in the billions of cycles.

As new information is gained on the outer space environment, it is fed into all component development programs. Until a thorough understanding of the environment is obtained and extensive ground simulation techniques are developed, it is very difficult to have a full measure of confidence in the action of equipment in space. In the meantime, continued component refinement is the only course of action.

#### CONCLUSION

Component development programs met the early requirements of the space age by a logical extension of the current activity. However, as more stringent requirements for more complex and reliable systems are evolved, a more dynamic and specific component development program is required.

The Signal Corps is continually pursuing every problem area to provide equipment designers with the components they need when they need them.

The many programs required to provide the greatly increased state of the art necessary for full utilization of the space potential must be started now to meet requirements five and ten years from now. Clear and continuing definition of system requirements as they are evolved by the system designers is a necessity for progressive component program planning. With this information and the proper program emphasis, there is every reason to hope that these technological barriers will be broken down in time for useful application.

# Power Sources Designed For Space\*

W. SHORR†, D. LINDEN†, AND A. F. DANIEL†

**Summary**—New, improved and more reliable power sources will have to be developed if anticipated, space-oriented, requirements for higher power and longer life are to be satisfied. Conversion systems employing chemical, solar and nuclear energies are described and their prospects for further improvement discussed.

## INTRODUCTION

THE projected auxiliary electrical power requirements of electrical and electronic equipment in artificial satellites are expected to exceed the kilowatt level, with a required lifetime of at least one year, within the next 2 to 3 years. The most ambitious power source built thus far for a space vehicle was rated at only 25 watts. This was the solar converter array designed for Explorer VI, the "paddle-wheel" satellite. New and better energy conversion devices will be required if power sources are to be available that are compatible with system requirements. Chemical, nuclear and solar energy are the three prime sources of energy which will fulfill these new power re-

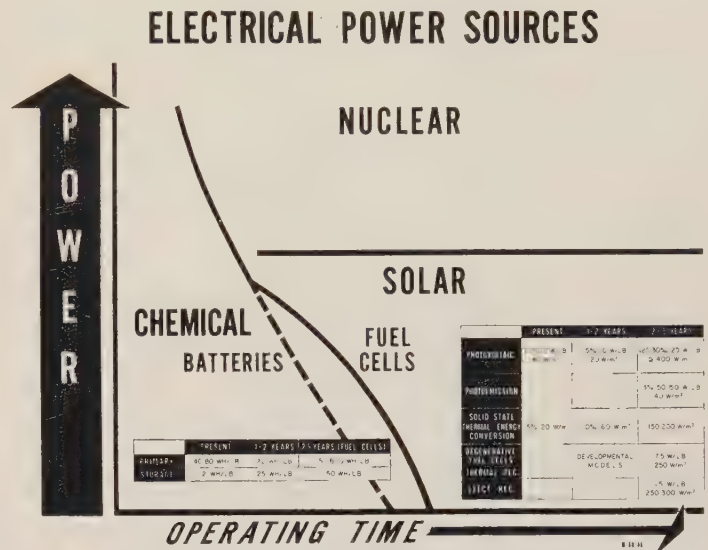


Fig. 1—Areas of usefulness for chemical, solar and nuclear energy sources.

	Chemical	Nuclear	Solar
Chief advantages	<ol style="list-style-type: none"> <li>1) High power/weight ratio.</li> <li>2) Proven and reliable.</li> <li>3) Controllable discharge rate and time.</li> <li>4) Good for storage of energy.</li> <li>5) Best for short-term applications.</li> <li>6) Low cost.</li> </ol>	<ol style="list-style-type: none"> <li>1) Highest energy density.</li> <li>2) Operation independent of temperature and many other environmental influences.</li> </ol>	<ol style="list-style-type: none"> <li>1) Free, inexhaustible source of energy.</li> <li>2) Long life, limited only by converting device.</li> <li>3) High energy-weight ratio.</li> </ol>
Disadvantages	<ol style="list-style-type: none"> <li>1) High weight-energy ratio.</li> <li>2) Temperature dependent.</li> <li>3) Limited shelf life.</li> </ol>	<ol style="list-style-type: none"> <li>1) Radiation can require heavy shielding.</li> <li>2) Problem of heat dissipation.</li> <li>3) High cost.</li> </ol>	<ol style="list-style-type: none"> <li>1) Operation only when collector is light-oriented.</li> <li>2) Requires energy storage systems for "round-the-clock" operation.</li> <li>3) May require auxiliary power device for handling peak loads.</li> <li>4) Requires large area for energy collection—low power density.</li> </ol>
Method of conversion of electrical energy	<ol style="list-style-type: none"> <li>1) Electrochemical <ol style="list-style-type: none"> <li>a) Batteries</li> <li>b) Fuel cells</li> </ol> </li> <li>2) Via thermal energy</li> </ol>	<ol style="list-style-type: none"> <li>1) Direct conversion</li> <li>2) Nucleo-galvanic</li> <li>3) Via thermal energy <ol style="list-style-type: none"> <li>a) Solid-state devices (thermo-electric, thermionic)</li> <li>b) Chemical</li> <li>c) Mechanical</li> </ol> </li> </ol>	<ol style="list-style-type: none"> <li>1) Via light energy <ol style="list-style-type: none"> <li>a) Photoelectric (solid state)</li> <li>b) Photogalvanic</li> </ol> </li> <li>2) Via thermal energy</li> </ol>

Fig. 2—Comparison of energy sources

quirements. Each of these sources has attractive characteristics and each will be used to advantage.

The areas of usefulness and the characteristics of chemical, solar and nuclear energy conversion devices are respectively compared in Figs. 1 and 2.

## CHEMICAL CONVERSION

The primary-type chemical battery, because of its excellent reliable performance and the highest known power-to-weight ratio for short-term service, has been the system most used in satellites. Its continued use, however, will be limited to applications requiring high watt per pound for relatively short operating lifetimes.

The chemical storage battery at present represents the most compact energy storage device known. In this role,

\* Manuscript received by the IRE, February 1, 1960.

† U. S. Army Signal Res. and Dev. Lab., Fort Monmouth, N. J.



it will continue to be an essential adjunct to solar and thermal energy conversion systems to furnish power on dark side of the orbit and during peak power requirements. The hermetically sealed nickel-cadmium battery, because of its high cycle life, is the best of this type; it has accomplished over 11,000 shallow (20 per cent of rated capacity) charge and discharge cycles and has a rated energy/weight ratio of 10–12 watt-hours per pound. Investigations in the zinc-silver oxide and cadmium-silver oxide systems to increase the energy/weight ratio and to improve reliability and cycle life should result in the development of storage batteries with at least two- to four-fold improvement.

Another means of converting chemical energy into electricity is the fuel cell. This is a device which is similar to the galvanic cell except that fuels are fed into the cell on demand and are not an integral part of the structure. Fuel cells may be classified into two main groups: continuously fed galvanic systems and regenerative galvanic systems.

In continuously fed galvanic systems, the lifetime of the system is limited to the amount of fuel stored in the accompanying container. Conversion efficiency may be as high as 90 per cent and the theoretical watt-hours per pound, of the hydrogen and oxygen active materials is over 1600. Practical cells with 150 to 800 watt-hours per pound should be available within 2 to 5 years.

If continuous, or intermittent, power is required for extended periods of time, continuously-fed fuel cell systems will have to be replaced with regenerative galvanic systems which receive their regeneration energy from solar or nuclear energy. In such systems, the fuel and oxidant necessary to operate the galvanic system are regenerated from the cell reaction product by the energy introduced from outside the system. The over-all efficiencies attainable are determined by the regenerative process used and are lower than those of the continuously-fed galvanic systems. The regenerative process may be carried out by electrolytic, thermal, photochemical and radiochemical methods.

None of the regenerative fuel cell systems have progressed to the point where practical structures have been fabricated. Not only have the basic problems proven difficult, but the auxiliary hardware associated with closed cycle regenerative systems becomes quite complex, and operation in zero gravity further complicates practical solutions. Despite these difficulties, its high power-to-weight ratio at extended life operation makes the regenerative fuel cell one of the promising power sources for space application.

#### SOLAR CONVERSION

One of the most useful energy conversion devices for providing power in space is the photovoltaic converter, or solar cell. It has been used successfully in Vanguard I, Explorer VI, Explorer VII and in Sputnik III and will be the power source for other planned satellites. The power source in Vanguard I, designed and fabricated by

USASRDL personnel, represents the first demonstration of a solar battery as a practical source of power for space application. (See Fig. 3.) March 17, 1960, will record the second year of continuous power generation by this device. The present solar cell is a silicon *p-n* junction device which converts solar radiation directly into electrical energy. Commercially available cells can accomplish this with an efficiency of about 10 per cent; instances of efficiencies as high as 14 per cent have been reported. Thus, assuming 10 per cent conversion in outer space, the 1400 watts/m<sup>2</sup> of available solar radiation is convertible to 14 milliwatts of electrical energy for each square centimeter of active cell surface. However, full output power is not realized because of a number of degrading factors: 1) temperature, 2) erosion from micrometeorites, 3) type and duty cycle of orbit, 4) oriented or nonoriented satellite, and 5) structural. Correcting for these factors, the cell output power is reduced to 8 mw/cm<sup>2</sup>. In the rated 5-watt solar converter array designed for Explorer VII, the power-to-weight ratio did not exceed 1/4 watt per pound. (See Fig. 4.) Had orientation been possible in this satellite, the ratio of 1.5 watts per pound would have been realized, since it would not have been necessary to repeat the power source six times in order to assure exposure of sufficient cells to the solar beam adequate to generate the required output power.

Developments current in silicon solar cells indicate that conversion efficiencies exceeding 12 per cent should be available in production cells in about a year and at considerably reduced cost. The anticipated need for kilowatt level power sources will necessitate the use of large, lightweight expansible and oriented cell arrays, using spectrally selective coatings, new materials and techniques, and whose over-all efficiency would range from 15 to as high as 20 per cent.

The photoemissive diode is another solar conversion device having practical implications for space power applications. Recent design studies have indicated that conversion efficiencies of about one per cent and a very desirable power/weight ratio of 50 watts per pound should be realized early. An efficiency of 3 per cent and a ratio of 100 watts per pound appears to be quite feasible with further development.

#### THERMAL CONVERSION

It is very probable that the production of high levels of power for use in space will rely chiefly on thermal conversion systems. The heat sources will be radioisotopes and solar concentrators for the lower range of power and nuclear reactors for the higher range. The conversion devices will be thermoelectric and thermionic generators, various type of dynamic, vapor cycle heat engines and regenerative fuel cells. The magnetohydrodynamic generator may become an important system for high power generation; its development, however, is still in its infancy.

Two increasingly important thermal energy conversion

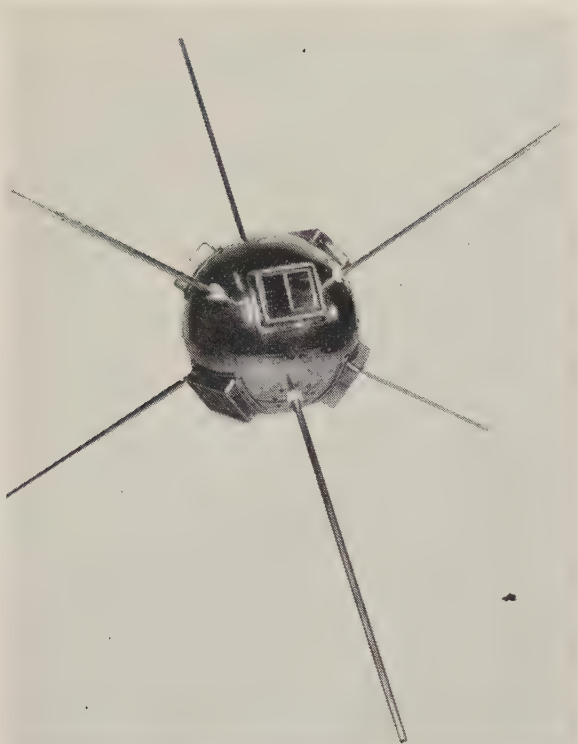


Fig. 3—Model of Vanguard satellite with solar clusters.

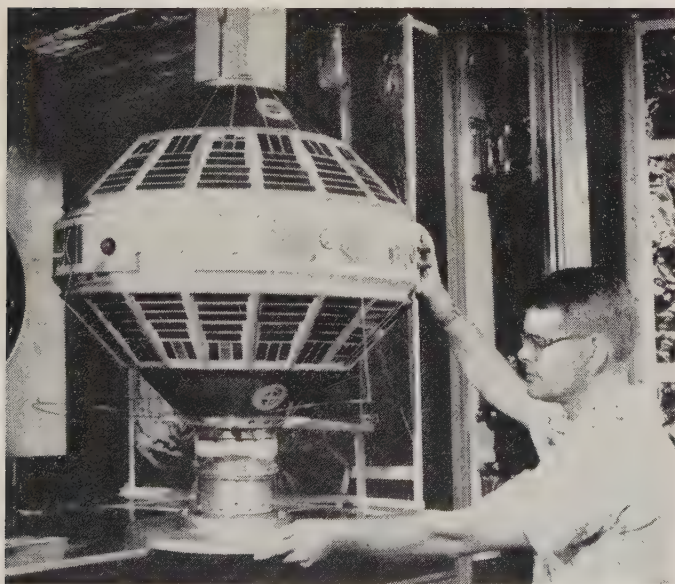


Fig. 4—Solar cell power supply employed on Explorer VII satellite.

devices are the thermoelectric and thermionic converters. No moving parts are involved in their conversion processes and consequently their lifetime should be inherently long with a high degree of reliability.

Thermoelectric generators have been developed with power outputs from 10 to 100 watts, with conventional fuels being used as the heat source, the over-all power-to-weight ratio being 5 watts per pound. Radioisotope powered generators have been built of which SNAP III is the

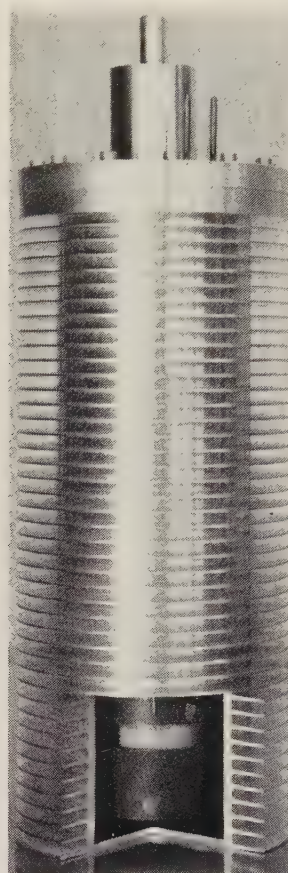


Fig. 5—Gas-fired model of thermionic converter being developed by the Thermo Electron Engineering Corporation.

best known. (See Fig. 5.) This generator, with a rated output of 5 electrical watts, was powered by a Polonium-210 heat source. It weighed 5 pounds and showed an over-all efficiency of over 5 per cent. The estimated watt-hours per pound for the first half-life of the isotope was given as 1600. Radiation hazards associated with the use of radioisotope heat sources pose a problem which will require special handling procedures.

Rapid developments in semiconductor and intermetallic compounds and in generator design and technology are expected to result in a two-fold improvement in the watts per pound ratio to about 10 watts per pound and in over-all efficiency to about 7–12 per cent.

The thermionic converter is basically a diode which converts thermal energy to electricity through the principle of the Edison Effect. Technologically, the thermionic converter is not as advanced as the thermoelectric generator; however its Carnot efficiency should be considerably higher than the thermoelectric generator because of its higher temperature of operation. Whereas the thermoelectric generator, because of present-day material shortcomings, is limited to an input temperature of 700°C, the thermionic converter operates at temperatures exceeding 1000°C, rejecting heat at about 600°C.

Space-charge effects and the need for long-life, high-temperature emitters are two major problems in the de-



velopment of thermionic converters capable of generating high output power at high efficiency. The vacuum diode with close-spaced electrodes and the plasma diode are two approaches by which space-charge effects may be minimized. High-temperature cathodes with long life expectancy are still to be developed.

Close-spaced diodes can now be made with output power of 5–10 watts at an efficiency of 6–10 per cent. A design analysis has been made of an isotope powered thermionic converter which, for a power output of 100 watts, predicts an efficiency of 10–15 per cent and a weight of approximately 20 pounds. A solar powered converter with a rated power of 1200 watts would have a probable efficiency of 9.6 per cent and weight approximately 44 pounds, exclusive of the weight of the collector, orientation and storage systems. A model of a close-spaced, gas fueled thermionic generator is shown in Fig. 6.

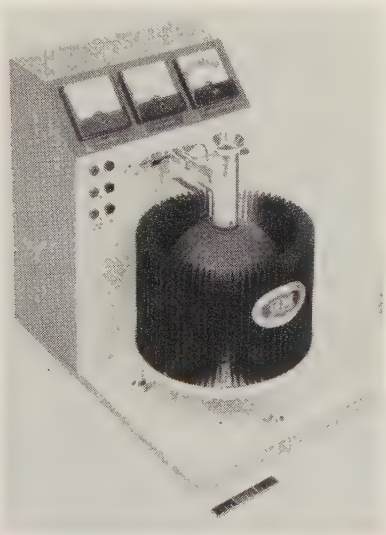


Fig. 6—Five-watt, gas-fired thermoelectric generator developed by 3 M company.

Since the thermionic converter rejects heat at a temperature usable by the thermoelectric generator, it should be possible to match the two devices so that a greater portion of the input heat may be converted to electrical energy with an increase in total system efficiency. With suitable design, the converter efficiency may be boosted to as high as 17 per cent.

#### ELECTRICAL TO ELECTRICAL CONVERSION

The electrical and electronic equipment aboard the space vehicle will require specific voltages and currents, ac or dc with varying degrees of regulation and control, to perform their necessary functions. Since these outputs may not be readily available directly from the power source, they must be provided by other means.

The transistorized power converter, because of its high efficiency, low weight, small volume, and inherent reliability, has been able to fulfill the needs until now. Its limitations with respect to operating temperature, magnitude

of voltage and current, power dissipation and radiation resistance, will have to be studied in the attempt to improve the dynamic characteristics of the transistorized converter if it is to meet the stringent future requirements. Transistorized power converters have been designed by USASRD personnel to meet the highly-specialized power, weight and volume requirements for the cosmic ray experiments in the Explorer satellites, for Project Score and for other satellites not yet launched.

Considerable improvement is envisaged by the application of silicon controlled rectifiers, or silicon power transistors, which will increase the upper operating temperature limit. The silicone controlled rectifier will also enable the converter to operate at higher switching frequencies with higher power ratings, thus permitting greater miniaturization and weight reduction. Investigation of nondissipative regulating systems will result in reduction of heat generation of the converter with consequent improvement in efficiency.

#### CONCLUSION

Much work remains to be done before devices employing chemical, solar or nuclear energy can be designed to meet space applications demanding kilowatts of power. It may be predicted, however, that chemical energy systems will be used in short-term applications, for peak load requirements and for energy storage. Solar energy systems will fulfill requirements for power in the low range and for long operational life; and, finally, the needs for high-level power will be met by nuclear energy systems.

#### REFERENCES

- [1] H. K. Ziegler, "Scientific Uses of Earth Satellites," J. Van Allen, Ed., University of Michigan Press, Ann Arbor, pp. 55–57; 1956.
- [2] H. K. Ziegler, "Solar power sources for satellite applications," in "Annals of the IGY," Pergamon Press, New York, N. Y., vol. 6, pts. 1–5, 3.3.3., pp. 300–304; 1958.
- [3] H. A. Zahl, H. K. Ziegler, and A. F. Daniel, "Energy in space: pounds vs. power," *Chem. Engrg. News*, vol. 37, pp. 96–99, 133; May 18, 1959.
- [4] H. A. Zahl and H. K. Ziegler, "Power sources for satellites and space vehicles," in "Annals of the IGY," Pergamon Press, New York, N. Y., vol. 9, p. 292; 1960.
- [5] A. D. Steele, "A thermoelectric generator," *Proc. Thirteenth Annual Power Sources Conf.*, Atlantic City, N. J., April 28–30, 1959, Power Sources Div., USASRD, Fort Monmouth, N. J., pp. 36–39; 1959.
- [6] V. C. Wilson, "Thermionic emission," *ibid.*, pp. 41–45.
- [7] G. N. Hatsopolous, "Comparison of thermoelectric and thermionic conversion," *ibid.*, pp. 46–49.
- [8] M. Telkes, "Collection and concentration of solar energy for thermal applications," *ibid.*, pp. 69–72.
- [9] H. Hunger, "Fuel cells—introductions, concepts and survey," *ibid.*, pp. 105–108.
- [10] E. Yeager, "Review of the art and future trends in fuel cell systems," *Proc. Seminar on Advanced Energy Sources and Conversion Techniques*, Pasadena, Calif., November 3–7, 1958, ASTIA Doc. No. AD209301, pp. 69–81; 1959.
- [11] P. Rappaport, "The photovoltaic effect and its utilization," *ibid.*, pp. 127–137.
- [12] P. Duwez, "The collection and concentration of solar energy for thermal applications," *ibid.*, pp. 123–126.
- [13] D. Linden and A. F. Daniel, "New power sources for space electronics," *Electronics*, pp. 43–47; March 20, 1959.
- [14] A. F. Daniel, "Solar batteries," *Proc. IRE*, vol. 48, pp. 636–641; April, 1960.

# Launching Procedures for Space Vehicles\*

DANIEL D. COLLINS†

**Summary**—Operations conducted at a launching site on any space vehicle program are a result of all contributions to the launching operation team from the many sources of origin concerned with the vehicle. Recognizably, therefore, these contributions vary from contractor to contractor.

The following paper is based on the general launching techniques developed and followed by one of the contractors at the Atlantic Missile Range.

Launching procedures are the recommended methods and operations necessary in testing, checking and preparing a space vehicle for flight. They are the culmination of all previous experiences, studies and tests formed into a written chronological schedule to check and test each critical flight component and operation in proper sequence. The procedures are accomplished by a group of engineers, technicians and various other specialists organized into a well-coordinated team.

THE labors of a space vehicle launching team are both complex and routine, with the primary goal the attainment of the particular mission assigned to the vehicle. To achieve a successful launching and flight that satisfies the exacting criteria for a successful space mission, the launching team must predetermine which components and which integral systems of the vehicle require the most assiduous testing and those which require only a perfunctory check. Armed with this foreknowledge, the team then prepares a work schedule which distributes the work load so that personnel may perform their testing and checking without hampering the over-all launching preparations.

After a space vehicle is received at the launching site, it is inspected for damage which may have been incurred during transportation to the site and examined to verify the existence of, or provisions for, mounting all the components alleged to be on board. Following this inspection, the vehicle is assembled and weighed. Components not on board at the time of weighing are or have been weighed separately. The center of gravity (CG) of the dry vehicle is then determined and compared with the values calculated at the manufacturing site. Upon termination of weighing and CG determination activities, the vehicle is placed on a custom-built trailer for transportation to the launching pad.

The vehicle, on arrival at its assigned launching pad, is lifted from the trailer by the servicing structure's hoisting mechanism and placed carefully and accurately on the launching table. The launching table is then adjusted to align the vehicle vertically with reference to the local plumb line and then rotated to the precalculated launching azimuth. Upon completion of these alignment checks, the

vehicle is again weighed to compare the launching table scale readings with the weight readings taken in the assembly area. This is done to insure that the dry weight of the vehicle does not exceed that weight assumed in calculating the preflight trajectory.

The vehicle is connected to ground power and the receiving and transmitting antennas are tuned before the vehicle is surrounded by the servicing structure. Upon completion of these tuning adjustments, the servicing structure is rolled up to the vehicle and working platforms are adjusted to the level of the instrumentation compartment, the guidance compartment, and the upper stages with payload. During this time, the vehicle is connected to pneumatic lines and blockhouse measuring cables. After the working platforms are in place, the complete measuring cable setup is installed connecting the vehicle with the measuring trailer which has been moved into position alongside the servicing structure. These cables join in a predetermined order the recorders in the measuring trailer and the adapter boxes, which are plugged into the output of the various measuring devices installed on board. The output of these measuring devices will be transmitted over the telemetering system during the flight or during some portion of the flight. To eliminate excessive RF radiation, which would severely handicap normal activities around the launching site during preflight checkouts, the output of some measuring devices is carried by hard wire to blockhouse recorders.

The vehicle and its payload are now put through intensive measurement calibrations, leakage tests, powerplant checks, and pressurization tests. The measurement calibrations are compared with the calibration curves prepared at the manufacturing site and, if necessary, new calibration curves are drawn to reflect the data obtained from the calibration made at the launching site. All pneumatic tubing and joints are checked for leaks, and adjustments are made as dictated by the type of leak detected. The power plant is inspected visually for rust, foreign material, proper valve operation, etc., to insure that no damage was incurred while preparing and shipping the vehicle from the manufacturing site to the launching site. Upon completion of the leakage tests and any subsequent adjustments, the vehicle's whole pneumatic system with pressure bottles and fuel and oxidizer tanks is pressurized to pre-launch values. A simulation of launching is then conducted to operate the valves in the proper functional sequence.

Many closed loop RF checks are run with the calibration of all measurements and the functional operation of the entire vehicle pneumatic system, thereby determining if interference exists between any of the RF systems, the electrical networks, and the mechanical systems.

\* Manuscript received by the IRE, February 1, 1960.

† U.S. Army Ballistic Missile Agency, Missile Firing Lab., Cape Canaveral, Fla.



Satisfactory completion of the aforementioned closed loop RF checks is necessary before open loop RF tests are run. During the open loop RF tests, any interference between on-board systems and ground RF instrumentation systems may be detected and corrected before entering the final phases of vehicle preflight checkout.

A highly important procedure, and the prelude to the final preflight systems tests, is the destruct-command receiver (DCR) test. This test is conducted with radiation from the launching site destruct-command transmitter to insure proper functional control and compatibility with the DCR and its related vehicle components. Satisfactory completion of this test is mandatory before the launching team will receive permission from the launching site control agency to begin the launch countdown. Subsequent to the DCR test, other RF radiation tests are run with the DCR system active, but not connected to the destruct block, to satisfy the launching team and the launch site control agency that no interference exists between other RF systems and the DCR system.

To alleviate any preflight concern about the guidance and control systems employed to position the vehicle and payload at a point in space with the required velocity to achieve either orbital or space flight, a test is run with only the components associated with either the guidance or control systems active in the vehicle. In this test, the vehicle is connected to ground power and the telemetry system is used to transmit component operation from the vehicle to the ground telemetry receiving station. As in all open loop RF radiation, frequency clearance must be obtained from the launch site control agency before this test is run.

Next, to assure the vehicle is properly connected to internal power supply and that all inverters will stabilize after transfer to internal power, a test is run, simulating launch conditions with telemetry RF radiation. To accomplish this, the vehicle's on-board networks are activated by ground power and then switched to internal power. If this is completed satisfactorily, the vehicle is disconnected from all plugs connected to ground equipment. When this occurs, all systems which are a part of the on-board networks react as they would if a launching had occurred, and any variation from normal operation can be detected.

During the time when various vehicle systems are being checked, the ground electronic and optical tracking and the recording systems are closely inspected and operational reliability insured in preparation for the preflight and flight tests. These ground systems tests are conducted separately from the vehicles tests and since some RF radiation is necessary to insure operational reliability, close coordination is mandatory to prevent damage to vehicle components and possible hazards to human life. Electronic tracking systems such as the SCR 584 Mod II radar operating in the *S* band of frequencies, the AN/FPS-16 radar operating in the *C* band of frequencies, the UDOP (UHF Dovap) and DOVAP (VHF) CW tracking systems using the radio Doppler technique for determination

of vehicle velocity and position, the beat-beat systems—a real-time flight safety display utilizing radiation emanating from the on-board DOVAP transponder and the telemetering transmitter, and the microlock payload tracking and telemetering system are used with the flight of the space vehicle. Maintenance of these systems is a daily routine, but when support of a flight test is requested, each system goes through a carefully prepared check-out procedure to insure high quality data acquisition and the best attainable reliability during the vehicle's flight.

The type of optical tracking systems used depends on the time of day the launch is to occur and on what on-board components are carried to supply the tracking source for these systems. Systems used with the launch of space vehicles have been the CZR-1 Fixed Ribbon-Frame Camera for early launch phase high accuracy acceleration measurements, the Askania Kth 53 Cine-Theodolite for powered flight phase position and velocity determination, and the Wild BC-4 Ballistic Camera for nighttime very high accuracy position determination utilizing some light source emanating from the vehicle. In addition to these metric camera systems, various other documentary or engineering sequential-type fixed or tracking cameras are used for day or night close-in coverage. The ROTI or IGOR-type long focal length tracking cameras are used for long-range daytime documentary or event coverage. Each of these optical systems requires regular maintenance servicing to insure reliable operation, and most require some type of calibration or check-out during the launch countdown. However, except for checkout of the on-board flash tube or the continuity circuit checks on the photoflash cartridge panel, none of the optical tracking systems conduct any systems checks in coordination with the check-out of the vehicle.

During the time period in which all the foregoing calibration, checks, and test activities are conducted, other personnel within the launching team are at work insuring that adequate supplies of fuel, oxidizer, pressurizing gases, replacement parts, etc. are available. Thus, no delays in the launching procedure will be incurred should any of these items be required. Other personnel are requesting the launching site and downrange controlling agency to provide such special instrumentation as is necessary to record telemetry, photograph upper stage burning, or provide real-time position and velocity from systems such as Microlock. Still others are checking calibration records, reading preflight telemetry oscillographs, redrawing calibration curves as required, and requesting special data reduction of the space vehicle telemetry records, camera films and plates, and electronic tracking systems deemed necessary in advance of the actual launch. Another element of the launching team is photographing each preparatory step of the launch procedure for documentation of all critical phases of the procedure.

There are three final steps in the vehicle checkout before launch can be requested by the director of the launching team.

The first, the cluster interference test, has a two-fold purpose:

- 1) to insure that no interference exists with the payload microlock signal either from the payload itself and the RF systems on the carrier vehicle, or from the ground RF systems,
- 2) to provide a final check on the balance of the rotating mass comprising the upper stages and payload and the influence of rotation on the equipment and the antenna pattern.

This test may be run as two tests if the circumstances warrant. During the interference test, all RF systems to be used during the flight of the vehicle are operated simultaneously and any interference on any RF system is noted for correction before the next test. Any unbalance noted by recording vibrations induced from rotation is also corrected.

The second step, the simulated flight test, is run as close as possible to the launch day to attempt to eliminate any changes to on-board components between this test and the launch countdown. As the test name indicates, operations are conducted as if it were an actual launch countdown. All RF systems are again active and the vehicle is transferred from ground power to internal power as in launch operations. A simulated launch is performed and all internal systems are operated in the sequence they would be expected to occur if in actual flight. Upon completion of this test, the telemetry records are carefully reviewed to check for deviations from normal operation. These deviations, whether explainable or not, are corrected even to the extent of rerunning the test if necessary. The telemetry data are then compared to the calibration data. If any discrepancy exists, the measurement may be recalibrated. All other RF systems must indicate satisfactory operation of beacons or transponders in connection with the ground equipment before the space vehicle may be said to be ready for the launch countdown.

The final step in preparations leading to the launch of the space vehicle is the launch countdown. However, before the launch countdown begins, a wide variety of preparatory work must be accomplished. This consists largely of notifying support personnel when to deliver pyrotechnic devices to the pad, checking operation of fire fighting equipment in the pad and blockhouse area, checking relief valve settings, installing the destruct prima-cord and one-shot relays, and safety wiring all measuring adaptors, special valves and pressure switches. When the launch countdown is started, the space vehicle is as well prepared for its assigned mission as the decades of rocket launching experience acquired by the veterans of this launching team can assure.

The basic concept of the countdown is to provide an orderly sequence of checks on vehicle components and range instrumentation readiness. Any time lost due to deviations from the countdown must either be made up or a "hold" in the count called until the deviation is corrected. It is always the goal of personnel participating in the

countdown to have their function or their equipment ready when required by the countdown schedule.

Actual activities during the launch countdown are very similar to that conducted during the simulated flight test. However, this time the vehicle is loaded with fuel and oxidizer, the igniter for the rocket engine is installed, the destruct prima-cord is connected electrically, the explosive bolts for separation are set in place, and the igniter squibs on the upper stages are installed. These and other similar exceptions differentiate a simulated flight test from a launch countdown.

Upon completion of the vehicle prelaunch checks and preparations and completion of tracking systems checks, the launch site flight safety officer gives the "clear to launch" command. From this time on to the "firing command" order, all operations must be performed with exactitude and no deviations can be tolerated without calling a "hold" in the count.

Giving the order, "firing command," activates the waiting components in the vehicle. This is the penultimate of all the work and preparation that has preceded this event. All vehicle internal operations are dependent on the proper sequence of a variety of events with the main events being the pressurizing of the fuel tank, the oxidizer tank, the oxidizer start tank, and the fuel start tank. Within seconds of fuel start tank pressurization, the space vehicle's booster engine ignites and moments later the vehicle lifts from the launching table. This is the culmination of the launching team's main effort.

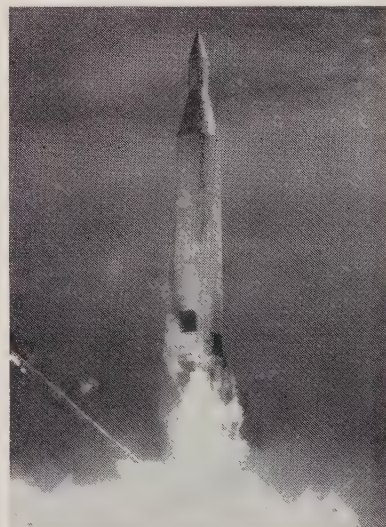


Fig. 1.

However, before the team will relax they must know how well the vehicle performed and whether or not all components met expectations. And finally, they must know whether or not the space vehicle was successful in placing the payload in orbit or in free space flight.

With assurances from the RF tracking system and the Microlock tracking system that all went well, then, and only then, will the launching team relax and look forward to another space vehicle launching.



## From an Early Sputnik Diary\*

HAROLD A. ZAHL†

**Summary**—Like almost everyone else in the world, personnel of the U. S. Army Signal Research and Development Laboratory (USASRD), Fort Monmouth, N. J. were caught by surprise when the U.S.S.R. successfully launched earth satellites in October and November, 1957. The narrative which follows portrays some of the happenings in our environment when the BEEP-BEEPS descended upon us. I should mention, however, that any humor the reader may see in the latter-day remarks which constitute this diary was certainly nonexistent during the long, dreary 40 days and 40 nights when, in the wilderness of outer space, we were "wrestling" with these electronic invaders. It is only in retrospect that we can now smile.

**D**URING the period from 1955 to late 1957, in our office coffee breaks, we also poured out many discussions on Astro-Electronics, combined with amateur speculation on international subjects, all on the highest serendipic plane of course, reaching a variety of new highs or lows, from the stars down to mere mortals, depending on whether you wanted to make the deuces wild, or as it turned out, the one-eyed jacks, too!

Because of our Laboratory participation in the IGY Earth Satellite Program, we were in a good position to watch the warm-up as the U. S. prepared to make what we thought would be the first significant pitch to space in the artificial earth satellite game. We had two years lead through the IGY or rather, we thought we had—time enough for the country to be dignified and really peaceful about its preparations.

Many of our debates centered eruditely about these questions; suppose the Soviets could beat us to space. Would they dare do it, realizing such an action might trigger the U. S. off to an order of magnitude greater defense effort, or wouldn't it be smarter for them to perfect their big missiles secretly and let us coast along complacently, thinking we were far ahead in space stuff and other things implied?

These debates seesawed back and forth endlessly—no one ever won; no one ever lost; but the coffee was good!

Then, one pleasant evening in 1957, October 4, to be precise, I retired very early, having had only two hours sleep the night before,<sup>1</sup> when with the suddenness of a small rubber carnival balloon bursting, Ivan the Necromancer rudely set off an alarm clock which both literally and figuratively was heard around the world. Electrified by this news, Hans Ziegler called my number but the household slept on. Hans then called Bill Stroud, who tried my number again, this time with success, and having wakened me, he picked me up and the two of us drove rapidly 20 miles to the home of Edward Rich in Farmingdale, N. J. There at

2148 hours, I heard the first of the BEEPS. Ed Rich was all set for this drama, for he had a Collins R-390 warmed up as part of a communications net which kept contact with a Laboratory team firing IGY rockets at Fort Churchill, Canada. We made tape recordings (and downed a bottle of medicinal Bourbon, too) as we listened through most of the night in sleepy dismay and amazement. Long after midnight, with many rudely-awakening phone calls, I set up an emergency meeting in my office at 0800 hours, Saturday, October 5, calling in 20 top Signal Corps communications people for consultation.

Together, we pondered what should be done with these stray 20- and 40-mc signals coming in at us from above and from every direction.

Our decision was simple . . . we would ourselves declare a state of National Emergency due to an "invasion." This also served to "legalize" our many subsequent actions which the more upright among us (like Major General Earle F. Cook and Colonel Paul W. Albert) were concerned about. After all, we had no legal project set up for tracking Russian satellites. We knew the IGY net, then at 108 mc, would take days for conversion to the Soviet frequencies, but within our own Laboratory, we had an immediate potential, and Duty called desperately.

By Saturday noon, October 5, our small select group of Signal Corps R & D personnel at Fort Monmouth knew their jobs. They also knew that no overtime was authorized, and knew, furthermore, that they were to arrange, within their own resources, ways and means for keeping their respective parts of our new research program running at 24 hours a day, seven days a week, until we knew all there was to be learned from the mysterious electronic invader carrying the hammer and the sickle.

Hans Ziegler was assigned the role of USASRD Task Master, alias Simon Legree, but working with volunteer slaves. Norman Field was anointed as his Man Friday. My office was "accepted" as Headquarters through "squatters' rights" protocol, and Hans was merrily on his way toward a new U. S. Government marathon work-record of a 400-hour month with your author providing the aspirin and a few slaps on the back thrown in for extra.

Communications Department with Bob Kulinyi and Lloyd Manamon directing, soon had our Deal site listening and recording both frequencies with Collins R-390's and R-220's. Fred Dickson alerted his global Radio Propagation Agency potential, and soon receivers at the ionospheric stations at Adak, Alaska, Grand Bahama Island, Fletcher Ice Island (T-3) in the Arctic Ocean, White Sands, N. M., Thule, and Okinawa were gathering data around the clock. "Bud" Waite, of Antarctic fame, started recording events with a receiver he had at home. Our Surveillance Department tuned up the Diana Moon Radar, and our Meteorological Division put another special re-

\* Manuscript received by the PGMIL, February 1, 1960.

† U. S. Army Signal Res. and Dev. Lab., Fort Monmouth, N. J.

<sup>1</sup> This was an entirely different project and is none of the reader's business.

ceiver on the air. Our Frequency Control Division started checking frequencies, Doppler shifts, etc., against masers, no less. Even the Army's Paul Siple in the Antarctic was listening and recording.

But perhaps most important of all during these early hours on October 5 were the efforts of a few of our Countermeasures people operating an experimental direction-finding station at Collingswood, N. J. In the open, and in freezing weather, Bill Gould, Harold Jaffe and associates, day after day, all through the long nights, week after week, gave out bearing information—information vitally needed by the Vanguard Computing Center at NRL to determine orbits and make predictions. Yet, the Soviet had kicked off, but before we could really play in the game, we first had to *find* the ball.

For weeks, Ziegler called the Vanguard Computing Center at least every recorded orbit, and often two or three times in between, and on many occasions kept the toll line open as Alpha completely circumnavigated that bit of cosmic dust we call Earth. Some people, looking for a smile, even accused Hans of having bought a share of AT&T stock and trying to run up his dividends.

The Vanguard Computing Center at NRL was, of course, flooded with thousands of phone calls from all over the U. S., but just hearing the signal soon had little orbital determination value. Until optical fixes from the Smithsonian, Moon-Watch and the Minitrack System started operating, the direction-finding data from Jaffe were all-important, and we fed his angles and time to the greedy computer in Washington as fast as we gathered them.

But it was not easy, and peculiar situations often arose. For example, as the orbit was first being roughed out, a "mysterious force" (quoting blazing Washington newspaper headlines) suddenly appeared, pointed to a two-minute discrepancy in predicted orbit time. Alpha seemed to be where it wasn't. Were there really new forces? Could Newton and Kepler possibly have been wrong?

This two-minute differential was very conspicuous in the data our direction finder reported to the Computing Center. Accordingly, a decision was made in Washington to try this correction in the machine. But somewhere in the transmission of our data, the sign was unfortunately reversed, and when compensation using these data was attempted, the discrepancy jumped from two to four minutes and "the force" thus grew bigger and ever more mysterious. The computer, however, was given another chance with the suggested correction applied in the reverse direction. Immediately, all was well. Our bad actor was only someone's sleepiness, the 24-hour working day being a novelty even in Government circles. Kepler again became a respected authority.

As the long days and nights passed, finally out of confusion came the Sputnik ephemeris, and the IBM brain at the Vanguard Computing Center finally had all the input needed. The little intruder became a visible and scheduled sunrise and sunset spectacle to those of the nation who watched and/or got up before breakfast, or delayed cock-tails.

On a very personal side: One frosty morning early in October, I set a bridge table on our lawn and shiveringly served orange juice, wheat cakes, bacon, coffee and/or milk to my wife and three youngsters (2, 6 and 8 years). Precisely at 0551, I was saying that it should be in the north, moving across our view toward the south, when Chris (6) interrupted me and said, "Dad, what is that twinkling moving star?" He pointed to the north. It was Alpha, all right.

For several minutes we breathed the exciting air of adventure and discovery, as one of the greatest of all man-made spectacles majestically sailed across our view. Few in the U. S. had yet seen the satellite, so we were particularly thrilled. Hours later, Buzzy, the oldest, gave a lecture on satellites to his third grade class, while Chris lectured similarly in the first grade. The baby was asleep again.

By, now, our little Army volunteer group at Fort Monmouth had grown to a strength of 120 people and the ROYAL ORDER OF SPUTNIK CHASERS (ROOSCH) came into being—sweat, tears, success, failure, no sleep, no extra compensation (and who cared), family problems, curiosity and patriotism all wrapped into one. But even with their tiredness, the volunteers acquired a sense of new importance and felt proud to be aboard, sailing into the unknown of outerspace electronics. With added help now coming more easily, we listened and watched as Sputnik's batteries started to run down. We knew our long vigil would soon end, with the forgotten word of sleep wending its way back into our vocabulary—we hoped. Our primary interest now became one of learning, particularly propagation, as much as we could from the two excellent mobile transmitters so kindly provided, at no cost, by the Soviet. Important data were being accumulated at the biggest bargain rate since Marconi turned on his first spark transmitter.

But Ivan was cruel!

We had just caught up on loss of sleep from Alpha when he launched Beta, and Laika's heart beats throbbed as loudly through our loudspeaker as did ours through our shirts. Actually, we heard Laika's stethoscopic signature briefly during only one of the earliest orbits, but it was an unmistakable signal (0429–0430, November 3, 1957).

Army Signal Corps personnel were the first to hear this new intruder, Beta, as it came over the North American continent. We were ready,<sup>2</sup> and alert technically, albeit, and ironically, our own Technical Information Staff lacked official permission to release the news of its entry over our continent, and the hour was 0250. The Pentagon was not yet ready for the space maze.

George Moise of our Technical Information Division quite innocently, however, called one of the wire services and asked, "Did anyone hear the new Russian satellite over the U. S. before our reception at 0250 hours?" This

<sup>2</sup> I should qualify the statement somewhat. U. S. radio announced the launching at about 0200 on November 3. At the same time, it happens there was also a good party going on having some of our honorable Sputnik Chasers in attendance. Being "ready" and going to work quickly thus meant only telling the wife or girlfriend to find another way home—ROOSCH business was calling!



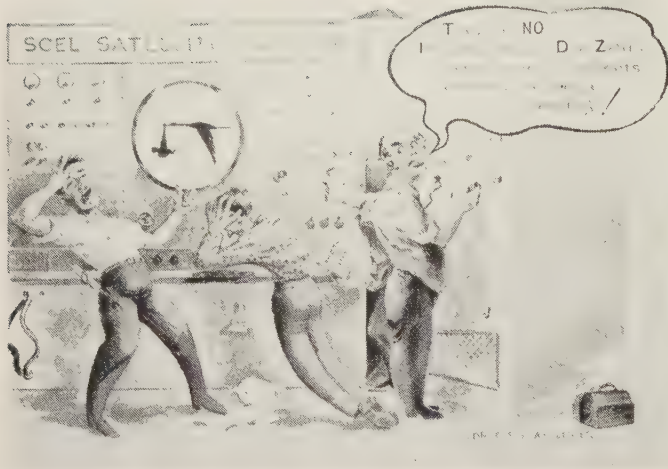


Fig. 1—The author's staff, with help of artist B. H. Christenson, anticipate the astro-electronics age, as the author's wife anticipates the arrival of an offspring. This sketch was subsequently used as a "launching card," beating the Sputniks by almost two years.

was just a simple question, of course, and the wire services are supposed to give out information.

"What!" came the reply. "No—but, but, but—you've got a story!"

And so he did. But our George was saved from possible reprimand, for almost simultaneously, Len Rokaw, responsible for the harassment of three echelons of Pentagon hierarchy, received official permission to release the facts on our first hearing. Rokaw and Moise certainly owe beers to an unnamed General (and two Colonels in chain-of-command) who was awakened at his home at 0300 and who authorized the news release. And there are those, too, who say they heard the OK given twice, once by phone and then again, 10 minutes later, as the sound wave from Washington arrived in New Jersey. From such stuff come commendations or reprimands; it's the way the coin falls.

But again, just hearing the signal hardly awakened the interest of the Computer in Washington. It yawned and with mathematical preciseness said, "Serve me with apogees, perigees, angles and time, please. I am not clairvoyant." And the computer had cause, since actually for a few early hours, some U. S. radio broadcasters had the satellite going in a peculiar and most unusual direction. Ziegler was very worried over the peculiar course.

"Look at Jaffe's direction finding data, Harold," he said to me. "You heard the last broadcast—something is lousy!"

And it was!

Our first bearing data were then quickly sent to the Vanguard Computing Center where, combined with Mini-track data coming in, the course of the satellite was established and then correctly and officially announced. We are sure, however, that the theoretical acceleration involved in our paper reversal of the direction of this particular bird did not bother Laika much. Had she known, she probably would have been very much amused by the entire incident.

After all, "hot dogs" are an American invention.

And so it went. We finally established an authorized project. Military personnel were brought in to help in our new 24-hour tracking schedule. At Deal alone, the "Mayor" of that activity, Lloyd Manamon, recorded many miles of tape containing good data—priceless for future reference. In fact, today the Deal library, of all satellite recordings, is the most complete in the world.

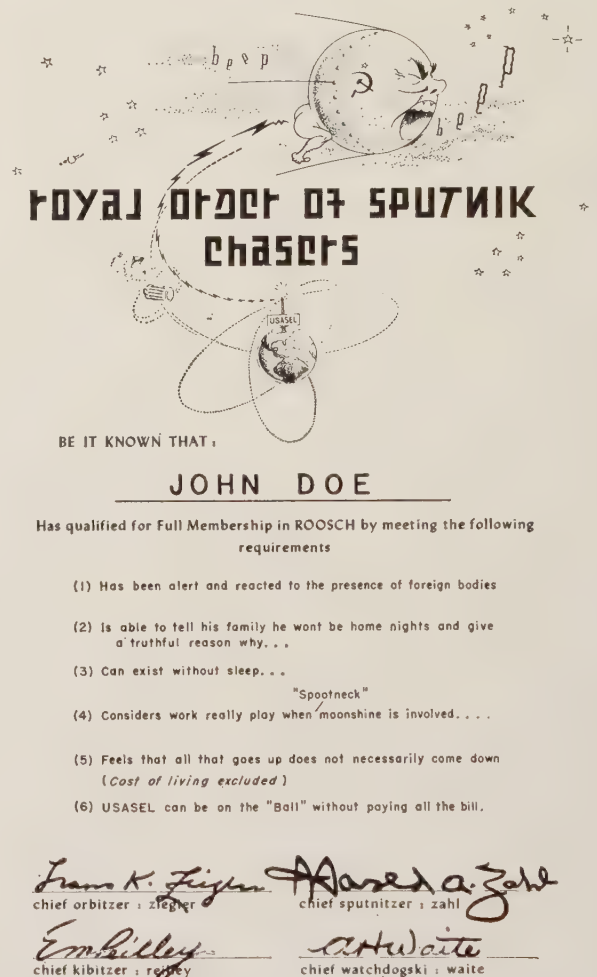


Fig. 2—In lieu of numerous letters of commendation, a ROOSCH Diploma was given to all Signal Corps employees who donated more than 100 hours of service during the trying days of Sputnik I and II.

It is now 1960. Many tracking systems the world over can now do, and do much better, the things we fought so hard for over a period of 40 days in late 1957. We even do it now almost "stereophonically and in full color." We rest while the receivers and recording equipment work on almost automatically, and children of ROOSCH parents again recognize their fathers. But before I close, I must point out that the Army Signal Corps group was only one of several others in the U. S. which we know experienced the same emotions and worked as hard toward the same end as did we. I am sure the chronology of these activities would add fascinating chapters to the history of the first earth satellites. But they are separate stories and should be written by others.

# Army Participation in Project Vanguard\*

W. E. SMITHERMAN†

**Summary**—The Army was responsible for the installation and maintenance of six Minitrack stations for Project Vanguard. In addition, the Army responsibility included the electrical tracking of the artificial satellites from these stations.

This paper outlines the actions taken by the Army in fulfilling these responsibilities.

THE scientific program for launching an unmanned, earth-circling, instrumented earth satellite was stimulated by a resolution passed by the Special Committee planning the International Geophysical Year (IGY) at its Rome meeting during October, 1954. The IGY had been established as July 1, 1957 through December 31, 1958. The artificial earth satellite project was sponsored by the National Academy of Sciences and the National Science Foundation as part of the United States program for participation in the IGY.

The IGY satellite program, known as Project Vanguard, was comprised of four operational phases. First, the satellite must be launched. Secondly, the satellite must be tracked and observed. Thirdly, the information obtained from the satellite must be refined to useful facts. Finally, the processed data must be given to those who can use it. The U. S. Army—particularly through its Signal Corps and Corps of Engineers—has been especially active in the second phase in support of Project Vanguard, and in the last phase for its own geodetic and mapping missions conducted by the Army Map Service (AMS). This paper describes Army participation in Project Vanguard.

On September 9, 1955, Secretary Wilson announced Department of Defense responsibility in a tri-service program to launch a scientific satellite during the IGY. He assigned management of the technical program to the Department of the Navy. On September 27, 1955, the Secretary of the Navy directed the Chief of Naval Research, who, in turn, assigned responsibility to the Naval Research Laboratory (NRL), to execute the Navy's portion of the program. Between March 27 and May 11, 1956 a Site Selection Team composed of representatives of the Army's Corps of Engineers and Signal Corps and the NRL made an extensive reconnaissance to locate suitable Minitrack station sites. This team was accompanied in South America by a representative of the Inter-American Geodetic Survey (IAGS), a Corps of Engineer agency cooperating in a mapping program with 17 Latin American nations. The following site selection criteria were established by NRL and adhered to by this team.

- 1) The minimum area for each site was 750 by 750 feet.
- 2) The Minitrack stations were to be located generally along the 75th meridian in northern Florida, Cuba, and the Panama Canal Zone in the northern hemisphere; at the equator; and at 12°, 24°, and 34° in the southern hemisphere.
- 3) Sites were to be on virgin ground with no fill; however, grading was permissible to attain difference of elevation of plus or minus 5 feet.
- 4) Adjacent terrain height should be under 10° elevation for at least ½ mile, with a permissible increase to 20° at 5 miles.
- 5) There should be adequate road net to accommodate required vehicular traffic.
- 6) The sites should be at least two miles from high tension lines, large power plants or large power users.
- 7) The sites should be at least 5 miles from airways or airports unless tight aircraft control could be effected during tracking events.
- 8) The sites should be within one hour's travel time from a major population center.
- 9) Good optical sighting conditions were desirable.
- 10) All stations must be tied into the existing geodetic triangulation net.

Using these criteria the team selected sites at Fort Stewart, Georgia (selected because of airways congestion in northern Florida); Batista Field, Havana, Cuba; Rio Hata, Republic of Panama; Paramo de Cotopaxi, Quito, Ecuador; Pampa de Ancon, Lima, Peru; Salar del Carmen, Antofagasta, Chile; and Peldehune Military Reservation, Santiago, Chile.

Of these, the Rio Hata site was later abandoned since observations from this station would have been largely duplicated by those of the Navy stations at San Diego, California, and Antigua, British West Indies.

In addition to selecting suitable sites for tracking stations, the team obtained assurances that the Vanguard tracking program could be accomplished in Cuba and South America as an extension of the activities of IAGS during the IGY without revision of the basic IAGS cooperative agreements.

At the request of the Naval Research Laboratory, the Chief of Engineers, in September, 1956, initiated construction of the six Minitrack stations, by contracts awarded to private firms and administered by the Savannah and Jacksonville District Engineers and the Panama Area Engineer. With the exception of basic local materials, such as form lumber and concrete, all materials needed for the station construction, such as prefabricated buildings, antenna posts and rails, electrical conduit and wire, etc., were furnished directly to each station site by the Government.

\* Manuscript received by the PGMIL, February 1, 1960. Contributory authorship of Capt. Harold N. Acrivos, C. E., U.S.A., is hereby acknowledged.

† Signal Officer, Autilles Command, San Juan, P. R. Formerly with Army Map Service, Corps of Engineers, Washington, D. C.



A prerequisite to station construction was astronomic and geodetic surveys to precisely locate the station sites with respect to existing first-order triangulation nets. These surveys were accomplished by the Army Map Service, the U. S. Coast and Geodetic Survey and the IAGS, in co-operation with the geodetic agencies of Cuba, Ecuador, Peru, and Chile. Computations to adjust these survey positions to a common Vanguard datum were accomplished by the Army Map Service. In addition to the precise location of the site, the precise location of the station center in geodetic and astronomic terms was also required in order that the antenna system might be oriented and constructed in a true geodetic position. Since the precision of the observations, and consequently the final data, from each station is directly determined by the accuracy of the antenna pattern, a brief description of the location and orientation criteria will be of interest.

- 1) Position Accuracy—plus or minus 0.05 foot per mile with respect to the existing first-order triangulation net.
- 2) Direction Accuracy—plus or minus three seconds of arc with respect to geodetic north.
- 3) System Level Accuracy—plus or minus  $\frac{1}{8}$  inch in 500 feet.

By Department of the Army letter (subject: "Army Participation in Project Vanguard," dated October 16, 1956), the Chief of Engineers was assigned responsibility for executing the following specific Army Functions under guidance from the NRL and the Chief Signal Officer:

- 1) acquisition of real estate and construction of essential facilities for the tracking stations,
- 2) provision of all necessary equipment not furnished by the Navy,
- 3) installation, maintenance, and operation of tracking, telemetering, and communications equipment at the tracking stations,
- 4) provision of communication facilities to pass the tracking data from various tracking stations to the data-processing center operated by the Navy in Washington, D.C.
- 5) provision of trained personnel to operate the tracking stations and communications system.

The same Department of the Army letter assigned responsibilities to

- 1) the Chief Signal Officer for supporting the Chief of Engineers as necessary,
- 2) The Commanding Generals, Continental Army Command and U. S. Army Caribbean, for providing routine administrative and logistic support in their respective areas, and
- 3) The Deputy Chief of Staff for Personnel for providing required personnel spaces.

The responsibility for the implementation of the Vanguard mission, with the exception of land acquisition and station construction, was assigned by the Chief of Engineers to the Commanding Officer, Army Map Service. In order to carry out this responsibility, a separate operational element, designated Project Vanguard Task Force, was established at AMS.

In addition to the Vanguard mission, the Task Force was assigned cognizance of the AMS Project BETTY. This project was initiated and operated to use electronic observations of artificial satellites for geodetic purposes and was, therefore, directly related to and dependent upon the Vanguard program.

Project Vanguard Task Force became operational on February 1, 1957. It consisted of

- 1) one Colonel, Corps of Engineers, Task Force Chief,
- 2) one civilian secretary,
- 3) one Lt. Colonel, Signal Corps, Chief, Project Vanguard, AMS,
- 4) The 523rd Engineer Detachment which had been transferred from Fort Bliss, Texas, to form the nucleus of the Task Force. The commanding officer of the 523rd was designated Chief, Project BETTY.

By this time, station construction was under way, Signal Corps engineering of the basic communications system was well advanced, and the initial contingent of military personnel were under orders to the Army Map Service. The Task Force settled immediately into the problems of completing plans and arranging for specialized training for the station personnel.

The NRL established a school for Minitrack and telem-



Fig. 1—This photograph shows the layout of the tracking components at a Minitrack station. The top of the photo is east. A line drawn through the centers of the upper and lower antennas would pass through the center of the system (in the small white building) in a precise geodetic north-south direction. The other antenna axis is precisely  $90^\circ$  from this, and constitutes an east-west direction. Each leg of the cross, to the antenna centers, is 250 feet in length.

The small building in the center of the antenna field houses an astronomical camera used in station calibration. The trailer at the right center of the photo houses receiving, amplifying, time-standard, and recording equipment of the Minitrack system. Connections to the antennas are buried pressurized coaxial cables.

The portion of the station shown in these photos is typical of all stations. Not shown, but also a part of each station, are a headquarters building, a power shelter unit, a telemetry receiving antenna trainable within limits in an east-west direction, and a telemetry turn-on antenna. Telemetering command turn-on and receiving and recording equipment are in the headquarters building. Antennas for radio communications, where used, are outside the station compound. All areas are fenced for traffic exclusion rather than security.



etry familiarization. The station chiefs (Army captains), all enlisted electronic technicians of the original contingent, six civilian technicians provided under an Army contract, a number of civilian engineers provided under a Navy contract, and a number of NRL personnel—including the scientists to be assigned to the Army Stations—were trained in 4- to 5-week courses in this school.

As the Minitrack vans were delivered to the NRL, each team participated in the acceptance check of its tracking and telemetry equipment. This included actual operation of the equipment using the antennas at the Navy's Blossom Point, Maryland, prototype station. Signal sources were the sun, radio stars, and airplane-borne simulated satellites.

Amateur radio equipment was provided for each team as an alternate communication system. While seldom needed as an alternate means, this equipment proved to be worth much more than its cost as a means of inter-station discussion of problems as well as for conference-type discussions with NRL and the Task Force. The added morale value of a "phone patch" to home and other "ham" radio activities was tremendous.

The Task Force accepted the job, at the request of NRL, of accomplishing lease of all commercial teletypewriter circuits required for Vanguard. The total system for which the Army Map Service was ultimately responsible consisted of a separate radio teletypewriter circuit to each Latin American station plus 16 leased commercial lines connecting stations and control points in the U.S.

Arrangements were made with the U. S. Army Signal Engineering Agency to provide installation teams for the radio equipment. NRL provided similar teams for the tracking equipment. Arrivals of these teams were planned so that they could be mutually supporting, with both receiving assistance from the station personnel.

In July and August, 1957, station teams moved to their respective sites.

Many small problems occurred in the field, generally of the "brush fire" variety. Lost and slow shipments, parts of shipments, and a variety of other activities kept the "wires hot." It was necessary for the station chiefs to find their own solutions to many local problems. The experience and familiarity of the IAGS personnel with local conditions and resources were of valuable aid during this period.

It quickly became apparent that, in initial planning, too much dependence had been placed on local procuring of material and services. In the case of support to power units, this was particularly true since it had been expected that practically all parts could be bought locally. It was found that almost none were available. In addition, it was found that a single 30-kilowatt power unit would not carry the station load and maintain satisfactory voltage regulation. It was necessary, therefore, to operate two units in parallel at all times. This greatly increased maintenance problems and seriously reduced the standby power capability. AMS initiated two actions to relieve this situation:

- 1) secured approval for, procured, and shipped an additional 45-kilowatt power unit to each station,
- 2) prepared a maintenance parts list and provided the stations with an extensive stock of parts for the original

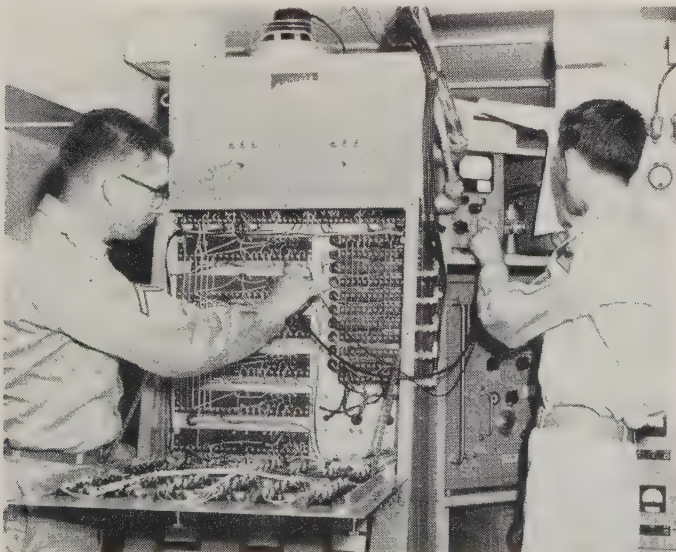


Fig. 2—Checking equipment. Pfc. Steven Durkovic (left) and Sp-3 John H. Fields check voltage on receiver control panel in trailer van housing the intricate Minitrack equipment at Vanguard Observation Station, Fort Stewart, Ga.

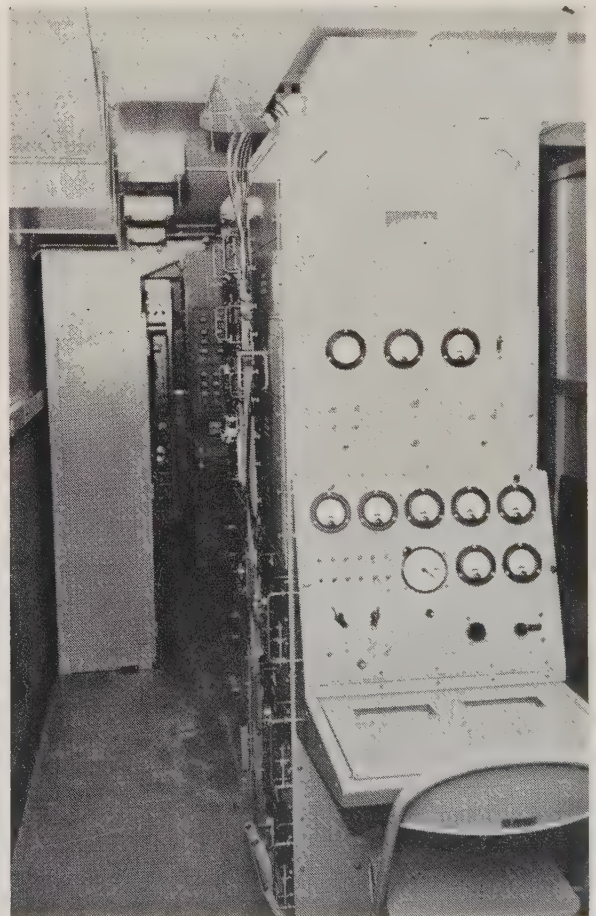


Fig. 3—Rear of trailer, looking forward to towed end. Center island of racks houses time-synchronization and phase-measuring systems.



30-kilowatt units as well as the added 45-kilowatt units.

As the system neared operational readiness, material was prepared and sent to the stations for on-the-job training and testing of team abilities. Chart recordings of simulated satellite passes were made at Blossom Point. These were duplicated at AMS and shipped in coded packages to the several stations. It was planned that dry runs would be conducted, under the control of NRL, using these charts for checking of the teams' abilities to read-out and transmit the tracking data. It was expected that these tests should be conducted in the months of October and November, so that the stations would be ready for the first satellite launching event in early December, 1957.

Tracking began, however, without benefit of these training tests with the unpredicted launching on October 4, 1957 of Sputnik I—the first artificial earth satellite. Direct communications had been established to Fort Stewart and Antofagasta. Other stations were nearly ready, but had to be reached by various slower means, such as commercial cable, the IAGS radio net, amateur radio, and long-distance telephone to pass on the scant technical information available about the Soviet satellite. No preparation had been made for either detection or tracking at the frequencies used. Emergency equipment alterations and antennas were designed. Station teams and installation crews worked around the clock for several days to make the necessary modifications. A special shipment of radio receivers was sent by air to all stations, and within a few days all stations were capable of limited tracking at the Sputnik frequencies. The data obtained could only be considered approximate at best. On October 26, the Sputnik radio faded. It was immediately realized that the "wettest dry run in history" has been a blessing in disguise. The shake-down under pressure, and the realization that they could do the job, did wonders for team and individual morale. It was also apparent that tracking might be required without advance prediction and that the Task Force must be prepared for anything. This realization was extremely fortunate since, on November 3, 1957, the Russians launched the second Sputnik. During the six days of its

radio life, tracking operations—while still crude—began to approach the routine, and the data obtained was considered much more reliable.

January 31, 1958 saw the successful launching of the first United States satellite—Explorer I. There is no doubt that this was a great day for the Army. It was also a great day for the Vanguard Task Force. At long last, there was a tracking job to be done which approximated that for which elaborate preparations had been made.

On Saint Patrick's Day in 1958 the long awaited Vanguard I satellite was put into orbit. Although much derided as the "grapefruit," the orbit of this four-pound sphere was superior to previous ones and the personnel of the Task Force rejoiced with NRL at the vindication of its planning. Thanks to the experience gained on the Explorer, station teams were able to track Vanguard I so successfully that, after a few days, the computer was able to determine the orbit with a high degree of accuracy and the requirement for rapid data was relaxed.

The launching of Explorer III, on March 26, 1958, proved the validity of planning for full-time tracking. There were three U. S. satellites in orbit and all were transmitting a trackable signal. Instead of 3 or 4 passes a day, each station was now recording 10 to 15. This busy period lasted for almost two months. By the end of that time satellite tracking was a routine business for which each station team was well qualified.

Of the other satellites put into orbit during the period of Army participation in IGY, only 1958 Zeta caused any excitement. This one, Project SCORE, was launched in almost complete secrecy. It was only after completion of its first orbit, and the subsequent public announcement, that the Task Force was given its radio frequencies, which were such as to require complete retuning of the Minitrack system. Nevertheless, Vanguard stations recorded the third, and tracked the fourth and subsequent passes. This was a considerable tribute to the capabilities of the station teams to meet and deal quickly with the unexpected.

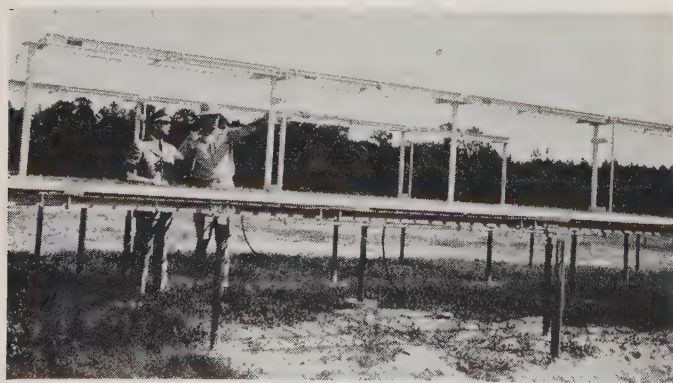


Fig. 4—Lt. Col. W. E. Smitherman, Chief, Project Vanguard, AMS, and Captain Warren L. Hurst, officer in charge, Vanguard Observation Station No. 2, inspect Minitrack antenna at Fort Stewart, Ga.

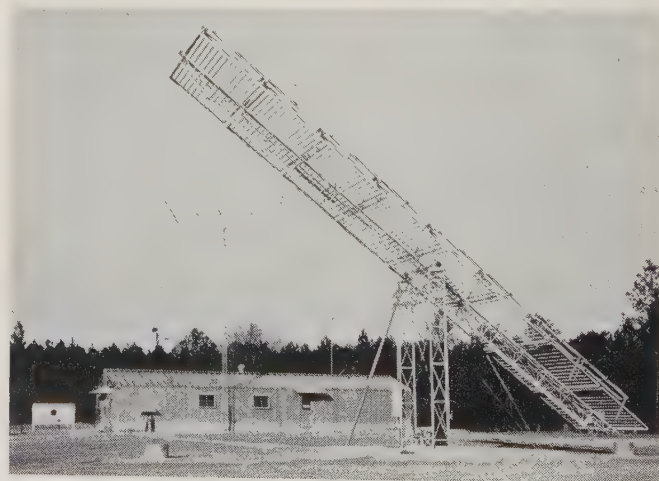


Fig. 5—Telemetry antenna, in foreground, tilted to the east. Amateur antenna next to operations building.

Extensive modifications to the Fort Stewart station began in mid-1958. These were changes that made the station part of a special-purpose east-west fence and effectively removed it from the IGY Minitrack system.

The Cuba station experienced some anxious times during the early days of 1959 when the Government of Cuba was overthrown by the "26th of July" revolutionary movement. The station was closed on New Year's Day as a precautionary measure, and reopened on January 6. No damage occurred to the station nor was it molested in any way.

The 85th Congress, by the National Aeronautics and Space Act of 1958, established the National Aeronautics

and Space Administration (NASA). Executive Order of the President, dated October 1, 1958, transferred to the NASA all functions of the Department of Defense with respect to Project Vanguard. On March 1, 1959, the transfer had been completed and the stations were in NASA hands. Of course, no change is completed so abruptly. There were actions in progress, such as supplies already in the pipeline, which had to be pursued to conclusion. Operationally, however, the Army had accomplished its mission of helping to track the earth's first nine artificial satellites, and thereby had contributed towards the satisfaction of man's curiosity concerning his environment.

## The Signal Corps Astro-Observation Center, Fort Monmouth, N. J.\*

L. H. MANAMON† AND A. S. GROSS†

**Summary**—Many months of active participation in the satellite and missile observation program have resulted in a number of new and improved concepts which have been put to practical use in the establishment of the U.S. Army Signal Research and Development Laboratory's Astro-Observation Center, Fort Monmouth, N. J.

This paper will describe the capabilities of the Research and Development station and several of the instrumentation techniques in use, including the use of phase-locked audio-frequency tracking filters, and high-speed digital readout equipment for precision Doppler measurements.

The extreme flexibility of frequency coverage of the station has been of exceptional value in the rapid acquisition of signals transmitted from foreign satellites and space probes.

### INTRODUCTION

THE U. S. Army Signal Research and Development Laboratory operates an advance design satellite and missile observation station known as the USASRDL Astro-Observation Center near Fort Monmouth, N. J., to study wave propagation phenomena associated with radio transmissions from space objects.

This facility consists of two stations; one is located at the center of a 208-acre tract of land previously used by the Bell Telephone Laboratories as a fixed site for early transoceanic radio telephone experiments. The property, called the Deal area, has been employed by USASRDL since 1953 as a site for testing and evaluating newly developed Signal Corps receiving systems, and for wave propagation research. The second station is located on Shark River near Belmar, N. J., and is the original site

of the first moon radar contact made by the Signal Corps in 1946. Called the Aircraft Warning Area for its early history in aircraft detection research during World War II, it is more commonly called the Diana Site since the first moon radar reflections were received.

When the Soviet Union launched the first artificial earth satellite, Sputnik I, on October 4, 1957, the Deal station embarked on a new phase of operation, that of satellite observation. Existing station equipment permitted the reception and recording of transmissions on 20.005 and 40.002 mc. A total of 273 orbits of Sputnik I were observed and recorded covering approximately 500 hours of continuous monitoring. As the space program continued to grow, so did the instrumentation and the concept of this portion of the observation center. Improved instrumentation was added to the station during the early part of 1959 (Figs. 1 and 2). Currently, the station operates on a 24 hour per day basis, and to date has recorded over 12,000 orbits of all satellites, foreign and domestic. The recordings, both Doppler and amplitude, have been cataloged and placed on file in the station's library for analysis and are available for reference by interested research groups. Many important results on radio transmission from space and ionospheric parameters have been observed and reported elsewhere.

During the past two years an extended effort has been put into the investigation and improvement of satellite and missile Doppler measuring equipment, with the view of developing a system which affords extreme flexibility of frequency coverage. Such a system has been designed and is in operation at the USASRDL Astro-Observation Station.

\* Manuscript received by the PGMIL, February 1, 1960.

† U. S. Army Signal Res. and Dev. Lab., Fort Monmouth, N. J.





Fig. 1—USASRD Astro-Observation Center. Over-all view, showing interior of operations room.

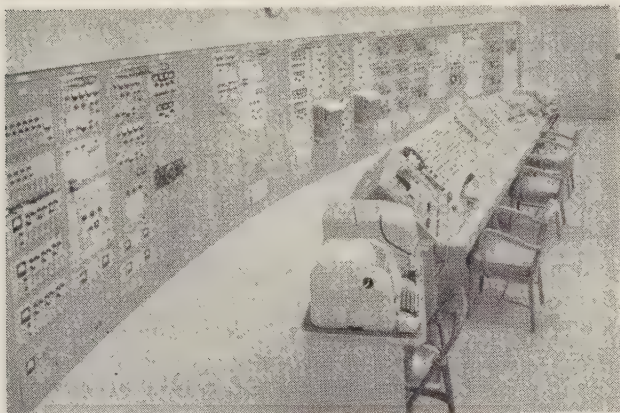


Fig. 2—USASRD Astro-Observation Center. Over-all view, showing interior of instrument room.

The frequency coverage of the station is currently covering the range 15 kc to 900 mc. Within this range it is possible to make precision Doppler measurements at random frequencies with automatic digital readout accuracies of 1 part in  $10^8$ .

#### DEAL STATION DOPPLER MEASUREMENT SYSTEM

The low intensity of signals being transmitted from earth satellites or space probes requires that methods be employed at the ground station to greatly improve the signal-to-noise ratio of the Doppler signal by obtaining a reduction in circuit bandwidth. In effect, an electronic band-pass filter whose center frequency automatically tracks the Doppler signal frequency fulfills this requirement.<sup>1</sup>

The tracking system presently in use at this station employs a phase-locked, audio-frequency electronic tracking filter with adjustable bandwidths between 2.5 and 50 cps which permits lock-on capabilities at signal input levels as much as 30 db below the noise. The center frequency of the electronic band-pass filter tracks the input frequency by means of a phase-locked servo loop. Easily accessible controls allow for immediate adjustment of bandwidths

under dynamic flight conditions, thus it is possible to take advantage of the maximum signal-to-noise ratio by permitting the use of the narrowest possible bandwidth without losing lock.

The tracking filter may be used with any receiver combination capable of detecting the incoming signal which is heterodyned against a precise frequency standard and mixed at the input to the receiver. The heterodyned note produced by the mixing of the incoming signal with the frequency standard may be anywhere in the range of 100 to 20,000 cycles. The audio output of the receiver containing this signal is fed to the input of the tracking filter. This level is usually about 3 volts rms. The output of the tracking filter now contains a sinusoidal wave form which is varying in frequency as the received Doppler frequency. The maximum tracking error over the entire range of the filter is less than 0.02 degree and so can be neglected for all practical cases. The resultant frequency is counted and recorded on magnetic tape for future reference. The tracking filter block diagram is shown in Fig. 3.

The system as described so far lends itself very satisfactorily as a means of detecting and recording the Doppler shift of a satellite or missile in flight. However, the great speeds at which these vehicles travel allow little time for the manual conversion of the recorded data for rapid transmission to computer centers. The requirement for such a system has resulted in the development of a digital data readout unit which has the capability of recording frequency measurements simultaneously with real time, both in printed numerals and in coded perforations at the rate of 60 digits per second.<sup>2</sup>

Frequencies are alternately measured by two 10-mc electronic counters, and time is measured in hours, minutes, and seconds by a 24-hour digital clock driven by a 100-kc frequency standard. Two or more stations at widely separated locations may be phased together by means of a Digital Phase Shifter which permits the clock and the counter gates to be synchronized within plus or minus 1 msec of the standard time signals being transmitted by the Bureau of Standards Station WWV, or from any other reference standard. Start and stop control pulses for the two electronic counters are derived from a common electronic switch in the digital phase shifter. The gate of either one electronic counter or the other is open at all times except for the transition time of the switch gates. (Less than 1  $\mu$ sec.) The time between adjacent stop and start signals is one second, with accuracy equal to the 100-kc reference standard. Digital readout is recorded in printed form on a standard three-inch paper tape. A punch coupler-perforator combination records identical data in coded perforations on standard teletype tape for transmission over wire line circuits. When the tape produced by the tape perforator is fed into a standard teletype punched tape reader, a teletype page printer will produce columns of figures.

<sup>1</sup> Phase-lock tracking filter, product of Interstate Electronics Corp., Anaheim, Calif.

<sup>2</sup> Digital Data System DY-5236A, mfd. for USASRD by Dymec Inc., Palo Alto, Calif.

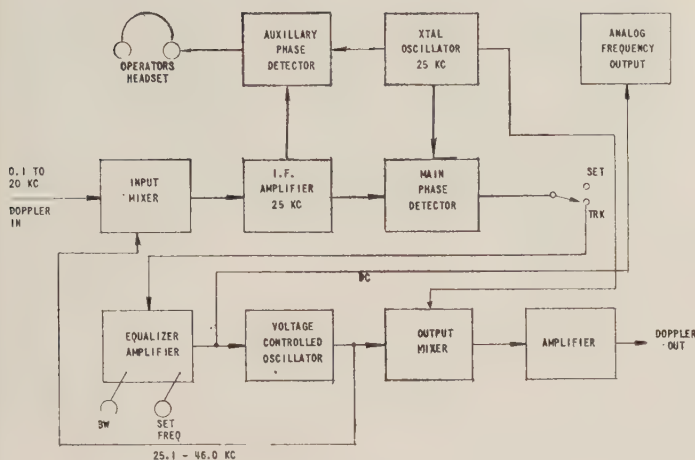


Fig. 3—Tracking filter block diagram.

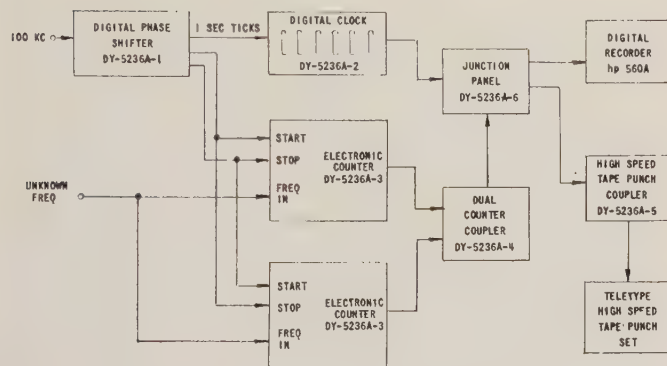


Fig. 4—Digital data system DY-5236A, frequency measurement.

Each line reading horizontally will contain six digits of time in hours, minutes, and seconds followed by a space and then a series of eight digits representing the Doppler frequency from the electronic counters. Fig. 4 shows a block diagram of the complete digital Data System DY-5236A.

It must not be overlooked that the accuracy of this system is strictly dependent on the accuracy of the injection oscillator employed. Serious consideration should be taken, therefore, in the selection of a suitable frequency standard for this purpose. It is highly desirable that the frequency standard selected be capable of variable frequency output which can be multiplied to cover the frequency range of the Doppler system. For this purpose, the USASRDL station employs a group of frequency synthesizers with a basic range of 30 cps to 30 mc in steps of 10 cps, locked-in with an external 100-kc frequency standard.<sup>3</sup> The synthesizers are also capable of continuous variable frequency output in between the 10-cycle points with somewhat reduced accuracy. The output voltage is sinusoidal, free from spurious frequencies, and adjustable between 0.1 mv and 1 volt, which is used to drive frequency multipliers up to the systems limit of 900 mc. Local frequency standards

are calibrated against a 100-kc signal transmitted over cable facilities from the main laboratory's Atomichron, located approximately four miles away. Plans are currently being formulated to drive the synthesizers directly from the remote Atomichron for improved accuracy.

The output of the frequency multipliers is passed through attenuators to the inputs of standard Signal Corps R390A/URR receivers with converters continuously tunable to 55.0 mc. The remainder of the VHF and UHF ranges up to 900.0 mc are covered by the use of commercially available special-purpose receivers.<sup>4</sup> The LF range (15–1500 kc) is monitored by the use of standard Signal Corps R 389/URR receivers.

The extreme flexibility of frequency coverage of this system offsets to a great extent the current limitation of 20,000 cycles of Doppler excursion. However, full Doppler excursion can be had up to 375 mc at velocities of 18.2K mph. The circuitry of the tracking filter readily lends itself to modification for this increased excursion. It is contemplated that such a modification will be initiated in the near future.

This system has been of invaluable use at USASRDL for immediate acquisition and measurement of Doppler shift of foreign satellites and space probes operating at various frequencies throughout the spectrum, whereas fixed frequency microlock systems have been unable to meet this challenge. The use of these techniques has been instrumental in immediate evaluation of the success or failure of space vehicles launched from Cape Canaveral. This is especially true for those launchings made in a northeasterly direction.

#### SIGNAL LEVEL MEASUREMENTS

During the course of observing signals transmitted from earth satellites and space probes, it has become more important to obtain a permanent record of the behavior of propagated radio signals as they pass through the ionosphere. Instrumentation has been set up at the USASRDL Observation Center to provide for the permanent recording of such signals for use by propagation study groups.

The instrumentation for this project required the modification of the AGC circuits of the R390-A/URR receivers to remove all delay so that the slightest change in signal would cause a change in AGC voltage, and would in turn activate a recorder. In reality, the R390-A receiver is used as a recording voltmeter. The modification is a relatively simple one resulting in a change in the AGC voltage curve as illustrated in Fig. 5. The curves shown are representative of the AGC voltage change of the R390 receiver operating without the addition of VHF converters, which materially increases the gain of the system.

Eight-channel Sanborn recorders are provided for read-out of the relative strength of the received signal. One-second time markers are recorded on the extreme edge of

<sup>3</sup> Rhode & Schwarz frequency synthesizers types XUA and XUB, with associated frequency standards and multipliers.

<sup>4</sup> Nems Clark 1302A (55-260MC), range extension units REU-300 (250-900 mc).



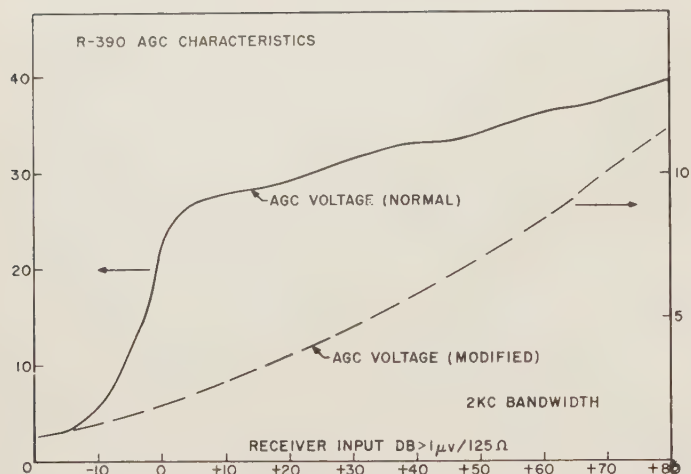


Fig. 5—Normal and modified receiver AGC characteristics.

the chart which accurately marks the time of events recorded on the main channels of the recorder. Each recording is identified and indexed to the corresponding Doppler recording for the particular event being observed, and then is filed in the station's library for further reference. As mentioned previously, the library now contains over 12,000 recordings dating back to the early orbits of Sputnik I. This represents the most complete reference library of its type known to exist in the entire country, if not the entire scientific world.

#### TELEMETRY RECEIVING SYSTEM

In order to meet the operational commitments in a station of this size, it was planned that the basic design of the station include adequate telemetry receiving facilities with sufficient channels to accommodate all future demands.

The telemetry system currently in use at the USASRD station consists of ten channels of encoder-decoder equipment coupled to the output of a bank of Nems-Clark telemetry receivers equipped for crystal-controlled operation on any one of 44 assigned RF channels within the band 225 to 260 mc.<sup>5</sup>

The outputs of ten subcarrier oscillators are fed to Sanborn chart recorders and to magnetic tape recorders. Ten audio-frequency discriminators are available for the playback of magnetic tapes, or to decode telemetry data from signals received from satellites or space probes.

#### ANTENNA FACILITIES

A wide variety of antennas are used at the USASRD station. Generally, several antenna systems are used on each intercept depending on the particular experiment in progress. The normal complement of antennas consists of horizontal and vertical polarized high gain Yagis, circular polarized Yagis, and broad-band conical helices with right- and left-hand polarization.

#### DIANA STATION

The Diana station is a basic research facility for the study of wave propagation, communications, and radio astronomy research. At this site, as described previously, the first moon radar echoes were received. At the present, routine moon transmissions to the University of Illinois, are undertaken to determine the electron content of the ionosphere and the diurnal and seasonal variations. Measurement of the Faraday rotation of lunar radio echoes on a frequency of 151 mc are used to determine the time variation in the total ionospheric electron content. Absolute values of ionospheric electron content are determined from these measurements in conjunction with information on the electron content below the  $F^2$  peak computed from vertical incidence sounding data.<sup>6</sup>

The Diana station has undertaken many other experiments, for example, the determination of upper usable frequencies for ionospheric scatter, meteor scatter, and the calibration of "Minitrack" receiving systems in the western hemisphere by moon relay at 108 mc. Numerous verifications of reception of these signals were received from radio amateurs throughout the world. A specially designed verification card was sent to all stations reporting reception of the moon-bounce signal (Fig. 6). Radio astronomy techniques now usable for space probe tracking were developed, and many of the first parametric amplifiers were used at this site.

The antennas at the Diana station, Fig. 7, consist of 50- and 60-foot paraboloidal antennas. The 50-foot antenna has an azimuth-elevation mount, a maximum speed of rotation of 0.5 degree per second with a positional accuracy of 0.1 degree. Its use is limited by the steel mesh reflecting surface to frequencies below 1500 mc. The transmission line is a 6 1/8-inch rigid coaxial line capable of withstanding high-power RF transmission. The 50-foot system serves a dual purpose as a radar transmitting system for moon studies, propagation experiments and the like; and as a receiving system equipped with parametric amplifiers for space probe tracking. Dipole feeds at the focal point of the dish are changed for each frequency, although one triple feed covering 108 mc, the telemetry band at 240 mc, and 960 mc is available.

The Diana and Deal stations are integrated by the use of a microwave link which has the capability of handling several data channels. Precision Doppler measurements can be made at Deal from the Diana 50-foot antenna, by transmitting over this microwave link the audio output of the receivers containing the heterodyned note produced by the mixing of the incoming signal with a frequency standard. Tracking filters at the main station accept this signal, and the Doppler is automatically printed out by the Dymec system described earlier in this paper.

<sup>5</sup> Telemetry equipment mfg. by Hallamore Electronics Co., Anaheim, Calif.

<sup>6</sup> S. J. Bauer and F. B. Daniels, "Measurements of ionospheric electron content by lunar radio technique," *J. Geophys. Res.*, vol. 64, pp. 1371-1376; October 10, 1959.

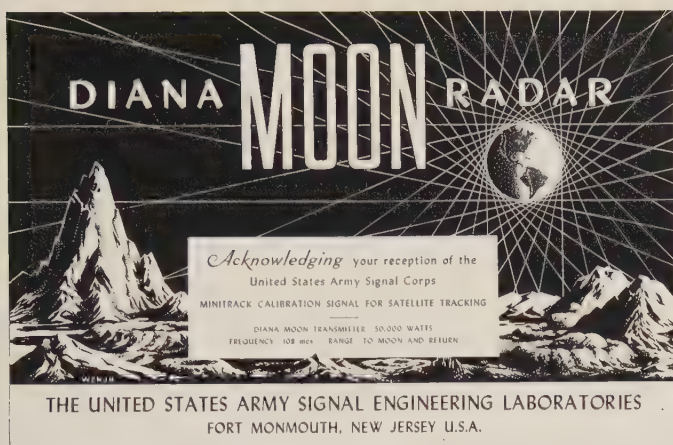


Fig. 6—Verification card sent to stations reporting reception of moon bounce signals.



Fig. 7—50- and 60-foot paraboloidal antennas at Diana station.

In addition to the 50-foot antenna, a 60-foot parabola is also available for use. Marked success was achieved using the 60-foot antenna on the Russian Lunik II shot, as well as on the Pioneer space probes. This 60-foot parabola is also of the azimuth-elevation type with a rotational speed of 10 degrees per second. The reflector has an aluminum mesh usable as high as 3000 mc. The antenna will automatically track any device transmitting in the 225-mc to 250-mc region to within 0.1 degree accuracy.

Two transmitters are in use for the propagation experiments. One operates at 151.11 mc with 50-kw power

output in the CW mode. Pulse widths from 600  $\mu$ sec to 4 seconds at various repetition rates are available. The second radar operates at 413.25 mc, with 20 kw in the CW mode and 50 kw peak in pulse operation. Pulse widths from 6 to 2000  $\mu$ sec are available at various repetition rates.

These equipments have been instrumental in determining significant results in radar range errors, refractive errors, and as previously noted, in ionospheric densities. Experimentation on detection of high altitude nuclear blasts and the determination of parameters affecting tropospheric, ionospheric, and meteor scatter communications have also been investigated.

The data taken by the Astro-Observation Center have provided scientific results in many aspects. For instance, they serve to determine the tumbling and spinning of the satellites, the natural decay of the satellites spin rate, and ionospheric parameters.<sup>7</sup> These results will be valuable for the design of future controlled aspect satellites and space vehicles, and of satellite communications systems.

The planning of a receiving station possessing the versatility of the USASRDL station encompasses the compilation of many ideas and a wide variety of experiences. Primary consideration must be given to unlimited flexibility and ease of operation. For example, on missile launchings maximum effort is placed on the accurate acquisition of Doppler data which must be transmitted to a network of computer centers. Once the satellite is determined to be in orbit, a complete change of data acquisition techniques is required. Instrumentation must be switched instantaneously with the least possible confusion in the instrumentation area.

With this country's growing capability, leading to the launching of bigger and more sophisticated satellites, a research program to keep this type of ground station up to the state of the art is also underway. Research tasks for the development of wide-band antenna feeds, wide tuning range parametric amplifiers, electronic scanning techniques, and other investigations to increase the capabilities of ground tracking stations are underway. As these techniques and equipments are developed, they will be tested at the Astro-Observation Center before installation at other stations around the world.

<sup>7</sup> P. R. Arendt, "Review of USASRDL satellite propagation studies," this issue, p. 357.



# Tracking in Space by DOPLOC\*

L. G. DEBEY†

**Summary**—A satellite and space vehicle tracking system of the Doppler type, known as DOPLOC, is described. The characteristics of the heart of the system, a phase-locked tracking filter, are discussed from the viewpoints of bandwidth, signal-to-noise ratio, and accuracy of Doppler frequency measurement. System sensitivity to low energy signals is shown to be  $2 \times 10^{-20}$  watts at a bandwidth of 1 cps. Tracking ranges vs frequency are given for constant gain and constant aperture antennas. The advantages of DOPLOC in satellite tracking programs are briefly discussed.

## INTRODUCTION

A NUMBER of acronyms have made their appearance in the technical literature over a period of several years. DOPLOC, derived from DOPpler phase LOCK, is but one of many such names coined to permit quick reference to a particular system of equipment. It is a type of radiometric tracking system designed particularly for obtaining trajectory or orbit information from missiles, satellites, or space vehicles in flight. As its name implies, it is based on the use of Doppler techniques enhanced by correlation detection methods which employ narrow-band, electronic, frequency tracking filters. The purpose of this paper is to describe briefly the DOPLOC system and to discuss some of its more important advantages in detecting and tracking low energy level signals received from satellites and space vehicles.

Instrumentation systems based on the Doppler principle have been in use for many years, primarily as precision tracking devices at the various guided missile test ranges. The first such system to attain wide application was the Doppler Velocity and Position (DOVAP) system developed by the Army Ordnance's Ballistic Research Laboratories in 1945 for use at White Sands Missile Range. Doppler systems of the DOVAP type are beacon systems; *i.e.*, a missile-borne receiver-transmitter is used to amplify and retransmit a CW signal originating at a ground transmitting station. The chief advantage of such a system lies in the fact that the frequency and wavelength of the radiation are accurately known.

## THE DOPLOC SYSTEM

Doppler systems, like radars, may also be used without cooperative beacons in the satellite. With beacons, signal levels are relatively high, whereas without beacons energy must be reflected from the satellite, requiring either high power illuminating transmitters or greatly reduced tracking range. Because of the high sensitivity of the DOPLOC system, it may be used advantageously in reflection Doppler applications. For the purposes of this paper, however, its use with a beacon will be described.

The vehicle to be tracked is assumed to carry a small radio transmitter. The frequency of the signal from the transmitter, as received at a DOPLOC ground station, is compared with a stable local oscillator (STALO) and the change in frequency vs time (Doppler shift) is measured and recorded. Fig. 1 shows a simplified block diagram of a typical DOPLOC receiving system. All components are commercially available items which have conventional characteristics except the phase-locked tracking filter. The tracking filter is the heart of the system and provides the special characteristics which permit detection of very low energy signals. It has been described by Richard.<sup>1</sup> Some of its more important characteristics will be reviewed briefly here as a prelude to a discussion of its application to the space tracking problem.

## THE TRACKING FILTER

The principle of operation of the tracking filter is shown in Fig. 2. The phase of the input signal is compared with that of a voltage-controlled oscillator (VCO), an error voltage is developed, and, after filtering in an equalizer network, is used to control the frequency and phase of the VCO. This electronic servo system has been designed to yield essentially zero tracking error for constant rate of change of frequency. The small errors which do exist are due to inability to synthesize perfectly the theoretically correct third-order transfer function on which the design of the filter was based.

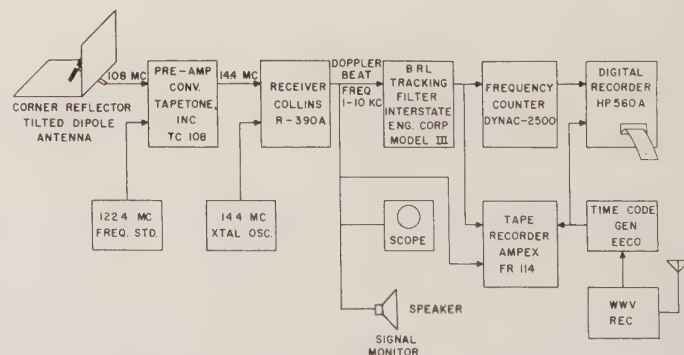


Fig. 1—108-mc DOPLOC station. Basic Doppler satellite tracking station using BRL tracking filter.

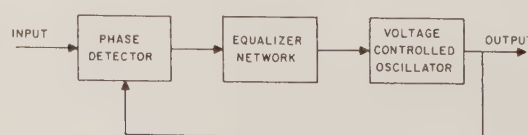


Fig. 2—Basic tracking filter system.

\* Manuscript received by the PGMIL, February 1, 1960.

† Ballistic Res. Labs., Aberdeen Proving Ground, Md.

<sup>1</sup> V. W. Richard, "The DOPLOC Tracking Filter," Ballistic Res. Lab., Aberdeen Proving Ground, Md., BRL Rept. No. 1173; October, 1958.

The response of the filter to a step function of rate of change of frequency  $\dot{f}$  from 0 to 5 cps is shown in Fig. 3 for a nominal filter bandwidth of 5 cps. Note that after the initial transient of error signal the latter drops to a value corresponding to a tracking phase error of about five degrees. It has been shown by Katz and Honey<sup>2</sup> that the bandwidth of the filter may be determined from

$$B = 1.38 \sqrt{\frac{\dot{f}}{E}} \quad (1)$$

where  $B$  = bandwidth in cps,  $E$  = peak phase transient in radians, and  $\dot{f}$  = amplitude of  $\dot{f}$  step function in cps. Thus

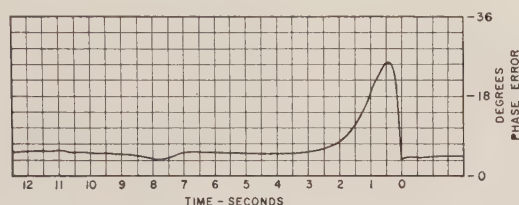


Fig. 3—Measured transient phase error vs time.

from Fig. 3 the actual bandwidth may be calculated and found to be 4.4 cps. Final calibration of the filter is accomplished by this method.

The signal-to-noise improvement is a function of the ratio of tracking filter bandwidth to input bandwidth. Amplitude noise at the input to the filter is converted to phase noise at the output of the filter. Katz and Honey<sup>2</sup> have shown that

$$\left(\frac{N}{S}\right)_0 = \sqrt{2} \theta_0$$

where  $\theta_0$  = rms phase jitter in output signal expressed in radians. For a given maximum output phase jitter, the maximum tolerable noise-to-signal ratio at the input to the filter will be

$$\left(\frac{N}{S}\right)_i = \sqrt{2} \theta_0 \sqrt{\frac{B_i}{B_0}}$$

It has been found by experiment that  $\theta_0 = 1/2$  radian is the maximum jitter that will permit essentially continuous tracking without an occasional peak phase excursion causing the filter to drop lock, and corresponds to a 6-db output signal-to-noise ratio. Fig. 4 relates  $(N/S)_i$  to filter bandwidth for  $\theta_0 = 1$ ,  $1/2$ , and  $1/4$  radians.

Of the several sources of radio noise, the two of greatest importance in space tracking are internal receiver noise and cosmic noise. It is assumed that man-made noise can be held within tolerable limits through careful selection of receiving sites and good engineering practices.

<sup>2</sup>L. Katz and R. Honey, "Phase-lock Tracking Filter," Interstate Engineering Co., Anaheim, Calif., Final Engrg. Rept. for the Ballistic Res. Labs., May 22, 1957.

In a Doppler system the Doppler frequency  $f_d$  and rate of change of frequency  $\dot{f}_d$  is proportional to the carrier frequency  $f_c$ . Eq. (1) shows that the bandwidth required in the filter to maintain lock is proportional to the square root of  $\dot{f}_d$ . The output noise power will therefore increase as the square root of the carrier frequency assuming a constant receiver noise figure. The noise at the receiver output due to galactic sources varies as  $f^{-1.8}$ . Fig. 5 shows the internal receiver and galactic noise magnitudes as functions of frequency referred to the receiver input. This figure also shows the received signal power required, for output signal-to-noise ratio of 0 db, and two examples of the tracking range capability of the DOPLOC system. The assumed values of the parameters are within the current state of the art.

The first example assumes a fixed and relatively low antenna gain. For low altitude satellites, where the angular velocity of the satellite with respect to a receiving site is high, antenna tracking is not always practical and nearly omnidirectional antennas are desirable. If narrow beam antennas are used in such a way that the duration of received signal is a function of beamwidth, as in search or acquisition operations, the maximum gain will be a func-

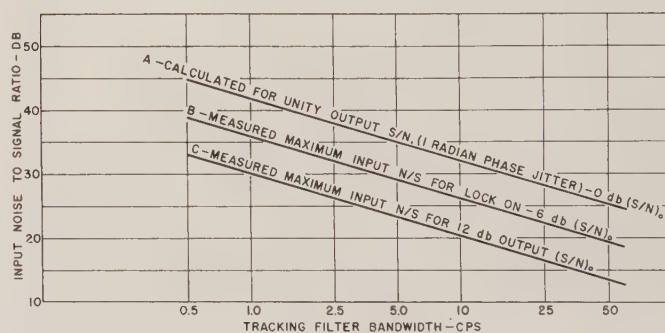


Fig. 4—Signal-to-noise improvement by BRL tracking filter. Tracking filter bandwidth vs input noise-to-signal ratio.

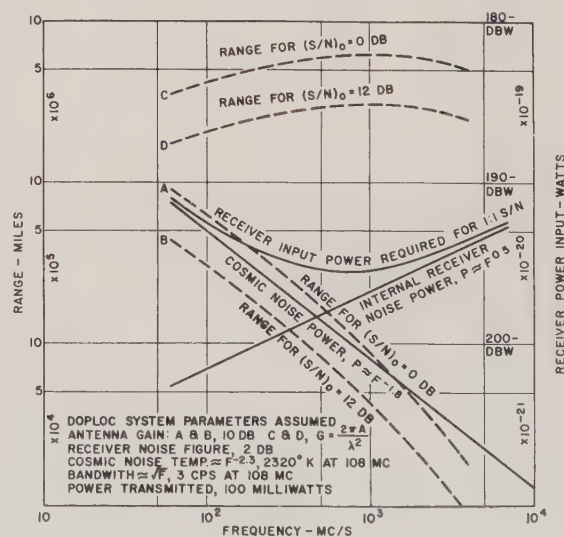


Fig. 5—Noise, receiver signal input power, and tracking range vs frequency.



tion of minimum beamwidth. Since the beamwidth determines the duration of signal, which in turn fixes the integration time available for determining frequency, there will be a lower limit of beamwidth which will yield the desired accuracy of frequency measurement as will be shown later [see (6)].

In the second example, a constant antenna aperture is assumed and the gain increases with frequency. Such antennas are applicable to the space probe problem where angular velocities are very low over long intervals of time and very narrow beamwidth antennas may be tracked successfully. The gain in such cases is limited only by the tolerable physical size of the antenna structure. A parabolic antenna with a diameter of 100 feet has been assumed for this case.

From Fig. 5 it is apparent that Doppler systems having antennas with fixed maximum gains should be operated at the lowest frequency compatible with the tolerable errors caused by the ionosphere if maximum tracking range is to be achieved. On the other hand, a system with antennas of fixed maximum size will realize maximum tracking range with a frequency near 900 mc.

#### FREQUENCY COVERAGE

The frequencies that have been used for space-earth communication and tracking have ranged from about 20 mc to 1000 mc. In general, each different satellite or space probe project makes use of a different frequency. Unlike other frequency or phase-locked systems, in which the entire receiver is in the feedback loop and hence must be carefully adjusted to optimize the transfer function for each significant change in frequency, the DOPLOC system maintains its basic characteristics throughout the 55- to 970-mc range for which equipment is currently available.

#### AUTOMATIC LOCK-ON

Typical Doppler frequencies resulting from satellite tracking may range from 2 to 14 kc for a carrier frequency of 108 mc. Special techniques are required to search this frequency range, detect the signal buried in noise, adjust the tracking filter VCO to the signal frequency, and lock it in phase with the signal. For slowly varying Doppler frequencies these operations may be accomplished by a human operator. For high rates of change of frequency, rapid, automatic, methods are desirable. A comb filter frequency search device has been developed and used successfully to perform these operations. Selected narrow frequency bands (1 to 50 cps) in the 2- to 14-kc band are tested periodically for presence of signal, and when signal is observed in any such narrow band the tracking filter VCO is shifted electronically to this frequency and locked to it. For the model currently in use, 120 bands are scanned every 1.2 seconds. Most Doppler signals can be acquired in a few scan cycles. A newer automatic lock-on system of this same general type has been developed to permit scanning 1200 bands in the 2- to 14-kc

range in 0.1 second, thus assuring automatic lock-on to any signal which the tracking filter can track.

#### FREQUENCY MEASUREMENT

In a Doppler system the basic measurement is one of frequency, and the accuracy to which frequency can be measured is a direct indication of the figure of merit of the system. The error to be expected in frequency measurements using the tracking filter may be derived from the expression previously given for output phase jitter. The input and output noise to signal voltage ratios are related by

$$\left(\frac{N}{S}\right)_i = \left(\frac{N}{S}\right)_0 \sqrt{\frac{B_i}{B_0}} \quad (3)$$

Substituting in (2),

$$\theta_0 = \frac{1}{\sqrt{2} \left(\frac{S}{N}\right)_0} \quad (4)$$

$\theta_0$  is the rms value of the phase noise on the output of the filter and constitutes the error that will be made in measuring phase at the beginning and at the end of any interval  $T_i$  over which the frequency  $f$  is to be averaged. If the total change of phase of the signal during the interval  $T_i$  is  $\phi = 2\pi f T_i$ , then the rms error in frequency measurement will be

$$\Delta f = \frac{\sqrt{2} \theta_0}{\phi} \times f \quad (5)$$

Substituting for  $\theta$  and  $\phi$

$$\Delta f = \frac{\sqrt{2}}{\sqrt{2} \left(\frac{S}{N}\right)_0} \times \frac{1}{2\pi f T_i} \times f = \frac{1}{2\pi T_i \left(\frac{S}{N}\right)_0} \quad (6)$$

For a typical integration time of 0.5 second and a 12-db output signal-to-noise ratio,  $\Delta f$  is 0.08 cps. This is the rms value of uncertainty of frequency measurement.

Experimental tests have been conducted in an attempt to confirm the validity of (6). The standard deviations of  $\Delta f$  for tracking filter input noise-to-signal ratios of 0, 6, 12, and 24 db were determined and the experimental value of the constant in (6) was derived. The average value of the constant for the four signal-to-noise ratios was found to be 0.157 as compared to the theoretical value of  $\frac{1}{2}\pi = 0.159$ , a discrepancy of approximately one per cent. The values quoted are for the case where  $f = 10$  kc,  $B = 10$  cps, and  $T_i = 0.1$  second. Further tests will be required to evaluate completely the frequency measuring capability of the DOPLOC system, but from these preliminary results it appears that frequency can be measured to within very close limits of theoretically attainable values.

#### DOPLOC RESULTS

The results of hundreds of tracking operations at a frequency of 108 mc have shown that the peak random scat-

ter of individual frequency measurements is about 2.5 cps. In view of the demonstrated ability of the receiving and frequency measuring equipment to measure the frequency of noisy signals with a standard deviation of frequency error considerably smaller than the observed scatter, it appears that the conclusion must be drawn that the observed scatter in frequency is due to perturbations introduced by the propagating medium. Inhomogeneity of the ionosphere is most likely the biggest contributing factor, although antenna phase perturbations caused by gyrations of the satellite in flight also contribute to the total phase noise.

The DOPLOC system has been used extensively in space tracking operations. Starting with the first United States satellite, it has provided precise information on the velocity history of selected portions of the trajectories of all but a very few of the satellites and space probes that have been launched. The inherent high sensitivity of the DOPLOC system to signals of very low energy ( $2 \times 10^{-20}$  watts,  $-197$  dbw or  $0.001 \mu\text{v}$  across  $50$  ohms for  $1$ -cps bandwidth) has permitted the use of conventional low gain, wide coverage antennas to achieve horizon to horizon tracking at ranges in excess of  $25,000$  miles. The system has been found to track properly to within a few decibels of theoretical limits, a characteristic due in large part to the careful design and high stability of the phase-locked tracking filter. Operationally, it has been found to be practical to change bandwidths, over the selectable range of  $1$  to  $50$  cps, in accordance with the information content of the signal, and thus to achieve maximum signal-to-noise ratios.

DOPLOC data have been used in a number of ways. Digital data obtained in real time during the launch phase have been transmitted via double parity check data transmission systems to computing centers for use in establishing the orbit injection parameters. Data from passes of a satellite within line-of-sight of the stations have been similarly used by computing centers for improving the orbit parameters previously determined. More recently, Doppler data from a single pass of a satellite over two stations have

been used to determine completely the orbit parameters. The analytical methods employed in obtaining the orbit are reported by Patton.<sup>3</sup> Patton's method will also yield orbit solutions with data taken from a single Doppler station, and tests of the method using simulated error-free data have demonstrated the feasibility of establishing orbit parameters after only a few minutes of high-speed computer time. The key to successful determination of orbits with real data lies in obtaining data with small values of random and systematic error. Of the injection parameters which define a particular orbit, the velocity parameters are of greatest importance, particularly when only a small segment of the orbit is subject to measurement. Doppler systems thus have distinct advantages over systems which measure position and derive velocity component by differentiating independent position measurements. The DOPLOC system, because of its high resolution and accuracy in velocity measurement, ranks among the best of available satellite trajectory determining systems, and because of its narrow band characteristics, potentially it has the greatest tracking range of any system now in use or contemplated, assuming the same characteristics for other systems.

Over the span of time since the first guided missile was fired in this country, there have been often-repeated predictions that one or more of the more sophisticated radars, interferometers or other tracking systems would replace Doppler systems in precision tracking applications. Far more sophisticated and complex systems now have been developed, and second-generation systems are in the research and development stage. In spite of the technological advancements in these areas, Doppler systems continue to be the choice of many missile system designers for obtaining the most needed information concerning flight performance. There is no indication that contemplated developments in these other fields will replace the Doppler systems which will grow out of systems of the current DOPLOC type.

---

<sup>3</sup> R. B. Patton, Jr., "Orbit determination from single pass Doppler observations," this issue, p. 336.



# Orbit Determination from Single Pass Doppler Observations\*

R. B. PATTON, JR.†

**Summary**—This paper presents a method for determining the orbit of a satellite by observing, in the course of a single pass, the Doppler shift in the frequency of a CW signal transmitted from the ground and reflected by the satellite to one or more ground-based receivers at remote sites. The method is sufficiently general that, with minor modification, it may be applied to any type of satellite or ICBM tracking measurements. The computation consists of improving approximations for initial position and velocity components by successive differential corrections which are obtained from a least squares treatment of an over-determined system of condition equations while imposing elliptic motion as a constraint. Methods for obtaining approximations for the initial position and velocity components are likewise discussed. Results are presented for computations with typical input data.

## INTRODUCTION

BY observing the Doppler shift in a CW signal, an orbit may be determined from a few minutes of data recorded in the course of a single pass of a satellite. It is immaterial whether the source of the signal is an air-borne transmitter in the satellite or ground-based instrumentation. However, while the latter requires a more complex over-all instrumentation system, it both simplifies and increases the reliability of the computing methods which are involved in the data reduction process. The method of solution, which is presented herein, has been developed for a system with a ground-based transmitter, but it may be readily applied to observations from a system in which the signal source is carried in the satellite. Indeed, with minor modification, the method may be applied to any type of satellite or ICBM tracking measurements, since it consists essentially of standard least squares and differential correction techniques.

Inasmuch as it was desired to develop a rapid, as well as reliable, method of determining the orbit of a satellite tracked by a Doppler system employing a minimum of instrumentation, emphasis was initially directed toward the development of a solution for a set of data recorded at a single receiver during a single pass of the satellite. To strengthen the geometry of the system, and therefore the solution, the single receiver requirement was relaxed, but the limitation of single pass measurements was considered essential. This results in a relatively short time interval of observation which in turn permits several simplifying assumptions. First, while the Earth is treated geometrically as an ellipsoid, dynamically it is considered to be spherical. In addition, drag as well as ionospheric and atmospheric refraction

may be neglected without serious loss in accuracy. This reduces the problem to one of determining the six parameters of a Keplerian orbit from data recorded by a Doppler system with a ground-based transmitter. Observations from such a system will be referred to in this paper as passive data, as opposed to active data which would be obtained from a system that included an air-borne transmitter as an integral part of the tracking instrumentation. From a data reduction point of view, there are several distinct advantages in having the transmitter on the Earth's surface. Of primary interest are the following.

- 1) Both the transmitter frequency and drift may be accurately measured if the signal source is ground-based whereas they become additional unknowns for any system that includes an air-borne transmitter. Moreover, they are weakly determined when treated as unknowns in the latter system, and in turn, they seriously degrade the accuracy with which the orbital parameters are determined.
- 2) Measurements by a single receiver are insufficient for a reliable solution when the transmitter is carried by the satellite. On the other hand, single receiver solutions are frequently possible with passive data so that reductions may still be obtained even when several receiving sites of a multi-receiver system may fail to record data.
- 3) Increased reliability is obtained through the complete elimination of air-borne equipment.

## DESCRIPTION OF OBSERVED DATA

In order to arrive at a computing method, it was necessary to consider the various forms in which the data may be recorded. The observations consist of either Doppler frequency or the Doppler period, which may be readily converted to frequency. In the sense in which it is used here, Doppler frequency is defined to be the frequency obtained by beating a local oscillator against the received signal reflected from the satellite and then correcting the output for the bias introduced by the difference in frequency between the transmitter and the local oscillator. If the Doppler frequency is plotted as a function of time, one obtains a curve of the form plotted in Fig. 1(a), usually referred to as an *S* curve. The asymmetry is typical for a system in which the ground-based transmitter and receiver are separated by an appreciable distance and the orbit is not symmetrical with respect to the base line joining the two instrumentation sites. If observations are recorded at

\* Manuscript received by the PGMIL, February 1, 1960.

† U. S. Army Ballistic Res. Labs., Aberdeen Proving Ground, Md.

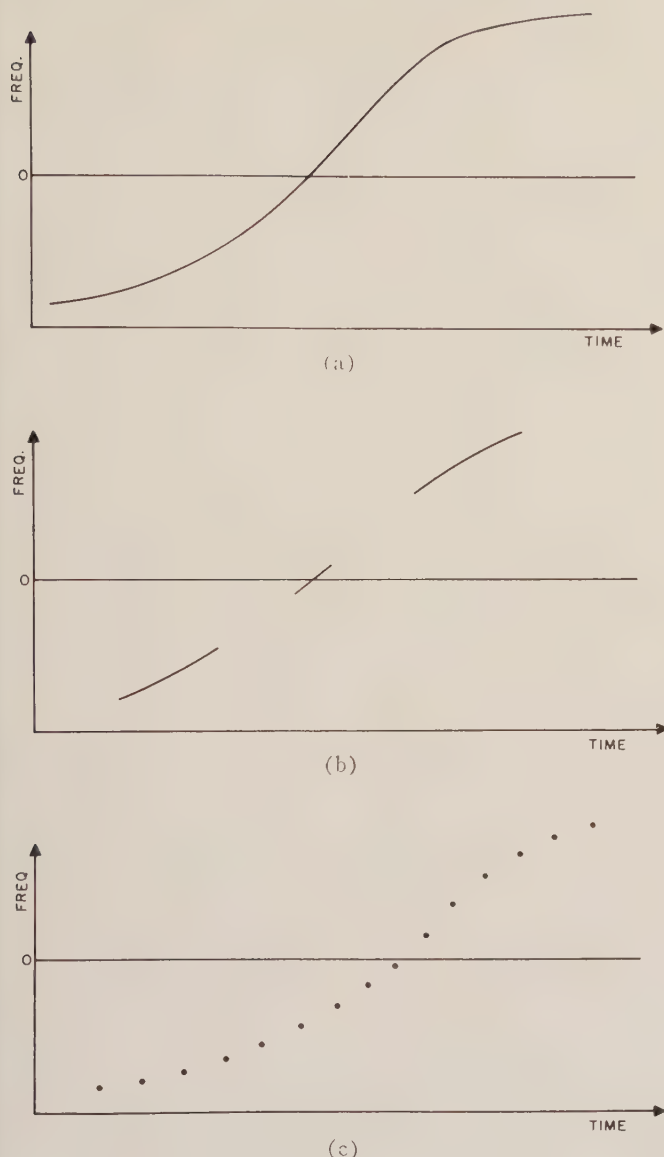


Fig. 1—Doppler frequency-time curves.

frequent intervals, such as one per second, Fig. 1(a) illustrates a typical set of data available for computer input. However, in order to conserve power, it may be necessary to use antenna systems consisting of three narrow, fan-shaped beams which would provide continuous data at intermittent intervals as in Fig. 1(b). A third possibility consists of discrete observations at regular intervals as shown in Fig. 1(c). Such data could be obtained by a system which scanned the sky with a narrow, fan-shaped beam.

Any of these sets of data may be used readily as input for the computing procedure. Whenever possible, this input consists of the total cycle count rather than the Doppler frequency, *i.e.*, the area under the curves or arcs of curves presented in Fig. 1(a) and 1(b). Hence, this method of solution is based, in a sense, upon every

available observation rather than upon a selected few of the total observations (which would be the case if the computing input were limited to a representative number of frequency measurements). Experience has shown this to yield a very significant gain with regard to the accuracy and convergent properties of the solution.

### THE SOLUTION

The method of solution consists of fitting a computed curve to a set of Doppler observations by a least squares technique in which a compatible set of approximations to the six orbital parameters are derived and then improved by repeatedly applying differential corrections until convergence is achieved. Keplerian motion is assumed. The equations of condition are derived from the Taylor expansion about that point which consists of the approximate values of the six orbital parameters. All second and higher order terms of the expansion are neglected. Convergence is greatly dependent upon the set of parameters which are selected to describe the orbit. Not every set of orbital parameters will yield normal equations which are sufficiently independent to permit a solution with this method. It has been found that parameters consisting of position and velocity components for a given time readily yield a convergent solution, whereas a set comprising the semi-major axis, eccentricity, mean anomaly at epoch, inclination, right ascension of the ascending node, and argument of perigee proved to be altogether hopeless.

As stated previously, the observations will consist either of Doppler frequency as a function of time, or period measurements which may be converted to Doppler frequency. The desired computer input, on the other hand, is the total cycle count. When a continuous record of observations is recorded for a substantial period of time, the total cycle count may be obtained by the simple process of summation over time intervals that, in general, will be of several seconds duration. If  $\lambda$  is the wavelength of the radiated signal and  $N_{ij}$  the total number of Doppler cycles resulting at the  $i$ th receiver from the motion of the satellite between times  $t_j$  and  $t_{j+1}$ , it follows that  $v_{ij} \equiv \lambda N_{ij}$  is a measure of the total change in path length from the transmitter to the satellite to the  $i$ th receiver between times  $t_j$  and  $t_{j+1}$ . Let  $g_{ij}$  be defined as the actual change in path length. It follows from Fig. 2 that:

$$g_{ij} = (TS_{j+1} + R_i S_{j+1}) - (TS_j + R_i S_j), \quad (1)$$

where  $T$  is the transmitting site,  $R_i$  the location of the  $i$ th receiver,  $S_{j+1}$  the position of the satellite at time  $t_{j+1}$ , and  $S_j$  the position of the satellite at time  $t_j$ . In the event that the observations consist only of discrete measurements of frequency, the same definitions will apply, but the time interval from  $t_j$  to  $t_{j+1}$  will be limited to one second.



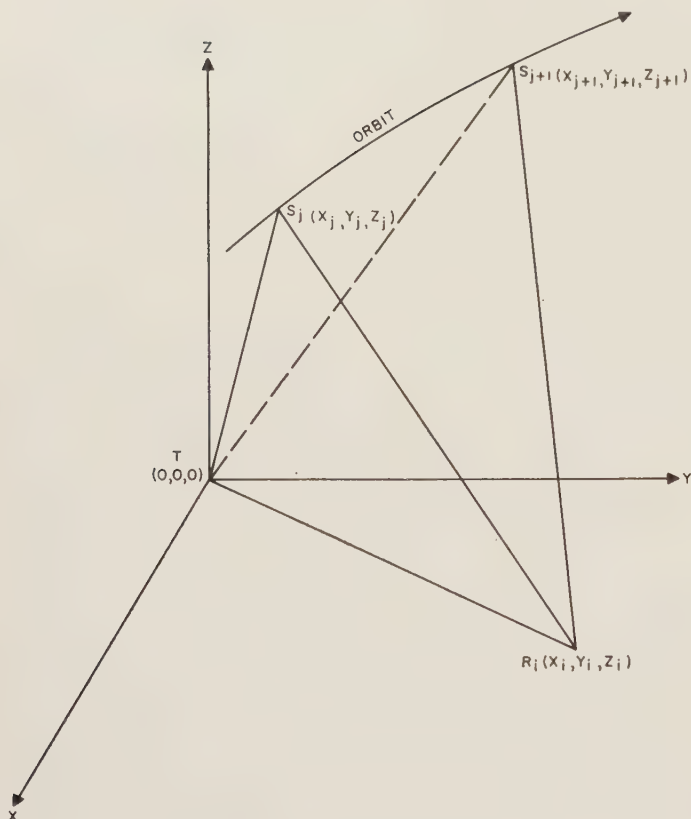


Fig. 2—Problem geometry.

The solution consists of improving a set of position and velocity components which have been approximated for a specific time. The latter will be defined as  $t_0$ , and as a matter of convenience, it is generally taken as the time at which tracking is initiated. Although the location of the coordinate system in which the position and velocity vectors are defined is relatively immaterial from the standpoint of convergence, a system fixed with respect to the Earth's surface does provide two distinct advantages. First, the function  $g_{ij}$  is somewhat simplified since the coordinates of the instrumentation sites remain fixed with respect to time. Of greater significance, however, is the fact that the method may be altered to accept other types of measurements for input by merely changing the definition of the function  $g_{ij}$  and correspondingly, the expressions for its derivatives, with no additional modification to the balance of the procedure which in fact, constitutes the major portion of the computing process.

The set of initial approximations for the position and velocity components are defined for time  $t_0$  as  $(x_0, y_0, z_0, \dot{x}_0, \dot{y}_0, \dot{z}_0)$ . The reference frame is the  $xyz$ -coordinate system which is defined in the following section. If second and higher order terms are omitted from the Taylor expansion about the point  $(x_0, y_0, z_0, \dot{x}_0, \dot{y}_0, \dot{z}_0)$ , the equations of condition may be written in matrix form,

$$\Delta V = J \Delta X, \quad (2)$$

where

$$J \equiv \left( \frac{\partial g_{ij}}{\partial x_0}, \frac{\partial g_{ij}}{\partial y_0}, \frac{\partial g_{ij}}{\partial z_0}, \frac{\partial g_{ij}}{\partial \dot{x}_0}, \frac{\partial g_{ij}}{\partial \dot{y}_0}, \frac{\partial g_{ij}}{\partial \dot{z}_0} \right),$$

$$\Delta V \equiv (\Delta v_{ij}) = (v_{ij} - g_{ij}), \quad (3)$$

$$\Delta X \equiv \begin{bmatrix} \Delta x_0 \\ \Delta y_0 \\ \Delta z_0 \\ \Delta \dot{x}_0 \\ \Delta \dot{y}_0 \\ \Delta \dot{z}_0 \end{bmatrix},$$

for all values of  $i$  and  $j$ . Hence,  $J$  is a matrix of order  $(i \cdot j \times 6)$ ,  $\Delta V$  a matrix of order  $(i \cdot j \times 1)$ , and  $\Delta X$  a matrix of order  $(6 \times 1)$ . Since there are six unknowns, a minimum of six equations are required for a solution. In practice, sufficient data are available to provide an over-determined system, thus permitting the least squares solution,

$$\Delta X = (J^* J)^{-1} J^* \Delta V, \quad (4)$$

where  $J^*$  is the transpose of the Jacobian  $J$ . Finally, improved values for the initial conditions are obtained from

$$X + \Delta X,$$

where

$$X \equiv \begin{bmatrix} x_0 \\ y_0 \\ z_0 \\ \dot{x}_0 \\ \dot{y}_0 \\ \dot{z}_0 \end{bmatrix}.$$

As a matter of convenience, no subscripts were introduced to indicate iteration; but at this point, the improved values of  $X$  are used for the initial point and the process is iterated until convergence is achieved.

#### EVALUATION OF $\Delta V$

Since the function  $g_{ij}$  cannot be expressed readily in terms of  $X$  directly, the evaluation is obtained implicitly. An ephemeris is computed for the assumed values of the position and velocity vectors at time  $t_0$ . Then using (1),  $g_{ij}$  may be evaluated for all values of  $i$  and  $j$ .

In the process of this evaluation, it is expedient to use two rectangular coordinate systems in addition to the Earth-bound system whose origin is at the transmitting site. Referring to Fig. 3, these coordinate systems are defined as follows.

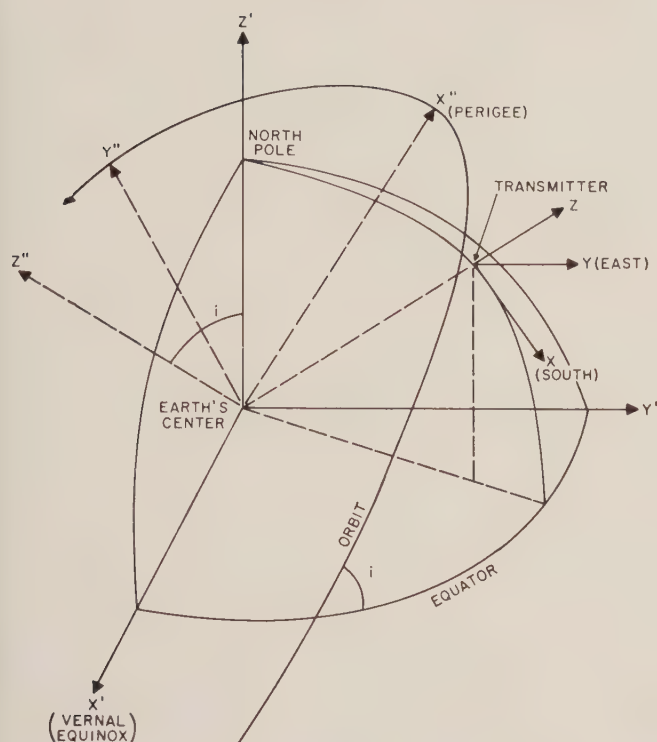


Fig. 3—Coordinate systems.

- 1) The  $xyz$ -coordinate system is a right-hand rectangular system with the origin on the Earth's surface at the transmitter. The  $x$  axis is positive south, the  $y$  axis is positive east and the  $z$  axis is normal to the Earth's surface at the transmitting site.
- 2) The  $x'y'z'$ -coordinate system is a right-hand rectangular system with the origin at the Earth's center. The  $x'$  axis lies in the plane of the equator and is positive in the direction of the vernal equinox, while the positive  $z'$  axis passes through the north pole. The  $y'$  axis is chosen so as to complete a right-hand system.
- 3) The  $x''y''z''$ -coordinate system is likewise a right-hand rectangular system with the origin at the Earth's center. The  $x''y''$  plane lies in the orbital plane of the satellite, with the positive  $x''$  axis in the direction of perigee. The positive  $z''$  axis forms with the positive  $z'$  axis an angle equal to the inclination of the orbital plane to the plane of the equator. The  $y''$  axis is chosen so as to complete a right-hand system.

The first step in this phase of the computation consists of computing values for the initial position and velocity components in the  $x'y'z'$ -coordinate system. This may be achieved by one rotation and one translation which are independent of time, and a second rotation which varies with time. Let the notation  $R_i(\alpha)$  indicate the matrix performing a rotation through an angle  $\alpha$  about the  $i$ th axis of the frame of reference such that the angle is positive when the rotation is in the

right-hand direction and  $i$  is equal to 1, 2, or 3, according to whether the rotation is about the  $x$ ,  $y$ , or  $z$  axis respectively. The desired transformation follows,

$$\begin{pmatrix} x_0' \\ y_0' \\ z_0' \end{pmatrix} = R_3(-\theta_0)R_2(\phi - 90^\circ) \left( \begin{pmatrix} x_0 \\ y_0 \\ z_0 \end{pmatrix} + \begin{pmatrix} \rho_\phi \sin \Delta \\ 0 \\ \rho_\phi \cos \Delta \end{pmatrix} \right), \quad (5)$$

$$\begin{pmatrix} \dot{x}_0' \\ \dot{y}_0' \\ \dot{z}_0' \end{pmatrix} = R_3(-\theta_0)R_2(\phi - 90^\circ) \left( \begin{pmatrix} \dot{x}_0 \\ \dot{y}_0 \\ \dot{z}_0 \end{pmatrix} + R_3(-\theta_0)R_2(\phi - 90^\circ) \begin{pmatrix} \dot{x}_0 \\ \dot{y}_0 \\ \dot{z}_0 \end{pmatrix} \right), \quad (6)$$

where

- $\dot{R}_3(-\theta_0) \equiv$  the time derivative of  $R_3(-\theta_j)$  when  $\theta_j = \theta_0$ ,  
 $\theta_j \equiv$  the right ascension of the transmitting site at time  $t_j$ ,  
 $\phi \equiv$  the geodetic latitude of the transmitting site,  
 $\rho_\phi \equiv$  the radius vector from the Earth's center to a point on the Earth's sea level surface at the latitude  $\phi$ ,  
 $\Delta \equiv$  the difference between the geodetic and geocentric latitudes at the transmitting site.

The next step in the computation involves the evaluation of the following orbital parameters:

- $a \equiv$  semi-major axis,  
 $e \equiv$  eccentricity,  
 $\sigma \equiv$  mean anomaly at epoch,  
 $i \equiv$  inclination,  
 $\Omega \equiv$  right ascension of the ascending node,  
 $\omega \equiv$  argument of perigee.

The evaluation of these orbital parameters is obtained from the following equations:<sup>1</sup>

$$r_0 = \sqrt{(x_0')^2 + (y_0')^2 + (z_0')^2}, \quad (7)$$

$$v_0 = \sqrt{(\dot{x}_0')^2 + (\dot{y}_0')^2 + (\dot{z}_0')^2}, \quad (8)$$

$$r_0 \dot{r}_0 = x_0' \dot{x}_0' + y_0' \dot{y}_0' + z_0' \dot{z}_0', \quad (9)$$

$$\mu = gR^2,$$

<sup>1</sup> Derived by Dr. B. Garfinkel, Ballistic Res. Labs., Aberdeen Proving Ground, Md.



where  $g$  is the mean gravitational constant and  $R$  is the radius of the Earth, which is assumed to be spherical in the development of the equations,

$$a = \frac{\mu r_0}{2\mu - r_0 v_0^2}, \quad (10)$$

$$e = \left| \frac{(r_0 \dot{r}_0)^2}{\mu a} + \left(1 - \frac{r_0}{a}\right)^2 \right|^{1/2}, \quad (11)$$

$$E_0 = \tan^{-1} \left\{ \frac{r_0 \dot{r}_0}{\sqrt{\mu a} \left(1 - \frac{r_0}{a}\right)} \right\} + \frac{\pi}{2} \left\{ 1 - \operatorname{sgn} \left(1 - \frac{r_0}{a}\right) \right\}, \quad (12)$$

where

$$\operatorname{sgn} \left(1 - \frac{r_0}{a}\right) \equiv 1 \quad \text{if} \quad \left(1 - \frac{r_0}{a}\right) > 0,$$

$$\operatorname{sgn} \left(1 - \frac{r_0}{a}\right) \equiv -1 \quad \text{if} \quad \left(1 - \frac{r_0}{a}\right) < 0,$$

$$n = \sqrt{\frac{\mu}{a^3}}, \quad (13)$$

$$\sigma = E_0 - e \sin E_0 - n t_0, \quad (14)$$

$$\dot{r}_1 = y_0' \dot{z}_0' - z_0' \dot{y}_0', \quad (15)$$

$$\dot{r}_2 = z_0' \dot{x}_0' - x_0' \dot{z}_0', \quad (16)$$

$$h_3 = x_0' \dot{y}_0' - y_0' \dot{x}_0', \quad (17)$$

$$h = \sqrt{h_1^2 + h_2^2 + h_3^2}, \quad (18)$$

$$k_1 = \frac{h_1}{h}, \quad (19)$$

$$k_2 = \frac{h_2}{h}, \quad (20)$$

$$k_3 = \frac{h_3}{h}, \quad (21)$$

$$T = \sqrt{h_1^2 + h_2^2}, \quad (22)$$

$$N_1 = -\frac{h_2}{T}, \quad (23)$$

$$N_2 = \frac{h_1}{T}, \quad (24)$$

$$\dot{r}_i = \cos^{-1} k_3, \quad \text{where} \quad 0 \leq i \leq \pi, \quad (25)$$

$$\bar{x} = a(\cos E_0 - e), \quad (26)$$

$$\bar{y} = a(\sin E_0) \sqrt{1 - e^2}, \quad (27)$$

$$r_0 \cdot N = x_0' N_1 + y_0' N_2, \quad (28)$$

$$r_0 \times k \cdot N = N_1(y_0' k_3 - z_0' k_2) + N_2(z_0' k_1 - x_0' k_3), \quad (29)$$

$$\omega = (-1)^p \cos^{-1} \left\{ \frac{\bar{x}(r_0 \cdot N) + \bar{y}(r_0 \times k \cdot N)}{r_0^2} \right\}, \quad (30)$$

where

$$p = \left\{ \frac{1 - \operatorname{sgn} [\bar{x} z_0' + \bar{y}(x_0' k_2 - y_0' k_1)]}{2} \right\}, \quad (31)$$

$$\Omega = (-1)^q \cos^{-1} N_1,$$

where

$$q = \left\{ \frac{1 - \operatorname{sgn} N_2}{2} \right\}.$$

Having obtained values for  $a$ ,  $e$ ,  $\sigma$ ,  $i$ ,  $\Omega$ , and  $\omega$ ,  $g_{ij}$  may be evaluated for each time of observation. The first step in the computing procedure consists of solving for the eccentric anomaly  $E_j$  in Kepler's equation,

$$E_j - e \sin E_j = n t_j + \sigma. \quad (32)$$

The position of the satellite as a function of time is determined in the  $x''y''z''$ -coordinate system.

$$f_j = 2 \tan^{-1} \left[ \sqrt{\frac{1+e}{1-e}} \tan \left( \frac{E_j}{2} \right) \right]; \quad (33)$$

$$r_j = a(1 - e \cos E_j); \quad (34)$$

$$x_j'' = r_j \cos f_j; \quad (35)$$

$$y_j'' = r_j \sin f_j. \quad (36)$$

$z_j''$  is zero according to the definition of the  $x''y''z''$ -coordinate system. A transformation to the  $x'y'z'$  coordinates can be achieved by three rotations as follows:

$$\begin{bmatrix} x_j' \\ y_j' \\ z_j' \end{bmatrix} = R_3(-\Omega) R_1(-i) R_3(-\omega) \begin{bmatrix} x_j'' \\ y_j'' \\ 0 \end{bmatrix}. \quad (37)$$

Finally the position in the  $xyz$ -coordinate system may be obtained by two additional rotations and a translation.

$$\begin{bmatrix} x_j \\ y_j \\ z_j \end{bmatrix} = R_2(90^\circ - \phi) R_3(\theta_j) \begin{bmatrix} x_j' \\ y_j' \\ z_j' \end{bmatrix} - \begin{bmatrix} \rho_\phi \sin \Delta \\ 0 \\ \rho_\phi \cos \Delta \end{bmatrix}. \quad (38)$$

Referring to (1),  $g_{ij}$  may be then expressed in terms of the satellite's positions at time  $t_j$  and  $t_{j+1}$ .

$$g_{ij} = \sqrt{x_{j+1}^2 + y_{j+1}^2 + z_{j+1}^2} + \sqrt{(x_{j+1} - x_i)^2 + (y_{j+1} - y_i)^2 + (z_{j+1} - z_i)^2} - \sqrt{x_j^2 + y_j^2 + z_j^2} - \sqrt{(x_j - x_i)^2 + (y_j - y_i)^2 + (z_j - z_i)^2}, \quad (39)$$

where  $(x_i, y_i, z_i)$  is the surveyed position of the  $i$ th receiver. Finally, the residuals  $\Delta v_{ij}$  may be determined from

$$\Delta v_{ij} = v_{ij} - g_{ij}. \quad (40)$$

### EVALUATION OF $J$

Having evaluated the vector  $\Delta V$ , there remains the problem of determining the Jacobian  $J$ . The necessary differentiation may be carried out numerically, but the computing time will be reduced and the accuracy increased if the derivatives are evaluated from analytical expressions. Recalling that for all values of  $i$  and  $j$ ,

$$J \equiv J \begin{pmatrix} g_{10}, \dots, g_{ij}, \dots \\ x_0, y_0, z_0, \dot{x}_0, \dot{y}_0, \dot{z}_0 \end{pmatrix},$$

let

$$J = J_1 J_2 J_3 J_4,$$

where

$$J_1 \equiv \begin{pmatrix} g_{10}, \dots, g_{ij}, \dots \\ x_{j+1}, y_{j+1}, z_{j+1}, x_j, y_j, z_j \end{pmatrix}, \quad (41)$$

$$J_2 \equiv \begin{pmatrix} x_{j+1}, y_{j+1}, z_{j+1}, x_j, y_j, z_j \\ a, e, \sigma, \omega, \Omega, i \end{pmatrix}, \quad (42)$$

$$J_3 \equiv \begin{pmatrix} a, e, \sigma, \omega, \Omega, i \\ x'_0, y'_0, z'_0, \dot{x}'_0, \dot{y}'_0, \dot{z}'_0 \end{pmatrix}, \quad (43)$$

$$J_4 \equiv \begin{pmatrix} x'_0, y'_0, z'_0, \dot{x}'_0, \dot{y}'_0, \dot{z}'_0 \\ x_0, y_0, z_0, \dot{x}_0, \dot{y}_0, \dot{z}_0 \end{pmatrix}. \quad (44)$$

The orders of the above matrices are ( $i \cdot j \times 6$ ) for  $J_1$ , and ( $6 \times 6$ ) for  $J_2$ ,  $J_3$ , and  $J_4$ . A distinct advantage of this method of evaluating  $J$  results from the fact that the function  $g_{ij}$  appears only in  $J_1$ . Hence, if the solution is applied to other types of measurements, only  $J_1$  needs revision for the appropriate evaluation of  $J$ . This is trivial compared to the effort required to derive the derivatives contained in  $J_2$  and  $J_3$ . The expressions for many of the elements of these Jacobian matrices are rather long and involved, and therefore will not be presented here, but the complete results are reported in [1].

### INITIAL APPROXIMATIONS

Of primary importance to the success of the method that has been presented, is the capability of establishing a compatible set of initial approximations which are sufficiently close to the actual values to permit convergence of the computing process. It has been determined that the computation will converge with input consisting of data from a single receiver system, if the base line from the transmitter to the receiver is not excessively short, and the initial approximation to  $(x_0, y_0, z_0, \dot{x}_0, \dot{y}_0, \dot{z}_0)$  is moderately accurate. For example, with base lines of the order of 400 miles and either continuous or intermittent observations over time intervals of approximately five minutes, convergence may reasonably be expected when the error in each coordinate of the initial estimate is not in excess of 50 to 75 miles and the velocity components are correct to within  $\frac{1}{2}$  to 1 mile per second. For a two-receiver system, on the other hand, an accuracy of 150 to 200 miles in each coordinate and 1 to 2 miles per

second in each velocity component has been found sufficient to secure convergence. The computing process has occasionally converged with larger initial errors, but the figures presented are intended to specify limits within which convergence may reasonably be assured.

Clearly, a supporting computation to furnish moderately accurate initial approximations is essential to the successful application of the computing method. Several approaches to this phase of the problem have been considered, but one in particular is preferred. It involves using an analog computer to fit a computed curve to an observed Doppler frequency-time curve. In the fitting procedure, the boundary values of a second-order differential equation are systematically varied until the computed  $S$  curve matches the observed  $S$  curve. The differential equation has been derived on the basis of a circular orbit and a nonrotating Earth. The initial approximations for the position and velocity components, which serve as input for the primary computation, are then computed from the results obtained by the curve fitting procedure. A variation of this method consists of plotting a frequency-time curve for the observed data and then matching this to the appropriate member of a large family of  $S$  curves previously computed for various circular orbits. Both methods have been successfully employed.

The following definitions will be useful in the derivation of the differential equation used in the fitting procedure.

$R_T$   $\equiv$  the radius vector from the Earth's center to the transmitting site.

$r_j$   $\equiv$  the radius vector from the Earth's center to the position of the satellite at time  $t_j$ .

$\beta_j$   $\equiv$  the angle between  $R_T$  and  $r_j$ .

$(x_T'', y_T'', z_T'')$   $\equiv$  the position of the transmitting site.

$(x_j'', y_j'', 0)$   $\equiv$  the position of the satellite at time  $t_j$ .

$\rho_j$   $\equiv$  the distance from the transmitting site to the satellite at time  $t_j$ .

$\rho_{ij}$   $\equiv$  the distance from the  $i$ th receiver to the satellite at time  $t_j$ .

$H$   $\equiv$  the altitude of the satellite above the Earth's surface.

$v$   $\equiv$  the velocity of the satellite.

To simplify the problem, certain assumptions have been made:

- 1) the satellite moves in a circular Keplerian orbit,
- 2)  $\beta_j$  is relatively small throughout the period of observation,
- 3) the Earth is not rotating.

A number of useful relationships may be derived as a result of these assumptions.

$$|r_j| = r = R + H,$$

where  $H$  is constant.



$$v = nr = \sqrt{(\dot{x}_j'')^2 + (\dot{y}_j'')^2}$$

$$\left( \frac{R}{R+H} \right) = \left( \frac{Rv^2}{\mu} \right)$$

$$\ddot{x}_j'' = -n^2 x_j''; \quad \ddot{y}_j'' = -n^2 y_j''$$

$$\cos \beta_j \approx 1.$$

$$R_T = \text{constant}.$$

The reference frame for this derivation is the  $x''y''z''$ -coordinate system which has been defined previously. It follows from the definition of  $\rho_j$  that

$$\rho_j = \sqrt{(\dot{x}_j'' - x_T'')^2 + (\dot{y}_j'' - y_T'')^2 + (\dot{z}_T'')^2}. \quad (45)$$

Differentiating twice with respect to time yields

$$\dot{\rho}_j^2 + \rho_j \ddot{\rho}_j = (\dot{x}_j'')^2 + (\dot{y}_j'')^2 + \ddot{x}_j''(x_j'' - x_T'') + \ddot{y}_j''(y_j'' - y_T''), \quad (46)$$

which may be simplified to

$$\begin{aligned} \dot{\rho}_j^2 + \rho_j \ddot{\rho}_j &= v^2 - n^2(r^2 - x_j''x_T'' - y_j''y_T''), \\ &= n^2(R_T \cdot r_j), \\ &= n^2 r R \cos \beta, \\ &= v^2 \left( \frac{R}{R+H} \right) \cos \beta, \\ &= \frac{Rv^4}{\mu} \cos \beta, \\ &\approx \frac{Rv^4}{\mu}. \end{aligned}$$

It follows that

$$\ddot{\rho}_j \approx \frac{\frac{Rv^4}{\mu} - \dot{\rho}_j^2}{\rho_j}. \quad (47)$$

A similar expression may be derived for  $\ddot{\rho}_{ij}$ . Recalling the definition for  $g_{ij}$ , we conclude that

$$\ddot{g}_{ij} \approx \frac{A - \dot{\rho}_j^2}{\rho_j} + \frac{A - \dot{\rho}_{ij}^2}{\rho_{ij}}, \quad (48)$$

where

$$A = \frac{Rv^4}{\mu}.$$

The initial step in the fitting process on the analog computer consists of approximating  $A$ ,  $\rho_0$ ,  $\rho_{i0}$ ,  $\dot{\rho}_0$ , and  $\dot{\rho}_{i0}$ , then computing and plotting that curve for  $\ddot{g}_{ij}$ , which satisfies (48) while observing the constraints  $\ddot{g}_{i0} = \ddot{v}_{i0}$  and  $\dot{g}_{i0} = \dot{v}_{i0}$ . The five parameters are adjusted systematically until a sufficiently good fit is obtained. The final value for  $A$  may be used to determine the velocity from which the altitude may be estimated on the basis of a circular orbit, but this has not been particularly successful for highly eccentric orbits. The preferred procedure is to assume that  $\dot{z}_0 = 0$  and  $z_0 = \bar{z}$ ,

where  $\bar{z}$  is an estimate of the altitude based on experience. The former is always an adequate approximation while the latter may usually be estimated to within 100 to 200 miles by merely observing the general characteristics of the  $S$  curve. In the event that the original estimate of  $z_0$  proves to be so poor that it prevents convergence, a series of values for  $\bar{z}$  may be tried without becoming involved in excessive computation. Estimates for  $x_0$  and  $y_0$  are obtained by solving the equations

$$\begin{cases} x_0^2 + y_0^2 + \bar{z}^2 = \rho_0^2, \\ (x_0 - x_i)^2 + (y_0 - y_i)^2 + (\bar{z} - z_i)^2 = \rho_{i0}^2. \end{cases} \quad (49)$$

Differentiating  $\rho_j$  and  $\rho_{ij}$  with respect to time yields, for  $j=0$  and  $\dot{z}_0=0$ ,

$$\begin{cases} x_0 \dot{x}_0 + y_0 \dot{y}_0 = \rho_0 \dot{\rho}_0, \\ (x_0 - x_i) \dot{x}_0 + (y_0 - y_i) \dot{y}_0 = \rho_{i0} \dot{\rho}_{i0}, \end{cases} \quad (50)$$

which may be solved for  $\dot{x}_0$  and  $\dot{y}_0$ . This completes the computing procedure for the desired set of initial approximations.

#### COMPUTATIONAL RESULTS

Numerous convergent solutions have been obtained with both simulated and actual field data serving as computer input. Since the latter are of major interest, the discussion will be restricted to results obtained from real data. This method of solution was developed specifically for the DOPLOC system, which is reported upon by deBey.<sup>2</sup> The interim version of this Doppler system complex consists of a 50-kw continuous wave illuminator transmitter station located at Fort Sill, Okla., and two DOPLOC receiving stations, one at White Sands Missile Range (WSMR) and a second at Forrest City, Ark. To conserve power, the antenna system has been limited to three narrow, fan-shaped beams which provide continuous data at intermittent intervals as illustrated in Fig. 1(b). The present results were obtained from observations which were recorded during a period when the WSMR receiver was inoperable and, therefore, are derived from data recorded by a single receiver in the course of a single pass over the instrumentation site. Included with the DOPLOC results are orbital parameters which were determined and published by the National Space Surveillance Control Center (Space Track). As an aid in comparing the two sets of determinations, the Space Track parameters have been converted to the epoch times of the DOPLOC reductions.

The initial successful solution with field data from the DOPLOC system was achieved for Revolution 9937 of Sputnik III. Measurements were recorded for 28 seconds in the south antenna beam of the system, 7 seconds in the center beam, and 12 seconds in the north beam,

<sup>2</sup> L. G. deBey, "Tracking in space by DOPLOC," this issue, p. 332.

with two gaps in the data of 75 seconds each. Thus, observations were recorded for a total of 47 seconds within a time interval of 3 minutes and 17 seconds. On the first pass through the computing machine, the computation converged in three iterations to initial position and velocity components that were equivalent to the following orbital parameters:

$$\begin{aligned}a &= 4149 \text{ miles,} \\e &= 0.0153, \\\sigma &= 288.04^\circ, \\i &= 65.37^\circ, \\\Omega &= 178.24^\circ, \\\omega &= 104.62^\circ.\end{aligned}$$

For comparison, the orbital parameters reported in Space Track Bulletin No. 230 for 1958 Delta II (Sputnik III) were used to compute the value of the parameters for the same epoch time as that of the solution. The results are as follows:

$$\begin{aligned}a &= 4111 \text{ miles,} \\e &= 0.0130, \\\sigma &= 257.78^\circ, \\i &= 65.06^\circ, \\\Omega &= 178.22^\circ, \\\omega &= 137.95^\circ.\end{aligned}$$

In comparing the DOPLOC and Space Track solutions, it will be noted that there is reasonably good

agreement in the values for  $a$ ,  $e$ ,  $i$ , and  $\Omega$ , particularly for the latter two. This is characteristic of the single-pass solution when the eccentricity is small and the computational input is limited to Doppler frequency. Since the orbit is almost circular,  $\sigma$  and  $\omega$  are less significant than the other parameters and likewise, are more difficult for either system to determine accurately. However, as a result of the small eccentricity, the sum of  $\omega$  and  $\sigma$  is a rather good approximation to the angular distance along the orbit from the nodal point to the position of the satellite at epoch time and as such, provides a basis of comparison between the two systems. In the DOPLOC solution,  $(\omega + \sigma) = 32.66^\circ$  while the Space Track determination yields a value of  $35.73^\circ$ , a difference of  $3.07^\circ$  between the two sets of results. To summarize, when limited to single-pass, single-receiver observations, the DOPLOC system provides an excellent determination of the orientation of the orbital plane, a good determination of the shape of the orbit, and a fair-to-poor determination of the orientation of the ellipse within the orbital plane.

Occasionally, excellent results have been obtained for both  $\sigma$  and  $\omega$ ; but in general, the interim DOPLOC system with its present limitations fails to provide consistently good evaluations of these two quantities. Therefore, in presenting the remaining DOPLOC reductions,  $\sigma$  and  $\omega$  have been eliminated from further consideration. Results have been indicated in Table I for six revolutions of Discoverer XI, including number 172 which was the last known revolution of this satellite. As a matter of interest, the position determined by the

TABLE I  
COMPARISON OF DOPLOC AND SPACE TRACK RESULTS FOR DISCOVERER XI

	Revolution Number	$a$ (miles)	$e$	$i$ (degrees)	$\Omega$ (degrees)	Total Amount of Data (seconds)	Interval of Observation (seconds)
DOPLOC	30	4186	0.0295	80.15	215.92	35	123
Space Track		4189	0.0291	80.01	215.84		
Difference		-3	0.0004	0.14	0.08		
DOPLOC	124	4115	0.0198	80.31	207.50	44	138
Space Track		4135	0.0203	80.10	207.27		
Difference		-20	-0.0005	0.21	0.23		
DOPLOC	140	4138	0.0198	80.44	205.22	55	141
Space Track		4121	0.0178	80.10	205.78		
Difference		17	0.0020	0.34	-0.56		
DOPLOC	156	4143	0.0300	80.79	204.50	25	117
Space Track		4108	0.0148	80.10	204.30		
Difference		35	0.0152	0.69	0.20		
DOPLOC	165	4037	0.0111	79.99	203.63	49	165
Space Track		4099	0.0128	80.10	203.50		
Difference		-62	-0.0017	-0.11	0.13		
DOPLOC	172	4093	0.0189	80.44	203.18	35	90
Space Track		4091	0.0111	80.10	202.84		
Difference		2	0.0078	0.34	0.34		



interim DOPLOC system for this pass indicated an altitude of 82 miles as the satellite crossed the base line 55 miles west of Forrest City. To provide a basis for evaluation of the DOPLOC results, orbital parameters, obtained by converting Space Track determinations to the appropriate epoch times, have been included in the table. Table I also contains a listing of the amount of data available for each reduction in addition to the total time interval within which the observations were collected.

#### CONCLUSION

This method of solution has been shown to be both practical and useful by numerous successful applications with real as well as simulated data. Although results have been presented for passive data only, the computing procedure has been altered slightly and applied to active data with considerable success. Computing times are reasonable since convergent solutions have required from 20 to 40 minutes on the ORDVAC with the coding in floating decimal, whereas more modern machines would perform the same computation in 2 to 4 minutes. This method allows the determination of a relatively accurate set of orbital parameters with as little as 1.5 to 3 minutes of intermittent observations from a single receiver when the signal source is a ground-based transmitter. While multi-receiver systems provide numerous distinct advantages, it has been shown that it is possible to obtain, routinely, quite satisfactory results with observations from a single receiver.

It should be emphasized that solutions have been ob-

tained for actual field data, and further that such solutions were completely independent of other measuring systems. Results from the latter were used only for comparison and did not enter any phase of the computations leading to these solutions.

In conclusion, the method is general and therefore, need not be confined to either Doppler observations or Keplerian orbits. For more complex orbits, it may be desirable to replace analytical with numerical differentiation and it will, of course, be necessary to modify the computation for the ephemeris; otherwise the solution will be fundamentally the same. Insofar as the use of other types of observations are concerned, only  $J_1$  and  $g_{ij}$  need be modified to allow the method to be applied to observations from any satellite or ICBM tracking system, provided the limitation of Keplerian orbits is retained.

#### ACKNOWLEDGMENT

The author is indebted to Dr. Boris Garfinkel for many helpful suggestions.

#### BIBLIOGRAPHY

- [1] R. B. Patton, Jr., "A Method of Solution for the Determination of Satellite Orbital Parameters from DOPLOC Measurements," Ballistic Res. Labs., Aberdeen Proving Ground, Md., Memo. Rept. No. 1237; September, 1959.
- [2] W. H. Guier and G. C. Weiffenbach, "Theoretical Analysis of Doppler Radio Signals from Earth Satellites," Appl. Phys. Lab., Silver Spring, Md., Bumblebee Rept. No. 276; April, 1958.
- [3] R. C. Davis, "Techniques for the Statistical Analysis of Continuous-Wave Doppler Data," U. S. Naval Ord. Test Station, China Lake, Calif., NAVORD Rept. 1312; April, 1951.
- [4] F. R. Moulton, "An Introduction to Celestial Mechanics," Macmillan & Co., Ltd., New York, N. Y.; 1902.

# Comparison of Precalculated Orbital Elements of the Army Explorer Satellites with the Actual Elements Derived from Observations\*

H. G. L. KRAUSE† AND R. N. DEWITT†

**Summary**—Based on precalculated data for the position and velocity vector of the injection points for the Explorers I through V, orbital elements are derived and compared with the actual orbital elements at injection time, calculated from position and velocity data obtained from radar measurements. Calculations are also made for the different orbital periods of a satellite perturbed by the Earth's oblateness. For Explorer I, it is shown that the actual orbital elements derived from tracking observations agree well with the actual elements derived from early astronomical observations.

## INTRODUCTION

THE PURPOSE of this paper is to present a method for obtaining a complete set of precalculated and observed injection point data of artificial earth satellites from available flight trajectory calculations and evaluation of radar determined trajectory data; and, further, to show the determination of the orbital elements of artificial earth satellites from the space-fixed injection point data. This general method is numerically applied to the five Army satellites of type "Explorer," which were put into orbit by booster missiles of the Juno I family, namely, modified Redstone missiles of the Army Ballistic Missile Agency (ABMA), Redstone Arsenal, Huntsville, Ala. The senior author of this paper used this method to precalculate orbital elements for Explorer I shortly before it was launched.

## GENERAL THEORY

A multistage rocket booster, carrying a small satellite, is fired at lift-off time  $t_0$  from the launching pad  $L$  (with its coordinates  $r_0, \phi_0, \lambda_0$ ) in a direction with an azimuth angle  $\chi_0$ . Usually there are given the geodetic (geographical) latitude  $\phi_0$ , the geographic longitude  $\lambda_0$ , and the altitude  $y_0$  of the launching pad. Taking as best values for the equatorial radius  $a_e$  and the flattening (oblateness)  $f$  of the earth,

$$a_e = 6378150 \pm 70 \text{ m}; \quad 1/f = 298.2 \pm 0.2,$$

(corresponding to the selected data  $a_e = 6378270 \pm 70 \text{ m}$ ;  $1/f = 297.0 \pm 1.2$  according to Herrick, Baker, and Hilton<sup>1</sup>) then it follows for the square of the eccentricity of the Earth's meridian ellipse that

$$e_e^2 = \frac{a_e^2 - c_e^2}{a_e^2} = f(2 - f) = 0.006\,695\,662\,46,$$

and for the polar radius,

$$c_e = a_e \sqrt{1 - e_e^2} = a_e(1 - f) = 6356\,761.161 \text{ m}.$$

The geocentric latitude  $\phi$  can now be obtained from the geodetic one by means of the accurate relation,

$$\tan \phi = (1 - e_e^2) \tan \varphi \equiv (1 - f)^2 \tan \varphi \quad (1)$$

or from the series development

$$\phi - \varphi = -m \sin 2\varphi + \frac{m^2}{2} \sin 4\varphi - \frac{m^3}{3} \sin 6\varphi \pm \dots \quad (1a)$$

where

$$m = \frac{e_e^2}{2 - e_e^2} = 0.003\,359\,076\,852.$$

The Earth's radius is then obtained from

$$R = a_e \sqrt{\frac{1 - e_e^2(2 - e_e^2) \sin^2 \varphi}{1 - e_e^2 \sin^2 \varphi}} = \frac{c_e}{\sqrt{1 - e_e^2 \cos^2 \phi}}, \quad (2)$$

or the power series development

$$\begin{aligned} \frac{R}{c_e} &= 1 + \frac{e_e^2}{2} \cos^2 \phi + \frac{3}{2} \left( \frac{e_e^2}{2} \cos^2 \phi \right)^2 \\ &+ \frac{5}{2} \left( \frac{e_e^2}{2} \cos^2 \phi \right)^3 + \dots \end{aligned} \quad (2a)$$

The radius vector is then  $r = R + y$ .

By integration of the equations of motion for the different rocket stages or by evaluation of radar measurements, the following data are obtained for the burn-out point  $B$  (or the cut-off point, if complete control is possible) of the last stage, which is the injection point for the orbit of the satellite, namely the flight time  $t_i - t_0$ , the velocity  $v_i$ , the flight path angle  $\theta_i$  (with respect to the local vertical), the altitude  $y_i$  and the ground range  $x_i$  measured along the curved Earth's surface from the launching pad  $L$  to the sub-injection point  $B'$ . It is not the task of this paper to show how actual injection point data can be found from evaluation of radar measurements or how predicted injection point data are obtained by integration of the equations of motion for the satellite boosters.

Having these data now available from flight evaluation reports, it is necessary to derive the complete position vector of the injection point, namely,  $r_i = R_i + y_i$ ,  $\phi_i, \lambda_i$ , and also the velocity azimuth angle  $\chi_i$ , the angle which the velocity vector makes with the local meridian. Making an estimate for the geocentric latitude  $\phi_i$  of the

\* Manuscript received by the PGMIL, February 1, 1960.

† Future Projects Design Branch, Structures and Mechanics Lab., U. S. Army Ballistic Missile Agency, Redstone Arsenal, Ala.

<sup>1</sup> S. Herrick, R. M. L. Baker, Jr. and C. G. Hilton, "Gravitational and Related Constants for Accurate Space Navigation," American Rocket Society Preprint No. 497-57, III+63 pp., October, 1957. Also *Proc. Eighth International Astronautical Congress*, Barcelona, Spain; October 6-12, 1957.





$$\begin{cases} v_r^* = v_i^* \cos \theta_i^* & = v_i \cos \theta_i \\ v_\chi^* = v_i^* \sin \theta_i^* \sin \chi_i^* & = v_i \sin \theta_i \sin \chi_i + \Omega r_i \cos \phi_i, \\ v_\phi^* = v_i^* \sin \theta_i^* \cos \chi_i^* & = v_i \sin \theta_i \cos \chi_i \end{cases} \quad (9)$$

or transformed,

$$\begin{cases} v_i^* \cos \theta_i^* & = v_i \cos \theta_i \\ v_i^* \sin \theta_i^* \cos (\chi_i^* - \chi_i) & = v_i \sin \theta_i + \Omega r_i \cos \phi_i \sin \chi_i, \\ v_i^* \sin \theta_i^* \sin (\chi_i^* - \chi_i) & = \Omega r_i \cos \phi_i \cos \chi_i. \end{cases} \quad (10)$$

From these relations, the following equations can be derived:

$$\begin{cases} v_i^* \sin \theta_i^* = \sqrt{(v_i \sin \theta_i)^2 + \Omega r_i \cos \phi_i (2v_i \sin \theta_i \sin \chi_i + \Omega r_i \cos \phi_i)} \\ v_i^* & = \sqrt{v_i^2 + \Omega r_i \cos \phi_i (2v_i \sin \theta_i \sin \chi_i + \Omega r_i \cos \phi_i)} \end{cases} \quad (11)$$

$$\begin{cases} \cos \theta_i^* = \frac{\cos \theta_i}{v_i^*/v_i} = \frac{\cos \theta_i}{\sqrt{1 + \frac{\Omega r_i \cos \phi_i}{v_i^2} (2v_i \sin \theta_i \sin \chi_i + \Omega r_i \cos \phi_i)}} \\ \tan \theta_i^* = \tan \theta_i \left( \frac{v_i^* \sin \theta_i^*}{v_i \sin \theta_i} \right) = \tan \theta_i \sqrt{1 + \frac{\Omega r_i \cos \phi_i}{(v_i \sin \theta_i)^2} (2v_i \sin \theta_i \sin \chi_i + \Omega r_i \cos \phi_i)}, \end{cases} \quad (12)$$

$$\begin{cases} \tan \chi_i^* = \tan \chi_i + \frac{\Omega r_i \cos \phi_i}{v_i \sin \theta_i \cos \chi_i} = \tan \chi_i \left[ 1 + \frac{\Omega r_i \cos \phi_i}{v_i \sin \theta_i \sin \chi_i} \right] \\ \cot (\chi_i^* - \chi_i) = \tan \chi_i + \frac{v_i \sin \theta_i}{\Omega r_i \cos \phi_i \cos \chi_i} = \tan \chi_i \left[ 1 + \frac{v_i \sin \theta_i}{\Omega r_i \cos \phi_i \sin \chi_i} \right]. \end{cases} \quad (13)$$

Most of these relations were already given by Krause, *et al.*<sup>3</sup> The simplest way for numerical calculations seems to be the following system:

$$\begin{aligned} v_i^*/v_i &= \sqrt{1 + \left( \frac{\Omega r_i \cos \phi_i}{v_i} \right)^2 \cdot \left( \frac{2}{A} + 1 \right)} \\ \cos \theta_i^* &= \frac{\cos \theta_i}{v_i^*/v_i} \\ \tan \chi_i^* &= \tan \chi_i [1 + A], \end{aligned} \quad (14)$$

where

$$A = \frac{\Omega r_i \cos \phi_i}{v_i \sin \theta_i \sin \chi_i}. \quad (15)$$

Having now the space-fixed velocity vector ( $v_i^*$ ,  $\theta_i^*$ ,  $\chi_i^*$ ), we need the space-fixed position vector ( $v_i$ ,  $\alpha_i$ ,  $\delta_i$ ), where  $\alpha_i$  is the right ascension and  $\delta_i$  the declination of the satellite at injection time. The declination is simply equal to the geocentric latitude of the sub-injection point (sub-satellite point at injection time) on the Earth's surface, where the satellite can be seen at the zenith. Thus,

$$\delta_i = \phi_i. \quad (16)$$

In order to calculate  $\alpha$ , the fundamental relation

$$\alpha = \Theta - \tau \quad (17)$$

is used, where  $\Theta$  is the local sidereal time and  $\tau$  the hour angle. At the moment when the satellite passes the local

<sup>3</sup> *Ibid.*, pp. 73 and 74.



meridian ( $\tau=0$ ), the right ascension  $\alpha$  of the satellite is equal to the local sidereal time  $\Theta$ . By means of "The American Ephemeris and Nautical Almanac" it is easy to calculate the local sidereal time  $\Theta$  or the hour angle  $\tau$  of the vernal equinox ( $\alpha=0$ ) for any local civil time  $t$  and meridian with geographic longitude  $\lambda$ . At first it is necessary to know the conversion factor from mean solar time intervals to sidereal time intervals. This factor  $\dot{\Theta}=d\Theta/dt$  is practically equal to the angular velocity  $\Omega$  of the earth's rotation, when the small difference due to the precessional motion of the vernal equinox is neglected. Thus

$$\begin{aligned}\dot{\Theta} &= 1.002\,737\,9093 \text{ d}^*/\text{d}(\text{h}^*/\text{h}) \\ &= 15.041\,068\,639 \text{ }^\circ/\text{h} \\ &= 0.0000729211585 \text{ rad/sec;} \\ (P &= 86164^{\text{d}}.09054),\end{aligned}\quad (18)$$

while

$$\begin{aligned}\Omega &= 1.0027378025 \text{ rot./d} = 15.041067038 \text{ }^\circ/\text{h} \\ &= 0.0000729211508 \text{ rad/sec;} \\ (p &= 86164^{\text{d}}.09971).\end{aligned}\quad (18a)$$

The hour angle  $\tau$  of the mean sun is also the Astronomical Time or the mean solar time beginning at noon, while the Civil Time is the mean solar time beginning at midnight. Thus the local Civil Time is

$$t = \tau + 12^{\text{h}},$$

and using (17)

$$\alpha = \Theta - \tau = \Theta - (t - 12^{\text{h}})\dot{\Theta}.$$

Therefore,

$$\Theta - \dot{\Theta} \cdot t = \Theta_{\text{Gr}} - \dot{\Theta} t_{\text{U.T.}} = \Theta_{\text{Gr}, 0^{\text{h}}\text{U.T.}} = \alpha - 12^{\text{h}}\dot{\Theta}, \quad (19)$$

where  $\Theta_{\text{Gr}}$  is Sidereal Time Greenwich and  $t_{\text{U.T.}}$  means Universal Time or the time referred to the Greenwich meridian ( $t_{\text{Gr}}$ ). Thus

$$t - t_{\text{U.T.}} = \frac{\lambda}{15} [\text{h}]$$

is given by the longitude correction, from which

$$\Theta - \Theta_{\text{Gr}} = \dot{\Theta}(t - t_{\text{U.T.}}) = \dot{\Theta} \frac{\lambda}{15} [\text{h}^*] \quad (20)$$

follows immediately. Combining now (19) and (20), there follows finally

$$\begin{aligned}\alpha &= \Theta = \Theta_{\text{Gr}} + \dot{\Theta} \frac{\lambda}{15} = \Theta_{\text{Gr}, 0^{\text{h}}\text{U.T.}} + \dot{\Theta} \cdot t \\ &= \Theta_{\text{Gr}, 0^{\text{h}}\text{U.T.}} + \dot{\Theta} \left( t_{\text{U.T.}} + \frac{\lambda}{15} \right).\end{aligned}\quad (21)$$

The Sidereal Time Greenwich at midnight,  $\Theta_{\text{Gr}, 0^{\text{h}}\text{U.T.}}$ , can be taken from "The American Ephemeris and Nautical Almanac" for every day of the year. In reality, this is the apparent or true sidereal time and the nutation in right ascension ( $< 1^{\text{s}}$ ) must be subtracted to obtain the mean or uniform sidereal time. After having applied the time and longitude correction, the nutation in right ascension for this local time must be added. However, the two corrections due to nutation in right ascension partially cancel each other, because the daily change is so small. The right ascension of the injection point is therefore

$$\begin{aligned}\alpha_i[h^*] &= \Theta_i \\ &= \left[ \Theta_{\text{Gr}, 0^{\text{h}}\text{U.T.}} + 1.002\,737\,9093 \left( t_{\text{U.T.}} + \frac{\lambda}{15} \right) \right]_i\end{aligned}\quad (22)$$

or

$$\begin{aligned}\alpha_i[^\circ] &= \left[ 15\Theta_{\text{Gr}, 0^{\text{h}}\text{U.T.}} + 15.041\,068\,639 \left( t_{\text{U.T.}} + \frac{\lambda}{15} \right) \right]_i.\end{aligned}\quad (23)$$

The six space-fixed injection point data  $r_i$ ,  $\alpha_i$ ,  $\delta_i$ ,  $v_i^*$ ,  $\theta_i^*$ ,  $\chi_i^*$  give now the six orbital elements for the elliptical, inclined satellite orbit with the injection time  $t_i$  as epoch. Introducing the dimensionless velocity parameter

$$Q_i^* = \left( \frac{v_i^*}{v_{\text{cir}}} \right)_i^2 = \frac{v_i^{*2} r_i}{\mu} = -2 \frac{E_{\text{kin}}}{E_{\text{pot}}} > 1, \quad (24)$$

with

$$\mu = GM = 398\,613.52 \frac{\text{km}^3}{\text{sec}^2}.$$

according to the paper of Herrick, Baker, and Hilton<sup>1</sup> ( $G$ , Newton's gravitational constant,  $M$ , the mass of the Earth), the six orbital elements are:

1) the semi-major axis which determines the size of the orbit,

$$a = \frac{r_i}{2 - Q_i^*}; \quad (25)$$

2) the eccentricity which determines the shape of the orbit,

$$e = \sqrt{1 - Q_i^*(2 - Q_i^*) \sin^2 \theta_i^*} \geq Q_i^* - 1; \quad (26)$$

3) the argument of perigee (arc distance of the perigee from the ascending node) which determines the position of the line of apsides (prolongated major axis of the orbit)

$$\omega = -\tan^{-1} \left\{ \frac{Q_i^* \sin \theta_i^* \cos \theta_i^*}{Q_i^* \sin^2 \theta_i^* - 1} \right\} + \tan^{-1} \left\{ \frac{\tan \delta_i}{\cos \chi_i^*} \right\}; \quad (27)$$

4) the perigee time (when the Earth satellite passes the point nearest to the Earth's center) which determines the position of the satellite in its orbit,

$$t_p = t_i - \sqrt{\frac{r_i^3}{\mu(2 - Q_i^*)^2}} \left[ \tan^{-1} \left\{ \frac{\sqrt{Q_i^*(2 - Q_i^*)} \cos \theta_i^*}{Q_i^* - 1} \right\} - \sqrt{Q_i^*(2 - Q_i^*)} \cos \theta_i^* \right]; \quad (28)$$

5) the inclination of the orbit to the Earth's equator which determines, together with the following orbit element, the position of the orbit plane with respect to a space-fixed reference plane (celestial equator) and a space-fixed origin (vernal equinox),

$$\gamma = \cos^{-1} \{ \cos \delta_i \sin \chi_i^* \}; \quad (29)$$

6) the right ascension of the ascending node (arc distance of the intersection line of the orbit plane with the equator from the vernal equinox)

$$\alpha_\Omega = \alpha_i - \tan^{-1} \{ \sin \delta_i \tan \chi_i^* \}. \quad (30)$$

All these formulas follow very easily from relations given in Krause.<sup>4</sup> Formulas (25) and (26) are given by (117) of that paper.<sup>4</sup> The true anomaly  $w_i$ , the eccentric anomaly  $E_i$ , and the mean anomaly  $M_i$  of the injection

point can be determined using (120), (121) and (62) of Krause.<sup>4</sup>

$$\begin{cases} e \sin w_i = \frac{p}{r_i} \cot \theta_i^* = Q_i^* \sin \theta_i^* \cos \theta_i^* \\ e \cos w_i = \frac{p}{r_i} - 1 = Q_i^* \sin^2 \theta_i^* - 1. \end{cases} \quad (31)$$

Then

$$\begin{cases} e \sin E_i = \sqrt{1 - e^2} \cot \theta_i^* = \sqrt{Q_i^*(2 - Q_i^*)} \cos \theta_i^* \\ e \cos E_i = 1 - \frac{r_i}{a} = Q_i^* - 1 \end{cases} \quad (32)$$

and

$$M_i = n(t_i - t_p) = nt_i + \sigma = E_i - e \sin E_i. \quad (33)$$

This last equation gives now the time  $t_p$  for perigee passage. Eqs. (1) through (9) of Krause<sup>4</sup> can now be applied. We select the following three equations for the determination of the orbital elements  $\omega$ ,  $\gamma$ , and  $\alpha_\Omega$ :

$$\tan(\omega + w_i) = \frac{\tan \delta_i}{\cos \chi_i^*} \begin{cases} \sin(\omega + w_i) = \frac{\sin \delta_i}{\sin \gamma} \\ \cos(\omega + w_i) = \frac{\cos \delta_i \cos \chi_i^*}{\sin \gamma}, \end{cases} \quad (34)$$

$$\cos \gamma = \cos \delta_i \sin \chi_i^*, \quad (35)$$

$$\tan(\alpha_i - \alpha_\Omega) = \frac{\sin \delta_i}{\cot \chi_i^*} \begin{cases} \sin(\alpha_i - \alpha_\Omega) = \frac{\sin \delta_i \sin \chi_i^*}{\sin \gamma} \\ \cos(\alpha_i - \alpha_\Omega) = \frac{\cos \chi_i^*}{\sin \gamma}. \end{cases} \quad (36)$$

The additional formulas only serve to determine the quadrant in which the angles are located. Because  $0 \leq \gamma \leq 180^\circ$  and  $|\delta_i| = |\phi_i| \leq 90^\circ$ , we always have  $\sin \gamma \geq 0$  and  $\cos \delta_i \geq 0$ .

Taking into consideration the secular perturbations of the satellite orbit due to the Earth's oblateness, we have<sup>4</sup> for the sidereal, tropical, anomalistic and nodical mean motions

$$\begin{aligned} n_{\text{sid}} &\approx n_{\text{trop}} = L = n_0 + \dot{\epsilon} = n_0 + \dot{\sigma} + \dot{\pi} \\ &= n_0 + \dot{\sigma} + \dot{\omega} + \cos \gamma \dot{\alpha}_\Omega \\ &= n_{\text{anom}} + \dot{\pi} = n_{\text{nod}} + \cos \gamma \dot{\alpha}_\Omega \end{aligned}$$

<sup>4</sup> H. G. L. Krause, "The Secular and Periodic Perturbations of the Orbit of an Artificial Earth Satellite," paper presented at the Seventh International Astronautical Congress, Rome, Italy; September 17-22, 1956. (Army Ballistics Missile Agency translation from the German by S. Nelson, 59 pp.)



$$= n_0 \left\{ 1 + J \left( \frac{a_e}{p_0} \right)^2 (1 + \sqrt{1 - e_0^2}) \cdot \left( 1 - \frac{3}{2} \sin^2 \gamma_0 \right) \right\}, \quad (37)$$

$$n_{\text{anom}} = \dot{M} = n_0 + \dot{\sigma}$$

$$= n_0 \left\{ 1 + J \left( \frac{a_e}{p_0} \right)^2 \sqrt{1 - e_0^2} \cdot \left( 1 - \frac{3}{2} \sin^2 \gamma_0 \right) \right\}, \quad (38)$$

$$n_{\text{nod}} = n_0 + \dot{\sigma} + \dot{\omega} = n_{\text{anom}} + \dot{\omega}$$

$$= n_0 \left\{ 1 + J \left( \frac{a_e}{p_0} \right)^2 \left[ \sqrt{1 - e_0^2} \cdot \left( 1 - \frac{3}{2} \sin^2 \gamma_0 \right) + \left( 2 - \frac{5}{2} \sin^2 \gamma_0 \right) \right] \right\}. \quad (39)$$

The subscript 0 means that the orbital elements refer to the unperturbed motion.

$$J = 0.001628$$

is the oblateness factor which was used for the Earth.

#### LIST OF SYMBOLS

$a_e$ = equatorial radius of the Earth. $c_e$ = polar radius of the Earth. $e_e$ = eccentricity of an Earth meridian. $f$ = flattening (oblateness) of the Earth. $R$ = radius of the Earth for latitude $\phi$ . $\varphi$ = geodetic (geographic) latitude. $\phi$ = geocentric latitude. $\lambda$ = geographic longitude (from Greenwich positive to $E$ in the direction of the Earth's rotation). $t$ = time. $x$ = ground range. $\psi = x/\bar{R}$ = ground range angle ( $\bar{R}$ mean Earth's radius for this arc). $y$ = altitude above sea level. $r = R + y$ = radius vector. $v$ = velocity. $\theta$ = flight path angle (with respect to the local vertical). $\alpha$ = azimuth angle (from $N$ to $E$ in a clockwise direction). $v_{\text{cir}}$ = local circular velocity. $\Omega$ = angular velocity of the Earth's rotation. $\mu = GM$ = constant of Kepler's 3rd law ( $G$ , Newton's gravitational constant; $M$ , mass of the Earth). $\delta$ = declination. $\alpha$ = right ascension (from the vernal equinox, positive in the direction of the Earth's rotation). $\Theta$ = sidereal time. $\tau$ = hour angle. $Q = (v/v_{\text{cir}})^2$ = dimensionless velocity parameter. $a$ = semi-major axis. $e$ = eccentricity. $t_p$ = time of perigee passage. $\omega$ = argument of perigee. $\gamma$ = inclination to the Earth's equator. $\alpha_n$ = right ascension of the ascending node. $p$ = half-parameter (semi-latus rectum). $C = \sqrt{\mu p}$ = constant of Kepler's second law. $n$ = orbital mean motion. $P = 2\pi/n$ = orbital period. $w$ = true anomaly. $E$ = eccentric anomaly. $M$ = mean anomaly.	<p>Earth constants.</p> <p>Eulerian orientation angles of the Earth-fixed position vector.</p> <p>Eulerian orientation angles of the velocity vector.</p> <p>Eulerian orientation angles of the space-fixed position-vector.</p> <p>Orbital elements.</p> <p>Additional orbital parameters.</p> <p>Time variables.</p>
--	--

## Subscripts

0 = conditions at launching point (launching pad).  
*i* = conditions at injection point (burnout of last stage).  
*p* = conditions at perigee point.  
*a* = conditions at apogee point.

## Superscript

\* = space-fixed data of the velocity vector.

## Pad #5

$\varphi_0 = 28^\circ 26' 20''.8987 = 28^\circ.439\ 138\ 53.$   
 $\phi_0 = 28^\circ.278\ 247\ 67.$   
 $\lambda_0 = -80^\circ 34' 24''.6758 = -80^\circ.573\ 521\ 06\ (W).$   
 $R_0 = 6373\ 331\ \text{m}.$   
 $y_0 = 3.527\ \text{m}\ (11.571\ \text{feet}).$   
 $r_0 = 6373\ 335\ \text{m}.$   
 $\chi_0 = 44^\circ; \bar{R} = 6372\ 523\ \text{m}.$

APPLICATION OF THE THEORY TO THE  
ARMY EXPLORERS

For the numerical calculations the following constants for the two launching pads were used.

## Pad #26A

$\varphi_0 = 28^\circ 26' 39''.673 = 28^\circ.444\ 353\ 6.$   
 $\phi_0 = 28^\circ.283\ 441\ 0.$   
 $\lambda_0 = -80^\circ 34' 14''.682 = -80^\circ.570\ 745\ 0\ (W).$   
 $R_0 = 6373\ 329\ \text{m}.$   
 $y_0 = 3.694\ \text{m}\ (12.12\ \text{feet}).$   
 $r_0 = 6373\ 333\ \text{m}.$   
 $\chi_0 = 110^\circ; \bar{R} = 6373\ 735\ \text{m}.$

The actual and the predicted data for velocity  $v_i$ , flight path angle  $\theta_i$ , altitude  $y_i$ , and ground range  $x_i$ , at injection point of the Army Explorers were taken from Speer.<sup>5</sup> Application of the above theory leads to Tables I-VIII for actual and predicted orbital elements.

<sup>5</sup> F. Speer, "Aeroballistics Evaluation of Test Flight Jupiter C-29<sup>6</sup> 26, 24, 44, 47," Army Ballistics Missile Agency, Redstone Arsenal, Ala., Repts. No. DA-M-321-58, DA-M-11-58, DA-M-29, DA-M-64-58; 1958. (Secret reports.)

TABLE I  
CHARACTERISTIC LAUNCHING DATA FOR THE ARMY EXPLORERS

Satellite	Explorer I	Explorer II	Explorer III	Explorer IV	Explorer V
IGY name	1958 $\alpha$	—	1958 $\gamma$	1958 $\epsilon$	—
Booster missile of the Juno I family	RS-29	RS-26	RS-24	RS-44	RS-47
Weight of satellite (pounds)	18.13	18.83	18.53	25.76	25.76
Orbiting weight (pounds)	30.66	31.36	31.00	37.16	37.16
Launching time (EST)	January 31, 1958	March 5, 1958	March 26, 1958	July 26, 1958	August 24, 1958
Launching pad (AFMTC)	22 <sup>h</sup> 47 <sup>m</sup> 56 <sup>s</sup>	13 <sup>h</sup> 27 <sup>m</sup> 59 <sup>s</sup>	12 <sup>h</sup> 38 <sup>m</sup> 03 <sup>s</sup>	10 <sup>h</sup> 00 <sup>m</sup> 17 <sup>s</sup>	01 <sup>h</sup> 17 <sup>m</sup> 22 <sup>s</sup>
Launching azimuth	26A 110°	26A 110°	26A 110°	5 44°	5 44°

Note: Explorer VII was excluded because it was primarily a NASA contribution to the IGY, even though the booster was furnished by the Army.

TABLE II  
PREDICTED DATA

Explorer	I	II	III	IV	V
$x_i$ (km)	764.648	751.90	788.65	777.20	783.08
$\psi_i = x_i / \bar{R}$ (rad)	0.1199686	0.1179685	0.1237344	0.1219611	0.1228838
$\phi_i = \delta_i$ (°)	6.87369	6.75910	7.08946	6.98786	7.04072
$\lambda_i - \lambda_0$ (°)	25.74594	25.79115	25.67977	33.18231	33.21838
$\lambda_i$ (°)	7.17256	7.05564	7.33344	5.79546	5.84165
$\lambda_i$ (h)	-73.398185	-73.51511	-73.23731	-74.77806	-74.73187
$R_i$ (km)	-4.893212	-4.901007	-4.882487	-4.985204	-4.982125
$y_i$ (km)	6374.098	6374.084	6374.117	6371.657	6371.708
$r_i$ (km)	352.100	352.100	351.760	287.100	282.290
$v_i$ (m/s)	6726.198	6726.184	6725.877	6658.757	6653.998
$\theta_i$ (°)	7684.5	7646.8	7714.30	8058.3	8054.29
$\chi_i$ (°)	89.87	89.90	89.93	89.98	90.00
$t_0$ (EST)	113.2621	113.2113	113.3361	46.9660	46.9913
$t_i - t_0$ (sec)	January 31, 1958	March 5, 1958	March 26, 1958	July 26, 1958	August 24, 1958
$t_i$ (UT)	22 <sup>h</sup> 47 <sup>m</sup> 56 <sup>s</sup> .60	13 <sup>h</sup> 27 <sup>m</sup> 59 <sup>s</sup> .36	12 <sup>h</sup> 38 <sup>m</sup> 03 <sup>s</sup> .98	10 <sup>h</sup> 00 <sup>m</sup> 17 <sup>s</sup> .83	01 <sup>h</sup> 17 <sup>m</sup> 22 <sup>s</sup> .77
	419.28	417.90	423.000	386.28	383.62
	February 1, 1958	March 5, 1958	March 26, 1958	July 26, 1958	August 24, 1958
	03 <sup>h</sup> 54 <sup>m</sup> 55 <sup>s</sup> .88	18 <sup>h</sup> 34 <sup>m</sup> 57 <sup>s</sup> .26	17 <sup>h</sup> 45 <sup>m</sup> 06 <sup>s</sup> .98	15 <sup>h</sup> 06 <sup>m</sup> 44 <sup>s</sup> .11	06 <sup>h</sup> 23 <sup>m</sup> 46 <sup>s</sup> .39



TABLE III  
PREDICTED DATA

Explorer	I	II	III	IV	V
$\lambda_i$	$-04^{\circ}53^{\circ}35^{\circ}.56$	$-04^{\circ}54^{\circ}03^{\circ}.63$	$-04^{\circ}52^{\circ}56^{\circ}.95$	$-04^{\circ}59^{\circ}06^{\circ}.73$	$-04^{\circ}58^{\circ}55^{\circ}.65$
$t_i + \lambda_i$	$-00^{\circ}58^{\circ}39^{\circ}.68$ $-9^{\circ}.64$	$13^{\circ}40^{\circ}53^{\circ}.63$ $02^{\circ}14^{\circ}.85$	$12^{\circ}52^{\circ}10^{\circ}.03$ $02^{\circ}06^{\circ}.85$	$10^{\circ}07^{\circ}37^{\circ}.38$ $01^{\circ}39^{\circ}.82$	$01^{\circ}24^{\circ}50^{\circ}.74$ $13^{\circ}.94$
$\Theta_{Gr}, 0^{\circ}UT$	$-00^{\circ}58^{\circ}49^{\circ}.32$ $08^{\circ}42^{\circ}46^{\circ}.83$	$13^{\circ}43^{\circ}08^{\circ}.48$ $10^{\circ}48^{\circ}56^{\circ}.55$	$12^{\circ}54^{\circ}16^{\circ}.88$ $12^{\circ}11^{\circ}44^{\circ}.12$	$10^{\circ}09^{\circ}17^{\circ}.20$ $20^{\circ}12^{\circ}43^{\circ}.85$	$01^{\circ}25^{\circ}04^{\circ}.68$ $22^{\circ}07^{\circ}03^{\circ}.93$
$\Theta_i$	$07^{\circ}43^{\circ}57^{\circ}.51$	$0^{\circ}32^{\circ}05^{\circ}.03$	$01^{\circ}06^{\circ}01^{\circ}.00$	$06^{\circ}22^{\circ}01^{\circ}.05$	$23^{\circ}32^{\circ}08^{\circ}.61$
$\alpha_i$	$115^{\circ}59'22''.65$	$8^{\circ}1'15''.45$	$16^{\circ}30'15''.00$	$95^{\circ}30'15''.75$	$353^{\circ}2'9''.15$
$\alpha_i$ (°)	115.98962	8.02096	16.50417	95.504375	353.03587
$v_i^*$ (m/s)	8092.26	8054.56	8122.05	8359.95	8355.71
$\theta_i^*$ (°)	89.8766	89.9051	89.9366	89.9807	90.0000
$\chi_i^*$ (°)	112.0266	111.9730	112.1008	48.8671	48.8903
$v_{air}$ (m/s)	7698.24	7698.24	7698.42	7909.52	7739.89
$Q_i^*$	1.104987	1.094712	1.113083	1.167477	1.165461
$w_i$ (°)	1.29325	1.10717	0.61764	0.18083	0
$E_i$ (°)	1.16374	1.00716	0.55157	0.15556	0
$M_i$ (°)	1.04155	0.91176	0.48919	0.12950	0

TABLE IV  
PREDICTED DATA

Explorer	I	II	III	IV	V
$n$ (rad/sec)	0.0009690939	0.0009858318	0.0009560417	0.0008826341	0.0008867925
$n$ (°/sec)	0.05552499	0.05648400	0.05477715	0.05057121	0.05080947
$t_i - t_p$ (sec)	18.76	16.14	8.93	2.56	0
$a$ (km)	7515.192	7429.886	7583.438	7998.285	7973.261
$e$	0.10501	0.09473	0.11309	0.16748	0.16546
$\omega$ (°)	126.57800	126.6439	127.42451	44.64946	44.88375
$t_p$ (UT)	February 1, 1958	March 5, 1958	March 26, 1958	July 26, 1958	August 24, 1958
$\gamma$ (°)	03 <sup>h</sup> 54 <sup>m</sup> 37 <sup>s</sup> .12	18 <sup>h</sup> 34 <sup>m</sup> 41 <sup>s</sup> .12	17 <sup>h</sup> 44 <sup>m</sup> 58 <sup>s</sup> .05	15 <sup>h</sup> 06 <sup>m</sup> 41 <sup>s</sup> .55	06 <sup>h</sup> 23 <sup>m</sup> 46 <sup>s</sup> .39
$\alpha_{\Omega}$ (°)	33.3858	33.3860	33.3831	50.9228	50.9256
$P$	343.0259	235.1799	243.3646	62.4307	320.9162
$p$ (km)	108 <sup>m</sup> 3 <sup>s</sup> .57	106 <sup>m</sup> 13 <sup>s</sup> .49	109 <sup>m</sup> 32 <sup>s</sup> .08	118 <sup>m</sup> 38 <sup>s</sup> .68	118 <sup>m</sup> 05 <sup>s</sup> .29
$C$ (km <sup>2</sup> /sec)	7432.324	7363.216	7486.453	7773.943	7754.975
$r_p$ (km)	54430.001	54176.353	54637.844	55666.857	55598.900
$v_p$ (m/s)	6726.035	6726.075	6725.837	6658.752	6653.998
$r_a$ (km)	8092.43	8054.68	8122.09	8359.95	8355.71
$v_a$ (m/s)	8304.350	8133.696	8441.038	9337.818	9292.524
	6554.40	6660.73	6471.70	5961.44	5983.19

TABLE V  
ACTUAL DATA

Explorer	I	II	III	IV	V
$x_i$ (km)	806.934	697.237	808.04	756.90	775.04
$\psi_i = x_i / \bar{R}$ (rad)	0.1266030	0.1093922	0.1267775	0.1187756	0.1216222
$\psi_i = \delta_i$ (°)	7.25382	6.26771	7.26376	6.80534	6.96844
$\lambda_i - \lambda_0$ (°)	25.59531	25.98396	25.59135	33.05765	33.16903
$\lambda_i$ (°)	7.55978	6.55324	7.56989	5.63628	5.77850
$\lambda_i$ (h)	-73.01096	-74.01750	-73.00085	-74.93724	-74.79502
$R_i$ (km)	-4.867397	-4.934500	-4.866724	-4.995816	-4.986335
$y_i$ (km)	6374.142	6374.091	6374.143	6371.763	6371.725
$r_i$ (km)	366.510	378.399	388.410	265.200	284.370
$v_i$ (m/s)	6740.652	6752.490	6762.553	6636.963	6656.095
$\theta_i$ (°)	7800.9	5457.7	7796.51	7922.5	7597.53
$\chi_i$ (°)	89.10	89.09	84.45	90.40	97.98
$t_0$ (EST)	113.4298	112.9920	113.4341	46.8791	46.9568
$t_i - t_0$ (seconds)	January 31, 1958	March 5, 1958	March 26, 1958	July 26, 1958	August 24, 1958
	22 <sup>h</sup> 47 <sup>m</sup> 56 <sup>s</sup> .60	13 <sup>h</sup> 27 <sup>m</sup> 59 <sup>s</sup> .36	12 <sup>h</sup> 38 <sup>m</sup> 03 <sup>s</sup> .985	10 <sup>h</sup> 00 <sup>m</sup> 17 <sup>s</sup> .83	01 <sup>h</sup> 17 <sup>m</sup> 22 <sup>s</sup> .77
	428.56	406.41	423.015	386.40	383.73
$t_i$ (UT)	February 1, 1958	March 5, 1958	March 26, 1958	July 26, 1958	August 24, 1958
	03 <sup>h</sup> 55 <sup>m</sup> 05 <sup>s</sup> .16	18 <sup>h</sup> 34 <sup>m</sup> 45 <sup>s</sup> .77	17 <sup>h</sup> 45 <sup>m</sup> 07 <sup>s</sup> .00	15 <sup>h</sup> 06 <sup>m</sup> 44 <sup>s</sup> .23	06 <sup>h</sup> 23 <sup>m</sup> 46 <sup>s</sup> .50

TABLE VI  
ACTUAL DATA

Explorer	I	II	III	IV	V
$\lambda_i$	$-04^h52^m02^s.63$	$-04^h56^m04^s.20$	$-04^h52^m00^s.80$	$-04^h59^m44^s.94$	$-04^h59^m10^s.81$
$t_i + \lambda_i$	$-00^h56^m57^s.47$ $-9^s.36$	$13^h38^m41^s.57$ $2^m14^s.49$	$12^h53^m06^s.80$ $2^m07^s.00$	$10^h06^m59^s.29$ $1^m39.71$	$01^h24^m35^s.69$ $13^s.90$
$\Theta_{Gr}, 0^mUT$	$-00^h57^m06^s.83$ $08^h42^m46^s.83$	$13^h40^m56^s.06$ $10^h48^m56^s.55$	$12^h55^m13^s.80$ $12^h11^m44^s.12$	$10^h08^m39^s.00$ $20^h12^m43^s.85$	$01^h24^m49^s.59$ $22^h07^m03^s.93$
$\Theta_i$	$07^h45^m40^s.00$	$00^h29^m52^s.61$	$01^h06^m57^s.92$	$06^h21^m22^s.85$	$23^h31^m53^s.52$
$\alpha_i$	$116^\circ24'59''.99$	$7^\circ28'9''.14$	$16^\circ44'28''.79$	$95^\circ20'42''.79$	$352^\circ58'22''.84$
$\alpha_i$ (°)	116.41666	7.46921	16.74133	95.34522	352.97301
$v_i^*$ (m/s)	8209.49	5867.66	8204.67	8223.24	7896.56
$\theta_i^*$ (°)	89.1448	89.1536	84.7269	90.3854	97.6759
$\chi_i^*$ (°)	112.1994	111.3034	112.1936	48.8122	48.9874
$v_{oir}$ (m/s)	7689.98	7683.23	7677.52	7749.81	7738.67
$Q_i^* = v_i^* r_i / \mu$	1.139679	0.583232	1.142039	1.125910	1.041222
$E_i$ (°)	6.95415		38.28807	-3.44453	
$E_i$ (°)	6.03904		32.63808	-3.03467	
$M_i$ (°)	5.19225		27.42581	-2.65237	

TABLE VII  
ACTUAL DATA

Explorer	I	II	III	IV	V
$n$ (rad/sec)	0.0009103610		0.0009022178	0.0009542369	
$n$ (°/sec)	0.05215984		0.05169327	0.05467375	
$t_i - t_p$ (sec)	99.54		530.55	-51.31	
$a$ (km)	7835.047		7882.120	7592.996	
$e$	0.14046		0.16867	0.12609	
$\omega$ (°)	123.40437		92.13665	40.08543	
$t_p$ (UT)	February 1, 1958		March 26, 1958	July 26, 1958	
$\gamma$ (°)	03 <sup>h</sup> 53 <sup>m</sup> 25 <sup>s</sup> .62		17 <sup>h</sup> 36 <sup>m</sup> 16 <sup>s</sup> .45	15 <sup>h</sup> 07 <sup>m</sup> 35 <sup>s</sup> .54	
$\alpha_\Omega$ (°)	33.3828		33.3760	50.8958	
$P$	343.0485		243.3773	63.4072	
$p$ (km)	115 <sup>m</sup> 01 <sup>s</sup> .86		116 <sup>m</sup> 04 <sup>s</sup> .16	109 <sup>m</sup> 44 <sup>s</sup> .51	
$\dot{p}$ (km)	7680.471		7657.867	7472.284	
$C$ (km <sup>2</sup> /sec)	55331.183		55249.702	54576.125	
$r_p$ (km)	6734.545		6552.613	6635.620	
$v_p$ (m/s)	8216.02		8431.71	8224.72	
$r_a$ (km)	8935.549		9211.628	8550.372	
$v_a$ (m/s)	6192.25		5997.82	6382.90	

TABLE VIII  
MOTION OF EXPLORERS PERTURBED BY  
EARTH'S OBLATENESS

	Explorer I	Explorer III	Explorer IV
$\dot{\alpha}_\Omega$ [°/sec]	-0.00004890	-0.00004875	-0.00004090
$\dot{\omega}$ [°/sec]	0.00007280	0.00007259	0.00003207
$\dot{\sigma}$ [°/sec]	0.00003165	0.00003142	0.00000622
$\dot{\pi}$ [°/sec]	0.00003197	0.00003188	0.00005787
$\dot{\epsilon}$ [°/sec]	0.00006362	0.00006330	0.00006409
$n_{trop}$ [°/sec]	0.05222346	0.05175657	0.05473784
$P_{trop}$ [Min-Sec]	114 <sup>m</sup> 53.45 <sup>s</sup>	115 <sup>m</sup> 55.62 <sup>s</sup>	109 <sup>m</sup> 36.78 <sup>s</sup>
$n_{anom}$ [°/sec]	0.05219149	0.05172469	0.05467997
$P_{anom}$ [Min-Sec]	114 <sup>m</sup> 57.66 <sup>s</sup>	115 <sup>m</sup> 59.93 <sup>s</sup>	109 <sup>m</sup> 43.74 <sup>s</sup>
$n_{nod}$ [°/sec]	0.05226429	0.05179728	0.05471204
$P_{nod}$ [Min-Sec]	114 <sup>m</sup> 48.06 <sup>s</sup>	115 <sup>m</sup> 50.16 <sup>s</sup>	109 <sup>m</sup> 39.90 <sup>s</sup>



## CONCLUSIONS

A comparison of actual and precalculated orbital elements shows that the position of the orbital plane in space, given by the elements  $\alpha_\Omega$  and  $\gamma$ , is not very sensitive to changes of injection-point data, if the same lift-off time is taken for the comparison. The other orbital elements  $a$ ,  $e$ ,  $\omega$ ,  $t_p$  are very sensitive, especially to changes of the injection-point velocity vector.

The deviations of the actual space-fixed velocity vector at injection time from the local circular velocity vector are very interesting. Table IX shows these deviations with the perigee altitude  $y_p$  (for all artificial earth satellites, the perigee is very near to the injection point so that  $y_p = r_p - R_i$  and  $y_a = r_a - R_i$ ) and the lifetime  $t_L$ .

Table IX shows very clearly that Explorer II was unable to go into orbit because it had sub-circular velocity in the injection point ( $Q_i^* < 1$ ) due to the fact

that the fourth stage failed to ignite. On the other hand, Explorer V had super-circular velocity ( $Q_i^* > 1$ ) at burnout of the fourth stage (injection point). However, due to a collision of the separated upper stages with the burned out booster, these stages showed a wrong spatial attitude and, thus, were fired into a wrong direction ( $\theta_i^* = 97^\circ.68$ ). This resulted in an elliptic orbit ( $e = 0.14$ ) with a semi-major axis about 750 km lower than those of the other Explorers. This means that Explorer V had to follow an elliptic orbit intersecting the earth's surface ( $y_p < 0$ ). Also, the air drag encountered by the satellite accelerated its descent.

The actual orbital elements derived in this report are based on flight parameters obtained by evaluation of radar tracking observations and telemetry data. As shown in Table X for Explorer I, they agree well with the actual orbital elements derived from early astronomical observations.

TABLE IX  
SOME CHARACTERISTIC ORBIT DATA

Explorer	I	II	III	IV	V
$v_i^* - v_{cir}(\text{m/s})$	+519.44	-1815.57	+527.15	+473.43	+157.89
$\theta_i^* - 90^\circ$	-0.86	-0.85	-5.27	+0.39	+7.68
$Q_i^* = \frac{v_i^{*2}}{v_{cir}^2}$	1.1397	0.5832	1.1420	1.1259	1.0412
$a$ (km)	7835.047	—	7882.120	7592.996	6942.269
$e$	0.14046	—	0.16867	0.12609	0.13968
$y_p$ (km)	360.403	—	178.470	263.857	-399.152
$t_L$ (d)	$\approx 2000$	0	92	454	0
Duration of Existence	January 31, 1958 to ?	—	March 26, 1958 to June 28, 1958	July 26, 1958 to October 23, 1959	—

TABLE X  
COMPARISON OF THE ORBITAL ELEMENTS DERIVED FROM TRACKING OBSERVATIONS WITH THOSE DERIVED FROM EARLY ASTRONOMICAL OBSERVATIONS (EXPLORER I)

Orbital Element	ABMA (Present Report)	Naval Research Laboratory (Harvard Card 1393)	Smithsonian Astrophysical Observatory (Harvard Card 1404)	Vanguard Control Center (Teletype)
$a$ (km)	7835.047	7831.2	7829.3	7829.20
$e$	0.14046	0.14052	0.139	0.13989
$\omega$ ( $^\circ$ )	123.404	120.76	120.0	121.68
$t_p$ (UT)	February 1, 1958 3 <sup>h</sup> 53 <sup>m</sup> 25 <sup>s</sup> .6	February 1, 1958 3 <sup>h</sup> 53 <sup>m</sup> 18 <sup>s</sup> .8	February 1, 1958 3 <sup>h</sup> 52 <sup>m</sup> 53 <sup>s</sup>	February 1, 1958 3 <sup>h</sup> 53 <sup>m</sup> 23 <sup>s</sup> .1
$\gamma$ ( $^\circ$ )	33.383	33.58	33.19	33.43
$\alpha_\Omega$ ( $^\circ$ )	343.049	342.95	343.4	343.00
$P$ (min)	115.031	114.95 (nod)	114.94	114.94 (anom)
$y_p$ (km)	360.403	352.45	361.01	360.00
$y_a$ (km)	2561.407	2554.0	2541.7	2551.0
Epoch (UT)	1958 February 1.163254	1958 February 1.165278	1958 February 1.16182	1958 February 1.16330
$M_E$ ( $^\circ$ )	5.192	14.68	0	5.54

# Tracking Experiments with Pioneer IV\*

T. A. BARR† AND C. A. LUNDQUIST†

**Summary**—Several organizations participated in a program for testing receiver techniques used in tracking the low power transmitters carried on the space probe Pioneer IV. A meeting was held and presentations were made on each system tested.

This paper presents a summary and comparison of the results of the receiving techniques used to track the Pioneer IV. It also gives a brief description of the transmitter and antenna used on Pioneer IV.

## INTRODUCTION

TWO space probes were executed for the National Aeronautics and Space Administration (NASA) through a joint program by the Jet Propulsion Laboratory (JPL) of the California Institute of Technology and the Army Ballistic Missile Agency (ABMA). The first of the probes, Pioneer III, was launched at 0545 U.T., December 6, 1958 and reached an altitude of 108,700 km before returning to the earth about 1943 U.T., December 7, 1958. The second probe, launched at 0511 U.T., March 3, 1959, passed within 60,000 km of the moon and went into an orbit around the sun, becoming Artificial Planet 2 ("The Moon Probe Pioneer IV" [4]).

In this joint program, ABMA had the responsibility for the preparation of the first stage of the Juno II vehicles used to launch the probes. The second, third, and fourth stages, and the probes themselves with their instrumentation, were prepared by JPL. Some of the scientific instrumentation for detecting energetic charged particles was supplied by the State University of Iowa. Personnel of both JPL and ABMA participated in the launch operations. The determination, immediately after launch, of the initial position and velocity vector with which the probes began their free flight was made by ABMA. The long-term tracking, orbit determination, and data acquisition programs were executed by JPL until the probe ceased to transmit radio signals [3].

While JPL was carrying out this prime tracking program on Pioneer IV, ABMA was able to participate in some more speculative experiments in tracking low power transmitters over great distances. Several organizations in addition to ABMA had expressed a desire to test various receiver techniques using the radio signal from Pioneer IV as a source. The other organizations were the Ballistic Research Laboratories, Aberdeen Proving Ground, Md.; the General Electric Company, Schenectady, N.Y.; the International Telephone and Telegraph Company, Nutley, N.J.; and the University of Illinois, Urbana.

The activities of these groups were coordinated by ABMA. Predictions of probe positions as a function of time were supplied to each participating group. On April 16 and 17, 1959, a meeting of representatives from the participating organizations was held at ABMA to facilitate the exchange of information. Presentations were made on each receiving system tested, and the results were discussed. A summary and comparison of these results follows.

## PROBE INSTRUMENTATION

Shortly after burnout of the final stage of the launching vehicle, the payload package containing the instrumentation was separated from the final stage rocket. This package (Fig. 1) weighed 13.4 pounds. Two flexible wires were released to reduce the spin rate of the payload from 480 to 11 revolutions per minute.

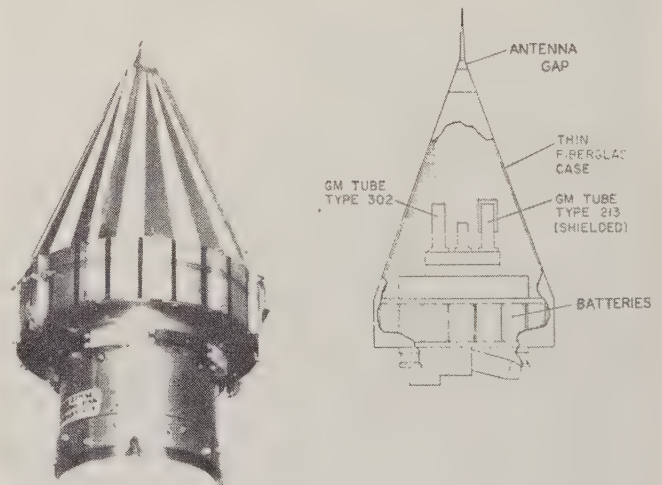


Fig. 1—Pioneer IV payload.

The transmitter on the package operated at a frequency of 960.05 mc, with a transmitted power of about 180 milliwatts. Its operating lifetime was limited by the total energy available from the mercury batteries it carried. In the case of Pioneer IV, the transmitter operated for 82 hours.

The antenna for the transmitter was a dipole, consisting of an aluminum spike 3 inches long mounted on the apex of a conducting cone 20 inches long and about 9 inches in diameter at the base. The spike served as one element of the dipole and the cone as the second.

The signal was phase-modulated. Three subcarrier telem-

\* Manuscript received by the PGMIL, February 1, 1960.

† U. S. Army Ballistic Missile Agency, Redstone Arsenal, Huntsville, Ala.



etry channels were used, with center frequencies of 400 cps, 560 cps, and 730 cps.

Data from two radiation detectors [7], an optical scan device, and temperature measurements were transmitted by the telemetry system.

#### ORBIT OF PIONEER IV

Burnout of the last rocket stage of the launching vehicle occurred about 270 seconds after liftoff, at approximately  $74^{\circ}\text{W}$  longitude and  $28.5^{\circ}\text{N}$  latitude. Shortly thereafter, because of its high eastward launch velocity, the probe passed beneath the south-eastern horizon for all stations in the continental United States. Some three to six hours after launch, depending on station location in the U. S., it reappeared above the same horizon. The probe, having lost much of its original velocity because of the gravitational attraction of the earth, was then moving at an angular rate less than the rotation of the earth. The probe appeared to cross the sky from east to west as the earth rotated beneath it, and about 13 or 14 hours after launch it passed below the western horizon for the stations participating in the experiment (see Fig. 2).

About one-half day later, it again came above the eastern horizon and was within radio sight for about another half day.

About 41 hours after launch, the probe made its closest approach to the moon, passing  $7.2^{\circ}$  to the east and  $5.7^{\circ}$  south of the moon.

The probe rose above the eastern horizon for the stations for a third time at about 1000 U.T., March 5, and again set below the western horizon one-half day later. It rose in the east once more about 1000 U.T., March 6. During this period of visibility from the United States, after 82 hours of operation, the batteries were exhausted and the transmission ceased. At this time, the artificial planet was some 655,000 km, almost twice the distance of the moon, from the earth.

The artificial planet is calculated to have a 395-day year. Its closest approach to the sun is 148 million km, and its greatest distance is 170 million km.

#### TRACKING STATIONS

Four tracking stations, excluding the JPL facilities, participated in the tracking experiment with Pioneer IV. Each of the stations was also set up to measure one-way Doppler frequencies during the injection phase of the probe flight. These stations attempted to track the probe as long as sufficient signal was available.

These stations, their locations, and the equipment tested were:

ABMA-ITT, Huntsville, Ala., parametric amplifier (low sideband converter).

General Electric Company, Schenectady, N. Y., parametric amplifier (thru converter).

University of Illinois, Urbana, Dicke radiometer.

BRL, Aberdeen, Md., phase-lock tracking receiver.

Although they were designed to perform the same basic function, the stations evolved distinctive design concepts. Each facility was fabricated mostly from equipment available and served to demonstrate each organization's approach to the problem.

The novel method adopted by the University of Illinois used a Dicke radiometer similar to systems used by radio astronomers [2]. Fig 3 is a block diagram of the system. The antenna is a 28-foot dish with a "logarithmic periodic" type feed. By a comparison switch, the RF mixer is connected alternately to the antenna output and to a noise source. In the actual apparatus, a symmetrical square wave is used alternately to switch from the antenna to the noise source. The switch output is fed to a conventional mixer with a noise figure of 7.0 db at 1000 mc. The mixer output is normally fed to an R-390A receiver, the output of which feeds a Krohn Hite 30-cps filter followed by a phase-sensitive detector. In the phase-sensitive detector, the converted noise source output is subtracted from the converted antenna output. The difference voltage is then amplified and integrated in an integrator with an adjustable time constant. Finally, the integrator output is recorded on a chart recorder to produce the system output. The comparison switch and the phase-sensitive detector must be synchronized exactly. This is accomplished by driving both by the same square wave.

The sensitivity of the system is limited by the time con-

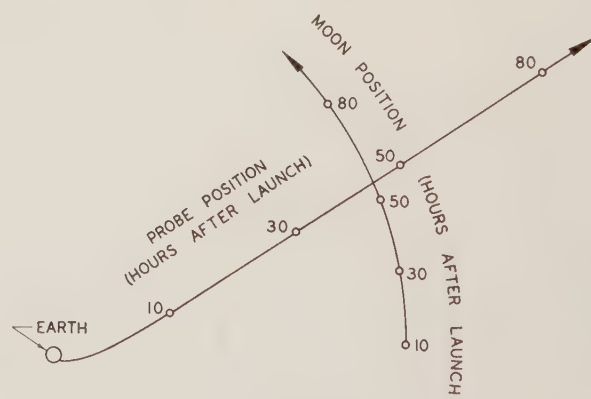


Fig. 2—Motion of Pioneer IV in space.

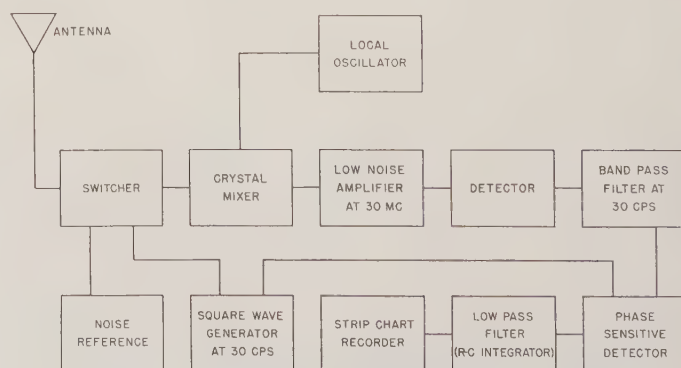


Fig. 3—University of Illinois Dicke radiometer system.

stant of the integrator, and by the stability of the noise source and the dc amplifier. Assuming these last two effects to be controlled adequately, the sensitivity varies as the square root of the time constant. Thus, the sensitivity of any receiving system could be improved by a factor equal to the square root of the ratio of the over-all bandwidth of the original system to the bandwidth of the Dicke system, less a loss of 3 db in the comparison switch.

The parameters of the Illinois system at 960 mc are:

Antenna: 28 feet, 37-db gain, linearly polarized.  
 Mixer noise figure: 7.0 db.  
 Integrator time constant:  $\frac{1}{2}$  second to 1 minute.  
 Switching rate: 30 cps.  
 Intermediate frequency: 30 mc.  
 IF bandwidth: 100 cps to 2 mc.

Assuming an IF bandwidth of  $\frac{1}{2}$  kc, the minimum detectable coherent signal with this antenna and noise figure is about  $10^{-17}$  w/m<sup>2</sup> without the Dicke comparison system. If the Dicke system is activated, with an integration time of ten seconds, the minimum detectable signal is reduced by a factor of 50.

Since the bandwidth is extremely small, the Dicke system is useless for receiving telemetry. An improvement in signal-to-noise ratio implies a considerable integration time and hence a limitation on the angular tracking rate that can be achieved.

The system used by the General Electric Company consisted of a parametric thru-converter with a measured noise figure of 2.0 db [1]. An 18-foot dish antenna with a gain of 32 db, linearly polarized, fed the amplifier. The block diagram of the receiver is shown in Fig. 4. The signal from the antenna is applied to the parametric amplifier, and then to a low noise crystal mixer which has a 6-db noise figure. The local oscillator signal is derived from a phase-lock system so that its frequency is exactly 30 mc higher than the receiver frequency. The 30-mc output of the mixer is amplified in a conventional IF strip and converted to 455 kc in a type R-390A communications receiver which has an unusually stable local oscillator. The phase of the 455-kc IF output from the receiver is compared with the phase of a stable 455-kc standard frequency in two phase comparators. One compares the IF signal in phase with the standard and the other compares in-phase quadrature. The phase comparator develops a voltage proportional to phase difference and also provides demodulation of the composite telemetry subcarriers from the phase-modulated carrier. The quadrature phase comparator provides a dc voltage proportional to the signal amplitude. The dc output of the in-phase comparator is applied to a loop filter and then to a voltage-controlled oscillator (VCO) that has a frequency of 55.0028 mc but which varies slightly from this frequency in accordance with the voltage from the loop filter. The

output of the 55-mc oscillator is multiplied 18 times to 990.05 mc, plus or minus the Doppler shift. The 990-mc signal is used to provide exact 30-mc difference frequency output changes at exactly 1/18th the rate of the received frequency. The VCO is mixed with a stable 55-mc standard to produce an audio tone suitable for direct counting. The audio tone is recorded on a two-channel tape recorder together with time from WWV. Telemetry signals are also recorded on magnetic tape using a 4-kc bandwidth filter.

Some of the facilities used by General Electric were made available by the Air Force Cambridge Research Directorate for whom General Electric is conducting a satellite tracking study.

The station at Huntsville was a joint undertaking between ABMA and ITT [5]. The parametric amplifier was supplied by ITT, and the rest of the system was supplied by ABMA. A block diagram of the station is shown in Fig. 5. A 14-foot circularly polarized dish antenna is used to feed the receiver input. The dish was mounted on a modified 584 pedestal connected to a manually directed servo. Since the angular rates of tracking were low, the operator could position the dish with an over-all error of  $\pm \frac{1}{2}$  degree. During the last few hours of tracking when the signal was very low, angle readout deteriorated to 2 degrees.

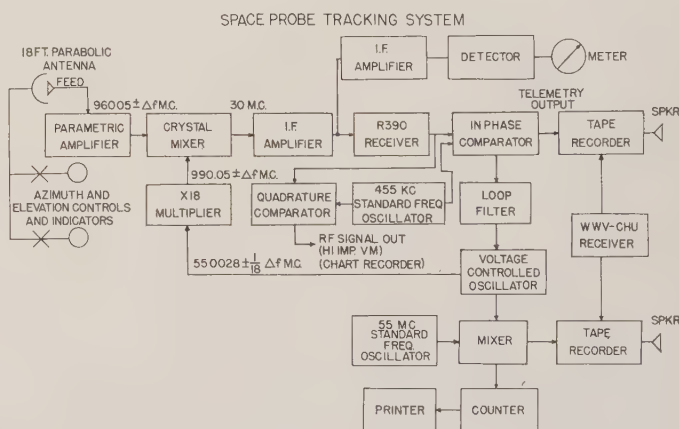


Fig. 4—General Electric Company station.

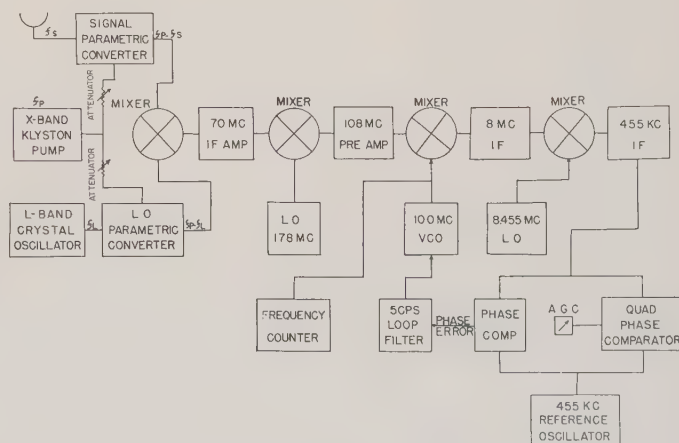


Fig. 5.—ABMA-ITT station.



The antenna was connected through a short section of low-loss transmission line to the parametric amplifier, and its output fed directly to a narrow band phase-lock tracking receiver. The telemetry and signal level outputs of the receiver were continuously recorded during the tracking operation.

The incoming signal is converted to the difference between the pump frequency less the signal frequency in the first capacitor diode converter. This is mixed with the local oscillator signal generated by the second L.O. parametric converter. Both converters use the same pump source. By using the same pump, inherent klystron frequency jitter is canceled out. The hardware for signal parametric amplifier input included an impedance matching system to match the 50-ohm antenna output.

The outputs from both parametric converters are mixed and amplified thru a 70-mc IF amplifier. Its output is mixed with a 178-mc crystal-controlled local oscillator to produce 108 mc, which is fed to a conventional phase-lock tracking receiver, with its inherent bandwidth advantage. The use of two crystal-controlled oscillators reduced substantially the frequency stability of the system, and deteriorated the Doppler readout over the three-day tracking period. The noise figure of the ITT parametric amplifier was established by conventional techniques using an argon noise source. A cross check was performed by comparing the signal background noise generated as the sun crossed the main antenna lobe and comparing the difference with a conventional receiver, whose noise figure had been previously established in the laboratory. The cross check agreed within  $\pm 1/4$  db. Over-all sensitivity of  $-158$  dbm was achieved with a loop bandwidth of 5 cps.

The station located at the Ballistic Research Laboratory, Aberdeen, Md., used a conventional phase-locked tracking receiver with a variable loop filter bandwidth of 10 or 30 cps. The 30-cps filter was used during the upper stage burning, or maximum Doppler shift portion of the flight. A block diagram is shown in Fig. 6. Except for the operating frequency, the equipment closely resembled a typical 108-mc microlock satellite tracking system [6].

RESULTS

Because of equipment malfunction, principally in the local injection oscillator, the University of Illinois station did not receive the signal from the probe. Unfortunately, no opportunity to repeat the experiment has been available since Pioneer IV. However, the over-all sensitivity of the system was later checked using the sun as source.

The station at the Ballistic Research Laboratory employed what might be called typical equipment for a high quality satellite tracking station. Much experience had been gained with this and similar stations on previous satellite experiments. The principal mission of the station on the Pioneer IV experiment was acquisition of Doppler frequencies during the burning of the three solid propellant rocket stages. However, in addition, the station was able to track the probe until it passed over the eastern horizon 12 minutes after launch at a range of about 5000 km. The signal was not received when the probe reappeared. The performance of this station was significant as a standard with which to compare the performance of the more advanced systems.

The ABMA-ITT station tracked the probe during its periods of visibility on March 3, and again on its reappearance above the eastern horizon on the following day. About noon, Huntsville time, on March 4, the signal was lost in the increased background noise when the antenna was looking, roughly, in the direction of the sun. No attempt was made to reacquire the signal after this loss.

Most outstanding was the performance of the General Electric station. The signal was received during every period of visibility until exhaustion of the batteries when the probe was 655,000 km from the earth. This range was below the ultimate extrapolated range capability of this station.

The specifications and performance of each of the stations are summarized in Table I.

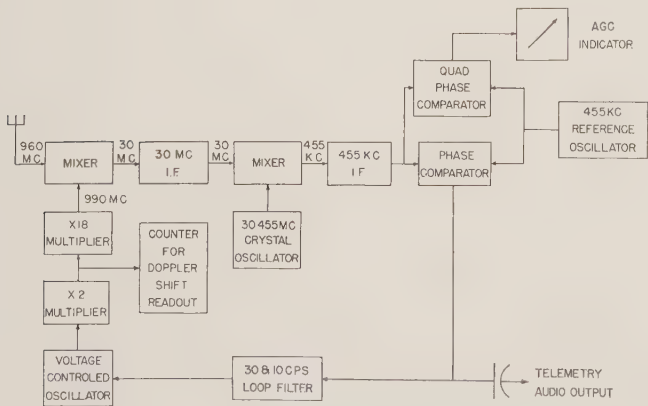


Fig. 6—BRL station.

TABLE I

Station	Antenna	Sensitivity	Noise Figure	Range Tracked
BRL, Aberdeen, Md.	6-foot dish, circular polarization, 23 db	145 dbm	7.5 db	5,000 km
ABMA-ITT, Huntsville, Ala.	14-foot dish, circular polarization, 31 db	161 dbm	1.5 db	350,000 km
GE, Schenectady, N. Y.	18-foot dish, linear polarization, 32 db	161 dbm	2.0 db	655,000 km
University of Illinois, Urbana, Ill.	28-foot dish, linear polarization, 37 db	$5 \times 10^{-18}$ watts per meter	7.0 db	equipment malfunction

The experience with the two systems employing parametric amplifiers followed by a phase-lock tracking receiver dramatically illustrated the substantial range capability possible with such a system.

The use of the parametric amplifier was responsible for approximately doubling the range of the basic phase-lock system.

From a practical standpoint, the experiment demonstrated that parametric amplifiers can be operated satisfactorily over extended periods of time, with only minor adjustments to maintain a low noise figure.

Such a parametric amplifier can be used even with a modest size antenna for quite ambitious projects.

#### BIBLIOGRAPHY

- [1] R. E. Anderson and A. D. French, "Tracking Pioneer IV beyond the moon," 1959 IRE NATIONAL CONVENTION RECORD, pt. 5, pp. 152-157.
- [2] M. E. Armstrong, G. W. Swenson, Jr., R. L. Sydnor, and H. D. Webb, "The Use of Radio Noise from the Sun for Calibrating Radio Receiving Systems," presented at 1959 National Electronics Conf., Chicago, Ill.; October 12-14, 1959.
- [3] A. R. Hibbs, M. Eimer, and R. Stevens, "Tracking the Moon Probes," presented at COSPAR First International Space Science Symp., Nice, France; January, 1960.
- [4] "The Moon Probe Pioneer IV," undated NASA-JPL booklet.
- [5] W. C. Pittman, "A parametric amplifier in space-probe tracking," *Astronautics*, vol. 4, pp. 40-44; August, 1959.
- [6] H. L. Richter, Jr., "The Microlock radio-tracking system," *Annals of the IGY*, vol. 6, pp. 410-417; 1958.
- [7] J. A. Van Allen and L. A. Frank, "Radiation measurements to 658,300 km with Pioneer IV," *Nature*, vol. 184, pp. 219-224; July 25, 1959.

## Review of USASRDL Satellite Propagation Studies\*

P. R. ARENDT†

**Summary**—The U. S. Army Signal Research and Development Laboratory has been engaged in a series of analyses of satellite radio propagation. Some examples of the observations and their interpretation are given. Details have been published elsewhere in individual reports.

THROUGH the continuous observation of all artificial earth satellites performed at the Astro-Observation Center of the Laboratory a series of studies on radio propagation and other phenomena related to outer space communications have been carried out. This type of passive experiment often suffers from lack of initial information regarding the satellite's radio transmitting features. It is essential to know in advance not only the frequency of the vehicle's transmission but also its antenna pattern, antenna gain, polarization and modulation of the signal, transmitter power, and the spinning or tumbling characteristics of the vehicle. For more elaborate evaluation a most precise ephemeris of the satellite is necessary. Therefore, during the initial period of the work a certain amount of detective labor was necessary. For example, it is difficult *a priori* to differentiate between signal fadeouts caused by an unknown antenna pattern of a vehicle spinning with unknown frequency and fadeouts caused by polarization fadings originated by unknown variations of the magneto-ionic effects along the ray paths. Furthermore, the recording operations are facilitated by the knowledge of expected position, of predicted time of intercept, and of expected Doppler shift range.

Part of the propagation studies is devoted to analysis of

the refractive effects of the ionosphere which alter the propagation path with regard to its length, curvature, and direction. A typical example for this effect is shown in Fig. 1 (an early recording of Sputnik I). The signal strength observed at 20 and at 40 mc is plotted vs time. The signals at 20 mc suffer more from refraction than at 40 mc. Thus, the 20-mc signal arrives first, but fades shortly thereafter. Then both signals appear and remain during the entire line of sight passage. Under favorable ionospheric and orbital conditions one can observe 20-mc signals propagated from the antipode between two line-of-sight passages. Also under sporadic conditions the 40-mc signal was heard normally when the 20-mc signal was missing. Obviously the 20-mc signal must have been refracted or reflected into outer space. For detailed interpretation of such phenomena it is obvious that at least some information on the ephemeris of the satellite is necessary.

The different curvature of the path is also demonstrated with polarization fading. Fig. 2 is an observation of this effect. Here a 20-mc signal of Sputnik III is recorded simultaneously with its first harmonic on 40 mc. According to theory, if the propagation paths were identical the time intervals between fadeouts should be proportional to the square of the frequency. However, this observation indicates, like so many others, that this relationship is not maintained with precision in this frequency range. The duration of the 20-mc fading normally differs about  $\pm 20$  per cent (and often far more) from that predicted from the 40-mc fading period. These observations suggest a very large divergence of the two ray paths.

The refraction effects cause deviations of the direction of the propagation path from the satellite to the observer.

\* Manuscript received by the PGMIL, February 1, 1960.

† Inst. for Exploratory Res., U.S. Army Signal Res. and Dev. Lab., Fort Monmouth, N.J.



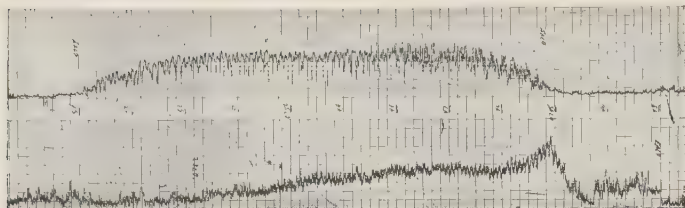


Fig. 1—Different times of initial intercept at the two frequencies of Sputnik I; 40 mc (top); 20 mc (bottom); October 13, 1957, about 07 hours EST; time from right to left, time marks in minutes.

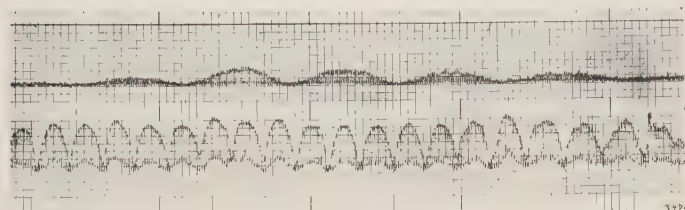
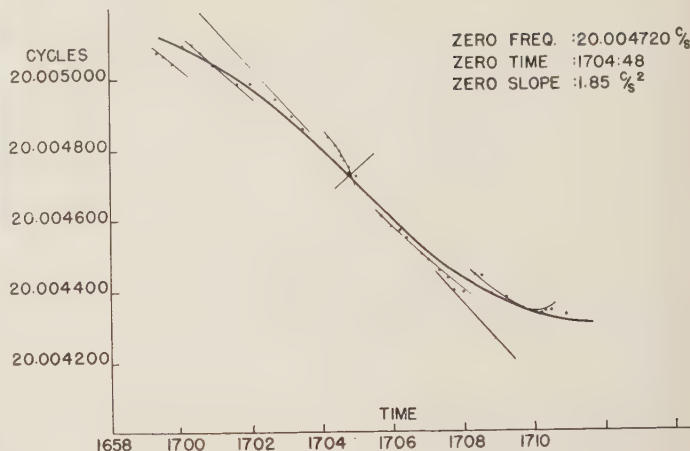


Fig. 2—Polarization fading of Sputnik III, orbit 3476; January 21, 1959, 0705 hours EST; vertical dipoles for receiver; 1 second per frame, time from right to left; 40 mc (top), 20 mc (bottom).

Thus the angle formed by this path and by the vector velocity of the satellite suffers sporadic deviations. Such spatial scintillations of the radio beam cause variations of the received Doppler frequency. Examples of these frequency scintillations are shown in Fig. 3. Their origin is presumed to be the same inhomogeneities of the ionosphere which have been studied by means of amplitude scintillation of radio stars. Direction finding has disclosed correlated deviations in the received azimuth bearings. The frequency scintillations are more frequent and more pronounced with the lower satellite frequencies (20-mc range) than with 100 mc. However, they have been observed in the 250-mc range, in the few observations made to date. These scintillation effects must be considered in precision frequency measurements, in Doppler tracking and when directive antennas are used at the vehicle or on the ground.

As a result of a continuous study of the frequency scintillations based on some 250 passages, a qualitative index in terms of the magnitude of the frequency deviations has been derived. This index has been prepared in order to attempt correlation of this measure of ionospheric activity with other geophysical and solar measurements (Fig. 4).

Other studies of a long-range nature have indicated the decay of the spin rate of Vanguard I. In the case of this satellite in which some 5000 passages within range of Fort Monmouth, N. J., have been observed, a very precise set of measurements has given detailed knowledge on the spin decay process. This decay is of exponential character; however, an anomaly in the decay rate was observed during winter solstice 1958.



SATELLITE  $\delta$  1958, 11 JUNE 58 ORBIT # 372

Fig. 3—Frequency scintillations and slope deviations on 20 mc; Sputnik III; orbit 372, June 11, 1958, about 1700 hours GMT.

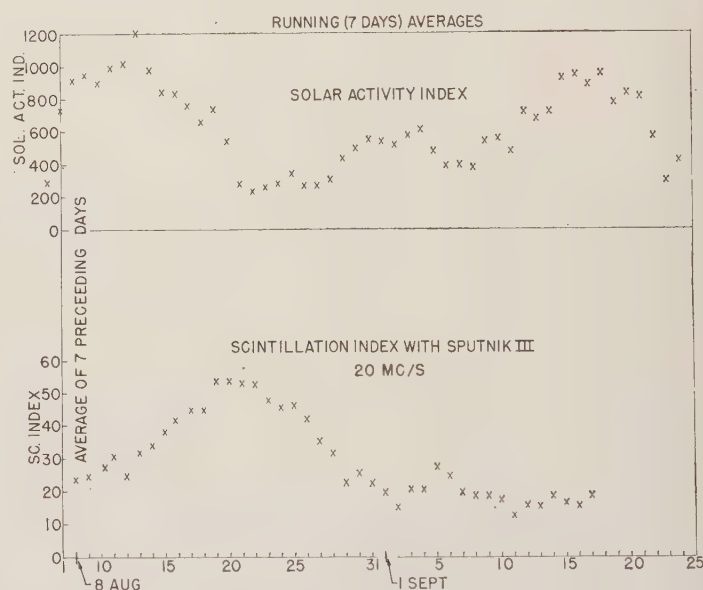


Fig. 4—Running averages of optical solar activity index and of scintillation index during August and September, 1958.

The studies of the above phenomena have created a better understanding of outer space radio propagation. They have led to various proposals for improved tracking, precision Doppler measurements, satellite navigation, and attitude observation. Concepts for satellite communication systems have been derived which permit continuous communication in spite of satellite spin or ionospheric changes. The program of signal analysis will be continued at the U. S. Army Signal Research and Development Laboratory in the future. Certain anomalies still exist without adequate explanation, showing that true knowledge of the ionosphere and its statistical behavior, although improved by this observation, is still limited.

# Analysis of Satellite Motion from Radio Reception\*

FRIEDRICH O. VONBUN†

**Summary**—This paper presents an analysis of a radio signal originating from a tumbling and rotating earth satellite. An equation is derived for the relative motion of the unit position vector pointing from the observer to the satellite with respect to the satellite coordinate system. From this, the amplitude variation of the ground received radio signal is calculated. It is further shown how a recording of this amplitude variation can be used to calculate the tumbling angle of the satellite in space. A simple example is given in which this angle between the normal of the plane of a satellite turnstile antenna system and a fixed axis in space is determined with the help of AGC recording. These recordings can be made either with linear or circular polarized receiving antenna. For future stabilized satellites, these derived equations can be used as an easy check of the operational condition of the stabilization system itself.

## I. INTRODUCTION

FOR satellites carrying photographic equipment as, for instance, in the case of the U. S. Army Cloud Cover Satellite, it is important that the "position" of the satellite with respect to an axis fixed in space is known in order that the photographed area on the earth may be determined. It is the purpose of this paper to develop equations which allow one to calculate this "position" based upon giving recordings from a satellite on the ground.

Bolljahn,<sup>1</sup> with the assumption that rotation is the only motion of a satellite, has shown how this rotation influences a radio signal, received on the ground from a satellite, in amplitude and frequency.

In this paper, equations are derived for the general movement of the unit position vector, with respect to the satellite coordinate system, pointing from the satellite to the observer. These equations can then be used to calculate the "modulation" of the radio frequency signal originating from a rotating and tumbling satellite. It is further shown how this information, given, for instance, in the form of an AGC recording, can be used to determine the tumbling angle of a satellite.

## II. THE SATELLITE ANTENNA

### A. Turnstile Antenna

In most of the launched satellites, turnstile antennas, which are crossed half-wave dipoles fed 90° out of phase, are used to communicate with stations on the earth. This type of an antenna has the advantage that no zero-field zones occur as in the case of only a single dipole.

To assure the continuity of this paper a brief intimation is given for the calculation of the antenna field.

The far field radiation of a turnstile antenna can easily be calculated from<sup>2</sup>

$$\mathbf{E} = c p_1 (\mathbf{r}_0 \times (\mathbf{r}_0 \times \mathbf{p}_{01})) + c p_2 (\mathbf{r}_0 \times (\mathbf{r}_0 \times \mathbf{p}_{02})), \quad (1)$$

where  $c$  is a function proportional to  $1/r$ , the inverse distance between observer and dipole;  $p_1$  and  $p_2$  are the magnitudes of the dipole moments;  $\mathbf{p}_{01}$  and  $\mathbf{p}_{02}$  are the unit vectors of the dipole moments directed in the positive sense of the  $x$  and  $y$  axes respectively; and  $\mathbf{r}_0$  is the unit vector directed from the origin, where the dipoles are located, to the observer.<sup>1</sup> By a simple calculation from (1) using the relation  $p_2 = j p_1$  and  $p_1 = p$  for a turnstile antenna, one obtains, for the  $\varphi$  and  $\vartheta$  component of the electric field in spherical coordinates,

$$\begin{aligned} E_\varphi &= j c p e^{j\varphi} \mathbf{e}_{\varphi 0}, \\ E_\vartheta &= c p e^{j\varphi} \cos \vartheta \cdot \mathbf{e}_{\vartheta 0}, \end{aligned} \quad (2)$$

where  $\mathbf{e}_{\varphi 0}$  and  $\mathbf{e}_{\vartheta 0}$  are the unit vectors in the  $\varphi$  and  $\vartheta$  directions. (See Fig. 1.) Examining (2), one sees immediately that the magnitude of the field of this antenna does not depend on the angle  $\varphi$ . The only amplitude variation comes from the angle  $\vartheta$  which is a function of time when the satellite is rotating and tumbling.

It is the function

$$\cos \vartheta(t) = (\mathbf{n}_0 \cdot \mathbf{r}_0) \quad (3)$$

which contains the information of the satellite movement and which will be calculated later.

### B. Dipole Antenna

In case the satellite is equipped with only a simple dipole  $\mathbf{p}_0$  directed along the  $z$  axis, shown as a dashed line in Fig. 1, the far field reads

$$\mathbf{E} = c p (\mathbf{r}_0 \times (\mathbf{r}_0 \times \mathbf{p}_0)), \quad (4)$$

or, in component form,

$$\begin{aligned} E_\vartheta &= c p \sin \vartheta \cdot \mathbf{e}_{\vartheta 0} \\ E_\varphi &= 0. \end{aligned} \quad (4a)$$

Also in this case, only the angle  $\vartheta(t)$  is of importance as far as the variation of the amplitude with time is concerned. Eq. (3) can therefore be used to analyze the signal variation since

$$\mathbf{E} = E_\vartheta = c p \sqrt{1 - \cos^2 \vartheta} \cdot \mathbf{e}_{\vartheta 0}$$

represents the far field for a single dipole.

\* Manuscript received by the PGMIL, February 1, 1960.

† NASA, Goddard Space Flight Center, Washington, D. C. Formerly at Frequency Control Div., U. S. Army Signal Res. and Dev. Lab., Fort Monmouth, N. J.

<sup>1</sup> J. T. Bolljahn, "Effects of satellite spin on ground-received signal," IRE TRANS. ON ANTENNAS AND PROPAGATION, vol. AP-6, pp. 260-267; July, 1958.

<sup>2</sup> J. A. Stratton, "Electromagnetic Theory," McGraw-Hill Book Co., Inc., New York, N. Y., p. 435; 1941.



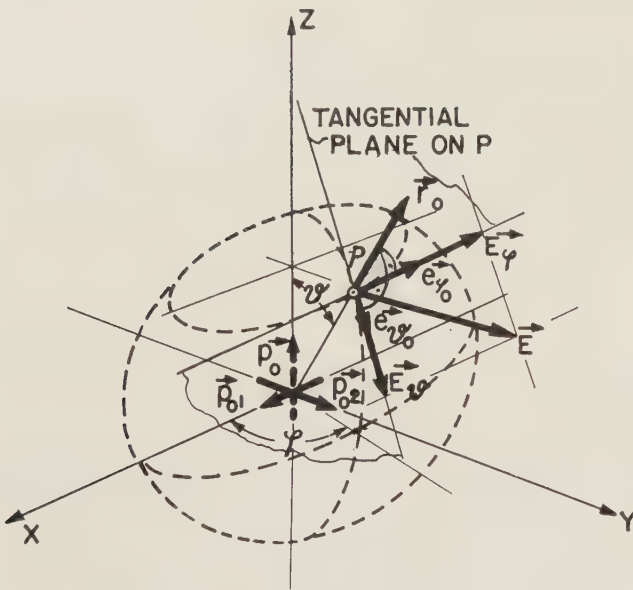


Fig. 1—Spherical coordinates to describe the far field of a turnstile antenna.

### III. GENERAL MOTION OF THE UNIT VECTOR OF OBSERVATION FOR A TUMBLING AND SPINNING SATELLITE

The motion of the unit position unit vector  $r_0$  shall be calculated with the help of Fig. 2. This is a schematic drawing showing the unit vectors of the dipole moments  $p_{01}, p_{02}$ , the normal of the antenna plane  $n_0$ , the tumbling axis  $h_0$ , the axis of rotation  $s_0$ , and the position vector  $r_0''$ , which is the position vector  $r_0$  after its relative motion in respect to  $h_0$  and  $s_0$ .

In order to simplify the mathematics involved, it is assumed that the satellite is fixed in space and that the unit position vector  $r_0$  performs the motion. More specifically:

- 1) The tumbling motion of  $s_0$  around  $h_0$  with a fixed  $r_0$  shall be replaced by a rotation of  $r_0$  around  $h_0$ , giving  $r_0'$  as shown in Fig. 3(a).
- 2) The rotation of the satellite around the axis  $s_0$  with a fixed  $r_0'$  shall be replaced by a rotation of  $r_0'$  around  $s_0$  giving  $r_0''$  as shown in Fig. 3(b).

From vector analysis it can readily be shown that the rotation of one vector around another can be represented by

$$r_0' = (h_0 \cdot r_0)(1 - \cos \Omega t)h_0 + r_0 \cos \Omega t + (h_0 \times r_0) \sin \Omega t, \quad (5)$$

and similarly

$$r_0'' = (s_0 \cdot r_0')(1 - \cos \omega t^*)s_0 + r_0' \cos \omega t^* + (s_0 \times r_0') \sin \omega t^*, \quad (6)$$

where  $\Omega t$  is the rotational angle of the tumbling motion and  $\omega t^*$  that of the rotation of the satellite as indicated

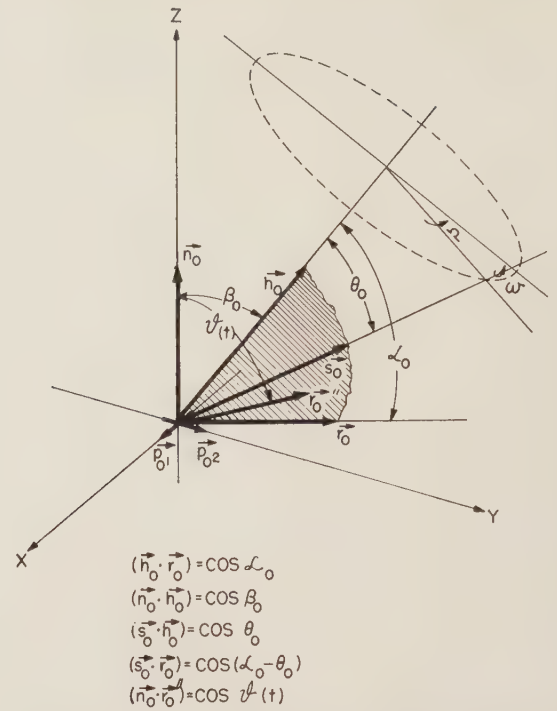


Fig. 2—Unit vectors in the satellite coordinate system.

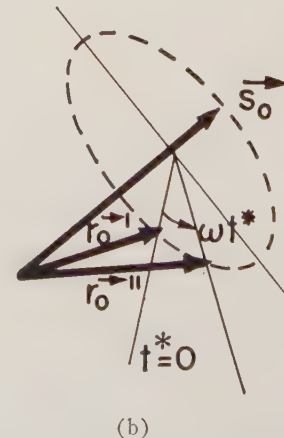
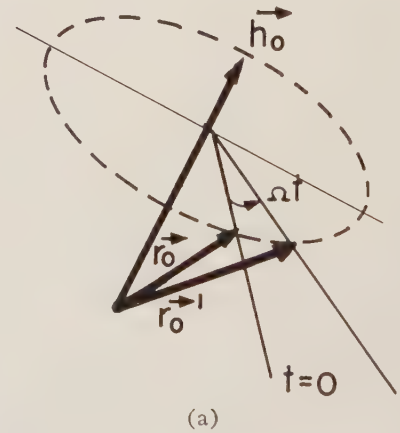


Fig. 3—Rotational and tumbling motion of the unit position vector  $r_0$ .

in Fig. 3(a) and Fig. 3(b). Since these two rotations are independent of one another, the time describing the angular motions must be different, that is for  $\Omega t = 0$ , with  $\Omega \neq 0$  the rotational motion  $\omega t^*$  took place already or vice versa.

Since  $\mathbf{r}_0$  rotates around  $\mathbf{s}_0$ , the time can be chosen so that for  $t^* = (t - t_0)$ ,  $\mathbf{h}_0$ ,  $\mathbf{s}_0$  and  $\mathbf{r}_0$  are coplanar vectors, thus simplifying the equation for  $\mathbf{r}_0''$ . This, of course, does not restrict the generality of this equation for  $\mathbf{r}_0''$  since  $\mathbf{h}_0$ ,  $\mathbf{s}_0$  and  $\mathbf{r}_0$  are constants. One obtains now for  $\mathbf{r}_0''$ , from (5) and (6), after some manipulation,

$$\begin{aligned} \mathbf{r}_0'' = & \{ (\mathbf{h}_0 \cdot \mathbf{r}_0)(1 - \cos \Omega t)(\mathbf{s}_0 \cdot \mathbf{h}_0) + (\mathbf{s}_0 \cdot \mathbf{r}_0) \cos \Omega t \} \cdot \\ & \cdot (1 - \cos \omega t^*) \mathbf{s}_0 + (\mathbf{h}_0 \cdot \mathbf{r}_0)(1 - \cos \Omega t) \mathbf{h}_0 \cos \omega t^* \\ & + \mathbf{r}_0 \cos \Omega t \cos \omega t^* + (\mathbf{h}_0 \times \mathbf{r}_0) \sin \Omega t \cos \omega t^* \\ & + (\mathbf{h}_0 \cdot \mathbf{r}_0)(1 - \cos \Omega t)(\mathbf{s}_0 \times \mathbf{h}_0) \sin \omega t^* \\ & + (\mathbf{s}_0 \times \mathbf{r}_0) \cos \Omega t \sin \omega t^* \\ & + (\mathbf{s}_0 \times (\mathbf{h}_0 \times \mathbf{r}_0)) \sin \Omega t \sin \omega t^*. \end{aligned} \quad (7)$$

Eq. (7) represents the general relative motion of the unit position vector  $\mathbf{r}_0$  for a tumbling and rotating satellite. Eq. (7) is restricted to satellite motion over a small arc only, since  $\mathbf{r}_0$  is considered to be a constant in this derivation. A motion of  $\mathbf{r}_0$  over an arc of  $\pi/20$  will not introduce a large error into (7), as can be seen from Figs. 2, 3(a), and 3(b). A satellite of a slant range of 1000 km can, therefore, move approximately 150 km (approximately 20 seconds) without violating the validity of (7). As is shown later, this small movement is adequate for determining the tumbling angle.

A considerable simplification of (7) and therefore of (3) can be obtained by assuming that the axis of rotation  $\mathbf{s}_0$  and the normal of the antenna plane  $\mathbf{n}_0$  coincide. That is

$$\mathbf{n}_0 = \mathbf{s}_0, \quad (8)$$

which is valid for satellites where the moments of inertia are

$$I_x = I_y < I_z.$$

The function  $\cos \vartheta$  can now be calculated using (3), (7), and (8), as follows:

$$\cos \vartheta = (\mathbf{h}_0 \cdot \mathbf{r}_0)(\mathbf{n}_0 \cdot \mathbf{h}_0)(1 - \cos \Omega t) + (\mathbf{n}_0 \cdot \mathbf{r}_0) \cos \Omega t. \quad (9)$$

This equation can, of course, be obtained by simply rotating  $\mathbf{r}_0$  around  $\mathbf{h}_0$ , as was done similarly in obtaining (5) and (6).

With the help of Fig. 4(a) one sees immediately that

$$\begin{aligned} (\mathbf{h}_0 \cdot \mathbf{r}_0) &= \cos \alpha_0 = c_1, \\ (\mathbf{n}_0 \cdot \mathbf{h}_0) &= \cos \theta_0 = c_2, \\ (\mathbf{n}_0 \cdot \mathbf{r}_0) &= \cos(\alpha_0 - \theta_0) = c_1 c_2 + \sqrt{1 - c_1^2} \sqrt{1 - c_2^2}. \end{aligned} \quad (10)$$

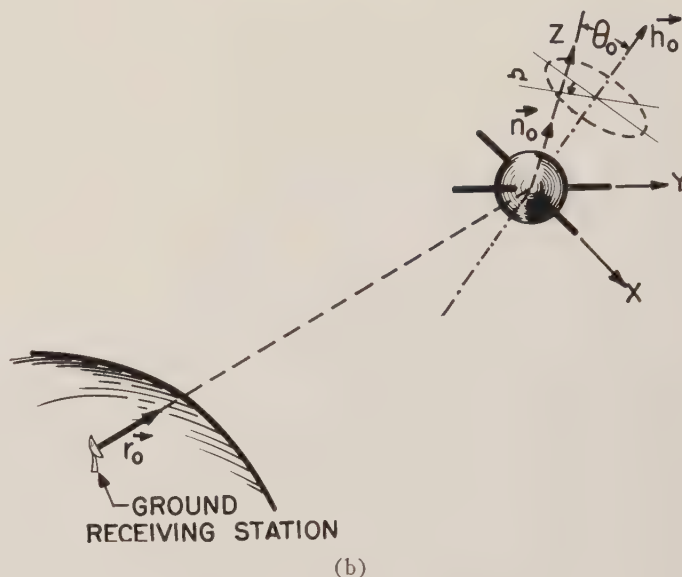
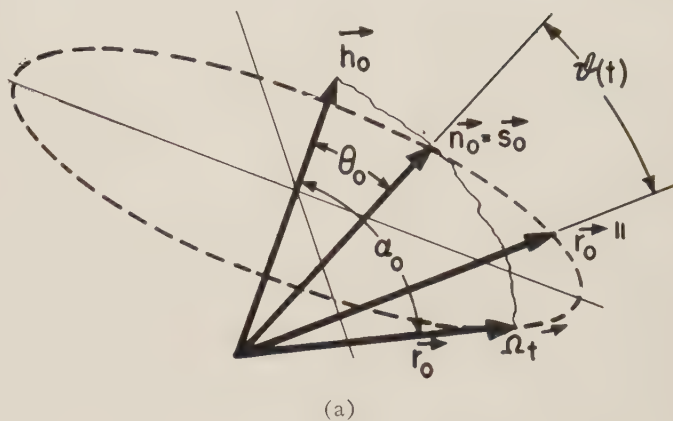


Fig. 4—(a) Unit vectors describing the relative tumbling motion of the normal of the antenna plane  $\mathbf{n}_0$  around a fixed axis  $\mathbf{h}_0$  in space. (b) Over-all view of the tumbling satellite.

Introducing (10) into (9) one finally gets for this particular case,

$$\cos \vartheta = a + b \cos \Omega t, \quad (11)$$

where

$$\begin{aligned} a &= c_1 \cdot c_2 \\ b &= \sqrt{1 - c_1^2} \sqrt{1 - c_2^2}. \end{aligned}$$

Eq. (11) is the final equation for the angle  $\vartheta$  which will later be used to determine the tumbling angle  $\theta_0$  shown in Figs. 2, 4(a), and 4(b). Note that (11) no longer contains the spin frequency  $\omega$ , which means that the satellite spin cannot be determined in this case.

#### IV. THE RECEIVED SIGNAL ON THE GROUND

Assume, as an example, that a satellite equipped with a "turnstile antenna system" is spinning with an angular frequency  $\omega$  and tumbling with  $\Omega$  as shown in Figs. 2, 4(a), and 4(b).



The received voltage amplitude  $V$  of the radio signal will now be calculated for two cases where the main beam of the receiving antenna is pointed towards the satellite, as shown in Fig. 4(b).

#### A. Linearly Polarized Receiving Antennas

From Fig. 5 one can see that the complex voltage  $V_c$  of a linear antenna represented by the unit vector  $\mathbf{m}_0$  is given by the scalar product of the complex electric field vector  $\mathbf{E}$  and  $\mathbf{m}_0$ . Thus

$$V_c = G((\mathbf{E}_\varphi + \mathbf{E}_\vartheta) \cdot \mathbf{m}_0), \quad (12)$$

where  $G$  is the total voltage gain of the receiving system. With the help of (2) and

$$\begin{aligned} (\mathbf{e}_{\vartheta 0} \cdot \mathbf{m}_0) &= \sin \delta_\varphi = \sigma = \cos \delta_\vartheta, \\ (\mathbf{e}_{\varphi 0} \cdot \mathbf{m}_0) &= \cos \delta_\varphi = \sqrt{1 - \sigma^2}, \end{aligned} \quad (13)$$

as shown in Fig. 5, one obtains for the received voltage

$$V = \chi \sqrt{1 - \sigma^2 + \sigma^2 \cos^2 \vartheta(t)}, \quad (12a)$$

where

$$\chi = Gc\rho.$$

#### B. A Circularly Polarized Receiving Antenna

This can be a pair of crossed dipoles fed  $90^\circ$  out of phase, or a helical antenna. The received voltage in this case is only dependent on the magnitude of the incoming electric field strength. Thus

$$V = G|\mathbf{E}| = Gc\rho|j\mathbf{e}_{\varphi 0} + \cos \vartheta \cdot \mathbf{e}_{\vartheta 0}|,$$

or

$$V = \chi \sqrt{1 + \cos^2 \vartheta(t)}, \quad (14)$$

where

$$\chi = Gc\rho.$$

The same can easily be done in a similar fashion for a satellite with a dipole antenna, (4a), and will not be further treated here.

### V. DETERMINATION OF THE TUMBLING ANGLE WITH THE HELP OF THE RECORDED SIGNAL ON THE GROUND

#### A. Linearly Polarized Receiving Antenna

Eq. (12a) will now be utilized to determine the tumbling angle  $\theta_0$ .

In order to evaluate (12a) to obtain  $\theta_0$  and  $\alpha_0$ , one has to consider  $\sigma$  as a constant. This can be assumed true only if a recording of  $V$  over a short period of time is considered, say 10 to 20 seconds, for a slant range of 1000 km and for a satellite in a quasi-equatorial orbit. The reason here is not the constancy of  $r_0$  alone, as described before, but the constancy of the Faraday rotation<sup>3,4</sup> for this condition. This is an even more stringent

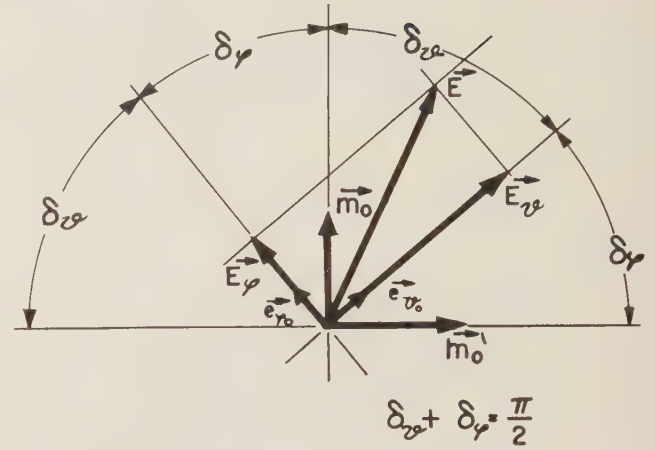


Fig. 5—Vectors representing the far field of the satellite antenna,  $\mathbf{E}$ , and the dipoles  $\mathbf{m}_0$  and  $\mathbf{m}_0'$  of the receiving antennas.

requirement, since one has no control whatsoever over the change of the axis of the elliptically polarized signal, due to this Faraday rotation. However, for a quasi-polar orbit, the change in Faraday rotation during the observation time could introduce a significant error using linearly polarized receiving antennas.

For simpler evaluation of (12a) in view of (11) it is better to work with  $V^2$  instead of  $V$  itself. Squaring (12a) and introducing (11), one obtains for an antenna system  $A$ ,

$$V^2 = g_0 + g_1 \cos \Omega t + g_2 \cos 2\Omega t, \quad (12b)$$

where

$$\begin{aligned} g_0 &= \chi^2(1 - \sigma^2) + (a^2 + \frac{1}{2}b^2)\chi^2\sigma^2, \\ g_1 &= 2\chi^2\sigma^2 a \cdot b, \\ g_2 &= \frac{1}{2}\chi^2\sigma^2 b^2. \end{aligned}$$

The  $g_0$ ,  $g_1$ , and  $g_2$ , are actually given values which can easily be obtained by a harmonic analysis of the square of the received voltage. One of the possible forms of  $V^2$  is shown in Fig. 6 together with the harmonics given by (12b). The information contained in (12b), namely the tumbling angle  $\theta_0$ , is absorbed in the values  $a$  and  $b$ , as can be seen from (10) and (11).

There are actually four unknowns in (12b)  $\chi$ ,  $\sigma$ ,  $a$  and  $b$ , but only three equations. ( $\chi$  is not easy to calculate in advance since the uncertainty in  $p$ , or in the radiated power, after the satellite is launched, is too large.) A second antenna  $A'$  (recording) is therefore needed. Assume one uses another dipole  $\mathbf{m}_0'$  perpendicular to  $\mathbf{m}_0$ , as shown in Fig. 5 and a receiver with the same gain. Then  $\chi' = \chi$  (for simplicity only). Also,

$$\begin{aligned} \sigma' &= (1 - \sigma^2), \\ (1 - \sigma'^2) &= \sigma^2. \end{aligned} \quad (15)$$

The two recordings obtained at the same receiving station yield, in view of (12b) and (15),

<sup>3</sup> Private communication with Dr. S. Bauer of the U. S. Army Signal Res. and Dev. Lab., Fort Monmouth, N. J.

<sup>4</sup> I. Daniels and S. Bauer, "The ionospheric Faraday effect and its application," *J. Franklin Inst.*, vol. 267, pp. 187-200; March, 1959.

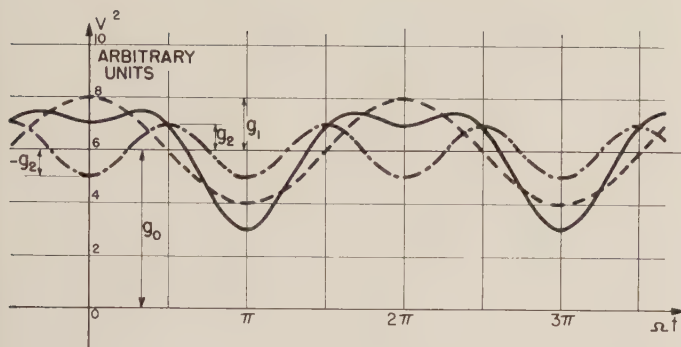


Fig. 6—A possible recording of the received power of a tumbling and rotating satellite. ( $g_0$ ,  $g_1$ , and  $g_2$  are the mean power and amplitudes of the first and second harmonics of the observed modulation respectively.)

$$V^2 = g_0 + g_1 \cos \Omega t + g_2 \cos 2\Omega t, \quad (16)$$

$$V'^2 = g_0' + g_1' \cos \Omega t + g_2' \cos 2\Omega t,$$

where

$$g_0 = \chi^2(1 - \sigma^2) + (a^2 + \frac{1}{2}b^2)\chi^2\sigma^2,$$

$$g_1 = 2\chi^2\sigma^2 ab,$$

$$g_2 = \frac{1}{2}\chi^2\sigma^2 b^2,$$

and

$$g_0' = \chi^2\sigma^2 + (a^2 + \frac{1}{2}b^2)\chi^2(1 - \sigma^2),$$

$$g_1' = 2\chi^2(1 - \sigma^2)ab,$$

$$g_2' = \frac{1}{2}\chi^2(1 - \sigma^2)b^2.$$

This can easily be achieved by using a dual channel recorder where each output of the system  $A$  and  $A'$  can be separately recorded. (The same recorder gain, of course, has to be used.)

From (16), only four equations are really necessary to calculate  $a$  and  $b$ . One obtains, after a simple calculation,

$$a = \pm \frac{\sqrt{2}}{4} \cdot \frac{g_1}{g_2} \cdot \left[ \frac{g_2'}{g_0 - g_2 - \frac{1}{8}g_1^2/g_2} \right]^{1/2},$$

$$b = \pm \left[ \frac{2g_2'}{g_0 - g_2 - \frac{1}{8}g_1^2/g_2} \right]^{1/2}. \quad (17)$$

Since  $a$  and  $b$  are now expressed by (17) in terms of the given values  $g_0$ ,  $g_1$ , and  $g_2$ , the tumbling angle  $\theta_0$  and the constant angle  $\alpha_0$  can be calculated.

From (11) one obtains

$$c_2 = \cos \theta_0 = \pm a \left\{ \frac{1}{2}(1 + a^2 - b^2) \right. \\ \left. \pm \left[ \frac{1}{4}(1 + a^2 - b^2) - a^2 \right]^{1/2} \right\}^{-1/2},$$

$$c_1 = \cos \alpha_0 = \pm \left\{ \frac{1}{2}(1 + a^2 - b^2) \right. \\ \left. \pm \left[ \frac{1}{4}(1 + a^2 - b^2) - a^2 \right]^{1/2} \right\}^{1/2}. \quad (18)$$

### B. A Circularly Polarized Receiving Antenna

Also in this case it is simpler to work with the squared values  $V^2$  of the received signal. From (14) and (11) one obtains a similar equation to the one for linearly polarized antenna, namely,

$$V^2 = g_0 + g_1 \cos \Omega t + g_2 \cos 2\Omega t, \quad (19)$$

where

$$g_0 = \chi^2 + \chi^2(a^2 + \frac{1}{2}b^2),$$

$$g_1 = 2\chi^2 ab,$$

$$g_2 = \frac{1}{2}\chi^2 b^2.$$

Here, three equations are available from one recording for the three unknowns  $\chi$ ,  $a$ , and  $b$ . From (19) one obtains

$$a = \pm \frac{\sqrt{2}}{4} \left[ \frac{g_1^2/g_2}{g_0 - g_2 - \frac{1}{8}g_1^2/g_2} \right]^{1/2},$$

$$b = \pm \left[ \frac{2g_2}{g_0 - g_2 - \frac{1}{8}g_1^2/g_2} \right]^{1/2}. \quad (20)$$

Eq. (18) can again be used for calculating  $\theta_0$  and  $\alpha_0$  respectively. As far as this analysis is concerned, at least over the short period of recording, the angle  $\alpha_0$  is a value dependent on the position of the receiving station, as previously described, and therefore different for each station while  $\theta_0$  is a constant.

## VI. CONCLUSIONS

The equation of motion for the unit position vector for a tumbling and spinning satellite is general and can be used for any kind of vehicle. From the simplified example presented one can see how the amplitude recordings can be used to determine the tumbling angle. It is also shown that it is more accurate, as well as more simple, to use circularly polarized receiving antennas since, in this case, any Faraday rotation of the incoming radiation does not influence the characteristic of the recordings.

For future stabilized satellites, this method can also be used to test the operating condition of the stabilization system after launching.

## VII. ACKNOWLEDGMENT

The author acknowledges helpful discussions, in the early stage of this paper, with Dr. R. Stampfl, Dr. A. Stroud, Dr. R. Hanel, and W. Bandeen of the National Aeronautics and Space Administration, Goddard Space Flight Center, Washington, D. C.

The many valuable suggestions and criticism offered by the author's colleague, Dr. H. H. Plotkin, during preparation of this article, are acknowledged with appreciation.



# World-Wide Clock Synchronization\*

F. H. REDER† AND G. M. R. WINKLER‡

**Summary**—To satisfy already existing needs for higher precision in various time measurements, a world-wide system of synchronized clocks is required.

One possible method for accomplishing such a system, the transportation of operating precision clocks, is discussed. Particular consideration is given to the use of atomic clocks in this connection, and methods of maintenance of synchronization by means of phase tracking of a central master clock via VLF transmissions are reviewed. Project WOSAC, a Signal Corps project of world-wide synchronization of atomic clocks based upon the principles discussed, is outlined and results already achieved are described.

## INTRODUCTION

SOME satellite and missile tracking methods, certain secure communication systems, scientific studies of propagation phenomena, etc., require precise synchronization to  $\pm 1$  microsecond or better of widely separated clocks. Present radio time transmissions furnish time with a precision of up to  $\pm 100$  microseconds, depending upon distance and propagation conditions. Very distant stations, however, cannot yet be synchronized to better than several milliseconds either because they receive a common signal which is randomly shifted in phase, or because they cannot receive the same central station and have therefore to rely on different transmissions. Different standard-time transmissions in general are not in synchronization to better than a few milliseconds with the notable exceptions of the two pairs WWV-WWVH ( $\pm 500$  microseconds)<sup>1,2</sup> and NBA-GBR (on an experimental basis).

Several methods have been proposed to improve the accuracy of clock synchronization. One method involves the use of LF or VLF timing signals with or without retransmission from the slave station.<sup>3</sup> Another method consists of transporting a very stable clock among all stations to be synchronized.

Range requirements dictate the use of VLF in the first case, but pulsing a VLF transmitter is problematic due to the high  $Q$  of VLF antennas. It is believed that the National Bureau of Standards is pursuing this approach.<sup>4</sup>

The clock transportation method, on the other hand, promises highest attainable accuracy but puts very severe requirements upon the environmental performance characteristics of the clock to be transported and might become quite expensive if many widely separated clock sites are involved. Extensive work on atomic frequency standards during the past several years has brought about a deeper understanding of the various points of view in regard to "Atomic Clocks,"<sup>5,6</sup> and has also produced a wealth of information about the performance of available commercial and military cesium beam frequency standards.<sup>7-9</sup> This method deserves, therefore, serious consideration.

It is the purpose of this paper to describe a feasibility study of world-wide synchronization of atomic clocks (Project WOSAC). The accuracy of synchronization using presently available equipment is expected to approach  $\pm 1$  microsecond.

WOSAC was initiated by the U. S. Army Signal Research and Development Laboratory in the summer of 1959, and is carried out in close cooperation with J. A. Pierce of Cruft Laboratory, Navy Electronics Laboratory, Rome Air Development Center, Air Force Missile Test Center at the Patrick Air Force Base, and the British Post Office. WOSAC is based upon establishing synchronism of widely separated atomic clocks by the clock transportation method, and maintaining the synchronism by phase tracking VLF transmission signals controlled by the master clock. After a general discussion of atomic clocks and their applications, and a brief consideration of the use of VLF transmissions for maintaining slave stations in synchronism with the master clock, Project WOSAC is outlined in detail and the results already achieved are reported.

## ATOMIC CLOCKS

The error,  $E$ , of a clock after a time,  $T$ , is usually expressed by:

$$E = E_0 + R \cdot T + \frac{1}{2} AT^2, \quad (1)$$

\* Manuscript received by the PGMIL, February 1, 1960.

† Frequency Control Div., U. S. Army Signal Res. and Dev. Lab., Fort Monmouth, N. J.

<sup>1</sup> Natl. Bur. of Standards, "Standard Frequencies and Time Signals WWV and WWVH," Letter Circular LC 1012, Boulder Labs.; June, 1956.

<sup>2</sup> Natl. Phys. Lab., "Standard-frequency transmissions," *Electronic Radio Engr.*, vol. 36, pp. 117-118; March, 1959.

<sup>3</sup> A. H. Morgan, "Precise Time Synchronization of Widely Separated Clocks," Natl. Bur. of Standards, Boulder, Colo., Tech. Note No. 22; July, 1959.

<sup>4</sup> A. D. Walt, *et al.*, "A Study of Power Requirements and Choice of an Optimum Frequency for a World Wide Standard Frequency Broadcasting Station," Natl. Bur. of Standards, Boulder, Colo., Rept. No. 6023; November 10, 1958.

<sup>5</sup> L. Essen and J. V. L. Parry, "The cesium resonator as a standard of frequency and time," *Phil. Trans. Roy. Soc. (London)*, vol. 250, pp. 45-69; August 8, 1957.

<sup>6</sup> B. Deaux, "Etalons de frequence," *Astronom. J.*, vol. 64, pp. 116-119; April, 1959.

<sup>7</sup> J. Holloway, W. Mainberger, F. H. Reder, G. M. R. Winkler, L. Essen, and J. V. L. Parry, "Comparison and evaluation of cesium atomic beam frequency standards," *Proc. IRE*, vol. 47, pp. 1730-1736; October, 1959.

<sup>8</sup> F. H. Reder and S. Roth, "Performance of a Cs beam frequency standard," *Proc. 11th Annual Symp. on Frequency Control*, Asbury Park, N. J., pp. 385-401; May 7-9, 1957.

<sup>9</sup> R. Bridgman, G. M. R. Winkler, and F. H. Reder, "Synchronized clock experiment," *Proc. 13th Annual Symp. on Frequency Control*, Asbury Park, N. J., pp. 342-349; May, 1959.

where  $E_0$  is the initial error,  $R$  is the clock rate (original fractional frequency offset), and  $A$  is the acceleration (fractional drift rate) of the clock. These coefficients,  $R$  and  $A$ , as small as they are for an atomic clock, unfortunately cannot be neglected if a long-term clock synchronization to  $\pm 1$  microsecond is required. For example, let us take a cesium beam clock. We have to consider influences upon the atomic frequency itself (magnetic  $C$  field), influences which change the observation conditions of the atomic frequency (phasing of the two Ramsey cavities, presence of sidebands in the exciting signal, etc.), and influences in the servo loop which change the locking point (presence of a second harmonic in the modulation signal, change in the drift rate of the quartz crystal flywheel, etc.). These influences either are constant or vary with time in a systematic or random way. Constant influences introduce  $R$ , which represents the constant fractional frequency offset between two individually adjusted models. A frequency adjustment of two standards will reduce but not eliminate  $R$ . Rapid variations of influences may best be described by changes in  $R$ . Slowly varying influences can be represented by  $A$ .<sup>10</sup> Trouble arises in clock operation mainly from unpredictable systematically changing influences, which are, *e.g.*, caused by changing environmental conditions or aging of electronic components and mechanical structures, because in cases of clock operation interruptions for adjustments<sup>9</sup> cannot be tolerated (in contrast to the operation of a frequency standard), and we will have no other means to find out about systematic changes. This constitutes the limit for the accuracy of the clock transportation method. To give an idea about the order of magnitudes involved, these systematic changes in  $R$  are smaller than  $10^{-10}$  for presently available equipment (*e.g.*, National Company's Atomichron NC-1001) if the apparatus is kept on reasonably constant line voltage and temperature. Values of  $A$  for various changes of conditions may be found in the literature.<sup>8</sup>

The question can be raised which of the several types of atomic clocks is best suited for the purpose of the flying clock, the master clock, and the slave clocks. Only the cesium beam frequency standard mentioned above is commercially available. It has demonstrated over the past four years that it is capable of producing by far the highest accuracy and stability. Only its large size (7-foot rack) and sensitivity to rotational movements have presented problems in certain mobile applications. Its rotation sensitivity is caused by the beam deflecting action of Coriolis forces which make the atoms miss the particle detector and drive the system out of lock. Rotations slower than  $90^\circ$  per 15 seconds, of the large

NC-1001 Atomichron, around an axis normal to the beam direction are harmless. Work on new models of considerably reduced size (less than 2 cubic feet) is in progress [AF 33(600)-36067, AF 33(600)-39025, DA 36-039-SC-73283].

In the future, other highly stable frequency standards based on the maser principle,<sup>11</sup> or on the gas cell method using optical pumping and optical detection, might come on the market. It is easy to see that passive devices, *e.g.*, the cesium beam apparatus or the gas cell, are principally superior for any long-time clock operation over the active maser devices. The active standards suffer from the disadvantage that their frequency is subject to pulling by the tuned resonance structures employed. It may be true that one can keep this influence constant, but the same amount of care observed in the operation of a passive device will produce better results simply because there is one less disturbing influence. However, the active systems do have advantages in respect to short time stability<sup>12</sup> and insensitivity to extreme environmental conditions.<sup>13</sup> The gas cell standard using buffer gases<sup>14,15</sup> for line-width reduction has the probable advantage of low weight and power consumption, and small size, but its frequency is subject to shifting effects of the buffer gases.<sup>16</sup> For the same reason, the frequency may also be more strongly influenced by the electronics (power shift, modulation-sensitivity, etc.) than is the case in a cesium beam device. This overshadows a little the hope that it might at least become a cheap secondary standard of high stability, which will in the long run stand up to the competition by the best quartz crystal standards. We believe, therefore, that the cesium beam device is now, and will also remain at least for the near future, the best choice for an atomic clock in synchronization experiments.

Most atomic frequency control devices have been used in the past to calibrate the rate of high precision quartz crystal clocks since it is postulated that the observation of a natural constant, as the oscillation frequency of the cesium atom under specified conditions, will at least yield a uniform time scale. This is already very valuable because crystal clocks alone or in conjunction with the rotation of the earth cannot produce

<sup>11</sup> R. C. Mockler, *et al.*, "The ammonia maser as an atomic frequency and time standard," IRE TRANS. ON INSTRUMENTATION, vol. I-7, pp. 201-202; December, 1958.

<sup>12</sup> A. Morgan and J. A. Barnes, "Short time stability of a quartz crystal oscillator as measured with an ammonia maser," PROC. IRE, vol. 47, p. 1782; October, 1959.

<sup>13</sup> F. H. Reder and C. Bickart, "A missile borne maser frequency standard," Proc. 13th Annual Symp. on Frequency Control, pp. 546-565; May, 1959.

<sup>14</sup> R. H. Dicke, "Effect of collisions on Doppler width," Phys. Rev., vol. 89, pp. 472-473; January 15, 1953.

<sup>15</sup> P. L. Bender, *et al.*, "Optical detection of narrow Rb<sup>87</sup> hyperfine absorption line," Phys. Rev. Letters, vol. 1, pp. 311-313; November 1, 1958.

<sup>16</sup> M. Ardit, *et al.*, "Frequency shift of the zero field hyperfine splitting of Cs<sup>133</sup> produced by various buffer gases," Phys. Rev., vol. 112, pp. 449-450; October 15, 1958.

<sup>10</sup> F. H. Reder, "Proposed feasibility study of frequency shift in sealed atomic beam frequency standards," PROC. IRE, vol. 47, pp. 1656-1657; September, 1959.



a uniform time scale.<sup>17-24</sup> It can even be assumed that for most practical purposes this atomic time scale will have no acceleration with respect to the uniform Ephemeris Time (ET), which is derived from gravitational celestial phenomena.

The time scale of the Model NC-1001 Atomichron, however, differs from ET because this standard refers its output frequencies to a cesium zero field frequency,  $f = 9,192.631840$  mc, instead of using the measured value of  $9,192.631770$  mc.<sup>21</sup> Our clock, therefore, is slow by  $74.5 \times 10^{-10}$  with respect to ET including the effect of the magnetic  $C$  field (1.5 cps). The various forms of Universal Time,  $UT$ ,  $UT_1$  and  $UT_2$ , and also sidereal time, which are all time systems in respect to the varying rotation of the earth, have no significance for our problems here, as valuable as they still are for geodesy, celestial navigation and the civic life.  $UT_2$  is presently slow in respect to ET by more than 2 ms per day and seems to slow down further.

The poor accuracy of about 0.1 second of an epoch, if given in ET, on the other hand, makes the adoption of a separate time system necessary for each net of electronically synchronized stations. These time systems are obviously independent of the astronomical relationships. In practice, this has been the case in all precision range-timing systems for several years. A world-wide net of synchronized stations, as envisioned in Project WOSAC, creates a new point of view only insofar as it does not deal with centrally distributed timing pulses, but relies on a free-running clock at each station with only initial synchronization, and on cautious use of phase information via VLF transmissions, as we shall see later. Our "semi-independent" clocks must be good enough (parts in  $10^{11}$  or better) to bridge the relatively long time intervals for determining any necessary correction.

The clock adjustments, when they become necessary, are carried out with respect to rate and phase. The dependency of the cesium resonance frequency upon the  $C$  field is given by<sup>5</sup>

$$f = f_0 + 427 \cdot (B^2), \quad (2)$$

<sup>17</sup> W. Markowitz, "Uniform Time," U. S. Naval Observatory, 6 pp.; April 29, 1957.

<sup>18</sup> W. Markowitz, "On the Calibration of Atomic Standards of Frequency," U. S. Naval Observatory; August 19, 1957.

<sup>19</sup> W. Markowitz, "Variation in the speed of rotation of the earth since June, 1955," *Nature*, vol. 181, p. 1054; April 12, 1958.

<sup>20</sup> W. Markowitz, "The Second of Ephemeris Time," U. S. Naval Observatory; July 26, 1958.

<sup>21</sup> W. Markowitz, et al., "Frequency of cesium in terms of ephemeris time," *Phys. Rev. Letters*, vol. 1, p. 204; August 1, 1958.

<sup>22</sup> W. Markowitz, "Astronomical and atomic times," U. S. Naval Observatory; March 9, 1959.

<sup>23</sup> W. Markowitz, "The system of atomic time," *Proc. 13th Annual Symp. on Frequency Control*, Asbury Park, N. J., pp. 316-317; May, 1959.

<sup>24</sup> National Bureau of Standards, "National standards of time and frequency in the United States," *Proc. IRE*, vol. 48, pp. 105-106; January, 1960.

( $B$  in gauss and  $f$  in cps), and can conveniently be used for a very fine control of the rate of an atomic clock in respect to a "master" clock. The phase of the clock may be set, for instance, by means of a continuously variable phase shifter (resolver type) in the 100-kc channel.

The difference in terminology between a clock and a frequency standard is rather subtle but useful. If one uses the apparatus to compare frequencies (derivatives) directly then it should be called frequency standard, and if the emphasis is on phase or time measurements one should speak about a clock. In the latter case, a counting device is added to the frequency standard.

Since all atomic frequency standards already employ a crystal oscillator of their own, it should be quite unnecessary to use an additional crystal oscillator and to calibrate it from time to time in terms of the atomic standard, provided the atomic standard has sufficient reliability to keep the clock in operation. Such a calibration procedure is bound to introduce additional errors, especially if the rate of the crystal clock is adjusted frequently. The change of rate of a crystal oscillator may produce long-lasting after-effects with subsequent unaccountable time errors. In addition, it is against the principles not to control continuously a quantity (phase of the crystal clock) but discontinuously its derivative only.<sup>25</sup> However, atomic frequency standards can, by their very nature, hardly ever reach the reliability of the much simpler quartz crystal oscillator. One answer to this problem is, of course, redundancy engineering to utilize the high accuracy of atomic standards and the excellent reliability of a quartz crystal flywheel oscillator in one system.<sup>26</sup> This measure is especially important for the central clock which also controls the VLF transmission. It is not absolutely necessary for the "slave" clocks because they can maintain synchronism with somewhat reduced accuracy by VLF phase tracking during the time of breakdown of the atomic frequency standard. The basic principle of the clock, described previously by Winkler,<sup>26</sup> is simple. An electronic device keeps a reliable quartz crystal oscillator (flywheel) phase-locked to the average output signal of several atomic standards. Whenever an atomic standard falls out of lock its input signal is automatically removed from the locking device, and the quartz crystal oscillator locks on to the mean signal from the remaining atomic devices.

## VLF TRANSMISSIONS

VLF transmissions have been used for precision fre-

<sup>25</sup> V. A. Rubtsov, "On the equivalency between sampled data and continuous control systems," *Automation Express*, vol. 1, p. 38; February, 1959.

<sup>26</sup> G. M. R. Winkler, "A superior atomic clock for continuous long time operation," *Proc. 14th Annual Symp. on Frequency Control*, Atlantic City, N. J.; June 2, 1960.

quency measurements for several years.<sup>27-36</sup> This frequency range has the particular advantage of comparatively small changes of the transmission medium characteristics, but VLF signals cannot be pulsed with a high degree of accuracy since the bandwidth of the antennas is in the order of 50-100 cps only. It is rather the carrier itself which advantageously can provide the timing information. The features of main interest for our purpose are: 1) the low propagation loss, 2) the diurnal phase variation, and 3) the sudden phase disturbances. Although a study<sup>4</sup> revealed the advantages of the frequency range around 20 kc with respect to efficiency, transmitter power, noise, and greatest coverage, the range around 10 kc will probably be better for timing purposes.<sup>33</sup>

Pierce has convincingly demonstrated<sup>31</sup> that, except for the periods of sunset or sunrise over the transmission path, the phase of a VLF signal remains remarkably stable (with an approximate 5-hour standard deviation of 2 microseconds for the transatlantic GBR signal). Sudden disturbances which are more pronounced during the night time<sup>27</sup> have been observed with effects upon the received frequency of up to  $6p:10^8$ .<sup>32</sup> These severe disturbances seem to be very rare, however.

Disturbances are, in principle, changes in the propagation time or, as they are observed, phase shifts around an invariant value. Pierce has used this criterion successfully to distinguish the propagational phase shifts which must come back to the average value, from the "secular" phase shifts caused by changes of the oscillator frequency which will increase with time.<sup>31</sup> If frequency measurements are made without regard to this criterion by choosing arbitrary end points to determine the quantity

$$\Delta\Omega = \frac{\Delta\phi}{\Delta t},$$

<sup>27</sup> J. A. Pierce, "Intercontinental frequency comparison by very low frequency radio transmission," *PROC. IRE*, vol. 45, pp. 794-803; June, 1957.

<sup>28</sup> J. A. Pierce, "Recent long distance frequency comparisons," *IRE TRANS. ON INSTRUMENTATION*, vol. I-7, pp. 207-210; December, 1958.

<sup>29</sup> D. D. Crombie, A. H. Allan, and M. Newman, "Phase variations of 16-kc transmissions from Rugby as received in New Zealand," *Proc. IEE*, vol. 105, pp. 301-304; May, 1958.

<sup>30</sup> J. A. Pierce, "The diurnal carrier phase variation of a 16-kc transatlantic signal," *Proc. IRE*, vol. 43, pp. 584-588; May, 1955.

<sup>31</sup> J. A. Pierce, "Frequency standards for research in radio wave propagation," *Proc. 13th Annual Symp. on Frequency Control*, Asbury Park, N. J., pp. 318-341; May, 1959.

<sup>32</sup> J. A. Pierce, "VLF phase shifts associated with the disturbance of February 23, 1956," *J. Geophys. Res.*, vol. 61, pp. 475-483; September, 1956.

<sup>33</sup> C. J. Casselman, D. P. Heritage, and M. L. Tibbals, "VLF propagation measurements for the Radux Omega navigation system," *PROC. IRE*, vol. 47, pp. 829-839; May, 1959.

<sup>34</sup> W. Markowitz, "Time Service Notice No. 7," U. S. Naval Observatory; June 19, 1959.

<sup>35</sup> S. N. Kalra, "Frequency measurement of standard frequency transmissions against caesium beam resonator standard," *Can. J. Phys.*, vol. 37, pp. 1328-1329; November, 1959.

<sup>36</sup> B. Decaux and A. Gabry, "Comparison of atomic frequency standards by means of myriametric wave transmissions," *Compt. rend. Acad. Sci., Paris*, vol. 249, November 23, 1959. (In French.)

then obviously the resolution<sup>37</sup> of the frequency measurement will be very poor.

Therefore, it seems to be quite possible to use a highly stable (atomically controlled) VLF transmission to keep a slave clock in synchronism with a central master clock. The requirement is only that the slave clocks be very stable because one cannot make corrections more frequently than about once a day. The important point is that one deals here with a phase lock with a very long time constant, and that good judgment is required.

This latter "circuit element" is not easily represented electronically, but the phase tracking operation can be facilitated to a good degree by use of a diurnal simulator, as used by Pierce.<sup>27</sup>

A side aspect of the experiments under consideration is the question of the value of the phase velocity of VLF transmissions as a function of frequency, direction (reciprocity law), surface condition, and season. Such measurements can be carried out conveniently during the clock transportation when the slave clocks are initially synchronized with the master clock, by counting the number of wavelengths over the clock distances. It may be interesting to note earlier attempts to measure propagation velocities in the VLF range by a different method.<sup>38</sup>

#### DETAILS ON PROJECT WOSAC

In order to demonstrate the feasibility of world-wide clock synchronization by initial synchronization with a flying clock and maintenance of synchronism by VLF phase tracking, it was decided to break up Project WOSAC into five tasks:

- 1) study of the influence of the propagation medium on the phase stability of a transatlantic VLF signal (Task GBR<sup>39</sup>),
- 2) experiments with directly Atomichron-controlled LF transmitters (Task V-II<sup>39</sup>),
- 3) study of very long distance propagation effects using a directly Atomichron-controlled high-power VLF transmitter (Task "Hawaii"<sup>39</sup>),
- 4) feasibility study of high precision time transfer by flying atomic clocks (Task V-I<sup>39</sup>), and
- 5) attempt to demonstrate maximum-range clock synchronization, and measurement of VLF propagation velocities (Task V-III<sup>39</sup>).

<sup>37</sup> G. M. R. Winkler, "Short time stability measurements on frequency standards and the notion of resolution," *PROC. IRE*, vol. 47, p. 101; January, 1959.

<sup>38</sup> Ia. L. Al'pert and S. V. Borodina, "On the speed of propagation of electromagnetic waves at audio frequencies," *JETP (USSR)*, vol. 33, pp. 1305-1307; November, 1957.

<sup>39</sup> The abbreviations represent the old task identifications which were used when Project WOSAC was set up in the summer of 1959.



## TASK GBR

The phase of the quartz crystal controlled 16-kc VLF signal, GBR, radiated by the Rugby station with an output power of 50 kw, was monitored in the past by Cruft Laboratory<sup>27-31</sup> and NRL<sup>40</sup> with reference to Atomichrons 112 and 110, respectively. The determination of the frequency of the controlling quartz crystal oscillator and of the influence of the propagation medium on the phase of the GBR signal was obstructed by the vagaries of the crystal oscillator and by other phase changing influences in the Rugby transmission system. To separate clearly the propagation effects from perturbations introduced by the transmission facilities, and to determine the ultimate accuracy of VLF frequency transfer over a path of medium length (about 5200 km), task GBR was set up by USASRDL in close cooperation with the British Post Office, and with J. A. Pierce of Cruft Laboratory who suggested this experiment.

A monitoring station was installed in September, 1959 at Banbury (40 km from Rugby) which was equipped with apparatus (Fig. 1) similar to that used by Pierce at the other side of the Atlantic Ocean. The station consisted of Atomichrons 111 and 117, frequency dividers, a precision scope, and a film camera.<sup>27</sup> This way it was possible to measure the phase of the GBR signal with reference to Atomichron 111 at the beginning of the path and with reference to Atomichron 112 at the end of the path. Combining the results from the two stations demonstrated convincingly the rather small effect of the propagation medium on the average frequency. Calculating<sup>41</sup> the average frequency from the change in phase during the daytime transmission gave a standard deviation of 3 parts in  $10^{11}$ . For nighttime transmission the standard deviation was 4 parts in  $10^{11}$ , and for a 24-hour averaging period it was 2.5 parts in  $10^{11}$  which confirmed very well Pierce's prediction.<sup>31</sup> Since the period of daylight over the whole transmission path becomes shorter on the northern hemisphere during the winter, the accuracy of frequency determined from a single daylight transmission decreases in winter time. On the other side, it is known that magnetic activity exerts a larger influence on the phase stability of the VLF signal during nighttime propagation.<sup>31</sup> Phase changes appearing simultaneously on the records of both stations were interpreted as having been caused by sudden changes in the transmission system, e.g., one phase jump occurred (as the log book of the transmitter revealed afterwards) when the transmitter was shut down for a short period. Details on the results of this very successful experiment, which was brought to a conclusion on October 30, 1959, will be published elsewhere.<sup>41</sup>

<sup>40</sup> J. A. Murray and H. F. Hastings, "Long Distance Comparison of Frequency Standards," Report of NRL Progress; June, 1958.

<sup>41</sup> J. A. Pierce, et al., "The GBR experiment: a transatlantic frequency comparison between Cs controlled oscillations," paper in preparation for submission to *Nature*, 1960.

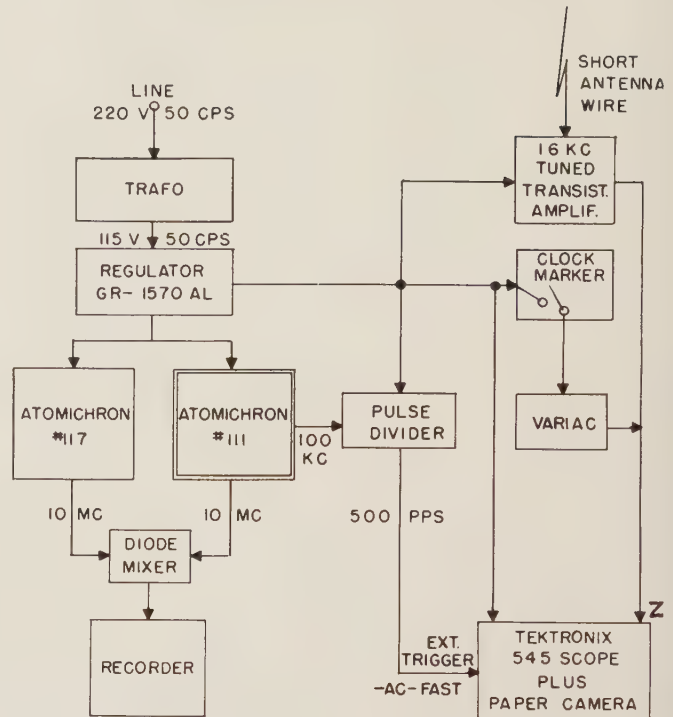


Fig. 1—Block diagram of the monitoring station for the 16-kc GBR transmission, at Banbury, England (GBR).

#### DIRECT ATOMICHRON CONTROL OF LF TRANSMITTERS (V-II)

It was clear from the beginning that the procedure followed in Task GBR was the most economical one to reach the limited goal of this task, but that it required a direct control of a VLF station by atomic clocks in order to fulfill the final aim of Project WOSAC. Such direct control of the Rugby GBR station was not practicable at the time in view of this transmitter's mission.

Other VLF stations were also not available at this time for the purpose of evaluating their performance under direct Atomichron control. Existing LF facilities at Fort Monmouth were, therefore, chosen to put a  $33\frac{1}{3}$ -kc transmitter in operation at Oakhurst, N. J., and a  $133\frac{1}{3}$ -kc transmitter at Earle, N. J. Both are controlled by a single Atomichron by way of microwave links in order to gain experience with Atomichron control of transmitters, to evaluate phase control for the emitted signals, to aid in Task V-I, and to provide two simultaneously Atomichron-controlled signals for propagation studies and accurate frequency-transfer to other places in the eastern part of the U.S.

A block diagram of the complete final transmission facilities at Fort Monmouth is given in Fig. 2. The  $133\frac{1}{3}$ -kc Earle transmitter has been in operation since October, 1959, on an experimental basis, using a simple flat top antenna which radiates only about 30 watts of power. The call sign A5XA is given every 10 minutes. During October and November, the  $133\frac{1}{3}$ -kc signal was monitored by Pierce with respect to Atomichron 112. Standard deviations for one-hour phase measurements.

were as good as 0.05 microsecond for daylight operation and 0.25 microsecond for nighttime operation. The results of the various runs are listed in Table I.

The daylight results raise the question if the remaining errors were mainly due to instabilities of the propagation medium or of the Atomichrons. To decide the question, one new atomic beam standard each (USASRDL Contract DA36-039 SC-74863) will be in-

stalled temporarily at both ends of the propagation path (Fort Monmouth—Harvard) sometime in August, 1960. The new models are expected to have a higher stability.

The furthest point at which the signal was definitely identified was at the Ohio State University, Columbus. This is not enough range for Task V-I. During December and January, the Earle transmitter was, therefore, modified and now uses a top-loaded, 186-feet high, base-fed tower. An increase of radiated power by 15 db will make it possible to receive the A5XA signals at Cape Canaveral for the synchronization experiment V-I.

The  $33\frac{1}{3}$ -kc Oakhurst transmitter was completed January 10, 1960, and was put into operation during the same month. Ten kw of power are fed into a 400-foot high, loop-excited tower. The radiated power is expected to be about 2 watts. It will have the same call sign as the Earle transmitter. The power amplifier for this station was supplied by NRL, and parts of the tuning unit by NEL.

It is tentatively planned that one or both Fort Monmouth transmitters will be put on a regular transmission schedule beginning in February, until the summer of 1960 for allowing a long-term evaluation of propagation characteristics.

#### DIRECT ATOMICHRON CONTROL OF HIGH-POWER VLF STATIONS ("HAWAII")

Task V-II has already given excellent results with direct Atomichron control of the  $133\frac{1}{3}$ -kc transmitter. The next logical step is, therefore, to establish direct Atomichron-control of a high-power VLF transmitter for

- 1) an experiment supplemental to GBR, to get information on phase stability and accuracy of frequency transfer over distances from 8000 to 20,000 km,

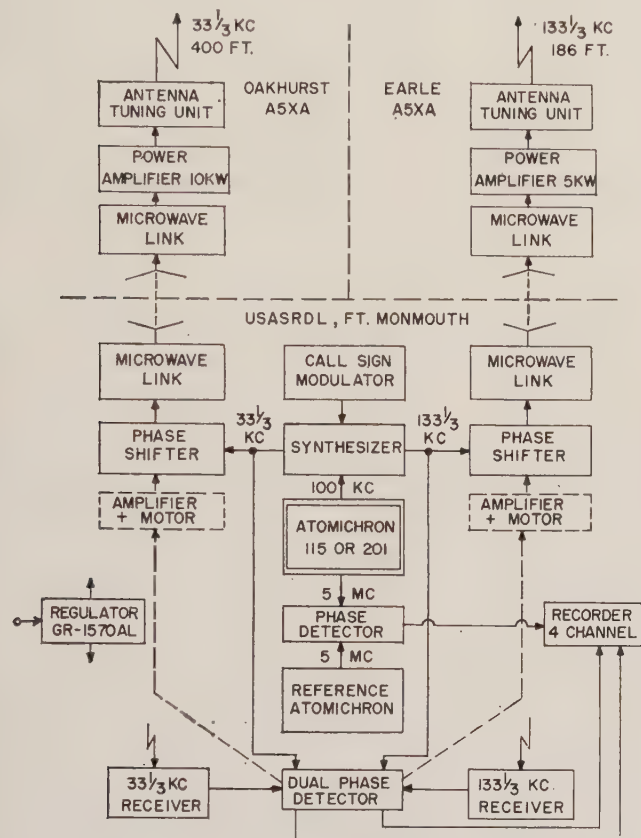


Fig. 2—Block diagram of the control equipment for the two USASRDL LF stations Earle ( $133\frac{1}{3}$  kc) and Oakhurst ( $33\frac{1}{3}$  kc) (V-II).

TABLE I

STABILITY OF THE DIRECTLY ATOMICHRON-CONTROLLED A5XA ( $133\frac{1}{3}$  KC) SIGNAL IN TERMS OF ATOMICHRON 112 AT CRUFT LABORATORY. DATA ON LABORATORY COMPARISONS OF ATOMICHRONS AT USASRDL ARE ADDED AT THE END OF THE TABLE

Date	Atomichrons	Hours of Comparison	Inherent Averaging Time	$\Delta f/f \cdot 10^{11}$	$\sigma \times 10^{11}$	$p \times 10^{12}$
October 22	8-112	6, day	1 hour	- 1.4	1.5	6.0
October 28	8-112	6, day	1 hour	- 3.4	1.0	4.0
October 29	8-112	6, day	1 hour	- 5.2	2.1	8.5
November 4-5	115-112	2, day	10 minutes	- 2.8	8.5	25.0
November 4-5	8-112	2, day	1 hour	- 1.0		
November 4-5	8-112	3, day	10 minutes	- 3.0		
November 4-5	8-112	17	4 hours	14.2	11.2	50.0
November 4-5	201-112	2, day	10 minutes	0.5	5.5	16.0
November 4-5	119-112	2, day	1 hour	- 7.0		
November 12-13	201-112	26	5 hours	- 8.1	1.8	4.0
November 12-13	201-112	8, day	1 hour	- 7.1	1.6	5.5
November 4-5	123-201	10		26.7	3.2	9.0
November 7-8	119- 8	13	1 hour	8.7	0.5	0.8
November 7-8	8-201	22	1 hour	- 4.9	0.3	0.1
November 12-13	118-201	29	$\frac{1}{2}$ hour	12.5	0.5	0.6
November 12-13	115-201	29	1 hour	2.6	0.5	0.9
November 12-13	8-201	29	$\frac{3}{4}$ hour	8.7	1.6	2.5

Note: Data computed from averaging frequencies instead of phase values.



2) the evaluation of direct Atomichron-control of a high power VLF station with respect to instrumentation problems and phase stability of the radiated signal in the vicinity of the transmitter,

3) providing two VLF stations necessary for project V-III,

4) establishing experimental Atomichron-controlled VLF signals which can be received everywhere on earth for large-scale intercomparison of atomic frequency standards (tentative).

One Atomichron and some necessary accessories will be shipped to Hawaii in January, for installation at the Haiku transmitter site according to the block diagram in the upper part of Fig. 7. In the same way, another Atomichron and accessories will be installed at the Forrestport VLF transmitter site.

The transmitters are capable of radiating between 100–1000 watts at selected frequencies within the 10–20-kc band. They are, in general, used on a time sharing basis for experiments with the Navy Radux-Omega Navigation System,<sup>33</sup> but will be available for WOSAC at certain times during the Spring of 1960. The time sharing cycle has a period of 5 seconds, with four intervals of operation of 0.9, 1.0, 1.1, and 1.2 second length and four switching intervals of 0.2 second length each. This pattern serves for identification. Electronic commutators, driven by the frequency standards at the two sites, and proper synthesizers allow a variety of combinations of operation times and frequencies of the two transmitters. The frequencies 10.2, 14.2 and 18.2 kc were chosen for WOSAC in view of task V-III.

At first, a few test transmissions on 12.5 kc will enable Cruft Laboratory and USASRD to get information on the phase stability of the signals received at Harvard and Fort Monmouth. In June the signals will be used for project V-III and during the course of this experiment, the phase of the 14.2-kc signal from Hawaii will be monitored at a distance of roughly 30 km with respect to another Atomichron (Fig. 7). The 14.2-kc signal from Forrestport will be monitored at RADC (Fig. 6).

#### HIGH PRECISION TIME TRANSFER BY FLYING ATOMIC CLOCKS (V-I)

Before any synchronization by air transportation of an atomic clock could be attempted, it was necessary to determine whether the presently available Atomichron NC1001 would operate properly in a flying airplane. This model was designed for use in a normal laboratory environment, and it was very questionable, indeed, whether a flight experiment would be successful. As previously explained, atomic standards of the beam tube type are strongly affected by Coriolis forces if the beam axis is subjected to certain rotational motions. To reduce this effect, it is advisable to mount the Atomichron parallel to the axis of the fuselage. However, the design of the cesium oven in the NC1001 does not permit

its operation below an angle of 5° between beam axis and the horizontal plane; otherwise the liquid cesium would flow through the fine channels of the effuser into the beam tube and destroy the beam directivity.

The horizontal mount of the Atomichron had also an adverse effect on the servo control mechanism since the shock mounts of the crystal oscillator and its control mechanism were designed for operation of the equipment in a vertical position only. The horizontal mount caused an intolerable braking of the servo motor, which shifted the locking point on the resonance curve and decreased the stability of the standard. The problem was solved by mounting the NC1001 under an angle of 15° between beam axis and axis of the fuselage, and by modifying the mount of the crystal oscillator chassis as shown elsewhere.<sup>42</sup>

We felt, however, that despite these and other difficulties in using a laboratory standard in the plane environment, only the most precise clock, operated under the best achievable conditions could produce the desired results.

The first flight tests of the NC1001 were made in November, 1959. An R4D (DC-3) Signal Corps plane was available for flights around Monmouth County Airport, N. J. Power for the plane clock was supplied by a Diesel engine generator when the plane was on the ground, and by the plane power supply when the aircraft engines were in operation. Fig. 3 shows a block diagram of the measurement system. A voltage regulator took care of the necessary voltage control, particularly because of the unavoidable switching from one to the other power source. The 100-kc output signal and the second pulses from the divider were transferred via a microwave link from the airport to the Signal Laboratory. The 100-kc signal was used in addition to the second pulses to increase the resolution<sup>43</sup> and speed of the synchronization process. The pulses, on the other hand, were necessary to remove any ambiguities and to represent the actual clock outputs. Synchronization was accomplished within a few hours by adjusting the

<sup>42</sup> F. H. Reder and G. M. R. Winkler, "Preliminary flight tests of an atomic clock," *Nature*, vol. 186, pp. 592–593; May 21, 1960.

<sup>43</sup> The comparison of two sinusoidal signals can best be achieved by the phase detector—phase shifter method as employed also in the Radux Omega system (see footnote 33). The shaft angle position of the phase shifter can be directly calibrated in terms of the accumulated time difference. It is much simpler, but less convenient to record directly the sinusoidal output voltage from the phase detector

$$V = V_{\max} \sin(\Delta\phi),$$

and to derive the time difference of the clocks from

$$E = \frac{\Delta\phi}{\Omega} = \frac{1}{\Omega} \arcsin \left( \frac{V}{V_{\max}} \right) \quad (3)$$

( $\Delta\phi$  is the phase angle difference, and  $\Omega$  the angular frequency). The "instantaneous" relative frequency offset or rate,  $R$ , is then

$$R = \frac{\Delta\Omega}{\Omega} = \frac{1}{\Omega} \left[ 1 - \left( \frac{V}{V_{\max}} \right)^2 \right]^{-1/2} \frac{d}{dt} \left( \frac{V}{V_{\max}} \right), \quad (4)$$

where  $d/dt(V/V_m)$  is the slope of the recorded line. See also footnote 37.







continuity and uninterrupted transmission when either the link or the Forrestport frequency standard should fail.

Fig. 7 shows a block diagram of the slave clocks used at Hawaii and at location  $X$ , and of the Atomichron control circuit for the Haiku transmitter.

Fig. 8 gives the block diagram of the measurement system used in the jet plane. Two flying clocks are kept in synchronism so that either one may fail without disturbing the mission. An OMNI Range receiver feeds markers to the recording scope whenever the plane passes over an OMNI Range fixed point, in order to correlate geographical distance with electrical distance measured by the NAVARHO system.<sup>44</sup> The rest of the equipment is similar to that used during GBR and V-I.

The following flights are anticipated.

1) One round trip, Rome-Hawaii-Rome, to synchronize the clock at Hickam field and to measure propagation velocities. For the flight Rome-Hawaii, the transmission schedule will be, Haiku on 10.2 kc for 0.9 second, Forrestport on 10.2 kc for 1.0 second, then Haiku on 14.2 kc for 1.1 seconds and Forrestport at 14.2 kc for 1.2 seconds. For the return trip, the 10.2-kc frequency will be replaced by 18.2 kc.

2) A round-trip, Rome-location  $X$ -Rome, will follow to synchronize the clock at location  $X$ , to check the reciprocity law for the Forrestport (Rome)-Balboa path in North-South direction at 18.2 kc, and to make phase velocity measurements over the rest of the flight path. The transmission schedule for the latter experiment will be on a similar time sharing basis as explained above. The 18-kc NBA transmission will be recorded with an extra system not shown in Fig. 8.

3) A second round trip, Rome-Hawaii-Rome, to recheck synchronization of the Hawaii Clock and to repeat the reciprocity experiment in East-West-East directions.

4) A round trip, Rome-Balboa-Rome, to repeat the reciprocity experiment in North-South-North direction.

For the evaluation of recordings taken during the flight the following parameters are introduced:

$R$ =rate of the plane clock,

$A$ =acceleration of plane clock in seconds<sup>-1</sup>,

$\Omega$ =VLF angular frequency in radian per second,

$c_{0(s)}(x)$ =instantaneous VLF propagation velocity, in km per second, as a function of plane distance,  $x$ , from master clock (the subscript, 0, is used for waves coming from the direction  $x=0$ , and the subscript  $s$ , for waves propagating into the opposite flight direction),

$V(x)$ =instantaneous velocity of the airplane in direction  $S$ , in kilometers per second,

$s$ =shortest distance in kilometers between the two ground clocks,

$T$ =flight time in seconds to cover the distance  $s$ ,

$\tau$ =VLF propagation time in seconds for the distance  $s$ ,

$\phi_{0(s)}(t)$ =accumulated phase, in radians, of the beat-note as recorded in the airplane (indices have the same meaning as above).

A simple analysis then gives:

$$\begin{aligned} \frac{\phi_{0(s)}(T)}{\Omega} &= (RT + \frac{1}{2}AT^2) + (-) \int_0^T \frac{V(x)}{c_{0(s)}(x)} dt, \\ &= E(T) + (-) \frac{s}{\langle c_{0(s)} \rangle}. \end{aligned} \quad (5)$$

The first term represents the clock error,  $E$ , in seconds, accumulated at the time  $T$ . Its value cannot be determined accurately, but it can be estimated by continuing the phase recording after the plane has landed. The behavior of this phase recording will indicate what type of interpolation for the interval,  $0 \leq t \leq T$ , should be used. If the atomic clock in the plane behaves as expected,  $E$  should be negligible for flight times less than one day. The integral of the second term of (5) may be evaluated by replacing the unknown function,  $c=c(x)$ , by its average,  $\langle c \rangle$ , over the flight path. A better approximation may be calculated by applying (5) to each path element determined by two successive OMNI Range stations.

Other useful relations are derivable from (5), as follows.

Propagation time from  $x=0$  to  $x=s$ :

$$\tau_0 = \frac{\phi_0(T)}{\Omega} - E \approx \frac{\phi_0(T)}{\Omega}, \quad \text{seconds.} \quad (6a)$$

Propagation time from  $x=s$  to  $x=0$ :

$$\tau_s = \frac{-\phi_s(T)}{\Omega} + E \approx \frac{-\phi_s(T)}{\Omega}, \quad \text{seconds.} \quad (6b)$$

Average VLF propagation velocity from  $x=0$  to  $x=s$ :

$$\langle c_0 \rangle = \frac{\Omega s}{\phi_0(T) - E\Omega} \approx \frac{\Omega s}{\phi_0(T)}, \quad \text{km/s.} \quad (7a)$$

Average VLF propagation velocity from  $x=s$  to  $x=0$ :

$$\langle c_s \rangle = \frac{\Omega s}{-\phi_s(T) + E\Omega} \approx \frac{\Omega s}{-\phi_s(T)}, \quad \text{km/s.} \quad (7b)$$

The accuracy of these velocity determinations depends, of course, on the accuracy to which the geographical distance can be measured.

<sup>44</sup> O. Goldberg, Report on NAVARHO Evaluation, Contract AF30-(635)-4487, Final Report, Pickard and Burns, Inc., Needham, Mass.; 1957.



The discrepancy between the two propagation velocity values, in violation of the reciprocity law, may be expressed by

$$\frac{|\langle c_0 \rangle - \langle c_s \rangle|}{\frac{1}{2}(\langle c_0 \rangle + \langle c_s \rangle)} = 2 \frac{|(-\phi_s - \phi_0) + 2E\Omega|}{-\phi_s + \phi_0}$$

$$= 2 \frac{|-\phi_s - \phi_0|}{-\phi_s + \phi_0} \quad (8)$$

The final phase of project WOSAC is scheduled to begin, June, 1960, and to last for about one month.

#### CONCLUSION

The first part of Project WOSAC ended with the successful demonstration that phase tracking of the transatlantic 16-kc GBR signal allows long-range frequency transfer to an accuracy of  $2.5p:10^{11}$  (standard deviation for a 24-hour averaging period). The evaluation of the directly Atomichron-controlled LF station, A5XA, indicated that further improvements might be possible by using direct control of VLF stations by the improved models of the atomic cesium standard. The results from the first flight experiments with atomic beam standards justify the hope that the world-wide clock

synchronization experiments scheduled for the near future will approach the projected goal of synchronization to the order of a microsecond.

#### ACKNOWLEDGMENT

A project of this scope could not be successful without active support from many individuals and organizations. The authors wish to acknowledge the generous support by Rome Air Development Center (O. G. Tallman and G. T. Clawson), Navy Electronics Laboratory (M. C. Tibbals), Air Force Missile Test Center at the Patrick Air Force Base (Capt F. L. Hafer), British Post Office (R. L. Corke, W. N. Genna), and Naval Research Laboratory (C. Young).

The authors are particularly indebted to Prof. J. A. Pierce of Cruft Laboratory, Harvard University, for his invaluable guidance in a project which is largely based on his fundamental research work.

Within our own organization, the U. S. Army Signal Research and Development Laboratory, the authors appreciate the lively interest taken in the project by all echelons of command, in particular by W. L. Doxey, Dr. E. A. Gerber, and J. M. Havel.

Finally, it is a pleasure to acknowledge the enthusiastic help extended by all personnel of the Atomic Resonance Branch, and W. L. Sage of the Communications Department.

# Contributors

P. R. Arendt was born in 1900 in Dresden, Germany. He received a Ph.D. degree in physics from the University of Berlin, Germany, in 1924 where he studied under Planck, Einstein, Haber, and Hahn.



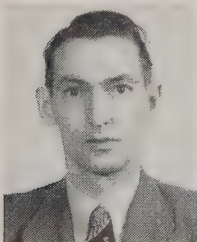
P. R. ARENDT

From 1924 to 1929 he did R&D work for Siemens & Halske A.G., Berlin, on multiple carrier, picture telegraphy over loaded cables, and acoustical standards. He was with ITT in London, Paris, and Berlin from 1929 to 1935 as chief engineer of the Berlin associates of ITT, and did engineering and research in all fields of communications, including magnetic sound recording, wired wireless, common frequency broadcasting. From 1935 to 1957 he was associated with Allgemeine Elektrizitäts Gesellschaft in Berlin and in Frankfurt where he was technical director concerned with the supervision of R&D activities and of patent policy of the concern's associated companies (Telefunken and Osram). He also acted as consultant to the president of the Board and during the war he inaugurated the production of an infrared proximity fuze for the V-2. He has been with the U. S. Army Signal Research and Development Laboratory, Institute for Exploratory Research, Fort Monmouth, N.J., from 1957 to the present. He is Chairman of the Radiation Effects Committee and is especially interested in research on satellite radio propagation.

He has been awarded several patents, two of which are a metallic conductor covered with ferrites and a nuclear power reactor for direct conversion of nuclear energy into electricity.

Dr. Arendt is a member of the American Nuclear Society and of Deutsche Physikalische Gesellschaft. He is listed in *Who is Who in Atoms*, London.

Hans Joachim aufm Kampe was born in Essen, Germany, on December 10, 1912. He received the M.S. and Ph.D. degrees in 1936 and 1941, respectively, from Technical University, Darmstadt, Germany.



H. J. AUFM KAMPE

From 1936 to 1945, he was an atmospheric research physicist at a research institute for aeronautics at Darmstadt and Ayring, Germany, where he worked in synoptic

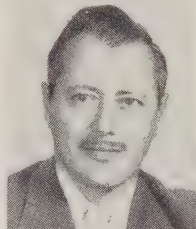
meteorology, micrometeorology, cloud-physics, aerology, solar radiation, and instrument development.

From 1946 to 1948, he was an atmospheric research physicist at the Central Meteorological Office of the Northwest German Weather Service at Hamburg, Germany. He is responsible for the starting of an atmospheric physics observatory.

From 1948 to the present he has been an atmospheric research physicist at USASRDL, Fort Monmouth, N. J., where he has been involved in, and supervising, research in various fields of atmospheric physics such as dynamics of the atmosphere, cloud physics, atmospheric electricity, and upper-air physics. His present position is as chief of the Atmospheric Physics Branch of the Meteorological Division at USASRDL.

Dr. aufm Kampe is a member of the American Meteorological Society and the American Geophysical Union.

Charles L. Barker, Jr., was born on July 1, 1918, in Maplewood, N. J. He attended the University of Tampa, Fla., and The University of Michigan at Ann Arbor, receiving the B.S. degree in aeronautical engineering from the latter.



C. L. BARKER, JR.

In 1941, following six months employment in the armament engineering section of the Glenn L. Martin Company, Baltimore, Md., he served four years with the Corps of Engineers during World War II. After separation he returned to the Martin Company Engineering Department, working on the Martin 202 and 404 aircraft. In 1948, he moved into the solid propellant, rocket and explosives area, joining the Air Force Missile Test Center, Fla., in 1952 with the Matador Field Test Program for the Martin Company.

In 1953 he accepted a position with the Rocket Development Laboratories, Redstone Arsenal, Ala., as chief of the Design Section where he remained until transferring in 1955 to the Air Munitions Development Laboratories at Eglin Air Force Base as chief of the Rocket Branch. In early 1958 he was transferred to the Army Ballistic Missile Agency, Redstone Arsenal, assuming the position as chief of the Astronautical Engineering Section, Future Projects Branch, Development Operations Division.

Mr. Barker is a member of the American Ordnance Association.

Thomas A. Barr was born in Gary, W. Va., on July 20, 1929. He received his education in electrical engineering at Bluefield College. From 1945 to 1948 he worked for several broadcasting stations, principally installing FM transmitting equipment.

In 1948 he joined the General Electric Company at Fort Bliss, Texas, assigned to the Army missile program, where he participated in the design of antenna and telemetry systems for the Hermes missile. In 1950 he was transferred to Huntsville, Ala., and placed in charge of antenna development for the Redstone missile.

In 1951 he joined Redstone Arsenal as Chief of the Antenna Development Unit for the Redstone and Jupiter missiles. He has been engaged in the design of several specialized antennas for missile nose cones and satellites. In 1960 he was appointed assistant to the Chief of the Radio Frequency Systems Section of the Army Ballistic Missile Agency. He has a patent pending on a dual frequency slot antenna.

Rodolfo M. Barraza was born on May 29, 1928, in Mesilla, N. M. He attended New Mexico State University, Las Cruces, prior to joining Dr. von Braun's team with which he has been working since February, 1949.



R. M. BARRAZA

He worked in the Army Ballistic Missile Agency Guidance and Control Laboratory for nine years, performing design engineering of rudder drives, actuators, servomotors, relay devices and main distributors for the missile network. In May, 1958, he transferred to Structures and Mechanics Laboratory as assistant recovery project engineer, and is presently the recovery project engineer for Development Operations Division.

James E. Bartow (S'51-A'53-M'57) was born in Port Jefferson, N. Y., on October 10, 1930. He received the B.E.E. degree from Rensselaer Polytechnic Institute, Troy, N. Y., in 1952.



J. E. BARTOW

In 1952 he joined the U. S. Army Signal Research and Development Laboratory, Fort Monmouth, N. J., where he has been involved in the design of radio relay and tropo-



ospheric scatter systems and holds a patent for a calculator for determining scatter circuit performance. He joined the Astro-Communication Branch of USASRD in 1959 and is currently involved in the design of satellite communication systems.



N. J. BEYERS

atmospheric electricity.

Mr. Beyers is a member of the American Meteorological Society.

Josef Boehm was born in Unterhimmel near Steyr, Austria, on August 7, 1908. He received the B.S. and M.S. degrees in mechanical engineering from the Technical University at Dresden, Germany.



J. BOEHM

During 1933-1934, he was employed in German industry in the field of automatic machinery. For the following five years, he was research associate in the department of kinematics and automatic machinery at the Technical University. In 1939, he joined Dr. Wernher von Braun at the German Rocketry Center at Peenemuende, where he was in charge of design engineering for control systems of long-range rockets. After coming to this country in 1945, he worked for the Army Ordnance Corps at Aberdeen Proving Ground, Md., and at Fort Bliss, Tex. In 1950, he joined the Guided Missile Development Division at Redstone Arsenal, Huntsville, Ala. Mr. Boehm is presently chief of the Electro-Mechanical Engineering Branch, Guidance and Control Laboratory, Development Operations Division, Army Ballistic Missile Agency at Huntsville. He made essential pioneer contributions to the development of artificial earth satellites. Mr. Boehm was in charge of designing and testing a complete satellite which formed the basis for Explorer I, built by the Jet Propulsion Laboratory of Pasadena,

Calif. He was project engineer for the successfully launched Explorers IV and VII.

Mr. Boehm is a member of the American Rocket Society.

Hans A. Bomke was born in Berlin, Germany, in 1910. He attended the University of Berlin, majoring in physics, mathematics, and medicine, and was awarded the Ph.D. degree.



H. A. BOMKE

After the war, he held several scientific positions in Europe and in the United States.

In 1952, he joined the U. S. Army Signal Research and Development Laboratory, Fort Monmouth, N.J., where he is now Director of Exploratory Research Division S. His scientific interests have been in the fields of research in atomic physics, gas discharges, microwaves, radiation dosimetry, and geophysics.

Dr. Bomke is a member of the Optical Society of America, the American Rocket Society, and the American Geophysical Union.

Samuel P. Brown (SM'59) was born in Greensburg, Pa., on November 25, 1921. He received the B.S. degree in electrical engineering from Pennsylvania State University in 1942, and the M.S. degree in electrical engineering from Rutgers University, New Brunswick, N. J., in 1950. As part of his army electronics training, he completed courses in radio and radar techniques at the General Electric Company, Schenectady, N.Y.



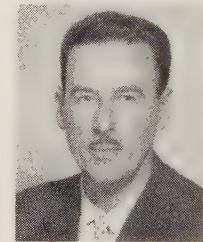
S. P. BROWN

While in military service, he was responsible for the system and field evaluation of newly-developed microwave radio relay systems at the Signal Corps Ground Signal Agency. Subsequently, he engaged in military technical intelligence activities regarding Japanese radio equipments. Upon his release from active military service in 1946, he joined the U. S. Army Signal Research and Development Laboratory, Fort Monmouth, N. J., where his current assign-

ment is director, Astro-Electronics Division. In 1955, he was promoted to the rank of Major in the U. S. Army Reserve, Signal Corps.

Since 1946, Mr. Brown has been active in the development of military radio relay, tropospheric scatter, and time division multiplex systems. During 1958, he was deputy director of the U. S. Army's program leading to the communication system embodied in Project Score with specific responsibility for the system design and integration into the Atlas missile.

Herbert I. Butler (M'45) was born in New York, N. Y., on July 24, 1914. He studied electrical engineering at the Polytechnic Institute of Brooklyn, N. Y., and received the B.S. degree in physics in 1939 from Monmouth College, West Long Branch, N. J.



H. I. BUTLER

In 1941 he joined the U. S. Army Signal Research and Development Laboratory, Fort Monmouth, N. J., and engaged in research and development of radio direction finders, and intercept and countermeasures equipment. In 1958, he was appointed by USASRD to the Ad Hoc Committee on Meteorology formed by the Advanced Research Projects Agency, in which capacity he has served as the engineering coordinator for Project TIROS. At present he is chief of the Astro-Instrumentation Branch of the Astro-Electronics Division, USASRD.

Mr. Butler is a licensed professional engineer in the state of New Jersey.

Gerald A. Champlin, Major, U. S. Army (MC), was born in Chicago, Ill., on September 12, 1923. After graduation from the St. Louis University Medical School, he specialized in surgery.

In 1954 he began active service with the U. S. Army as chief of surgery at Fort Eustis, Va. From 1958 to 1959, he was chief of the Bio-Astronautics Research Unit, AOMC. He took flight surgeon training at Pensacola, Fla., and is now Aviation Medical Officer at the U. S. Army headquarters at Heidelberg, Germany.

George Q. Clark was born in Overton, Tex., on September 30, 1928. He did undergraduate work at Texas A & M College,

and received the B.S. degree in physics in 1957 from Texas Western College, El Paso.

He was employed as research engineer-scientist at the Schellenger Research Laboratory at Texas Western College while serving as instructor in the Department of Physics and Mathematics. In 1958 he accepted employment with the Missile Geophysics Division of U. S. Army Signal Missile Support Agency at

White Sands Missile Range, N. M. Since that time he has been working in the field of atmospheric physics. His chief area of interest in this field lies between the balloon and satellite altitudes. At this time he is serving as nose cone scientist and chief of the Fort Greely, Alaska, Meteorological Rocket Team.

Mr. Clark is a member of the American Meteorological Society and the American Rocket Society.

❖

Daniel D. Collins was born on July 8, 1925, in Bradenton, Fla. He received the B.A. degree in mathematics from Harding College, Searcy, Ark., in 1949. In 1956, after working for the Bureau of Docks and Yards Engineering Office at the Key West Naval Base, Fla., he became a research engineer with the Flight Instrumentation, Planning and Analysis Section of the U. S. Army Ballistic Missile

Agency's Missile Firing Laboratory, Cape Canaveral, Fla. Mr. Collins has participated in missile flight instrumentation and measurement planning for Army Redstone, Jupiter, Juno II and Jupiter C research and development firings at Cape Canaveral.

❖

Henry A. Curtis (A'47-M'55) was born in Cincinnati, Ohio, in 1919. He received the B.A. degree in chemistry from San Diego State College, Calif., and subsequently obtained engineering experience at Ryan Aeronautical Company, San Diego, and Fluor Corporation, Los Angeles, Calif.

In 1947 he joined the staff of the Jet Propulsion Laboratory, California Institute of Technol-

ogy, Pasadena, where he is now chief of the Electronic Devices Section.

Mr. Curtis is a member of Sigma Xi.

❖

Arthur F. Daniel was born in Birmingham, Ala., on September 27, 1905. He received the B.S. degree in chemistry from the University of North Carolina, Chapel Hill, in 1927, and the M.S. degree in physics in 1928. He was a Coffin Fellow at the University of Chicago in 1929.



A. F. DANIEL

From 1929 to 1932, he was a research associate in electrical engineering at Harvard University, Cambridge, Mass. He was affiliated with General Chemical Company, Long Island, N. Y., until 1935 and T. A. Edison, Inc., West Orange, N. J., until 1941, when he joined the Signal Corps Laboratory, Fort Monmouth, N. J. He is currently director of the Power Sources Division of the Electronic Components Research Department at the U. S. Army Signal Research and Development Laboratory, Fort Monmouth.

Mr. Daniel is a member of the American Chemical Society, the Electrochemical Society, and the American Physical Society.

❖

L. Gerard deBey was born in Orange City, Iowa, on March 8, 1912. He received the B.S.E.E. degree from the University of South Dakota, Vermillion, in 1933 and the M.S.E. degree from Purdue University, Lafayette, Ind., in 1942.



L. G. DEBEY

From 1934 to 1936 he was employed as research assistant by the Purdue University Research Foundation in early television developments. In 1936 he joined the transmitter division of RCA. He returned to Purdue University in 1938 as a research assistant, working in the field of aircraft navigation, blind landing, and radio noise suppression. He joined the staff of the Ballistic Research Laboratories, Aberdeen Proving Ground, Md., in 1942 as head of the Electronic Measurements Group. He is currently chief of the Electronic Measurements Branch. His activities have included development, during 1942-1945, of precision instrumentation for obtaining bombing table data, and directing a research and development program, from 1945 to 1954, to provide all instrumentation and data reduction equipment for the first guided missile test range, White Sands Proving Ground. He developed the first Doppler velocity and position instrumentation (DOVAP) now used at all

United States test ranges. In 1952 he initiated research leading to current Doppler satellite tracking and upper atmosphere research instrumentation. He has served on numerous Department of Defense committees in advisory capacity in the field of guided missile and satellite instrumentation.

❖

Robert N. DeWitt was born on June 27, 1936, in Lake Charles, La. He received the B.S. degree in physics and mathematics from Southwestern Louisiana Institute, Lafayette, in 1958. Upon graduation, he joined the Army Ballistic Missile Agency, Redstone Arsenal, Ala., as a physicist in radar systems analysis. After eight months, he became an assistant to Dr. H. G. L. Krause, working in the fields of celestial mechanics and



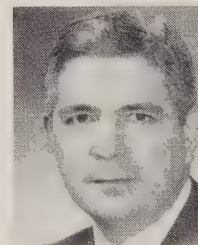
R. N. DEWITT

rocket dynamics. At present, he is concentrating on the field of low-trust acceleration motion.

Mr. DeWitt holds membership in the American Rocket Society, the British Interplanetary Society, and the Rocket City Astronomical Association.

❖

Frederic H. Dickson (S'38-A'43-M'55) was born in Bristol, Colo., on January 10, 1916. He received the B.S. degree in electrical engineering from Oregon State College, in 1939, where he was a graduate assistant in electrical engineering until 1940. Prior to entering the military service in 1942, he was an instructor in the Air Corps Technical Schools. He served as an assistant radio officer, Allied



F. H. DICKSON

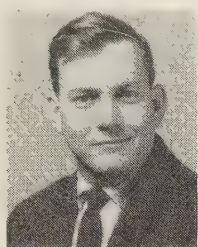
Forces Headquarters, and as assistant signal officer, Fifteenth Army Group, European Theater, and returned from overseas as Executive Officer and later Commanding Officer of the Signal Corps Radio Propagation Unit.

After being discharged from the military service in 1946, he joined the Office of the Chief Signal Officer, Washington, D. C., and became chief of the Radio Propagation Section in 1950. In 1954, he became director of the U. S. Army Signal Radio Propagation Agency, Fort Monmouth, N. J., which is engaged in application engineering and operational research in the field of radio wave propagation.

Mr. Dickson is a member of the U.S.A. National Committee of URSI, and is International Vice Chairman of Commission IV. He is a registered professional engineer in the District of Columbia.



Sanford W. Downs, Jr., was born in Amory, Miss., on March 14, 1930. He received the B.E.E. degree from Auburn University, Ala., in 1951.

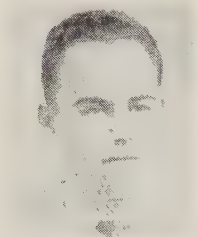


S. W. DOWNS, JR.

Mr. Downs is a member of Tau Beta Pi and Eta Kappa Nu.



Louis D. Duncan was born on July 26, 1934, in Jonesboro, Ark. He received the Bachelor of Science degree in mathematics from Arkansas State College in 1956, and the M.S. degree from St. Louis University, Mo., in 1958.



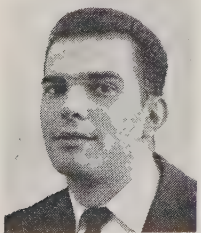
L. D. DUNCAN

He held the position of graduate assistant in mathematics at St. Louis University. He was then employed as a mathematician in the field of flight testing by McDonnell Aircraft Company, St. Louis, Mo., from 1956 to 1957. Since 1958, he has been with the U. S. Army Signal Missile Support Agency, White Sands Missile Range, N. M., as a research mathematician in the field of ballistics and related meteorological studies.

Mr. Duncan is a member of Sigma Phi Epsilon and the American Meteorological Society.



Arthur Engelman was born in New York, N. Y. on March 17, 1930. He received the B.S. degree in 1950 from the College of the City of New York, N. Y., and the M.S. degree in 1951 from New York University.



A. ENGELMAN

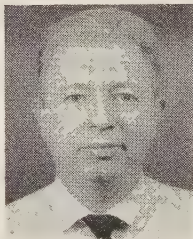
He is presently employed in the Chemical Physics Department of the Aeronomy Division of Geophysics Corporation of America as a staff engineer and is currently working on electron cloud study. He was previously employed from 1950 to 1952 and 1954 to 1955 as a research assistant in the

Meteorology Department of New York University, during which time he worked on several Army and Air Force research projects. From 1952 to 1954 he served as company executive officer for the U. S. Army Corps of Engineers. He later was employed as project engineer at Rome Air Development Center, Rome, N.Y., from 1955 to 1957, working on propagation aspects of WS 219-L, 117-L, 107-A, 222-A, etc. From 1957 to 1959 he was employed by Raytheon Missile Systems Division as a senior engineer on AICBM.

He is a member of the American Meteorological Society and the American Geophysical Union.



John P. Eyraud (S'52-M'55) was born in Temple City, Calif., on December 6, 1929. He received the B.S. degree in mathematics from the California State Polytechnic College, San Luis Obispo, in 1955.



J. P. EYRAUD

Since 1955 he has been employed at the Jet Propulsion Laboratory, Pasadena, Calif., as a research engineer in the Flight Telemetry Group. His efforts there have been primarily in airborne instrumentation for the following programs: Loki rocket, Corporal missile, Jupiter-C, Explorer satellite, and, currently, the Sergeant missile program.



William Fishbein was born in New York, N. Y., in 1927. He received the B.S. degree in electrical engineering from the College of the City of New York in 1948. He attended Rutgers University, New Brunswick, N. J., and received the M.S. degree in electrical engineering in 1955.



W. FISHBEIN

From 1948 to 1950, he worked at the New York Naval Shipyard in the design of shore communications stations. From 1950 to 1952, he was in the U. S. Army Signal Corps where he served as an engineer at the Signal Corps Laboratories at Fort Monmouth, N. J. Since 1952, he has been with the U. S. Army Signal Research and Development Laboratory. He is presently chief of the Radar Division's Applied Research Section which is engaged in the development of advanced techniques for army radars.

Mr. Fishbein is a member of Eta Kappa Nu.

Siegfried J. Gerathewohl was born in Ebersbach, Germany, on September 11, 1909. He studied psychology and physiology at the Saxony Institute of Technology, Dresden, Germany, where he received the Ph.D. degree in 1936.



S. J. GERATHEWOHL

After many years as a scientist with the German Air Force, he joined the staff of the School of Aviation Medicine, Randolph Air Force Base, Tex., in 1947. He is now chief of the Bio-Astronautics Research Office, U. S. Army Medical Research and Development Command, OTSG, at the Army Ballistic Missile Agency, Redstone Arsenal, Ala.



Bill B. Greever was born in Tazewell, Va., on August 12, 1922. He received the B.S. degree in mechanical engineering in



B. B. GREEVER

1946 from Virginia Polytechnic Institute, Blacksburg, and did graduate work at George Washington University, Washington, D. C., in engineering administration.

In 1947 he joined the Buick Division of the General Motors Corporation, Flint, Mich., where he worked in research and development. From 1948 through 1952, he was associated with automotive dealerships in a managerial capacity. He served three years on the staff of the Bureau of Yards and Docks, Department of the Navy.

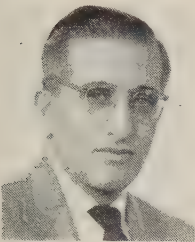
Mr. Greever joined the Army Ballistic Missile Agency at Huntsville, Ala., in 1956. He was assigned to liaison work with the Jet Propulsion Laboratory in connection with the Juno I program, and later became assistant project engineer on Juno I. Since 1958 he has been project engineer on the Juno II program.



Alan Sterling Gross was born in New York, N. Y., on August 3, 1921. He attended Townsend Harris in New York, and the College of the City of New York, receiving the B.S.E.E. degree from the latter in 1941.

After graduation, he began work at the Signal Corps Laboratories at Fort Monmouth, N. J., as a research engineer. From 1943 to 1946, he served as a line radar officer in the U. S. Navy. During this period he received advanced electronics training at

Bowdoin College, Brunswick, Me., and M.I.T., Cambridge, Mass., and was then assigned as OC of a ground control approach radar on Guam, Okinawa, and in China. After the war he returned to USASRDL where he worked on radar to the moon (Diana), and the long-range propagation of radio waves. He designed the moon radar diorama which is still on exhibit at the Smithsonian Institution, Washington, D. C. During this period, he was a member of the DOD Arctic Ionospheric Advisory Committee, the DOD Arctic Tropospheric Advisory Committee, and Deputy Member to the Research and Development Board, Panel on Antennas and Propagation. He directed the Diana group through the initial program of "check-out" and calibration of the world-wide Vanguard Minitrack stations utilizing moon reflections; and was also instrumental in the detection of dark satellites by the high-power scatter techniques. With the advent of Sputnik, tracking of all the various deep space probes, including the latest Russian Luniks, was begun. An R&D program was also inaugurated to develop new equipment and techniques for future ground tracking systems. At present he is chief of the Astro-Observation and Analysis Branch, with responsibility for the implementation, installation, and research and development connected with the world-wide ground tracking network for ARPA. He also directs the Astro-Observation Center at Fort Monmouth, comprising the Deal Observation Station and the Diana Tracking Facility.



A. S. GROSS

Rudolf A. Hanel (A'55) was born on July 14, 1922, in Austria. He received his professional education at the Institute of Technology, Department of Physics, Vienna, Austria (Dipl. Ing. 1950; Dr. Tech., 1953). Between 1950 and 1953 he served as a research assistant in the Department of Communications at the same Institute where he was engaged in electronic and ultrasonic research.



R. A. HANEL

In 1953, he joined the U. S. Army Signal Corps Engineering Laboratory, Fort Monmouth, N. J., and worked on various acoustical and optical topics. He had an active part in the development of the Vanguard II satellite instrumentation. Since 1959, he has been a member of the

Goddard Space Flight Center, National Aeronautics and Space Administration, Washington, D.C.

Dr. Hanel is the author of various papers and a patent in the fields of acoustics, transistor circuitry optics and thermal topics.



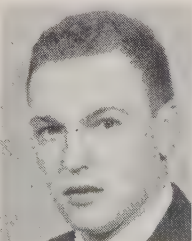
G. B. HELLER

Gerhard B. Heller was born in Eschwege, Germany, on January 24, 1914. He received the B.S. degree from the University of Göttingen, Germany, and the M.S. degree from the Institute of Technology, Darmstadt, Germany. From 1940 to 1945 he worked at Peenemuende on power plant research and development for the V-2 and the Wasserfall missiles. He came to the United States in 1945 and worked on Project Hermes at Fort Bliss, Texas. He continued this work at the Guided Missile Development Division, Redstone Arsenal, Ala. after joining the organization in 1950. Throughout 1953 and 1954 he contributed to the Orbiter Project.

He has been with the Development Operations Division of the Army Ballistic Missile Agency since 1956, and has been active in thermodynamic problems of Jupiter re-entry, and temperature control for satellites. He is presently Deputy Director of the Research Projects Laboratory and is supervising supporting research in fields of high-temperature plasma phenomena, and environmental conditions for satellites. The Development Operations Division is now the Marshall Space Flight Center of the National Aeronautics and Space Administration. Mr. Heller joined NASA during the organizational transfer.

He is a member of the American Rocket Society, Rocket City Astronomical Association, and the American Chemical Society.

William G. Huber was born on June 24, 1931, in Chicago, Ill. He received the B.S. degree in mechanical engineering from the University of Illinois, Urbana, and the M.S. degree in armament engineering from the U. S. Air Force Institute of Technology, Dayton, Ohio.

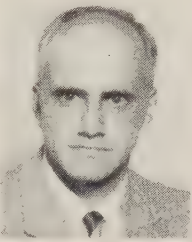


W. G. HUBER

He served four and one-half years with the U. S. Air Force prior to accepting the position he now holds as an

aeronautical research engineer in charge of the Operations and Logistics Unit of the Future Projects Design Branch, Structures and Mechanics Laboratory. This is one of ten Laboratories making up the Army Ballistic Missile Agency's Development Operations Division which is an element of the U. S. Army Ordnance Missile Command.

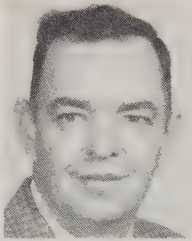
Donald L. Jacoby (M'46) was born in New York, N. Y., on July 8, 1920. He received the B.S. degree in electrical engineering from Columbia University, New York, N. Y., in 1941, and the M.S. degree in electrical engineering from Rutgers University, New Brunswick, N. J., in 1950.



D. L. JACOBY

He has been employed at the U. S. Army Signal Research and Development Laboratory, Fort Monmouth, N. J., since 1941, with the exception of three years spent as a radar officer in the U. S. Navy. He has been engaged in research and development programs in fields of multiplexing, radio relay and tropospheric scatter, and, until recently, was chief of the Radio Relay Branch of the Transmission Facilities Division. He has authored several papers and holds a patent on "Pulse Code Modulation." He is currently deputy director of the Astro-Electronics Division, USASRDL, with responsibility for directing programs in satellite communications, satellite instrumentation and tracking.

Otha Jean was born in Fayetteville, Tenn., on June 21, 1927. Mr. Jean received the B.S. degree in mathematics from Murfreesboro State College, Tenn., in 1951. From 1951 to 1957 he taught in the Tennessee public school system. From 1957 to the present he has been employed as a mathematician in the Aeroballistics Laboratory of Army Ballistic Missile Agency, Huntsville, Ala. It has been Mr. Jean's



O. JEAN

responsibility to lay out the trajectories of the Army's space probes. At present, he is acting section chief of the Space Projects Section, Future Projects Analysis Branch.



Kenneth R. Jenkins was born in Quanah, Tex., on October 6, 1920. He attended La-Salle University, Chicago, Ill., for two years prior to entering the U. S. Army as a meteorologist, serving principally in the Aleutian Islands. From 1946 through 1956 he was employed as a meteorologist with the U. S. Weather Bureau at Laredo, Tex., and Amarillo, Tex. During this period he did extension work with



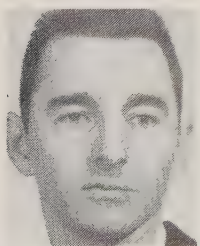
K. R. JENKINS

Pennsylvania State University.

Late in 1956 he transferred to the U. S. Army Signal Missile Support Agency, White Sands Missile Range, N. M., serving as research and development meteorologist. In 1957 he supervised the initiation of Signal Corps meteorological rocket firings at White Sands Missile Range. He is presently chief of the Rocket Section of the Missile Geophysics Division, and is supervising the firing of meteorological rockets at Fort Churchill, Canada, and Fort Greely, Alaska, and furnishing technical assistance in sounding rocket firings at Wallops Island, Va., Point Mugu, Calif., Cape Canaveral, Fla., Eglin Air Force Base, Fla., and other projected sites under the Meteorological Rocket Network.

Mr. Jenkins is a member of the American Meteorological Society, the American Rocket Society, and the National Geographic Society.

Jerry L. Johnson was born in Okmulgee, Okla. on November 28, 1932. He received the B.S. degree from Murray State College, Ky., in 1954.



J. L. JOHNSON

He entered the military service in 1954 and was assigned to the Aero-Medical Field Laboratory at Holloman AFB, N. M., where he participated in the space biology and biodynamics programs. Leaving the service in 1958, he became a member of U. S. Army Ballistic Missile Agency, Huntsville, Ala., where he is currently responsible for astrobiological instrumentation research and development.

Werner D. Kahn was born in Germany, on May 26, 1930. He received the B.S. degree in 1952 and the M.S. degree in 1955,

both in mathematics, from the University of Illinois, Urbana. The latter degree was awarded while he was on active duty with the U. S. Air Force.

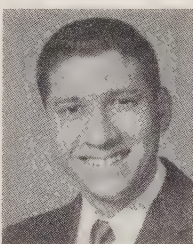


W. D. KAHN

He joined the Army Map Service in August, 1956, upon leaving the USAF. Since that time his principal research has been in the field of radio interferometry as applied to geodesy.

Mr. Kahn is a member of the American Mathematical Society, the American Astronomical Society, and the Association for Computing Machinery.

George N. Krassner (S'48-M'59) was born in New York, N. Y., on January 22, 1929. He received the B.E.E. degree from the College of the City of New York in 1950, and the M.S.E.E. degree from The University of Michigan, Ann Arbor, in 1951, specializing in microwave communications.



G. N. KRASSNER

While performing graduate studies, he was awarded both a teaching fellowship and a research assistantship.

Except for a two-year period in military service, he has been employed at the U. S. Army Signal Research and Development Laboratory, Fort Monmouth, N. J., since 1951. He has been engaged primarily in development of military communication systems, including tactical radio relay, tropospheric scatter, airborne communications, and satellite communication. He performed much of the initial systems design of the first communications satellite, Project Score, and is presently chief of the technical staff of the Astro-Electronics Division of this Laboratory.

Mr. Krassner is a member of Tau Beta Pi and Eta Kappa Nu.

Helmut G. L. Krause was born November 10, 1911, at Koenigsberg, Prussia. He studied from 1932 to 1937 at the University of Koenigsberg, where he obtained the M.S. and the Ph.D. degrees in astronomy, physics, and mathematics in 1938. Since April, 1937, he has worked as a research scientist at the Observatories of Koenigsberg and Hamburg-Bergedorf, the Institute of Ballistics

of the Technical Air Force Academy at Berlin-Gatow, the Carl Zeiss plant at Jena, and the Institute of Theoretical Physics of the University of Jena. He worked as a technical physicist of a large chemical factory at Hamburg. In October, 1951, working also professionally in the fields of rocketry and astronautics, he was employed as chief ballistics and aerodynamicist at the Astronautical Research Institute in Stuttgart, and as chief aerodynamicist and thermodynamicist at the Research Institute for Physics of Jet Propulsion at the Stuttgart Airport.

Since June, 1957, he has been serving as aeronautical research engineer in the capacity of special assistant to the chief of the Future Projects Design Branch of the Army Ballistic Missile Agency, Redstone Arsenal, Ala.

He has written approximately thirty comprehensive theoretical research papers in the field of rocket ballistics, supersonic aerodynamics, aerodynamic heat transfer, thermodynamics of dissociated gases, free-flight dynamics, and perturbation theory of celestial bodies.

Dr. Krause holds membership in the Institute of the Aeronautical Sciences, the American Rocket Society, the American Astronomical Society, the American Astronautical Society, the British Interplanetary Society, the German Astronomical Society, the German Society for Rocket Technology and Space Flight (Scientific Director for 1952 and 1953), and the German Rocket Museum Society.

In 1951, he received the first Ernst Heinkel Space Flight Award.

Herman F. Kurtz, Jr., was born in Macon, Ga., on April 1, 1935. He received the B.A. and M.A. degrees in physics from Vanderbilt University, Nashville, Tenn., in 1956 and 1957, respectively.



H. F. KURTZ, JR.

He has been with the Army Ballistic Missile Agency since 1958, and is presently acting chief of the Space Flight Section, Flight Evaluation Branch, of the Aeroballistics Laboratory.

This Section is responsible for the upper stage and orbital evaluation of ABMA space vehicle flights, including early orbit determination. He is the author of a number of ABMA technical reports.

Mr. Kurtz is a member of the American Rocket Society.



John H. Licht was born in 1930, in Union, N. J. He received the B.S. degree in civil engineering and the M.S. degree in mechanical engineering from Newark College of Engineering, N. J., in 1951 and 1957, respectively. He is a licensed professional engineer in the state of New Jersey.

In 1951 he was employed by the U. S. Army Signal Research and Development Laboratory, Fort Monmouth, N. J.,

where he was a project engineer working on computer mechanisms and atomic test mechanical instrumentation. He was responsible for the design and development of the Vanguard II and Atlas-Score satellite tape recorders and mechanical phases of the instrumentation.

Since October, 1959, he has worked for the Meteorology Branch of the National Aeronautics and Space Administration, Washington, D. C., where at present he heads a mechanical engineering group, engaged in design and development of mechanical instrumentation.

David Linden was born in New York, N. Y., on January 6, 1923. He received the B.S. degree in chemistry from the College of the City of New York in 1942, and the M.S. degree, also in chemistry, from the Polytechnic Institute of Brooklyn, N. Y., in 1950.

He has been employed at the U. S. Army Signal Research and Development Laboratory, Fort Monmouth, N. J., since 1942 and is presently deputy director of the Power Sources Division of the Electronic Components Research Department there.

Mr. Linden is a member of the American Chemical Society and the Electrochemical Society.

Charles A. Lundquist was born in Webster, S. D., on March 26, 1928. He received the B.S. degree in engineering physics from South Dakota State College, Brookings, in 1949, and the Ph.D. degree in physics from the University of Kansas, Lawrence, in 1953.

He held the position of assistant professor of engineering research at Pennsylvania State University, University Park, for a year before entering military service. From 1954 to 1956 he served as a physicist in the Technical Feasibility Study Office at Red-

stone Arsenal, Ala. Upon his discharge from military service in 1956 he accepted civilian employment at Redstone Arsenal with the

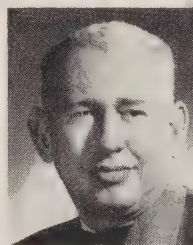


C. A. LUNDQUIST

Army Ballistic Missile Agency. He is presently chief of the Physics and Astrophysics Branch of the Research Projects Laboratory.

Dr. Lundquist is a member of the American Physical Society, the American Geophysical Union, and the National Speleological Society.

Lloyd H. Manamon was born on September 14, 1915, in Wareham, Mass. He studied electrical engineering at Northeastern University, Boston,



L. H. MANAMON

Mass., from 1933 to 1936. After four years experience in industry, he joined the Federal Security Agency in 1941. In 1942, he transferred to the Vehicular Radio Section of the Signal Corps Laboratories, Fort Monmouth, N. J., where he was concerned with the development of vehicular radio equipment at Squier Laboratory. He remained in that position until 1945, at which time he was assigned as project engineer to the Field Engineering Section, Coles Laboratory. He received the War Department Commendation from the Office of the Chief Signal Officer in 1946. In 1953, he was assigned to the Long Range Radio Branch as a section chief in charge of communication facilities and systems evaluation. He joined the staff of the Astro-Electronics Division in 1959, and has been in charge of the USASRD Astro-Observation Center at Deal, N. J., since that date.

Mr. Manamon is a member of the Armed Forces Communications and Electronics Association.

Frederick F. Marmo was born on October 25, 1920, in Boston, Mass. He received the B.A. degree, magna cum laude, from Boston University, Mass., and the M.S. and Ph.D. degrees from Harvard University, Cambridge, Mass., all in chemical physics, in 1949, 1951, and 1954, respectively.

He is manager of the Chemical Physics Department in the Aeronomy Division of the Geophysics Corporation of America. From 1951 through 1958 he was associated with the Geophysics Research Directorate of

the Air Force Cambridge Research Center where he was branch chief and project officer. His responsibilities lie in the area of



F. F. MARMO

scientific direction of upper atmosphere photochemical research using laboratory techniques and rockets in addition to studies pertinent to planetary atmosphere. The concept of artificial electron clouds is attributed to Dr. Marmo. He and his colleagues were the first to produce an artificial electron cloud, and between May, 1957, and September, 1958, eight successful pioneer-type experiments designed to investigate the possibility of utilization of artificial electron clouds for practical communication purposes were performed.

Dr. Marmo is a member of Phi Beta Kappa, the American Rocket Society, and the American Physical Society.

Donald H. Marx (S'49-A'51-M'56) was born in Miami, Fla., on July 21, 1927. He received the B.S. degree in electrical engineering from the

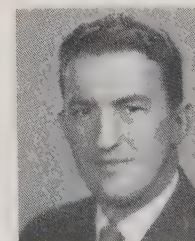


D. H. MARX

Newark College of Engineering, N. J., in 1951, and the M.S. degree from Rutgers University, New Brunswick, N. J., in 1955.

Since 1950, he has been employed by the U. S. Army Signal Research and Development Laboratory, Fort Monmouth, N. J., working in the fields of radar countermeasures, radio direction finding, and communication satellites.

Clifford D. May, Jr., (M'57) was born in Des Moines, Iowa, on May 19, 1922. He received training in electrical engineering at the State University of Iowa, Ames,



C. D. MAY, JR.

and the Chicago Signal Schools, Ill.

He joined the Signal Corps as a civilian employee radar technician in 1942 and has served continuously in various technical and engineering positions since that time. Two



years of his career were spent on active military duty in the Signal Corps. In 1945, he joined the U. S. Army Communication Agency where he served as chief, Electronics Maintenance Unit until 1951. At that time, he joined Army Communications Service Division, Office of the Chief Signal Officer, as a staff communication specialist engaged in communication systems planning. In July, 1958, he was appointed technical director, ACSO, OCSigO, where he is currently serving.

He has received numerous decorations and awards during his Signal Corps career, including the Exceptional Civilian Service Award, Meritorious Civilian Service Award, and the Award for Sustained Superior Performance. He has contributed significantly to the success of the Army's UNICOM program and the national communication satellite program.

Mr. May is a member of the Association of the United States Army. He is a licensed radio amateur.



Marjorie E. McLardie was born in Brunswick, Ga., in 1925. She attended Georgia Institute of Technology, Atlanta, Texas Western College, El Paso, and did extension work with Pennsylvania State University.



M. E. McLARDIE

She served as meteorologist for the Weather Bureau from 1945 to 1956 in Georgia, Florida, Alabama, and New Mexico. In 1956, she transferred to the U. S. Army Signal Missile Support Agency (SMSA), White Sands Missile Range, N. M., serving as a research and development meteorologist. In 1957, she supervised the initiation of a meteorological tower at White Sands Missile Range. She is presently supervising research and development studies and the meteorological support of tactical missile firings at the SMSA Missile Geophysics Research Tower.

Miss McLardie is a member of the American Meteorological Society and the American Rocket Society.



James P. McNaul (M'57) was born in Madison, Wis., on August 20, 1933. He received the B.S. degree in electrical engineering from the University of Wisconsin, Madison, in 1956. He worked as a field engineer for Square D Company, Milwaukee, Wis., before being commissioned in the Signal Corps in May, 1956.

His first assignment was at the U. S. Army Signal Research and Development Laboratory (USASRDL), Fort Monmouth, N. J., as assistant project officer of Project MONMOUTH, a communications system

and frequency compatibility study. He served in this capacity until May, 1958, when he joined the technical staff of the Electronic

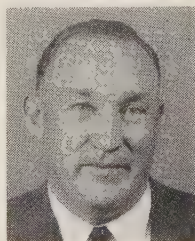


J. P. MCNAUL

Components Research Department of USASRDL. Since reverting to civilian status, he has continued in that position with responsibilities in the application of components to communication systems.



Mr. McNaul is a member of the Armed Forces Communications and Electronics Association, and Kappa Eta Kappa. He has served as Chairman of the Professional Group on Radio Frequency Interference.



W. D. MERRICK

William D. Merrick was born on November 6, 1917, in San Francisco, Calif. He received the B. S. degree in electrical engineering from the California Institute of Technology in 1939. In 1951 he joined the Jet Propulsion Laboratory as a research engineer and worked on optical and electromechanical systems in connection with radar guidance of the Corporal missile. Since 1954 he has been a supervisor of the inertial components research group and has been responsible for work conducted on gyroscopes, stable platforms, and optical equipment. He has also been responsible for the design, construction, and installation of the 85-foot antenna at the JPL Goldstone tracking station.

Mr. Merrick is a member of the Instrument Society of America and the Optical Society of America.



John C. Mester (S'48-A'51) was born in Baltimore, Md., on January 15, 1927. After serving two years in the United



J. C. MESTER

States Navy, he graduated from the University of Maryland, College Park, receiving the B.S. degree in electrical engineering in 1948, and the M.A. degree in mathematics in 1951.

Since 1950, he has been a mathematician at the Army Ballistic Research Laboratories, Aberdeen Proving Ground, Md.

He has worked on the error analysis

of electronic tracking systems and on missile guidance problems, especially on the application of digital and analog computer techniques. His interest has ranged over many related fields including the propagation of electromagnetic waves through the ionosphere.

Mr. Mester is a member of the American Geophysical Union and an alternate member of the Working Group on Upper Atmosphere Rocket Research.



Thomas P. Mottley was born in New York, N. Y., on April 23, 1914. He graduated from the U. S. Army Signal Corps Wartime Radar School, Fort Monmouth, N. J., and attended Monmouth College, West Long Branch, N. J.



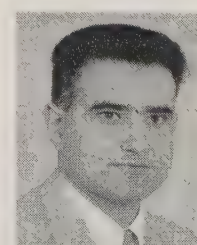
T. P. MOTTLEY

He served as project engineer with the U. S. Air Force, Watson Laboratories (now Rome Air Development Center), Rome, N. Y., on an improvement program for USAF Ground Controlled Approach Radar System. During the course of this work, he received an Air Materiel Command AF citation for the design and development of special-purpose indicators for application on ground control approach systems. In 1950, he became associated with the U. S. Army Signal Research and Development Laboratory, in Fort Monmouth, serving as assistant chief of the Measurements Section, where he worked on special test equipment for germanium diode testers and storage tube evaluation equipment design. From 1956-1958, he was chief of the Vulnerability Measurements Section of the Countermeasures Division, USASRDL, on a susceptibility test program of classified radar and communications programs. He is now engineer for the USASRDL on communication satellite projects.

Mr. Mottley is the co-inventor of a patented design for an automatic oscillographic antenna-pattern recording system.



Wilhelm Nordberg was born on March 30, 1930 in Fehring. He received the Ph.D. degree in physics from the University of



W. NORDBERG

Graz, Austria. He also assisted in research activities on ionospheric physics and wave propagation in the ionosphere at the University's Institute for Meteorology and Geophysics.

In 1953, Dr. Nordberg joined the Atmospheric Physics Section of the U. S.



Army Signal Research and Development Laboratory, Fort Monmouth, N. J., where he participated in upper atmosphere research programs for six years. He transferred to the National Aeronautics and Space Administration, Washington, D. C., in July, 1959, and is now conducting atmospheric research projects in the Meteorology Branch of Goddard Space Flight Center.



R. B. Patton, Jr., was born in Pittsburgh, Pa., on August 15, 1918. He received the B.S. degree in education from the University of Pittsburgh, Pa., in 1940. From 1941 to 1946, he was on active duty with the U. S. Army Air Force. He studied meteorology at M.I.T., Cambridge, Mass., from 1941 to 1942, while on this tour of duty. From 1946 to 1948 he studied mathematics in the Graduate School of the University of Pittsburgh and also lectured at the University.



R. B. PATTON, JR.

Since 1948, he has been a member of the Ballistic Research Laboratories, Aberdeen Proving Ground, Md., where he has specialized in the development of mathematical methods for the reduction of missile and satellite tracking data. He is currently in charge of the Performance Evaluation Section, and a member of the Ballistic Research Laboratories' scientific staff.

Mr. Patton is a member of Sigma Pi Sigma and Kappa Phi Kappa.



Sol Perlman (M'45-SM'52) was born in Brooklyn, N. Y., on April 22, 1906. He received the E.E. degree in 1929 and the M.E.E. degree in 1947, from the Polytechnic Institute of Brooklyn.



S. PERLMAN

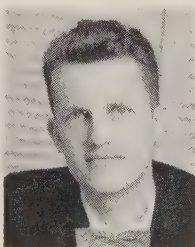
From 1929 to 1941, he worked for private industry. Part of that time, in business for himself, he did equipment design and manufacturing on electronic test equipment, antennas, and hearing aids. From 1941 to 1945, he was employed by Signal Corps Procurement, Philadelphia, Pa., as a field engineer on transmitter tubes and radio transmitters. From 1945 to 1949, he was employed, in turn, as equipment engineer in a transmitter tube plant, senior engineer on television receiver development, and electronic engineer on the manufacture of wire recording business office dictating

machines. In May, 1949, he became an electronic engineer in the radar laboratory of Watson Laboratories, U. S. Air Force, Easton, N. J. In January, 1951, he moved to the Rome Air Development Center, Griffiss Air Force Base, Rome, N. Y., as chief of the radar data handling unit, and later as chief of the special circuits unit, both in the radar laboratory. His work included development of radar data remoting and control systems for search, height finding and IFF radars and, later, as consultant on transistor circuitry and nonlinear circuit applications for RADC. In March, 1956, he transferred to the U. S. Army Signal Radio Propagation Agency, Fort Monmouth, N. J., as chief of the analysis engineering division. He has participated in studies of tropospheric scatter problems of interference, frequencies for space vehicle communication, and application of the digital computer to MUF-LUF computations.

Mr. Perlman is a member of the American Institute of Electrical Engineers, American Geophysical Union, and the American Association for the Advancement of Science.



Eberhardt Rechtin (S'45-A'49-SM'55) was born in Orange, N. J., on January 16, 1926. He received the B.S. degree in 1946, and the Ph.D. degree in 1950 from California Institute of Technology.



E. RECHTIN

He joined the Jet Propulsion Laboratory the same year and participated in the early development of the U. S. missile and space programs. He has specialized in range instrumentation, missile radio guidance, information and filter theory, secure communications, and extreme-range communications. Dr. Rechtin has directed much of the JPL effort in space communications and tracking, specifically the Microlock system for satellites and the TRACE system used on the Army Pioneer for lunar communication.

He received the Westinghouse Science Talent Award in 1943, was a Cole Fellow in 1947, and a National Science Fellow in 1948. He is Chairman of the Avionics Panel of the NATO Advisory Group on Aeronautical Research and Development, which is devoted to international cooperation in space programs, and is a member of Sigma Xi and Tau Beta Pi.



Friedrich H. Reder (A'54) was born in Garsten, Upper Austria, on December 9, 1919. He received the Cand. Ing. degree in technical physics from the Institute of Technology, Graz, Austria, in 1947, and the Ph.D.

degree in physics from the University of Graz in 1949.

From 1948 to 1950, he was scientific assistant at the Physics Institute of the University of Graz, and worked on microwave cavity methods for determining the dielectric constant of solids and liquids, and in interference microscopy. From 1950 to 1951, he held a research fellowship at M.I.T., Cambridge, Mass., where he was



F. H. REDER

engaged in studying microwave gas discharge phenomena in pure helium gas. From 1951 to 1953, he worked on gas discharge projects and high-vacuum techniques at the University of Graz and at the Shell Research Laboratory, Amsterdam, The Netherlands. Since 1953 he has been with the Frequency Control Division of the U. S. Army Signal Research and Development Laboratory, Fort Monmouth, N. J., where he is now chief of the Atomic Resonance Branch, and in charge of research and development work on atomic and molecular frequency control.

Dr. Reder is a member of the American Physical Society.



Henry L. Richter, Jr. (SM'58) was born in Long Beach, Calif., in 1927. He received the B. S. degree in chemistry in 1952 and the Ph.D. degree with a chemistry major and electrical engineering and physics minors in 1955, both from the California Institute of Technology, Pasadena.



H. L. RICHTER, JR.

He has been with the Jet Propulsion Laboratory, Pasadena, Calif., since 1955. Since 1959 he has been chief of the Space Instruments Section and previously was supervisor of the new circuit elements and stable oscillator research groups.

Dr. Richter is a member of the American Radio Relay League and is coordinator for Amateur Radio Participation in the IGY satellite-tracking program.



Otto E. Rittenbach was born in May 1922, in Herrnskretsch, Czechoslovakia. From 1938 to 1941, he attended the City College of Technology in Tetschen-Bodenbach, Czechoslovakia, and from 1946 to 1952, he attended the Institute of Technology in Braunschweig, West Germany.

From 1942 to 1945, he worked for the Civil Service of the German Navy in the torpedo research plants in Eckernförde, and



Gotenhafen, Germany, and in the Elac plant in Kiel, Germany. There he developed and evaluated electronic implements for submarines and torpedoes.



O. E. RITTENBACH

From 1953 to 1958, he was employed by the Communications Department of Siemens and Halske in Munich, Germany, where he worked on the development of television program transmission equipment for the 625-line standard, in particular the TV modulator bay.

In June, 1958, Mr. Rittenbach joined the U. S. Army Signal Research and Development Laboratory, Fort Monmouth, N. J. He is engaged in theoretical and experimental investigation of the application of correlation techniques to radar.



Thelma A. Robinson was born in Murphy, Miss., on February 6, 1928. She received the B.S. degree in mathematics from Tougaloo College, Miss., in 1948, the M.S. degree in mathematics from Howard University, Washington, D. C., in 1950, and has done further graduate work at George Washington University in Washington, D. C.

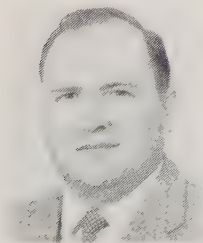


T. A. ROBINSON

In 1950 and 1951, she taught mathematics at Bethune-Cookman College, Daytona Beach, Fla. In 1952, she joined the Department of Mathematics at Southern University, Baton Rouge, La. Since 1953, she has been employed as a mathematician at the Army Map Service in Washington, D. C., where she has been engaged in geodetic research.



James E. Rorex was born in Cherokee, Ala., on May 21, 1925. He received the B.S.E.E. degree from the University of Alabama, Tuscaloosa, in 1949.



J. E. ROREX

From 1943 to 1945, he served as a pilot in the Army Air Corps. He taught radar for two years and worked for a consulting engineering company for one year before joining the Army Ballistic Missile Agency (ABMA) in 1952. Until January, 1959, he was assigned to

ABMA's Missile Firing Laboratory at Cape Canaveral, Fla., where he was chief of the RF and Telemetry Section and was responsible for development of telemetry test procedures and equipment used in flight testing the Redstone and Jupiter missiles.

In January, 1959, he was transferred to Huntsville, Ala., as chief, Radio Telemetry Section of Guidance and Control Laboratory, where he has been responsible for the development of ABMA's airborne telemetry equipment.

Mr. Rorex is a member of the AIEE.



Harry O. Ruppe was born on May 3, 1929, in Leipzig, Germany. He studied theoretical physics and mathematics at the University of Leipzig and the Technical University at Berlin-Charlottenburg, receiving the B.S. and M.S. degrees from the latter.



H. O. RUPPE

Upon completion of his studies he served as assistant on supersonic aerodynamics to the professor of theoretical physics at The Free University at Berlin-Steglitz from 1955 to 1957. He was a consultant on solid propellant rocket motor development in the engineering office of the German firm Sommerkorn, in Frankfurt, from 1956 to 1957.

He came to the United States in October, 1957, and has been employed at the Army Ballistic Missile Agency, Redstone Arsenal, Ala. At present he is chief of the Lunar and Interplanetary Flight Unit in the Structures and Mechanics Laboratory.

Mr. Ruppe is a member of DGRG, a German Society for Rockets and Space Flight, the American Rocket Society, and is a Fellow of the British Interplanetary Society.



William J. Russell, Jr., (A'46-M'55) was born in Minneapolis, Minn., on July 9, 1921. He received the B.S. degree from the California Institute of Technology, Pasadena, in 1946.



W. J. RUSSELL, JR.

He served in the U. S. Army Signal Corps from 1943 to 1946, and has been employed since that time as a propagation engineer, electronic scientist, and project engineer for the U. S. Army Signal Radio Propagation Agency, now at Fort Monmouth, N. J.

Mr. Russell is a licensed professional engineer in the state of New Jersey.

Dan Schneiderman was born in Baltimore, Md., on February 23, 1922. In 1949 he received the B.S. degree in electrical engineering at the University of California, Berkeley.



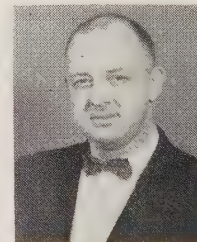
D. SCHNEIDERMAN

He joined the Jet Propulsion Laboratory, California Institute of Technology, Pasadena, in 1950 and has been active in research and development of digital computer components and techniques, radio-inertial guidance and analog computer systems, and was in charge of the Payload Group for Pioneers III and IV.

Mr. Schneiderman is now engineering supervisor of the Spacecraft Systems Design Group at JPL.



Russell D. Shelton was born in Junction City, Ky., on February 17, 1925. He received the B.S. degree from Eastern Kentucky State College, Richmond, Ky., in 1947. He received the M.S. degree in 1950, and the Ph.D. degree in 1953 from the University of Tennessee, Knoxville.



R. D. SHELTON

He served as a senior nuclear engineer in the Aircraft Nuclear Propulsion Group, Convair, Fort Worth, Tex., from 1953 to 1954. From 1954 to 1955 he was project nuclear engineer in the Advanced Nuclear Studies Group for Convair. From 1955 to 1958 he worked for the Admiral Corporation in Chicago as executive physicist in the Radiation Effects Group. He joined the Army Ballistic Missile Agency in 1958. He is presently serving as chief of the Nuclear Physics Branch in the Research Projects Laboratory. He has been engaged in the administration of research in thermoelectric refrigeration, nuclear instrumentation, fission plate design, and nuclear facility design.

Dr. Shelton has published numerous papers in the fields of radiation effects on electronic components, shielding techniques, ground scattering phenomena, and molecular spectroscopy.



William Shorr was born in New York, N. Y., on February 1, 1907. He received the B.S. degree in chemistry from New York University in 1931.

In 1942, he joined the Signal Corps Lab-



oratory, Fort Monmouth, N. J., and has been active in power sources research and development since that time. His present title is Deputy Chief of the Power Engineering Branch, Power Sources Division, Electronic Components Research Department.

He is a member of the American Chemical Society and the Electrochemical Society.



W. SHORR



W. E. Smitherman was born February 9, 1915, in East Bend, N. C. He is a Lieutenant Colonel in the U. S. Army, and an officer in the Signal Corps, where he has served in various capacities both in the United States and the European Command. He is presently Signal Officer of the Antilles Command, San Juan, Puerto Rico.

Lt. Col. Smitherman was awarded the Commendation Ribbon with Metal Pen-

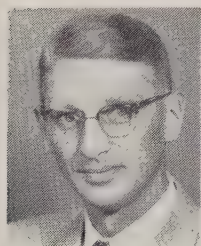
dant for meritorious achievement, for his services as assistant projects officer, AMS Project Vanguard Task Force and as chief, AMS Project Vanguard, from February 4, 1957 to February 28, 1959.



Fridtjof A. Speer was born in Berlin, Germany, on August 23, 1923. He received the Ph.D. degree in physics from Technical University, Berlin, in 1953, and was assistant professor of experimental physics for three years.

A former member of the Peenemunde rocket development group, he signed a contract with the U.S. Army and came to this country in 1955. Since then he has been with the Development Operations Division of the Army Ballistic Missile Agency, where he is presently chief of the Flight Evaluation Branch, Aeroballistics Laboratory. He is in charge of the ABMA early orbit determinations, and is responsible for the evaluation of all ABMA ballistic missile and space vehicle flights. He is the author of several German publications in the field of semiconductors and has published some 30 ABMA technical reports.

Dr. Speer is a member of the American Rocket Society.



F. A. SPEER

Charles S. Spooner, Jr., was born December 1, 1915, in Thomasville, Ga. He received the B.S.F. and M.F. degrees in 1938 and 1939 respectively, from The University of Michigan, Ann Arbor. During World War II, he served as a Naval Intelligence Officer and he presently holds the rank of Lt. Colonel, USAR.

In 1946 Mr. Spooner began an eight-year service as chief of the Relief

Map Division of the Army Map Service, Washington, D. C. In 1954 he assumed the duties of assistant chief of the Operations and Planning Staff, responsible for advising on all operational aspects of the Army Map Service. In 1956 he assumed the duties of chief of the Technical Developments Staff at the Army Map Service. This staff is comprised of a small group of senior scientists and engineers engaged in the planning and execution of advanced research programs in geodesy and topographic mapping.

Mr. Spooner is a member of the Washington Academy of Sciences, the American Society of Photogrammetry, and the American Congress on Surveying and Mapping.



Rudolf A. Stampfl (A'54) was born on January 21, 1926, and is a native of Vienna, Austria. He attended the Institute of Technology, Vienna, from which he received the B.S., M.S., and Ph.D. degrees in communications and electronics.

He came to the United States in 1953, and from 1953-1959 was employed by the U. S. Army Signal Research and Development Laboratory, Fort Monmouth, N.J.,

first as a systems engineer on surveillance systems, and then with a team which designed the Vanguard II experiment. Since 1959, Dr. Stampfl has been employed by the National Aeronautics and Space Administration, Washington, D. C., as deputy head of the Meteorology Branch.



Sidney Sternberg was born in New York, N. Y., on May 27, 1921. He received the B.S. degree in physics from the College of the City of New York in 1943, and the M.S.E.E. degree from New York University in 1949.

During World War II, he served as a radar officer in the U. S. Navy. From 1946 to 1950, he was employed by the Office of

Naval Research, Washington, D.C., where he made significant contributions in computer research. He joined the RCA Laboratories, Princeton, N.J., in 1951, where he was initially engaged in research programs typified by the Typhoon computer and the Dynamic Systems Synthesizer, and later was in charge of satellite studies and design projects. He received the RCA Laboratories Research

Achievement Award both in 1953 and 1955.

Mr. Sternberg's connection with space technology dates back to the early days of satellite systems. In 1955, when a previous study of the use of television techniques in space reconnaissance systems was broadened into a research study for an over-all space reconnaissance system, he was placed in charge of the Information Systems portion of the program. He subsequently became project manager of a feasibility study leading to a design project for a television reconnaissance satellite system.

He joined the Astro-Electronic Products (AEP) Division of RCA upon its formation in 1958, as manager of satellite projects. He is presently chief engineer and has directed much of the pioneering effort on the development of electronic space systems. Under his management, AEP is conducting study, development, and construction programs on earth satellite systems, space probes, rocket propulsion systems, secondary (payload) power systems, and specialized satellite components. Two notable developments achieved under his direction are those portions of the ground and space-borne communication equipment for Project Score (the talking satellite) and the satellite and ground equipment for the recently launched TIROS I, for which Astro-Electronic Division of RCA was the contractor.

Mr. Sternberg is a member of Sigma Xi and the American Rocket Society.



Robertson Stevens (M'53) was born in San Diego, Calif., on August 7, 1922. He received the B. S. degree from the U. S.

Naval Academy, Annapolis, Md., in 1945 and the M. S. degree in electrical engineering from the University of California at Berkeley in 1949. He joined the Jet Propulsion Laboratory of California Institute of Technology in 1949 as a research engineer.

Since 1958 he has been chief of the guidance techniques research section, where he is responsible for research and development in the fields of



S. STERNBERG



R. STEVENS



antennas and microwaves, masers and parametric devices, inertial and optical guidance components, gas bearing development, and molecular aggregate devices. He was in charge of the JPL effort which resulted in the design, installation, and operation of the Goldstone tracking station during the Pioneer III and IV experiments.

Mr. Stevens is a member of Sigma Xi.



William G. Stroud, Jr., was born on March 5, 1922, in Philadelphia, Pa. He received the B.S. degree from the Pennsylvania State University,



W. G. STROUD, JR.

where he worked as a research assistant in organic chemistry, the M.S. degree from the University of Chicago, Ill., where he worked as a research assistant in physics, and the M.A. degree from Princeton University, N.J. where he also served as a research

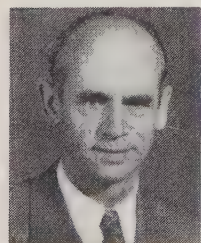
assistant in physics.

From 1943-1945 he worked on the Manhattan Project at the Los Alamos Scientific Laboratory, Los Alamos, N. M.; from 1950-1959 he was a physicist with the U. S. Army Signal Research and Development Laboratory, Fort Monmouth, N. J.; and since April, 1959 he has headed the Meteorology Branch, Goddard Space Flight Center, National Aeronautics and Space Administration, Washington, D. C. He has authored or co-authored over 28 articles and technical papers on cosmic ray physics, upper atmosphere physics, infrared, and satellite applications.

Mr. Stroud is a member of the American Physical Society and the American Rocket Society.



Ernst Stuhlinger (A'54) was born in Niederrimbach, Germany, on December 19, 1913. He received the Doctorate degree in physics at the University of Tuebingen, Germany, in 1936.



E. STUHLINGER

He was appointed assistant professor of the physics department at the Berlin Institute of Technology and was a member of the faculty there from 1936 to 1941. He worked closely with Dr. Hans Geiger, devel-

oper of the Geiger counter, for seven years. From 1939 to 1941, he also was a member of

a research group conducting studies in nuclear physics. In the spring of 1943, he joined the Rocket Development Center at Peenemuende, where he carried on research in connection with the development of guidance and control systems for the V-2 guided missile. Dr. Stuhlinger came to the United States in 1946, and until 1950 conducted research and development work on guided missiles at Fort Bliss, Texas. He also assisted in high-altitude research firings of V-2 missiles at White Sands Proving Ground, N. M. Since 1950, he has been a member of the guided missile team at Redstone Arsenal, Huntsville, Ala., where he is presently director of the Research Projects Laboratory at the Army Ballistic Missile Agency. He has gained wide recognition in recent years for his feasibility and design studies of electrical propulsion systems.

Dr. Stuhlinger is a Fellow of the American Rocket Society and of the American Astronautical Society. He is also an Honorary Member of the German Society for Rocket Techniques. He received his American citizenship in April, 1955.



Walter P. Teetsel (S'52-A'53-M'58) was born in Union City, N. J., on March 28, 1927. He received the B.S. degree in electrical engineering from the Drexel Institute of Technology, Philadelphia, Pa., in 1952, and the M.S. degree from Rutgers University, New Brunswick, N. J., in 1955.



W. P. TEETSEL

Since 1952, he has been employed by the U. S. Army Signal Research and Development Laboratory, Fort Monmouth, N.J., working in the guided missile range instrumentation and satellite communication fields.

Mr. Teetsel is a member of Phi Kappa Phi, Tau Beta Pi, and Eta Kappa Nu.



Reg Thomas (A'47-M'52) was born on October 2, 1920, in Wickliffe, Ky. He was a warranted communications technician in the U. S. Marine Corps during World War II, serving as radio and wire chief, and received the B.S. degree in engineering from American Institute of Engineering, Chicago, Ill., in 1949.



R. THOMAS

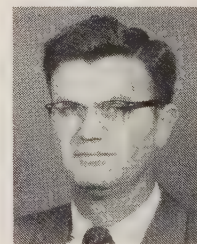
From 1949 to 1954, Mr. Thomas was associated with Cook Research Lab-

oratories, Chicago, Ill., and worked in the field of electronic and photographic instrumentation of high-speed rocket sleds and test missiles. This work included the design and development of magnetic tape recording and playback equipment for use in missile instrumentation, and methods of correlating electronic and photographic data from missile and sled tests. During this period he was also Wing Communications Officer of the Illinois Wing of the Civil Air Patrol, assigned to Civilian Defense.

Since 1954, he has been employed by Bendix-Pacific Division of Bendix Aviation Corporation, Hollywood, Calif., in the field of digital data handling and transmission. He has been project engineer on digital telemetering networks, industrial automation equipment, and data acquisition and logging systems. At present he is project engineer on the White Sands Missile Range Digital Meteorological Data Logging System.



Arthur W. Thompson (M'55) was born in Louisville, Ky., on February 6, 1924. He received the B.S. degree in physics and mathematics from Western Kentucky College, Bowling Green, Ky., in 1949.



A. W. THOMPSON

After a year with Land Air, Inc., at Holloman Air Force Base, he joined the White Sands Group of New Mexico A & M College in 1951. From 1954 until 1956, he was employed by the Electronic Warfare Division, White Sands Signal Corps Agency. While in New Mexico, he worked on development of proximity fuzes and fuze instrumentation for Corporal and Talos missiles. He joined the Army Ballistic Missile Agency at Redstone Arsenal, Huntsville, Ala., in 1956. He is presently chief of the Systems and Instrumentation Section in the Research Projects Laboratory. He has worked on tracking and telemetering requirements for the Explorer satellites and is now doing similar work for future satellite projects.

He is a member of the American Rocket Society.



Walter K. Victor was born in 1922 in New York, N. Y. He attended the University of Texas in Austin, and received the B. S. degree in mechanical engineering in 1942.

Prior to his military service, he was with the Sperry Gyroscope Company, Brooklyn, N. Y., working on airborne computer and fire-control systems. During the war he served with the Air Corps as a pilot instructor.

Since September, 1953, he has been associated with the Jet Propulsion Laboratory, Pasadena, Calif., where he is head of the communications systems research section. Mr. Victor was responsible for the flight and ground electronic instrumentation for the Army Explorer Satellite Program. He was also responsible for the communications system design for Pioneer probes III and IV.



W. K. VICTOR

Mr. Victor is a member of Tau Beta Pi and Sigma Xi.

Friedrich O. Vonbun (M'60) was born in Vienna, Austria, on June 22, 1925. He received the M.S. degree at the Institute of Technology, Vienna, in 1952, and the Ph.D. degree in physics at the Institute of Technology, Graz, Austria, in 1957.



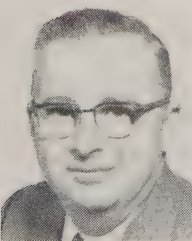
F. O. VONBUN

He joined the U. S. Army Signal Research and Development Laboratory (USASRDL), Fort Monmouth, N. J., early in 1953 as a research physicist. For two years, he was engaged in research work in the field of microwave antennas. In 1955, he joined the Frequency Control Division of USASRDL and was engaged in work in atomic and molecular resonance devices. He is at present consulting scientist of the Frequency Control Division.

In May, 1960, Dr. Vonbun joined the National Aeronautics and Space Administration, Goddard Space Flight Center, in Washington, D. C. He is at present consultant to the Tracking Systems Division at Goddard and is engaged in research and development work in the fields of radio and optical tracking, propagation of electromagnetic waves through the ionosphere, radio telemetry and geophysics.

Dr. Vonbun is a member of the American Physical Society.

Joseph R. Walsh was born in Somerville, N. J., on October 5, 1909. He received the B.S. degree in mechanical engineering from Lehigh University, Bethlehem, Pa., in 1931, and the M.S. degree in meteorology from California Institute of Technology, Pasadena, in 1943.



J. R. WALSH

He worked with the Department of Commerce from 1932-1940 doing surveying and construction, and from 1941

to the present, four years of which were spent in military service, he has been with the Signal Corps as a mechanical engineer engaged in research and development on equipment and techniques in the field of meteorology.

His present position is deputy chief, Meteorological Techniques Branch, Meteorological Division, USASRDL, Fort Monmouth, N. J.

Mr. Walsh is a professional meteorologist and is a member of the American Meteorological Society.

Willis L. Webb was born in Nevada, Tex., on July 9, 1923. He received the B.S. degree in mathematics from Southern Methodist University, Dallas, Tex., after undergraduate work at Reed College, Portland, Ore., and Harvard University, Cambridge, Mass.



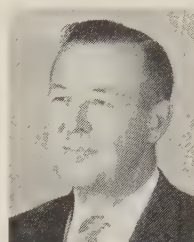
W. L. WEBB

His activities as a meteorologist have ranged from routine meteorological and river forecasting at Weather Bureau offices in atmospheric physics.

The period from September, 1942, to March, 1952, was spent in Weather Bureau stations in Tulsa, Okla., and in Big Spring and Dallas, Tex., with three years military leave to the Air Force Weather Service. In March, 1952, he moved to the Weather Bureau's Physical Research Division in Washington, D. C. His research efforts were directed toward atmospheric effects on the nation's missile program through work at the White Sands Missile Range with the U. S. Army Signal Missile Support Agency from February, 1955, to the present time. His early studies centered around missile acoustics, while implementation of a network of meteorological rocket sounding stations has been a major activity during the last few years. He is chairman of the Meteorological Rocket Network Committee of the Inter-Range Instrumentation Group, Meteorological Working Group, which is charged with coordination of the efforts of several diverse groups involved in this program. He is currently chief of the Atmospheric Propagation Branch of the Signal Agency at White Sands. The Branch is engaged in studies in acoustic and electromagnetic propagation as well as the development of balloon platforms, rocket systems, and sensors to make the required measurements.

Perry L. White was born on June 4, 1917, in Gans, Okla. He received the B.S. degree in education, with a physical science major, from Oklahoma State University,

Stillwater, in 1946. Later, in 1950, he received the M.S. degree in education administration, with a physical science minor, from the same university.



P. L. WHITE

From 1942-1946, he served as a radar maintenance technician in the U. S. Army. The following academic year was spent in teaching physics and chemistry at Oklahoma State University; during this time, he began work with the University Research Foundation as a research assistant working on the development of MIRAN (Missile Ranging Only Tracking System). In 1951, Mr. White left the University to work at White Sands Missile Range, White Sands, N. M. Since that time, he has done design work in servomechanisms, analog computers, radar, and associated data-handling equipment. Presently chief of the Laboratory Branch there, he is responsible for the research and development work in the Radar Division of the U. S. Army Signal Missile Support Agency.

Edward S. Wilbarger, Jr., Captain, U. S. Army (MSC), was born in Billings, Mont., on February 21, 1931. He received the B.S. degree in civil engineering from the Virginia Military Institute, Lexington, in 1952, and the M.S. degree in physics from the U. S. Naval Postgraduate School, Monterey, Calif., in 1956. He then worked on preventive medicine.

In 1959, he was assigned as engineer-physicist to the Bio-Astronautics Research Office, AOMC. He is presently with the Nuclear Power Division, Office of the Chief Engineer, Department of the Army, Washington, D. C.

Gernot M. R. Winkler was born in Bruck, Austria, on October 17, 1922. He received the Ph.D. degree from the University of Graz, Austria, in 1952. He was on the staff of the Astronomical Observatory in Graz, as assistant to the director, from 1949 to 1953. He was employed in industry from 1953 to 1956.



G. M. R. WINKLER

Dr. Winkler came to this country in 1956 and joined the Frequency Control Division, U. S. Army Signal Research and Development Laboratory, Fort Monmouth,



N. J., as a consulting physicist. He has been engaged with various developments in the field of microwave electronics and precision frequency and time measurements.



Richard S. Young was born in Southampton, N. Y. on March 6, 1927. He received the B.A. degree from Gettysburg College, Pa., in 1948 and the Ph.D. degree from Florida State University, Tallahassee, in 1955.



R. S. YOUNG

He was employed in the Cancer Research Division of Lederle Laboratories, Inc., Pearl River, N. Y., and also worked in the cancer research field in the Pharmacology Division of the Federal Food and Drug Administration, Washington, D. C. For the past

year he has been assigned in the area of astrobiology in the Army Ballistic Missile Agency, Huntsville, Ala.

He is the author of scientific papers in the fields of experimental embryology and biochemistry. He has taught at Athens College, Athens, Ala., and in the Huntsville extension of the University of Alabama.

Dr. Young is a member of Phi Sigma, Sigma Xi, the American Association for the Advancement of Science, and the Society for Experimental Biology and Medicine.



Harold A. Zahl (A'39-SM'46-F'50) was born on August 24, 1904, in Chatsworth, Ill. He received the B.S. degree from North Central College, Naperville, Ill., in 1927, the M.S. degree in 1929 and the Ph.D. degree in physics in 1931 from the State University of Iowa, Iowa City.

From 1927 to 1931 he was a research assistant at Iowa. In 1931 he became a re-

search physicist at the U. S. Army Signal Research and Development Laboratory in Fort Monmouth, N. J., where he has been director of research since 1948. From 1942 to 1946, he was an officer in the Signal Corps, and as a Lieutenant Colonel was involved in the work with the Bikini Atomic Tests in 1946. In the same year, he received the Legion of Merit. He is the author of 50 technical publications in the



H. A. ZAHL

fields of molecular and atomic physics, X rays, acoustics, thermodynamics, and astro-electronics. He has had patents issued for work in radar, communications, electron tubes, infrared and aircraft instruments.

Dr. Zahl is a Fellow of the American Physical Society and is also a member of the Armed Forces Communications Association.







## INFORMATION FOR AUTHORS

The PGMIL TRANSACTIONS is intended to bridge the gap between the various disciplines contributing to military electronics. Since this includes most of the branches of electronics, the military, and many fields which are associated with but not actually within the realm of electronics, it is essential that the papers published be of broad interest. The emphasis should be on readable, thought-provoking material that stimulates an attitude of open mindedness and curiosity.

Papers are solicited in the following general subject categories:

**Military sciences**—Military science fiction, famous battles involving electronics, basic problem areas of military electronics.

**Technical survey**—Tutorial technical papers on radar, communications, navigation, systems and operations research, etc.

**Integrating papers**—Integration of concepts common to several fields, as for example, wave phenomena, information theory, etc.

**Physical sciences**—Fundamentals of modern physics that may influence the future of military electronics.

**Mathematical concepts**—Applications and implications of modern mathematical methods.

**Associated subjects**—Survey of fields that are neither military nor electronic but which are important to the advancement of military electronics.

**Manufacturing**—Industrial and military problems of reliability, quality control, etc.

It is requested that each paper be submitted in duplicate. Standard IRE practice should be followed in preparation of the manuscript and illustrations. Papers should be sent to James Q. Brantley, Jr., or Donald R. Rhodes, PGMIL Editors, P.O. Box 6904, Orlando, Fla.

## INVITATION TO MEMBERSHIP IN PGMIL

Members of the IRE may join the Professional Group on Military Electronics as active, voting members by payment of the annual fee of \$2.00. Nonmembers of the IRE who qualify may become nonvoting affiliates under the new IRE Affiliate Plan by payment of an annual fee of \$4.50 in addition to the assessment of the Group. All applications for membership affiliation should be addressed to the Chairman of the PGMIL Membership Committee, William M. Richardson, The Ramo-Wooldridge Corporation, 1300 Connecticut Ave., Washington 6, D.C., or to IRE Headquarters.



## INSTITUTIONAL LISTINGS

The IRE Professional Group on Military Electronics is grateful for the assistance given by the firms listed below, and invites application for Institutional Listings from other firms interested in the field of Military Electronics.

ELECTRONIC COMMUNICATIONS INC., 1501 72nd St., No., St. Petersburg, Fla.  
Systems Development, Advanced Communications, Data Link, Countermeasures, Special Purpose Computers

PHILCO CORP., Government and Industrial Div., 4700 Wissahickon Ave., Philadelphia 44, Pa.  
Microwave, Radar, Computers, Guided Missiles, Space Instrumentation, and Other Military Electronics Systems

THE RAMO-WOOLDRIDGE LABORATORIES, 8433 Fallbrook Ave., Canoga Park, Calif.  
Electronic Systems Technology and Intellectronics Laboratories

TEXAS INSTRUMENTS INCORPORATED, Apparatus Div., 600 Lemmon Ave., Dallas 9, Tex.  
Missile Electronics, Submarine Detection Systems, Electronic Surveillance Systems, Heavy Radar

The charge for an Institutional Listing is \$75.00 per issue or \$225.00 for four consecutive issues. Applications for Institutional Listings and checks (made out to the Institute of Radio Engineers) should be sent to Mr. L. G. Cumming, Technical Secretary, Institute of Radio Engineers, 1 East 79th Street, New York 21, N. Y.